

THE JOURNAL OF PHYSICAL CHEMISTRY

Registered in U. S. Patent Office © Copyright, 1968, by the American Chemical Society

VOLUME 72, NUMBER 3 MARCH 15, 1968

Isopiestic Measurements of the Osmotic and Activity Coefficients for the Systems $\text{HClO}_4\text{-LiClO}_4\text{-H}_2\text{O}$, $\text{HClO}_4\text{-NaClO}_4\text{-H}_2\text{O}$, and $\text{LiClO}_4\text{-NaClO}_4\text{-H}_2\text{O}$ ¹

by R. M. Rush and J. S. Johnson

Chemistry Division, Oak Ridge National Laboratory, Oak Ridge, Tennessee 37830 (Received October 9, 1967)

Isopiestic measurements of the osmotic coefficients are presented for the systems $\text{HClO}_4\text{-LiClO}_4\text{-H}_2\text{O}$, $\text{HClO}_4\text{-NaClO}_4\text{-H}_2\text{O}$, and $\text{LiClO}_4\text{-NaClO}_4\text{-H}_2\text{O}$. Parameters obtained from these results are used to derive the activity coefficients in the mixtures. Estimates of the activity coefficients in the mixtures may be made from information on the limiting two-component systems with an error of 7% or less at concentrations up to 5 *m*. The systems $\text{HClO}_4\text{-LiClO}_4\text{-H}_2\text{O}$ and $\text{LiClO}_4\text{-NaClO}_4\text{-H}_2\text{O}$ obey Harned's rule for both components reasonably well over the concentration range studied. For the system $\text{HClO}_4\text{-NaClO}_4\text{-H}_2\text{O}$ the deviations are greater, especially at the higher concentrations.

The importance of variations of free energies from ideality in chemical equilibria and kinetics is well appreciated. Information concerning these variations is of interest not only for its implications concerning the basic nature of solutions, but also for its fundamental importance in, for example, the study of complexing reactions, estimation of molecular weights by thermodynamic methods, and interpretation of reaction rate data. For aqueous solutions of electrolytes, there is a vast body of data available for two-component systems at 25°. Most cases of practical interest, however, involve mixtures of electrolytes, and it is here that there is a scarcity of data. There is not enough information on many important systems even to allow a check of various plausible procedures for estimation of multicomponent activity coefficients from values of the limiting two-component solutions.

We have been interested for some time in three-component systems, and a few years back, we tested equilibrium ultracentrifugation as a technique for studies in this area.² Recently we have started using the isopiestic method. The first system studied was a multicomponent system of solutions having the approximate composition of sea water.³ Because of their importance as inert media for various studies, we intend to study the behavior of various perchlorate

mixtures. This paper presents the first results of such an investigation: the systems $\text{HClO}_4\text{-LiClO}_4\text{-H}_2\text{O}$, $\text{HClO}_4\text{-NaClO}_4\text{-H}_2\text{O}$, and $\text{LiClO}_4\text{-NaClO}_4\text{-H}_2\text{O}$.

Experimental Section

Materials. Stock solutions of NaCl were prepared from reagent grade crystals dried overnight at 200°. The concentrations of the solutions were calculated from the weights of dried salt. Analysis of these solutions by measurement of the density to 5 parts/100,000 and comparison with the data of Wirth⁴ gave differences in molality of 0.10% or less.

A stock solution of H_2SO_4 was prepared from reagent grade concentrated acid. The solution was analyzed by weight titration against Na_2CO_3 . Weight titration against a concentrated NaOH solution which had been standardized against potassium acid phthalate gave results about 0.6% higher than the Na_2CO_3 titration. Since the direct titration with Na_2CO_3 involved fewer

(1) Research sponsored by the U. S. Atomic Energy Commission under contract with the Union Carbide Corp.

(2) R. M. Rush and J. S. Johnson, *J. Phys. Chem.*, **68**, 2321 (1964).

(3) R. M. Rush and J. S. Johnson, *J. Chem. Eng. Data*, **11**, 590 (1966).

(4) H. E. Wirth, R. E. Lindstrom, and J. N. Johnson, *J. Phys. Chem.*, **67**, 2339 (1963).

manipulations and gave more consistent results when the H_2SO_4 solutions were compared isopiesticly with the NaCl solutions, we used the concentration as determined by this method.

A stock solution of HClO_4 was prepared from reagent grade concentrated acid. The solution was analyzed by weight titration against Na_2CO_3 . Weight titration against a concentrated NaOH solution which had been standardized against potassium acid phthalate gave results about 0.6% higher than the Na_2CO_3 titration. We used the concentration as determined by the direct titration with Na_2CO_3 , for the same reasons as noted above for H_2SO_4 . Analysis by dilution, measurement of the density to 5 parts/100,000, and comparison with the data of Wirth⁴ gave a molality 0.07% lower than the value obtained from the direct titration with Na_2CO_3 .

A stock solution of LiClO_4 was prepared by neutralizing reagent grade HClO_4 with solid reagent grade LiOH to a pH of 4.5. The solution was analyzed by evaporation of a sample to dryness, heating at 200°, and weighing as LiClO_4 .

A stock solution of NaClO_4 was prepared by neutralizing concentrated reagent grade HClO_4 with solid reagent grade NaOH to a pH of 4.5. The solution was analyzed by evaporation of a sample to dryness, heating at 110°, and weighing as NaClO_4 . Analysis by dilution, measurement of the density to 5 parts/100,000, and comparison with the data of Wirth⁴ gave a molality 0.02% lower than that obtained by evaporation to dryness.

Solutions of the various perchlorate mixtures were prepared by weight from the above solutions. Distilled water, passed through a mixed-bed ion-exchange column, was used for the preparation of all solutions.

Apparatus and Procedure. The apparatus and procedure have been described previously.³ The temperature of the bath varied 0.01° or less during the course of an equilibration except for four points where the variation was 0.02°. The temperature of the bath at equilibrium varied from one equilibration run to another within the range of 24.99–25.01°.

Following the weighing of the 12 dishes, the first dish was weighed again; the difference between the two weighings was 0.01% of the weight of the solution, or less. All weights were corrected to their weights *in vacuo*. The dishes were allowed to equilibrate for 2–7 days.

For each set of equilibrations, there were at least two dishes containing the same solution, except as noted in the tables. The maximum difference in concentration among the replicate dishes was 0.1%.

The reference material was NaCl up to the limit of its solubility and H_2SO_4 for higher concentrations. The osmotic coefficients of these electrolytes were taken from the tables given by Robinson and Stokes.⁵

Table I: Isopiestic Concentrations for the Two-Component Systems^a

	$m_{\text{H}_2\text{SO}_4}$	m_{HClO_4}	m_{NaClO_4}
A	8.5700	8.3130	17.902 ^b
	7.2386	7.2122	14.218 ^b
	5.7762	5.8971	10.473 ^b
	4.5470	4.7036	7.6032 ^b
	3.4117	3.5449	5.2181 ^b
	2.3218	2.4042	3.1973 ^b
D	8.3244	8.1180	17.193
	5.3034	5.4478	9.3323
	3.5829	3.7231	5.5585
	2.4574	2.5477	3.4328
H	8.4064	8.1892	17.426
	7.7388	7.6427	15.571
	7.1752	7.1637	14.048
	6.2800	6.3680	11.722
	5.5858	5.7213	10.007
	4.3945	4.5540	7.2651
	3.3180	3.4499	5.0320
	2.4825	2.5748	3.4761

^a H_2SO_4 as reference material. ^b One dish only.

Table II: Isopiestic Concentrations for the Two-Component Systems^a

	m_{NaCl}	m_{HClO_4}	m_{LiClO_4}	m_{NaClO_4}
B	5.3454	4.0087		6.1283
	4.2536	3.2931		4.7440
	2.9916	2.4240		3.2280
	2.2088	1.8563		2.3362
	1.5771	1.3747		1.6389 ^b
C	1.6304	1.4150		1.6964
	1.1303	1.0150		1.1603
	0.8191	0.7538		0.8340
	0.5915	0.5552		0.5988
E	5.9796		4.4666	
	5.1742		3.9166	
	3.8196		2.9714	
	2.8004		2.2462	
	1.9970		1.6569 ^b	
F	5.7563		4.3176	
	4.9916		3.7924	
	4.1008		3.1710	
	3.2162		2.5468	
	2.3548		1.9224	
	1.7073		1.4364	
G	2.6685		2.1516	
	2.1380		1.7631	
	1.5503		1.3202	
	1.1544		1.0103	
	0.8378		0.7528	

^a NaCl as reference material. ^b One dish only.

(5) R. A. Robinson and R. H. Stokes, "Electrolyte Solutions," 2nd ed, revised, Butterworth and Co. Ltd., London, 1965.

Results

The isopiestic molalities for the limiting two-component systems, HClO₄-H₂O, LiClO₄-H₂O, and NaClO₄-H₂O, are given in Tables I and II. The isopiestic molalities and the osmotic coefficients for the three-component systems, HClO₄-LiClO₄-H₂O, HClO₄-NaClO₄-H₂O, and LiClO₄-NaClO₄-H₂O, are given in Tables III-VI.

Table III: Isopiestic Concentrations and Osmotic Coefficients for the System HClO₄(A)-LiClO₄(B)-H₂O

	<i>m</i> _{NaCl}	<i>m</i>	<i>y</i> _B	φ (obsd)
E	5.9796	4.4224	0.2509	1.7145
		4.4366	0.4997	1.7090
		4.4513	0.7474	1.7033
	5.1742	3.9010	0.2509	1.5991
		3.9043	0.4997	1.5977
		3.9100	0.7474	1.5954
	3.8196	2.9880	0.2509	1.4093
		2.9802	0.4997	1.4130
		2.9746	0.7474	1.4157
	2.8004	2.2725	0.2509	1.2711
		2.2609	0.4997	1.2776
		2.2518	0.7474	1.2828
1.9970	1.6834	0.2509	1.1657	
	1.6728	0.4997	1.1731	
	1.6637	0.7474	1.1795	

Treatment of Results

In the interpretation of the above data, we follow the procedure of Scatchard,⁶ who starts with the excess free energy, *G*^e. The excess free energy is the total free energy of the solution less that of the components in their standard state, and less the ideal free energy represented by the concentration terms. Scatchard uses the dimensionless form, *G*^e/*RT*, where *R* is the gas constant and *T* is the absolute temperature. He expresses it as a sum of contributions calculated from the limiting two-component solutions (*A* terms, solute indicated by single subscript), contributions involving concentrations of two solute components (a series of *B* terms, the solutes indicated by a double subscript),

(6) G. Scatchard, *J. Amer. Chem. Soc.*, **83**, 2636 (1961). For the convenience of readers who may wish to follow the development in detail, we list several misprints in the equations. Equation 1 should read: $G^e/RT = (G - G^*)/RT + \sum_i n_i(1 - \ln n_i/n_0w_0) = \sum_i n_i A_i \sqrt{I} + \sum_{ij} n_i n_j (B_{ij} + C_{ij} \sqrt{I})/n_0w_0 + \sum_{ijk} n_i n_j n_k (D_{ijk} + E_{ijk} \sqrt{I})/(n_0w_0)^2 + \dots$. The first line of eq 8 should read: $-\partial(G^e/RT \sum_i n_i^*)/\partial(\ln n_0w_0) = (\sum_{ij} n_i m_j / \sum_i m_i^*)(\phi - 1) = \dots$. The final factor in eq 15 should be y_B^3 . The equations on p 2639 should read: $B_{AB}^{(0,2)} - \beta_{AB}^{(0,2)} + 3(B_{AB}^{(1,2)} - \beta_{AB}^{(1,2)}) = -1/2(\beta_{AB}^{(0,2)} + 3\beta_{AB}^{(1,2)})$, $(\nu_B m_B / I_B) \ln y_B = A_B + \alpha_B + [-(\alpha_B - \alpha_A) + \beta_{AB}^{(0,1)} + 4\beta_{AB}^{(0,2)}/3] y_A - \beta_{AB}^{(0,2)} y_A^2$ (17). The correlation of Harned's symbols with Scatchard's, on p 2640, should be: $\alpha_{12} - j[(\alpha_B - \alpha_A) + \beta_{AB}^{(0,1)} + 2\beta_{AB}^{(0,2)}/3]/2.303 \nu_A I, \alpha_{21}^{(0)} - k[(\alpha_A - \alpha_B) + \beta_{AB}^{(0,1)} + 4\beta_{AB}^{(0,2)}/3]/2.303 \nu_B I, \beta_{21} + k\beta_{AB}^{(0,2)}/2.303 \nu_B I^2$. In the section concerning the Debye-Hückel treatment, it should be noted that $\mathcal{D} = 2(-1.17)$ for aqueous solution at 25°.

Table IV: Isopiestic Concentrations and Osmotic Coefficients for the System HClO₄(A)-NaClO₄(B)-H₂O^a

	<i>m</i> _{H₂SO₄}	<i>m</i>	<i>y</i> _B	φ (obsd)
A	8.5700	9.5588	0.2486	2.3548
		11.3156	0.5005	1.9892
		13.8616	0.7493	1.6238
	7.2386	8.1744	0.2486	2.1319
		9.5044	0.5005	1.8336
		11.3730	0.7493	1.5323
	5.7762	6.5680	0.2486	1.8666
		7.4696	0.5005	1.6413
		8.6928	0.7493	1.4104
	4.5470	5.1536	0.2486	1.6331
		5.7437	0.5005	1.4653
		6.5180	0.7493	1.2913
3.4117	3.8176	0.2486	1.4169	
	4.1682	0.5005	1.2978	
	4.6144	0.7493	1.1723	
2.3218	2.5398	0.2486	1.2218	
	2.7113	0.5005	1.1445	
	2.9222	0.7493	1.0619	
H	8.4064	9.3976	0.2486	2.3267
		11.0989	0.5007	1.9700
		13.5577	0.7496	1.6127
7.7388	8.7077	0.2486	2.2169	
	10.1928	0.5007	1.8939	
	12.3084	0.7496	1.5684	
7.1752	8.1110	0.2486	2.1191	
	9.4192	0.5007	1.8248	
	11.2588	0.7496	1.5266	
6.2800	7.1348	0.2486	1.9580	
	8.1760	0.5007	1.7086	
	9.6088	0.7496	1.4539	
5.5858	6.3551	0.2486	1.8300	
	7.2034	0.5007	1.6145	
	8.3514	0.7496	1.3925	
4.3945	4.9770	0.2486	1.6026	
	5.5206	0.5007	1.4448	
	6.2561	0.7496	1.2749	
3.3180	3.7080	0.2486	1.3989	
	4.0402	0.5007	1.2836	
	4.4633	0.7496	1.1619	
2.4825	2.7272	0.2486	1.2480	
	2.9206	0.5007	1.1653	
	3.1616	0.7496	1.0765	

^a H₂SO₄ as reference material.

and higher terms for systems with more than three components. Concentrations are expressed in ionic strength units. The *A*'s and *B*'s are functions of temperature and pressure, and ionic strength. For convenience in computation, we have expanded these parameters a little differently than Scatchard. Our *A* for each electrolyte consists of a Debye-Hückel term

Table V: Isopiestic Concentrations and Osmotic Coefficients for the System $\text{HClO}_4(\text{A})\text{-NaClO}_4(\text{B})\text{-H}_2\text{O}^a$

	m_{NaCl}	m	y_{B}	ϕ (obsd)
B	5.3454	4.3479	0.2486	1.4985
		4.7850	0.5005	1.3617
		5.3502	0.7493	1.2178
	4.2536	3.5320	0.2486	1.3666
		3.8369	0.5005	1.2580
		4.2236	0.7493	1.1429
	2.9916	2.5611	0.2486	1.2196
		2.7338	0.5005	1.1426
		2.9480	0.7493	1.0596
	2.2088	1.9398	0.2486	1.1327
		2.0444	0.5005	1.0747
		2.1716	0.7493	1.0118
1.5771	1.4218	0.2486	1.0655	
	1.4807	0.5005	1.0231	
	1.5509	0.7493	0.9768	
C	1.6304	1.4656	0.2486	1.0716
		1.5282	0.5005	1.0277
		1.6026	0.7493	0.9800
	1.1303	1.0416	0.2486	1.0206
		1.0748	0.5005	0.9891
		1.1132	0.7493	0.9550
	0.8191	0.7688	0.2486	0.9902
		0.7875	0.5005	0.9667
		0.8084	0.7493	0.9417
	0.5915	0.5635	0.2486	0.9695
		0.5739	0.5005	0.9519
		0.5852	0.7493	0.9335

^a NaCl as a reference material.

and a power series in I . As many B terms are used as are necessary to represent the three-component data; each of our B terms is an integral power series in I (see eq 8 and 9).

By differentiation of appropriate excess-energy functions with respect to amount of solvent, an expression involving the osmotic coefficient, ϕ , of the solutions is obtained; by differentiating with respect to number of moles of component J , an expression for the activity coefficient, $\gamma_{\pm J}$, is obtained. (Guggenheim⁷ has used a similar procedure in a discussion of mixtures of 1:1 electrolytes, although his discussion was limited to concentrations at which power-series terms linear in concentration are adequate.) These equations involve the A and B coefficients and their partial derivatives, α and β , with respect to $\ln I$. The coefficients in the equations for ϕ necessary to fit experimental data are also the coefficients in the $\ln \gamma_{\pm}$ equations, and activity coefficients can be evaluated from ϕ for two- and three-component solutions without going through the cumbersome conventional integration procedure, with the difficulties it involves near the limit of zero concentration. This treatment, instead,

Table VI: Isopiestic Concentrations and Osmotic Coefficients for the System $\text{LiClO}_4(\text{A})\text{-NaClO}_4(\text{B})\text{-H}_2\text{O}$

	m_{NaCl}	m	y_{B}	ϕ (obsd)
F	5.7563	4.6958	0.2509	1.5332
		5.1715	0.4982	1.3922
		5.8212	0.7562	1.2368
	4.9916	4.1018	0.2509	1.4499
		4.4881	0.4982	1.3251
		5.0087	0.7562	1.1874
	4.1008	3.4056	0.2509	1.3527
		3.6946	0.4982	1.2468
		4.0782	0.7562	1.1296
	3.2162	2.7105	0.2509	1.2571
		2.9122	0.4982	1.1700
		3.1734	0.7562	1.0737
2.3548	2.0279	0.2509	1.1652	
	2.1534	0.4982	1.0973	
	2.3122	0.7562	1.0219	
1.7073	1.5046	0.2509	1.0974	
	1.5804	0.4982	1.0448	
	1.6739	0.7562	0.9864	
G	2.6685	2.2780	0.2509	1.1983
		2.4294	0.4982	1.1237
		2.6244	0.7562	1.0402
	2.1380	1.8541	0.2509	1.1423
		1.9620	0.4982	1.0795
		2.0980	0.7562	1.0095
	1.5503	1.3760	0.2509	1.0808
		1.4408	0.4982	1.0322
		1.5206	0.7562	0.9780
	1.1544	1.0453	0.2509	1.0398
		1.0858	0.4982	1.0010
		1.1338	0.7562	0.9586
0.8378	0.7736	0.2509	1.0072	
	0.7974	0.4982	0.9772	
	0.8246	0.7562	0.9449	

implicitly makes use of the known Debye-Hückel expressions for ϕ and $\ln \gamma_{\pm}$ in dilute solutions.

The equation for ϕ of a three-component mixture is (ref 6, eq 14)

$$\phi = 1 + \frac{I}{\nu_A m_A + \nu_B m_B} \left\{ \alpha_A + (\alpha_B - \alpha_A) y_B + \beta_{AB}^{(0)} y_B (1 - y_B) + \beta_{AB}^{(1)} y_B (1 - y_B) (1 - 2y_B) \right\} \quad (1)$$

where

$$\alpha_J = \frac{2S}{a_J^3 I} \left[1 + a_J I^{1/2} - \frac{1}{1 + a_J I^{1/2}} - 2 \ln (1 + a_J I^{1/2}) \right] + a_J^{(1)} I + a_J^{(2)} I^2 + a_J^{(3)} I^3 + a_J^{(4)} I^4 \quad (2)$$

(7) E. A. Guggenheim, "Applications of Statistical Mechanics," Clarendon Press, Oxford, 1966.

Table VII: a Parameters for the Two-Component Systems (Eq 2)

	$a^{(1)}$	$a^{(2)}$	$a^{(3)}$	$a^{(4)}$	σ
1a HClO ₄ , all data	0.23770	0.03666	-0.00204	0.000046	0.0022
1b HClO ₄ , NaCl as reference material	0.2588	0.01164	0.00600	-0.000740	0.0005
2 LiClO ₄	0.3434	-0.01570	0.00678	-0.000666	0.0007
3a NaClO ₄ , all data	0.00894	0.01102	-0.000950	0.0000236	0.0030
3b NaClO ₄ , NaCl as reference material	0.00172	0.01276	-0.000890	0 ^a	0.0005

^a Not varied; fixed at zero.

$$\beta_{AB}^{(0)} = b_{AB}^{(0,1)}I + b_{AB}^{(0,2)}I^2 + b_{AB}^{(0,3)}I^3 \quad (3)$$

$$\beta_{AB}^{(1)} = b_{AB}^{(1,2)}I^2 + b_{AB}^{(1,3)}I^3 \quad (4)$$

and where y_J is the ionic strength fraction I_J/I for any component J, \mathbf{a}_J is the distance of closest approach parameter for any component J, ν_J is the number of ions per molecule of component J, I is the ionic strength on the molality scale, and $S = -1.17082$ (aqueous solutions at 25°). For a mixture of two 1:1 electrolytes, $I/(\nu_A m_A + \nu_B m_B) = 0.5$ and $I = m = m_A + m_B$, the total molality. It should be noted that our $b_{AB}^{(j,i)}$ are Scatchard's $\beta_{AB}^{(j,i)}/I^i$.

The equations for the activity coefficients of components A and B are (ref 6, eq 15)

$$\ln \gamma_{\pm A} = \frac{I_A}{\nu_A m_A} [A_A + \alpha_A + (\alpha_B - \alpha_A) y_B + \beta_{AB}^{(0)} y_B + (B_{AB}^{(0)} - \beta_{AB}^{(0)}) y_B^2 + \beta_{AB}^{(1)} y_B + 3(B_{AB}^{(1)} - \beta_{AB}^{(1)}) y_B^2 - 2(2B_{AB}^{(1)} - \beta_{AB}^{(1)}) y_B^3] \quad (5)$$

$$\ln \gamma_{\pm B} = \frac{I_B}{\nu_B m_B} [A_B + \alpha_B + (\alpha_A - \alpha_B) y_A + \beta_{AB}^{(0)} y_A + (B_{AB}^{(0)} - \beta_{AB}^{(0)}) y_A^2 - \beta_{AB}^{(1)} y_A - 3(B_{AB}^{(1)} - \beta_{AB}^{(1)}) y_A^2 + 2(2B_{AB}^{(1)} - \beta_{AB}^{(1)}) y_A^3] \quad (6)$$

where

$$(A_J + \alpha_J) = \frac{2SI^{1/2}}{1 + \mathbf{a}_J I^{1/2}} + 2\mathbf{a}_J^{(1)}I + \frac{3}{2}\mathbf{a}_J^{(2)}I^2 + \frac{4}{3}\mathbf{a}_J^{(3)}I^3 + \frac{5}{4}\mathbf{a}_J^{(4)}I^4 \quad (7)$$

$$B_{AB}^{(0)} = b_{AB}^{(0,1)}I + \frac{1}{2}b_{AB}^{(0,2)}I^2 + \frac{1}{3}b_{AB}^{(0,3)}I^3 \quad (8)$$

$$B_{AB}^{(1)} = \frac{1}{2}b_{AB}^{(1,2)}I^2 + \frac{1}{3}b_{AB}^{(1,3)}I^3 \quad (9)$$

For a mixture of 1:1 electrolytes $I_A/\nu_A m_A = I_B/\nu_B m_B = 0.5$.

The values of the power-series coefficients, $\mathbf{a}_J^{(2)}$, and the distance of closest approach parameter, \mathbf{a}_J , in eq 2 are obtained from the osmotic coefficients of the individual components, in this study by the method of least squares. These coefficients can then be used in eq 7 to calculate the contribution of the individual

components to the activity coefficients. The osmotic coefficients for the mixture are then used to obtain the b coefficients of eq 3 and 4, again by the method of least squares. These in turn define the B coefficients of eq 8 and 9.

It should be noted that, since the Debye-Hückel contributions of the two-component systems appear only in the A and α terms, the distance of closest approach parameter need not be the same for the two components of the mixture.

Discussion

Two-Component Systems. The values of the a coefficients for the two-component systems are given in Table VII. The deviations from the fitted equations are shown in Figure 1. In all cases, a satisfactory fit could be obtained with \mathbf{a} fixed at the value 1.5. The standard deviation, $\sigma = [\sum d^2/(n - k)]^{1/2}$, where d is the deviation, n is the number of observations, k is the number of variable parameters, and the summation is overall observations, is also given in this table.

1. HClO₄. Two sets of parameters are given in Table VII for HClO₄. The solubility of LiClO₄ limits

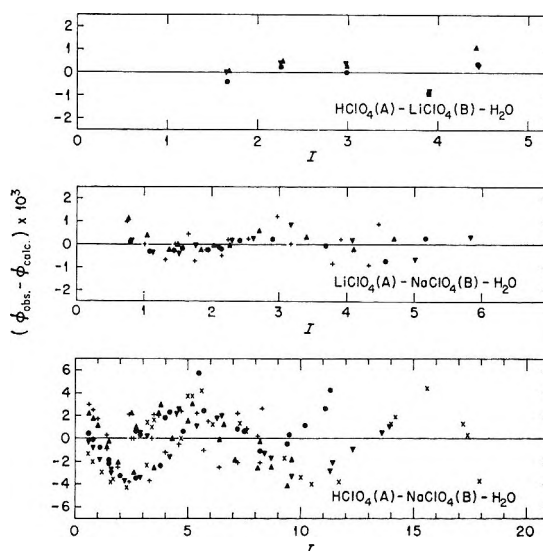


Figure 1. Deviations of osmotic coefficients for two- and three-component data from fitted equations (symbol, y_B : +, 0.0; \blacktriangle , 0.25; \bullet , 0.5; \blacktriangledown , 0.75; \times , 1.0).

the concentration range of mixtures containing this salt to approximately the range covered by NaCl as the reference salt. Parameters for HClO₄ were derived for the entire range of concentrations and for the concentration range covered by NaCl as reference salt. In both cases, the osmotic coefficients calculated with these parameters agree with those tabulated by Robinson and Stokes⁵ with an average deviation without regard to sign of 0.003 and a maximum deviation of 0.009 in ϕ .

2. *LiClO₄*. The osmotic coefficients derived from the parameters given in Table VII agree with those tabulated by Robinson and Stokes,⁵ with an average deviation of 0.003 and a maximum deviation of 0.013 in ϕ .

3. *NaClO₄*. As with HClO₄, a separate set of parameters was derived for the data with NaCl as the reference material. Literature values for the osmotic coefficients of NaClO₄ go up to only 6 *m*.⁵ Within this range, our values agree with those tabulated by Robinson and Stokes⁵ with an average deviation of 0.003 and a maximum deviation of 0.005 in ϕ . Table VIII gives values of the osmotic coefficients and activity coefficients of NaClO₄ at even molalities from 6 to 18 *m* as a supplement to the tables in the literature.⁵ The data in this table were calculated using parameter set 3a of Table VII.

Table VIII: Osmotic and Activity Coefficients for NaClO₄ at High Concentrations

<i>m</i>	ϕ	γ_{\pm}	<i>m</i>	ϕ	γ_{\pm}
6	1.0579	0.684	13	1.2118	0.887
7	1.0888	0.713	14	1.2218	0.910
8	1.1174	0.744	15	1.2306	0.933
9	1.1430	0.775	16	1.2392	0.955
10	1.1653	0.805	17	1.2493	0.979
11	1.1841	0.834	18	1.2626	1.007
12	1.1994	0.862			

From the above discussion, it is clear that our measurements on the two-component systems are in satisfactory agreement with values in the literature, thus lending confidence to the accuracy of our three-component values.

Three-Component Systems. The values of the *b* parameters for the three-component systems are given in Table IX. The deviations from the fitted equations are also shown in Figure 1. For each system, fits were obtained using combinations of parameters other than those shown in the table. The sets of parameters given in Table IX are those with the least number of parameters which do not represent a significant increase in the standard deviation (σ).

In considering the activity coefficients in the mix-

Table IX: *b* Parameters for the Three-Component Systems (Eq 3 and 4)

	HClO ₄ (A)- LiClO ₄ (B)	HClO ₄ (A)- NaClO ₄ (B)	LiClO ₄ (A)- NaClO ₄ (B)
Two-component parameters ^a	1b, 2	1a, 3a	2, 3b
$b_{AB}^{(0.1)}$	0.0308	0.0609	0.0158
$b_{AB}^{(0.2)}$	-0.00637	-0.03213	-0.0202
$b_{AB}^{(0.3)}$	0 ^b	0.000319	0.00105
$b_{AB}^{(1.2)}$	0 ^b	0 ^b	0.00420
$b_{AB}^{(1.3)}$	0 ^b	-0.000513	-0.00097
σ	0.0006	0.0022	0.0004

^a See Table VII. ^b Not varied; fixed at zero.

tures, it is convenient to define a deviation function δ such that

$$\delta_J = \log \gamma_{\pm J} - (\log \gamma_{\pm J})_{\alpha} \quad (10)$$

where $(\log \gamma_{\pm J})_{\alpha}$ is obtained from eq 5 or 6 using only the parameters for the limiting two-component systems, *i.e.*, with the *b* coefficients all equal to zero. Thus

$$\delta_A = \frac{I_A}{\nu_A m_A} [\beta_{AB}^{(0)} y_B + (B_{AB}^{(0)} - \beta_{AB}^{(0)}) y_B^2 + \beta_{AB}^{(1)} y_B + 3(B_{AB}^{(1)} - \beta_{AB}^{(1)}) y_B^2 - 2(2B_{AB}^{(1)} - \beta_{AB}^{(1)}) y_B^3] \times 0.4343 \quad (11)$$

$$\delta_B = \frac{I_B}{\nu_B m_B} [\beta_{AB}^{(0)} y_A + (B_{AB}^{(0)} - \beta_{AB}^{(0)}) y_A^2 - \beta_{AB}^{(1)} y_A - 3(B_{AB}^{(1)} - \beta_{AB}^{(1)}) y_A^2 + 2(2B_{AB}^{(1)} - \beta_{AB}^{(1)}) y_A^3] \times 0.4343 \quad (12)$$

This deviation function indicates how well the activity coefficients in the mixture can be estimated from the limiting two-component osmotic coefficient data. By the Brønsted rule (as extended by Scatchard) for obtaining activity coefficients of electrolytes in mixed solutions, $\delta = 0$, and the value of δ can be taken as a measure of the success of this rule. In addition, it is possible to observe how well a given component obeys Harned's rule.⁸ A plot of δ as a function of ionic strength fraction at a given ionic strength should be linear if Harned's rule is obeyed for the component in question.

1. *HClO₄-LiClO₄-H₂O*. This system was investigated over a shorter range of concentrations, partly because of the limited solubility of LiClO₄ and partly because of the proximity of the osmotic coefficients of HClO₄ and LiClO₄. The osmotic coefficients of this system can be fitted quite well with only the two cross parameters $b_{AB}^{(0.1)}$ and $b_{AB}^{(0.2)}$ (see Table IX). The behavior of the deviation function δ at ionic strengths

(8) H. S. Harned and B. B. Owen, "The Physical Chemistry of Electrolytic Solutions," 3rd ed, Reinhold Publishing Corp., New York, N. Y., 1958, Chapter 14.

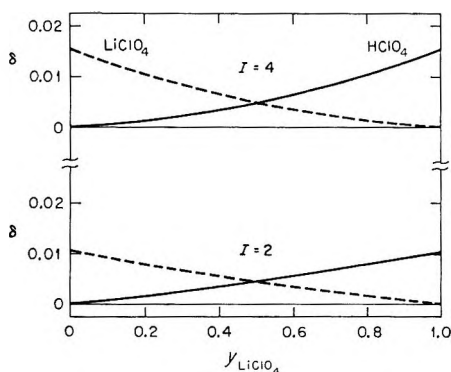


Figure 2. Deviation function, δ , for the system $\text{HClO}_4\text{-LiClO}_4\text{-H}_2\text{O}$.

2 and 4 is shown in Figure 2. As can be seen in this figure, the maximum error in approximating the activity coefficients from the limiting two-component data is 2% in γ_{\pm} at $I = 2$ and 4% at $I = 4$. The maximum deviation from linearity (Harned's rule) is 0.1% in γ_{\pm} at $I = 4$ and even less at $I = 2$. It is apparent from Figure 2 and from eq 11 and 12 that, if $\beta_{AB}^{(1)}$ is zero, the δ functions for the two components of the mixture are mirror images.

2. $\text{HClO}_4\text{-NaClO}_4\text{-H}_2\text{O}$. Because of the high solubility of HClO_4 and NaClO_4 , this system was investigated over the greatest range of concentrations (0.6–14 m). This system can be represented adequately with four cross parameters, $b_{AB}^{(0,1)}$, $b_{AB}^{(0,2)}$, $b_{AB}^{(0,3)}$, and $b_{AB}^{(1,3)}$ (see Table IX). Inclusion of the parameter $b_{AB}^{(1,2)}$ did not improve the standard deviation (σ). Fixing $b_{AB}^{(0,3)}$ at zero produced almost as good a fit ($\sigma = 0.0028$) as that given in Table IX. The behavior of the deviation function, δ , at three ionic strengths is shown in Figure 3. The maximum error in approximating the activity coefficients from the limiting two-component data is 2, 7, and 50% in γ_{\pm} at $I = 1, 5$, and 9, respectively. The maximum deviation from linearity at these same ionic strengths is 0.3, 6, and 20% in γ_{\pm} , respectively. It is clear from Figure 3 that the deviation from linearity (Harned's rule) is greater for the activity coefficient of HClO_4 than for that of NaClO_4 .

3. $\text{LiClO}_4\text{-NaClO}_4\text{-H}_2\text{O}$. Investigation of this system was also limited by the solubility of LiClO_4 . Since the osmotic coefficients of LiClO_4 and NaClO_4 are quite different, the investigation was extended to lower concentrations than with the $\text{HClO}_4\text{-LiClO}_4\text{-H}_2\text{O}$ system. This system requires all five cross parameters (see Table IX) for the best fit to the data, although the fit is almost as good ($\sigma = 0.0009$) using only the two parameters $b_{AB}^{(0,1)}$ and $b_{AB}^{(0,2)}$. The behavior of the deviation function, δ , at three ionic strengths is shown in Figure 4. The maximum error in approximating the activity coefficients from the limiting two-component data is 0.4, 2, and 7% in γ_{\pm} at $I = 1, 3$, and 5, respectively. The maximum deviation from linearity at

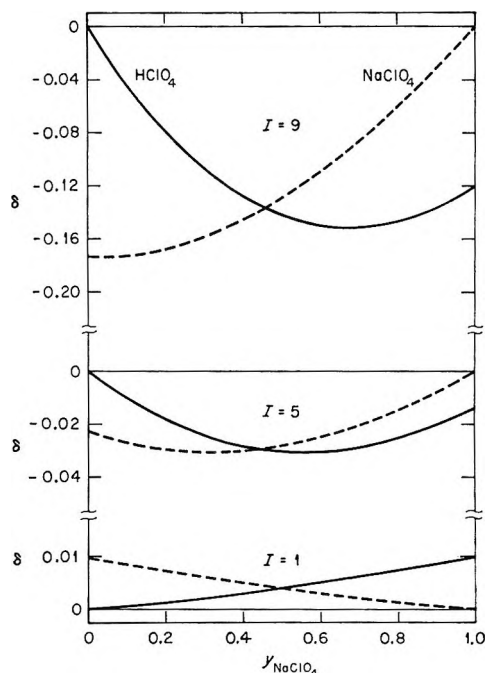


Figure 3. Deviation function, δ , for the system $\text{HClO}_4\text{-NaClO}_4\text{-H}_2\text{O}$.

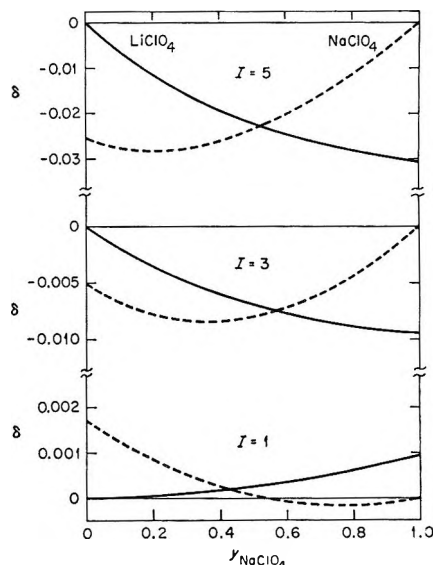


Figure 4. Deviation function, δ , for the system $\text{LiClO}_4\text{-NaClO}_4\text{-H}_2\text{O}$.

these same ionic strengths is 0.2, 1, and 2% in γ_{\pm} , respectively.

From the above discussion, it is apparent that the equations given by Scatchard provide an adequate and convenient means of representing the osmotic coefficients of three-component mixtures. In addition, these equations provide a simple method for the calculation of the activity coefficients that is not dependent on an integration to zero concentration, as is the case with the McKay-Perring method.⁹ We have re-

(9) H. A. C. McKay and J. K. Perring, *Trans. Faraday Soc.*, **49**, 163 (1953).

cently shown that the Scatchard approach, as outlined above, agrees well with the McKay-Perring method for the system NaCl-KCl-H₂O.¹⁰

The Scatchard equations also provide a convenient way of approximating the osmotic or activity coefficients in the three-component mixture from the data on the limiting two-component systems alone. Guggenheim⁷ also has found for many dilute solutions of 1:1 electrolytes that activity coefficients for mixtures can be estimated to a good approximation from two-component data. In the examples given here, the error in γ_{\pm} introduced by this approximation is, at most, 7% at ionic strengths up to five. For the one system studied at higher concentrations, HClO₄-

NaClO₄-H₂O, this approximation produces a much greater error. For the systems HClO₄-LiClO₄-H₂O and LiClO₄-NaClO₄-H₂O, Harned's rule is followed for both components within a few per cent up to $I = 5$. For the system HClO₄-NaClO₄-H₂O, the deviation from Harned's rule is quite noticeable even at $I = 5$. The activity coefficients of HClO₄ show a greater deviation than those of NaClO₄.

Acknowledgments. We express our appreciation to Professor George Scatchard for helpful discussions and to Neva Harrison for technical assistance.

(10) R. M. Rush and R. A. Robinson, *J. Tenn. Acad. Sci.*, in press

Photodecomposition of Aqueous Solutions of Barium Azide

by V. R. Pai Verneker¹ and M. Blais

Explosives Laboratory, Feltman Research Laboratories, Picatinny Arsenal, Dover, New Jersey 07801
(Received March 6, 1967)

The kinetics of gas evolution and the formation of ammonia, hydrazine, and hydroxylamine when aqueous solutions of barium azide are photolyzed with light from a low-pressure mercury lamp are investigated as a function of intensity, time of irradiation, and the concentration of the solution. Earlier work on the change in pH of such solutions as a function of time of irradiation by Bonnemay has been repeated. Results indicate that the pH rises steeply and finally attains a constant value. In extremely dilute solutions, if the reaction is followed to completion, the pH eventually begins to decrease. A possible explanation as to why Bonnemay found that the reaction is heterogeneous in certain concentration ranges is included. This is discussed in the light of the possible interference of CO₂ and of the photodecomposition of secondary products.

Introduction

Studies on the photodecomposition of aqueous solutions of azides have been undertaken by Gleu,² Bonnemay,³ and Shinohara, *et al.*⁴ The latter workers added mercuric salt to the azide solution before photolyzing. During photolysis the hydrogen atoms formed ($N_3^- + H_2O \xrightarrow{h\nu} H + OH^- + N_2$) reduce the mercuric salt and give mercurous azide; the pH of the solution remains unchanged. The experimental conditions, such as degassing of the solution, description of light source, *etc.*, which we find to be of great importance in these studies, are explicitly described by Shinohara, *et al.*⁴ The other workers, Gleu² and Bonnemay,³ do not describe their conditions in detail, although they both studied the photolysis of aqueous solutions of NaN₃ without any intentional use of a scavenger. Gleu² used as a light source a Hg lamp which was immersed in the experimental solution, the solution being contained in a closed vessel at a constant temperature.

He analyzed only the final products of decomposition. The products of decomposition are N₂H₄, NH₄OH, NH₂OH, N₂, and a trace of H₂, and are independent of the pH of the solution. Bonnemay did not immerse the Hg lamp in the solution but used a quartz vessel as a container and a low-pressure mercury lamp as an external source ($\lambda \sim 2537 \text{ \AA}$). He followed the reaction by observing the destruction of azide ions (colorimetrically, using FeCl₃) and the increase in the pH using a pH meter. He found that in the concentration range 2.3 *N* to saturation the reaction is homogeneous and does not depend on the vessel used. The reaction has the following characteristics. There is an induction period (pH ~ 9), a rapid rise in the pH, a

(1) Address correspondence to this author at the Research Institute for Advanced Studies, Baltimore, Md. 21227.

(2) K. Gleu, *Ber. Bunsenges. Phys. Chem.*, **61**, 702 (1928).

(3) M. Bonnemay, *J. Chem. Phys.*, **41**, 18 (1944).

(4) K. Shinohara, T. Shida, and N. Saito, *ibid.*, **38**, 1985 (1963).

region of fairly constant pH (~ 10.5), and a second rise followed by a constant pH region (~ 11.8). In the medium concentration range (1 to $1 \times 10^{-3} M$), the reaction is heterogeneous. In some cases, plots of pH *vs.* time are similar to those in the strong concentration range, but in other cases, after the induction period, the pH rises to a constant value of 12 without any intermediate step. This behavior is attributed to the vessel. In the weak concentration range (below $0.001 N$) the pH, after the induction period, rises to a constant value which depends on the concentration of the starting solution. The reaction is homogeneous.

Although Bonnemay has made a systematic study of the reaction as it proceeds (the depletion of the azide ion and the production of the OH^-), the results are rather puzzling because the photochemical reaction is homogeneous in certain concentration ranges and heterogeneous in other ranges. In this paper a study is made of the production and destruction of the products during the course of the reaction.

Experimental Section

Water used in all the experiments was triply distilled. Barium azide was prepared by passing hydrazoic acid gas, prepared by the Reitzner method, into an aqueous solution of barium carbonate of spectroscopic grade. The radiation source was one or more Spectroline quartz pencil lamps, manufactured by Black Light East Corp, Westbury, N. Y. The output of the lamps is principally 2537 \AA , with a small component of 1849 \AA . The light intensity was varied by changing the number of the lamps calibrated with a thermopile. The experiments were all done at a constant temperature of 20° and in 1 atm of helium, nitrogen, oxygen, or carbon dioxide.

A known amount of the solution (degassed in all the experiments except when it was desirable to show the effect of not degassing) was put into a double-walled quartz vessel, and air or water was passed between the walls. The lamp used in this work, or any low-pressure mercury lamp, emits light of wavelength 1849 \AA ($\sim 2.0\%$) in addition to the major component, 2537 \AA ($\sim 98\%$). A water filter reduces the intensity of 1849-\AA light by 90–95%, whereas 2537-\AA light is reduced by only 10%. The electrodes to measure the pH or a thermometer were inserted into the solution. The light source was kept outside the vessel and was warmed up for at least 20 min before a run. The fraction of the light absorbed by the solutions was dependent on the concentration of the azide ions. The light traveled a 6-cm path of the experimental solution. The gas evolved as a result of photolysis was measured by the displacement method and the pH was recorded on a pH meter. Samples of the solution were taken at intervals with a syringe and analyzed for the products formed. At the end of the experiments when the light was turned off (Figure 1) the azide was all decomposed.

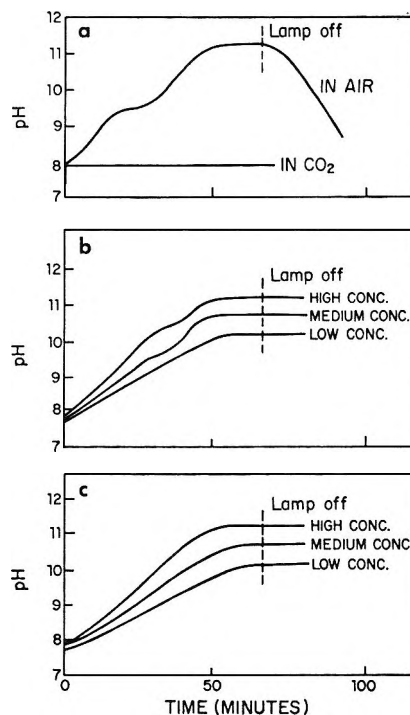


Figure 1. Photolysis of barium azide solutions: (a) in air and CO_2 atmosphere; (b) nondegassed solutions in O_2 , N_2 , or He atmosphere; (c) degassed solutions in O_2 , N_2 , or He atmosphere.

Results

The photolysis in air of barium azide dissolved in triply distilled water (not degassed) was followed from the pH change with the following results. The pH increased, stayed constant for a while (depending on the concentration), and then increased again until it attained a constant value. When the light was switched off, the pH decreased slowly, sometimes returning to its initial value and at times reaching an even lower value. However, when the experiments were performed in an atmosphere of CO_2 , the pH did not change at all, although the azide was decomposed. Furthermore, when the experiments were done in an atmosphere of nitrogen, oxygen, or helium, the value of the pH did not fall when the light was switched off. Figure 1 summarizes the results of the different experiments carried out in different atmospheres. When nondegassed solutions of a higher concentration were employed, the intermediate step was observed in a plot of pH *vs.* time of irradiation, but these were not detected with degassed solutions as shown in Figure 1.

Reproducible results were obtained only if the solutions saturated with nitrogen were carefully degassed before measurements were made.

In weak concentrations of the order of $10^{-5} M$ and with air used to cool the quartz cell (so as to maintain the temperature constant), it was found that the pH, after rising and attaining a constant value for a while, started to fall. This effect was not observed if a water filter to remove the 1849-\AA light was placed between the

mercury lamp and the cell instead of the air. This is shown in Figure 2.

The photolyzed solutions were subjected to analysis at various stages of decomposition. The analyses were carried out according to the methods of Kelly and Smith,⁵ Pesez and Petit,⁶ Bremner,⁷ and Blais.⁸ No detectable amounts of $\text{NH}_2\text{-NH}_2$ or NH_2OH were found. The products of decomposition were principally OH^- and NH_3 and N_2 gas, but small amounts of H_2 were also found. The ammonia concentration decreased after reaching a steady value, when light of wavelength 2537 and 1849 Å was used as the photolyzing source, as is shown in Figure 3. In Figure 4 the NH_3 concentration is plotted as a function of intensity, and it is shown that the rate of formation of NH_3 was proportional to the intensity of the source ($\lambda \sim 2537 \text{ \AA}$). Figure 5 gives plots of: (a) depletion of N_3^- , (b) increase in pH, (c) gas evolution, and (d) NH_3 formation as a function of the time of irradiation. Figure 6 gives plots of the rate of formation or depletion of the products *vs.* the intensity of light. Tables I and II give the yields of products resulting from the decomposition of barium azide solutions in the presence of nitrogen and helium, respectively.

Table I: Photolysis of $\text{Ba}(\text{N}_3)_2$ in Nitrogen (1 atm)^a

Time of irradiation, min	Total azide ion depleted, $\times 10^{-4}$ mol	Total N_2 , ^b $\times 10^{-4}$ mol	Total NH_3 , ^b $\times 10^{-4}$ mol	Total N_2 formed, $\times 10^{-4}$ mol	Total NH_3 formed, $\times 10^{-4}$ mol
30	0.68	0.91	0.23	0.70	0.67
60	1.31	1.73	0.43	1.37	1.46
120	2.86	3.81	0.95	2.92	2.81

^a Concentration, $5 \times 10^{-2} \text{ M}$. ^b Calculated from azides depleted according to eq 1 and 2.

Table II: Photolysis of $\text{Ba}(\text{N}_3)_2$ in Helium (1 atm)^a

Time of irradiation, min	Total azide ion depleted, $\times 10^{-4}$ mol	Total N_2 , ^b $\times 10^{-4}$ mol	Total NH_3 , ^b $\times 10^{-4}$ mol	Total N_2 formed, $\times 10^{-4}$ mol	Total NH_3 formed, $\times 10^{-4}$ mol
30	1.35	1.80	0.45	0.20	0.74
60	1.99	2.64	0.66	0.69	1.71
120	3.43	4.56	1.14	1.98	2.32
360	7.05	9.40	2.35	6.03	4.80

^a Concentration, $5 \times 10^{-2} \text{ M}$. ^b Calculated from azide depleted according to eq 1 and 2.

Discussion

The results presented in Figure 1 clearly indicate that photolysis of aqueous solutions of barium azide is a homogeneous reaction and is independent of the reac-

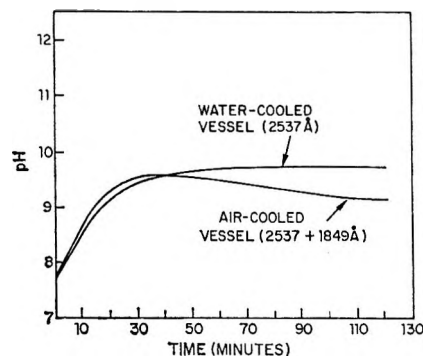


Figure 2. Effect of 1849-Å radiation on the pH of barium azide solution ($5 \times 10^{-6} \text{ M}$).

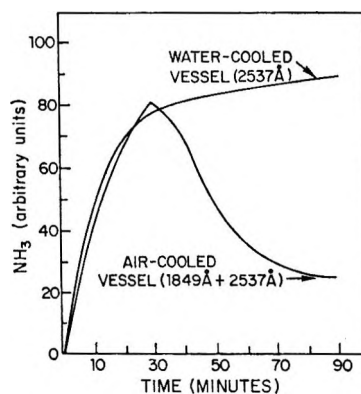


Figure 3. Formation and decomposition of ammonia ($5 \times 10^{-6} \text{ M}$).

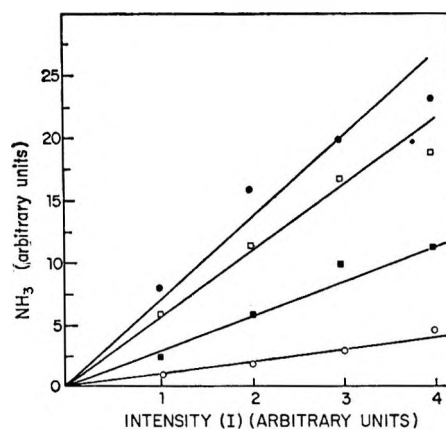


Figure 4. Rate of formation of ammonia as a function of light intensity ($5 \times 10^{-5} \text{ M}$): \circ , 5 min; \blacksquare , 10 min; \square , 15 min; \bullet , 20 min.

tion vessel. pH *vs.* time is a smooth curve with no breaks in between. This is true for all the concentrations studied. However, the reaction is strongly affected by impurities such as carbon dioxide. Bon-

(5) P. Kelly and M. Smith, *J. Chem. Soc.*, 1497 (1961).

(6) M. Pesez and A. Petit, *Bull. Soc. Chim. France*, 122 (1947).

(7) J. M. Bremner, *Analyst*, **79**, 198 (1954).

(8) M. Blais, *Microchem. J.*, **7**, 464 (1963).

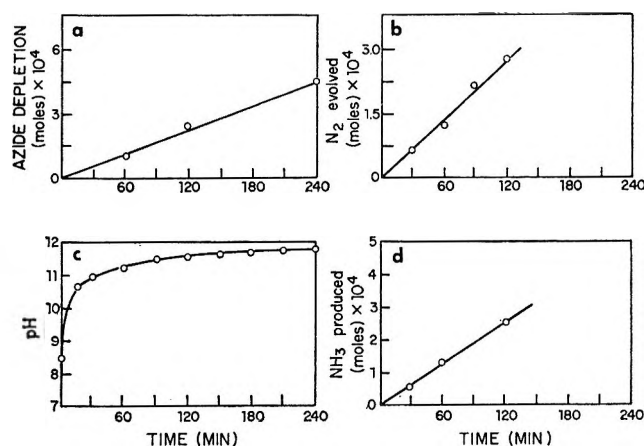


Figure 5. Photolysis of aqueous BaN_6 solutions ($5 \times 10^{-2} M$ degassed in N_2 atmosphere): (a) azide depletion vs. time of irradiation; (b) gas evolution vs. time of irradiation; (c) increase in pH vs. time of irradiation; (d) ammonia formation vs. time of irradiation.

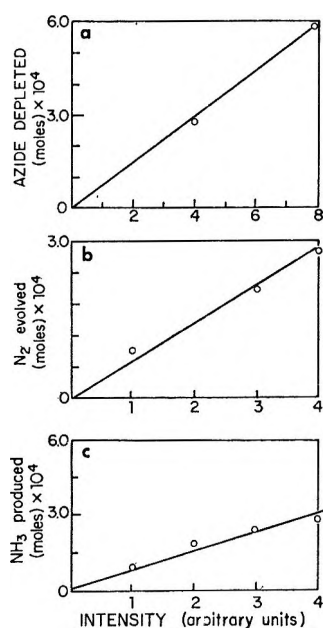


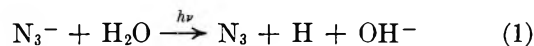
Figure 6. Photolysis of aqueous BaN_6 solutions ($5 \times 10^{-2} M$ degassed in N_2 atmosphere): (a) azide depletion vs. light intensity; (b) gas evolution vs. light intensity; (c) ammonia formation vs. light intensity.

nemay,³ who reports that the reaction is heterogeneous in the medium concentration range, does not specify whether his solutions were degassed or not. His results can be understood, if he worked with nondegassed or improperly degassed solutions. Bonnemay³ also reports that there is an induction period in the reaction, but no induction period was observed in the present experiments if the lamp was warmed up properly. The present results indicate that if one photolyzes an aqueous solution of barium azide under proper experimental conditions (thorough degassing and proper warming up of the lamp) and uses only light of wavelength 2537 \AA , the pH increases steadily until it attains

a constant value. However, if the irradiation source contains light of wavelength 1849 \AA , the pH decreases steadily after reaching the constant value, as shown in Figure 2.

Ammonia is found to absorb in the region of 2100 \AA . It is possible that light of wavelength 1849 \AA photolyzes NH_3 very efficiently, and this explains the drop in the pH shown in Figure 2.

Figure 3 shows how the concentration of NH_3 is controlled by light of wavelength 1849 \AA . The time at which the pH starts decreasing (Figure 2) and the time at which NH_3 concentration falls off (Figure 3) agree very well, suggesting that the drop in pH is caused by the photodecomposition of NH_3 . One also sees (Figure 4) that if light of wavelength 2537 \AA is used as a photolyzing source, the rate of formation of NH_3 is proportional to the intensity of the light. In the concentration range of $10^{-5} M$, the method used does not give a quantitative estimation of the total gas evolved, but estimates are given for other concentrations (Figures 5 and 6). The fact that the NH_3 concentration is proportional to the intensity could be explained by the following reactions proposed by Shinohara, *et al.*⁴

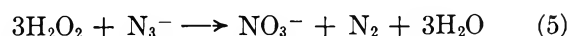


The mechanism requires that $\text{N}_2:\text{NH}_3$ ratio to be 4:1. However, the results in Table I (N_2 atmosphere) indicate that the $\text{N}_2:\text{NH}_3$ ratio is roughly 1:1. Further, there seems to be a quantitative agreement between the azide depleted and the products formed. When the experiment is done in an atmosphere of helium (Table II), the absolute yields are lower, and the ratio of $\text{N}_2:\text{NH}_3$ is still not 4:1.

The present results therefore necessitate a mechanism in which $\text{N}_2:\text{NH}_3$ ratio is 1:1 and the products are directly proportional to the intensity of the light source. A tentative speculation would be



the hydrogen peroxide subsequently reacting in accordance with the mechanism proposed by Shinohara, *et al.*⁴



In summary, then, when an aqueous solution of barium azide is irradiated with light from a low-pressure mercury lamp, in an atmosphere of nitrogen or helium gas, the products of decomposition consist of OH^- , NH_3 , N_2 , and NO_3^- . In view of the fact that Gleu² did not specify his experimental conditions, it is difficult to explain why he found large quantities of hydrazine and hydroxylamine; further, he immersed the lamp into the aqueous solution of the azide. This could mean that

(1) all the light of wavelength 1849 Å is absorbed by the solution, and (2) a significant amount of heat is generated by the lamp. We have also shown why Bon-

nemay³ found that the photolytic reaction is homogeneous in certain concentrations while it is heterogeneous in other concentrations.

Study of the Explosive Behavior of Barium Azide

by V. R. Pai Verneker¹ and L. Avrami

Explosives Laboratory, Picatinny Arsenal, Dover, New Jersey (Received August 17, 1967)

A study has been made of the factors which affect sensitivity of barium azide. The data show that (1) sensitivity increases with surface area; (2) solvents used in the preparation affect the sensitivity; (3) aging of the material initially brings about a desensitization, which is then followed by sensitization to the original level; (4) barium metal, either added physically or produced thermally, in concentrations up to 0.1 mol %, causes sensitization; and (5) impurities such as Na⁺ or [Fe(N₃)]²⁺ sensitize barium azide. It has also been shown that different crystal structures can be obtained, depending on the method of preparation.

Introduction

A great deal of work has been done on the slow processes occurring in the photochemical and thermal decomposition of barium azide.²⁻⁹ It is possible, however, to observe inconsistencies in the published results. For instance, Thomas and Tompkins² found that the rate of thermal decomposition of barium azide decreased somewhat with the passage of time after its synthesis. Yerofeyev and Sviridov⁸ later repeated this experiment and found no deceleration but, on the contrary, observed an acceleration. The temperature at which barium azide explodes has been reported to be 217-221,¹⁰ 225,¹¹ and 152°.¹²

According to Ficheroule and Kovache,¹³ barium azide explodes 14% of the time with a 2-kg weight at a height of 40 in. In the impact tests conducted on BaN₆ at Picatinny with a 2-kg weight from a height of 9 in., we have observed two different types of results. One group of results clearly indicates a 50% value at 9 in., while the other group shows a maximum of 5% at the same height.

Most of the workers who have reported on barium azide have not specified the conditions under which the tests were conducted. These, very likely, can affect the explosive properties of the material. This paper is presented as a broad exploration of chemical events that are implicit in characterizing or modifying explosive sensitivity. Much of the quantitative effort remains to be done, but the results so far are interesting enough to be presented for comment. The object of the present work is to study how these properties of barium azide are influenced by (1) particle size, (2) method of preparation, (3) age of the material, *i.e.*,

time elapsed between preparation and sensitivity testing, (4) additives, *i.e.*, physical mixtures, (5) prior partial thermal decomposition, and (6) impurities.

Experimental Section

Preparation of Material. Barium azide was prepared by passing hydrazoic acid gas from a generator¹⁴ into an aqueous solution of spectral grade barium carbonate until the solution was free of carbonate. The pH was maintained between 3 and 4. Azide crystals were then obtained from this solution by one of the following methods. (a) The solution was allowed to evaporate in air. Crystals were removed and half of this amount was dried in air. This will be referred to in the text as

(1) Address correspondence to this author at the Research Institute for Advanced Studies, Baltimore, Md. 21227.

(2) J. G. N. Thomas and F. C. Tompkins, *Proc. Roy. Soc. (London)*, **A209**, 550 (1951).

(3) P. W. M. Jacobs, F. C. Tompkins, and D. A. Young, *Discussions Faraday Soc.*, **28**, 234 (1959).

(4) S. K. Deb, *Trans. Faraday Soc.*, **59**, 1423 (1963).

(5) P. W. M. Jacobs, F. C. Tompkins, and V. R. Pai Verneker, *J. Phys. Chem.*, **66**, 1113 (1962).

(6) P. W. M. Jacobs, J. Sheppard, and F. C. Tompkins, *International Symposium on Reactivity of Solids, Germany, 1964*.

(7) F. E. Harvey, *Trans. Faraday Soc.*, **29**, 653 (1933).

(8) B. V. Yerofeyev and V. V. Sviridov, *Inst. Khim. An BSSR. Nauchn. Rabot.*, **5**, 113 (1956).

(9) W. E. Garner and J. Maggs, *Proc. Roy. Soc. (London)*, **A172**, 299 (1939).

(10) T. Curtius and J. Risson, *J. Prakt. Chem.*, **58**, 261 (1898); *J. Chem. Soc.*, **76** II, 91 (1899).

(11) A. R. Hitch, *J. Amer. Chem. Soc.*, **40**, 1195 (1918).

(12) L. Wohler and F. Martin, *Z. Angew. Chem.*, **30**, 33 (1917).

(13) H. Ficheroule and A. Kovache, *Mol. Phys.*, **33**, 7 (1951).

(14) B. Reitzner and R. P. Manno, *Nature*, **198**, 991 (1963).

preparation 1. The other half was dried in a vacuum desiccator over P_2O_5 (preparation 2). (b) Acetone was added to the solution until all of the solid precipitated. This precipitate was then dried in air (preparation 3). (c) Ethyl alcohol was used as a precipitating agent and the precipitate dried in air (preparation 4). (d) Methyl alcohol was used as a precipitating agent and the crystals formed were dried in air (preparation 5). (e) A solution was saturated by evaporation at 95° and then cooled to 65° . Crystals thus obtained were separated and dried in air (preparation 6).

These different preparations were analyzed for barium and nitrogen content.¹⁵ The results, given in Table I, are within $\pm 1.0\%$. Crystal structures were not determined, but X-ray powder diffractograms were obtained, using the same particle size, to demonstrate identity of crystal structure (Table II). Impurity determinations were made by emission spectroscopy. Results, which are accurate to $\pm 50\%$, are listed in Table III. All the tests were done on materials having the same particle size, which was obtained by passing the samples through nylon sieves of known diameter. Because of the aging effect, which is dealt with in the Results section of this paper, many of the comparative tests had to be completed within a day or so. For this reason, it has not been possible to do all the tests involving all the methods at the same time.

Table I: Analysis of Barium Azide

Formula	Ba, %	N ₂ , %
BaN ₃ (theoret)	61.98	38.01
BaN ₃ ·H ₂ O (theoret)	57.32	35.15
Preparation no.	Ba, %	N ₂ , %
1	57.60	35.40
2	62.37	38.02
3	62.60	37.70
4	62.10	38.15
5	62.20	37.60
6	62.30	37.80

Normally, in the tests that were conducted, barium azide was prepared by adding ethyl alcohol to an aqueous solution of barium azide. The exception was in the study of the influence of the method of preparation on the sensitivity. Since the accuracy of chemical analysis was $\pm 1.0\%$, it is possible that the ethanol may have been incorporated in the azide. However, even if this were the case, it would be common to all samples. Whenever the samples were not used, they were stored in a desiccator in the dark. To study the aging effect at different temperatures, the samples were placed in evacuated glass vessels and then one set was main-

tained at liquid nitrogen temperature, another set at -25° , and still another at $+55^\circ$. These temperatures were selected arbitrarily.

For doping purposes, the dopant was added to the aqueous solution of barium azide, which was then precipitated by the addition of ethanol. Two dopants were used. (1) The starting solution contained 1 mol % NaN₃. The amount of sodium which was incorporated into the crystals and the manner of incorporation were not determined. (2) The starting solution contained ferric azide in desired concentration and the uptake of iron was determined by using Fe⁵⁹ tracer. Ferric azide was prepared by dissolving spectral grade iron in an aqueous solution of HN₃. From earlier work by Pai Verneker, *et al.* (which is being communicated to the Journal of Physical Chemistry), it was determined that iron is carried by barium azide *via* anomalous mixed crystal formation, *i.e.*, [FeN₃]²⁺ is homogeneously distributed within the crystal. All the solvents used in this work were of spectral grade.

To study the influence of additives on sensitivity, barium metal (99.5% as obtained from K & K Laboratories, Plainview, N. Y.) was ground in air and passed through nylon sieves. A particle size was selected and mixed with barium azide of the same particle size by shaking it mechanically for 6 hr.

To study the effect of prior thermal decomposition on sensitivity, a 50-mg sample (of a specific particle size) was decomposed thermally (temperature, 110°) in a conventional vacuum system. An alphasatron gauge served to measure the pressure of nitrogen gas evolved (a liquid nitrogen trap was included in the system to collect any condensibles). After the desired degree of decomposition was obtained, a part of the decomposed solid was dissolved in water to test for ammonia, to determine if any nitride was formed. No significant amount of ammonia was detected (colorimetrically). Since the volume of the vacuum system was known, the extent of decomposition could be calculated from the quantity of nitrogen gas evolved.

Methods for Measuring the Sensitivity. Altogether, five techniques were used as an index of sensitivity: (1) impact sensitivity test, (2) explosion temperature test, (3) friction sensitivity test, (4) differential thermal analysis (DTA), and (5) thermal decomposition. The choice of a particular technique for a particular experiment was mostly determined by the length of time which could be spent on that experiment. Of the five, impact and explosion temperature tests were used most often.

Impact Sensitivity Test. In measuring the sensitivity of explosives to impact, the Picatinny Arsenal impact machine¹⁶ was used. Although a full impact sensitivity curve was desirable,¹⁷ this was not possible, since many

(15) M. Blais, *Microchem. J.*, 7, 4 (1963).

Table II: Prominent 2θ Angles in X-Ray Powder Diffractograms of Different Preparations of BaN_6 (in Arbitrary Values of Intensity)

Reflection angle 2θ	Prep 1 (air dried)	Prep 2 (desiccator dried)	Prep 3 (acetone solution)	Prep 4 (ethanol solution)	Prep 5 (methanol solution)	Prep 6 (95–65°)
16.4	2	...
17.4	1.5	6.5	3
18.6	6.5	4	10	6	13	86
20.2	1	4.5	1
22.1	10.5	8	13	8.5	25.5	8
26.0	1.5	2	3.5	2	5.5	2.5
27.0	1	...
28.1	2	1.5	3	1.5	4	57
28.7	...	1	...	1	5	2
30.2	0.5	5.5	7.5
33.0	1.5	1.5	2.5	2	5	2.5
34.8	5	3.5	8	4.5	7.5	5
39.2	2	2	4	3	4	2
40.8	2.5	2.5	3.5	2.5	7	2.5
44.1	2	0.5
45.3	...	1	1	1	4	1.5
57.9	0.5	1.5	14

Table III: Spectrographic Analysis^{a,b} of BaN_6 Samples, ppm Weight

Impurity	Prep 1	Prep 2	Prep 3	Prep 4	Prep 5	Prep 6
Pb	20	20	20	30	30	20
Ca	5	5	20	20	20	20
Al	<10 (N)	<10 (T)	20	15	20	10
Cr	10	10	5	10	10	10
Cu	10	5	1000	5	10	10
Fe	70	30	50	20	20	20
Mg	5	5	5	5	5	5
Si	30	40	200	30	200	120
Ni	<5 (N)	<5 (N)	5	<5 (T)	5	5
Ag	<1 (N)	<1 (N)	<1 (T)	<1 (T)	<1 (T)	<1 (T)
Sn	<1 (N)	<1 (N)	5	<1 (N)	5	5
Mn	<1 (N)	<1 (N)	<1 (T)	<1 (T)	<1 (T)	<1 (T)

^a Only elements found are listed in the table. Alkali metals were sought and none were found above blank. Analysis performed by Battelle Memorial Institute. ^b (T) = trace; (N) = not traced.

of the comparative tests had to be completed within a day or so. Therefore, the number of heights per specified sample was limited to three.

Explosion Temperature Test. The apparatus used for this test has been described previously.¹⁶ Instead of determining the 5-sec point, an arbitrary temperature was selected and five samples were tested at that point. The average of the five samples was used as the time to explode at that point.

Friction Sensitivity Test. The friction sensitivity apparatus used was a modified version of the experimental type developed at the Explosives Research and Development Establishment (ERDE) at Waltham Abbey, England. An empirical estimate of friction sensitivity difference was attempted by subjecting the material to the forces involved when a free-swinging pendulum dropped from a selected height strikes the upper block of a clamped assembly, consisting of two

blocks coated with abrasive between which the azide is placed. The percentage fire value was determined from the results of ten tests performed at each specific height.

Differential Thermal Analysis (DTA). DTA measures the difference in temperature between a sample and an inert reference when both are heated at a uniform rate, thus indicating the physical or chemical changes that occur within the sample. The equipment used was a DuPont 900 differential thermal analyzer.

Gas Evolution via Thermal Decomposition. In this phase of the investigation, a 50-mg sample was placed in a glass container, which was in turn connected to a conventional vacuum system. The sample was heated

(16) A. J. Clear, Standard Laboratory Procedures for Sensitivity, Brisance and Stability of Explosives, Picatinny Arsenal Technical Report FRL-TR-25, Dover, N. J., Jan 1961.

(17) P. W. Levy, *Nature*, 182, 37 (1958).

by immersion in an oil bath which had been preheated to within a tenth of a degree of the desired temperature. An alphasatron gauge connected to the system measured the pressure of any gas that evolved. The materials were subjected to 120° for 0.5 hr (selected arbitrarily) and the amount of gas evolved during this period was used as an index of sensitivity.

Results and Discussion

Figures 1 and 2 present data showing the effect of surface area on the sensitivity of barium azide. The surface area was calculated by considering the particles of barium azide as spheres, and the particle sizes were selected by screening the azide through different nylon sieves. Figure 1 shows the data obtained in the impact sensitivity test and Figure 2 presents the data obtained by the explosion temperature method. In both cases, we see that sensitivity increases with surface area. In his work on the thermal decomposition of lead azide, Jach¹⁸ reports that the activation energy needed for the surface reaction is much less than that needed for the bulk reaction. This means that, for PbN_6 , an increase in surface area results in a decreased total reaction time. The results indicate the same behavior for barium azide.

The data on the X-ray powder diffractograms of barium azide prepared by the different methods appear in Table II. By examining the intensities of the Bragg reflections at various reflection angles, one can conclude that preparations 1, 2, and 3 have one crystal structure (called A) and preparations 4, 5, and 6 have a second crystal structure (called B).

Data on the sensitivity of the different preparations measured by the impact test, friction test, and explosion temperature appear in Figure 3. Of the preparations having crystal structure A, barium azide with the water of crystallization is the least sensitive, the azide precipitated from acetone is second in sensitivity, and the maximum sensitivity is shown by the azide which has lost its water of crystallization. Table III shows that the impurity contents of preparations 1, 2, and 3 are of the same magnitude, except that preparation 3 has 200 ppm of Si and 1000 ppm of Cu. If impurities influence the sensitivity, then preparation 3 should have either the maximum or the minimum sensitivity compared to preparations 1 and 2. However, it is between 1 and 2. This does not rule out the fact that impurities affect the sensitivity, but it signifies that there may be other factors which have a greater influence.

Of the preparations having crystal structure B, preparation 5 was the least sensitive. Preparations 4 and 6 have the same sensitivity as tested by friction and impact machines, but the explosion temperature test suggests that preparation 6 was more sensitive than preparation 4. Table III shows that preparations 4, 5, and 6 all have an impurity content of the same order

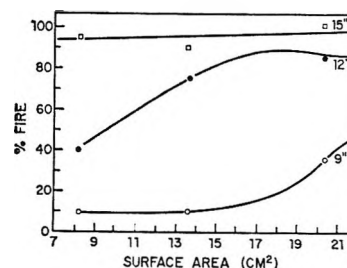


Figure 1. Impact sensitivity (2-kg drop weight) vs. surface area of barium azide. Each value is the result of 20 tests at each height.

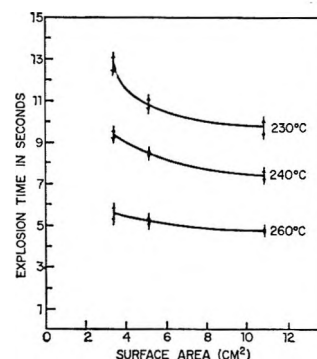


Figure 2. Time for BaN_6 to explode at indicated temperatures vs. surface area.

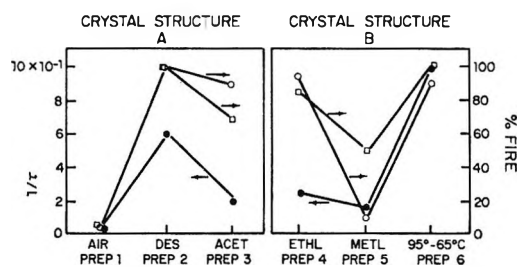


Figure 3. Sensitivity of BaN_6 as a function of the method of preparation: \times , $1/\tau$ for 290°; \square , friction sensitivity; \circ , impact sensitivity (2-kg drop weight) at 15 in. (20 tests at each point); \leftarrow or \rightarrow , points to vertical coordinate to which curve is relevant.

of magnitude except that preparations 5 and 6 have 200 and 120 ppm of Si, respectively. Preparation 4, on the other hand, has only 30 ppm of Si. This again shows that there may be factors other than the presence of impurities which have a more pronounced influence on sensitivity. Since all other factors, such as age, particle size, and storage conditions, were controlled, it seems probable that solvents used for crystallizing the azide play a role in determining the sensitivity of the material.

How the impact sensitivity of barium azide is influenced by the age of the material (time passed since its synthesis) is shown in Figure 4. The general trend seems to suggest that a desensitization process occurred

(18) J. Jach, *Trans. Faraday Soc.*, 59, 947 (1963).

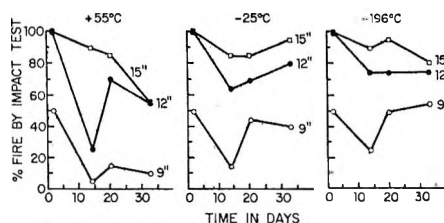


Figure 4. Aging effect of BaN_6 stored at different temperatures.

during the first 14 days, after which a sensitization process occurred. The data seem to suggest that the desensitization process is slowed down by storing the samples at low temperatures.

In Figure 5, data are presented indicating how the thermal sensitivity (explosion temperature) was influenced by the addition of barium metal. The particle size of the barium metal added was the same as that of the barium azide. The results indicate that when up to about 0.1% of barium metal is added, the sensitivity increases; however, on further addition, the sensitivity decreases. It is not clear why 1.0% barium metal should cause desensitization. Large amounts of metal may react with the azide to form the nitride.¹⁹ It should be pointed out here that in all experiments where BaN_6 was decomposed by impact testing or thermal means, the end product contained a significant amount of nitride.

The influence of prior thermal decomposition at 110° on the sensitivity as determined by the impact and explosion temperature tests is shown in Figure 6. Initially, there is a very significant sensitization, but when barium azide is thermally decomposed beyond 1%, a desensitization is evident. At low temperature (110°), thermal decomposition leads to the metal and nitrogen and no significant amount of nitride is formed.²⁰ Analogously, this experiment was similar to the previous one where a physical mixture of barium metal and barium azide was used. The graph does indicate that the greatest increase in sensitivity occurs at approximately the same percentage of thermally decomposed barium azide in both the impact and explosion temperature tests. The sensitization observed in the reactivity of barium azide either thermally decomposed or physically mixed with barium metal bears a distinct resemblance to the thermal decomposition of barium azide, where during the induction period metallic nuclei are formed which catalyze the reaction, usually known as the autocatalytic reaction (acceleratory region). The metal particles act as electron traps and thus increase the number of reacting azide radicals. Deb, *et al.*,²¹ have demonstrated that this can actually lead to a sensitized explosion. However, when produced in a large concentration, the metal, by virtue of its high specific heat, can act as a heat sink and inhibit the explosive decomposition.

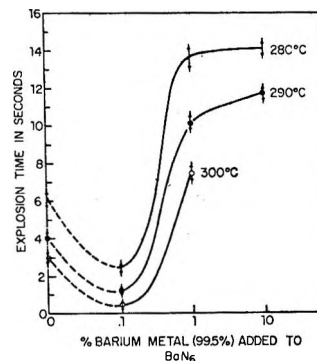


Figure 5. The effect of the addition of barium metal on the explosion times at indicated temperatures.

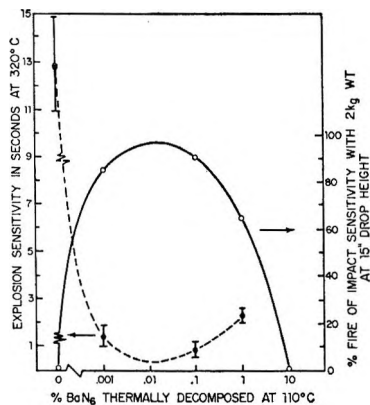


Figure 6. Sensitivity of BaN_6 partially thermally decomposed at 110° . Each impact test value is the result of 20 tests at the specified height.

The effect on impact sensitivity of doping barium azide with sodium as a function of aging is shown in Figure 7. The quantitative concentration of sodium in the crystals was not determined, but the reaction solution contained 1 mol% NaN_3 . The curves in Figure 7 indicate that for spectral grade undoped barium azide, the desensitizing phase has been completed and the sensitization process has started. In the sodium-doped barium azide, the desensitization was still in process or lengthened and the over-all sensitivity of the doped material was very much higher than that of the undoped barium azide. The impact sensitivity tests for this phase of the work were conducted at room temperature. One tentative explanation is that doping a divalent cationic compound with a monovalent cationic ion should produce vacancies in the crystal. One would then suspect that enhancing the vacancy concentration would enhance the impact sensitivity.²²

An effort was made to show quantitatively how barium azide doped with iron in the form of a com-

(19) W. E. Garner, "Chemistry of the Solid State," Butterworth and Co. Ltd., London, 1955, p 238.

(20) V. R. Pai Verneker and M. Blais, unpublished data.

(21) S. K. Deb, B. L. Evans, and A. D. Yoffe, 8th International Symposium on Combustion, 1962, p 829.

(22) P. F. Gray, T. C. Waddington, *Chem. Ind.*, 1255 (1955).

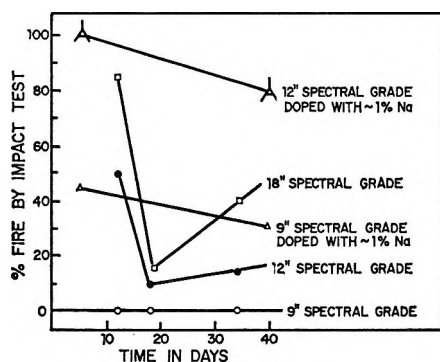


Figure 7. Effect of doping BaN_6 with Na^+ impurity on the impact sensitivity.

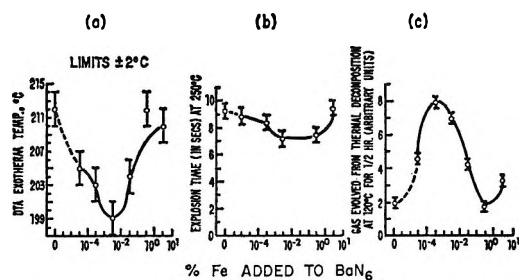


Figure 8. Effects on DTA exotherm; explosion time at 250° and gas evolution at 120° of doping BaN_6 with $[\text{Fe}(\text{N}_3)]^{2+}$.

plex $[\text{Fe}(\text{N}_3)]^{2+}$ is sensitized. The plots (Figure 8a, b, and c) show that the sensitization effect is observed in a slow thermal decomposition as well as a fast explosive process. The amount of doping is small and the maximum sensitization occurs when the doping is

of the order of 0.1 mol %. Beyond that a densitization goes into effect. A possible explanation may be that the sensitization results not because ferric azide is more explosive than barium azide but is due rather to an acceptor level introduced by $[\text{Fe}(\text{N}_3)]^{2+}$ in the band picture of barium azide. This seems very probable because barium azide doped with $[\text{Fe}(\text{N}_3)]^{2+}$ starts to absorb at $680 \text{ m}\mu$. Pai Verneker and Forsyth²³ have shown a similar sensitization in $\alpha\text{-PbN}_6$ doped with $[\text{Fe}(\text{N}_3)]^{2+}$ and a desensitization in $\alpha\text{-PbN}_6$ doped with Fe^{3+} . Doping with Fe^{3+} does not change the absorption edge of $\alpha\text{-PbN}_6$, whereas doping with $[\text{Fe}(\text{N}_3)]^{2+}$ does. In short, it is a solid-state process that is responsible for the sensitization.

In summary, we have shown that the following parameters affect the sensitivity of barium azide. (1) Sensitivity increases with the surface area. (2) Solvents which may get incorporated into the crystal affect the sensitivity of barium azide. (3) Aging of the material initially brings about a desensitization followed by sensitization. (4) Barium metal, either added physically or produced thermally up to 0.1 mol %, brings about sensitization. (5) Impurities like Na^+ or $[\text{Fe}(\text{N}_3)]^{2+}$ sensitize barium azide.

We have also shown that, depending on the method of preparation, two types of crystal structure are obtained. On analysis of the products of explosive decomposition caused by heat or impact, we have found a very significant amount of barium nitride.

(23) V. R. Pai Verneker and A. C. Forsyth, *J. Phys. Chem.*, **72**, 111 (1968).

Reductions by Monovalent Zinc, Cadmium, and Nickel Cations¹

by D. Meyerstein² and W. A. Mulac

Chemistry Division, Argonne National Laboratory, Argonne, Illinois 60439 (Received April 27, 1967)

The specific rates of reaction of Zn^+ , Cd^+ , and Ni^+ with O_2 , N_2O , H_2O_2 , NO_2^- , NO_3^- , BrO_3^- , IO_3^- , Cu^{2+} , and H_3O^+ have been determined. It has been found that the order of reactivity is $Zn^+ \geq Cd^+ \geq Ni^+$; this order is correlated with the electronic structure of the monovalent cations.

Introduction

It has been shown that the hydrated electrons produced in the radiolysis of water reduce divalent transition metal cations.³ The monovalent cations formed are unstable in aqueous solutions and it has been suggested that they disappear by disproportionation.^{4,5}

The redox potentials for the $M^{2+}-M^+$ couples have been estimated,⁶ suggesting that Zn^+ , Cd^+ , and Ni^+ should be powerful reductants. The rates of reaction of some of these monovalent cations with permanganate,⁷ oxygen,⁸ divalent lead ions,⁸ nitrous oxide,⁹ and hydrogen peroxide⁹ have been measured. It has also been shown that they dehalogenate certain haloaliphatic compounds.¹⁰

The absorption spectra of the monovalent cations have been measured,^{4,5,11,12} and it was found that the spectra of Zn^+ , Cd^+ , and Ni^+ have maxima in the same region. These absorption bands have been tentatively attributed to a charge transfer to solvent.^{5,11} However, Brown and Dainton¹² suggest that in the case of Cd^+ the absorption band originates from a $5^2P_{1/2}$ or $1/2 \leftarrow 5^2S_{1/2}$ transition.

The aim of the present work has been to obtain a better understanding of the chemical properties of the monovalent transition metal cations in aqueous solutions by a systematic study of the kinetics of reduction of different inorganic substrates by Zn^+ , Cd^+ , and Ni^+ .

Experimental Section

All solutions were prepared from triply distilled water and AR reagents without further treatment. Solutions of $2 \times 10^{-2} M$ of MSO_4 ($M = Zn^{2+}$, Cd^{2+} , or Ni^{2+}) and $1 \times 10^{-3} M$ methanol (added in order to scavenge the hydroxyl radicals thus inhibiting the reaction $M^+ + OH \rightarrow M^{2+} + OH^-$ and decreasing the amount of H_2O_2 formed by the pulse) have been used in all experiments unless otherwise stated. To these solutions, different oxidants have been added in the concentration range of 5×10^{-5} to $10^{-2} M$. The actual concentration used depended on the reactivity of M^+ and e_{aq}^- with the oxidants. The solutions were deaerated by shaking with argon gas in a syringe and then expelling the gas. This procedure was repeated

four times leaving a residual concentration of oxygen smaller than $3 \times 10^{-7} M$. Nitrous oxide saturated solutions were prepared by the same technique using pure nitrous oxide (Matheson), which was further purified by passing it, successively, through three traps containing basic solutions of pyrogallol and, finally, through a trap containing triply distilled water.

The pulse radiolytic experiments were carried out using a 0.4- μ sec, 15-MeV electron pulse from a linear accelerator, yielding a dose of $0.8-6 \times 10^{19}$ eV l^{-1} pulse⁻¹. Under the experimental conditions, all OH radicals formed by the pulse reacted with methanol, whereas the hydrated electrons reacted with M^{2+} to give M^+ . (In some experiments, a fraction of the hydrated electrons reacted with the oxidant; this fraction was always smaller than 30%.) The decay of M^+ was followed spectrophotometrically at 3130 Å using a multiple-reflection cell¹³ with a 4 cm long optical cell giving a 16-cm total light path. A 450-W xenon lamp was used as an analyzing light source, and a Bausch and Lomb monochromator followed by a 1P28 photomultiplier and a Type-555 Tetrax oscilloscope fitted with a Polaroid camera were used for recording the absorption changes in the solution.

In order to eliminate photochemistry of the solutes which might be induced by the analyzing light, a Corn-

(1) Based on work performed under the auspices of the U. S. Atomic Energy Commission.

(2) Nuclear Research Center, Negev, Israel.

(3) J. H. Baxendale and R. S. Dixon, *Proc. Chem. Soc.*, 148 (1963).

(4) G. E. Adams, J. H. Baxendale, and J. W. Boag, *ibid.*, 241 (1963).

(5) J. H. Baxendale, E. M. Fielden, and J. P. Keene, *Proc. Roy. Soc. (London)*, **A286**, 320 (1965).

(6) J. H. Baxendale and R. S. Dixon, *Z. Physik. Chem. (Frankfurt)*, **43**, 161 (1964).

(7) J. H. Baxendale, J. P. Keene, and D. A. Stott in "Pulse Radiolysis," Academic Press Inc., London, 1965, p 107.

(8) J. H. Baxendale, J. P. Keene, and D. A. Stott, *Chem. Commun.*, 715 (1966).

(9) G. V. Buxton, F. S. Dainton, and G. Thielens, *ibid.*, 201 (1967).

(10) M. Anbar and P. Neta, *J. Chem. Soc., A*, 841 (1967).

(11) T. Feldmann, A. Treinin, and V. Volterra, *J. Chem. Phys.*, **42**, 3366 (1965).

(12) D. M. Brown and F. S. Dainton, *Trans. Faraday Soc.*, **62**, 1139 (1966).

(13) J. Rabani, W. A. Mulac, and M. S. Matheson, *J. Phys. Chem.*, **69**, 53 (1965).

ing 0-53 filter absorbing the light below 300 $m\mu$ was introduced between the xenon lamp and the cell. Furthermore, a mechanical shutter was kept closed until shortly before the pulse.

The calculations were carried out using Chloe, an automatic photoelectronic scanner,¹⁴ for reading the Polaroid pictures and transferring the data to a magnetic tape which was then used in a computer program for the analysis of the kinetics.¹⁵ All traces were analyzed for first- and second-order decay, and pseudo-first-order rates were calculated when a good first-order decay plot was obtained for at least three half-lives. A correction for the decay of M^+ in the absence of oxidants was included when needed; this correction was always smaller than 15%. For every rate constant, at least ten traces were analyzed, which were obtained by pulse radiolyzing ten sample solutions, prepared by using at least two different stock solutions to dilute to several different concentrations. The maximum standard deviation in the results is 15%.

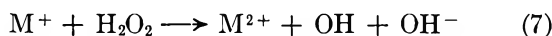
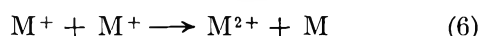
The steady-state radiolytic yield of I_2 from aqueous iodide solutions containing different concentrations of MSO_4 salts and saturated with N_2O have also been measured. The irradiations were carried out with a ^{60}Co source, and all experimental details are identical with those described elsewhere.¹⁶

Results and Discussion

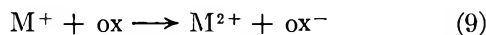
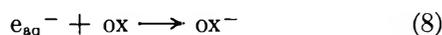
The radiolysis of water may be described by eq 1



the yields of the products being $G_{e_{aq}^-} = 2.6$, $G_{OH} = 2.6$, $G_H = 0.6$, $G_{H_2} = 0.45$, and $G_{H_2O_2} = 0.75$. In solutions containing MSO_4 salts and methanol, the following reactions are expected



It has been shown^{5,6} that for zinc, nickel, and cadmium ions, CH_2OH radicals do not react with M^{2+} or M^+ . The rate of reaction 7 is high for the cases of Zn^+ and Cd^+ (see Table I). When oxidants (ox) are added in concentrations low enough to avoid reaction 8, one can study the rate of reaction 9 by following the disappearance of M^+ .



The mechanism of the disappearance of Zn^+ , Cd^+ , and Ni^+ , in the absence of additive oxidants, has been

investigated. In all three cases, this mechanism is not governed by a pure second-order law, as would be expected from the disproportionation mechanism, eq 6. In the case of the Zn^+ and Cd^+ , additional contributions to their decay are expected due to their reactions (7) (at diffusion-controlled rates) with the "molecular hydrogen peroxide" formed by the pulse. As the amount of hydrogen peroxide formed is proportional to the pulse intensity, its effect on the rate of disappearance of M^+ is also proportional to the pulse intensity, giving the impression of a second-order rate of reaction. The rate of decay of Zn^+ is also dependent on the $ZnSO_4$ concentration, increasing with the salt concentration as expected for a reaction between two positively charged ions. (This effect was not investigated for Cd^+ and Ni^+ .) The mechanism of the disappearance of Ni^+ seems to be more complicated than those for Zn^+ and Cd^+ .

The decays of Zn^+ , Cd^+ , and Ni^+ under our experimental conditions (concentrations of 0.2–1.0 μM) are relatively slow, having half-lives longer than 100 μsec . It is possible by the addition of different oxidants to shorten these half-lives to 20 μsec and less, thus enabling the determination of the specific reaction rates of M^+ with these oxidants.

The specific rates of reaction of Zn^+ , Cd^+ , and Ni^+ with different inorganic substrates are summarized in Table I. The corresponding rates of reaction with hydrated electrons and hydrogen atoms are included for comparison. In addition to these values, the following upper limits for the rate constants of reduction by Zn^+ have been determined: $k_{Zn^+ + Cd^{2+}} < 1 \times 10^7 M^{-1} sec^{-1}$; $k_{Zn^+ + Ni^{2+}} < 5 \times 10^6 M^{-1} sec^{-1}$; $k_{Zn^+ + Co^{2+}} < 3 \times 10^6 M^{-1} sec^{-1}$, and $k_{Zn^+ + ClO_3^-} < 3 \times 10^6 M^{-1} sec^{-1}$.

It should be mentioned that all the rate constants measured are for solutions containing $2 \times 10^{-2} M$ of $M^{2+}SO_4^{2-}$, having, therefore, an ionic strength, μ , of 0.08 (neglecting the fact that some of the MSO_4 is not fully dissociated). The effect of changing the salt concentration (by changing the concentration of $ZnSO_4$ or by adding $NaClO_4$) on the rate of the $Zn^+ + NO_2^-$ reaction is shown in Figure 1, wherein $\log k$ is plotted against $\sqrt{\mu}/(1 + 1.33\sqrt{\mu})$ (μ was calculated neglecting the fact that part of the $ZnSO_4$ is not dissociated). The best straight line calculated using the least-mean-squares technique has a slope of -1.04 . This slope is in agreement with the theoretically required slope of -1.02 for much more dilute solutions. The value of

(14) The Chloe system was developed at the Argonne National Laboratory Applied Mathematics Division by an engineering group led by Donald Hodges. A detailed description of this machine is given by Donald Hodges, Technical Memorandum No. 61, Applied Mathematics Division, Argonne National Laboratory, Argonne, Ill., Nov 1963.

(15) M. C. Sauer, ANL-7146 Report, Argonne, Ill., 1966.

(16) M. Anbar, D. Meyerstein, and P. Neta, *J. Phys. Chem.*, **68**, 2967 (1964).

Table I: Specific Rates of Reaction of Monovalent Transition Metal Cations^a

Additive	Zn ⁺	Cd ⁺	Ni ⁺	e _{aq} ⁻	H
O ₂	2.4 × 10 ⁹ (3.3 × 10 ⁹) ^b	2.4 × 10 ⁹ (3.3 × 10 ⁹) ^b	1.4 × 10 ⁹ (2.2 × 10 ⁹) ^b	1.88 × 10 ¹⁰	2.6 × 10 ¹⁰
N ₂ O ^c	≤ 1.3 × 10 ⁷	≤ 2.0 × 10 ⁶ (1 × 10 ⁶) ^d	≤ 6.3 × 10 ⁶ (5.1 × 10 ⁷) ^d	5.6 × 10 ⁹	1.2 × 10 ⁴
H ₂ O ₂	1.80 × 10 ⁹	1.55 × 10 ⁹ (2.8 × 10 ⁹) ^d	4.3 × 10 ⁷ (2.1 × 10 ⁸) ^d	1.23 × 10 ¹⁰	1.6 × 10 ⁸
NO ₃ ⁻	2.1 × 10 ⁹	3.5 × 10 ⁸	≤ 1.4 × 10 ⁸ ^f	1.1 × 10 ¹⁰	1.7 × 10 ⁷
NO ₂ ⁻	2.2 × 10 ⁹	2.0 × 10 ⁹	1.50 × 10 ⁸	4.6 × 10 ⁹	6.0 × 10 ⁸
BrO ₃ ⁻	2.1 × 10 ⁹	1.25 × 10 ⁸	≤ 8.4 × 10 ⁶ ^f	2.1 × 10 ⁹	1.95 × 10 ⁹
IO ₃ ⁻	3.6 × 10 ⁹	2.3 × 10 ⁹	2.2 × 10 ⁸	7.7 × 10 ⁹	5.9 × 10 ⁹
Cu ²⁺	2.5 × 10 ⁸	1.2 × 10 ⁸	≤ 2.4 × 10 ⁷ ^f	3.3 × 10 ¹⁰	6.0 × 10 ⁸
H ₃ O ⁺	≤ 10 ⁶	≤ 10 ⁶	≤ 10 ⁵	2.3 × 10 ¹⁰	...

^a In units of $M^{-1} \text{sec}^{-1}$. All solutions contained 0.02 M MSO₄, $1 \times 10^{-3} M$ CH₃OH, plus the additive in different concentrations. The maximum standard deviation is 15%. The values in parentheses are from the literature. The rate constants for e_{aq}⁻ and H atoms are taken from tabulation by M. Anbar and P. Neta, *Intern. J. Appl. Radiation Isotopes*, **16**, 227 (1965). ^b From ref 10. ^c These solutions contained 1.0 M MSO₄. The concentration of N₂O was calculated from the solubility of N₂O, assuming that it is equivalent to that of 1.0 M MgSO₄ solutions; taken from A. E. Markham and K. A. Kobe, *J. Am. Chem. Soc.*, **63**, 449 (1941). As only saturated solutions were used and no check on linearity with concentration has been carried out, the rates are given only as upper limits. ^d From ref 9. ^e M. Anbar and P. Neta, unpublished results. ^f These oxidants affected the rate of disappearance of Ni⁺, but no good first-order plots were obtained. In the case of BrO₃⁻, the rate calculated from the initial part of the decay plots was constant in the concentration range $2.5\text{--}5 \times 10^{-3} M$.

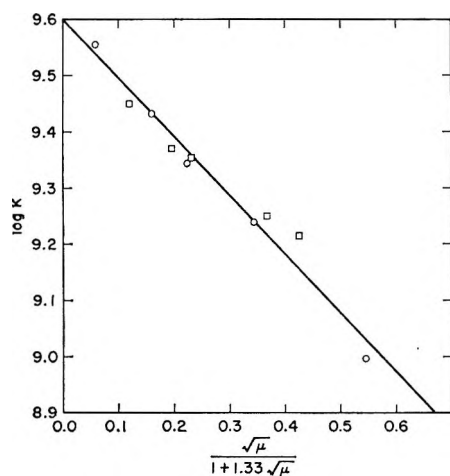


Figure 1. Salt effects on the rate of reaction of Zn⁺ with NO₂⁻ (all solutions contained $1 \times 10^{-4} M$ NaNO₂, $1 \times 10^{-3} M$ CH₃OH): O, different ZnSO₄ concentrations; □, $5 \times 10^{-3} M$ ZnSO₄ plus different concentrations of NaClO₄.

1.33 has been derived assuming a radius of encounter of 4 Å. (It is assumed that Zn⁺ is hydrated and has, therefore, a radius similar to that of Zn(H₂O)₆²⁺, which is approximately 3 Å.¹⁷ The radius of NO₂⁻ is about 1 Å.¹⁸) Changing the value used for the radius of Zn⁺ has only a minor effect on the slope. It can, therefore, be concluded that the charge of Zn⁺ is really plus unity, as has been assumed. In order to obtain the rates of reaction of M⁺ with the different anions at $\mu = 0$, the respective rate constants in Table I should be multiplied by approximately 1.6, and the rate of reaction with Cu²⁺ should be divided by 2.6.

In a recent work,⁸ $k_{\text{Zn}^+ + \text{Cd}^{2+}} = 8.3 \times 10^8 M^{-1}$

sec^{-1} and $k_{\text{Zn}^+ + \text{Ni}^{2+}} = 5 \times 10^7 M^{-1} \text{sec}^{-1}$ have been reported. If the reaction $\text{Zn}^+ + \text{Cd}^{2+} \rightarrow \text{Zn}^{2+} + \text{Cd}^+$ takes place, an increase in the optical density of the solution would be expected as $\epsilon_{\text{Cd}^+} > \epsilon_{\text{Zn}^+}$.⁵ No such increase was observed. If the reaction $\text{Zn}^+ + \text{Ni}^{2+} \rightarrow \text{Zn}^{2+} + \text{Ni}^+$ takes place, a sharp decrease of the optical density is expected (as $\epsilon_{\text{Zn}^+} > \epsilon_{\text{Ni}^+}$), followed by a much slower decay of Ni⁺. This has not been observed. The experiments were repeated using Zn(ClO₄)₂, Ni(ClO₄)₂, and Cd(ClO₄)₂, instead of the MSO₄ salts, in order to check whether complexing had any effect on the results, but no change in the decay pattern was observed. The reason for these discrepancies is not clear.

The specific rates of reaction of Zn⁺ with many oxidants are around $2 \times 10^9 M^{-1} \text{sec}^{-1}$. It is of interest to compare these rates with the calculated diffusion-controlled limits for these reactions. The diffusion-controlled limits have been calculated according to the Debye equation¹⁹

$$k_{\text{AB}} = \frac{4\pi r_{\text{AB}} D_{\text{AB}} N}{1000} \left\{ \frac{Z_{\text{A}} Z_{\text{B}} e^2}{r_{\text{AB}} E k T} \right. \\ \left. \left(\exp \left[\frac{Z_{\text{A}} Z_{\text{B}} e^2}{r_{\text{AB}} E k T} \right] - 1 \right) \right\} \quad (10)$$

The value in the braces is a correction term for reactions between charged molecules A and B (r_{AB} is

(17) W. Huckel, "Structural Chemistry of Inorganic Compounds," Elsevier Publishing Co., 1950, p 919.

(18) F. A. Cotton and G. Wilkins, "Advanced Inorganic Chemistry," Interscience Publishers, Inc., 1966, p 349.

(19) P. Debye, *Trans. Electrochem. Soc.*, **82**, 265 (1942).

Table II: A Comparison of Calculated Diffusion-Controlled and Experimental Rate Constants of Zn^+ Reactions^a

Oxidant	Diffusion coefficient of oxidant, $cm^2 sec^{-1}$	Radius of oxidant, Å	Calculated diffusion-controlled rate constant, $M^{-1} sec^{-1}$		Experimental rate constant, $M^{-1} sec^{-1}$
			$r_{Zn^+} = 3.0 \text{ Å}$	$r_{Zn^+} = 0.8 \text{ Å}$	
O_2	1.45×10^{-5b}	1.6 ^c	7.4×10^9	3.7×10^9	2.4×10^9
NO_2^-	0.7×10^{-5}	1.0	8.9×10^9	7.5×10^9	2.2×10^9
Cu^{2+}	0.7×10^{-5d}	3.0	1.5×10^9	0.4×10^9	2.6×10^9

^a A dielectric constant of 80 and a diffusion coefficient for Zn^+ of $0.7 \times 10^{-5} cm^2 sec^{-1}$ have been assumed throughout. ^b W. A. Roth and K. Scheel, Ed., "Landolt-Börnstein Physikalisch-Chemische Tabellen," 5th ed, 2nd suppl, Julius Springer, Berlin, 1931, p 198. ^c Averaged from van der Waals radii and interatomic distance of O_2 : L. Pauling, "The Nature of the Chemical Bond," 3rd ed, Cornell University Press, Ithaca, N. Y., 1960, p 518. ^d J. C. James and C. B. Monk, *Trans. Faraday Soc.*, **46**, 1041 (1950).

the encounter radius; D_{AB} , the total diffusion constant; N , Avogadro's number; Z_{Ae} and Z_{Be} , the charges of A and B; E , the dielectric constant; k , Boltzmann's constant; and T , the absolute temperature). Two extreme values for the radius of Zn^+ have been assumed: (1) a radius of 3.0 Å, assuming that Zn^+ is hydrated and has a radius similar to that of $Zn(H_2O)_6^{2+}$; ¹⁷ and (2) a radius of 0.8 Å, assuming that although Zn^+ is hydrated, the mechanism of its reactions requires the formation of a bond between the oxidant and Zn^+ (an inner-sphere mechanism) and, therefore, the effective radius is that of the unhydrated ion. The calculated diffusion-controlled and the experimental rate constants are summarized in Table II. It is clear that the reactions of Zn^+ with O_2 and H_2O_2 , as well as with NO_2^- , NO_3^- , BrO_3^- , and IO_3^- , after correcting for the salt effect, are diffusion controlled or approach this limit. The reactions of Zn^+ with N_2O and Cu^{2+} are definitely slower than the calculated diffusion-controlled limit.

The reactions of Cd^+ are, on the whole, slightly slower than the corresponding ones of Zn^+ , but only in the cases of the reaction rates with nitrate and bromate ions are the differences really significant. (The latter reaction rates are about an order of magnitude less than the diffusion-controlled limits.)

The reactions of Ni^+ are much slower than the others. Only the reaction rate of Ni^+ with oxygen approaches the diffusion-controlled limit, while a majority of the Ni^+ reactions were too slow to be measured.

The fact that the absorption bands of Zn^+ , Cd^+ , and Ni^+ are similar and that they have been attributed to charge transfer to solvent transitions^{5,11} might suggest that these ions would also react similarly in reductions involving a charge-transfer mechanism. We see, however, that there is a definite order of reactivity: $Zn^+ > Cd^+ \gg Ni^+$. This does not automatically imply that this is also the order for the redox potentials of the corresponding $M^{2+}-M^+$ couples. The order of reactivity can be explained by assuming that in Zn^+ the additional electron is located in an S orbital, where it would be relatively exposed, making Zn^+ a rapid reductant. The added electron in Cd^+ is also assumed

to be located in an S orbital, as suggested by esr studies.^{11,20} Its lower reactivity is reasonable, in view that it is expected that in the Zn, Cd, and Hg group the stability of lower oxidation states will increase with the atomic weight, and Hg^+ is really stable as a dimer in aqueous solutions. In Ni^+ , the added electron may enter the 3d shell. ESR studies have proved that the Ni^+ , formed by irradiating single crystals and glasses doped with Ni^{2+} , has a 3d⁹ configuration.^{11,21} Therefore, as the added electron is located in an inner orbital, it is reasonable that Ni^+ is less reactive than Zn^+ and Cd^+ . It is of interest to note that this order of reactivity is not the reverse of the order of reactivity of the hydrated electrons toward the corresponding divalent cations, there the order is $Cd^{2+} > Ni^{2+} > Zn^{2+}$.

Finally, it is of interest to compare the measured specific rates of reaction with the corresponding rates of reaction of the same oxidants with the hydrated electrons and hydrogen atoms. The M^+ cations react slowly with H_3O^+ , if they react with it at all, as opposed to the high reactivity of e_{aq}^- with H_3O^+ . The reason for this might be that the redox potential of M^+ is too low to allow reduction of H_3O^+ . In general, it seems that the reactivity of Ni^+ toward the compounds of Table I is more similar to that of H atoms than to that of e_{aq}^- . To a lesser extent, the same may also be true for Cd^+ (relatively low reactivity toward NO_3^- and N_2O) and Zn^+ (low reactivity toward N_2O), although here most of the rates are too near to the diffusion-controlled limit for obtaining a good comparison.

The very high reactivity of Zn^+ , Cd^+ , Ni^+ , e_{aq}^- , and H atoms toward oxygen is attributed to the biradical nature of the oxygen molecule.

The Reaction of M^+ with N_2O . It was of interest to investigate in greater detail the reactions of M^+ with N_2O . This reaction is expected to transfer a reducing agent (M^+) into an oxidizing agent (OH radicals). The effect of addition of MSO_4 on the radiolytic yield of iodine from iodide solutions saturated with N_2O has

(20) P. N. Moorthy and J. J. Weiss, *Nature*, **211**, 1317 (1964).

(21) W. Low and J. T. Suss, *Phys. Letters*, **7**, 310 (1963).

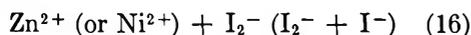
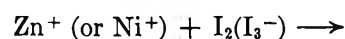
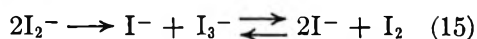
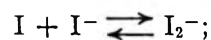
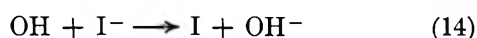
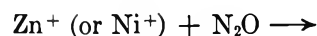
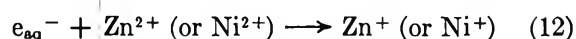
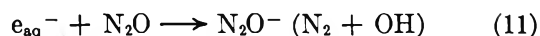
been studied as this system has been shown to be useful in measuring the hydroxyl radical yield.¹⁶ The results are summarized in Table III. The iodine yield is not linear with dose (the yields given are for a relatively low dose, 6700 rads, and the yield for a double dose has been up to 10% lower).

Table III: The Effect of Transition Metal Cations on the Radiolytic Iodine Yield from Iodide Solutions Saturated with Nitrous Oxide^a

Added salt concentration, <i>M</i>	<i>G(I₂)</i>		
	ZnSO ₄	NiSO ₄	CdSO ₄
...	1.60	1.60	1.60
1 × 10 ⁻³	1.53	1.65	1.35
1 × 10 ⁻²	1.80	1.75	0.67
1 × 10 ⁻¹	2.15	2.28	0.33
5 × 10 ⁻¹	2.88	2.77	0.22

^a Iodide concentration 1 × 10⁻³ *M*; dose 6700 rads; all solutions at pH 5.0–6.0; the maximal standard deviation of the *G(I₂)* values is ±0.10.

The results suggest that the following mechanism should be considered in the presence of Zn²⁺ and Ni²⁺.



From the known rate constants,²² $k_{e_{\text{aq}}^- + \text{N}_2\text{O}} = 5.6 \times 10^9 \text{ M}^{-1} \text{ sec}^{-1}$, $k_{e_{\text{aq}}^- + \text{Zn}^{2+}} = 1.5 \times 10^9 \text{ M}^{-1} \text{ sec}^{-1}$,

and $k_{e_{\text{aq}}^- + \text{Ni}^{2+}} = 2.2 \times 10^{10} \text{ M}^{-1} \text{ sec}^{-1}$, it is clear that, in the presence of the higher concentrations of Zn²⁺ or Ni²⁺, most of the hydrated electrons react via reaction 12. The fact that the results are not linear with dose may be explained by the competition between reactions 13 and 16. It is reasonable to assume that the rate constants for reaction 16 are $10^9 < k_{16} < 10^{10} \text{ M}^{-1} \text{ sec}^{-1}$. The yield of iodine after 6700 rads is approximately 10⁻⁵ *M*, and the N₂O concentration 2 × 10⁻² *M* and, therefore, the nonlinearity suggests that k_{13} is two to three orders of magnitude smaller than k_{16} , in agreement with the pulse-radiolytic experiments.

The increase of *G(I₂)* in the presence of Zn²⁺ and Ni²⁺ is believed to be connected with the scavenging of a small part of the precursors of the "molecular hydrogen," as well as some hydrated electrons which would otherwise recombine with hydroxyl radicals.

The effect of CdSO₄ on the iodine yield suggests that reaction 13 is much slower for Cd⁺ than for Zn⁺ or Ni⁺. However, the pulse radiolytic results indicated a good first-order decay of Cd⁺ in the presence of N₂O with a rate only three times slower than that for Ni⁺, which could hardly explain the difference in the effect on the iodine yield. The reason for this discrepancy is unknown. One plausible explanation is that the CdI⁺ complex formed ($\log K = 2.28$)²³ changes the chemical behavior of the system.

Acknowledgments. We are indebted to Dr. M. S. Matheson for his encouragement and discussions throughout this work, to Professor M. Anbar and Dr. E. H. Appelman for helpful discussions, and to Dr. M. C. Sauer for his assistance in the use of his computer program. We wish also to thank the Linac group for their careful operation and Mr. S. Petrek for maintaining the electronic equipment.

(22) J. H. Baxendale, *et al.*, *Nature*, **201**, 468 (1964).

(23) R. G. Bates and W. C. Vosburgh, *J. Am. Chem. Soc.*, **60**, 137 (1938).

Calorimetric Determination of the Heat of the Sodium-Lithium Ion-Exchange Reaction in Anhydrous Methanol

by A. Schwarz¹

Chemistry Department, Soreq Nuclear Research Centre, Yavne, Israel (Received May 16, 1967)

Calorimetric measurements at 25° of the heat of sodium-lithium ion exchange in methanol with a Dowex 50 W-X8 exchanger were combined with the selectivity data of the same resin to derive standard free energy, enthalpy, and entropy changes. The results are compared with data of a similar exchange system in water. The comparison shows that the fourfold increase in selectivity of sodium over lithium in methanol is due to a positive entropy change which may be attributed to a decrease in the solvation of sodium ions. This behavior suggests that ion-solvent interaction may become less important in determining ion-exchange selectivities when the dielectric constant of the solvent is reduced.

Introduction

Ion exchange in nonaqueous and mixed solvents has been receiving increasing attention in recent years.^{2a,3} Fairly extensive data⁴ exist on the behavior of different ions with the change of the solvent. Possibilities of enhancing and reversing selectivities have been reported.⁴ Even in isotopic separation, the resolution can be greatly improved by the addition of organic solvents.⁵ However, despite the considerable amount of work, from the present theory we are still far from able to predict equilibria in nonaqueous and mixed solvents to the extent possible with aqueous systems.

Calorimetric measurements by Boyd⁶⁻⁹ and co-workers and by others^{10,11} combined with selectivity data have proved to be a useful tool in aqueous ion-exchange work by providing an insight into the nature of ion binding in ion exchangers.

The present work was undertaken with the expectation that information on the sign and magnitude of the entropy and enthalpy of ion-exchange reactions in nonaqueous solvents will lead to a better understanding of the nature of ion binding in such systems. Methanol, with a dielectric constant of 32, was selected as it provides reasonable salt solubilities and has a water-like structure; also the relatively high dielectric constant could prevent imbibing of the co-ions.

Experimental Section

The calorimeter used in the heat measurements was similar in many respects to that described by Lindenbaum and Boyd.⁷ The container was an 800-ml cylindrical dewar flask mounted in a brass jacket equipped with a brass-Teflon cup which could be bolted to the jacket and sealed. The heat-sensing elements were two 2000 (nominal) Fenwal¹² thermistors having a temperature coefficient of $-3.9\%/^{\circ}\text{C}$. Due to the

lower heat capacity of methanol and because a Model 150 AR Kiethley amplifier was employed in the present study, the temperature sensitivity of the calorimeter was about $7 \times 10^{-6} \text{ }^{\circ}\text{C}$. The current through the thermistors was low enough so that self-heating was negligible. The reliability of the calorimeter was checked by measuring the heat of solution of crystalline KCl. Good agreement with literature data¹³ was observed.

Although the speed of aqueous ion exchange of singly charged cations at 25° in the resins used in this study is known to be quite high, this may not be so when methanol is used as a solvent; consequently, it was necessary to determine whether an ordinary calorimeter would be adequate. The results of exploratory rate studies, designed to duplicate the calorimeter measurements of sodium-lithium exchange, using an Na²² tracer are presented in Figure 1. These experiments were carried out by suspending a 1-g sample of the sodium resinate containing Na²² in pure dry methanol. The sodium-

- (1) Killed in action, Six-day Campaign, June 1967.
- (2) (a) R. W. Gable and H. A. Strobel, *J. Phys. Chem.*, **60**, 513 (1956); (b) R. G. Fessler and H. A. Strobel, *ibid.*, **67**, 2562 (1963).
- (3) J. Penciner, I. Eliezer, and Y. Marcus, *ibid.*, **69**, 2955 (1965).
- (4) F. Helfferich, "Ion Exchange," McGraw-Hill Book Co., Inc., New York, N. Y., 1962, Chapter 10.
- (5) H. Kakihana, *J. Chim. Phys.*, **60**, 81 (1963).
- (6) G. E. Boyd, F. Vaslow, and S. Lindenbaum, *J. Phys. Chem.*, **68**, 590 (1964).
- (7) S. Lindenbaum and G. E. Boyd, *ibid.*, **69**, 2374 (1965).
- (8) F. Vaslow and G. E. Boyd, *ibid.*, **70**, 2295 (1966).
- (9) K. E. Becker, S. Lindenbaum, and G. E. Boyd, *ibid.*, **70**, 3834 (1966).
- (10) E. H. Cruickshank and P. Meares, *Trans. Faraday Soc.*, **53**, 1289 (1957).
- (11) D. S. Flett and P. Meares, *J. Phys. Chem.*, **70**, 1841 (1966).
- (12) Fenwal Electronic, Inc., Framingham, Mass.
- (13) G. Somsen, J. Coops, and M. W. Talk, *Rec. Trav. Chim.*, **82**, 231 (1963).

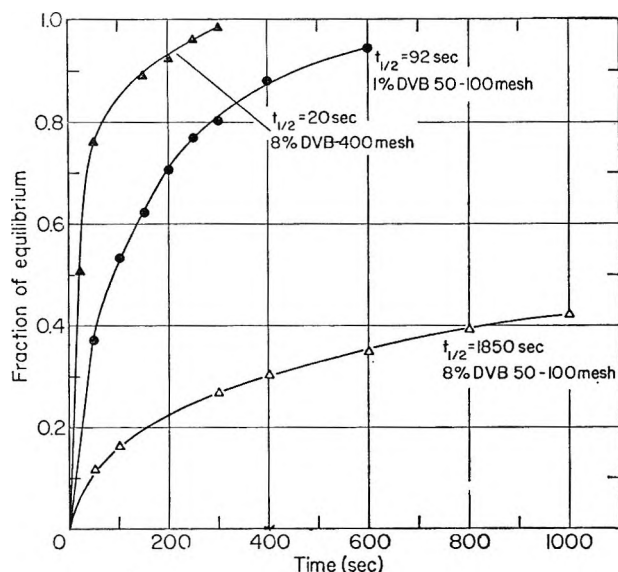


Figure 1. Fractional attainment of equilibrium in various Dowex 50 resins. Exchange reaction in methanol: $\text{RNa}^{22} + \text{LiCl} \rightleftharpoons \text{RLi} + \text{Na}^{22}$.

lithium exchange reaction was initiated by adding a solution of LiCl in methanol calculated to effect a final concentration of 0.1 *m* LiCl. The activity in the solution was counted as a function of time. The exchange in 8% DBV cross-linked 50-100 mesh resin was quite slow. However, with -400 mesh particles, a half-exchange time of 20 sec was observed. This rate is fast enough for a nonisothermal calorimeter with constant temperature environment. The reverse reaction, with -400 mesh particles, starting with the lithium form of the resin was also rapid as judged by the temperature history of the calorimeter. The smooth curves obtained in Figures 2 and 3, for both selectivity and heat data when starting from either sodium or lithium resin, also suggest that equilibrium is reached in a short time.

In a typical exchange reaction, methanol-saturated resin was weighed into the calorimeter pipet and covered by a 0.1 *m* methanolic solution whose composition was such that no ion exchange occurred. The calorimeter was filled with 500 ml of 0.1 *m* methanolic solution of sodium or lithium chloride or a mixture of the two electrolytes. At the end of a run, the resin was separated from the solution by filtration, the excess solution sucked, and the resin rinsed with pure methanol and eluted by 1.0 *M* aqueous HCl. Both the equilibrium methanol phase and the eluent were analyzed for sodium and lithium by flame spectrophotometry.

The number of equivalents of cation exchanged were computed from the initial and final mole fractions and the amount of resin used. This procedure eliminates the necessity for quantitative collection of fine particles.

Materials. The methanol (Fluka, Puriss grade) after drying with Linde molecular sieves contained 0.01 to 0.05% water as determined by Karl Fischer titration. The lithium chloride and sodium chloride were Baker

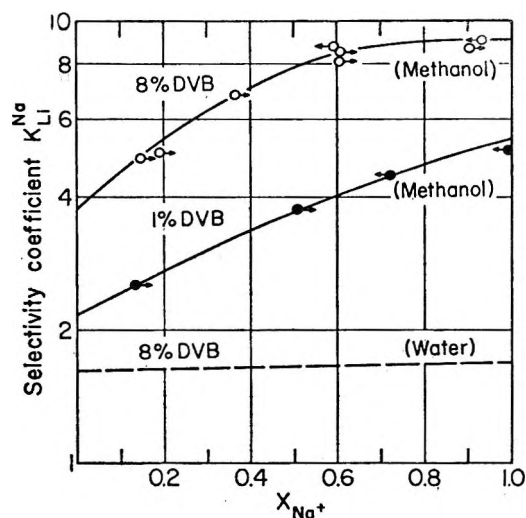


Figure 2. Selectivity coefficients for the sodium-lithium exchange with variously cross-linked Dowex 50 resins in methanol. Direction of approach to equilibrium is indicated by the arrows (data for water taken from ref 14).

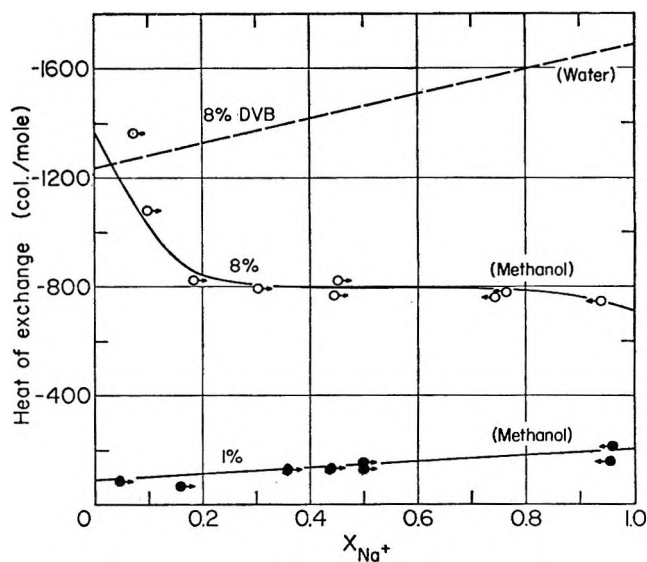


Figure 3. Differential heats of exchange of sodium with lithium ions on 1 and 8% cross-linked Dowex 50 resins. Circles indicate midpoints of chord for heats of partial exchange. Direction of approach to equilibrium is indicated by the arrows (data for water taken from ref 6).

analyzed reagents. The Dowex 50 cation-exchanger resin was conditioned before use by cycling between hydrogen and sodium or lithium with 2 *M* aqueous solutions of the corresponding salts. It was then washed with de-ionized water and next with methanol and dried to constant weight at 50° in a vacuum oven equipped with a liquid nitrogen trap. The capacity and methanol content of the resin used are shown in Table I.

Initial tests were made of the effect of small amounts of moisture on both the selectivity and the differential heat of exchange. A few runs were carefully carried out keeping the system as dry as possible, and in other runs

Table I: Resin Capacity and Solvent Content^a

	-RNa-		-RLi-	
	mequiv/g, dry	g of CH ₃ OH/g, dry	mequiv/g, dry	g of CH ₃ OH/g, dry
8% DVB	4.03	0.43	4.34	0.95
1% DVB	4.48	...	4.89	(2.76)

^a Equilibrated isopiastically with 0.1 *m* solutions of the corresponding salts.

water up to 1% by weight was added to the methanol. No significant changes in either the heat or the selectivity measurements were observed. This result is in agreement with data reported by Fessler and Strobel,^{2b} who studied the Na-Li selectivity coefficient in Dowex 50-X 8 resin in methanol-water mixtures as a function of the mixed solvent composition. According to their data K_{Li}^{Na} is nearly constant up to a water mole fraction of 0.1.

Results and Discussion

The dependence of the measured selectivity coefficient and the differential heats of sodium-lithium exchange for nominal 1 and 8% DVB cross-linked Dowex 50 exchangers on the equivalent fraction of Na⁺ ions is shown in Figures 2 and 3. Data for the exchange in water were taken from the literature.^{6,14} The differential heats and the selectivity coefficient increase with increased resin cross linking. In both methanol and water, heat is evolved in the preferential uptake of sodium. For the 8% DVB cross-linked resin more heat is evolved in water than in methanol while the preferential uptake of sodium over lithium is lower in water.

Another feature is the strong dependence of the selectivity coefficient on the resin equivalent fraction which increases nearly twofold when the resin becomes loaded with the preferred ion. From the Gable and Strobel^{2a} data for 8% DVB exchange, a value of 10.6 was obtained for K_{Li}^{Na} at $\bar{X}_{Na} = 0.5$ (or 9.6 as calculated from the K_H^{Li} and K_H^{Na}), while the value obtained in this study is 8.5. Considering that different batches of resin with different capacities are involved, the two sets of data are in reasonable agreement. The effect of capacity in this system is not known and although theory predicts an increase in selectivity with increasing capacity, PSSA resins behave differently. Cross-linked polyacrylic and pectinic acid exchangers, on the other hand, conform with the theory.¹⁵

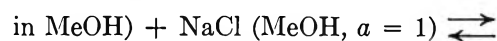
To facilitate the computation of ΔF and ΔH , the data shown in Figures 2 and 3 for the 8% DVB exchanger were fitted to least-squares quadratic equations with the following parameters

$$\log K_{Li}^{Na} = 0.544 + 1.019\bar{X}_{Na^+} - 0.628\bar{X}_{Na^+}^2$$

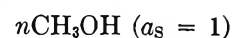
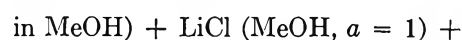
$$\partial\Delta H/\partial\bar{X}_{Na^+} = -1296 + 1839\bar{X}_{Na^+} - 1415\bar{X}_{Na^+}^2$$

The standard resin state⁶ chosen in this work is the homoionic exchanger in equilibrium with a 0.1 *m* methanolic alkali chloride solution having a common ion with the resin. The choice of 0.1 *m* electrolyte concentration is a compromise between the need to keep the electrolyte concentration in the liquid phase as low as possible (since 0.1 *m* in methanol may not be "dilute" enough in the sense of ideality) and the desire to keep the ratio of electrolyte to trace of moisture as high as possible. Standard thermodynamic quantities were computed for the hypothetical exchange reaction

LiR ($a = 1$, equilibrium with 0.1 *m* LiCl



NaR ($a = 1$, equilibrium with 0.1 *m* NaCl



where a_s is the activity of the solvent and n is the number of moles of methanol released or absorbed by the exchanger. The derivations of the integrated thermodynamic equilibrium constant from the selectivity coefficient and the standard heats from the integral heats of exchange is hampered by the lack of data on the behavior of electrolytes in nonaqueous solvents in general and in methanol in particular.

Another difficulty which had to be considered was the question whether the present case could adequately be described as a three-component system consisting of sodium resinate, lithium resinate, and methanol or that invasion by co-ions should not be neglected. Preliminary invasion studies showed that although electrolyte imbibement is stronger in methanol than in water, the pure 8% DVB lithium resinate at 0.1 *m* outside concentration gives a ratio of $\bar{m}_{LiCl}/m_{LiCl} = 0.1$, where \bar{m}_{LiCl} refers to the concentration of invaded electrolyte. Even higher ratios have been considered negligible.⁶ Similar small amounts of nonexchange electrolyte have been reported¹ for 8% DVB preparation in exchange studies carried out in methanol. For the 1% DVB cross-linked exchanger, invasion was found quite appreciable, and more information about the changes in solvent activity in the solid¹⁶ is needed before one can estimate the thermodynamic equilibrium constant for this resin. The 8% DVB data can adequately be treated by the formula

$$\Delta F^\circ = -2.303RT \int_0^1 \log \left(\frac{K_{Li}^{Na} \gamma_{\pm}^2(\text{LiCl})}{\gamma_{\pm}^2(\text{NaCl})} \right) dX_{Na^+}$$

The required activity coefficient ratio for correcting the selectivity coefficient in aqueous systems can be

(14) G. E. Myers and G. E. Boyd, *J. Phys. Chem.*, **60**, 521 (1956).

(15) S. Lindenbaum, C. F. Jumper, and G. E. Boyd, *ibid.*, **63**, 1924 (1959).

(16) G. L. Gains, Jr., and H. C. Thomas, *J. Chem. Phys.*, **21**, 714 (1953).

Table II: Thermodynamic Quantities of Ion-Exchange Reactions at 25° in Various Ion-Exchange Systems

Exchange ion	Solvent	Resin	Functional group	ΔG° , cal/mole	ΔH° , cal/mole	ΔS° , cal/mole	Ref
Na-Li	Methanol	Dowex 50-X8	SO ₃ ⁻	-1150	-781	1.2	Present work
Na-Li	Water	Dowex 50-X8	SO ₃ ⁻	-360	-1460	-3.6	6
Ag-Na	Water	Dowex 50-X8	SO ₃ ⁻	-830	110	3.1	8
Li-Cs	Water	PMA 10 DVB	COO ⁻	-134	404	1.8	7
Li-Cs	Water	Nuclear phosphonic acid	PO ₃ ⁻	-330	890	4.1	9

estimated following Boyd, *et al.*¹⁷ Thus the term $\log [\gamma_{\pm}^2(\text{LiCl})/\gamma_{\pm}^2(\text{NaCl})]$ for the aqueous ion exchange is only 6.86×10^{-3} and amounts to less than 3% of the selectivity term. One can approach the problem of estimating this term for methanol by the use of Harned's second rule,¹⁸ which may be stated as

$$\log \left[\frac{\gamma_{1(0)}}{\gamma_{2(0)}} \right]_{P,T,m} = \text{constant}$$

where $\gamma_{1(0)}$ and $\gamma_{2(0)}$ are the activity coefficients of the pure salt in water and in organic solvent-water mixtures. The rule has been verified up to 20% methanol in water¹⁸ and more recently¹⁹ up to 90% methanol in water. By further assuming that the rule may also approximately hold for dilute electrolyte mixtures, the same correction term may be applied for the activity coefficient ratio in both water and methanol.

The standard heats of exchange were calculated from the equation

$$\Delta H^\circ = \int_0^1 \left(\frac{\partial \Delta H}{\partial X_{\text{Na}^+}} \right) dX_{\text{Na}^+} - [\phi_L(\text{LiCl}) - \phi_L(\text{NaCl})]$$

The required $\Delta\phi_L$ values were obtained from the heat of dilution measurements on 0.1 *m* methanolic solutions of NaCl and LiCl. The lowest final concentration of both electrolytes was 1×10^{-3} *m*. Surprisingly, more heat was evolved on the dilution of NaCl than LiCl, and from these measurements, it was estimated that $\phi_L(\text{LiCl}) - \phi_L(\text{NaCl}) = -67$ cal/mole.

Table II compares the standard free energy, enthalpy, and entropy obtained in this study together with aqueous ion-exchange data from the literature. In the

alkali halide exchange reaction in PSSA and quaternary ammonium²⁰ type resins, heat was evolved in the uptake of the preferred ion while the entropy of the system decreased. Positive entropy changes were observed in weakly acid exchangers and for the Ag-Na exchange in PSSA; these were interpreted as indicating various forms of site binding or specific interaction between the resin functional group and the preferred ion. A comparison of the two sets of data on Na-Li exchange in water and methanol shows that the large increase in the selectivity for sodium in the latter solvent is due to the entropy term. A possible explanation is that the interaction of sodium ion with the sulfonate group is stabilized by the release of methanol molecules from their solvation sphere. The smaller lithium ion, on the other hand, enters the resin phase retaining its solvation sphere.

In conclusion, it seems that the positive entropy change observed in this study indicates that by lowering the dielectric constant of the medium, ion-solvent interaction may become less important in determining ion exchange selectivities.

Acknowledgment. The author wishes to thank Mr. J. Weiss for his assistance with the experimental work. Thanks are also due to Mrs. F. Padova for performing the flame spectrophotometric analysis.

(17) G. E. Boyd, S. Lindenbaum, and G. E. Myers, *J. Phys. Chem.*, **65**, 577 (1961).

(18) H. S. Harned, *ibid.*, **66**, 589 (1962).

(19) R. D. Lanier, *ibid.*, **69**, 2697 (1965).

(20) F. Vaslow and G. E. Boyd, *ibid.*, **70**, 2507 (1966).

A Comparison of Quinine Bisulfate and 9,10-Diphenylanthracene as Fluorescence Standards

by R. Rusakowicz and A. C. Testa

Department of Chemistry, St. John's University, Jamaica, New York 11432 (Received May 25, 1967)

A grating monochromator and photomultiplier which was calibrated with a lamp of known irradiance ($\mu\text{W}/\text{cm}^2 \text{ sec } 10 \text{ \AA}$) for the determination of relative fluorescence quantum yields was used to determine that the fluorescence quantum yield of 9,10-diphenylanthracene is 2.17 ± 0.10 times greater than the value for quinine bisulfate at room temperature. This result suggests the commonly used value of 0.55 for quinine bisulfate is too large. Using the upper limit of unity for 9,10-diphenylanthracene, the fluorescence quantum yield for quinine bisulfate is estimated to be 0.46 (16% lower than the accepted value). The fluorescence quantum yield ratio for 9,10-diphenylanthracene in degassed solutions of cyclohexane relative to air-saturated solutions was determined to be 1.41. The fluorescence yields for $3.33 \times 10^{-4} M$ anthracene in cyclohexane, relative to 9,10-diphenylanthracene, were determined to be 0.33 and 0.25 for degassed and air saturated solutions, respectively. A comparative fluorescence study of quinine sulfate and quinine bisulfate indicates that when the optical densities of the two molecules in solution are equal, they both exhibit indistinguishable fluorescence curves. The proportionality between intensity of fluorescence and concentration was observed for quinine bisulfate up to $10^{-4} M$, whereas linearity breaks down for quinine sulfate when the concentrations exceed $3 \times 10^{-5} M$.

Introduction

The application of quinine bisulfate in 0.1 *N* sulfuric acid as a fluorescence quantum yield reference compound is a generally accepted fact. Melhuish¹ has carefully studied this system, and the fluorescence quantum yield was determined to be 0.55. Recently, Drobnik and Yeagers² reported that the quantum yield of 2-aminopurine in neutral solutions at 160°K is 2.5 times larger than quinine sulfate at room temperature. These authors suggested that the quantum yield for quinine sulfate is probably 0.4 or less.

Another fluorescence standard which has been used is 9,10-diphenylanthracene (9,10-DPA), which was reported by Bowen and Sahu³ to have a quantum yield of unity. Berlman⁴ has found this compound a convenient standard to study the fluorescence of a large number of aromatic molecules. Although the fluorescence yields of some substituted anthracenes exhibit temperature dependence,^{5,6} which is attributed to the presence of a second triplet state (T_2) in the vicinity of the first excited singlet (S_1), this dependence does not apply to 9,10-DPA. Since there is no significant temperature dependence on the fluorescence of this molecule, it is not unexpected that Lim, *et al.*,⁵ have reported the fluorescence quantum yield of 9,10-DPA to be 1.00 ± 0.05 in EPA at 77°K.

In view of the ease of application of both compounds as fluorescence standards, it is expected that a consis-

tency exists between the ratios of the quantum yields for quinine bisulfate and 9,10-DPA. In this work, the ratio of quantum yields for these compounds was determined by two methods: (a) by comparison to a standard lamp of known irradiance ($\mu\text{W}/\text{cm}^2 \text{ sec } 10 \text{ \AA}$), and (b) by comparison of 9,10-DPA to quinine bisulfate as recommended by Melhuish.¹ The results of these experiments are described below.

Experimental Section

Materials. Reagent grade 9,10-DPA was recrystallized three times from ethanol and chloroform. Quinine sulfate (mol wt 783) and quinine bisulfate (mol wt 548) were obtained from K & K Laboratories, Plainview, N. Y., and recrystallized three times from water. Zone-refined anthracene was used without further purification. Quartz-distilled water was used for aqueous solutions and spectrograde cyclohexane for 9,10-DPA and anthracene. The extinction coefficients

(1) W. H. Melhuish, *J. Phys. Chem.*, **64**, 762 (1960); *N. Z. J. Sci. Tech.*, **B37-2**, 142 (1955).

(2) J. Drobnik and E. Yeagers, *J. Mol. Spectry.*, **19**, 454 (1966).

(3) E. J. Bowen and J. Sahu, *J. Phys. Chem.*, **63**, 4 (1959).

(4) I. B. Berlman, "Handbook of Fluorescence Spectra of Aromatic Molecules," Academic Press, New York, N. Y., 1965

(5) E. C. Lim, J. D. Laposa, and J. M. Yu, *J. Mol. Spectry.*, **19**, 412 (1966).

(6) R. G. Bennett and P. J. McCartin, *J. Chem. Phys.*, **44**, 1969 (1966).

determined with a Beckman DU spectrophotometer are 9,10-DPA, $\epsilon_{354} = 8.56 \times 10^3$, $\epsilon_{372} = 1.37 \times 10^4$, and $\epsilon_{392} = 1.32 \times 10^4$; quinine sulfate, $\epsilon_{346} = 1.04 \times 10^4$, $\epsilon_{368} = 6.20 \times 10^3$; and quinine bisulfate, $\epsilon_{368} = 3.46 \times 10^3$, these values agree satisfactorily with literature values.^{4,7}

Apparatus. An Aminco grating monochromator ($f/4.4$ aperture, reciprocal dispersion 6.6 $m\mu/mm$, 600 lines/mm, blaze at 5000 Å) was used in conjunction with an RCA-1P21 photomultiplier. The photomultiplier tube was powered by an Aminco microphotometer and the output was fed to a Moseley X-Y recorder (Model 7030A). The fluorescence signal entered the monochromator from a direction perpendicular to excitation, and monochromator entrance and exit slits remained constant at 0.2 mm for all measurements.

The excitation source was an Osram-100W/2 high-pressure mercury lamp which was placed at the focal point (1.5 in.) of a (1 in. in diameter) quartz lens. The excitation wavelength (366 $m\mu$) was isolated with a Schott (Jena Glaswerk, Mainz, Germany) interference filter distributed by Fish-Schurman Corporation, New Rochelle, N. Y. A Corning filter CS No. 3-75 was placed in front of the 1P21 tube to exclude the exciting wavelength.

The irradiance standard was obtained from Electro Optics Associates, Palo Alto, Calif., and its accuracy is $\pm 5\%$, relative to a National Bureau of Standards certified lamp.

All measurements were made with quartz spectrophotometric cells (1 cm). Degassed samples were sealed off at $<10^{-4}$ mm pressure after at least three alternate cycles of freezing and vacuum boiling.

The percentage of radiation absorbed by the samples was obtained in a single-beam light path, using the exciting source and filter. Radiation intensities were determined with the potassium ferrioxalate actinometer.⁸

A neutral density screen placed in front of and behind the sample cell block indicated that scattered radiation was not an important factor in our optical arrangement. The requirement of equivalent optical geometry, necessary for using the standard lamp, was attained by replacing the quartz sample cell with a front surface aluminized mirror. It was observed that the correction factors for the monochromator-photomultiplier arrangement were identical when calibrated with either the quinine bisulfate solution using Melhuish's¹ values or the standard lamp. Consequently, it appears that scattered light in the monochromator from the standard lamp is not significant.

Measurement of Fluorescence Quantum Yields

The quantum yield for a substance is given by the expression

$$\Phi_f = \frac{\int [dI_e(\bar{\nu})/d\bar{\nu}]d\bar{\nu}\Omega}{I_a} \quad (1)$$

where $[dI_e(\bar{\nu})/d\bar{\nu}]$ is the number of quanta emitting per unit area per unit time per wavenumber interval. I_a is the number of exciting quanta per second absorbed by the molecule of interest, and Ω represents the geometrical factor relating the fractional area of emitted radiation detected by the monochromator-photomultiplier system. When a standard lamp is used, the expression $[dI_e(\bar{\nu})/d\bar{\nu}]$ is related to the quantum output of the lamp, *i.e.*, $[dI_e(\bar{\nu})/d\bar{\nu}] = [dI_e(\bar{\nu})/d\bar{\nu}]_s(R_x/R_s)$, where $[dI_e(\bar{\nu})/d\bar{\nu}]_s$ represents the known output of the lamp, and R_x and R_s represent the photometer readings for the unknown solution and the standard lamp, respectively. The optical arrangement is, of course, held constant when relative measurements are made. The irradiance units of the standard lamp are $\mu W/cm^2$ sec 10^8 \AA , which can be converted to a quanta output, *i.e.*

$$dE/d\lambda(1/h\nu) = dI_e/d\lambda \quad (2)$$

where E is the energy rating from the lamp per wavelength interval and $h\nu$ is the energy per quantum. The term $dI_e/d\lambda$ represents the quanta output per unit area per unit time per wavelength interval. The relationship between $[dI_e(\bar{\nu})/d\bar{\nu}]$ and $[dI_e(\lambda)/d\lambda]$ is

$$[dI_e(\bar{\nu})/d\bar{\nu}] = [dI_e(\lambda)/d\lambda]_s \frac{d\lambda}{d\bar{\nu}} = - \left[\frac{dI_e(\lambda)}{d\lambda} \right]_s \lambda^2 \quad (3)$$

The final expression for the quantum yield of fluorescence is

$$\Phi_f = \frac{\int [dI_e(\bar{\nu})/d\bar{\nu}]_s (R_x/R_s) \Omega d\bar{\nu}}{I_a} \quad (4)$$

When relative quantum yields are measured, the geometric factor is eliminated, and the final working expression becomes

$$\frac{\Phi_1}{\Phi_2} = \frac{\int [dI_e(\bar{\nu})/d\bar{\nu}]_s (R_x/R_s) d\bar{\nu} I_a'}{\int [dI_e(\bar{\nu})/d\bar{\nu}]_s (R_x'/R_s') d\bar{\nu} I_a'} \quad (5)$$

where Φ_1 and Φ_2 are the fluorescence quantum yields of the two substances of interest, and the primed quantities refer to substance 2. The area under the corrected fluorescence curve is obtained with a planimeter. In our experiments the ratio of areas was measured.

There is a complication arising from the different solvents from which the fluorescence occurs, since 9,10-DPA was dissolved in cyclohexane and the quinine bisulfate in water. This correction was made with the expression^{9,10} (eq 6)

(7) J. W. Eastman, *Photochem. Photobiol.*, **6**, 55 (1967).

(8) C. G. Hatchard and C. A. Parker, *Proc. Roy. Soc. (London)*, **A235**, 518 (1956).

(9) J. J. Hermans and S. Levinson, *J. Opt. Soc. Am.*, **41**, 460 (1951).

(10) A. R. Horrocks, T. Medinger, and F. Wilkinson, *Photochem. Photobiol.*, **6**, 21 (1967).

$$\frac{\Phi_1}{\Phi_2} = \frac{n_1^2 A_1}{n_2^2 A_2} \quad (6)$$

were Φ , n , and A represent the fluorescence yield, index of refraction of the solvent, and the area of the corrected fluorescence envelope, respectively, for the two molecules.

Results

Since the direction of emission detection was at right angles to the excitation, the concentration of 9,10-DPA in cyclohexane was kept below $3.5 \times 10^{-5} M$ in order to minimize front-surface emission. The fluorescence of 9,10-DPA was measured for air-saturated solutions and for degassed solutions. The ratio of yields, Φ_f (degassed)/ Φ_f (air) is equal to 1.41, which agrees favorably with the value of 1.38 reported by Berلمان.⁴ The relative quantum-yield ratio for 9,10-DPA and quinine bisulfate was 2.07, when determined by comparison to the standard lamp.

In the second method using equal optical densities, the ratio of yields, Φ_f (DPA)/ Φ_f (QBS), was determined to be 2.27. These values include the refractive-index correction made with eq 6. If the quantum yield of 9,10-DPA in cyclohexane(degassed) is assigned the value unity, the fluorescence quantum yield value (upper limit) for quinine bisulfate becomes 0.46. It may be noted that lowering the quantum yield for 9,10-DPA lowers the quinine bisulfate yield. This value corroborates the recent investigation by Drobnik and Yeagers,² who suggested that the fluorescence yield of quinine sulfate is too large.

Since quinine sulfate (QS) and quinine bisulfate (QBS) are available, we compared the spectral characteristics of these two molecules, because incorrect usage has occurred in at least two recent investigations.^{2,7} Melhuish has recommended only the bisulfate as the fluorescence standard. The ratio of extinction coefficients for the two compounds at 366 m μ , $\epsilon_{QS}/\epsilon_{QBS}$, was determined to be 1.79 for concentrations up to $10^{-4} M$ in 0.1 N H₂SO₄. This ratio was also obtained when the intensity of fluorescence for the two compounds at the peak wavelength, 465 m μ , was plotted *vs.* concentration, provided that the concentration of QS was less than $3 \times 10^{-5} M$. In our experimental arrangement, the proportionality between fluorescence and concentration was not satisfactory when the concentration of QS exceeded $3 \times 10^{-5} M$. This non-linearity for QS is a source of positive error in the determination of relative fluorescence yields when $5 \times 10^{-5} M$ QS in 0.1 N H₂SO₄ is used instead of QBS. This fact may account for some error in the work of Drobnik and Yeagers;² however, our results with QBS still suggest that the fluorescence quantum yield recommended by Melhuish is too large. In contrast to the behavior of QS, the proportionality between intensity of fluorescence and concentration for QBS is linear up to $10^{-4} M$.

A convenient comparison of the two compounds is related by the fact that $5 \times 10^{-5} M$ QBS and $3 \times 10^{-5} M$ QS, each dissolved in 0.1 N H₂SO₄, exhibited the same fluorescence spectrum envelope. For this particular case in which the optical densities are the same, it is estimated that there is 23.5 $\mu\text{g/ml}$ QS to 27.4 $\mu\text{g/ml}$ QBS, since QS has a mol wt of 783 containing 83% quinine base, and QBS has mol wt of 548 containing 60% quinine base.¹¹ Thus, on the basis of percentage quinine present in each compound, there is 19.5 $\mu\text{g/ml}$ of quinine in QS and 16.4 $\mu\text{g/ml}$ in QBS. It follows that the two compounds are not optically equivalent.

The fluorescence of anthracene was also studied as a further proof of consistency. A solution of $3.33 \times 10^{-4} M$ anthracene in cyclohexane gave a fluorescence emission which was oxygen sensitive, as reported by Berلمان.⁴ The quantum yield we determined relative to 9,10-DPA is 0.33 in degassed solutions, which agrees with the value of 0.36 reported by Berلمان⁴ and the value of 0.30 reported by Parker and Joyce.¹² The ratio we obtained for degassed solutions relative to air-saturated solutions is 1.34, which compares favorably with the value of 1.25 reported by Berلمان.⁴

Although the largest uncertainty in our measurements is the distribution of energy from standard lamp, its accuracy is $\pm 5\%$. It is probably more realistic to estimate an accuracy of 10–15% in our data.

Discussion

The ratio of fluorescence quantum yields, Φ_f (DPA)/ Φ_f (QBS), determined in this work to be 2.17 ± 0.10 is significantly higher than the value of 1.82, which is predicted from Melhuish's value of 0.55 for quinine bisulfate. The results reported in this work, and those recently reported by Drobnik and Yeagers² suggest some uncertainty in the accepted value for the fluorescence yield of quinine bisulfate in 0.1 N H₂SO₄. It is noteworthy that in both cases the suggested value is less than 0.55.

Although our recommended value for quinine bisulfate is 0.46, the difference between our value and the currently accepted value may be due to uncertainties in the standard lamps used in this work and by Melhuish. The use of right-angle or front-surface detection of fluorescence should not be a source of error, provided concentrations are kept small in the former method. The possibility that quinine bisulfate samples may be different cautions against the use of quinine bisulfate as a standard and favors the use of 9,10-DPA.

The two examples (9,10-DPA and 2-aminopurine) of inconsistencies for quantum-yield ratios may not be

(11) A. Osol, G. Farrar, Jr., and R. Pratt, "The Dispensatory of the United States of America," J. B. Lippincott Co., Philadelphia, Pa., 1960, pp 1172, 1176.

(12) C. A. Parker and T. A. Joyce, *Trans. Faraday Soc.*, **62**, 2785 (1966).

considered significant; however, the possibility exists that other molecules may also show emission properties incompatible with the currently accepted value of 0.55 for the fluorescence yield of quinine bisulfate. The

authors hope that additional results from other researchers working with different molecules will help to evaluate the validity of the observations reported in this work.

Ion-Solvent Interaction. VI. A Thermodynamic Approach

to Preferential Solvation in Mixed Solvents^{1a}

by J. Padova^{1b}

Radiochemistry Department, Israel Atomic Energy Commission, Soreq Nuclear Research Center, Yavne, Israel
(Received May 29, 1967)

The thermodynamic treatment of a mixed fluid in an electrostatic field is applied to the calculation of preferential solvation in mixed solvents at infinite dilution. The preferential solvation is interpreted in terms of partial molar free energies of solvation and is compared with literature data.

Introduction

The preferential solvation shown by electrolytes in mixed solvents is a direct consequence of the specific interaction between an ion and one of the components of the mixed solvents. It may be defined as the relative change in the composition of the mixed solvent in the vicinity of the ion and may be expressed by

$$\frac{n_1/n_2}{n_1^0/n_2^0} = 10^\alpha \quad (1)$$

where n_1/n_2 is the mole ratio of the components in the vicinity of the ion, n_1^0/n_2^0 is the initial mole ratio of the components, and α will be called the index of preferential solvation. It is obvious that for $\alpha > 0$, the ion is selectively solvated by component 1; for $\alpha < 0$, the ion is selectively solvated by component 2; and for $\alpha = 0$ there is no preferential solvation.

Various attempts have been made to derive theoretical expressions for eq 1,²⁻⁵ assuming either an ideal mixture for the mixed solvent and the electrostatic contribution for the free energy to be given by Born's expression,² or an empirical correction for the change in the dielectric constant of the solution,³ or other experimental corrections.^{4,5}

It was now found possible to apply the thermodynamic treatment of a mixed fluid in an electrostatic field⁶ to the problem of calculating the preferential solvation, assuming the mixed solvent to be sorted

under the influence of the electric field caused by the presence of ions.

Theory

From electromagnetic theory, it is possible to show that the isothermic, isobaric electrostatic work done on a fluid is given by the expression⁷

$$W = \frac{1}{4\pi} \iint \bar{E} d\bar{D} dv \quad (2)$$

where \bar{E} and \bar{D} are the electric field and electric displacement vectors, respectively, and dv is the elementary volume.

From expression 2, the elementary electrical work done on the fluid is obtained as

$$dw = \frac{1}{4\pi} \left(\int \bar{E} d\bar{D} \right) dv$$

(1) (a) Presented in part at the XXXIII Meeting of the Israel Chemical Society Beler Sheva, Dec 1963; cf., J. Padova, *Israel J. Chem.*, **1**, 258 (1963). (b) Oak Ridge National Laboratory, Chemistry Division, Oak Ridge, Tenn. 37830.

(2) P. Debye, *Z. Physik. Chem.*, **130**, 56 (1927).

(3) G. Scatchard, *J. Chem. Phys.*, **9**, 34 (1941).

(4) (a) J. E. Ricci and G. J. Ness, *J. Am. Chem. Soc.*, **64**, 2305 (1942); (b) H. L. Clever and F. H. Verhoek, *J. Phys. Chem.*, **62**, 1961 (1958).

(5) I. F. Efremov, T. A. Probof'eva, and Yn. P. Syrnikov, *Zh. Fiz. Khim.*, **38**, 2258 (1964).

(6) H. S. Frank, *J. Chem. Phys.*, **23**, 2023 (1955).

(7) E.g., A. Prock and G. McConkey, "Topics in Chemical Physics," Elsevier Publishing Co., Amsterdam, 1962, p 11.

whence the increment in internal energy, dU , is obtained through the application of the first law of thermodynamics to an infinitesimal process

$$dU = TdS - PdV + \frac{1}{4\pi} \left(\int \bar{E} d\bar{D} \right) dv + \sum \mu_i dn_i \quad (3)$$

We may now define a characteristic function, H^* , analog to the enthalpy

$$H^* = U + Pv - \frac{v}{4\pi} \int \bar{E} d\bar{D}$$

and

$$dH^* = TdS + vdp - \frac{v}{4\pi} \bar{E} d\bar{D} + \sum \mu_i dn_i$$

and the analog Gibbs free energy, G^*

$$dG^* = -SdT + vdP - \frac{v\bar{E}}{4\pi} d\bar{D} + \sum \mu_i dn_i$$

introducing the differential dielectric constant, $\epsilon_d = dD/dE$, we obtain the fundamental equation

$$dG^* = -SdT + vdP - \frac{v\epsilon_d E}{4\pi} dE + \sum \mu_i dn_i \quad (4)$$

from which the desired relationships will be obtained in the usual way.

An earlier treatment⁶ assumed that the whole of the fluid sample under discussion is subject to the same (instantaneous) field strength. This has now been generalized, and eq 4 may be applied to a dielectric which is nonuniform in \bar{E} , since eq 2 allows for infinitesimal variations of \bar{E} and \bar{D} in the elementary volume, dv .

We are interested in the change of local composition in a mixture of solvents produced by the field of an ion. Equation 4 for a two component system is written as

$$dG^* = -SdT + vdP - \frac{v\epsilon_d E}{4\pi} dE + \mu_1 dn_1 + \mu_2 dn_2 \quad (5)$$

hence by cross differentiation

$$\left(\frac{\partial \mu_1}{\partial E} \right)_{P,T,n_1,n_2} = - \frac{1}{4\pi} \left[\frac{\partial (v\epsilon_d E)}{\partial n_1} \right]_{P,T,E,n_2} \quad (6)$$

or in terms of mole fractions N_1 and N_2

$$\left(\frac{\partial \mu_1}{\partial E} \right)_{P,T,N_1} = - \frac{E}{4\pi} \left[\epsilon_d \bar{V}_1 + N_2 V_m \left(\frac{\partial \epsilon_d}{\partial N_1} \right)_{P,T,E} \right] \quad (7)$$

where $v_m = v/(n_1 + n_2)$.

At constant temperature, μ_1 , P , E , and N_1 may be taken as a mutually dependent set of quantities, so that eq 8 follows.

$$d\mu_1 = \left(\frac{\partial \mu_1}{\partial P} \right)_{E,N_2,T} dP + \left(\frac{\partial \mu_1}{\partial E} \right)_{P,N_1,T} dE + \left(\frac{\partial \mu_1}{\partial N_1} \right)_{P,T,E} dN_1 \quad (8)$$

Since the changes in local composition produced by the field should be at constant chemical potentials μ_1 and μ_2 of the binary solvent, inside and outside the field, we obtain for $d\mu_1 = d\mu_2 = 0$

$$\left(\frac{\partial \mu_1}{\partial P} \right)_{E,N_1,T} \left(\frac{\partial P}{\partial E} \right)_{\mu_1,\mu_2} + \left(\frac{\partial \mu_1}{\partial E} \right)_{P,T,N_1} + \left(\frac{\partial \mu_1}{\partial N_1} \right)_{P,T,E} \left(\frac{\partial N_1}{\partial E} \right)_{\mu_1,\mu_2} = 0 \quad (9)$$

Making use of the Gibbs-Duhem relations

$$N_1 \left(\frac{\partial \mu_1}{\partial N_1} \right) + N_2 \left(\frac{\partial \mu_2}{\partial N_1} \right) = 0 \quad (10)$$

it may be shown that

$$\left(\frac{\partial N_1}{\partial E} \right)_{\mu_1,\mu_2,T} = \frac{Ev_m N_2}{4\pi} \left(\frac{\partial \epsilon_d}{\partial N_1} \right)_{P,E,T} \left(\frac{\partial \mu_1}{\partial N_1} \right)_{P,E,T}^{-1} \quad (11)$$

Rewriting eq 11 as

$$\left(\frac{\partial N_1}{\partial E} \right)_{\mu_1,\mu_2} = \frac{Ev}{4\pi} \left(\frac{\partial \epsilon_d}{\partial n_1} \right)_{P,T,E,n_2} \left(\frac{\partial \mu_1}{\partial N_1} \right)_{P,E,T}^{-1} \quad (12)$$

and dividing by N_1 gives

$$\left(\frac{\partial \ln N_1}{\partial E} \right)_{\mu_1,\mu_2} = \frac{Ev}{4\pi} \left(\frac{\partial \epsilon_d}{\partial n_1} \right)_{P,E,T,n_2} \left(\frac{\partial \mu_1}{\partial \ln N_1} \right)_{P,E,T}^{-1} \quad (13)$$

with a similar expression for

$$\left(\frac{\partial \ln N_2}{\partial E} \right)_{\mu_1,\mu_2}$$

where the relative change of composition per unit volume under the change of field strength dE is

$$\frac{1}{v} \left(\frac{\partial \ln N_1/N_2}{\partial E} \right)_{\mu_1,\mu_2} dE = \frac{1}{8\pi} \left(\frac{\partial \mu_1}{\partial \ln N_1} \right)_{P,E,T}^{-1} \times \left[\left(\frac{\partial \epsilon_d}{\partial n_1} \right)_{P,E,T,n_2} - \left(\frac{\partial \epsilon_d}{\partial n_2} \right)_{P,E,T,n_1} \right] d(E^2) \quad (14)$$

which gives for the change of composition in the vicinity of the ion ($r = r_e$) as compared to the composition outside the field ($r = \infty$)

$$\ln \frac{N_1}{N_2} - \ln \frac{N_1^0}{N_2^0} = \frac{1}{8\pi} \int_{r_e}^{\infty} 4\pi r^2 dr \int_0^{Er} \left(\frac{\partial \mu_1}{\partial \ln N_1} \right)_{P,E,T}^{-1} \times \left[\left(\frac{\partial \epsilon_d}{\partial n_1} \right)_{P,E,T,n_2} - \left(\frac{\partial \epsilon_d}{\partial n_2} \right)_{P,E,T,n_1} \right] d(E^2) \quad (15)$$

or

$$\ln \frac{N_1}{N_2} - \ln \frac{N_1^0}{N_2^0} = \frac{1}{2} \int_{r_e}^{\infty} r^2 dr \int_0^{Er} \left(\frac{\partial \mu_1}{\partial \ln N_1} \right)_{P,E,T}^{-1} \times \left[\left(\frac{\partial \epsilon_d}{\partial n_1} \right)_{P,E,T,n_2} - \left(\frac{\partial \epsilon_d}{\partial n_2} \right)_{P,E,T,n_1} \right] d(E^2) \quad (16)$$

which is the general expression for the sorting of mixed solvents by ions where N_i^0 is the value N_i outside the field, r_e is the intrinsic radius of the ion, and E_r is the field strength at the distance r . Various cases may be considered in evaluating eq 16.

First Case. The dielectric constant, ϵ , and the volume, v , are assumed to be independent of the field strength (which is true for weaker fields only); the binary mixture is assumed to form an ideal solution. Under these conditions, it is possible to integrate the right-hand side of eq 16, since

$$\mu_1 = \mu_1^0 + RT \ln N_1 \text{ and } \epsilon = \epsilon_d = \frac{dD}{dE}$$

$$\ln \frac{N_1}{N_2} - \ln \frac{N_1^0}{N_2^0} = \frac{vE^2}{8\pi RT} \left[\left(\frac{\partial \epsilon}{\partial n_1} \right)_{P,E,T,n_2} - \left(\frac{\partial \epsilon}{\partial n_2} \right)_{P,E,T,n_1} \right] \quad (17)$$

Substituting

$$v \left(\frac{\partial \epsilon}{\partial n_1} - \frac{\partial \epsilon}{\partial n_2} \right)_{P,T,E} = v_m \left(\frac{\partial \epsilon}{\partial N_1} \right)_{P,T,E}$$

where $v_m = v/(n_1 + n_2)$ gives

$$\ln \frac{N_1}{N_2} - \ln \frac{N_1^0}{N_2^0} = \frac{v_m^2 E^2}{8\pi RT} \left(\frac{\partial \epsilon}{\partial N_1} \right)_{P,T,E} \quad (18)$$

which is identical with the expression obtained by Frank.⁶ Substituting $E = (Ze)/(\epsilon r^2)$ in eq 17 gives

$$\ln \frac{N_1}{N_2} - \ln \frac{N_1^0}{N_2^0} = - \frac{vZ^2 e^2}{8\pi RT \epsilon^2 r^4} \left[\frac{\partial \epsilon}{\partial n_1} - \frac{\partial \epsilon}{\partial n_2} \right]_{P,E,T} \quad (19)$$

which may be compared with the similar equation²

$$v_1 \ln \frac{N_1}{N_1^0} - v_2 \ln \frac{N_2}{N_2^0} = \frac{Z^2 e^2}{8\pi RT \epsilon^2 r^4} \left(v_1 \frac{\partial \epsilon}{\partial \eta_1} - v_2 \frac{\partial \epsilon}{\partial \eta_2} \right) \quad (20)$$

where Z is the valence of the ion, e the electronic charge, and r the distance from the ion; η_1 and η_2 are the number of molecules per milliliter of the two substances, and v_1 and v_2 are molecular volumes defined by

$$\eta_1 v_1 + \eta_2 v_2 = 1$$

Frank⁶ has already shown that eq 20 is less general than eq 18 and that, qualitatively, it is possible to predict that in the immediate neighborhood of an ion, N_1/N_2 could change by several powers of ten, a rather complete sorting. This treatment, however, neglects electrostriction and dielectric saturation, even at infinitely dilute solutions, and cannot be used for finite salt concentrations.

Second Case. We shall now solve eq 16 for the case of organic solvents containing a large percentage of water, where it has been shown that the activity of the water is very nearly given by the water mole fraction in the solvent. However, the dielectric constant will be taken to be a function of the field strength. In this

case, $\mu_1 = \mu_1^0 + RT \ln N_1$ and eq 16 is transformed into

$$\ln \frac{N_1}{N_2} - \ln \frac{N_1^0}{N_2^0} = - \frac{1}{2RT} \int_{r_e}^{\infty} r^2 dr \int_0^{E_r} \left[\left(\frac{\partial \epsilon_d}{\partial n_1} \right)_{P,T,E,n_2} - \left(\frac{\partial \epsilon_d}{\partial n_2} \right)_{P,T,E,n_1} \right] d(E^2) \quad (21)$$

which may be interpreted as follows. The ionic free energy of solvation in a mixed solvent at infinite dilution, ΔG , may be formally described as

$$\Delta G = n_1 \overline{\Delta G}_1 + n_2 \overline{\Delta G}_2 \quad (22)$$

where $\overline{\Delta G}_i$ is a partial free energy of solvation of the ion in component i of the mixture.

It has been shown⁸ that the integral

$$\frac{1}{2} \int_{r_e}^{\infty} r^2 dr \int_0^{E_r} \epsilon_d d(E^2) \quad (23)$$

represents the electrostatic part of the ionic solvation free energy. The part $\frac{1}{2} \int_0^{E_r} \epsilon_d d(E^2)$ may be considered as the ionic-solvation free-energy density and the differential

$$\frac{\partial}{\partial n_1} \left[\int_0^{E_r} \epsilon_d d(E^2) \right]_{P,T,E,n_2} = \int_0^{E_r} \left(\frac{\partial \epsilon_d}{\partial n_1} \right)_{P,T,E,n_2} d(E^2)$$

as the partial ionic-solvation free-energy density in component 1 of the mixture. Hence the right side of eq 21 may be considered to represent the difference between the partial ionic-solvation free energies in components 1 and 2 of the binary solvent, and we may write

$$\ln \frac{N_1}{N_2} - \ln \frac{N_1^0}{N_2^0} = - \frac{1}{RT} (\overline{\Delta G}_1 - \overline{\Delta G}_2) \quad (24)$$

From eq 24, the ionic index of preferential solvation, α , is obtained

$$\alpha = - \frac{\overline{\Delta G}_1 - \overline{\Delta G}_2}{2.3RT} \quad (25)$$

We may now combine the ionic contributions of an electrolyte (ν_a , anions, and ν_c , cations) and obtain thereby a mean selective index, $\bar{\alpha}$, given by

$$\bar{\alpha} = \frac{\nu_a \alpha_a + \nu_c \alpha_c}{\nu} = - \frac{\overline{\Delta G}_1 - \overline{\Delta G}_2}{2.3\nu RT} \quad (26)$$

with $\nu = \nu_a + \nu_c$ and $\overline{\Delta G}_i$ is the partial molar free energy of solvation of the electrolyte in component i of the binary solvent.

It follows that the preferential solvation depends only on the difference between the partial molar free energy of the electrolyte in each component of the solvent mixture, since the sign of $\bar{\alpha}$ determines the solvent selectivity.

(8) J. Padova, *J. Chem. Phys.*, **39**, 1552 (1963).

Table I: Values of $\bar{\alpha}$ for Various Solvents as Compared to Water

Salt	Solvents								50% Dioxane- water
	NH ₃	N ₂ H ₄	CH ₃ OH	C ₂ H ₅ OH	C ₄ H ₉ OH	C ₆ H ₁₁ OH	(CH ₃) ₂ CO	HCOOH	
HCl	-5.58	-2.67	2.02	2.56	2.89	3.12	3.12	2.94	2.98
HBr	-6.73	-3.78	2.02	2.56	2.02	3.19	1.84	4.22	
HI	-7.58	-2.67	1.47	2.56	2.57	2.20	2.75	4.58	
HClO ₄									0.21
NaCl	1.47	1.09	1.28	1.83	3.07	4.71	6.78	-1.10	5.06
NaBr	0.32	0	1.28	1.83	2.2	4.78	5.50	0.18	
NaI	-0.55	1.10	0.73	1.83	2.75	3.79	6.42	0.55	
NaOH									6.45
NaNO ₃									3.59
LiCl	0.92	1.65	1.28	2.19	1.97	2.02	2.38	-0.73	4.21
LiBr	-0.23	0.55	1.28	2.19	1.10	2.09	1.10	0.54	
LiI	-1.08	1.65	0.73	2.19	1.65	1.10	2.02	0.92	
KCl	4.76	1.10	1.28	2.38	3.98	4.22	4.95	-0.55	5.06
KBr	3.61	0	1.28	2.38	3.12	4.29	3.67	0.73	4.14
KI	2.76	1.10	0.73	2.38	3.66	3.30	4.58	1.10	3.11
RbCl	2.93	1.28	1.83	2.93	5.63	4.22	5.50	0.55	4.81
RbBr	1.80	0.18	1.83	2.93	4.77	4.29	4.22	1.78	
RbI	0.92	1.28	1.28	2.93	5.31	3.30	5.13	2.20	
CsCl	4.76	0.92	1.83	2.67	3.26	3.67	3.85	-1.78	4.58
CaBr	3.57	-0.18	1.83	2.67	2.39	3.74	2.57	-0.52	
CsI	2.73	0.92	1.28	2.67	2.93	2.75	3.49	-0.13	
AgCl	-5.50	-6.23	2.20	2.38				-2.20	
AgBr	-6.65	-7.33	2.20	2.38				0.92	
AgI	-7.50	-6.23	1.65	2.38				-0.55	
CaCl ₂	6.98	2.44						0.49	
ZnCl ₂	-5.99	-3.66	4.40	5.86				1.84	
CdCl ₂	-4.03	-4.37	3.98	4.51				0.98	

The difference $\overline{\Delta G}_1 - \overline{\Delta G}_2$ could be rigorously obtained by applying the Backhuis-Roozeboom procedure to the free energy of solvation of the electrolyte per mole of mixed solvent.

However, because of the paucity of data for mixed solvents, the molal solvation free energy of the electrolyte in the pure component i of the mixed solvent has been used, since this has been shown⁹ to introduce only small errors in the calculation of the difference $\overline{\Delta G}_1 - \overline{\Delta G}_2$. The calculated values of $\bar{\alpha}$ are listed in Table I. All the values of the solvation free energy were taken from Izmailov,¹⁰ except those for the mixture of 50% dioxane-water, taken from Grunwald *et al.*,¹¹ who give a correct value for the difference $\overline{\Delta G}_1 - \overline{\Delta G}_2$.

From the table, it may be seen that, generally, salts will solvate water preferentially, except for mixtures of NH₃ + H₂O, N₂H₄ + H₂O, and HCOOH + H₂O. The negative values of $\bar{\alpha}$ in these cases indicate that chemical interaction is taking place (*e.g.*, ammine formation), which probably leads to complex formation; this tallies with the fact that lower free-energy states are more stable.

This assumption of selective solvation in interpreting data on conductance,¹²⁻¹⁵ solubility,^{4,5} thermodynamic association constant,¹⁶ viscosity,¹⁷ density,¹⁸ transference numbers,¹⁹ molar refraction,²⁰ ultraviolet and visible spectra,²¹ vapor-pressure data,¹¹ solvolysis

reactions,²² and emf¹⁰ is confirmed by results listed in Table I. In the cases where it was possible to prove

(9) J. Padova, to be published.

(10) A. N. Izmailov, "Electrochemistry of Solutions," Kharkov University, 1959.

(11) E. Grunwald, G. Beughman, and G. Kohnstam, *J. Am. Chem. Soc.*, **82**, 5802 (1960).

(12) (a) G. Atkinson, *ibid.*, **82**, 818 (1960); (b) C. J. Mallada and G. Atkinson, *ibid.*, **83**, 3759 (1961); (c) G. Atkinson and C. J. Mallada, *ibid.*, **84**, 721 (1962); (d) G. Atkinson and S. Petrucci, *ibid.*, **86**, 7 (1964).

(13) (a) N. Goldenberg, Ph.D. Thesis, University of Kansas, Kansas City, Kan., 1961; (b) A. Fratiello, Ph.D. Thesis, Brown University, Providence, R. I., 1962.

(14) A. Campbell and G. Debus, *Can. J. Chem.*, **34**, 1232 (1956).

(15) J. B. Hyne, *J. Am. Chem. Soc.*, **85**, 304 (1963).

(16) (a) H. K. Bodenseh and J. B. Ramsey, *J. Phys. Chem.*, **67**, 140 (1963); (b) Y. H. Imami, H. K. Bodenseh, and J. Ramsey, *J. Am. Chem. Soc.*, **83**, 4745 (1961); (c) A. d'Aprano and R. M. Fuoss, *J. Phys. Chem.*, **67**, 1704, 1871 (1963).

(17) J. Padova, *J. Chem. Phys.*, **38**, 2635 (1963).

(18) J. Padova, *ibid.*, **39**, 2599 (1963).

(19) (a) J. O. Wear and E. S. Amis, *J. Inorg. Nucl. Chem.*, **24**, 903 (1962); (b) R. K. Kay and A. Fratiello, *J. Phys. Chem.*, in press; (c) H. Schneider and M. Strehlow, *Z. Elektrochem.*, **66**, 309 (1962); (d) H. Strehlow and H. M. Koepf, *ibid.*, **69**, 674 (1965); (e) H. Schneider and H. Strehlow, *ibid.*, **69**, 574 (1965); (f) H. Schneider and H. Strehlow, *Z. Physik. Chem.*, **49**, 44 (1966).

(20) (a) S. Minc and W. Libus, *Roczn. Chem.*, **29**, 1073 (1955); (b) J. Padova, *Can. J. Chem.*, **43**, 458 (1965).

(21) (a) S. Minc and W. Libus, *Roczn. Chem.*, **30**, 945 (1956); (b) I. S. Pominov, *Zh. Fiz. Khim.*, **31**, 1926 (1957); (c) R. F. Pasternack and R. A. Plane, *Inorg. Chem.*, **4**, 1171 (1965).

that selective solvation is taking place, as in the nmr study of electrolytes in 50% dioxane–water mixtures,^{23a} all salts examined showed preferential solvation for water, contradicting the results obtained by Grunwald,¹¹ but in complete agreement with the results for $\bar{\alpha}$ in the table. Additional confirmation was obtained from the use of epr for MnSO_4 ,^{14d} in water–dioxane mixtures, the study of rate of exchange of solvent molecules for Cr(III) ,²⁴ high-resolution nmr of Cu^{2+} , Mn^{2+} , and Cr^{3+} ,²⁵ in ethanol–water and in methanol–water,^{26,27} and in pyridine–water;^{23b} all the nmr data²³ confirm the results listed in the table for the solvents usually examined, *i.e.*, methanol, acetone, ethanol, and dioxane.

It has been possible to predict preferential solvation in aqueous organic mixtures by using the thermody-

namic approach to the continuum theory of electrolytes in mixed solvents.

Acknowledgment. I wish to thank Professors H. S. Frank and A. Katchalsky for their reading of the manuscript and offering valuable comments.

(22) For review, see ref 14; R. Hudson, *Ber. Bunsenges Physik. Chem.*, **68**, 215 (1964).

(23) (a) A. Fratiello and D. C. Douglas, *J. Chem. Phys.*, **39**, 2017 (1963); (b) A. Fratiello and E. G. Christie, *Trans. Faraday Soc.*, **61**, 306 (1965); (c) A. Fratiello and D. P. Miller, *Mol. Phys.*, **11**, 37 (1966).

(24) J. C. Jayne and E. L. King, *J. Am. Chem. Soc.*, **86**, 3986 (1964).

(25) In. Ua. Shamonin and S. A. Yan, *Dokl. Akad. Nauk SSSR*, **152**, 677 (1963).

(26) J. H. Swinehart, T. E. Rogers, and M. Taube, *J. Chem. Phys.*, **38**, 393 (1963).

(27) T. E. Rogers, J. H. Swinehart, and M. Taube, unpublished results.

Calculation of Fractionation Factors for Carbon and Oxygen Isotopic

Exchange in the System Calcite–Carbon Dioxide–Water

by Y. Bottinga

Scripps Institution of Oceanography, University of California, San Diego, La Jolla, California 92037
(Received June 14, 1967)

Partition-function ratios for $\text{H}_2\text{O}^{18}/\text{H}_2\text{O}^{16}$, $\text{CO}^{18}_2/\text{CO}^{16}_2$, $\text{CaCO}^{18}_3/\text{CaCO}^{16}_3$, $\text{C}^{13}\text{O}_2/\text{C}^{12}\text{O}_2$, and $\text{CaC}^{13}\text{O}_3/\text{CaC}^{12}\text{O}_3$ have been calculated. Water vapor and carbon dioxide are treated as ideal gases, but vibrational anharmonicity effects are taken into account. The calcite partition function ratios were calculated by adopting the Giulotto–Loinger model for the acoustical, optical, and librational lattice modes; the orbital-valence force-field method was used for the carbonate ion vibrational frequencies. For oxygen isotopic exchange between CO_2 and calcite, the calculated fractionations can be expressed as $1000 \ln \alpha_0 = -3.2798 + (1.0611 \times 10^4/T) - (1.8034 \times 10^6/T^2)$, for the temperature interval 0–550°; for carbon exchange, the corresponding equation is $1000 \ln \alpha_C = -2.4612 + (7.6663 \times 10^3/T) - (2.9880 \times 10^6/T^2)$. The calculated fractionation factors for isotopic exchange in the systems carbon dioxide–calcite and carbon dioxide–water agree with the observed ones. The agreement is less satisfactory for the oxygen isotopic fractionations between calcite and water above 100°.

I. Introduction

A knowledge of isotopic fractionation factors is a prerequisite for understanding the stable isotope abundance patterns observed in nature. Fractionation factors for oxygen have been measured in several systems as a function of temperature.¹ Unfortunately, it is often difficult to measure fractionation factors at temperatures of geochemical interest in systems containing solids. Therefore, it is frequently necessary to extrapolate measured data over a considerable temperature interval. A theoretical treatment of the problem should produce guide lines for extrapolation

and may alleviate the need for experimental results in favorable cases.

After Urey² had published his important paper on isotopic exchange, several attempts were made to calculate the fractionation factors for isotopic exchange between condensed phases. McCrea³ published a brief account of calculations of the isotopic fractionation factors for carbon and oxygen exchange between calcite

(1) H. P. Taylor, *Trans. Amer. Geophys. Union*, **47**, 287 (1966).

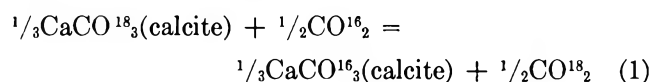
(2) H. C. Urey, *J. Chem. Soc.*, 562 (1947).

(3) J. M. McCrea, *J. Chem. Phys.*, **18**, 846 (1950).

and other phases. His calculated results do not agree with experimentally determined fractionations. In this paper, McCrea's work is discussed, and new calculations of fractionation factors for isotopic exchange in the system calcite-carbon dioxide-water are presented. All numerical results given in this paper were calculated on a CDC 3600 computer.

II. Calculation of Partition-Function Ratios

1. Gases. For the exchange reaction



the fractionation factor, α , is defined by

$$\alpha_{\text{O}} = (\text{O}^{18}/\text{O}^{16})_{\text{CO}_2} / (\text{O}^{18}/\text{O}^{16})_{\text{calcite}} \quad (2)$$

For carbon exchange in the analogous reaction one has

$$\alpha_{\text{C}} = (\text{C}^{13}/\text{C}^{12})_{\text{CO}_2} / (\text{C}^{13}/\text{C}^{12})_{\text{calcite}} \quad (3)$$

The fractionation factor can be calculated from the relation

$$\alpha_{\text{O}} = (Q^*/Q)_{\text{CO}_2}^{1/2} / (Q^*/Q)_{\text{calcite}}^{1/3} \quad (4)$$

where Q^*/Q stands for the partition-function ratio and the asterick indicates the presence of the heavy isotope. A detailed account of the above treatment can be found in many places: among others, Urey² and Dole.⁴ In going from eq 2 to 4, which corresponds to reaction 1, one has to assume a random distribution for the oxygen isotopes among the isotopically different carbonate ions in calcite and among the isotopically different carbon dioxide molecules. This assumption, the rule of the geometric mean, has been discussed by Bigeleisen^{5,6} and has been justified for carbon dioxide by Urey.² Formal justification for calcite requires a knowledge of the vibrational frequencies of all the isotopically different calcite unit cells, and such data are not available. As Bigeleisen⁶ shows, it is reasonable to assume that the rule of the geometric mean holds to the extent required for this paper, for structurally equivalent atoms other than hydrogen.

In this type of calculation, involving only ratios of partition functions for isotopically different molecules, the partition-function ratio is given, to a high degree of accuracy, by

$$Q^*/Q = (Q^*/Q)_{\text{trans}}(Q^*/Q)_{\text{rot}}(Q^*/Q)_{\text{vib}}$$

where the subscripts trans, rot, and vib stand for translational, rotational, and vibrational. For ideal gases one obtains

$$\begin{aligned} \ln(Q^*/Q) &= \ln(s^*/s) - 3n/2 \ln(m/m^*) + \\ &\sum_j \{ [(u_j - u_j^*)/2] + \ln[(1 - e^{-u_j})/(1 - e^{-u_j^*})] \} - \\ &\ln(u_j/u_j^*) \} d_j + ^{1/2}hc/(kT) \sum_{i < j} (x_{ij} - x_{ij}^*) d_i d_j + \\ &\ln[1 + hc/(kT) \sum_i d_i (d_i + 1) [x_{ii} e^{u_i} / (e^{u_i} - 1)^2 - \end{aligned}$$

$$\begin{aligned} &x_{ii}^* e^{u_i^*} / (e^{u_i^*} - 1)^2] + ^{1/2}hc/(kT) \sum_{i < j} d_i d_j \times \\ &\{ x_{ij} (e^{u_i} + e^{u_j}) / [(e^{u_i} - 1)(e^{u_j} - 1)] - \\ &x_{ij}^* (e^{u_i^*} + e^{u_j^*}) / [(e^{u_i^*} - 1)(e^{u_j^*} - 1)] \} \} \quad (5) \end{aligned}$$

In eq 5, $u_j = hc\omega_j/(kT)$, ω_j = zero-order frequency (in wave numbers) of the j th mode of vibration, x_{ij} = anharmonicity constant, d_i = degeneracy of the i th mode of vibration, s = symmetry number, n = number of exchanged atoms per molecule, and m = atomic mass of exchanged atom. T , k , h , and c have their usual meaning. Details about the first three terms (the harmonic part) in eq 5 can be found in Urey's paper. Vojta⁷ has treated the anharmonic part. The fourth term is the anharmonicity correction to the zero-point energy; it is an important term. The last term, the anharmonicity correction for the vibrational levels above the ground state, is complicated but quantitatively less important. Carbon dioxide and water vapor were treated as ideal gases, so that eq 5 could be applied. Table I illustrates the magnitude of the various terms in eq 5 for carbon dioxide. In Tables I and II, reduced partition-function ratios are listed. The reduced partition-function ratio is related to the normal partition-function ratio according to: $(Q^*/Q)_r = (Q^*/Q)(m/m^*)^{3n/2}$.

Table I: Reduced Partition Function Ratios for Carbon Dioxide

	Temp, °K			
	273.15	273.15	800	800
	Ln $(Q^*/Q)_r$			
	Oxygen	Carbon	Oxygen	Carbon
Harmonic terms	0.25382	0.20046	0.04739	0.04098
Zero-point anharmonic	-0.00331	-0.00327	-0.00113	-0.00112
Excited-level anharmonic	0.00010	0.00012	0.00025	0.00028
Total	0.25061	0.19732	0.04651	0.04014

The excited-level anharmonic correction is of the same order of magnitude as the presently attainable accuracy with which carbon and oxygen isotopic ratios may be measured in mass spectrometers.

2. *Solids.* Translations in solids are insignificant and rotations are normally absent or of a restricted nature. The restricted nature of the rotations makes it possible to treat them in this type of calculation as harmonic oscillations.⁸ The vibrational modes in

(4) M. Dole, "Introduction to Statistical Thermodynamics," Prentice-Hall, Inc., Englewood Cliffs, N. J., 1954.

(5) J. Bigeleisen, *J. Chem. Phys.*, **34**, 1485 (1961).

(6) J. Bigeleisen, *ibid.*, **23**, 2264 (1955).

(7) G. Vojta, *Ann. Physik*, **7**, 397 (1961).

(8) W. H. Stockmayer, *J. Chem. Phys.*, **27**, 321 (1957).

Table II: Reduced Partition-Function Ratios for Carbon Dioxide, Calcite, and Water Vapor

Temp, °C	Carbon dioxide		Calcite		Water vapor Oxygen ln (Q*/Q) _r
	Oxygen 1/2 ln (Q*/Q) _r	Carbon ln (Q*/Q) _r	Oxygen 1/2 ln (Q*/Q) _r	Carbon ln (Q*/Q) _r	
0	0.12530	0.19732	0.11404	0.21029	0.06822
25	0.11108	0.17558	0.09915	0.18570	0.06164
50	0.09919	0.15746	0.08693	0.16519	0.05608
75	0.08913	0.14215	0.07677	0.14787	0.05132
100	0.08053	0.12908	0.06824	0.13312	0.04721
125	0.07311	0.11779	0.06100	0.12044	0.04362
150	0.06666	0.10797	0.05482	0.10947	0.04046
175	0.06102	0.09936	0.04949	0.09990	0.03755
200	0.05606	0.09175	0.04486	0.09152	0.03516
225	0.05167	0.08450	0.04083	0.08414	0.03292
250	0.04777	0.07897	0.03729	0.07760	0.03090
275	0.04429	0.07356	0.03417	0.07179	0.02907
300	0.04116	0.06868	0.03140	0.06660	0.02740
325	0.03835	0.06427	0.02894	0.06200	0.02588
350	0.03581	0.06027	0.02673	0.05777	0.02449
375	0.03351	0.05662	0.02476	0.05400	0.02321
400	0.03141	0.05329	0.02298	0.05059	0.02203
425	0.02951	0.05024	0.02137	0.04749	0.02093
450	0.02776	0.04744	0.01992	0.04467	0.01992
475	0.02617	0.04487	0.01859	0.04209	0.01898
500	0.02470	0.04249	0.01739	0.03974	0.01811
525	0.02335	0.04030	0.01628	0.03758	0.01729
550	0.02211	0.03827	0.01527	0.03560	0.01653
575	0.02096	0.03638	0.01435	0.03377	0.01582
600	0.01989	0.03463	0.01349	0.03208	0.01515

calcite may be subdivided into external and internal modes. The external modes are the modes of the two-particle (calcium ion and carbonate ion) calcite lattice, while the modes of the carbonate ion are the internal ones. The external modes may be further subdivided into acoustical, optical, and librational modes. Calcium ions and carbonate ions vibrate in phase in the acoustical modes and out of phase in the optical modes. The librational modes correspond to the restricted rotations.

The contribution of the acoustical vibrations of the calcite lattice to the partition-function ratio has been evaluated by means of Debye functions. Optical and librational modes are treated by means of Einstein functions. Since there is no information on anharmonicity of the calcite spectrum, observed fundamentals were used instead of zero-order frequencies, and no anharmonic corrections were applied. The partition function-ratio for calcite becomes

$$\ln(Q^*/Q) = \sum_j \{ (u_j - u_j^*)/2 \} + \ln \{ (1 - e^{-u_j}) / (1 - e^{-u_j^*}) \} d_j + \sum_i \{ (3(u_i - u_i^*)/8) + \ln \{ (1 - e^{-u_i}) / (1 - e^{-u_i^*}) \} + D(u_i^*) - D(u_i) \} d_i \quad (6)$$

$$D(u_i) = (1/u_i)^3 \int_0^{u_i} x^3 dx / (e^x - 1)$$

Where j is the running index for the internal, optical,

and librational modes, and i indexes the acoustic modes. Table III gives some values of the terms contributing to the natural logarithm of the partition-function ratio for calcite and shows clearly that the lattice vibrations contribute significantly to the partition-function ratio.

Table III: Contributions to Calcite Partition-Function Ratios

	Temp, °K			
	273	273	800	800
	Ln (Q*/Q)		Oxygen	Carbon
Optical and rotational	0.30318	0.02154	0.27282	0.01957
Acoustic	0.04810	0.00741	0.04730	0.00729
Internal vibrational	0.52209	0.30179	0.25973	0.13101

III. Frequencies and Isotope Frequency Shifts

1. *Carbon Dioxide.* The degree of success of the calculations presented in this paper depends critically on the quality of the available spectral data. Exact vibrational constants are known for carbon dioxide. The constants used in this paper were measured by Courtoy.^{9,10} These constants were also used by

(9) C. P. Courtoy, *Can. J. Phys.*, **35**, 608 (1957).

(10) C. P. Courtoy, *Ann. Soc. Sci. Bruxelles*, **75**, 5 (1959).

Stull, *et al.*,¹¹ to calculate vibrational energy levels of the carbon dioxide molecule; their calculations showed good agreement with observed values. Courtroy measured the constants for C¹²O¹⁶₂ and for C¹³O¹⁶₂. The C¹²O¹⁸₂ frequencies were calculated from the C¹²O¹⁶₂ frequencies by means of the relations

$$\omega_1^*/\omega_1 = (m^{16}/m^{18})^{1/2}$$

$$\omega_2^*/\omega_2 = \{ [m^{16}(1 + 2m^{18}/m^{12})] / [m^{18}(1 + 2m^{16}/m^{12})] \}^{1/2}$$

$$\omega_3^*/\omega_3 = \omega_2^*/\omega_2$$

where m^{12} , m^{16} , and m^{18} stand, respectively, for the atomic masses of C¹², O¹⁶, and O¹⁸. The empirical relation¹²

$$x_{ij}^* = x_{ij}\omega_i^*\omega_j^*/\omega_i\omega_j$$

was used to calculate the anharmonicity constants for C¹²O¹⁸₂. The CO₂ vibrational constants used in this paper are listed in Table IV. The isotopic frequency shifts are equal to the ones listed by Urey.²

Table IV: CO₂ Vibrational Constants

Constant	Obsd C ¹² O ¹⁶ ₂ , cm ⁻¹	Obsd C ¹³ O ¹⁶ ₂ , cm ⁻¹	Calcd C ¹² O ¹⁸ ₂ , cm ⁻¹
ω_1	1354.91	1354.91	1277.25
ω_2	673.00	653.81	662.70
ω_3	2396.49	2328.22	2359.81
x_{11}	-3.75	-3.75	-3.33
x_{22}	-0.63	-0.64	-0.61
x_{33}	-12.63	-11.85	-12.25
x_{12}	3.65	3.50	3.39
x_{23}	-12.53	-11.75	-12.15
x_{13}	-19.37	-18.89	-17.98

2. *Water.* In previous calculations^{2,13} of partition-function ratios of H₂O¹⁶ over H₂O¹⁸, the water zero-order frequencies listed by Herzberg¹² were used. Recently, the vibrational constants for H₂O¹⁶ have been remeasured by Benedict, *et al.*¹⁴ Pinchas, *et al.*,¹⁵ have measured the observed fundamentals of D₂O¹⁸, but there are apparently no measurements of the H₂O¹⁸ spectrum.

Urey² has calculated the H₂O¹³ vibrational constants by assuming a valence force field. However, these frequencies lead to poor agreement between calculated and observed oxygen isotope fractionation in the system calcite-water and, more significantly, in the system carbon dioxide-water. Table V shows for the latter system the difference between Urey's calculated fractionation factor and the observed one. This difference is mainly due to Urey's water frequencies, since his carbon dioxide frequency shifts are the same as the ones in Table IV. Gompertz and Orville-Thomas¹⁶ used a quadratic potential function to calculate H₂O¹⁸ frequencies from H₂O¹⁶ data. Em-

ploying their calculated isotope shifts, one obtains results even worse than for Urey's isotope shifts.

Table V: Oxygen Isotopic Fractionation between Carbon dioxide-Water and Calcite-Water

System	Temp. °C	1000 ln α_0	Remarks
Calcite-water	0	34.4	a, b
Calcite-water	0	25.0	c
Calcite-water	0	34.4	d
Calcite-water	25	28.1	a, b
Calcite-water	25	20.3	c
Calcite-water	25	28.2	d
Carbon dioxide-water	25	39.9	e
Carbon dioxide-water	25	39.9	f
Carbon dioxide-water	25	40.9	g
Carbon dioxide-water	25	41.5	h
Carbon dioxide-water	25	37.4	i
Carbon dioxide-water	25	40.1	d

^a These data were taken from H. Craig (in press), who fitted a curve to the experimental data of Epstein, *et al.*, after these data were corrected for effects listed by Craig, [*Geochim. Cosmochim. Acta*, **12**, 133 (1957)]. ^b Measured: S. Epstein, R. Buchsbaum, H. A. Lowenstan, and H. C. Urey, *Bull. Geol. Soc. Amer.*, **64**, 1315 (1953). ^c Calculated: see ref 3. ^d Calculated: this paper. ^e Measured: W. Compston and S. Epstein, *Trans. Amer. Geophys. Union*, **39**, 511 (1958). ^f Measured: J. R. O'Neil and S. Epstein, *J. Geophys. Res.*, **71**, 4955 (1966). ^g Measured: M. Majzoub, *J. Chim. Phys.*, **563** (1966). ^h Measured: D. Staschewski, *Ber. Bunsenges Phys. Chem.*, **68**, 454 (1964). ⁱ Calculated: see ref 2.

Khachkuruzov¹⁷ has reanalyzed the published data on the spectrum of water, including the measurements made by Benedict, *et al.*,¹⁴ and deduced a new set of vibrational constants for H₂O¹⁶ and H₂O¹⁸. These constants have been used in this paper; they are tabulated in Table VI and compared with the constants determined by various other authors. (When this paper was submitted, one of the reviewers drew my attention to the recent treatment of the water molecule by D. Papoušek and J. Plíva [*Coll. Czech. Chem. Comm.*, **29**, 1973 (1964)], which appears to give very accurate force constants for several triatomic molecules. They obtained zero-order frequencies for H₂O and the deuteriated water molecules which do not differ greatly

(11) V. R. Stull, P. J. Wyatt, and G. N. Plass, *J. Chem. Phys.*, **37**, 1442 (1962).

(12) G. Herzberg, "Molecular Spectra and Molecular Structure," Vol. II, D. Van Nostrand Co. Inc., Princeton, N. J., 1945.

(13) S. C. Saxena, D. V. Batnagar, and S. Ramaswamy, *J. Chem. Eng. Data*, **7**, 240 (1962).

(14) W. S. Benedict, N. Gailar, and E. K. Plyler, *J. Chem. Phys.*, **24**, 1139 (1956).

(15) S. Pinchas, M. Halmann, and B. P. Stoicheff, *ibid.*, **31**, 1692 (1959).

(16) G. Gompertz and W. J. Orville-Thomas, *J. Phys. Chem.*, **63** 1331 (1959).

(17) G. A. Khachkuruzov, *Gosudarst. Inst. Prikl. Khim.*, **42**, 109 (1959).

Table VI: Comparison of Vibrational Constants for Water Vapor

	H_2O^{16} , cm^{-1}			H_2O^{18} , cm^{-1}		
	a	b	c	a	d	e
ω_1	3835.37	3832.17	3825.32	3827.59	3815.5	3804.8
ω_2	1647.59	1648.47	1653.91	1640.62	1647.8	1635.9
ω_3	3938.74	3942.53	3935.59	3922.69	3919.4	3905.8
x_{11}	-45.18	-42.576	-43.89	-45.00	-43.66	...
x_{12}	-15.14	-15.933	-20.02	-15.06	-19.89	...
x_{13}	-165.48	-165.824	-155.06	-164.47	-154.03	...
x_{22}	-17.04	-16.813	-19.5	-16.90	-19.36	...
x_{23}	-19.99	-20.332	-19.81	-19.82	-19.66	...
x_{33}	-44.62	-47.566	-46.37	-44.26	-45.99	...

^a Khachkuruzov.¹⁷ ^b Benedict, *et al.*¹⁴ ^c Herzberg.¹² ^d Urey.² ^e Gompertz and Orville-Thomas.¹⁶ The Kachkuruzov data were used in the present calculations.

from the values of Khachkuruzov, but they made no calculations for H_2O^{18} .)

3. *Calcite.* Various partial sets of calcite lattice vibrations have been published. Quantitative analysis of these data is rather rare. In this paper the calcite vibrational model developed by Giulotto and Loinger¹⁸ has been adopted. These authors solved the vibration problem for a single unit cell of calcite containing two molecules of CaCO_3 . One unit cell containing ten particles should have 30 degrees of freedom. In the Giulotto-Loinger model there are ten optical and librational modes, of which five are doubly degenerate, and two acoustical modes, the transverse one being degenerate. Hence the external modes account for 18 degrees of freedom. The remaining 12 degrees of freedom are taken up by the internal vibrations. The carbonate ion has four modes, of which two are doubly degenerate. By assuming that the unit cell is the vibrational unit in the calcite lattice, Giulotto and Loinger could also calculate the acoustical frequencies for the calcite lattice. From the equations given by these authors, the external frequencies of calcite were calculated and are given in Table VII.

Because the carbon isotope shift is rather small, the frequencies were calculated to four figures; this does not imply that these frequencies are accurate to four significant figures. In the oxygen case, only three figures were used. Table III shows that the variation with temperature of the lattice contribution to the partition-function ratio is relatively small. The reason for this is that the lattice modes are already excited to a large extent at room temperature. The internal frequencies are much larger than the external ones and far from totally excited at room temperature. They are mainly responsible for the temperature variation of the partition-function ratio. Hence the absolute magnitudes, as well as the isotope shifts, are of prime importance in the case of the internal frequencies, while in the case of the external frequencies, the exact magnitude of the frequencies is less important than the magnitude of the isotope shifts.

Table VII: External Frequencies of Calcite

Obsd CaCO_3 , cm^{-1}	Calcd $\text{CaC}^{12}\text{O}^{16}_3$, ^{a,b} cm^{-1}	Calcd $\text{CaC}^{12}\text{O}^{18}_3$, cm^{-1}	Calcd $\text{CaC}^{13}\text{O}^{16}_3$, cm^{-1}	Degen- eracy
282 ^a	282.2	266	281.9	2
155 ^a	155.1	147	154.0	2
357	397.2	388	396.0	1
106 ^a	106.1	100	106.1	1
330	345.3	334	344.9	2
106 ^a	110.9	111	110.6	2
...	256.5	249	256.1	2
...	269.1	255	267.4	1
...	99.1	94	98.9	1
...	294.6	295	294.6	1
...	104.3	101	103.8	2 ^c
...	142.1	137	141.4	1 ^c

^a Assumed in the original calculation by Giulotto and Loinger.¹⁸

^b These frequencies were also calculated by Giulotto and Loinger; their results differ slightly from the ones reported here. ^c Acoustical modes.

Table VIII gives a sample of the various sets of internal frequencies of the carbonate ion in the calcite lattice which have been published since 1955. Calculations were carried out using both the set quoted by Hexter¹⁹ and that given by Schroeder, *et al.*²⁰ The latter set gave slightly better results, and the calculations reported in this paper have been done with these frequencies. Internal frequencies for CaCO^{18}_3 or $\text{CaC}^{13}\text{O}_3$ have not yet been measured. Urey² attributes a set of frequencies for $\text{CO}^{18}_3^{2-}$ to Hibben. This statement is presumably a misprint, since Urey² outlines the way in which he himself estimated these frequencies. Beckmann, *et al.*,²¹ have calculated ν_1 , ν_3 , and ν_4 for $\text{C}^{12}\text{O}^{18}_3^{2-}$ and for $\text{C}^{14}\text{O}^{16}_3^{2-}$; their calculation

(18) L. Giulotto and A. Loinger, *Nuovo Cimento*, **8**, 475 (1951).

(19) R. M. Hexter, *Spectrochim. Acta*, **10**, 281 (1958).

(20) R. A. Schroeder, C. E. Wier, and E. R. Lippincott, *J. Res. Nat. Bur. Stand.*, **66A**, 407 (1962).

(21) L. Beckmann, L. Gutjahr, and R. Mecke, *Spectrochim. Acta*, **21**, 141 (1965).

Table VIII: Carbonate Ion Frequencies in the Calcite Lattice

ν_1 , cm ⁻¹	ν_2 , cm ⁻¹	ν_3 , cm ⁻¹	ν_4 , cm ⁻¹	Ref
1083	874; 855	1467	713; 700	a
1087	881	1432	712	b
1087	869	1432	714	c
1070	881	1460	712	d
...	860	1430	712	e

^a S. D. Ross and J. Goldsmith, *Spectrochim. Acta*, **2**, 781 (1964). ^b C. E. Weir and E. R. Lippincott, *J. Res. Nat. Bur. Stand.*, **65A**, 173 (1961). ^c See ref 19. ^d See ref 20. ^e J. Louisfert, *Compt. Rend.*, **241**, 940 (1955).

is based on an educated guess for one of the necessary force constants. Decius²² has observed the ν_2 frequency for C¹²O₃²⁻ and for C¹³O₃²⁻ in calcite; the respective values were 877.7 and 850 cm⁻¹.

In this paper the frequencies of the C¹³O₃²⁻ and C¹²O₃²⁻ carbonate ions (Table IX) were calculated by means of the orbital-valence force field proposed by Heath and Linnett²³ using a set of force constants calculated from the frequencies given by Schroeder, *et al.*²⁰ The calculated force constants were rather similar to those derived by Janz and Mikawa²⁴ by means of a Urey-Bradley field-type potential. It was assumed that the coupling between the internal and external frequencies is insignificant in calcite. This assumption can be justified on an *a priori* basis by the fact that the observed fundamentals of carbonate ion in aqueous solution are very similar to those of the carbonate ion in the calcite lattice.²³ The C¹³ isotope shift calculated for the second fundamental, 27.6 cm⁻¹, agrees with the value 27.7 cm⁻¹ observed by Decius, showing that in this case the isotopic frequency shift is unaffected by the external modes, as assumed.

Table IX: Internal Frequencies of Isotopic Calcite Species

Freq	Obsd CaC ¹² O ₃ , cm ⁻¹	Calcd CaC ¹² O ₃ , cm ⁻¹	Calcd CaC ¹³ O ₃ , cm ⁻¹
ν_1	1070	1008.67	1070.00
ν_2	881	871.13	853.38
ν_3	1460	1436.15	1419.74
ν_4	712	674.69	709.24

All effects of anharmonicity in calcite have to be neglected because of lack of information. However, these effects are, to a certain extent, included implicitly by the use of observed fundamentals instead of zero-order frequencies for all modes. Moreover the calcite frequencies are generally lower than those of CO₂ and H₂O, and thus the anharmonicity effects should be less significant than for the latter two molecules.

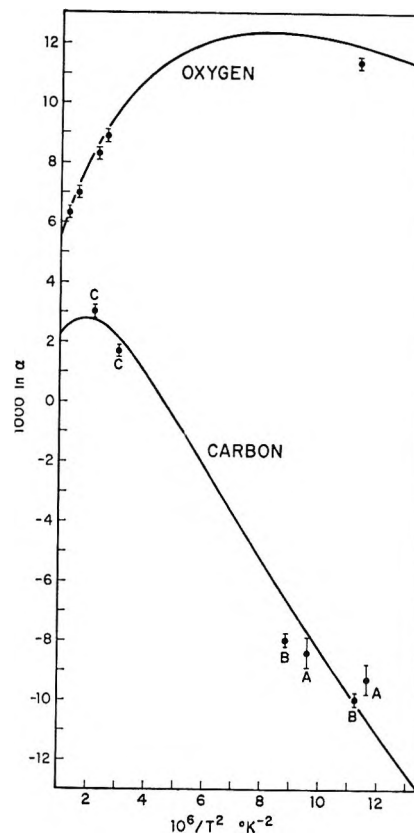


Figure 1. Calculated curves for oxygen and carbon isotope fractionation between CO₂ and calcite. The experimental points were measured by: J. C. Vogel, as quoted by R. O. Rye in his Ph.D. dissertation, Princeton University, Princeton, 1965 (carbon, A); P. Baertschi [*Schweiz. Mineral. Petrog. Mitt.*, **37**, 73 (1957)] (carbon, B); D. A. Northrop and R. N. Clayton [*J. Geol.*, **74**, 174 (1966)] (carbon, C); O'Neil and Epstein²⁵ (oxygen).

IV. Results

1. *Carbon Dioxide-Calcite.* Calculated fractionation factors for CO₂-CaCO₃ exchange are compared with experimental results of O'Neil and Epstein²⁵ on oxygen isotope exchange in Table X and with experimental data of various authors on carbon isotope exchange in Table XI. These comparisons are summarized in Figure 1, which shows that the present calculation is consistent with the experimental data over a large temperature range. The results for oxygen exchange are close to the experimental uncertainty of ± 0.2 ; experimental data on carbon exchange are less precise and the errors are difficult to estimate, but there is no indication of a systematic difference from the calculated values. The fractionation factor for oxygen exhibits a maximum near 348°K, and for carbon there is a maximum near 733°K. In carbon

(22) J. C. Decius, *J. Chem. Phys.*, **22**, 1946 (1954).

(23) D. F. Heath and J. W. Linnett, *Trans. Faraday Soc.*, **44**, 873 (1948).

(24) G. J. Janz and Y. Mikawa, *J. Mol. Spectrosc.*, **1**, 92 (1960).

(25) J. R. O'Neil and S. Epstein, *Science*, **152**, 198 (1966).

isotope exchange there is a crossover at 465°K. The cross-over point for oxygen exchange is below room temperature.

Table X: Fractionation Factors for Oxygen Exchange between Carbon Dioxide and Calcite

Temp, °K	Calcd 1000 ln α_O	Measured ^a 1000 ln α_O
298.15	11.9	11.4
623.15	9.1	8.9
673.15	8.4	8.2
793.15	7.1	7.0
883.15	6.3	6.4

^a O'Neil and Epstein;²⁵ experimental error is ± 0.2 .

Table XI: Fractionation Factors for Carbon Exchange between Carbon Dioxide and Calcite

Temp, °K	Calcd 1000 ln α_C	Measured 1000 ln α_C	Measured by
293	-10.7	-9.3 \pm 0.5	a
298	-10.1	-10.0	b
323	-7.7	-8.4 \pm 0.5	a
336	-6.6	-8.0	b
573	+2.1	+1.7	c
673	+2.7	+3.0	c

^a J. C. Vogel, as quoted by R. O. Rye in his Ph.D. Dissertation, Princeton University, Princeton, N. J., 1965. ^b P. Baertschi, *Schweiz. Mineral. Petrog. Mitt.*, **37**, 73 (1957). ^c D. A. Northrop and R. N. Clayton, *J. Geol.*, **74**, 174 (1966).

The calculated reduced partition-function ratios are tabulated *vs.* temperature in Table II. Fractionation factors calculated from these ratios were fit to the equation

$$1000 \ln \alpha = A + (B/T) + (C/T^2) \quad (7)$$

giving for oxygen

$$1000 \ln \alpha_O = -3.2798 + (1.0611 \times 10^4/T) - (1.8034 \times 10^6/T^2) \quad (8)$$

and for carbon

$$1000 \ln \alpha_C = -2.4612 + (7.6663 \times 10^3/T) - (2.9880 \times 10^6/T^2) \quad (9)$$

Least-square fits to equations using only the first and second or first and third terms of eq 7 were found to be inferior to eq 8. For example, using an equation of the type

$$1000 \ln \alpha = A + (C/T^2) \quad (10)$$

to fit the calculated fractionation factors for oxygen values of 1000 ln α_O which differ from the actual calculated values by -0.5 at 0°, by +2.1 at 200°, and

by +0.4 at 500°. The corresponding differences for eq 8 are only +0.1, +0.1, and +0.1, respectively. For carbon, a least-squares fit to eq 10 differs from the actual calculated values by -2.0, +1.3, and +0.7 at 0, 200, and 500°, compared to differences of -1.5, 0.2, and 0.3 obtained from eq 9.

2. *Water-Carbon Dioxide-Calcite.* The partition-function ratio for liquid water was obtained by multiplying partition-function ratio for water vapor (calculated from eq 5) with the fractionation factor for oxygen exchange between water and water vapor.^{26,27} The vapor pressure ratio of H₂O¹⁶:H₂O¹⁸, which is closely related to the fractionation factor, has been remeasured recently.^{28,29} The data of ref 26, 27, and 29 agree with each other to within the experimental error; they were preferred for this reason. Horibe and Craig²⁷ have fitted their data and those of Baertschi and Thürkauf²⁶ to the equation: $1000 \ln \alpha_v = (1.015 \times 10^6/T^2 - 2.30)$ (where α_v is the O¹⁸/O¹⁶ ratio in the liquid divided by the ratio in the vapor at equilibrium). In this paper 1000 ln α_v was taken to be 11.5 at 0° and 9.3 at 25°; these values were obtained by fitting a second-degree polynomial in 1/T to the data of Baertschi and Thürkauf, and Horibe and Craig.

The observed oxygen-fractionation factors are compared in Table V with the values calculated in this paper and by Urey² and McCrea.³ The calcite-water calculation is seen to be considerably improved by the present model. (If the values of 11.5 and 9.3 for 1000 ln α_v , obtained as described above, are used in the previous calculations cited in Table V, the discrepancy in their calculated values increases by 1.3 and 0.5 at 25 and 0°, respectively.)

V. Discussion

A brief discussion follows of the calculations by Urey² and McCrea³ whose results are given in Table V. Urey calculated ideal-gas partition-function ratios for the free carbonate ion and used these for the solid. The ν_1 and ν_2 frequency shifts are readily obtained and his values agree with those calculated here. However, his treatment of the ν_3 and ν_4 frequencies requires more information than is available from spectroscopic data because there are more unknowns than equations. Following a suggestion of Teller and Mayer, Urey, therefore, estimated the frequency shifts for carbon and oxygen by choosing three values for the ν_3 carbon shift, calculating the ν_4 carbon and both oxygen isotopic shifts required by his set of equations, and then selecting the resulting partition-function ratios

(26) P. Baertschi and M. Thürkauf, *Helv. Chim. Acta*, **43**, 80 (1960).

(27) Y. Horibe and H. Craig, unpublished data; measurement quoted in H. Craig, *et al.*, *J. Geophys. Res.*, **68**, 5079 (1963).

(28) O. V. Uvarov, N. M. Sokolov, and N. M. Zavoronkov, *Kernenergie*, **5**, 323 (1962).

(29) M. Szapiro, Ph.D. Dissertation, The Weizmann Institute of Science, Rehovoth, Israel, 1966.

which gave the best agreement for $\text{CO}_2\text{-CaCO}_3$ and $\text{CaCO}_3\text{-H}_2\text{O}$ fractionation with geochemical data. Craig³⁰ has shown that the geochemical carbon isotope data were incorrect for carbon dioxide and has pointed out that the partition-function ratios tabulated in column 8 of Urey's Table XVI are considerably better than those in column 7 which Urey chose.³¹ Frequency shifts from Urey's column 8 data for both carbon and oxygen ν_3 and ν_4 frequencies agree within 1 cm^{-1} with the frequency shifts calculated here in Table IX.

McCrea's³ treatment assumes that the rotational contribution to the partition-function ratio of calcite is equal to the translational contribution and uses optical and librational frequencies which differ from the ones used in this paper. He assumed that the optical, librational, and acoustical modes were triply degenerate. McCrea took the acoustical cut-off frequency from the work of Anderson,³² who measured the specific heat of calcite and deduced Debye and Einstein temperatures. However, Anderson's lowest specific heat measurement was near 50°K , which is too high to determine the acoustical cut-off frequency for calcite. McCrea used the carbonate ion frequency shifts estimated by Urey, as discussed above, and calculated isotopic shifts in the external modes by a somewhat *ad hoc* procedure. However, the major factor influencing the large difference in his results and the present ones is his assumption about the rotational contribution in calcite.

Tables VI and VIII illustrate, in a limited way, the variety of spectral information available; moreover, there are in the literature various partial sets of lattice frequencies for calcite (among others: Hexter,¹⁹ and Schroeder, *et al.*²⁰). The quality of these data is hard to judge. The 36-cm^{-1} librational frequency deduced by Schroeder, *et al.*, disagrees markedly with the available low-temperature specific-heat data for calcite. With a large choice of input information, it is not particularly difficult to calculate a fractionation factor for a given exchange reaction at a given temperature which virtually coincides with the observed factor. However, the calculations presented here agree with the experimental data over a large temperature interval and the calculated results are consistent with the possible fractionations among the three pairs of phases. The calculated oxygen fractionation in the system carbon dioxide-water is close to the average of the recently measured values of this quantity at 25° , the only temperature for which data are available.

The agreement between calculated and observed oxygen isotope fractionation factors in the system calcite-water is poorer than for the other systems treated. This is especially noticeable at higher temperatures where the values of $1000 \ln \alpha_0$ measured by Clayton³³ are consistently larger by about 2 ‰ than the ones calculated here and obtainable from the

data of Table XII. Possible causes of this discrepancy are the uncertainty in the vibrational constants of H_2O^{18} and the nonideality of water vapor. A meaningful comparison between the observed and calculated high-temperature fractionation factors in this system is difficult because of the uncertainty of the oxygen fractionation between water and water vapor at temperatures above 100°C . Of course, above the critical temperature of water, this fractionation becomes unity, but in the high-temperature exchange experiments³³ a $0.5\text{ M NH}_4\text{Cl}$ solution was used instead of pure water and the critical temperature of this solution is not known. The work by Sourirajan and Kennedy³⁴ on NaCl solutions suggests that the critical temperature of the solutions Clayton used will be higher than 374° .

At high temperatures the anharmonicity of the calcite frequencies will become important, and the partition-function ratio will approach unity faster than in the harmonic approximation. Therefore, the reliability of the calculations involving calcite will be decreased at high temperatures. On the other hand, the calculations may be used with confidence at low temperatures, where it may be impossible to obtain experimental results.

The present calculation for calcite partition-function ratios includes three principal assumptions: (1) the harmonic approximation, required by lack of data; (2) that coupling between internal and external modes of vibration does not significantly affect the isotopic frequency shifts, and (3) statistical distribution of O^{18} among the isotopically different calcite unit cells. The agreement between calculated and observed fractionation factors shows that no serious errors are introduced by these assumptions for carbon and oxygen exchange in the carbon dioxide-water-calcite system. The agreement for oxygen exchange between water and carbon dioxide is of special interest because of recent indications that the harmonic approximation for the molecules $\text{H}_2\text{O-HDO-D}_2\text{O}$ gives better agreement with observed data than the anharmonic treatment.³⁵⁻³⁸ The anharmonic correction for oxygen exchange between carbon dioxide and water amounts to only 1 ppt at 25° , and thus is barely significant. However, the anharmonic calculation does agree better with the experimental data.

Acknowledgments. I am grateful to Dr. H. Craig

(30) H. Craig, *Geochim. Cosmochim. Acta*, **3**, 53 (1953).

(31) H. Craig, personal communication, 1967.

(32) C. T. Anderson, *J. Am. Chem. Soc.*, **56**, 340 (1934).

(33) R. N. Clayton, *J. Chem. Phys.*, **34**, 724 (1961).

(34) S. Sourirajan and G. C. Kennedy, *Amer. J. Sci.*, **260**, 115 (1962).

(35) J. W. Pyper and F. A. Long, *J. Chem. Phys.*, **41**, 2213 (1964).

(36) R. E. Weston, Jr., *ibid.*, **42**, 2635 (1965).

(37) L. Friedman and V. J. Shiner, Jr., *ibid.*, **44**, 4639 (1966).

(38) J. W. Pyper, R. S. Newbury, and G. W. Barton, Jr., *ibid.*, **46**, 2253 (1967).

for discussion, criticism, and support of this work. Drs. G. Goles, S. Hart, H. C. Urey, and D. Weill read the paper and offered comments. The facilities of the Computer Center of the University of California,

San Diego, Calif., were used for the calculations; I thank Mrs. J. Hays for advice about the programming. This research was supported by the National Science Foundation, Grants GP-4547 and GP-3347.

Reactions of the Primary Reducing Species in the

Radiolysis of Liquid 2-Propanol¹

by J. C. Russell and G. R. Freeman

Chemistry Department, University of Alberta, Edmonton, Alberta, Canada (Received June 26, 1967)

A study has been made of the effects of temperature, acid, and nitrous oxide on the yield of hydrogen in the radiolysis of 2-propanol. The yields of free-ion solvated electrons and those that undergo geminate neutralization have been calculated to be $G(e_{\text{solv}}^-)_{\text{fi}} = 1.2$ (at 25°) and $G(\text{geminate neutralization}) = 2.8$ (at 25°). The fate of a portion of the electron yield equivalent to $G(e_{\text{solv}}^-) = 1.9$ is temperature dependent. At low temperatures, there is no hydrogen produced from this portion of the solvated electron yield. At temperatures above 140°, all of these electrons give rise to hydrogen. The results of electron scavenging reactions by nitrous oxide have been tested against a nonhomogeneous kinetics mechanism, with moderate success. Secondary reactions involving nitrous oxide produce large yields of nitrogen at high temperatures and high nitrous oxide concentrations.

Introduction

The radiolysis of the higher aliphatic alcohols has not been studied in the same detail as has that of methanol and ethanol. The radiolysis of ethanol exhibits a number of unusual features.^{2,3} A study of the primary reducing species in the radiolysis of 2-propanol should aid in understanding both ethanol radiolysis and alcohol radiolysis in general.

Sherman⁴ has suggested that in 2-propanol at room temperature, $G(e_{\text{solv}}^-) = 2.5$ and that the free-ion yield, $G(e_{\text{solv}}^-)_{\text{fi}} = 0.9$. He reported $G(\text{H}_2) = 4.0$. A consequence of the suggested mechanism is that $G(\text{H}) = 3.1$.⁴

Nitrous oxide in water is known to react with hydrated electrons with a high specific rate ($k(e_{\text{aq}}^- + \text{N}_2\text{O}) = 7 \times 10^9 \text{ M}^{-1} \text{ sec}^{-1}$).^{5,6} Nitrous oxide reacts much more slowly with hydrogen atoms in water ($k(\text{H} + \text{N}_2\text{O}) = 2 \times 10^6 \text{ M}^{-1} \text{ sec}^{-1}$).⁷ 2-Propanol would be expected to react rapidly with hydrogen atoms, so attack of the atoms on the nitrous oxide is probably of no consequence in propanol solvent.

Changing the temperature over a wide range causes large changes in the properties of a liquid such as 2-

propanol. The dielectric constant is particularly temperature dependent. Thus the present experiments were conducted over as wide a temperature range as was practicable.

Experimental Section

Most of the experimental methods used were identical with those used in an earlier study of the primary reducing species in ethanol.² All samples were irradiated with ⁶⁰Co γ radiation.

In the present work, some irradiations were performed at higher temperatures than those used previously.² Above 150°, the vapor pressure of 2-pro-

(1) This work received financial support from the National Research Council of Canada.

(2) J. C. Russell and G. R. Freeman, *J. Phys. Chem.*, **71**, 755 (1967).

(3) J. C. Russell and G. R. Freeman, *ibid.*, **72**, 816 (1968).

(4) W. V. Sherman, *ibid.*, **70**, 667 (1966).

(5) F. S. Dainton and D. B. Peterson, *Proc. Roy. Soc. (London)*, **A267**, 433 (1962).

(6) S. Gordon, E. J. Hart, M. S. Matheson, J. Rabani, and J. K. Thomas, *Discussions Faraday Soc.*, **36**, 193 (1963).

(7) F. S. Dainton and D. C. Walker, *Proc. Roy. Soc. (London)*, **A285**, 339 (1965).

panol rapidly exceeds that which may be contained by the glass cells used. The samples irradiated above 150° were placed in the usual glass cells in a steel pressure vessel partially filled with 2-propanol.⁸ The pressure vessel was placed in a small electrically heated oven and warmed to the desired temperature, allowed to equilibrate, and then irradiated. The temperature was measured with an indicating pyrometer which was calibrated against a mercury thermometer.

The design of the pressure vessel is shown in Figure 1. The walls were made as thin as practicable to minimize attenuation of the γ radiation. The vessel was machined from a bar of SPS-245 steel and heat treated to Rockwell C-30. The estimated bursting pressure of the vessel was approximately 650 atm before heat treatment and 1350 atm after heat treatment. The vessel was pressure tested on a hydraulic pressure system to 300 atm before use. Lead was found to be the most suitable gasket material, as a good seal is formed without the application of a high force through the screws in the head, and lead is not affected by temperature or radiation under the experimental conditions.

The 2-propanol which partially fills the pressure vessel exerts its vapor pressure on the glass sample cell, equalizing the interior and exterior pressures. Thus a glass cell may be used at very high over-all pressures. It was found to be necessary to flush the pressure vessel with nitrogen gas before closing it. At high temperatures and pressures, oxygen in the entrapped air oxidizes the alcohol, and the resulting acid rapidly attacks the steel. The vessel could be constructed from stainless steel, but this would require a greater wall thickness for the same strength.

The analysis for 2-chloropropane was made using techniques described elsewhere.³

Reagent grade 2-propanol from Fisher Scientific Company was treated with 2,4-dinitrophenylhydrazine, by a previously described technique,² in order to remove carbonyl impurities. It was then thoroughly degassed and stored under vacuum in a Pyrex vessel. All other materials were as previously described.²

Results

The yield of hydrogen from pure 2-propanol as a function of dose at 25° is shown in Figure 2. At a dose of 1.5×10^{17} eV/ml, the yield was $G(\text{H}_2) = 4.5$. All other experiments were performed at this dose, and all experiments were performed at a dose rate of 4.5×10^{17} eV/ml min.

Between -85 and 140°, the hydrogen yield increased roughly linearly with temperature from $G(\text{H}_2) = 3.6$ to 5.5. Higher temperatures, up to 225°, caused no further increase in yield (Figure 3).

The addition of hydrogen chloride caused different effects at different temperatures. Addition of acid at -85° caused $G(\text{H}_2)$ to increase from 3.6 to 5.1 at $[(\text{CH}_3)_2\text{CHOH}_2^+] = 0.03 M$, and it did not appear to

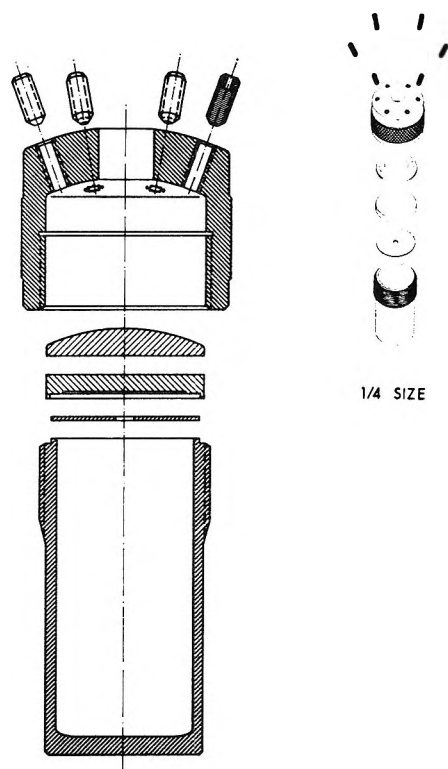


Figure 1. Steel pressure cell used for high-temperature irradiations. The diagram is drawn to scale and the inside diameter of the steel pressure cell is 5.1 cm.

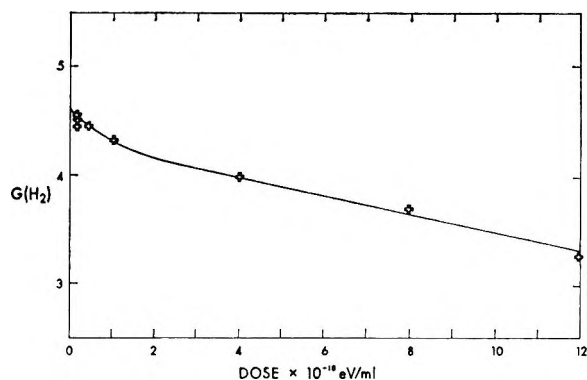


Figure 2. The yield of hydrogen as a function of dose at 25° and a dose rate of 4.5×10^{17} eV/ml min.

have reached a maximum (Figure 4). At 25°, $G(\text{H}_2)$ increased from 4.5 to 5.3 at 0.03 M $(\text{CH}_3)_2\text{CHOH}_2^+$ and also did not appear to have reached a maximum (Figure 5). At 140°, $G(\text{H}_2) = 5.5$, independent of acid concentration (Figure 6). Above 150°, addition of a high concentration of hydrogen chloride caused $G(\text{H}_2)$ to decrease by as much as 1.1 units at 1.4 M acid and 180° (Figures 7 and 8). At these higher temperatures, addition of a low concentration of hydrogen chloride caused no change in $G(\text{H}_2)$ (Figures 7 and 8).

(8) The authors are indebted to Dr. T. J. Hardwick for suggesting the principle of this technique.

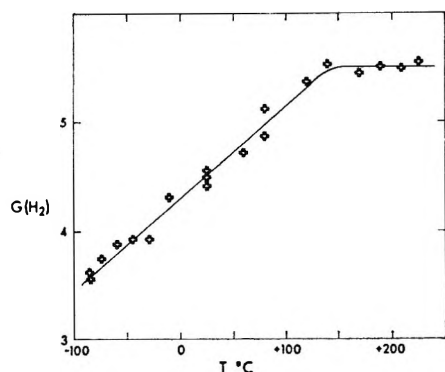


Figure 3. The yield of hydrogen as a function of temperature: dose = 1.5×10^{17} eV/ml.

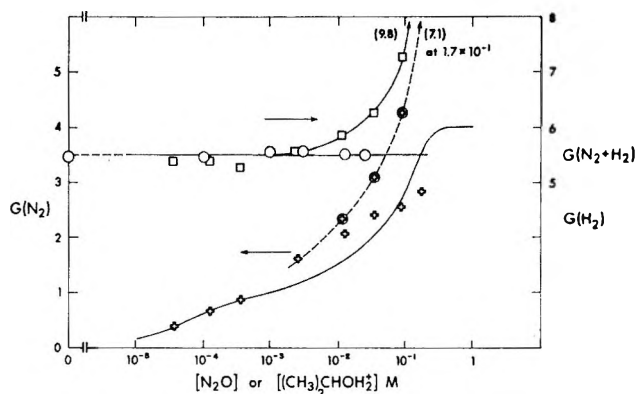


Figure 6. The effect of hydrogen chloride and nitrous oxide concentration at 140° : +, N_2 in the presence of nitrous oxide; ⊕, N_2 yields which required correction for secondary reaction; □, ($N_2 + H_2$) in the presence of nitrous oxide; ○, H_2 in the presence of hydrogen chloride.

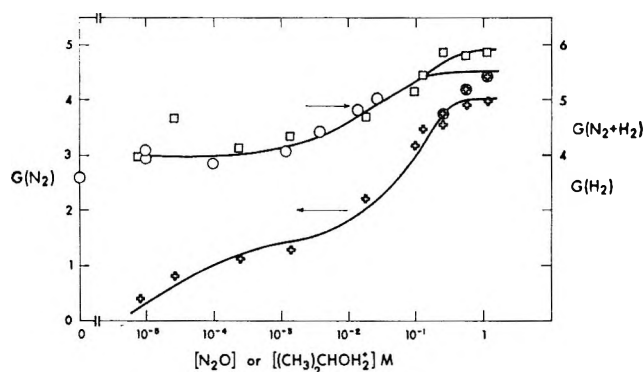


Figure 4. The effect of hydrogen chloride and nitrous oxide concentration at -85° : +, N_2 in the presence of nitrous oxide; ⊕, N_2 yields which required correction for secondary reaction; □, ($N_2 + H_2$) in the presence of nitrous oxide; and ○, H_2 in the presence of hydrogen chloride (this line has been extrapolated as discussed in the text).

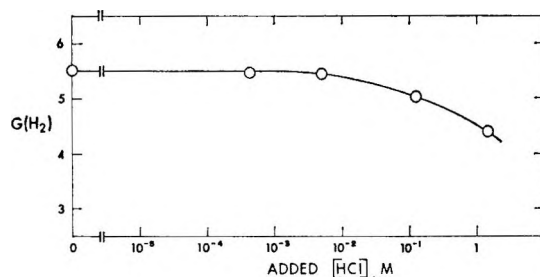


Figure 7. The yield of hydrogen at 180° as a function of added hydrogen chloride.

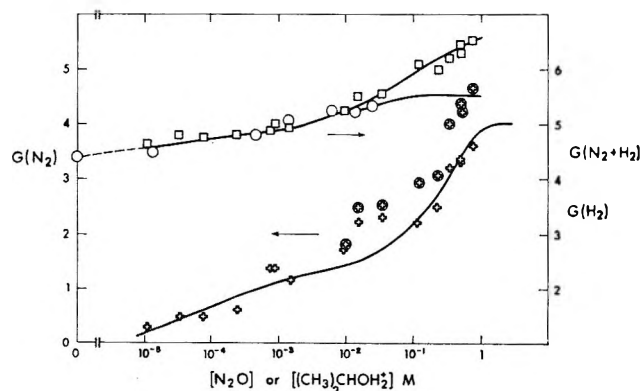


Figure 5. The effect of hydrogen chloride and nitrous oxide concentration at 25° : +, N_2 in the presence of nitrous oxide; ⊕, N_2 yields which required correction for secondary reaction; □, ($N_2 + H_2$) in the presence of nitrous oxide; and ○, H_2 in the presence of hydrogen chloride (this line has been extrapolated as discussed in the text).

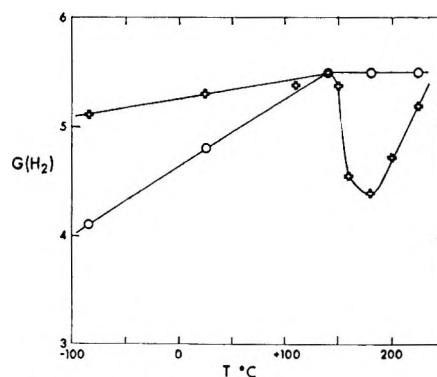


Figure 8. The yield of hydrogen in the presence of added hydrogen chloride as a function of temperature: +, $1.4 M$; and ○, $4 \times 10^{-4} M$ hydrogen chloride.

The concentration of hydrogen chloride in the samples was computed assuming that all the hydrogen chloride was dissolved in the propanol. The dissoci-

ation constant $K_{diss} = 4 \times 10^{-4}$ for hydrogen chloride in 2-propanol was calculated from the value $K_{diss} = 0.015$ in ethanol,^{9a} using an equation that relates the acid dissociation constant to the dielectric constant of

(9) (a) I. I. Bezzmann and F. H. Nerhock, *J. Am. Chem. Soc.*, **67**, 1330 (1945); (b) I. M. Kolthoff and S. Bruckenstein in "Treatise on Analytical Chemistry," Part I, Vol. 1, I. M. Kolthoff, P. J. Elving, and E. B. Sandell, Ed., Interscience Encyclopedia, Inc., New York, N. Y., 1959, Chapter 13, p 488.

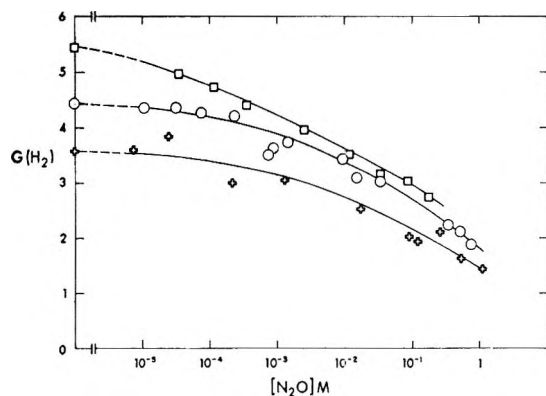


Figure 9. The yield of hydrogen as a function of nitrous oxide concentration: \square , 140° ; \circ , 25° ; and $+$, -85° .

the medium.^{9b} The concentrations of $(\text{CH}_3)_2\text{CHOH}_2^+$ for the data in Figures 4–6 have been calculated assuming this value of K_{diss} . The dissociation constants of weak acids in water and in aqueous–organic mixed solvents do not change rapidly with temperature. Furthermore, some dissociation constants increase and others decrease with increasing temperature.¹⁰ It is, therefore, assumed, for lack of anything better, that $K_{\text{diss}} = 4 \times 10^{-4}$ for hydrogen chloride in 2-propanol, independent of temperature.

Because of the decrease in $G(\text{H}_2)$ found at high temperatures and high acid concentration, and a similar effect found in ethanol accompanied by formation of ethyl chloride,³ samples were analyzed for 2-chloropropane. A sample containing 1.4 *M* added hydrogen chloride and treated as for irradiation at 170° was found afterwards to contain 1.1 *M* 2-chloropropane.

The addition of nitrous oxide to the propanol caused nitrogen to be formed (Figures 4–6) and the hydrogen yield to decrease (Figure 9). The sum $G(\text{H}_2 + \text{N}_2)$ increased with increasing nitrous oxide concentration. At -85 and 25° , this increase was very similar to the increase in $G(\text{H}_2)$ caused by addition of acid (Figures 4 and 5). At 140° , $G(\text{H}_2 + \text{N}_2)$ did not rise above 5.5 until the concentration of nitrous oxide exceeded 10^{-3} *M*. Above this concentration, $G(\text{N}_2)$ and $G(\text{H}_2 + \text{N}_2)$ rose very rapidly to high values (Figure 6).

The nitrogen yields are shown in Figures 4–6 both as measured and, in the high-concentration regions, as corrected by a method which will be discussed later. The lines through the nitrogen yields were calculated by the use of nonhomogeneous kinetics. These calculations will be discussed later. All other lines were drawn to suit the experimental points. The lines through the hydrogen yields as a function of acid concentration (Figures 4–6) were extrapolated to 1 *M* $(\text{CH}_3)_2\text{CHOH}_2^+$, as it was not possible to attain this concentration in practice. The extrapolation was made assuming that $G(\text{H}_2)$ did not exceed 5.5 at the lower temperatures, as it did not at 140° .

The hydrogen yield decreased with increasing nitrous

oxide concentration at all temperatures. The difference between the yields at -85° , 25° , and 140° decreased with increasing concentration of nitrous oxide (Figure 9).

The hydrogen yield was corrected for the hydrogen from direct radiolysis of the hydrogen chloride in those samples where the acid concentration was high enough to make this significant. The appropriate yield to use in these solutions was not known, so it was assumed that $G(\text{H}_2) = 6.5$ for the direct radiolysis of the acid.¹¹

The solubility of nitrous oxide in 2-propanol is not known. However, the solubility in 2-propanol is not likely to be radically different from that in ethanol, and thus the same values and techniques were used as for ethanol.^{2,12} At -85° , all the nitrous oxide was assumed to be dissolved in the 2-propanol.

A correction was made to the nitrogen yield for the direct radiolysis of nitrous oxide in the high-concentration solutions. It was assumed that the energy absorbed by the nitrous oxide was proportional to its electron fraction in the solution, and that $G(\text{N}_2) = 12.9$ for direct radiolysis.¹³

A study was also made of the effect of a high concentration of both hydrogen chloride and nitrous oxide. The results are shown in Table I.

Knowledge of the dielectric constant is required for the nonhomogeneous kinetics calculations of scavenging and free-ion solvated electron yields. The dielectric constant, ϵ , was measured over the temperature range -85 to $+80^\circ$ (Figure 10). An extrapolation of the curve was used to estimate ϵ at 140° . The values shown were determined at 1000 cps by a previously described method.²

Discussion

Reaction Mechanism. The present results are consistent with but more detailed than those previously published,⁴ and a more complex mechanism is required to explain them.

The yield of hydrogen is quite strongly dose dependent. Doses below 5×10^{17} eV/ml are required in order to be certain of observing initial effects. Sherman⁴ reported $G(\text{H}_2) = 4.0$ at room temperature and a dose of 5.8×10^{18} eV/ml. The present results indicate $G(\text{H}_2) = 3.85$ at this dose and 25° .

The yield of hydrogen increases with increasing temperature between -85 and 140° , and is constant at $G(\text{H}_2) = 5.5$ between 140 and 225° (Figure 3).

At 140° , the addition of as much as 1.4 *M* hydrogen

(10) H. S. Harned and B. B. Owen, "The Physical Chemistry of Electrolytic Solutions," 3rd ed, Reinhold Publishing Corp., New York, N. Y., 1958, pp 755–757.

(11) R. C. Rumfelt and D. A. Armstrong, *J. Phys. Chem.*, **68**, 761 (1964).

(12) International Critical Tables, McGraw-Hill Book Co., New York, N. Y., 1926.

(13) $G(\text{N}_2) = 12.9$ for liquid nitrous oxide at -88° : M. G. Robinson and G. R. Freeman, *J. Phys. Chem.*, in press.

Table I: The Effect of Acid on $G(\text{H}_2)$ and $G(\text{N}_2)$ at 25°

N_2O , M	HCl , M	$(\text{CH}_3)_2\text{CHOH}_2^+$, M	$\frac{[\text{N}_2\text{O}]}{3.5[\text{H}^+] + [\text{N}_2\text{O}]}$	$G(\text{N}_2)_0^a$	$G(\text{N}_2)_{\text{calcd}}^a$	$G(\text{N}_2)_{\text{exptl}}$	$G(\text{H}_2)$
0.16	1.4	0.024	0.66	3.45	2.3	2.7	3.5
0.16	0.14	0.0075	0.86	3.10	2.7	2.7	3.7
0.016	0.14	0.0075	0.38	2.40	0.91	0.5	5.0
0.016	0.0125	0.0023	0.67	2.15	1.4	1.2	4.2

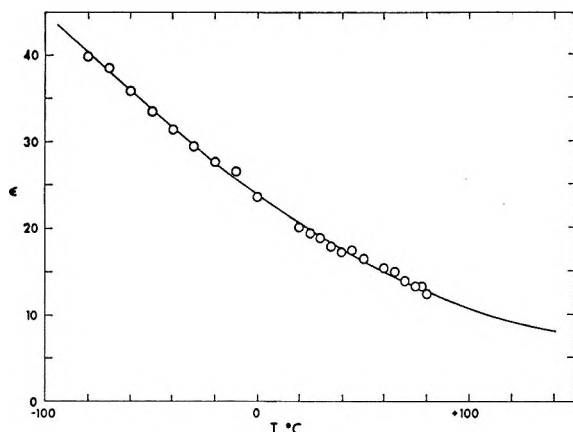
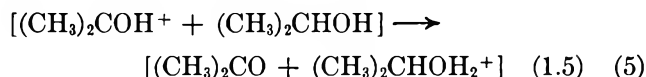
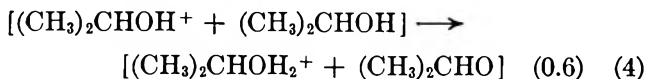
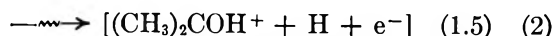
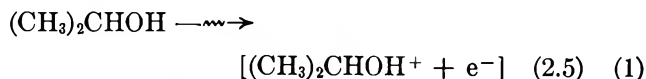
^a See eq. i.

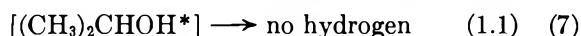
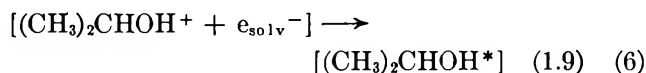
Figure 10. The dielectric constant as a function of temperature.

chloride (Figure 6) has no effect on $G(\text{H}_2)$, which remains at 5.5. However, at 25 and -85° the addition of high concentrations of hydrogen chloride causes $G(\text{H}_2)$ to increase nearly to $G(\text{H}_2) = 5.5$. It thus appears that the temperature-sensitive and acid-sensitive hydrogen precursors are the same. It would also appear that this hydrogen precursor is scavenged by nitrous oxide, as shown by the correspondance between the values of $G(\text{H}_2 + \text{N}_2)$ in the presence of nitrous oxide and $G(\text{H}_2)$ in the presence of acid at -85° (Figure 4). It is suggested that this hydrogen precursor is the solvated electron.

The mechanism which follows is based upon that proposed for ethanol.^{3,14} It is also based on consideration of the fate of ionic species in irradiated liquids, following a previously described approach.^{2,15} The brackets indicate that the species are inside a spur. The yields (G) specified in parentheses after each reaction refer to 25° and are based on the experimental yields and theoretical considerations.

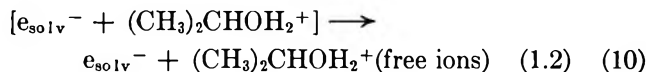
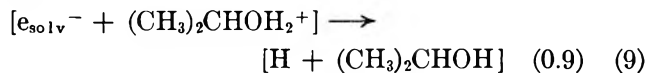


The solvated electrons in the spur appear to be involved in a reaction mechanism that is temperature dependent. This mechanism may be reactions 6–8. Reaction 6 must occur rapidly before reaction 4 takes place, and probably involves the less widely separated



ion–electron pairs.³ Reactions 6–8 could account for the observed temperature dependence of $G(\text{H}_2)$. The balance between reactions 7 and 8 is temperature dependent. At low temperatures reaction 7 is favored, and at 140° and higher temperatures, reaction 8 proceeds to the exclusion of reaction 7.

Those solvated electrons which do not undergo reaction 6 will either undergo reaction 9 or escape the spur to become free ions (reaction 10).



The yield of free-ion solvated electrons was calculated as previously described,² assuming $G(\text{total ionization}) = 4.0$. Those electrons which do not escape the spur undergo geminate neutralization (reactions 6 and 9). The same theory indicates that, at times less than 10^{-10} sec, the majority of the electrons have not yet undergone geminate recombination, and that they are therefore solvated before recombination takes place.

The hydrogen atoms attack the propanol.



The free-ion solvated electrons decay, giving rise to further hydrogen atoms.

(14) J. J. J. Myron and G. R. Freeman, *Can. J. Chem.*, **43**, 381 (1965).(15) G. R. Freeman, *J. Chem. Phys.*, **46**, 2822 (1967).

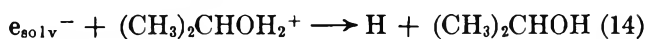


The product acetone is a good electron scavenger, as the addition of 0.68 *M* acetone was found to depress $G(\text{H}_2)$ to 2.0. Reaction 13 is probably responsible for



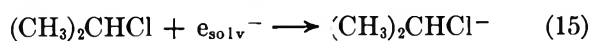
the observed dose dependence of $G(\text{H}_2)$. The experiments, other than the dose study, were conducted at a sufficiently low dose that reaction 13 was negligible.

The presence of acid would cause reaction 14 to be



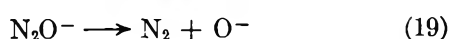
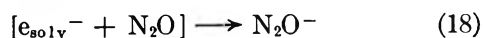
substituted for reaction 12. This would not alter the hydrogen yield, as it would not alter the number of hydrogen atoms formed. A high concentration of acid would also cause reaction 14 to interfere with reaction 6. At lower temperatures, this would cause an increase in $G(\text{H}_2)$ of as much as 1.9 units at -85° . A rise of 1.6 units was observed at -85° , and it is felt that the full increase of 1.9 units was not observed, due to the low degree of dissociation of hydrogen chloride in 2-propanol. Thus 1.4 *M* hydrogen chloride gives only approximately 0.09 *M* $(\text{CH}_3)_2\text{CHOH}_2^+$, a concentration which, by comparison with the calculations for nitrous oxide, would not be expected to completely scavenge the electrons in spurs.

At temperatures above 150° , virtually all the added hydrogen chloride was converted into 2-chloropropane and Figure 7 suggests that this compound scavenges electrons and inhibits hydrogen formation. Reactions 15 and 16 can account for the drop in $G(\text{H}_2)$ seen at high acid concentrations and high temperatures.



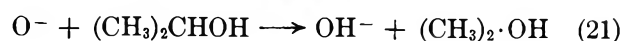
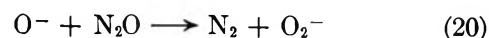
A similar pair of reactions appears to occur in ethanol under the same circumstances.³ It appears that 2-chloropropane is a less efficient electron scavenger than, and is formed at a lower rate than, ethyl chloride in ethanol. Below 150° , there is no evidence that 2-chloropropane interfered with the acid studies in 2-propanol, in contrast to the case of ethanol.³

Nitrous oxide reacts with the free-ion solvated electrons in the bulk of the liquid, and if present in sufficient concentration scavenges electrons within the spurs.

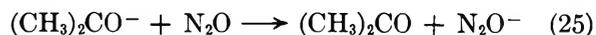
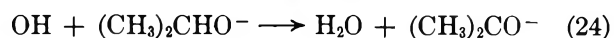
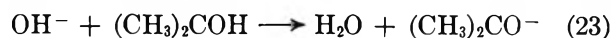


Reactions 17 and 18 increase the gas yield, $G(\text{H}_2 + \text{N}_2)$, only to the extent that they interfere with reaction 6. Such increase in $G(\text{H}_2 + \text{N}_2)$ should not give a yield greater than $G(\text{H}_2 + \text{N}_2) = 5.5$ at high concentrations of nitrous oxide. At -85° , $G(\text{H}_2 + \text{N}_2)$ rises to 5.9

at 1 *M* nitrous oxide, indicating that a small amount of nitrogen is being formed by reactions other than 17 and 18. At 25° , $G(\text{H}_2 + \text{N}_2) = 6.5$ on a gently rising curve at 0.8 *M* nitrous oxide, which was the maximum concentration which could be used. At 140° , $G(\text{H}_2 + \text{N}_2)$ shows no increase up to 2×10^{-3} *M* nitrous oxide, as expected from the previous mechanism, but above this concentration both $G(\text{N}_2)$ and $G(\text{H}_2 + \text{N}_2)$ rise rapidly in a manner which suggests the extensive occurrence of a secondary reaction at above 10^{-2} *M* nitrous oxide. Such a secondary reaction might be reaction 20 in competition with reaction 21 or 22.



However, reaction 20 apparently does not occur in ethanol³ and it probably cannot compete with 21 or 22 in propanol. The large nitrogen yields at high temperature and high nitrous oxide concentration might be due to the occurrence of a short chain reaction similar to that proposed for nitrous oxide-methylcyclohexane vapor mixtures.¹⁶ This would involve reaction 21 or 22, followed by 23 or 24, and then 25. A similar



series of reactions including reaction 25 has been proposed by Sherman¹⁷ to explain a chain reaction found in alkaline solutions of nitrous oxide in 2-propanol. There is a great need for knowledge of values of electron affinities of molecules and radicals, in the vapor phase and in solvents of various polarities, to help to decide the feasibility of reaction such as 25.

Using the values for the rate constants for the reactions $\text{H} + (\text{CH}_3)_2\text{CHOH}$,⁴ and $\text{H} + \text{N}_2\text{O}$,^{5,6} the expected contribution to the nitrogen yield from the reaction of $\text{H} + \text{N}_2\text{O}$ was calculated. This was found to be less than 10^{-2} $G(\text{H})$ under all experimental conditions.

Because of the occurrence of what is most probably a secondary reaction of nitrous oxide, it is necessary to apply a correction to the experimental nitrogen yields in order to obtain a reasonable measure of the number of solvated electrons scavenged. This was done by subtracting from $G(\text{N}_2)$ the difference between the nitrous oxide *vs.* $G(\text{H}_2 + \text{N}_2)$ and the acid *vs.* $G(\text{H}_2)$ curves (Figures 4-6). Since the low dissociation constant of the acid made experiments above 0.03 *M* $(\text{CH}_3)_2\text{CHOH}_2^+$ impractical, the $G(\text{H}_2)$ *vs.* acid curves

(16) W. H. Holtslander and G. R. Freeman, *Can. J. Chem.*, **45**, 1661 (1967).

(17) W. V. Sherman, *J. Phys. Chem.*, **71**, 1695 (1967).

were extrapolated. The assumption was made that at the lower temperature, $G(\text{H}_2)$ did not exceed 5.5, as it did not at 140°.

The presence of a high concentration of both acid and nitrous oxide would cause a competition of reactions 17 and 18 with reactions 9 and 14. This would cause both $G(\text{H}_2)$ and $G(\text{N}_2)$ to be between the values caused by the presence of either solute alone. The value of $k(e_{\text{solv}}^- + \text{H}^+)/k(e_{\text{solv}}^- + \text{N}_2\text{O})$ has been reported to be 3 in water,^{18a} in methanol, it was 7.9 at zero ionic strength and decreased to 1.3 at an ionic strength of 0.1.^{18b} Approximate agreement between calculated and experimental values of nitrogen yields from solutions containing both acid and nitrous oxide was obtained by assuming a value of 3.5 for this ratio in 2-propanol. The nitrogen yields were calculated using eq i and are reported in Table I.

$$G(\text{N}_2) = G(\text{N}_2)_0 \left(\frac{[\text{N}_2\text{O}]}{[\text{N}_2\text{O}] + 3.5[(\text{CH}_3)_2\text{CHOH}_2^+]} \right) \quad (\text{i})$$

$G(\text{N}_2)_0$ is the yield of nitrogen at a nitrous oxide concentration equal to $[\text{N}_2\text{O}] + 3.5[(\text{CH}_3)_2\text{CHOH}_2^+]$, uncorrected for any secondary reaction. The secondary reactions accounted for only 10% or less of the nitrogen formed at these concentrations of nitrous oxide in the absence of acid. Secondary reactions, such as eq 20–25, would also be inhibited by acid, so the error introduced by neglecting them in these calculations is small. Adjustment of the value of the ratio $k(e_{\text{solv}}^- + \text{H}^+)/k(e_{\text{solv}}^- + \text{N}_2\text{O})$ for the different ionic strengths, using a zero ionic-strength value of 14 and eq 1 of ref 19b, gave somewhat closer agreement between the calculated and experimental values of $G(\text{N}_2)$.

Within the uncertainties of the calculations, the results in Table I support the conclusion of Sherman⁴ that acid and nitrous oxide compete for the same species, namely solvated electrons.

The direct competition of acid and nitrous oxide for the same species in 2-propanol is slightly different from the case in ethanol. In ethanol, acid competes for all species with which nitrous oxide reacts, but it also reacts with a species with which nitrous oxide does not react.³

Nonhomogeneous Kinetics Calculations. The yield of free-ion solvated electrons and the scavenging effect of nitrous oxide were computed using nonhomogeneous kinetics, as previously described.^{2,15} A spectrum of $N(y)$ vs. y , the number of ion pairs formed with initial separation distance y , was computed for 2-propanol at each temperature.¹⁵ Data for the density of 2-propanol required for this computation have been measured by Costells and Bowden.¹⁹ The $N(y)$ spectrum permits calculation of ϕ_{fi} , the probability that a given pair of ions will become free ions, and Φ_- , the probability of reaction of an electron with a scavenger. The equations used for these calculations have been

previously described.² The yield of free-ion solvated electrons and the yield of nitrogen may be calculated by use of eq ii and iii.

$$G(e_{\text{solv}}^-)_{fi} = \frac{\Sigma N(y)\phi_{fi}}{\Sigma N(y)} G(\text{total ionization}) \quad (\text{ii})$$

$$G(\text{N}_2) = \frac{\Sigma N(y)\Phi_-}{\Sigma N(y)} G(\text{total ionization}) \quad (\text{iii})$$

The calculation of Φ_- involves an adjustable parameter^{2,15}

$$\beta_- = \frac{1}{u_+ + u_-} \left[\frac{b_- D_-}{\lambda_-^2} + \frac{b_s D_s}{\lambda_s^2} \right] \quad (\text{iv})$$

where D_- and D_s are the diffusion coefficients of the solvated electron and nitrous oxide, respectively, λ_- and λ_s are the respective average diffusive jump distances, b_- and b_s are the number of new neighbors encountered per jump, and u_+ and u_- are the mobilities of the positive and negative ions. Since these quantities are not known, β_- was adjusted to give the best fit with the experimental results.

The dielectric constant, ϵ , is required in order to calculate both ϕ_{fi} and Φ_- .¹⁵ The values of ϵ were taken from Figure 10. The values of β_- used for the present calculations are smaller, by approximately a factor of 4, from those found to be most suitable in a similar calculation for ethanol.³ This difference may be rationalized in terms of differences in the values of the quantities in eq iv. As in ethanol, the most suitable value of β_- varied with temperature ($\beta_- = 2.3 \times 10^{12}$ V/cm² at -85°, 2.4×10^{13} V/cm² at 25°, and 2.9×10^{13} V/cm² at 140°). This variation may be rationalized in terms of the variation of the quantities in eq iv.

In the low-concentration region below 10^{-3} M nitrous oxide, $G(\text{N}_2)$ was computed using eq v. $G(e_{\text{solv}}^-)_{fi}$ was calculated using equation ii and k_{17}/k_{12} was adjusted to

$$G(\text{N}_2) = G(e_{\text{solv}}^-)_{fi} \frac{k_{17}[\text{N}_2\text{O}]}{k_{12}[(\text{CH}_3)_2\text{CHOH}] + k_{17}[\text{N}_2\text{O}]} \quad (\text{v})$$

give the best fit with the experimental results. $G(e_{\text{solv}}^-)_{fi}$ was calculated to be 1.5 at -85°, 1.2 at 25°, and 0.8 at 140°. The values of the rate-constant ratio used were 3×10^5 at -85°, 1.6×10^5 at 25°, and 3×10^5 at 140°. Thus the ratio was essentially independent of the temperature, although the temperature range and hence the variation in viscosity and other factors is very large. The corresponding ratio of rate constants in ethanol was also insensitive to temperature.³ The value of $k_{17} = 7 \times 10^9$ M⁻¹ sec⁻¹ in water at 25°⁶

(18) (a) L. M. Dorfman and M. S. Matheson, *Progr. Reaction Kinetics* 3, 237 (1965); (b) G. V. Buxton, F. S. Dainton, and M. Hamnerli, *Trans. Faraday Soc.*, 63, 1191 (1967).

(19) J. M. Costells and S. T. Bowden, *Rec. Trav. Chim.*, 77, 36 (1958).

suggests that reaction 17 is nearly diffusion controlled. It therefore appears that the effect of temperature on reaction 12 is mainly a viscosity effect or is associated with the breaking of hydrogen bonds in the liquid structure.

Comments on the Yields of Primary Reducing Species

Dorfman, *et al.*,²⁰ have estimated the yield of free ion solvated electrons in 2-propanol to be $G(e_{\text{solv}}^-)_{\text{fi}} = 1.0 \pm 0.3$. The temperature to which this estimate refers was not specified, but is presumably about 25°. This measurement is in reasonably good agreement with the present value of $G(e_{\text{solv}}^-)_{\text{fi}} = 1.2$ at 25°.

The present results agree generally with those of Sherman.⁴ The variation of the yields with temperature, and the nonhomogeneous kinetics treatment of the scavenging of the solvated electrons, allow a fuller understanding of the radiolysis. Sherman⁴ estimated the yield of free-ion solvated electrons to be $G(e_{\text{solv}}^-)_{\text{fi}} = 0.9$ by the use of homogeneous kinetics. The nonhomogeneous kinetics calculations show that there is no sharp division between free-ion solvated electrons and those which undergo geminate neutralization in propanol. Thus it is not valid to use homogeneous kinetics to describe radiolytic scavenging in this system. Under the circumstances, the agreement between Sherman's value of $G(e_{\text{solv}}^-)_{\text{fi}} = 0.9$ and the present value of 1.2 is acceptable. Sherman² also estimated $G(e_{\text{solv}}^-)_{\text{T}} = 2.5$ by the use of homogeneous kinetics. In this case, as would be expected, the agreement with the present value of $G(e_{\text{solv}}^-)_{\text{T}} = 4.0$ is poor.

The present results and mechanism may be compared to those for ethanol.³ The yields in ethanol of $G(\text{H}) = 2.2$, $G(e_{\text{solv}}^-)_{\text{fi}} = 1.5$, and $G(\text{geminate neutralization}) = 2.5$ are similar to the values of $G(\text{H}) = 1.5$, $G(e_{\text{solv}}^-)_{\text{fi}} = 1.2$, and $G(\text{geminate neutralization}) = 2.8$ found for 2-propanol. The somewhat larger value for $G(e_{\text{solv}}^-)_{\text{fi}}$ in ethanol is to be expected in view of the somewhat larger value of ϵ for ethanol (25 compared to 19 for 2-propanol, at 25°). In both alcohols, there are temperature- and acid-sensitive hydrogen precursors. However, in 2-propanol these appear to be the same and to be solvated electrons, whereas in ethanol there are two additional species, one acid sensitive, and the other temperature sensitive. The solvated electrons appear to behave similarly in the two alcohols. The total hydrogen yield in ethanol at high temperatures and in the presence of acid is higher than in 2-propanol, because of the influence of the additional species.

It does not appear that secondary reactions of nitrous oxide occur in ethanol up to 145°. This is in contrast to 2-propanol, where there is a large secondary reaction at this temperature.

Comments on the First-Order Decay of e_{solv}^-

The activation energies for self diffusion in water,

ethanol, and 2-propanol are 4.6, 4.6, and 5.3 kcal/mol, respectively.²¹ Since reaction 17 appears to be nearly diffusion controlled and the ratio k_{17}/k_{12} is temperature independent, the activation energy of reaction 12 is also about 5 kcal/mol. If it is assumed that k_{17} has the same value in 2-propanol as in water, corrected for the difference in viscosity, the value of k_{12} at 25° would appear to be approximately $10^4 M^{-1} \text{sec}^{-1}$. This implies a half-life for the free-ion solvated electron in 2-propanol of approximately 5 μsec . This may be compared with a value of 7 μsec in ethanol at 25°.²

If the decomposition of a solvated electron to form a hydrogen atom and an alkoxide ion is considered to be a unimolecular reaction (reaction 12'), the entropy of



activation may be calculated by use of eq vi.²²

$$\begin{aligned} k_{12'} &= \frac{ekT}{h} e^{\Delta S \mp / R} e^{-E/RT} \\ &= 10^{13} e^{\Delta S \mp / R} e^{-E/RT} \quad (\text{vi}) \end{aligned}$$

Substituting the values of $k_{12'} = 1 \times 10^5 \text{sec}^{-1}$ and $E_{12'} = 5 \text{kcal/mol}$ into eq vi yields $\Delta S_{12'}^\ddagger = -20 \text{cal/deg mol}$. The entropies of activation for the corresponding decompositions of solvated electrons in ethanol and water (assuming the activation energy to be equal to that of diffusion²³) were also calculated and the values are listed in Table II. The entropies are all negative and large. This seems to indicate that a large amount of structural rearrangement occurs in each of the solvents during the reaction.

Table II: Entropies of Activation of the First-Order Decay of Solvated Electrons

Solvent	$k_{12'}$, sec ⁻¹	E , kcal/ mol ²¹	ΔS^\ddagger , cal/deg mol
2-Propanol	1×10^5	5	-20
Ethanol	1×10^{5a}	5	-20
Water	1×10^{3b}	5	-29

^a Calculated from data in ref 2. ^b Calculated from data by E. J. Hart, quoted by J. Rabani in "Solvated Electron," *Advances in Chemistry Series*, No. 50, American Chemical Society, Washington, D. C., 1965, p 251.

(20) M. C. Sauer, S. Arai, and L. M. Dorfman, *J. Chem. Phys.*, **42**, 708 (1965).

(21) H. J. V. Tyrrell, "Diffusion in Heat Flow and Liquids," Butterworth and Co. Ltd., London, 1961, p 155.

(22) A. A. Frost and R. G. Pearson, "Kinetics and Mechanism," John Wiley and Sons, New York, N. Y., 1953, p 98.

(23) (a) It might be better to relate the activation energy of reaction 12' to that of dielectric relaxation. However, the energies of activation of dielectric relaxation in 1-propanol^b and in water^c are also 5 kcal/mol at temperatures in the vicinity of 20°, so the results of the calculations would be the same; (b) S. K. Garg and C. P. Smyth, *J. Phys. Chem.*, **69**, 1294 (1965); (c) calculated from data in NBS Circular 589, p 6.

The Yields of the Primary Reducing Species in the Radiolysis of Liquid Ethanol¹

by J. C. Russell and G. R. Freeman

Chemistry Department, University of Alberta, Edmonton, Alberta, Canada (Received June 26, 1967)

The effects of high temperature, acid, and nitrous oxide on the radiolysis of liquid ethanol have been studied. The results indicate that at all temperatures, reaction between added hydrogen chloride and the ethanol takes place, and the resulting ethyl chloride seriously complicates the study of acid effects. In the light of the new results and better understanding of the effects of acid, previously published values of $G(N_2)$ from ethanolic nitrous oxide solutions have been reinterpreted in terms of the nonhomogeneous kinetics model. The new interpretation gives $G(H) = 2.2$, $G(e_{solv}^-)_{II} = 1.5$, and $G(\text{germinate neutralization}) = 2.5$. The unknown hydrogen precursors X and Y with yields $G(X) = 0.8$ and $G(Y) = 1.1$ were again found (cf. J. C. Russell and G. R. Freeman, *J. Phys. Chem.*, **71**, 755 (1967)).

Introduction

The reactions of the primary reducing species in γ -irradiated alcohols have been investigated and discussed by a number of authors.²⁻⁶ In a recent paper,⁶ the present authors reported the results of an investigation of the effects of temperature, hydrogen chloride, and nitrous oxide on the yields of hydrogen precursors in the γ radiolysis of ethanol. A similar investigation has been made of the yields of hydrogen precursors in the radiolysis of 2-propanol.⁷

A consideration of some of the unusual effects of hydrogen chloride on ethanol radiolysis, together with some inconsistencies between the model indicated by the 2-propanol results⁷ and the previously discussed model for ethanol,⁷ led to a further investigation of ethanol radiolysis. This further work was undertaken in the hope of clarifying the effect of acid on the radiolysis and obtaining better understanding of the yields of hydrogen precursors.

Experimental Section

The experimental methods used were identical with those used in the earlier study of ethanol radiolysis⁶ and in the study of 2-propanol radiolysis.⁷ All irradiations were performed with a ⁶⁰Co γ -ray source to a dose of 1.5×10^{17} eV/ml, on samples which were contained in sealed Pyrex cells.

Samples were raised to temperatures above 25° by two methods. The first, used for the experiments in this paper, unless otherwise noted, involved placing the glass sample cell in liquid ethanol contained in a steel pressure cell which was in turn placed in an electrically heated oven. The oven was heated to the desired temperature, 0.5 hr was allowed to elapse in

order to obtain thermal equilibrium, and the whole assembly was irradiated. This technique is described in more detail elsewhere.⁷ The second method, which has been previously described,⁶ involved placing the sample in a dewar vessel filled with glycerol, which had previously been heated. This technique permits a heating period of as little as 30 sec, followed by immediate irradiation (30 sec). However, it is not suitable for temperatures above 150°, as the glass sample cells will not withstand the vapor pressure of ethanol above this temperature. For example, the vapor pressure of ethanol at 240° is approximately 60 atm.

The analysis for ethyl chloride was performed by vapor-phase chromatography, using a 1,2,3-tris-2-cyanoethoxy propane on Chromosorb-W column. Helium carrier gas and a thermal conductivity detector were used.

Results

The yield of hydrogen from pure ethanol as a function of temperature is shown in Figure 1A. The results of previous work up to 150°⁶ are confirmed and extended to just above the critical temperature of ethanol ($T_c = 243^\circ$). The hydrogen yield is independent of temperature between -110 and 25°: $G(H_2) = 5.1$. Between

(1) This work received financial support from the National Research Council of Canada.

(2) G. E. Adams and R. D. Sedgwick, *Trans. Faraday Soc.*, **60**, 865 (1964).

(3) J. J. Myron and G. R. Freeman, *Can. J. Chem.*, **43**, 381 (1965).

(4) E. Hayon and M. Moreau, *J. Phys. Chem.*, **69**, 4053 (1965).

(5) W. V. Sherman, *ibid.*, **70**, 667 (1966).

(6) J. C. Russell and G. R. Freeman, *ibid.*, **71**, 755 (1967).

(7) J. C. Russell and G. R. Freeman, *ibid.*, **72**, 808 (1967).

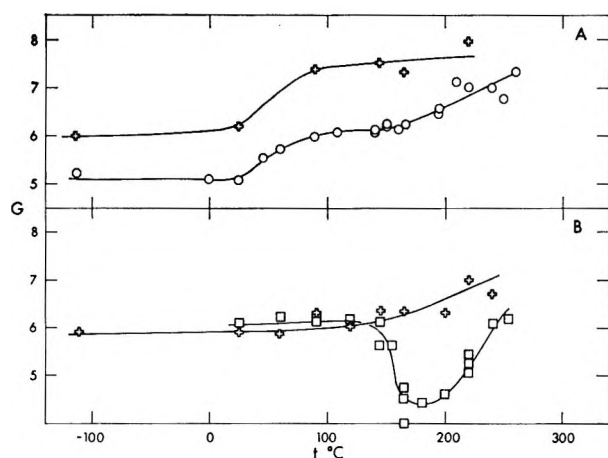


Figure 1. (A) The yield of hydrogen from pure ethanol, and of hydrogen plus nitrogen from 0.1 *M* nitrous oxide in ethanol, as a function of temperature: ○, $G(\text{H}_2)$; +, $G(\text{H}_2 + \text{N}_2)$. (B) The yield of hydrogen from ethanolic solutions of hydrogen chloride as a function of temperature: +, $3 \times 10^{-4} M$; □, 1.4 *M*.

25 and 100°, $G(\text{H}_2)$ increases, then becomes virtually independent of temperature up to 160°: $G(\text{H}_2) = 6.2$. At still higher temperatures, the hydrogen yield increases somewhat ($G(\text{H}_2) = 7.3$ at 250°), but there is no sudden increase at the critical temperature.

Values of $G(\text{H}_2 + \text{N}_2)$ from samples containing 0.1 *M* nitrous oxide are also shown in Figure 1A. The temperature dependence is similar to that of the hydrogen yield, with the possible exception that $G(\text{H}_2 + \text{N}_2)$ appears to increase only slightly between 140 and 220°.

In Figure 1B the hydrogen yields from ethanol containing hydrogen chloride (3×10^{-4} and 1.4 *M*) are shown as functions of temperature. The low concentration of hydrogen chloride caused an increase of 0.8 unit in $G(\text{H}_2)$ at 25°, but no increase was observed at temperatures greater than about 140°. The high concentration of hydrogen chloride caused a slightly greater increase in $G(\text{H}_2)$ than did the low concentration at 25°, but at 145° the yield was again the same as in pure ethanol. At temperatures greater than 145°, the hydrogen yield was actually decreased by the addition of 1.4 *M* hydrogen chloride; the decrease was 2.0 *G* units at 200°.

The effects of hydrogen chloride and sulfuric acid on the hydrogen yield at 25° are shown in Figure 2A. The observed effect of hydrogen chloride confirms the results of Fletcher.⁸ The effects of hydrogen chloride at 90, 145, 165, and 220° are shown in Figures 2B and 2C. At 25°, addition of $5 \times 10^{-6} M$ hydrogen chloride causes a rise in $G(\text{H}_2)$ of 0.8 unit. This effect has been ascribed to a species X.⁶ Higher concentrations of hydrogen chloride up to 1.4 *M* cause only a small increase in $G(\text{H}_2)$. However, addition of 1.4 *M* sulfuric acid causes a further increase in $G(\text{H}_2)$ of 0.6 unit. At higher temperatures, the effect of hydrogen chloride was found to decrease, becoming nil at 145°.

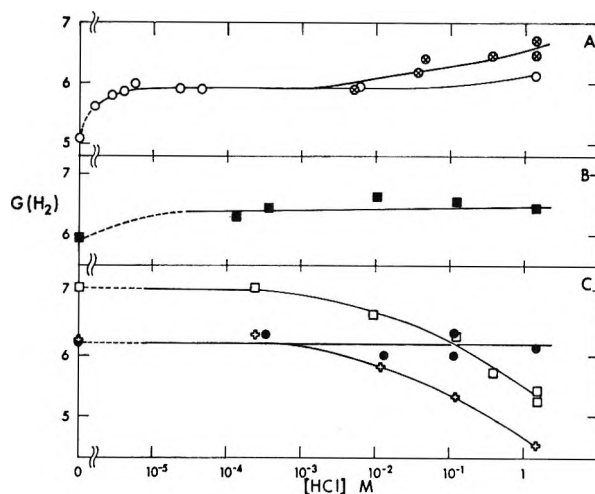


Figure 2. The yield of hydrogen as a function of acid concentration: A (25°): ○, HCl; □, H₂SO₄; B (90°); and C: ●, 145°; +, 165°; and □, 220°.

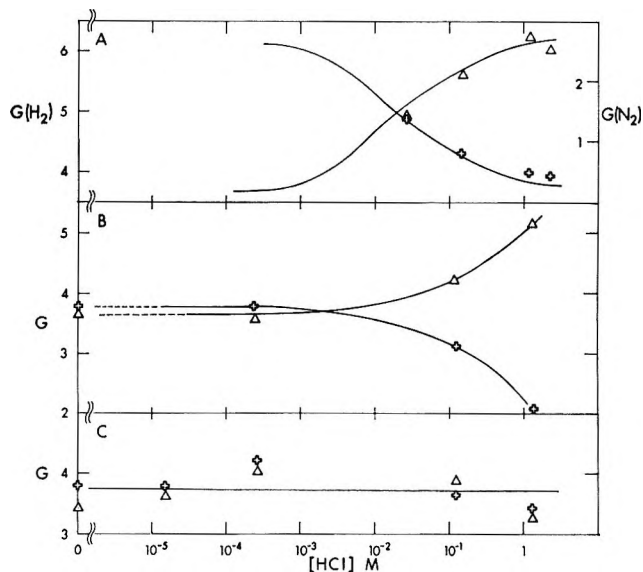


Figure 3. The yields of hydrogen and nitrogen from nitrous oxide solutions as function of the concentration of hydrogen chloride (Δ, H₂; +, N₂): A (25°, $4 \times 10^{-2} M$ N₂O; B (145°, $9.5 \times 10^{-2} M$ N₂O; and C (165°, $9 \times 10^{-2} M$ N₂O).

Above this temperature, a high concentration of hydrogen chloride caused a large decrease in $G(\text{H}_2)$, while a low concentration had no effect.

Competition studies between hydrogen chloride and nitrous oxide were performed in order to attempt to distinguish the effect of temperature on the different hydrogen precursors. The results at 25, 145, and 165° are shown in Figure 3. The data in Figure 3A (25°) were taken from a previous study,⁶ and the lines for $G(\text{N}_2)$ and $G(\text{H}_2)$ were calculated assuming $k(e_{\text{sol}^-} + \text{C}_2\text{H}_5\text{OH}_2^+)/k(e_{\text{sol}^-} + \text{N}_2\text{O}) = 2$, as was previously

(8) J. W. Fletcher, Ph.D. Thesis, University of Alberta, Edmonton, Alberta, Canada, 1967.

discussed.⁶ In Figures 3B and 3C, the lines were drawn to suit the experimental points. The competition studies between hydrogen chloride and nitrous oxide indicate that at 25° they compete for the same species, with the exception that nitrous oxide does not react with species X. At 165°, however, hydrogen chloride does not compete with nitrous oxide under our experimental conditions.

These unusual effects led to a search for ethyl chloride in hydrogen chloride containing samples, as it may be formed through a known reaction.⁹ In 1.4 M blank samples, treated and warmed in the same manner as irradiated samples, quantitative conversion of the acid to ethyl chloride was found at 165 and 230°. At 135°, 23% conversion was found, and even at 25° with no warming, 1.5×10^{-2} M ethyl chloride was found.

In the previous study of ethanol radiolysis,⁶ it was found that 10^{-4} M hydrogen chloride raised $G(\text{H}_2)$ by approximately 0.6 unit, even at 150°. Using the present technique, where the samples were heated in a pressure cell for 0.5 hr, this effect was not found. Repeat experiments, using the rapid heating technique previously used, gave results in agreement with the earlier results. This confirms that the formation of ethyl chloride from hydrogen chloride and ethanol inhibits the formation of hydrogen during radiolysis.

Discussion

The results are consistent with those reported earlier. Although the new information does not permit identification of species X and Y, it does clarify a number of points. In the light of these results, and those for 2-propanol,⁷ the previously obtained nitrogen yields⁶ require reinterpretation.

The hydrogen yield in pure ethanol increases with increasing temperature in the range 25–140°. This has been ascribed to the decomposition of an unknown species Y.⁶ At temperatures from 160 to 250°, a further increase in $G(\text{H}_2)$ of over 1 unit occurs. This is felt to have a different origin from the increase at lower temperatures.

In the present experiments, a low (4×10^{-4} M) concentration of hydrogen chloride raised $G(\text{H}_2)$ at 25° to 5.9, in agreement with the earlier results.⁶ However, at higher temperatures this increase disappeared (Figure 2). $G(\text{H}_2)$ did not show any temperature dependence, up to 150°, at this acid concentration. This is in disagreement with the previous results, where $G(\text{H}_2)$ increased between 25 and 150° in acidic ethanol.⁶ High concentrations of acid (1.4 M) at temperatures above 145° caused a decrease in $G(\text{H}_2)$ of as much as 2.0 units (Figure 2C).

The measurements of the ethyl chloride concentration in hydrogen chloride containing samples indicates that at 165° and higher temperatures, virtually all hydrogen chloride in the samples was converted into ethyl chloride

during the period of heating. The large concentration of ethyl chloride so produced would be expected to scavenge electrons and so reduce $G(\text{H}_2)$. At 145°, only about one-third of the added hydrogen chloride would have been converted into ethyl chloride, and thus one would expect a competition between $\text{C}_2\text{H}_5\text{OH}_2^+$ and ethyl chloride for the electrons, with one reaction tending to increase $G(\text{H}_2)$ and the other to decrease it. The independence of $G(\text{H}_2)$ on added hydrogen chloride at this temperature implies a balance between the two electron-scavenging reactions. Since this was in disagreement with the earlier results, the experiments were repeated using the previous technique with very rapid heating. The hydrogen yields then duplicated the earlier results. Thus, as would be expected, the length of time the samples were heated and the temperature influence the amount of ethyl chloride formed and thus $G(\text{H}_2)$.

Mineral acids scavenge electrons to form hydrogen, whereas nitrous oxide scavenges electrons to form nitrogen. The total gas-product yields should be nearly the same, whether acid or nitrous oxide is used as a scavenger. The fact that large concentrations of nitrous oxide caused the total gas-product yield to increase, whereas a large concentration of hydrogen chloride did not,⁶ led to the postulation of a secondary reaction between O^- and nitrous oxide to form nitrogen. The present results with sulfuric acid solutions show that high concentrations of acid do increase the total gas yield (Figure 2A) if an electron scavenger such as ethyl chloride, that does not form gaseous products, is absent from the solution. Ethyl sulfate is evidently a poor electron scavenger. The secondary reaction between O^- and nitrous oxide is not required to explain the present results; in fact, comparison of the results in the 2-propanol⁷ and ethanol systems at high temperature indicates that a secondary reaction with nitrous oxide does not occur in the ethanol system.

The foregoing considerations indicate that the corrections applied to the measured values of $G(\text{N}_2)$ in the earlier work⁶ were incorrect and the results require reinterpretation. The original uncorrected results for $G(\text{N}_2)$ as a function of nitrous oxide concentration are shown in Figures 4–7. The lines in Figures 4–7 were computed by the method discussed previously,⁶ but using slightly different values for the parameters. The calculations will be discussed later.

The mechanism which follows is essentially that previously presented,⁶ modified in some respects in view of the present results. It is based largely upon the same considerations as previously, including the theoretical treatment of the fate of ionic species in irradiated liquids.^{6,10} The specified yields (G) in

(9) C. R. Noller, "Chemistry of Organic Compounds," W. B. Saunders Co., Philadelphia, Pa., 1951.

(10) G. R. Freeman, *J. Chem. Phys.*, **46**, 2322 (1967).

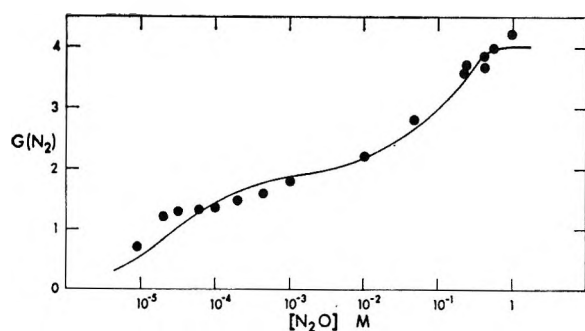


Figure 4. The nitrogen yields from nitrous oxide solutions at -112° . The solid line is calculated.

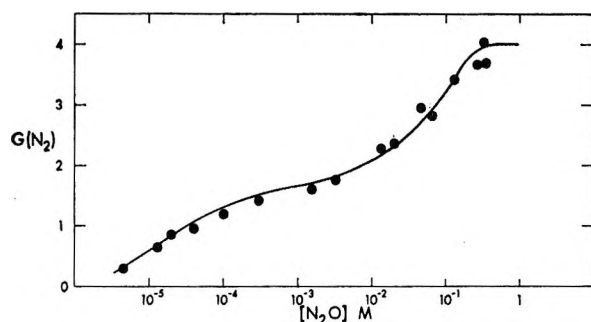


Figure 5. The nitrogen yields from nitrous oxide solutions at 25° . The solid line is calculated.

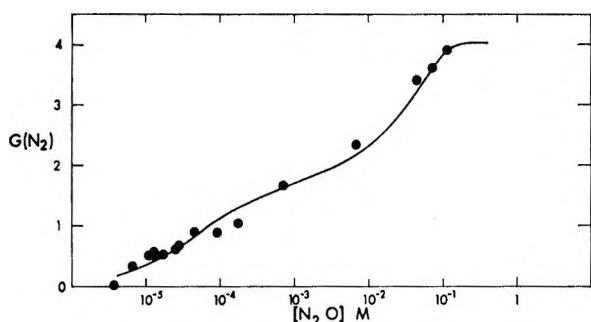


Figure 6. The nitrogen yields from nitrous oxide solutions at 90° . The solid line is calculated.

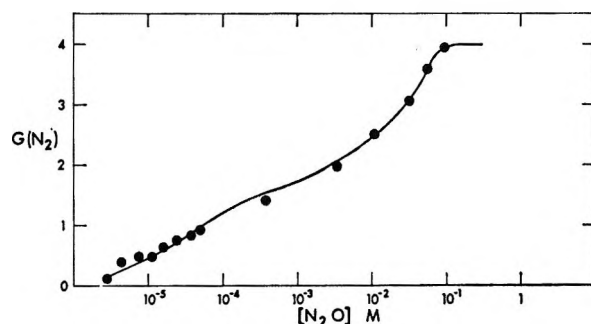
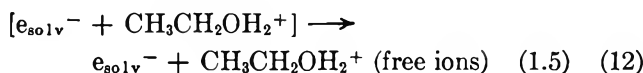
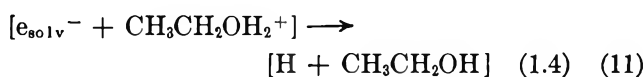
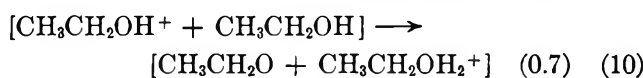
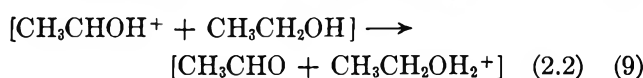
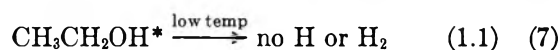
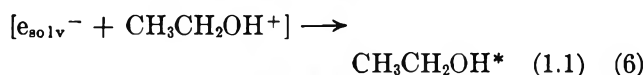
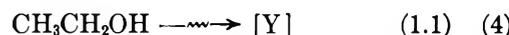
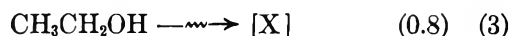


Figure 7. The nitrogen yields from nitrous oxide solutions at 145° . The solid line is calculated.

parentheses after the reactions refer to 25° , are based upon the experimental yields together with theoretical considerations, and have estimated uncertainties of 0.3

unit. The square brackets indicate that the species are inside a spur.

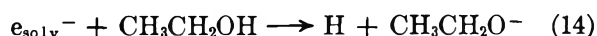


Reaction 2 involves a more energetic precursor than does reaction 1. Reaction 6 represents the rapid recombination of the less separated ion-electron pairs, which may result mainly from reaction 1 rather than from the higher-energy process in reaction 2.

The hydrogen atoms attack the ethanol.



The free-ion solvated electrons decay giving rise to further hydrogen atoms.



The addition of a low concentration of acid would cause reaction 14 to be replaced by reaction 15. However, this would not alter the observed yield of hydro-



gen. Since a small amount of acid does cause the hydrogen yield to increase, a reactive species has been postulated to undergo reactions 16 and 17.⁶

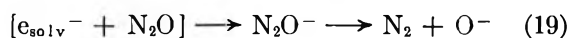
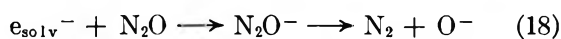


It has been shown⁶ that neither high temperatures nor high concentrations of nitrous oxide interfere with reaction 17. Because of this, X cannot be solvated electrons. At the low doses used, a very low concentration of acid ($5 \times 10^{-6} \text{ M}$) scavenges X completely.

This implies that even if the rate constant for reaction 17 is very large, X has a long lifetime, being of the order of 5×10^{-5} sec if $k_{17} = 10^{10} M^{-1} \text{sec}^{-1}$.

It appears that a high concentration of acid causes reaction 11 to interfere with reaction 6. This causes an increase in $G(\text{H}_2)$, in addition to that caused by reaction 17, as observed with the sulfuric acid solutions (Figure 2A).

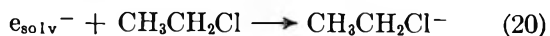
Nitrous oxide will react with the free-ion solvated electrons in the bulk of the liquid, and if present in sufficient concentration will scavenge electrons within the spurs. Reaction 18 should not increase $G(\text{H}_2 + \text{N}_2)$. However, at low temperatures reaction 19 will



cause $G(\text{H}_2 + \text{N}_2)$ to increase to the extent that it interferes with reaction 6.

In the presence of a high concentration of nitrous oxide and a low concentration of acid, $G(\text{H}_2 + \text{N}_2)$ should reflect the occurrence of both reactions 17 and 19. Thus $G(\text{H}_2 + \text{N}_2)$ should be above 5.9. Under these conditions $G(\text{H}_2 + \text{N}_2) = 7.2$ was found.⁶ The addition of a high concentration of sulfuric acid should cause $G(\text{H}_2)$ to increase to a similar value. However, acid should cause an effect only to the extent to which it dissociates into ions in the ethanol. The dissociation constant for sulfuric acid in ethanol is not known, but in water the constant is roughly one-tenth as large as that of hydrogen chloride.¹¹ In ethanol $K_{\text{diss}} = 0.015$ for hydrogen chloride.¹² On this basis, it is assumed that $K_{\text{diss}} \simeq 0.0012$ for the first ionization constant of sulfuric acid in ethanol. Thus 1.4 M sulfuric acid would give a concentration of $\text{CH}_3\text{CH}_2\text{OH}_2^+$ equal to $5 \times 10^{-2} M$. In the presence of $10^{-4} M$ hydrogen chloride and $5 \times 10^{-2} M$ nitrous oxide, $G(\text{H}_2 + \text{N}_2) = 6.8$. This compares favorably with $G(\text{H}_2) = 6.6$ found in the presence of 1.4 M sulfuric acid. The scavenging curves of nitrous oxide and acid therefore appear to be very similar, aside from the influence of species X.

The addition of a high concentration of hydrogen chloride appears to cause a small increase in $G(\text{H}_2)$ at room temperature. It is felt that this increase is not as large as would be expected because of interference by ethyl chloride through reaction 20. Reactions 20 and 21 serve to decrease $G(\text{H}_2)$ by removing solvated



electrons without production of hydrogen atoms. At 90°, where the concentration of ethyl chloride will be moderately high, the increase in $G(\text{H}_2)$ produced by hydrogen chloride is reduced to approximately 0.5 unit. At 145°, where the ethyl chloride concentration was estimated to be roughly one-third of the originally

added acid under the conditions of the experiment, there was no effect of added hydrogen chloride at any concentration. If the samples were warmed very rapidly, using the earlier technique so as to minimize ethyl chloride formation, an increase of $G(\text{H}_2) = 0.6$ was found, in agreement with the earlier results. This confirms that $G(\text{X})$ is not temperature sensitive. At 165° and higher temperatures, all of the added hydrogen chloride was converted into ethyl chloride. This caused $G(\text{H}_2)$ to fall by as much as 2.0 units through the influence of reactions 20 and 21. The curves for $G(\text{H}_2)$ vs. added hydrogen chloride at 165 and 220° are superimposable by a vertical shift. The influence of reaction 8 caused the over-all hydrogen yield to be greater at 220°, and the drop in $G(\text{H}_2)$ caused by the addition of large amounts of hydrogen chloride is due to scavenging of electrons by the resultant ethyl chloride (reaction 20).

The data in Figure 3A indicate, as previously discussed,⁶ that acid competes for all species with which nitrous oxide reacts. Figure 3B, which shows the results of a similar competition study at 145°, indicates that hydrogen chloride still competes for the same species as nitrous oxide, but that it is less efficient than at 25°. This is to be expected, as approximately one-third of the acid would have been converted into ethyl chloride, which would not tend to raise $G(\text{H}_2)$ at the expense of $G(\text{N}_2)$, but would rather be expected to decrease both. At 165°, where all the acid was converted into ethyl chloride, a competition should occur between ethyl chloride and nitrous oxide for the solvated electrons. This would be expected to reduce $G(\text{N}_2)$ at high concentrations of added acid. No such effect occurs and $G(\text{N}_2)$ was found to be independent of the added acid. This suggests that a reaction such as reaction 22 may occur in competition with reaction 21.



Such reactions involving electron transfer from one electron scavenger to another have been suggested to take place in vapor-phase methylcyclohexane¹³ and in aqueous solutions.^{13,14}

An alternate explanation for ethyl chloride not depressing $G(\text{N}_2)$ might be that $k(e_{\text{solv}}^- + \text{C}_2\text{H}_5\text{Cl}) \ll k(e_{\text{solv}}^- + \text{N}_2\text{O})$.

The temperature variation of $G(\text{H}_2)$ (Figure 1A) indicates that there is a species, which has been represented as Y, which is temperature sensitive. This has been previously discussed,⁶ and it has been shown that

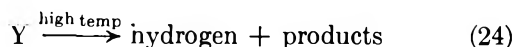
(11) "Handbook of Chemistry and Physics," 38th ed, Chemical Rubber Publishing Company, Cleveland, Ohio, 1956.

(12) I. I. Bezman and F. H. Nerhock, *J. Am. Chem. Soc.*, **67**, 1330 (1945).

(13) W. J. Holtzlander and G. R. Freeman, *Chem. Commun.*, 205 (1967).

(14) S. R. Logan and P. B. Wilmot, *ibid.*, 558 (1966).

it must undergo two different reactions, 23 and 24. At very high temperatures (above 150°) it appears that



some further source of hydrogen comes into play. Reactions 7 and 8 could account for this rise in $G(\text{H}_2)$. An implication of reactions 6–8 would be that at very high temperatures a high concentration of nitrous oxide would not cause $G(\text{H}_2 + \text{N}_2)$ to exceed $G(\text{H}_2)$ for pure ethanol. It was not possible to check this because experimental difficulties became very great above the critical temperature of ethanol.

The calculated values of $G(\text{N}_2)$ in Figures 4–7 were computed in the same manner as previously reported,⁶ with the omission of the correction for the assumed reaction of O^- with nitrous oxide. It now appears that this reaction does not occur in ethanol. A brief summary of the method of calculation also appears in ref 7. The calculations were performed assuming $G(\text{total ionization}) = 4.0$, and the adjustable parameter $\beta_- = 9.6 \times 10^{13} \text{ V/cm}^2$ at 25°. This value of β_- may be rationalized in terms of the following quantities, which are defined in the adjacent paper:⁷ $u_+ + u_- = 3 \times 10^{-3} \text{ cm}^2/\text{V sec}$, $b_- = 4$, $D_- = 3 \times 10^{-5} \text{ cm}^2/\text{sec}$, $\lambda_-^2 = 7 \times 10^{-16} \text{ cm}^2$, $r_0 = 1.0 \times 10^{-7} \text{ cm}$, $b_s = 4$, $D_s = 2 \times 10^{-5} \text{ cm}^2/\text{sec}$, and $\lambda_s^2 = 7 \times 10^{-16} \text{ cm}^2$. These quantities, especially D , will change with temperature. This variation is not precisely known, and the calculation is approximate. The most suitable value of β_- varied with temperature: $\beta_- = 3.2 \times 10^{13} \text{ V/cm}^2$ at -112° , $9.6 \times 10^{13} \text{ V/cm}^2$ at 25° ; $6.7 \times 10^{14} \text{ V/cm}^2$ at 90° , and $6.2 \times 10^{14} \text{ V/cm}^2$ at 145° . The best-fit values of k_{18}/k_{14} were 5.6×10^5 at -112° , 1.0×10^6 at 25° , 5.0×10^5 at 90° , and 5.4×10^5 at 145° . As was discussed previously,⁶ this ratio is essentially insensitive to temperature.

The calculated nitrogen yields agree very well with the experimental results. The agreement is better than the previous calculation to fit the results after application of the correction.⁶ The only parameters whose values were significantly altered from the previous calculation were $G(\text{total ionization}) = 4.0$ and $\beta_- = 9.6 \times 10^{13}$ at 25° , compared to the earlier values of 3.1 and 2.4×10^{13} , respectively. The larger values are consistent with those required to fit the nitrous oxide scavenging results in 2-propanol.⁷ The values of k_{18}/k_{14} are not significantly changed and are similar to

the equivalent values used in the 2-propanol calculations.

The values of $G(\text{free ion})$ determined in the calculations have been proportionately raised by the increased value of $G(\text{total ionization})$. The calculated values obtained were $G(\text{free ion}) = 1.9$ at -112° , 1.5 at 25° , 1.5 at 90° , and 1.6 at 145° . These are slightly larger than the corresponding values in 2-propanol.⁷ This is to be expected because of the higher dielectric constant of ethanol.

Other estimates of $G(e_{\text{soliv}}^-)_{\text{fi}}$ at about 25° have been made and these vary in the range $G(e_{\text{soliv}}^-)_{\text{fi}} = 1.0 \pm 0.3$.^{3,4,15} The uncertainties in all of the measurements and interpretations are so large that the lack of close agreement between the various estimates is not surprising.

The degree of reaction of hydrogen chloride with ethanol found and the very marked effects that this has on the radiolysis indicate that great caution must be exercised in such experiments. The characteristics of alcohols are evidently such as to make studies of the effect of acid on the radiolysis very difficult and virtually impossible at very high temperatures. It appears that ethyl sulfate is a less efficient electron scavenger than is ethyl chloride, and thus that sulfuric acid is a preferable acid to use. However, the known rapid rate of reaction with the alcohol⁹ changes the acid concentration from that added.

Summary

(1) The reactions of acids with alcohols complicate the study of the effects of acids on the radiolysis of alcohols.

(2) In the γ radiolysis of liquid ethanol at 25° , the following yields were estimated: $G(\text{total ionization}) = 4.0$, $G(e_{\text{soliv}}^-)_{\text{fi}} = 1.5$, $G(\text{H}) = 2.2$, $G(\text{X}) = 0.8$, and $G(\text{Y}) = 1.1$. $G(\text{H})$ represents the yield of reaction 2. Species X is sensitive to low concentrations of acid, but not to temperature in the range $25\text{--}100^\circ$, whereas the opposite is true for species Y. At very high temperatures, $>160^\circ$, an additional source of hydrogen becomes evident.

(3) Acid reacts with e_{soliv}^- and with X. Nitrous oxide reacts only with e_{sciv}^- .

(4) The nonhomogeneous kinetics model of charge scavenging fits the results. Two adjustable parameters are used in the model, and these were chosen to be $G(\text{total ionization})$ and β_- .

(15) I. A. Taub, D. A. Harter, M. C. Sauer, and L. M. Dorfman, *J. Chem. Phys.*, **41**, 979 (1964).

Proton Magnetic Resonance Studies of Mixed Aluminum Alkyls. I.

Aluminum Trialkyls¹

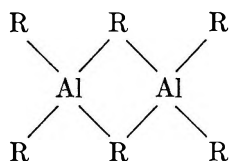
by Osamu Yamamoto and Kikuko Hayamizu

Government Chemical Industrial Research Institute, Tokyo, Japan (Received June 26, 1967)

The systems $\text{AlMe}_3\text{-AlEt}_3$, $\text{AlMe}_2\text{-Al}(n\text{-Pr})_2$, and $\text{AlMe}_2\text{-Al}(i\text{-Bu})_2$ were studied by means of pmr spectroscopy at room temperature as well as at low temperature. A bridge-bonding factor, defined as a measure of the tendency of an alkyl group to occupy the bridge position in the mixed dimer formed in the aluminum trialkyl mixture, was experimentally determined for ethyl, *n*-propyl, and isobutyl groups in the trialkylaluminum dimers as compared with methyl group and was found to be $1/6$, $1/7$, and $1/17$, respectively. It depends upon the bulkiness of the alkyl group. In terms of the bridge-bonding factor, the chemical shifts of the α -methyl and the α -methylene groups of the mixed dimers in the mixtures were calculated and compared with the experimental values. The equilibrium between the various dimers in each system was also discussed.

Introduction

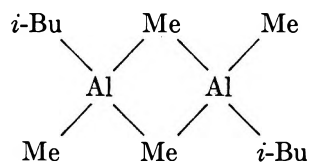
It is well known that the lower members of aluminum tri-*n*-alkyls associate into dimers with an alkyl bridge structure such as²



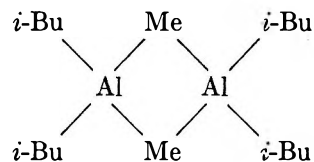
In the pmr spectra of these compounds, for example trimethyl aluminum, although there are two non-equivalent methyl groups in this structure, only one methyl signal is observed at room temperature. At sufficiently low temperature, however, two distinct signals are obtained, which may be assigned to the terminal and the bridge methyl groups, respectively. This fact was first observed by Muller and Pritchard³ and was explained as a rapid exchange between the terminal and the bridge methyl groups. It has been shown also that the same is true for other aluminum alkyls.^{4,5}

On the other hand, the stability of aluminum trialkyl dimers would be different from one to the other, and it is expected from the results of the vapor-pressure studies by Laubengayer and Gilliam⁶ that trimethylaluminum, the lowest member of aluminum trialkyls, is the most stable one.

Hoffmann⁷ found out from a cryoscopic study that a mixture of triisobutylaluminum and trimethylaluminum forms mixed dimer, such as



and



This is very interesting because, in general, branched aluminum alkyls have little tendency to form dimers.⁷ Hoffmann further studied the system by means of nmr spectroscopy⁸ and reported that the resultant mixed aluminum trialkyls are strongly associated by virtue of their methyl groups and the ratio of the bridge and the terminal methyl groups is dependent on the total concentration of methyl groups. He suggested from his nmr studies at room temperature that, in contrast to his earlier cryoscopic investigation and in spite of the rather weak bonding across an isobutyl group, a system of dimers with mixed-bonded ring, $>\text{Al} < \begin{smallmatrix} \text{Me} \\ i\text{-Bu} \end{smallmatrix} > \text{Al} <$, is energetically favored over a mixture of homogeneously methyl-bonded dimers and unaffected triisobutylaluminum. More recently, Ramey and his coworkers⁵ have studied the same system and added some discussion to Hoffmann's results about the exchange mechanism.

In the present work, to obtain more detailed infor-

- (1) A part of this work was presented at the International Symposium on Nuclear Magnetic Resonance, Tokyo, Japan, Sept 1965.
- (2) P. H. Lewis and R. E. Rundle, *J. Chem. Phys.*, **21**, 986 (1953).
- (3) N. Muller and D. E. Pritchard, *J. Am. Chem. Soc.*, **82**, 248 (1960).
- (4) O. Yamamoto, *Bull. Chem. Soc. Japan*, **37**, 1125 (1964).
- (5) K. C. Ramey, J. F. O'Brien, I. Hasegawa, and A. E. Borchert, *J. Phys. Chem.*, **69**, 3418 (1965).
- (6) A. W. Laubengayer and W. F. Gilliam, *J. Am. Chem. Soc.*, **63**, 477 (1941).
- (7) E. G. Hoffmann, *Ann. Chem.*, **629**, 104 (1960).
- (8) E. G. Hoffmann, *Trans. Faraday Soc.*, **58**, 642 (1962).

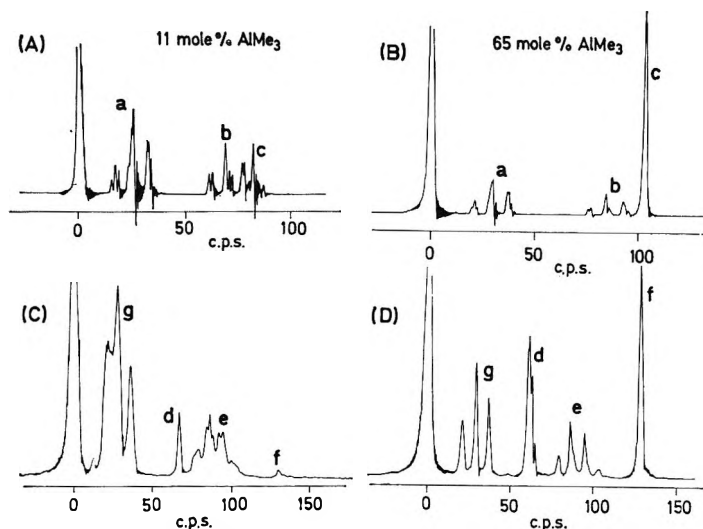


Figure 1. Nmr spectra of the mixtures of trimethylaluminum and triethylaluminum in cyclopentane at 60 Mcps. The chemical shifts are referred to the solvent, and a = β -CH₃, b = α -CH₂, c = α -CH₃, d = bridge-CH₃, e = terminal-CH₂, f = terminal-CH₃, and g = mixture of β -CH₃ and bridge-CH₂ signals. A and B are the room-temperature spectra of the mixtures in which mole ratios of AlMe₃:AlEt₃ are 11:89 and 65:35, respectively; C and D are the low-temperature spectra at about -75° corresponding to A and B, respectively.

mation about the trialkylaluminum mixtures, the systems Al(CH₃)₃-Al(C₂H₅)₃, Al(CH₃)₃-Al(*n*-C₃H₇)₃, and Al(CH₃)₃-Al(*i*-C₄H₉)₃ were studied by means of nmr spectroscopy, and the tendency for the alkyl groups in the aluminum compounds to form dimers was discussed. While in the former two systems, each of the components is a dimer in their pure state, in the latter system, one component is a dimer and the other a monomer in the isolated state.

Experimental Section

Trimethylaluminum and triethylaluminum were prepared by Pitzer and Gutowsky's method⁹ and Grosse and Mavity's method,¹⁰ respectively. Tri-*n*-propylaluminum and triisobutylaluminum were obtained from the Ethyl Corp., N. Y. Cyclopentane was used as a solvent. The solvent was dehydrated and purified by the conventional methods. Since aluminum alkyls are in general very reactive with air and moisture, the purified aluminum alkyls were transferred into cylindrical sample tubes, one after another, in an appropriate proportion to make a desired mixture in a high-vacuum line, a suitable amount of solvent was directly distilled therein, and then the tube was sealed off.

The nmr spectra were obtained by means of a Varian Associates DP-60 spectrometer operating at 60 Mcps with or without variable temperature accessories; the usual side-band technique was employed. The room-temperature spectra were obtained at $30 \pm 1^\circ$, and the low-temperature spectra were measured at a temperature between -78 and -73° .

The relative concentration of two aluminum alkyls in a given sample of mixture was determined by means of a Varian V-3521 nmr integrator. The total con-

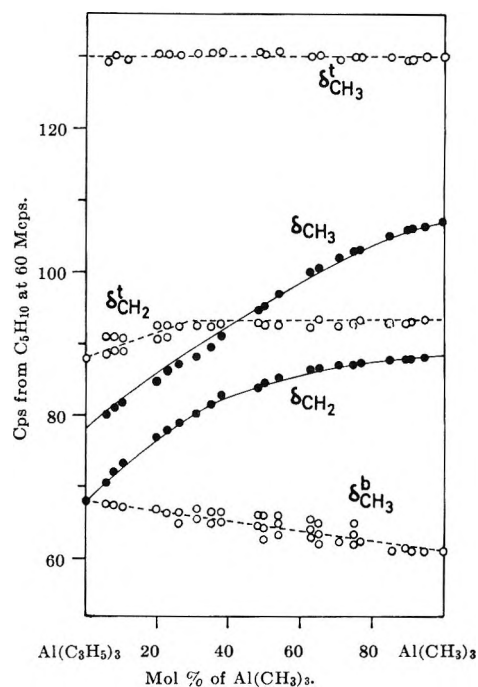


Figure 2. Chemical shifts of the signals in trimethylaluminum-triethylaluminum system at 60 Mcps: ●, signals at 30° ; ○, signals at about -75° ; —, calculated curves for δ CH₃ and δ CH₂; - - -, curves for δ CH₃^t, δ CH₃^b, and δ CH₂^t used in the calculation as corrections for $\Delta(n)$ CH₃ and $\Delta(n)$ CH₂.

centration of aluminum compounds in the samples was not so critically adjusted, provided that the samples

(9) K. S. Pitzer and H. S. Gutowsky, *J. Am. Chem. Soc.*, **68**, 2205 (1946).

(10) A. von Grosse and J. M. Mavity, *J. Org. Chem.*, **5**, 106 (1940).

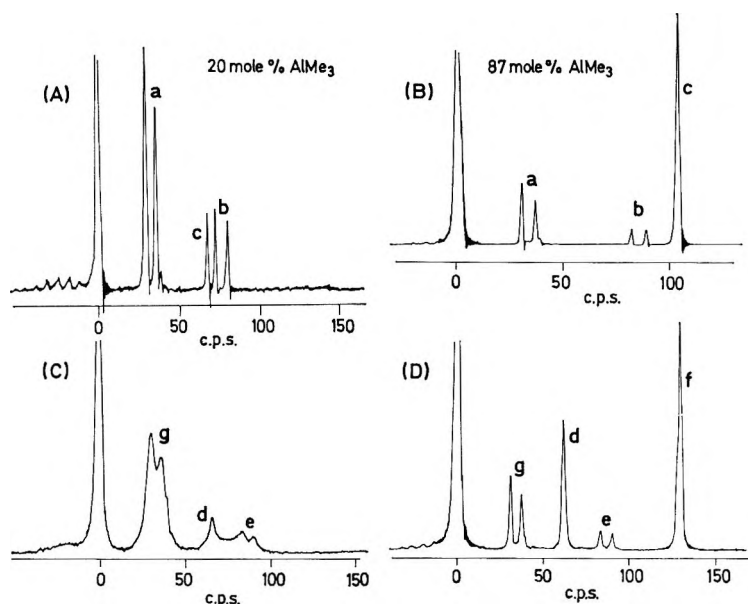


Figure 3. Nmr spectra of the mixtures of trimethylaluminum and triisobutylaluminum in cyclopentane at 60 Mcps. The chemical shifts are referred to the solvent, and a = γ -CH₃, b = α -CH₂, c = α -CH₃, d = bridge-CH₃, e = terminal-CH₂, f = terminal-CH₃, and g = the mixture of γ -CH₃ and bridge-CH₂ signals. A and B are the room-temperature spectra of the mixtures in which mole ratios of AlMe₃:Al(*i*-Bu)₃ are 20:80 and 87:13, respectively; C and D are the low-temperature spectra at about -75° corresponding to A and B, respectively.

remained liquid at a temperature as low as about -80° . They ranged from about 20 to 40 mol % of aluminum compounds.

Results

The System Trimethylaluminum-Triethylaluminum. The nmr spectra of mixtures of trimethylaluminum and triethylaluminum in cyclopentane at room temperature are shown in Figures 1A and B. Over the whole range of relative concentration between trimethyl- and triethylaluminum, the spectra display a single methyl signal and a single ethyl pattern. This indicates that the rapid exchange of the alkyl groups always takes place in the mixtures, as occurring in the pure dimers (*i.e.*, in trimethylaluminum³ and triethylaluminum⁴ alone). However, the chemical shift of each signal varies from one mixture to another. Let the shift of α -methyl (CH₃-Al<) signal and the shift of α -methylene (-CH₂-Al<) signal from solvent cyclopentane be δ_{CH_3} and δ_{CH_2} , respectively. The concentration dependences of δ_{CH_3} and δ_{CH_2} are such that the lower the concentration of triethylaluminum, the larger the δ_{CH_3} , and, at the same time, the larger the δ_{CH_2} .

At low temperature, the alkyl exchange becomes so slow that the bridge and the terminal signals of the α -methyl group and the terminal signal of the α -methylene group are distinctly observed as shown in Figures 1C and D. The low-temperature spectra also show small concentration dependences in the terminal α -methylene signal and in the bridge α -methyl signal. The positions of the bridge α -methyl signal at 0 (extrapolated value) and at 100 mol % of AlMe₃ differ by

about 7 cps. In the middle concentration range, the bridge signal of the α -methyl group consists of two to four lines. The intensity of each split line is dependent on the relative concentration of AlMe₃ and AlEt₃. The terminal α -methylene signal shows a similar concentration dependence and splittings (see Figure 1C), but in this case, the concentration dependence is limited within a smaller range; *i.e.*, it is observed only in the higher concentration range of AlEt₃.

The general behavior of the signals is shown in Figure 2.

*The System Trimethylaluminum-Tri-*n*-propylaluminum.* The spectral features and the over-all concentration dependences of δ_{CH_3} and δ_{CH_2} in the system AlMe₃-Al(*n*-Pr)₃ are almost the same as in the system AlMe₃-AlEt₃, except that in the present system an *n*-propyl signal appears in place of an ethyl signal.

The System Trimethylaluminum-Triisobutylaluminum. Figure 3 shows the nmr spectra of two different mixtures of AlMe₃ and Al(*i*-Bu)₃ in cyclopentane. In this case, we also have a single methyl signal and a single isobutyl pattern at room temperature. The bridge α -methyl signal also shows slight concentration dependence, but in this case the extent is smaller and the bridge α -methyl signal shows no splitting over the whole concentration range. Furthermore, unlike the system AlMe₃-AlEt₃, the terminal α -methyl signal splits into two peaks in the middle concentration range, while the terminal α -methylene signal does not split anywhere.

The chemical shifts of the α -methyl and the α -methylene signals are plotted against the relative concen-

tration of the two aluminum compounds in Figure 4. A notable feature in the present system is that the α -methyl signal shift at the zero concentration of AlMe_3 , $\delta_{\text{CH}_3}^0$, seems to coincide with the shift of the bridge α -methyl group, $\delta_{\text{CH}_3}^b$.

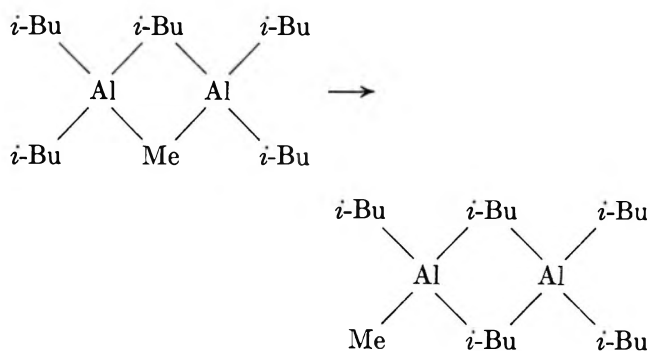
Discussion

As is the case in the usual exchange system, the signal of the α -methyl group, exchanging rapidly between the bridge and the terminal sites, appears at a position of the average between the shifts of the bridge and terminal signals weighted by the population of the methyl groups at each site. Thus, when the population of the methyl groups at the bridge site becomes larger as compared with pure trimethylaluminum dimer, the α -methyl signal is shifted to a lower field because the bridge α -methyl signal is at a lower field than the terminal α -methyl signal. The same is true for δ_{CH_2} . So the general concentration dependences of δ_{CH_3} and δ_{CH_2} in Figures 2 and 4 show that in the mixture systems at room temperature the methyl groups are found more frequently at the bridge rather than at the terminal positions, while the other alkyl groups are found more frequently at the terminal rather than the bridge positions.

The chemical shift of the bridge α -methyl group may be slightly different for different mixed dimer because of the different environments around the group in the dimer molecules. If in a given relative concentration the mixture contains various species of mixed dimers, and if an equilibrium would be reached between these various species depending upon the relative concentration of each component, the bridge α -methyl signal will be split into some lines corresponding to the presence of several mixed dimers contained in appreciable proportions. Thus the apparent concentration shift and the variation of the splitting of the bridge α -methyl group will result. Conversely, such a concentration dependence of the bridge α -methyl signal gives us evidence that there are various species of mixed dimers in the mixture, rather than only a single species of mixed dimer and a pure dimer. The concentration dependences of the terminal α -methyl and the α -methylene signals are also explained along a similar line.

As seen from Figure 2, in the system $\text{AlMe}_3\text{-AlEt}_3$, the α -methyl signal shift at the zero concentration of AlMe_3 , $\delta_{\text{CH}_3}^0$, is larger (by about 11 cps) than the bridge α -methyl signal, $\delta_{\text{CH}_3}^b$; and the α -methylene signal shift at the zero concentration of AlEt_3 , $\delta_{\text{CH}_2}^0$, is slightly smaller (by about 5 cps) than the terminal α -methylene signal shift, $\delta_{\text{CH}_2}^t$. It may be reasonable to assume that the reason why the difference between $\delta_{\text{CH}_3}^0$ and $\delta_{\text{CH}_3}^b$ does not vanish is due to the terminal methyl groups still present at very low concentration of AlMe_3 at room temperature. A similar discussion is also applicable to the difference between $\delta_{\text{CH}_2}^0$ and $\delta_{\text{CH}_2}^t$.

In the $\text{AlMe}_3\text{-Al}(i\text{-Bu})_3$ system, the difference between $\delta_{\text{CH}_2}^0$ and $\delta_{\text{CH}_2}^t$ is not zero. Thus even in the low concentration range of triisobutylaluminum, a part of the isobutyl groups is found at the bridge position at room temperature. On the other hand, $\delta_{\text{CH}_3}^0 - \delta_{\text{CH}_3}^b = 0$. This is explained by the instability of the isobutyl-isobutyl bridge. As was pointed out by Hoffmann,⁸ dimers with a mixed bonded ring, $>\text{Al}\langle_{\text{Me}}^{i\text{-Bu}}\rangle\text{Al}\langle$, can be present in the mixture system, while dimers with homogeneously isobutyl-bonded rings, $>\text{Al}\langle_{i\text{-Bu}}^{i\text{-Bu}}\rangle\text{Al}\langle$, can not, because of the bulkiness of the isobutyl group. Thus, for example, when a dimer, $\text{Al}_2\text{Me}(i\text{-Bu})_5$, with the methyl group at the bridge position undergoes exchange to form a dimer with the two bridge positions occupied by the isobutyl groups



the dimer dissociates into two monomers owing to instability of the isobutyl-isobutyl bridge. Then the methyl group again takes the bridge position after the monomers reassociate with each other or with a monomeric triisobutylaluminum. Thus the methyl group is always found at the bridge position. On the other hand, in the species with two or more methyl groups, at least one methyl group can take the terminal position by virtue of the methyl-isobutyl bridge. Since such species decrease in amount as the total concentration of the methyl groups decreases, the δ_{CH_3} curve will go down to the lower-field side rather than remain constant. In the limit of zero concentration of trimethylaluminum, only the species $\text{Al}_2\text{Me}(i\text{-Bu})_5$ will contribute to the δ_{CH_3} , and thus the α -methyl signal eventually coincides with the bridge α -methyl signal.

The Bridge-Bonding Factor. As stated above, the methyl group is more likely to occupy the bridge positions than the other alkyl group in a mixed dimer. Now, we define a quantity, the bridge-bonding factor, k , which is a measure of bridging tendency of the alkyl group in aluminum trialkyls. Let us assume that when two monomers associate into a dimer, or when a dimer undergoes exchange intramolecularly, as proposed by Muller and Pritchard,³ the chance for an alkyl group to occupy a bridge position is k times as many as that for a methyl group. Then the fractional population of

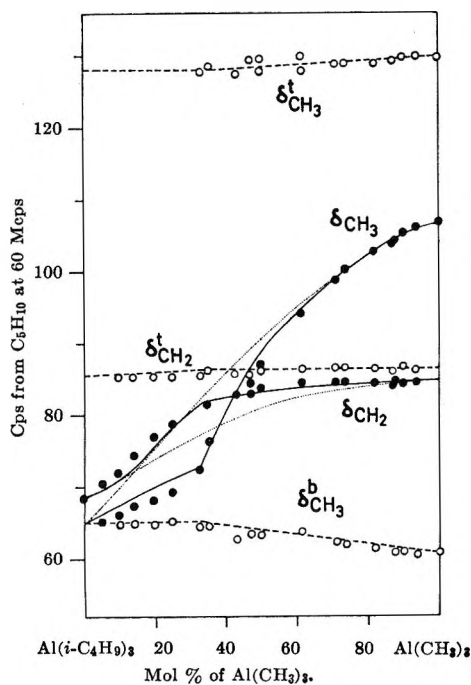


Figure 4. Chemical shifts of the signals in trimethyl aluminum-triisobutylaluminum system at 60 Mcps: ●, signals at 30°; ○, signals at about -75°; ·····, calculated curves for δ_{CH_3} and δ_{CH_2} with the statistical distribution assumption; —, calculated curves similar to above with the other distribution assumption; - - - -, curves for $\delta_{\text{CH}_3^t}$, $\delta_{\text{CH}_3^b}$, and $\delta_{\text{CH}_2^t}$ used in the calculation as corrections for $\Delta(n)\text{CH}_3$ and $\Delta(n)\text{CH}_2$.

methyl groups at the bridge position in a mixed dimer will be a function of k , and the α -methyl shift, δ_{CH_3} , can be calculated from the following formula

$$\delta_{\text{CH}_3} = \delta_{\text{CH}_3^t} - \frac{\sum_{n=1}^6 n f_n(p) Q_n(k) \Delta(n)\text{CH}_3}{\sum_{n=1}^6 n f_n(p)} \quad (1)$$

$$\Delta(n)\text{CH}_3 = \delta_{\text{CH}_3^t} - \delta_{\text{CH}_3^b}$$

for the n th dimer, where p is the formal mole fraction of AlMe_3 added in the mixture, $f_n(p)$ is the mole fraction of the n th dimer having n methyl groups and $(6-n)$ other alkyl groups, $Q_n(k)$ is the fractional population of methyl group at the bridge position in the n th dimer, and $\Delta(n)\text{CH}_3$ is the average separation between the terminal and the bridge α -methyl signal of the n th dimer. If $\delta_{\text{CH}_3^t}$ or $\delta_{\text{CH}_3^b}$ has any concentration dependence, appropriate correction must be made.

$Q_n(k)$ can be obtained by considering the probability for methyl groups to enter the bridge position in a pair of monomers. The probability to have two methyl groups at the bridge position is

$$P_2 = \frac{n}{n + (6-n)k} \frac{n-1}{(n-1) + (6-n)k} \quad (2)$$

and the probability to have one methyl group at the bridge position is

$$P_1 = \frac{n}{n + (6-n)k} \frac{(6-n)k}{(n-1) + (6-n)k} + \frac{(6-n)k}{n + (6-n)k} \frac{n}{n + (5-n)k} \quad (3)$$

Thus the fractional population of methyl group at the bridge position is given by

$$Q_n(k) = \frac{2P_2N + P_1N}{nN} = \frac{1}{n}(2P_2 + P_1) \quad (4)$$

where N is the number of n th dimer. As a special case, the 1-5 dimer, Al_2Me_5 , cannot have more than one bridge methyl group, and thus

$$Q_1(k) = P_1 = \frac{1 + 9k}{(1 + 4k)(1 + 5k)} \quad (5)$$

At the limit $p \rightarrow 0$, it may be reasonable to assume that only $f_1(p)$ is large compared with other $f_n(p)$'s; then we have

$$\delta_{\text{CH}_3}^0 = \lim_{p \rightarrow 0} \delta_{\text{CH}_3} = \delta_{\text{CH}_3^t} - Q_1(k) \Delta(1)\text{CH}_3 = \delta_{\text{CH}_3^t} - \frac{1 + 9k}{(1 + 4k)(1 + 5k)} \Delta(1)\text{CH}_3 \quad (6)$$

Thus k can be evaluated experimentally. From the data summarized in Table I, we obtain $k = 1/6$ for the ethyl group, and $1/7$ for the n -propyl group.

Table I: Chemical Shifts of the α -Methyl and the α -Methylene Signals at the Limits of the Relative Concentration^a

	AlMe_3 - AlEt_3	AlMe_3 - $\text{Al}(n\text{-Pr})_3$	AlMe_3 - $\text{Al}(i\text{-Bu})_3$
At the limit of zero concentration of AlMe_3			
$\delta_{\text{CH}_3}^0$	79	77	65
$\delta_{\text{CH}_3^t}$	130	130	Not observed
$\delta_{\text{CH}_3^b}$	68	68	65
$\delta_{\text{CH}_3}^0 - \delta_{\text{CH}_3^b}$	11	9	0
At the limit of zero concentration of the other trialkylaluminum			
$\delta_{\text{CH}_3}^0$	88.5		84.5
$\delta_{\text{CH}_2^t}$	93.5		86.5
$\delta_{\text{CH}_2^t} - \delta_{\text{CH}_2}^0$	5		2

^a Cycles per second from solvent C_5H_{10} at 60 Mcps.

Similar expressions also hold for δ_{CH_2} , but in this case k must be replaced by $k' = 1/k$ in the above formulas, and n , $Q_n(k)$, $f_n(p)$, etc., must be considered as those referred to other alkyl group. Then we can again obtain a k value from the δ_{CH_2} curve. However, an experimental ambiguity arose in $\delta_{\text{CH}_3^b}$, since it cannot be obtained explicitly from the low-temperature spectra.

From Figures 2 and 4, it is seen that $\Delta(n)\text{CH}_3$, de-

creases as the methyl groups are replaced one after another by another alkyl group. It eventually reaches about 62 cps at the limit of zero concentration of AlMe_3 in the system $\text{AlMe}_3\text{-AlEt}_3$. This value is considered as $\Delta(1)_{\text{CH}_3}$. The difference between the terminal and the bridge α -methylene signals of Al_2Et_6 , $\Delta(6)_{\text{CH}_2}$, can be calculated from its $\delta_{\text{CH}_2}^t$ and $\delta_{\text{CH}_2}^b$, and was found to be about 60 cps. It may be assumed that the difference between the terminal and the bridge signal of an alkyl group attached to an aluminum atom (but not each signal position) depends mainly upon the remaining alkyl groups in the dimer and is almost independent of the group itself. Thus $\Delta(1)_{\text{CH}_3}$ and $\Delta(6)_{\text{CH}_2}$ have almost the same value, because the remaining alkyl groups are all ethyl groups. By analogy, we can assume that $\Delta(1)_{\text{CH}_2}$ is almost equal to $\Delta(6)_{\text{CH}_2}$ (69 cps), because in this case the remaining alkyl groups are all methyl groups. Using this value as $\Delta(1)_{\text{CH}_2}$, the k value was also estimated to be $1/6$ from the δ_{CH_2} curve. The agreement of the two k values is satisfactory, and thus the k value can be obtained from either the δ_{CH_2} or the δ_{CH_3} curve.

The k value for isobutyl groups can be obtained only from the δ_{CH_2} curve, because $\delta_{\text{CH}_3}^a - \delta_{\text{CH}_3}^b = 0$. By use of the value of 69 cps for $\Delta(1)_{\text{CH}_2}$ also in this case, and of other necessary data summarized in Table I, we have $k = 1/17$ for the isobutyl group.

It is interesting to note that the bridge-bonding factor, k , is obtained at the limit of the relative concentration, and, therefore, it is independent of the actual distribution of the mixed dimers. In other words, even if the actual distribution in the system is not known, the bridge-bonding factor can be obtained provided that at the limit of zero concentration only the 1-5 or 5-1 dimer is predominantly present. The k value, of course, may be slightly dependent on temperature, thus k values reported here should be referred to the values at 30° .

Both trimethylaluminum and triethylaluminum are reported to be almost associated into dimer.⁷ However, the bridge-bonding factor of the ethyl group is $1/6$; *i.e.*, the tendency of a methyl group to occupy the bridge position is six times as large as that of an ethyl group. This is probably due to the steric effect of the alkyl group. Thus the bridge-bonding factor of more bulky alkyl group is expected to be smaller, and this expectation has been confirmed by the k values obtained for *n*-propyl and isobutyl groups.

Distribution of the Mixed Dimers in the Trialkylaluminum Mixtures. Poole, *et al.*,¹¹ assumed for their calculation of the line width of ^{27}Al resonance spectra for the alkylaluminum mixture that the alkyl groups in each dimer are arranged in a random or statistical manner. If this assumption is valid, $f_n(p)$ is simply given by

$$f_n(p) = {}_6C_n p^n (1-p)^{6-n} \quad (7)$$

where ${}_6C_n$ is the binomial coefficient. The calculated curves with these $f_n(p)$'s and $k = 1/6$ from eq 1 are plotted in Figure 2 with the solid lines. For this calculation, the changes of $\Delta(n)_{\text{CH}_3}$ and $\Delta(n)_{\text{CH}_2}$ were assumed to be linear. In the calculation of the δ_{CH_2} curve, the weighted average of $\delta_{\text{CH}_2}^t$ was used in the range of lower concentration of AlMe_3 , where the splitting of the terminal α -methylene signals is observed. As seen from Figure 2, general agreement between the experimental and calculated curves is good.

The $Q_n(k)$'s for $\text{Al}_2\text{Me}_n(i\text{-Bu})_{6-n}$ have different forms from those given in eq 4 and 5, because in the present case at least one methyl group must always be contained in the bridge positions. Hence $Q_n(k)$'s should be modified in such a manner that in calculating the probabilities P_1 and P_2 there is no contribution from the isobutyl group in the homogeneously isobutyl-bonded ring. (But such a modification is not necessary for the 5-1 dimer, $\text{Al}_2\text{Me}_5(i\text{-Bu})$, which has only one isobutyl group.)

With this modified $Q_n(k)$, the curves for the δ_{CH_3} and δ_{CH_2} were calculated and plotted in Figure 4 with dotted lines, assuming the statistical distribution as in $\text{AlMe}_3\text{-AlEt}_3$. In the calculation, pure triisobutylaluminum is assumed to have monomeric form, and the exchange between monomeric $\text{Al}(i\text{-Bu})_3$ and the mixed dimers is also taken into account. However, the calculated curves largely deviate from the observed values. The main factor contributing to the deviation seems to be the statistical distribution assumption. In contrast with $\text{AlMe}_3\text{-AlEt}_3$, the present system contains $\text{Al}(i\text{-Bu})_3$ monomer, and in the statistical distribution assumption the monomer is equally probable as the other dimers except in the statistical weight, but actually the bridging tendency of methyl group would be so great that monomeric $\text{Al}(i\text{-Bu})_3$ would be consumed to form mixed dimers in more amount than that expected from the simple statistical distribution. Then the over-all fractional population of the methyl group at the bridge position is increased, which in turn makes the δ_{CH_2} curve shift to a lower field and at the same time the δ_{CH_3} curve to a higher field.

To make situation clearer, we assumed that in the range of the mole ratio of $\text{AlMe}_3:\text{Al}(i\text{-Bu})_3$ smaller than 1:2, only 1-5 and 2-4 dimers as well as $\text{Al}(i\text{-Bu})_3$ monomer are present, and above the mole ratio of 1:2, 1-5 dimer and $\text{Al}(i\text{-Bu})_3$ monomer are absent. With this model and assuming the statistical distribution between the existing species, the δ_{CH_3} and the δ_{CH_2} curves were calculated and plotted in Figure 4 with solid lines. It will be seen that the agreement with the experimental values becomes much improved as compared with the previous calculated curves. Ac-

(11) C. P. Poole, Jr., H. E. Swift, and J. F. Itzel, Jr., *J. Chem. Phys.*, **42**, 2576 (1965).

tually, however, a slight disagreement is still observed, and some perturbation to the above assumed distribution is expected, especially in the lower concentration range of AlMe_3 .

The assumption used here is supported by the following experimental fact. It was found that below about 33.3 mol % of AlMe_3 a broad signal appears between the bridge α -methyl signal and the terminal α -methylene signal in the low-temperature spectra, as shown in Figure 3C. The broad signal can be assigned to a mixture of the terminal α -methylene signal of $\text{Al}_2\text{Me}(i\text{-Bu})_5$ and the α -methylene signal of monomeric $\text{Al}(i\text{-Bu})_3$. Because of the instability of the mixed bonded ring as compared with the homogeneously methyl-bonded ring, weaker thermal motion may cause the instable mixed bonded ring to be broken. Thus, even when the exchange in the mixed dimers having two or more methyl groups becomes slow enough to make the bridge and the terminal signals sufficiently sharp in a certain temperature range, the exchange between monomeric $\text{Al}(i\text{-Bu})_3$ and 1-5 dimer or between 1-5 dimers themselves will not yet be slow so that the α -methylene signals of these species may collapse to the broad signal. While the mixed bonded ring is always

present in 1-5 dimer, the other mixed dimers have configurations with the homogeneously methyl-bonded ring which are sufficiently stable to thermal motion at a temperature as low as -75° . These species will show a sharp terminal α -methylene signal, which can be seen from Figure 3C as superposed on the broad signal at the higher-field side.

On the other hand, such a broad signal is not found above 33.3 mol % of AlMe_3 . If the monomer and 1-5 dimer are absent, as assumed above, all species present can have the homogeneously methyl-bonded ring in certain configurations. Although these latter dimers may take configurations with the mixed bonded ring, once the dimers are set to a configuration with homogeneously methyl-bonded ring after a number of exchange, they will no longer undergo exchange at a temperature of about -75° , and the collapsed signal will not be observed. Thus the experimental fact supports the assumption made in the calculation of the δ_{CH_3} and δ_{CH_2} curves in $\text{AlMe}_3\text{-Al}(i\text{-Bu})_3$ system.

Acknowledgment. The authors are indebted to Mr. M. Yanagisawa, Mr. H. Sato, and Mr. S. Murakami for their help in carrying out the experiments.

Dilute Solution Properties of Styrene-Methyl Methacrylate Random Copolymers

by Tadao Kotaka, Yoji Murakami, and Hiroshi Inagaki

Institute for Chemical Research, Kyoto University, Takatsuki, Osaka, Japan (Received June 30, 1967)

The results of an extensive study on dilute solution properties of three series of styrene-methyl methacrylate random copolymers are described. The copolymers are prepared by a free radical polymerization method (conversion = less than 10%) and subsequently fractionated by use of a butanone-diisopropyl ether system. The characterization of the fractions is made by combustion analysis, by osmometry, and by light-scattering methods. The Θ temperatures for the copolymers are determined as the temperatures at which the osmotic second virial coefficient $A_2 = 0$ in cyclohexanol and 2-ethoxyethanol. Measurements of intrinsic viscosity, $[\eta]$, under the Θ conditions show that $[\eta]_{\Theta}$ is proportional to $M^{1/2}$ (M , the molecular weight) in the copolymer solutions. Measurements of $[\eta]$ are also made in toluene, 1-chloro-*n*-butane, and diethyl malonate, which have typically different solvent powers toward the parent homopolymers. All the $[\eta]$, A_2 , and M data are examined on the basis of the current excluded volume theories. Then the short-range and the long-range interaction parameters, A and B , are estimated for each copolymer-solvent pair, and their dependences on the monomer composition are examined in relation with those of the parent homopolymers. It is found that the values of $A^2 = (\langle S^2 \rangle_0 / M)$, with $\langle S^2 \rangle_0$ being the unperturbed mean-square molecular radius, are larger than the simple composition averages of those of the parent homopolymers. The parameter B shows the presence of repulsive interactions between the unlike monomer units.

Introduction

Recent advances in the studies on the properties of dilute polymer solutions have made it clear that the conformational and thermodynamic properties of flexible macromolecules may be described essentially by two independent parameters.¹⁻³ They are the short-range and the long-range interaction parameters, and are related, respectively, to the unperturbed average dimension⁴ and to the excluded-volume effect¹ of a given polymer in a given environment. The adequacy of the basic assumptions of the two-parameter statistical-mechanical theories has been substantiated by experiments.^{1-3,5-7} Of importance is the fact that these two parameters can be determined, in principle, consistently from adequate experimental data such as the molecular weight dependences of second virial coefficient,^{6,8} of mean-square statistical radius,^{3,6} of intrinsic viscosity,^{3,7,9-11} etc. In fact, several graphical procedures for making such analyses have been proposed so far, still leaving certain points of dispute among them though.

In view of the current status of the two-parameter theories, it would be an interesting problem to extend the theories to examine the dilute solution properties of copolymers. Difficulties in copolymer studies would arise from an obvious fact that there are (even for a simple binary copolymer) at least three factors: the molecular weight, the monomer composition, and the mode of monomer arrangements, for specifying a

copolymer sample. In addition, the heterogeneities with respect to these three factors would further complicate the problem. Therefore, any copolymer materials should first be well characterized in these respects.¹²

For our study, we selected copolymers of styrene (ST) and methyl methacrylate (MMA) for several reasons. First of all, the properties of the parent homopolymers, polystyrene (PST) and poly(methyl methacrylate) (PMMA), have been most extensively studied

(1) P. J. Flory, "Principles of Polymer Chemistry," Cornell University Press, Ithaca, N. Y., 1953.

(2) W. H. Stockmayer, *Makromol. Chem.*, **35**, 54 (1960).

(3) See, for example, M. Kurata and W. H. Stockmayer, *Fortschr. Hochpolym. Forsch.*, **3**, 196 (1963).

(4) See, for example, M. V. Volkenstein, "Configurational Statistics of Polymer Chain," Moscow and Leningrad, Academy of Sciences, U. S. S. R., 1959; T. M. Birshtein and O. B. Ptitsyn, "Conformations of Macromolecules," Nauk, Moscow, 1964.

(5) H. Inagaki, H. Suzuki, M. Fujii, and T. Matsuo, *J. Phys. Chem.*, **70**, 1718 (1966).

(6) (a) G. C. Berry, *J. Polymer Sci.*, **B4**, 161 (1966); (b) G. C. Berry, *J. Chem. Phys.*, **44**, 4550 (1966).

(7) G. C. Berry, *ibid.*, **46**, 1338 (1967).

(8) M. Kurata, M. Fukatsu, H. Sotobayashi, and H. Yamakawa, *ibid.*, **41**, 139 (1964).

(9) W. H. Stockmayer and M. Fixman, *J. Polymer Sci.*, **C1**, 137 (1963).

(10) H. Inagaki, H. Suzuki, and M. Kurata, *ibid.*, **C15**, 409 (1966).

(11) J. M. G. Cowie, *Polymer*, **7**, 487 (1966).

(12) See, for example, H. Benoit, *Ber. Bunsenges. Physik. Chem.*, **70**, 286 (1966).

in various solvents. Secondly, by the benefit of accumulated knowledge on the copolymerization kinetics of ST-MMA systems,¹³ random copolymers with a prescribed composition but with a negligible composition heterogeneity can be prepared by the free radical polymerization method. Thirdly, block copolymers with well characterized architecture can also be prepared by anionic polymerization methods,¹⁴ and thus the comparison of the ST-MMA random and block copolymers would become possible in due course.

In this report, we deal with the properties of the ST-MMA random copolymers, *i.e.*, those prepared by the free radical polymerization method. The studies of a similar nature have already been reported in several articles, notably by Stockmayer, Moore, Fixman, and Epstein¹⁵ and also by Utiyama.¹⁶ The present work supplements the previous works of these authors in greater detail.

Experimental Section

Materials. Commercial styrene monomer was washed several times with 10% NaOH solution and followed by repeated water washing to remove the alkali. The monomer was dried over CaCl₂, filtered, and stored over CaH₂ in a sealed vessel at about 4°. Just prior to use the monomer was distilled under a reduced N₂ atmosphere (12–14 mm pressure), and the middle fraction distilling at 38–40° was collected. Methyl methacrylate monomer was treated in the same way, except the middle fraction distilling at 40–41° under 82–83 mm of an N₂ atmosphere was collected.

Benzoylperoxide (BPO) was purified by recrystallizing it in methanol from chloroform solution; it was dried *in vacuo* at room temperature. All the solvents used for physicochemical measurements were carefully purified according to the standard procedures appropriate to each. Other solvents and nonsolvents used in large quantities for fractionation and subsequent purification were all purified by batch distillation.

Preparation and Fractionation of Copolymers. Five copolymer samples of (three) different compositions were prepared in bulk at 60° by using BPO as an initiator. In each polymerization, the reaction was terminated by cooling the mixture rapidly to room temperature and pouring it into an excess amount of methanol. The whole polymers obtained were purified by twofold precipitation from tetrahydrofuran (THF) or butanone solution into methanol, followed by vacuum drying at about 60°. MMA-rich copolymers often yielded somewhat sticky aggregates, even after vacuum drying. Therefore, they were further treated by redissolving them in benzene and subsequent freeze drying. The composition of each sample was determined from the carbon content by repeating the combustion analysis several times. Table I summarizes the copolymerization data.

Table I: Polymerization Data of ST-MMA Random Copolymers

Sample code	ST in feed, mol %	Amount of BPO, mol %	Time, min	Conversion, wt %	ST in products, mol %
SM3	21.5	0.0413	265	7.0	29.6
SM5	55.8	0.0444	270	5.1	55.9
SM5'	55.8	0.84	90	9.5	53.6
SM7	75.1	0.046	285	6.5	71.2
SM7'	75.1	0.90	85	10.0	70.1

Each whole polymer, coded as shown in Table I, was subjected to successive fractionating precipitation by using butanone and diisopropyl ether (DIPE) as solvent and precipitant,¹⁵ respectively, repeating the following procedures. The precipitant was added dropwise to the mixture at 30.0° with vigorous stirring, until the solution became sufficient cloudy. The temperature was raised (usually up to 50 ~ 55°) until the precipitates were redissolved. Then the temperature was gradually lowered to 30.0° with constant stirring overnight to ensure the equilibrium between phases. Finally the mixture was kept standing still until the phase separation was completed, and the precipitates were recovered. The conditions for the fractionation are listed in Table II. All the fractions were again

Table II: Conditions for the Copolymer Fractionation

Code	Amount of polymer, g	Polymer concn, g/100 ml, and γ values, vol fraction ^a		Number of fractions	Total recovery, wt %
		Initial	Final		
SM3	54.0	$c = 1.41$ $\gamma = 0.48$	0.085 0.74	12	95.5
SM5	41.0	$c = 1.35$ $\gamma = 0.51$	0.11 0.72	12	93.8
SM5'	35.0	$c = 1.39$ $\gamma = 0.68$... 0.83	6	...
SM7	51.0	$c = 1.09$ $\gamma = 0.57$	0.082 0.77	12	98.4
SM7'	37.0	$c = 1.36$ $\gamma = 0.70$... 0.84	6	...

^a γ = volume fraction of the nonsolvent. For the first fractions, the data show the condition under which the initial precipitation took place. The last fraction was recovered by adding large amount of methanol to the final solution.

(13) See, for example, G. E. Ham, Ed., "Copolymerization," Interscience Publishers, Inc., New York, N. Y., 1964.

(14) See, for example, M. Szwarc, and A. Rembaum, *J. Polymer Sci.*, **22**, 189 (1956); M. Baer, *ibid.*, **A2**, 417 (1964); D. Decker-Freyss, P. Rempp, and H. Benoit, *ibid.*, **B2**, 217 (1964).

(15) W. H. Stockmayer, L. D. Moore, Jr., M. Fixman, and B. N. Epstein, *ibid.*, **16**, 517 (1955).

(16) H. Utiyama, Dissertation, Kyoto University, Kyoto, Japan, 1963.

purified and their compositions were determined by the same procedures as for the whole polymers. Some of the fractions were used for the later measurements. Our laboratory stock of the parent homopolymers PST and PMMA were used, whenever necessary, for the sake of comparison.

Osmotic-Pressure Measurements. A Mechrolab high-speed membrane osmometer Model 502 with a variable temperature controller (Mechrolab, Mountain View, Calif.) was employed. Membranes used were ultracel-lafilter grade feinst or allerfeinst.

The latter were used for low molecular weight samples. The membranes were conditioned through 1-propanol to each relevant solvent before use. The data were obtained at 30.0° in either or both toluene and 1-chloro-*n*-butane (1-CB) solutions. The measurements were usually made at five or six different concentrations and the results were analyzed according to the equation¹

$$(\pi/C)^{1/2} = (RT/M_n)^{1/2}[1 + (A_2M_n/2)C]$$

where π is the osmotic pressure, C is the polymer concentration, M_n is the number average molecular weight, A_2 is the second virial coefficient, and R and T are the gas constant and the absolute temperature, respectively. Values obtained for M_n and A_2 are summarized in Table III.

Determination of Θ Temperatures. In order to find pure Θ solvents for ST-MMA copolymers, a variety of solvents were first examined by a simple cloud point test. For the test we used three random copolymer fractions with nearly equal M_n (one from each of the three series), and also PST and PMMA samples. In each case, a mixture of 15 mg of polymer and 3 ml of solvent was subjected to the cloud point test, within the temperature range from about 95° to room temperature. Several solvents were found to be promising.¹⁷ Two solvents, cyclohexanol¹⁸ (CHL) and 2-ethoxyethanol¹⁷ (2-EE), were chosen and the Θ temperatures were determined by osmotic-pressure measurements as the temperatures at which the osmotic second virial coefficient, A_2 , vanishes.¹ Values obtained for Θ and temperature coefficient of A_2 at Θ , $(\partial A_2/\partial T)_\Theta$, are given in Table IV.

Refractive-Index Increment and Light-Scattering Measurements. Specific refractive-index increments of PST, PMMA, and some of the copolymer fractions were measured with 436-m μ wavelength light in toluene, in dioxane, and in butanone at 30.0° by a Shimadzu (Debye type) differential refractometer equipped with a thermostated cell (Shimadzu-Seisakusho, Kyoto, Japan).

Light-scattering measurements were made by a Shimadzu (Brice type) light-scattering photometer equipped with a thermostated jacket.⁵ A cylindrical cell was used throughout the work. Scattering intensities were usually measured at 11 different angles, ranging from 30 to 150°, with vertically polarized light of 436-m μ

Table III: Results of Fractionation and Osmometric Data^a

Code	$10^{-4}M_n$	M_w/M_n^b	10^4A_2	
			TOL	1-CB
SM3-1	59.2	1.78	2.6	1.5
-5	44.0	...	2.8	1.3
-6	38.7	1.75	...	1.5
-7	35.4	...	3.0	1.4
-8	27.6	...	3.2	2.3
-9	18.1	1.52	3.7	1.7
-10	10.0	1.50	4.3	2.1
-11	4.67	...	3.7	...
(0.29 ± 0.01) ^c				
SM5-1	50.0	...	3.3	2.2
-2	46.0	1.62	3.1	2.1
-5	39.7	1.53	3.5	2.2
-6	35.0	...	3.6	2.2
-8	26.4	...	3.7	2.3
-9	22.6	...	3.6	2.6
-10	18.5	1.48	3.9	2.7
-11	9.66	...	4.1	3.4
SM5'-2	6.89	1.41	...	4.6
-4	4.80	1.40	...	4.6
-5	3.42	5.6
(0.56 ± 0.01) ^c				
SM7-2	43.2	1.26	2.9	2.1
-3	34.2	1.29	3.1	2.6
-6	27.4	...	4.0	3.0
-8	21.0	1.29	3.5	3.0
-9	18.1	3.3
-10	14.5	1.26	4.7	3.2
-11	6.67	...	4.1	5.8
SM7'-2	6.21	3.0
-4	4.73	4.1
-5	4.00	1.24	...	5.2
(0.70 ± 0.10) ^c				

^a Units: average ST content = mole fraction, and A_2 = ml mol/g². Abbreviations: TOL = toluene and 1-CB = 1-chloro-*n*-butane, all measured at 30.0°. ^b For M_w data, see Tables V and VI. ^c The numbers in parentheses are the average ST content.

wavelength (for both incident and scattered lights). The calibration procedures of the apparatus were described elsewhere.⁵

For some of the fractions, measurements were carried out in three solvents, butanone, dioxane, and toluene, at 30.0 ± 0.1°, and for some others only in butanone at 30.0 ± 0.1°. All the test solutions were prepared by keeping them at about 60° in sealed glass tubes for at least 2 days, with occasional shaking. The solutions were filtered through Grade m ultracel-lafilter directly into the light-scattering cell.

It has been known that the specific refractive index increment, ν of a binary copolymer can be usually ex-

(17) For a preliminary report, see T. Kotaka, H. Ohnuma, and Y. Murakami, *J. Phys. Chem.*, **70**, 4099 (1966).

(18) D. Froelich and H. Benoit, *Makromol. Chem.*, **92**, 224 (1966), reported values of Θ in CHL are 77.6° for PMMA, 83.5° for PST, 68.6° for azeotropic ST-MMA random copolymer, and 81.6° for equimolar (PST-PMMA) type block copolymer.

Table IV: Θ Temperatures and $(\partial A_2/\partial T)_\Theta$ for ST-MMA Random Copolymers

Code	ST content, mole fraction	Θ , °C and $10^6(\partial A_2/\partial T)_\Theta^a$	
		Cyclohexanol	2-Ethoxyethanol
PMMA 14M ^b	0.00	79.4 (2.5)	39.0 (0.80)
SM3-7	0.285	68.2 (2.3)	40.0 (0.46)
SM5-6	0.552	61.3 (1.3)	58.4 (0.52)
SM7-3	0.694	63.0 (1.3)	72.8 (0.70)
PST 16H ^b	1.00	81.8 (1.7)	Insoluble

^a Values in parentheses. ^b Prepared by anionic polymerization method by using Na-biphenyl as an initiator. Values of M_n are 7.21×10^4 for PMMA 14M and 20.6×10^4 for PST 16H.

pressed with a high precision as to be dependent linearly on the composition and independent of molecular weight, M^{15}

$$\nu = x\nu_1 + (1-x)\nu_2$$

where x is the weight fraction of monomer species I, and the subscripts 1 and 2 denote the quantities characteristic of the parent homopolymers I and II (in this study, PST and PMMA, respectively). The reduced scattering intensity, R_θ , at an scattering angle θ for a copolymer solution can be expressed, following the procedure of Zimm,¹⁹ as

$$\lim_{\theta \rightarrow 0} Kc/R_\theta = 1/M_{app} + 2(A_2')_{app}c + \dots$$

$$\lim_{c \rightarrow 0} Kc/R_\theta = (1/M_{app}) \times$$

$$\left[1 + \frac{4}{3} \left(\frac{2\pi n_0}{\lambda_0} \right)^2 \langle S^2 \rangle_{app} \sin^2(\theta/2) + \dots \right]$$

where $K = (4\pi^2/\lambda_0^4 N_a)(n_0\nu)^2$ is the well known light-scattering factor; λ_0 is the wavelength of light *in vacuo*; n_0 is the refractive index of the solvent; and N_a is the Avogadro number. In case of homopolymers, M_{app} , $(A_2')_{app}$, and $\langle S^2 \rangle_{app}$ are, respectively, equal to the weight-average molecular weight M_w ; the light-scattering second virial coefficient, A_2' ; and the z-average mean-square statistical radius, $\langle S^2 \rangle_z$, of the polymer chains.²⁰ These quantities for copolymers are apparent values and different from those of homopolymers^{12,15,21} if there is the slightest heterogeneity in the composition of the copolymer.

As far as the assumption of the linear dependence of ν on x is valid, M_{app} can be expressed as^{12,15}

$$M_{app} = M_w + 2[(\nu_1 - \nu_2)/\nu]P + [(\nu_1 - \nu_2)/\nu]^2 Q$$

$$\text{where } P = \sum_i \gamma_i M_i (x_i - x), \quad Q = \sum_i \gamma_i M_i (x_i - x)^2,$$

where γ_i is the weight fraction of component i whose molecular weight is M_i , and the composition is x_i ; $x = \sum_i \gamma_i x_i$ is the average composition of the sample (in weight fraction of component I). The parameters P

and Q represent the heterogeneity in composition; P relates to the composition variation with molecular weight, and Q to its broadness. For azeotropic copolymers, or more generally, for low-conversion copolymers of any composition, it is very likely that the composition variation with molecular weight is negligible and the broadness is also small.²² The assumptions lead to: $P = 0$, $Q = M_w \sum_i f_i (x_i - x)^2$,

where f_i is the weight fraction of all the components with x_i , regardless of their molecular weights. Thus, measurements of M_{app} in at least three solvents should allow one to determine M_w , P , and Q independently. If the composition heterogeneity is very small, measurements, even in a single solvent with large ν values, would allow one to determine M_w with a reasonable accuracy. The data were analyzed according to the above equations; the results are given in Tables V and VI.

Table V: Summary of Light Scattering M_{app} Data^a

Code	$10^{-4} M_{app}$			$10^{-4} M_w$	Q/M_w
	MEK	DOX	TOL		
SM3-1	111.1	112.9	163.9	105.8	0.06
-6	69.0	71.4	83.3	67.8	0.03
-9	27.0	28.2	...	27.6	0.00
SM5-2	74.6	87.7	100.0	74.5	0.13
-5	61.7	67.1	74.1	60.8	0.08
-10	26.6	28.6	27.0	27.7	0.00
SM7-2	57.1	62.5	74.5	54.4	0.23
-3	45.3	52.6	62.5	44.0	0.24
-8	28.2	30.8	35.7	27.0	0.17

^a Abbreviations: MEK = butanone, DOX = dioxane, and TOL = toluene, all measured at 30.0°.

Viscosity Measurements. The measurements were made by using three Ubbelohde dilution viscometers with flow times (for toluene at 30.0°) more than 200 sec/ml. Neither the kinetic-energy correction nor the non-Newtonian correction were found to be necessary. The temperature was kept within $\pm 0.02^\circ$ at each desired value. The intrinsic viscosity, $[\eta]$, was determined by using two types of viscosity-concentration plot, *i.e.*, η_{sp}/c and $(\ln \eta_r)/c$ vs. c , and by extrapolating them so as to yield a common intercept at $c = 0$

$$\eta_{sp}/c = [\eta] + k'[\eta]^2 c + O(c^2)$$

$$(\ln \eta_r)/c = [\eta] - (1/2 - k')[\eta]^2 c + O(c^2)$$

(19) B. H. Zimm, *J. Chem. Phys.*, **16**, 1093, 1099 (1948).

(20) H. C. Brinkman and J. J. Hermans, *ibid.*, **17**, 574 (1949); J. G. Kirkwood and R. J. Goldberg, *ibid.*, **18**, 54 (1950); W. H. Stockmayer, *ibid.*, **18**, 58 (1950).

(21) W. Bushuk and H. Benoit, *Compt. Rend.*, **244**, 3167 (1958); *Can. J. Chem.*, **36**, 1616 (1958); H. Benoit and C. Wippler, *J. Chim. Phys.*, **57**, 524 (1960).

(22) W. H. Stockmayer, *J. Chem. Phys.*, **13**, 199 (1945).

Table VI: Summary of Viscometric Data of ST-MMA Copolymers in Three Good Solvents and in Two Θ Solvents

Code	$10^{-4}M_w^a$	[η], dl/g ^b			[η], dl/g; $(10^4[\eta]/M_w^{1/2})^c$	
		TOL	DEM	1-CB	2-EE $T = 40.0^\circ$	CHL $T = 68.0^\circ$
SM3-1	105.8	2.01	1.42	1.15	0.628 (6.10)	0.636 (6.18)
-5	(77.4)	1.62	1.15	0.946	...	0.574 (6.54)
-6	67.8	1.43	1.09	0.865	0.512 (6.24)	...
-7	(60.6)	1.32	0.974	0.830	...	0.508 (6.55)
-8	(44.7)	0.996	0.774	0.666
-9	27.6	0.768	0.585	0.518	0.340 (6.48)	0.341 (6.50)
-10	15.0	0.507	0.379	0.360	0.264 (6.83)	0.270 (6.98)
-11	(7.05)	0.299	0.242
					$T = 60.0^\circ$	$T = 64.0^\circ$
SM5-1	(81.0)	1.96	1.15	1.36	...	0.670 (7.44)
-2	74.5	1.82	1.05	1.29	0.682 (7.92)	...
-5	60.8	1.61	0.984	1.12	0.622 (7.99)	...
-6	(53.5)	1.44	0.880	1.05	...	0.550 (7.54)
-8	(39.6)	1.13	0.740	0.846
-9	(33.4)	1.05	0.657	0.755	...	0.443 (7.68)
-10	27.7	0.877	0.589	0.663	0.408 (7.76)	...
-11	(13.7)	0.557	0.387
SM5'-2	9.71	0.434	0.314	0.335	...	0.221 (7.16)
-4	6.76	0.336	0.261	0.275	0.201 (7.76)	...
-5	(4.79)	0.262	0.193	0.220
					$T = 72.0^\circ$	$T = 64.0^\circ$
SM7-2	54.4	1.68	0.875	1.17	0.580 (7.88)	0.578 (7.84)
-3	44.0	1.47	0.770	1.03
-6	(35.2)	1.17	0.647	0.845
-8	27.0	0.949	0.555	0.726	0.401 (7.75)	0.380 (7.35)
-9	(23.0)	0.890	0.517	0.611
-10	18.3	0.707	0.441	0.556	0.332 (7.78)	0.320 (7.50)
-11	(8.40)	0.481	0.287
SM7'-2	(7.70)	0.386	0.261	0.310
-4	(5.86)	0.312	0.221	0.263
-5	4.96	0.276	0.206	0.237	0.171 (7.72)	0.166 (7.47)

^a Values in parentheses are those estimated from M_n data; see text. ^b Abbreviations: TOL = toluene, DEM = diethylmalonate, and 1-CB = 1-chloro-*n*-butane, all measured at 30.0°. ^c Abbreviations: 2-EE = 2-ethoxyethanol and CHL = cyclohexanol; values in parentheses are $10^4[\eta]/M_w^{1/2}$.

where η_{sp} is the specific viscosity, η_r is the relative viscosity, and k' is the Huggins constant. Values obtained for $[\eta]$ in various solvents are summarized in Table VI.

Results

Fractionation and Osmometric Data. Table III summarizes the results of fractionation and osmometric data. It is found from the results of elementary analysis that the composition fluctuation from one fraction to the other in each series is less than $\pm 1\%$. We assign the values (in mole fraction) 0.29 ± 0.01 for the fractions from SM3, 0.56 ± 0.01 for those from SM5 and SM5', and 0.70 ± 0.01 for those from SM7 and SM7', as the average ST contents. For some of the fractions, the values of M_w/M_n are also listed in Table III.

The fractionation procedure developed by Stockmayer, *et al.*,¹⁵ appears to be successful in fractionating

ST-MMA copolymers, according only to molecular weight but not to average composition. However, in view of achieving an efficient fractionation by molecular weight, the butanone-DIPE system appears to be less efficient for MMA-rich copolymers. As shown in Table III, the values of M_w/M_n are usually larger in SM3 fractions and smaller in SM7 fractions. A similar result was reported by Utiyama,¹⁶ who found a poor resolution of PMMA by molecular weights. In this respect, use of some other system might be desirable for MMA-rich copolymers.

Θ Temperatures. Table IV summarizes the results of Θ temperature determination in CHL and in 2-EE for the three copolymer fractions and two homopolymer samples,^{17,18} and Figure 1 shows plots of Θ vs. ST content m in the copolymers. It is interesting to note that the Θ temperatures in CHL of the copolymers are lower than either of those of PST and PMMA and have a minimum at nearly equimolar composition,

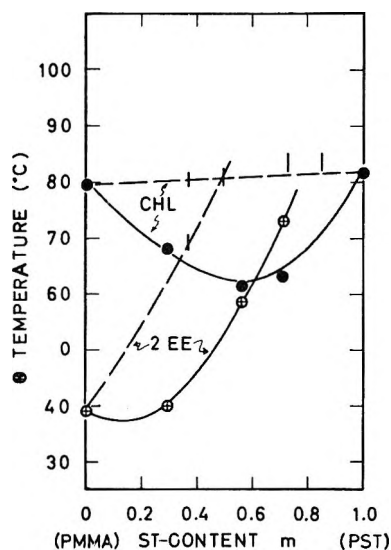


Figure 1. The θ temperatures of ST-MMA copolymers in cyclohexanol (CHL) and in 2-ethoxyethanol (2-EE) as functions of ST content (mole %) in the copolymers. The points represent data for the random copolymers and the homopolymers. Bold dashed curves represent those for block copolymers.¹⁷

while in 2-EE, which is a nonsolvent for PST, the θ temperatures appear to have a shallow minimum at MAA-rich composition and increase rapidly with increasing ST content. Figure 1 also shows our previous data of θ for ST-MMA block copolymers¹⁷ in these solvents. The composition dependences of θ for the block copolymers are quite different from those of the random copolymers. Detailed discussion on the behavior of the block copolymers will be reported in a later publication.

Specific Refractive-Index Increment and Light Scattering. Figure 2 shows the values of ν as functions of ST content x . The results were found to be expressed with good approximations by the relations (for 436-m μ light): $\nu = 0.232x + 0.133(1 - x)$ in butanone, 30.0°; $\nu = 0.184x + 0.071(1 - x)$ in dioxane, 30.0°; and $\nu = 0.113x + 0.004(1 - x)$ in toluene, 30.0°. The fluctuation in the values of ν from one fraction to the other was negligible as anticipated; the result corroborates that of the elementary analysis.

Table V summarizes the light-scattering data obtained in three solvents for some of the fractions from each series. Since we already found that the composition of each fraction in each series was virtually independent of molecular weight, we calculated M_w and Q by employing the assumption $P = 0$. We found that (i) the values of Q/M_w were reasonably small as anticipated, and (ii) the values of M_{app} obtained in butanone, in which ν is the largest among the three solvents, were close to the values of M_w . Therefore, subsequent measurements were carried out only in butanone at 30.0°. The values of M_w/M_n in each series derived from these data varied systematically with increasing M_n , and we found a correlation between M_w and M_n

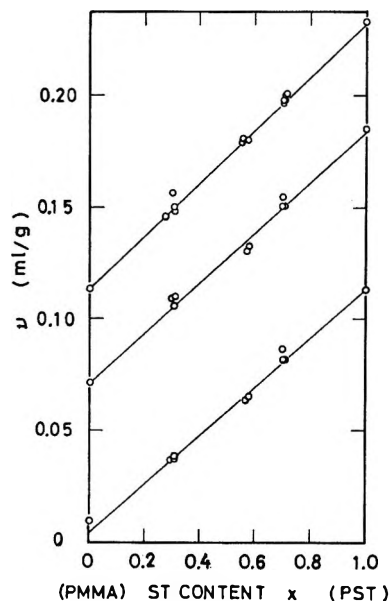


Figure 2. The specific refractive-index increments, ν , of ST-MMA copolymers as functions of ST content (wt %) in three solvents, *i.e.*, in 2-butanone, *p*-dioxane, and toluene, in order from top to bottom.

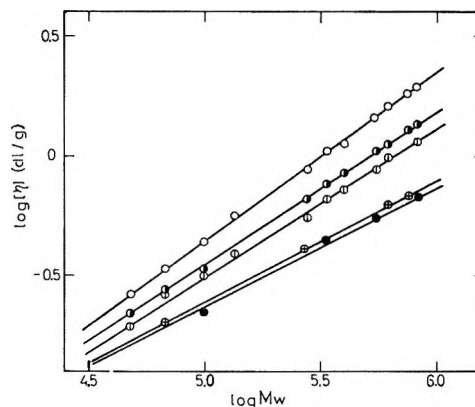


Figure 3. Intrinsic viscosity-molecular weight relationship for ST-MMA copolymers SM5 and 5' in toluene, O; in DEM, \square ; in 1-CB, \triangle ; all at 30.0°; in CHL at 64.0°, \bullet ; and in 2-EE at 60.0°, \oplus .

from plots of M_w/M_n vs. M_n . Then, we drew a smooth curve fitting the plots, and, by using this as the calibration curve we estimated M_w of other fractions from the M_n data. The values of M_w thus obtained are listed in Table VI, in which the values in parentheses are those estimated from the M_n data.

Intrinsic Viscosity. Table VI lists $[\eta]$ data obtained in the two θ solvents and in toluene, DEM, and 1-CB. By way of illustration, Figure 3 shows plots of $\log [\eta]$ vs. $\log M_w$ for SM5 and SM5' in these solvents. The plot for each solvent is fitted fairly well by a straight line over the range of M_w examined. All these data are summarized in the form of the Mark-Houwink-Sakurada relation, $[\eta] = K'M_w^a$. The values of K' and a are listed in Table VII. It is interesting to note that

the $[\eta]$ vs. M relations of the three copolymers are almost identical in toluene, which is a good solvent toward both of PST and PMMA. On the other hand, in 1-CB, which is a Θ solvent for PMMA ($\Theta = 35.4^\circ$),²³ the exponent a increases with increasing ST content. In DEM, which is a Θ solvent for PST ($\Theta = 35.9^\circ$),^{24,25} the tendency is apparently reversed. In the Θ solvents the exponents a are close to 0.5, as is always the case for any homopolymer- Θ solvent system.

Table VII: List of the Mark-Houwink-Sakurada Constants, $[\eta] = K'M_w^a$ of ST-MMA Copolymers in Various Solvents

Code (ST, mol fraction)	Solvent	$10^4 K'$	a
SM3 (0.29)	TOL	1.14	0.70
	DEM	1.57	0.66
	1-CB	2.65	0.60
	2-EE 40.0°	9.73	0.47
	CHL 68.0°	9.73	0.47
SM5 (0.56)	TOL	1.32	0.71
	DEM	2.49	0.62
	1-CB	2.49	0.63
	2-EE 60.0°	6.85	0.51
	CHL 64.0°	7.00	0.51
SM7 (0.70)	TOL	0.832	0.75
	DEM	3.13	0.60
	1-CB	1.76	0.67
	2-EE 72.0°	7.16	0.51
	CHL 64.0°	7.16	0.51

^a Measured at 30.0°, unless otherwise specified; for abbreviations, see Table VI.

Discussion

It is well established that for solutions of flexible chain (homo)polymers the effects of long-range interactions (the excluded volume effects) between non-bonded sequents—*i.e.*, those belonging to different polymer chains and those remotely separated by many other segments along the same polymer chain—should vanish under a special condition of solvent and temperature known as the Flory Θ condition.¹ Consequently, under the Θ condition, A_2 becomes zero and the polymer chains assume random flight configurations, the unperturbed dimensions being determined solely by the short-range interactions. The deviations of polymer dimensions and other properties, such as $[\eta]$, due to the excluded volume effects are usually expressed in terms of expansion factors such as

$$\alpha = (\langle S^2 \rangle / \langle S^2 \rangle_0)^{1/2}$$

$$\alpha_\eta = ([\eta] / [\eta]_\Theta)^{1/8}$$

with $\langle S^2 \rangle_0$ being the unperturbed mean-square statistical radius. The expansion factors are then ex-

pressed as functions of an excluded volume parameter z defined as

$$z = (B/A^3) M^{1/2} \quad (1)$$

with

$$A^2 = \langle S^2 \rangle_0 / M = a^2 / 6m_s \quad (2)$$

$$B = (1/4\pi)^{3/2} (\beta/m_s^2) \quad (3)$$

Here, A and B are the parameters representing the short-range and the long-range interactions, respectively; M is the molecular weight of the polymer; a^2 and m_s are the mean-square length and the molar weight of a segment of the statistical model; and β is the binary cluster integral between any pair of the segments and vanishes at $T = \Theta$. As far as one assumes that the intra- and the interchain long-range interactions are identical in nature, the A_2 is also expressed in terms of the parameters as defined by eq 1-3.^{1-3,26}

In case of extending such concepts to the studies on copolymer solutions, one ought to ask, first of all, whether the concepts of the Θ conditions may stand valid for copolymer solutions as well, and then to ask whether it is possible to apply the procedures proposed for homopolymer solutions to deduce the parameters A and B of copolymer solutions. The results of our preliminary study¹⁷ showed that the answers to the above questions are both affirmative, at least for solution of *random* copolymers, although the evidence is somewhat indirect. Thus, in this section we shall attempt to apply the proposed procedures to the present copolymer data.

Intrinsic Viscosity at Θ Conditions. At the Θ condition where $A_2 = 0$, the intrinsic viscosity, $[\eta]_\Theta$, may be written in the form

$$[\eta]_\Theta = K_0 M^{1/2} \quad (4)$$

where $K_0 = \Phi_0' (\langle S^2 \rangle_0 / M)^{3/2} = \Phi_0' A^3$; Φ_0' is the viscosity constant²⁷ at the Θ condition. Thus one would expect that $[\eta]_\Theta$ is proportional to $M^{1/2}$ so far as the statistics of random flight prevails at the Θ condition, and, hence, the K_0 may be regarded as constant. It is seen in Table VI that $[\eta]_\Theta / M_w^{1/2}$ is constant, or nearly constant, in each system, satisfying the relation given in eq 4. Figure 4 shows plots of $[\eta]_\Theta / M_w^{1/2}$ vs. $M_w^{1/2}$, from which values of K_0 may be readily estimated.

Use of eq 4 to deduce $\langle S^2 \rangle_0$ (or A^2) requires the knowledge of Φ_0' . As far as we are aware, such knowledge

(23) G. V. Schulz and R. Kirste, *Z. Physik. Chem.*, **30**, 171 (1961).

(24) T. A. Orofino and J. W. Mickey, Jr., *J. Chem. Phys.*, **38**, 2512 (1963); T. A. Orofino, *ibid.*, **45**, 4310 (1966).

(25) G. V. Schulz and H. Baumann, *Makromol. Chem.*, **60**, 120 (1963).

(26) B. H. Zimm, *J. Chem. Phys.*, **14**, 164 (1946); B. H. Zimm, W. H. Stockmayer, and M. Fixman, *ibid.*, **21**, 1716 (1953).

(27) P. J. Flory and T. G. Fox, *J. Am. Chem. Soc.*, **73**, 1904 (1951); see also ref 1, Chapter 14.

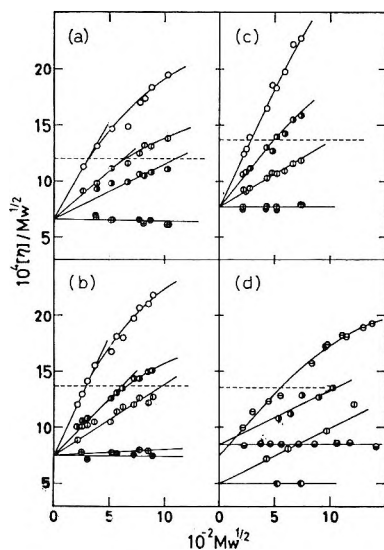


Figure 4. Plots of $[\eta]/M_w^{1/2}$ vs. $M_w^{1/2}$ for ST-MMA copolymers (a) SM3; (b) SM5 and 5'; and (c) SM7 and 7' in various solvents (for sample codes, see Table V; solvents are identified by the symbols as in Figure 3); and for (d) ST-MMA azeotropic copolymers in butanone at 25.0°, \ominus ;¹⁵ PST in 1-CB at 40.8°, \bullet ;¹⁶ and in cyclohexane at 34.5°, \ominus ;⁶ PMMA in DEM at 30.0°, \oplus ; and in 1-CB at 40.8°, \bullet .¹⁶ The dashed lines show the values of $\alpha_\eta^3 = 1.8$ for the copolymer data.

is not yet available for the ST-MMA copolymer- Θ solvent systems or any other copolymer systems. However, in view of the evidence that the Φ' constant of the copolymers in good solvents is in agreement with that for homopolymer-good solvent systems,^{15,16} it would not be unreasonable to employ the value of Φ'_0 currently established for homopolymer- Θ solvent systems. Thus, by employing the value of $10^{-21}\Phi'_0 = 39.4$ ($[\eta]$, dl/g) given by Pyun and Fixman,²⁸ we calculate $A^2 (= \langle S^2 \rangle_0/M_w)$ for the three copolymer samples. We also calculate the steric factor σ , which is a measure of the hindrance to internal rotations about the skeletal link and is defined as

$$\sigma = (A^2/A_f^2)^{1/2}$$

with A_f^2 being the mean-square statistical radius of a hypothetical freely rotating chain.^{3,4,29} All the values obtained are summarized in Table VIII.

Analysis of $[\eta]$ Data in Good Solvents. The intrinsic viscosity in good solvents may be written in the Flory-Fox viscosity equation²⁷

$$[\eta] = \Phi'(\langle S^2 \rangle/M)^{3/2} M^{1/2} \quad (5)$$

or by the more explanatory form

$$[\eta] = K_0 M^{1/2} \alpha_\eta^3 = K_0 M^{1/2} (\Phi'/\Phi'_0) \alpha^3 \quad (6)$$

Therefore, eq 6 combined with an appropriate expression for α_η^3 vs. z or for α^3 and (Φ'/Φ'_0) vs. z can be expected to allow an estimate of A and B from $[\eta]$ vs. M data for a given solvent. We test the present data by a few of the currently proposed methods^{5,7,10}

Table VIII: Values of the Parameters, K_0 , A^2 , and σ for ST-MMA Random Copolymers

Code	m	$10^4 K_0$, dl/g	$10^{18} A^2$, cm ²	σ
PMMA	0.00	5.0 ± 0.5	5.42 ± 0.30	1.87 ± 0.07
SM3	0.29	6.6 ± 0.2	6.52 ± 0.15	2.05 ± 0.02
SMA ^a	0.546	7.5	7.12	2.15
SM5, 5'	0.56	7.5 ± 0.2	7.12 ± 0.15	2.15 ± 0.02
SM7, 7'	0.70	7.7 ± 0.2	7.24 ± 0.15	2.17 ± 0.02
PST	1.00	8.0 ± 0.5	7.45 ± 0.30	2.22 ± 0.05

^a Data for ST-MMA azeotropic copolymer by Stockmayer, *et al.*¹⁵

in order (i) to estimate K_0 from the good solvent data to see if there is any specific solvent effect on K_0 , and then (ii) to estimate B for each copolymer-solvent pair.

The simplest and the easiest to manipulate among those methods is that due to Stockmayer and Fixman,⁹ which is written as

$$[\eta]/M^{1/2} = K_0 + 1.55\Phi'_0 B M^{1/2} \quad (7)$$

The numerical constant, 1.55, is so chosen as to attain agreement with first-order perturbation theory.^{30,31} The plots of $[\eta]/M_w^{1/2}$ vs. $M_w^{1/2}$ for the present and some other relevant data^{15,16} are shown in Figures 4a-d. It is to be noted that $[\eta]/M_w^{1/2}$ is not a linear function of $M_w^{1/2}$, particularly for toluene data. The use of eq 7 should be limited to rather poor solvent data; otherwise it would result in an overestimate of K_0 . Nevertheless, it is seen that the plots for each copolymer can be reasonably well extrapolated to $M_w^{1/2} = 0$, so as to yield a common value of K_0 .

Utiyama¹⁶ and Inagaki, Suzuki, and Kurata¹⁰ suggested a viscosity equation based on the Ptitsyn equation³² for α^2 vs. z combined with a semiempirical relation^{33,34} between α and α_η , such as $\alpha_\eta^3 = \alpha^{5/2}$. The equation due to Inagaki, *et al.*,¹⁰ reads

$$([\eta]/M^{1/2})^{4/5} = K_0^{4/5} \{ 3.68 + [1 + 9.36(B/A^3) M^{1/2}]^{2/3} \} / 4.68 \quad (8)$$

The authors further suggested that for very good solvent systems the unity in the right-hand side of eq 8 can be

(28) C. W. Pyun and M. Fixman, *J. Chem. Phys.*, **42**, 3838 (1965).

(29) For vinyl polymers, $10^8 A_f = 1.256/M_u^{1/2}$, with M_u being the molar weight of the repeating unit. For the ST-MMA copolymers with ST mole fraction m , we use $M_u = 104m + 100(1 - m)$.

(30) H. Yamakawa and M. Kurata, *J. Phys. Soc. Japan*, **13**, 94 (1958); M. Kurata and H. Yamakawa, *J. Chem. Phys.*, **29**, 311 (1958).

(31) M. Fixman, *ibid.*, **23**, 1656 (1955); **36**, 3123 (1962).

(32) O. B. Ptitsyn, *Vysokomol. Soedin.*, **3**, 1673 (1961); the equation is known to fit second-order perturbation theory.

(33) It is interesting to note that recent calculation by Fixman³⁴ is well approximated by the relation $\alpha_\eta^3 = \alpha^{2.62}$ over a considerably large span of z .

(34) M. Fixman, *J. Chem. Phys.*, **45**, 785, 793 (1966).

neglected with respect to $9.36z$, and plots of $([\eta]/M^{1/2})^{1/2}$ vs. $M^{1/2}$ can be extrapolated linearly to yield K_0 . The authors emphasize that the linear extrapolation should be applied only to good solvent data for which $\alpha_\eta^3 > 2.2$, and, hence, as such is complementary to eq 7. The present data are examined also by eq 8. We find that K_0 for toluene data are in good agreement with those determined in the Θ solvents. The plots for DEM and 1-CB solutions, both of which are poorer solvents than toluene, show nonlinear dependence on $M_w^{1/2}$, as anticipated.

Berry has proposed still another viscosity equation on the basis of his experimental data on the correlations of A_2 , $\langle S^2 \rangle$, $[\eta]$, and M for solutions of monodisperse polystyrene in decalin and in toluene.^{6,7} He suggested that nonlinear functions of $[\eta]/M^{1/2}$ vs. $M^{1/2}$, often encountered in good solvent systems, may be approximately split into two linear relations within the range of

$$[\eta]/M^{1/2} = K_0 + 0.60\Phi_0'BM^{1/2} \quad (9)$$

for $1 < \Delta_\eta^3 < 1.6$

$$[\eta]/M^{1/2} = 1.40K_0 + 0.30\Phi_0'BM^{1/2} \quad (10)$$

for $1.8 < \alpha_\eta^3 < 4$

α_η^3 specified as above. These equations retain the form of eq 7, but the constants are replaced by empirical ones. Therefore, so far as the estimates of K_0 are concerned, the conclusions are the same to those of eq 7. However this is obviously not true for the estimates of B . The author further suggested that these two equations may also be approximated by a single relation⁷

$$([\eta]/M^{1/2})^{1/2} = K_0^{1/2}\{1 + 0.42\Phi_0'B(M/[\eta])\} \quad (11)$$

The present data are also tested by eq 11; such plots are shown in Figure 5. Again we find that the plots for each copolymer can be extrapolated linearly to $M_w/[\eta] = 0$ to give the values of $K_0^{1/2}$ which are in practical agreement with each other and with those obtained in the Θ solvents, except for a few occasions. Such an exception is, for example, seen for the system SM7, 7' in toluene, in which an extrapolation placing emphasis on all the experimental points (*cf.* the dashed line in Figure 5c) would result in an unusually small value $K_0^{1/2}$. Although the origin of such a discrepancy is not clear, it appears that this does not reflect the specific solvent effect, but rather implies an inadequate use of eq 11 (*e.g.*, the range of M is not adequate).

As we have shown above, one can expect that the use of the different methods to complement each other would minimize the uncertainties in the estimate of K_0 . Then we may conclude that the values of K_0 (and presumably A) for the copolymers are not greatly influenced by the specific solvent effect and may be regarded as constant within the accuracy of, say, $\pm 10\%$.

Next we turn to the problem of estimating the values of B from $[\eta]$ vs. M data. Obviously any of the vis-

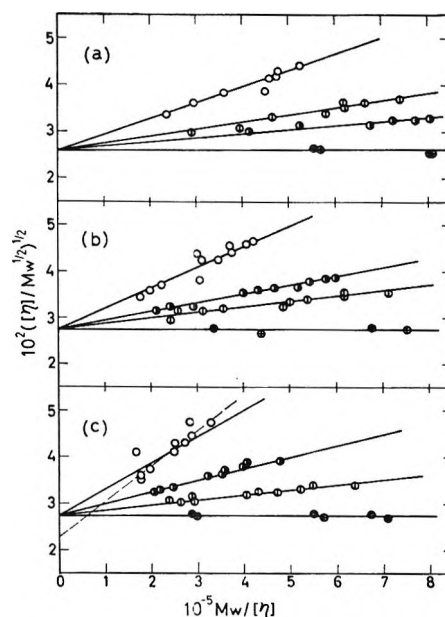


Figure 5. Plots of $([\eta]/M_w^{1/2})^{1/2}$ vs. $M_w/[\eta]$ for (a) SM3; (b) SM5 and 5'; and (c) SM7 and 7' in various solvents, as identified by the symbols as in Figure 3.

cosity equations, such as eq 7-11, can be expected to afford the estimates of B , but the results are never in agreement between those obtained by the different methods unlike for the estimates of K_0 . For example, if the results of eq 7 and 9 are compared, the latter equation predicts the values of B to be larger, by a factor of 2.58, than the former equation does for the same data. The situation is the same for other equations. Needless to say, it is not possible to judge from $[\eta]$ vs. M data alone as to which one of these different methods would yield most appropriate estimates of B . The question shall be discussed in the next section in relation with the analysis of A_2 vs. M data.

Analysis of A_2 Data. It is well known that A_2 in the vicinity of Θ may be written as

$$A_2 = 4\pi^{3/2}N_a B[1 + O(B)] \quad (12)$$

with

$$B = B_0(1 - \theta/T) \quad (13)$$

where B_0 is a parameter proportional to Flory's entropy of mixing parameter.¹ Hence, one can estimate values of B in the vicinity of Θ by using eq 12 combined with the temperature coefficient of A_2 at $T = \Theta$.

$$(\partial A_2/\partial T)_{T=\Theta} = (4\pi^{3/2}N_a/\Theta)B_0$$

The data in cyclohexanol are analyzed by these equations; values of B are given in Table IX, where T is arbitrarily taken as 80.0° .

It has been shown that the interaction parameters for good solvent systems can be deduced from A_2 vs. M data, just as from $[\eta]$ vs. M data, by using an appropriate closed expression for A_2 as a function of A , B ,

Table IX: Values of Long-Range Interaction Parameters B from $[\eta]$ and A_2 Data

Code	Solvent ^a	$10^{10}B$	
		From $[\eta]$ (eq 11)	From A_2 ^b
PMMA	TOL	60.5 ^c	...
	DEM	21.1	...
	1-CB	0	0
	CHL (80°)	...	0.7
SM3	TOL	82.3	120 ± 10
	DEM	50.0	...
	1-CB	21.5	27 + 5
	CHL (80°)	...	20
SM5, 5'	TOL	97.0	140 ± 10
	DEM	25.0	...
	1-CB	43.0	60 ± 10
	CHL (80°)	...	17
SM7, 7'	TOL	120	140 ± 10
	DEM	24.0	...
	1-CB	55.6	70 ± 10
	CHL (80°)	...	16
PST	TOL	107.5 ^c	110 ^c
	DEM	0	...
	1-CB	38.0 ^d	...
	CHL (80°)	...	-2.3

^a For abbreviations, see Table VI. ^b Data for CHL are treated by eq 12 and 13 taking arbitrarily $T = 80^\circ$; others are treated by the correlations of A_2 vs. M proposed by Berry.⁶ ^c Data in ref 6 and 7. ^d Data in ref 16.

and z .⁸ Such expressions may be most conveniently cast into the form³⁵

$$A_2M^{1/2} \equiv \Psi(\bar{z})(\langle S^2 \rangle / M)^{1/2} = \Psi(\bar{z})A^3\alpha^3 \quad (14)$$

$$\bar{z} = z/\alpha^3 \quad (15)$$

The function $\Psi(\bar{z})$, representing the extent of mutual penetration of approaching polymer coils,⁸ is known to be a function which in general increases monotonically from zero (at $\bar{z} = 0$, the Θ condition) and reaches an asymptotic limit as \bar{z} increases. A number of approximate expressions³⁶ for $\Psi(\bar{z})$ have been proposed so far, and any of the appropriate combinations of $\Psi(\bar{z})$ and α^3 can be expected to afford estimates of A and B from A_2 vs. M data in good solvents. Each of these equations predicts more or less different dependence of $A_2M^{1/2}$ on z , and thus the application of the different equations to a given set of A_2 vs. M data obviously yields different estimates of (B/A^3) value; the situation is the same as we are confronted with the analysis of the α_η^3 vs. z relations. Again it is not possible to judge from A_2 vs. M data alone which one of them is the most appropriate.

As far as one assumes that both the intrachain and the interchain long-range interactions are identical in nature, one would expect that the values of B derived from different sources, $[\eta]$ and A_2 data, should be in

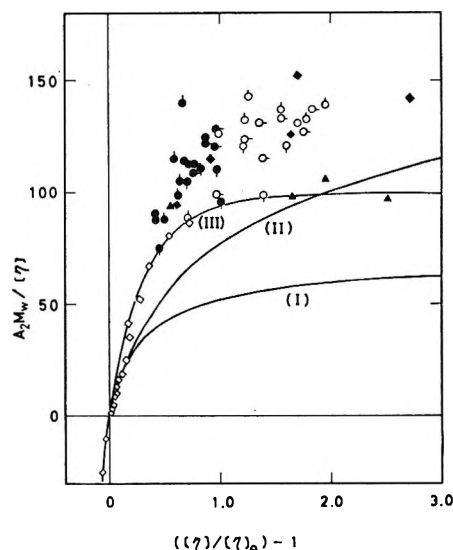


Figure 6. Plots of $A_2M_w/[\eta]$ vs. $[\eta]/[\eta]_\Theta - 1$ for ST-MMA copolymers in toluene and in 1-CB (solvents are identified by the symbols as in Figure 3, and the polymers by pip up for SM3, pip right for SM5 and 5', and pip down for SM7 and 7'); and for PST in toluene^{6,7} (\blacktriangle), PMMA in 1-CB²³ (\diamond), and also in other good solvents²³ (\blacklozenge). Curves I and II represent theoretical correlations predicted by the Fixman-type approximations and by the Ptitsyn-type approximations,⁸ and curve III represents empirical correlation due to Berry^{6,7} (see text).

agreement with each other (of course, if the particular combination of the theories on $[\eta]$ and A_2 employed for the analysis is adequate). The correlation between $[\eta]$ and A_2 can be most conveniently examined by the familiar dimensionless ratio of $A_2M/[\eta] = [\Psi(\bar{z})/\Phi_0']$ (α^3/α_η^3) as a function of, say, $([\eta]/[\eta]_\Theta) - 1 = \alpha_\eta^3 - 1$. Figure 6 shows such plots for the present copolymer data together with relevant homopolymer data. Figure 6 also shows two theoretical curves (referred to as curve I and II), which are constructed by combining the $[\eta]$ equations (7 and 8) with two of the variation theories on A_2 both due to Kurata, *et al.* [eq 74–76, and eq 10 and 101 in ref 8], respectively. Thus the first combination, curve I, is essentially related to the Fixman variation theory³¹ of the excluded effect, and the second one, curve II, to the Ptitsyn variation theory.³² Figure 6 also shows a curve due to Berry's empirical correlations^{6,7} (referred to as curve III), which is constructed by combining Berry's A_2 equation [*e.g.*, eq 1 and 2 in ref 6a, or eq 7, 13, and 20 in ref 6b] and the $[\eta]$ equation (11).

Certain interesting features emerge from the figure. First of all, it is seen that the experimental points show

(35) In eq 15, the expansion factor, α , for an isolated chain should be replaced by an expansion factor, α_2 , for a chain in a bimolecular cluster. They are often approximated as $\alpha_2 = \alpha$. For detailed discussion, see ref 3, 6, and 8.

(36) We do not list all the references here. Summaries and detailed discussion on them are found in several articles. See, for example, ref 2, 3, 6, and 8.

a fairly definite tendency, in spite of the fact that they include both the copolymer and homopolymer data from different sources. Thus the behavior of the homopolymers and the random copolymers are indistinguishable in this respect. Curve I appears to predict correct behavior in the vicinity of the origin and a subsequent rapid approach to an asymptotic limit. However, the theoretical limit of $A_2M/[\eta] = 60$ is far too small in comparison with the observed value of about 100–140. Consequently, the analysis based on eq 7 and the corresponding A_2 equation [e.g., eq 88 in ref 8], both of which are essentially based on the Fixman type approximation for the excluded volume effect,³¹ would result in the inconsistency between the viscometric and osmometric B values, namely the former is smaller than the latter by a factor of 2, at least.

Curve II also appears to predict correct initial behavior and subsequent increase of $A_2M/[\eta]$ up to about 120, which is about a right order of magnitude.³⁷ However, a rather significant discrepancy between the theory and the experiments is found in the range of intermediate values of α_η^3 , namely, the experimental values appear to approach to the asymptotic limit more rapidly than does the theoretical curve II. Hence it would be expected that the analysis based on eq 8 and the corresponding A_2 equation [e.g., such as eq 10 and 101 in ref 8] would result in a larger discrepancy between the viscometric and the osmometric values of B for moderately good solvent systems, rather than for very good solvent systems. In fact, from the analyses of the present data by these equations, we find that for 1-CB solutions the values of B by the A_2 method are about twice as large as those by the $[\eta]$ method, and for toluene solutions, the former are about 20–50% larger than the latter.

The inconsistencies found in the above two cases appears to be too large to be disregarded simply by attributing them to the usual poor experimental accuracy of A_2 data. This sort of inconsistency has already been reported for several homopolymer systems^{5–8} and is apparently real in the copolymer systems. To explain these inconsistencies between the theories and the experiments, a refinement of the theories of the excluded volume effect appears to be necessary. More recent theories^{34, 38, 39} show that the functions $\alpha(z)$ and $\alpha_\eta(z)$, which are consistent with the perturbation theories^{30, 31} in the vicinity of $z = 0$, increase more slowly in the range of large Z than the behavior predicted, for example, by the Ptitsyn equation or by eq 8.

Finally, curve III appears to represent most closely the general tendency of the observed behavior of $A_2M/[\eta]$ vs. $([\eta]/[\eta]_0) - 1$, besides in the vicinity of the origin.⁴⁰ This apparent success may not be surprising, since curve III plotted in this form is nothing else but Berry's experimental data themselves. Then perhaps

the difference found between the asymptotic values of $A_2M/[\eta]$ in Berry's data (about 100) and in the present data (about 130–140) should deserve more careful examination. The difference between them would be expected to result in the discrepancy in the estimates of B by the two methods using Berry's equations by a factor of 20–40%. A most likely reason one would think of is the difference in the polydispersity of the samples. It has been known that the heterogeneity correction usually requires the reduction of Φ_0' by a factor of a few to 10%.^{1, 3} which increases the limit of $A_2M/[\eta]$ by the same factor. The fact that the present A_2 data are obtained by osmometry could be another reason; usually the osmometric A_2 are slightly larger than the light-scattering A_2' , particularly for polydisperse samples. Anyway, in view of achieving consistent estimates of the values of B from both $[\eta]$ and A_2 data, the use of eq 11 and the A_2 equations proposed by Berry [e.g., eq 1 and 2 in ref 6a] would be expected to give most satisfactory results. The results of the estimates of B for the present systems are given in Table IX.

The Short-Range and the Long-Range Interaction Parameters as Functions of Monomer Composition. Figure 7a shows plots of the steric factor, σ^2 , vs. ST content m taken from the data in Table VIII. Previously Stockmayer, *et al.*,¹⁵ proposed a simple relation for the values of A^2 of a binary copolymer as

$$A^2 = x(A^2)_1 + (1 - x)(A^2)_2 \quad (16)$$

where the subscripts 1 and 2 again denote the quantities characteristic to the parent homopolymers (in this case PST and PMMA, respectively). Equation 16 can be readily rewritten as

$$\sigma^2 = m(\sigma^2)_1 + (1 - m)(\sigma^2)_2 \quad (16')$$

Apparently the experimental values are slightly larger than those expected from (16'). The characteristic ratio of the ST-MMA copolymer continuously increases with increasing ST content. Brant, Miller, and Flory⁴¹ reported that for the random coil configurations of copolypeptides, for example, of glycine-alanine copolymer, introduction of minor proportion of glycine residues into poly-L-alanine brings about a

(37) The subsequent slow but unlimited increase of curve II is apparently the result of the assumption that $\alpha_\eta^3 = \alpha^{5/2}$ in eq 8, which would be valid in the range of initial to intermediate values of α_η^3 , but would lose its significance in the range of very large α_η^3 . The present data do not cover such a range of large α_η^3 , hence we disregard this behavior of curve II.

(38) Z. Alexandrowicz, IUPAC Symposium on Macromolecular Chemistry, Tokyo-Kyoto, 1966, preprint VI-20.

(39) H. Yamakawa, private communication.

(40) The large initial slope of curve III is apparently the result of the use of eq 11 for constructing the curve. The $[\eta]$, eq 11, is supposed to be good only for data confined in good solvents and with large M .

(41) D. A. Brant, W. G. Miller, and P. J. Flory, *J. Mol. Biol.*, **23**, 47 (1967); W. G. Miller, D. A. Brant, and P. J. Flory, *ibid.*, **23**, 67 (1967).

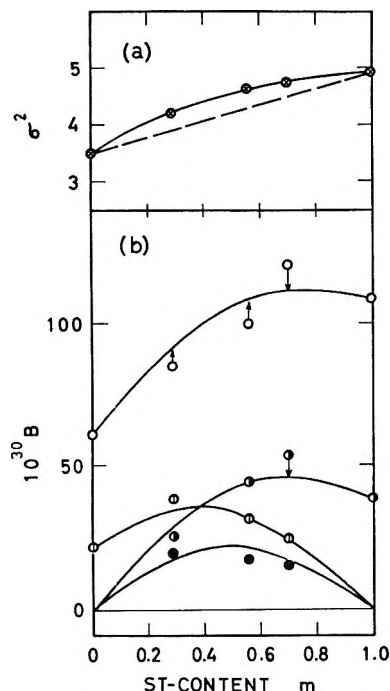


Figure 7. (a) Plots of the steric factor σ^2 vs. ST content m ; the dashed line represents the plots due to eq 16'; (b) plots of the long-range interaction parameter B vs. m in various solvents as identified by the symbols as in Figure 3. Solid curves represent the plots due to eq 17'.

disproportionately large decrease in the average chain dimensions. Apparently introduction of ST units into PMMA chains results in an opposite effect, *i.e.*, a disproportionately large increase in the average dimensions. Utiyama¹⁶ also reported the similar tendency for the ST-MMA random copolymers, and even the appearance of a maximum in the A^2 vs. m relation. This result might presumably be due to overestimation of K_0 (and hence of A^2), which were obtained from $[\eta]$ data in a good solvent, but not by $[\eta]_0$ data as in the present study. Obviously, the unperturbed dimensions of copolymers are a function of the monomer composition, the sequence length distribution, and the stereochemical configurations.^{4,41} Miller, Brant, and Flory⁴¹ have treated the effects of these factors theoretically for random-coil copolypeptides, in which the choice of approximate representation of the dependence of the conformation energy on bond rotation angles is essential. For ST-MMA copolymers, it has been suggested that the analysis of the sequence length distribution and the stereochemical configurations is partly possible from the knowledge of the monomer reactivity ratios¹³ and nmr spectra.⁴² However, the knowledge of the conformational energy functions is not yet available, and the analysis of the type such as suggested by Miller, *et al.*,⁴¹ is not applicable for the ST-MMA copolymers. Previously Utiyama¹⁶ suggested, by avoiding the estimation of the conformational energy functions, that the unperturbed dimensions of copolymer chains may be described

by six different parameters, each ascribed to one of the six different types of triadic sequences (*e.g.*, I-I-I, I-I-II, I-II-I, etc.). More recently, Nomura and Iwachido⁴³ suggested that the unperturbed dimensions may be described by three parameters each ascribed to one of the diadic sequences, and hence the deviations of σ^2 from those given by eq 16', *i.e.*, the extra short-range interactions, are assumed to be proportional to the population of diadic sequence of unlike monomers. These types of analyses, however, have little theoretical foundations and it is difficult to evaluate the significance of the parameters derived by those procedures. The quantitative analyses on the dependence of the unperturbed dimensions of copolymers on the molecular factors, such as mentioned above, are subject to further investigation on both experimental and theoretical aspects.

We now turn to the question on the long-range interaction parameters. As we have discussed in the previous section, the proposed theories for estimating B appear to be unsatisfactory and, hence, the values of B listed in Table IX would have only limited significance. Nevertheless, the data (or any other set of data estimated by different methods) distinctly show the presence of extra long-range interactions and their dependences on composition might have some qualitative significance. Figure 7 shows plots of B vs. m taken from Table IX. In Figure 7, the maxima are seen at nearly equimolar composition in toluene and in CHL solutions, and in other solvents, 1-CB and DEM, the maximum positions shift to the good solvent sides, namely, in 1-CB to the ST-rich side and in DEM to the MMA-rich side.

Stockmayer, *et al.*,¹⁵ and Utiyama¹⁶ suggested that the parameter B for a random (binary) copolymer may be written as a quadratic function of composition as

$$B = m^2 B_1 + (1 - m)^2 B_2 + 2m(1 - m) B_{12} \quad (17)$$

where B_{12} is a parameter representing the (long-range) interactions between unlike monomers. As a zeroth-order approximation, the extra interaction term, $\Delta B_{12} = B_{12} - (B_1 + B_2)/2$, is supposed to be dependent on the solvent only through its molal volume and is characteristic to the type of monomer species.^{15,18} We calculated the values of B_{12} from the data such as listed in Table IX and obtained $10^{30} B_{12} = 125$ for toluene solutions, 60 for DEM solutions, 69 for 1-CB solutions, and 40 for CHL (80°) solutions. From these values, the extra interaction parameters ΔB_{12} are calculated as $10^{30} \Delta B_{12} = 41$ in toluene, 50 in DEM, 50 in 1-CB, and

(42) See, for example, U. Johnsen, *Ber. Bunsenges. Physik. Chem.*, **70**, 320 (1966).

(43) H. Nomura and T. Iwachido, IUPAC Symposium on Macromolecular Chemistry, Tokyo-Kyoto, 1966, preprint VI-52.

40 in CHL. The values of B for the ST-MMA copolymers in various solvents may be approximated as

$$B = mB_1 + (1 - m) B_2 + 2m(1 - m) 10^{-30}(45 \pm 5) \quad (17')$$

The solid curves in Figure 7b show the relations given by eq 17' with the values of B_1 and B_2 , such as shown in Table IX. It appears that the crudest assumption in the form of eq 17 for the long-range interaction parameter B for the random copolymer is reasonably

satisfactory. The positive value of ΔB_{12} implies the existence of repulsive interactions between ST and MMA units. The result is reasonably understood by the fact that PST and PMMA are incompatible with each other.¹⁵

Acknowledgment. We wish to thank Messrs H. Suzuki and H. Ohnuma for their competent help in carrying out the experiments. We are indebted to Dr. H. Utiyama for disclosing to us the valuable results of his unpublished experiments. Y. M. wishes to thank Teijin and Co. for a fellowship grant.

Diffuse Double Layer of Weak Electrolytes with Field Dissociation

by Gilles G. Susbielles and Paul Delahay

Department of Chemistry, New York University, New York, New York 10003 (Received July 10, 1967)

The differential capacity of the diffuse double layer and the difference of potential across the diffuse double layer are computed as functions of the charge density on the metal for a metal in contact with a weak electrolyte. Field dissociation is considered without restriction on the field, and the field dependence of the dielectric constant in the diffuse double layer is introduced. The solution is obtained by numerical analysis after transformation into an initial value problem. Initial values are obtained by a perturbation treatment similar to but not identical with that reported by Bass. Application is made to 0.1 M acetic acid in water and to 0.5 M potassium acetate in glacial acetic acid. Departure from the Gouy-Chapman theory, as a result of field dissociation, is rather small for aqueous solution but significant for glacial acetic acid (20-30% change of differential capacity of diffuse double layer).

The effect of dissociation of a weak electrolyte on its diffuse double layer at an interface with a metal was recently treated by Bass.¹ This problem was also attacked by Sanfeld and Steichen-Sanfeld,² by means of a local thermodynamic method,² with the aim of calculating the dissociation constant in the double layer for a small charge density. The Bass treatment is applicable only for a small charge density on the electrode, as it uses a small perturbation method. This author calculated that the integral capacity of the diffuse double layer at the point of zero charge is changed only by 0.03 $\mu\text{F cm}^{-2}$ as a result of the field dissociation for 1 M acetic acid in water. The field effect should increase with the charge density. It is determined here by numerical analysis, without the limitation imposed by a small perturbation method for a 1-1 weak electrolyte. The Onsager equation for field dissociation is introduced in its Bessel function form, and variation of the dielectric constant in the diffuse double layer is taken into account.

Statement of Problem. The problem is clearly stated by Bass¹ and is formulated by the following system of

differential equations (his eq 14) written in this author's notations (see Appendix)

$$-d(p + n)/d\xi + f(p - n) - ads/d\xi = 0 \quad (1)$$

$$-d(p - n)/d\xi + f(p + n) - bds/d\xi = 0 \quad (2)$$

$$d^2s/d\xi^2 = R(\chi s - np) \quad (3)$$

$$df/d\xi = (1/2)(p - n) \quad (4)$$

The boundary conditions are discussed by Bass and are for $\xi \rightarrow \infty$: $n = 1$, $p = 1$, $f = 0$, $s = c_0(\infty)/c(\infty)$, and $\chi = K_0/c(\infty) = c(\infty)/c_0(\infty)$. The last two conditions are not independent ones if one selects the first three conditions as independent ones. Moreover, the flux of neutral species must be equal to zero for $\xi = 0$ and $\xi \rightarrow \infty$. The last condition for $\xi \rightarrow \infty$ is not an independent one.

The problem is to calculate the differential capacity of the diffuse double layer and the difference of poten-

(1) L. Bass, *Trans. Faraday Soc.*, **62**, 1900 (1966).

(2) A. Sanfeld and A. Steichen-Sanfeld, *ibid.*, **62**, 1907 (1966).

tial across the diffuse double layer as functions of the charge density on the electrode. Four independent conditions are stated above, and prescribing the charge density gives a fifth condition. This is all that is needed, since the system of eq 1-4 includes three differential equations of the first order and one equation of the second order.

We must know from the start the dependence of the dissociation constant, K , as a function of the field, E , contained in function χ . We shall use Onsager's result in its Bessel function form,^{3,4} which is valid without limitation on the field. We also must consider the dependence of the dielectric constant, ϵ (see parameter λ) on the field. We shall use the empirical equation proposed and tested by Grahame.^{5,6}

Initiation of the Solution by a Perturbation Method for Small-Field Dissociation

Since three independent boundary conditions are given for $\xi \rightarrow \infty$, the solution must be initiated for large values of ξ for a selected value of the charge density on the metal. The solution is then obtained step by step to $\xi = 0$ and is adjusted by iteration to satisfy the following conditions: (a) the flux of the neutral species at $\xi = 0$ must be equal to zero; and (b) the charge density on the metal, as computed by application of Gauss' theorem, must be equal to the value initially selected.

The field is very small for sufficiently large values of ξ , and Bass' perturbation method can be applied to initiate the solution. This method was applied in a somewhat different way than its original version and will be discussed. The functions n , p , f , s , and χ are written as the sum of their values at $\xi \rightarrow \infty$ plus a term corresponding to the Gouy-Chapman theory plus a term accounting for field dissociation. Thus

$$p = 1 - k_1 \exp(-\xi) + p^{(2)} \quad (5)$$

$$n = 1 + k_1 \exp(-\xi) + n^{(2)} \quad (6)$$

$$f = k_1 \exp(-\xi) + f^{(2)} \quad (7)$$

$$s = c_0(\infty)/c(\infty) + s^{(2)} \quad (8)$$

$$\chi = [c(\infty)/c_0(\infty)] \{1 + r |k_1| \exp(-\xi) + (1/3)r^2 k_1^2 \exp(-2\xi) + rf^{(2)}\} \quad (9)$$

where k_1 is an arbitrarily selected constant $p^{(2)}$, $n^{(2)}$, $f^{(2)}$, and $s^{(2)}$ are the terms corresponding to field dissociation. It is to be noted that once k_1 is selected, the charge density on the electrode is determined by the Gouy-Chapman theory. Equation 9 is an expanded form of Onsager's equation for the effect of field dissociation. It is stressed that this expansion is valid only when $r |k_1| \exp(-\xi)$ is so small that the next term to those included in eq 9 is negligible. This condition for the application of eq 9 can always be fulfilled, regardless of the charge density on the electrode, because it suffices to select a sufficiently large value of ξ . The advance

beyond Bass at this stage consists in the retention of the term rf^2 .

Introduction of eq 5-9 into eq 1-4 yields, on neglecting terms of order, $\exp(-2\xi)$

$$-d[p^{(2)} + n^{(2)}]/d\xi - ads^{(2)}/d\xi = 0 \quad (10)$$

$$-d[p^{(2)} - n^{(2)}]/d\xi + 2f^{(2)} - bds^{(2)}/d\xi = 0 \quad (11)$$

$$df^{(2)}/d\xi = (1/2)[p^{(2)} - n^{(2)}] \quad (12)$$

$$d^2s^{(2)}/d\xi^2 = R \{r |k_1| \exp(-\xi) + rf^{(2)} + [c(\infty)/c_0(\infty)] s^{(2)} - [p^{(2)} + n^{(2)}]\} \quad (13)$$

Elimination of $p^{(2)}$ and $n^{(2)}$ yields a system of two differential equations of the second order in $f^{(2)}$ and $s^{(2)}$. Further elimination results in the equation

$$d^4s^{(2)}/d\xi^4 - (1 + \alpha^2) d^2s^{(2)}/d\xi^2 + \alpha^2 s^{(2)} = -(b/2) Rr ds^{(2)}/d\xi \quad (14)$$

A solution of the form $\exp(m\xi)$ is introduced in eq 14 and the parameter m thus obeys the equation

$$(m^2 - 1)(m^2 - \alpha^2) = -(b/2) Rrm \quad (15)$$

for which only the negative roots need be retained. The positive roots were introduced artificially by double differentiation. The left-hand side of eq 15 is represented by the curve in Figure 1 and the right-hand side by a straight line, the slope of which depends on the sign of b . In the case treated by Bass,¹ the slope of this line is so small⁷ that the solutions are very near the intersections of the curve with the abscissa axis, namely $m = -1$ and $m = -\alpha$.

Thus the solution of eq 14 is of the form

$$s^{(2)} = k_2 \exp(m_1\xi) + k_3 \exp(m_2\xi) \quad (16)$$

where m_1 and m_2 are the negative roots of eq 15; k_2 and k_3 are constants which must be such that the flux of neutral species at $\xi = 0$ is equal to zero, and the charge density on the electrode, as computed by application of the Gauss theorem, has the same value as the charge density corresponding to the initially selected value of k_1 in eq 5-9. These constants are adjusted by trial and error, and the validity of the above two conditions is verified, once the complete solution is obtained by numerical analysis (see below).

Once $s^{(2)}$ is determined, one computes $f^{(2)}$ by returning to the system of eq 10-13, from which one has eliminated $p^{(2)}$ and $n^{(2)}$, *i.e.*, from

(3) H. S. Harned and B. B. Owen, "The Physical Chemistry of Electrolytic Solutions," 2nd ed, Reinhold Publishing Co., New York, N. Y., 1950, p 111, eq 4, 7, 26.

(4) The linearized form used by Bass¹ is only valid for low field and cannot be applied here in the general solution.

(5) D. C. Grahame, *J. Chem. Phys.*, **18**, 903 (1950); see eq 17.

(6) The value $m = 0.5$ was selected in the application of the Grahame equation. Other parameters were the same as those selected by this author.

(7) Values considered by Bass were: $\alpha = 5^{1/2}$, $a = 1$, $b = -1$, $R = 5$, and $r = 0.07$.

$$d^2f^{(2)}/d\xi^{(2)} - f^{(2)} + (b/\varepsilon) ds^{(2)}/d\xi = 0 \quad (17)$$

The functions p^2 and n^2 are then readily obtained.

The above solution is more general than the one given by Bass,¹ because no restriction is imposed on r [although there is a restriction imposed on $r|k_1| \exp(-\xi)$; see above]. Bass also did not impose the condition that the charge density on the electrode, at open circuit, should remain the same when field dissociation is allowed to occur. Thus, one condition was lacking in his solution, as he noted.⁸

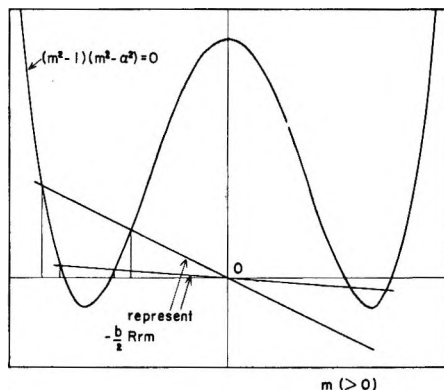


Figure 1. Diagram pertaining to eq 15. Intercepts of curve with abscissa axis are: $-\alpha$, -1 , $+1$, $+\alpha$ ($\alpha > 0$). The line with the smaller slope corresponds to a case analogous to that treated by Bass.¹

Solution by Numerical Analysis for any Field Dissociation

The above treatment yields the solution of the system of eq 1-4 for one large value of ξ . Further treatment involves the solution of an initial value problem for the system of eq 1-4, using the just computed solution as initial values. It is convenient to transform eq 1-4 into a new system having as independent variable $v = \exp(-\xi)$, thus changing the ξ domain into v domain extending from 1 to 0. Equations 1-4 then become

$$d(p + n)/dv + f(p - n)/v + ads/dv = 0 \quad (18)$$

$$d(p - n)/dv + f(p + n)/v + bds/dv = 0 \quad (19)$$

$$df/dv = -(p - n)/2v \quad (20)$$

$$vds/dv + v^2d^2s/dv^2 = R(\chi s - pn) \quad (21)$$

The Runge-Kutta method⁹ with a fourth-order approximation was applied in the following examples, using for K , as was already noted, the complete Onsager equation before expansion. Moreover, a field-dependent dielectric constant, as previously indicated, was used throughout the calculation. An iteration procedure was applied to determine the proper values of the constants k_2 and k_3 of eq 16 which satisfy the conditions stated below that equation. The charge density on the metal was computed by numerical integral by means of Gauss'

theorem using a field-dependent dielectric constant. Likewise, the difference of potential across the diffuse double layer was obtained by numerical integration of the field.

As an additional check, it was verified that the solution obtained by numerical analysis verified the particular solution of eq 1-4 already given by Bass (his eq 15), namely

$$2 - (p + n) + f^2 + ac_0(\infty)/c(\infty) - as = 0 \quad (22)$$

The differential capacity of the diffuse double layer was calculated by

$$C = (1/f)(df/dx) \quad (23)$$

$$= -(p - n)/2\lambda f$$

A complete program using 150,000 memory units for the CDC6600 computer is available.¹⁰ This program includes subroutines for integration of the field and the charge density by the Gauss method. This method requires interpolation and its use requires of the order of 50,000 memory units. A less precise integration method was not desirable because of error accumulation, especially because the field effect is not very large.

Application

The above method of calculation was applied to 0.1 M acetic acid in water and to 0.5 M potassium acetate in glacial acetic acid. These two examples are representative of solvents with high and low dielectric constant, respectively. Results are summarized in Tables I and II.

The intervals in the numerical calculations were the same for both cases and were in the v domain: 800 intervals for $1/8000 \leq v \leq 0.1$ and 720 intervals for $0.1 \leq v \leq 1$. The smaller intervals for the low values of v were required because of the singularity for $v = 0$. These numbers of intervals were sufficient to obtain five significant figures, even for $v = 1$, *i.e.*, in the region where the field varies rapidly with distance. The total computer time for these two cases was approximately 4 hr, including some substantial preliminary calculations. Determination of k_2 and k_3 by trial and error required repeated running of the program, especially for the first point, and accounted for a major share of the computer time.

Table I shows that the effect of field dissociation is

(8) He stated¹ just below his eq 24: "the theoretical value of $f^{(2)}(0)$ cannot be obtained without specific assumptions about the mechanism by which the space charge is generated." Professor Bass stated in a private communication that our condition is certainly a reasonable and useful one, but he is not certain that it is necessarily true independently of the mechanism by which the unperturbed double layer is established.

(9) J. M. McCormick and M. G. Salvadori, "Numerical Methods in FORTRAN," Prentice-Hall, Inc., Englewood Cliffs, N. J., 1964, pp 100-102.

(10) G. G. Susbielles and P. Delahay, Technical Report No. 4 to the Office of Naval Research, Contract Nonr-285(65), New York University, New York, N. Y., June 1967.

Table I: Comparison of Differential Capacity C , and Difference Potential, ϕ_2 , across Diffuse Double Layer for the Gouy-Chapman Theory and Present Work for 0.1 M Acetic Acid^a

Charge density on metal, $\mu\text{C cm}^{-2}$	ϕ_2 (G-C), mv	ϕ_2 (this work), mv	C (G-C), $\mu\text{F cm}^{-2}$	C (this work), $\mu\text{F cm}^{-2}$
0	0	b	8.3425	8.4296
0.4268	45.136	44.452	11.773	11.905
0.8558	74.10 \pm	72.691	18.628	18.795
1.7131	107.60	105.32	34.371	34.637
2.5679	127.97	125.23	50.671	51.264
3.4123	142.43	139.38	66.937	68.230
4.2728	153.91	150.48	83.580	86.040
5.1178	163.14	159.67	99.959	104.23

^a $T = 25^\circ$, $D_+ = 9 \times 10^{-5} \text{ cm}^2 \text{ sec}^{-1}$, $D_- = D_0 = 1.1 \times 10^{-5} \text{ cm}^2 \text{ sec}^{-1}$, $\lambda = 33.54 \text{ \AA}$, $K_0 = 1.764 \times 10^{-5} \text{ mol l.}^{-1}$, and $\epsilon = 78.56$. All data are the same as those selected by Bass,¹ except those involving the concentration. (His results pertain to 1 M acetic acid.) ^b Not computed because too close to zero.

Table II: Same Comparison as in Table I but for 0.5 M Potassium Acetate in Glacial Acetic Acid^a

Charge density on metal, $\mu\text{C cm}^{-2}$	ϕ_2 (G-C), mv	ϕ_2 (this work), mv	C (G-C), $\mu\text{F cm}^{-2}$	C (this work), $\mu\text{F cm}^{-2}$
0	0	...	1.5648	1.9099
0.1000	53.487	42.366	2.4934	2.9886
0.1957	83.360	63.195	4.1195	4.8072
0.2656	98.147	74.708	5.4028	6.2521
0.4043	119.09	94.973	8.0234	9.3544
0.5373	133.49	105.76	10.574	12.785
0.6268	141.33	110.82	12.300	15.456
0.7188	148.32	116.82	14.070	18.267

^a $T = 25^\circ$, $D_+ = 1.958 \times 10^{-5} \text{ cm}^2 \text{ sec}^{-1}$, $D_- = 1.090 \times 10^{-5} \text{ cm}^2 \text{ sec}^{-1}$, $D_0 = 1.024 \times 10^{-5} \text{ cm}^2 \text{ sec}^{-1}$, $\lambda = 35.06 \text{ \AA}$, $K_0 = 7.1 \times 10^{-7} \text{ mol l.}^{-1}$, and $\epsilon = 6.20$. The diffusion coefficients are only rough estimates and are equal to those for the ions and molecule in water. This is certainly incorrect, but values are not available. Note that the D 's could be multiplied by a constant without affecting the results. (See definition of a , b , and R .)

not negligible, but certainly not large. It should be noted that the capacity in Table I pertains only to the diffuse double layer. Since this capacity is in series with that of the compact double layer (near 20 $\mu\text{F cm}^{-2}$), experimental capacities should not be affected by more than 1%, at the most, for the upper range of the charges in Table I.

Table II for glacial acetic acid shows a much more pronounced effect than for aqueous solution. Calculations

were not carried out for higher charge densities because the relative increase of the differential capacity with charge density varies quite slowly.

The extent of field dissociation depends on the parameter b , i.e., on $D_0(1/D_+ - 1/D_-)$. The effect becomes larger when $1/D_+ - 1/D_-$ increases. The situation, from this point of view, is more favorable for the case of Table I than for that of Table II, but the high dielectric constant of the solvent in Table I renders field dissociation quite minor.

Finally, the following points should be noted:¹¹ (a) the validity of Onsager's theory is limited to dilute solutions (perhaps $<10^{-2} \text{ mol l.}^{-1}$); (b) consideration of a variable dielectric constant is not in complete agreement with Onsager's theory; and (c) Onsager used the activity dissociation constant whereas Bass and we introduced the concentration dissociation constant.

Acknowledgment. This work was supported by the Office of Naval Research. The authors are indebted to Professor L. Bass, University of Queensland, for most helpful comments.

Appendix: Notations

a	$D_0(1/D_+ + 1/D_-)$
b	$D_0(1/D_+ - 1/D_-)$
c_{\pm}	Concentration of cation or anion
$c(\infty)$	Bulk concentration of cation or anion
c_0	Concentration of neutral species
$c_0(\infty)$	Bulk concentration of neutral species
D_{\pm}	Diffusion coefficient of cation or anion
D_0	Diffusion coefficient of neutral species
$\pm e$	Charge of cation or anion
E	$-\text{grad } \phi$ (ϕ potential; $\phi \rightarrow 0$ for $\xi \rightarrow \infty$)
f	$eE\lambda/kT$
k	Boltzmann constant
K	Dissociation constant of weak electrolyte
K_0	Dissociation constant of weak electrolyte in the bulk of solution
n	$c_-/c(\infty)$
p	$c_+/c(\infty)$
r	$e^2/2\epsilon\lambda kT$
R	$\lambda^2 A c(\infty)/D_0 (= (D_+ + D_-)/2D_0$ according to Onsager; see Bass ¹)
s	$c_0/c(\infty)$
T	Absolute temperature
v	$\exp(-\xi)$
α	$+\{R[c(\infty)/c_0(\infty) + a]\}^{1/2}$
ϵ	Dielectric constant
λ	$[\epsilon kT/8\pi e^2 c(\infty)]^{1/2}$
ξ	x/λ (x distance from plane of closest approach)
χ	$K/c(\infty)$

(11) We are indebted to one of the referees for calling these points to our attention.

The Effect of Hydrogen Bonding on the Kinetics of the Urethane Reaction

by Adolf E. Oberth and Rolf S. Bruenner

Solid Propellant Research Division, Aerojet-General Corporation, Sacramento, California 95813 (Received July 18, 1967)

It is shown that the rate of the uncatalyzed urethane reaction depends essentially on the concentration of the polymeric (self-associated) alcohol. Solvents, by breaking down the polymer, cause a retardation of the reaction rate, the magnitude of which can be related directly to the hydrogen-bonding power of the solvent. The high reactivity of the polymeric alcohol is attributed to the polarization (weakening) of the H-O bond in the polymer. The degree of polarization, as indicated by the shift of the H-O absorption band to lower frequencies, is even more pronounced in amine-alcohol complexes, which, accordingly, are strong catalysts for the urethane reaction. Infrared studies have shown that the formation of the amine-alcohol complex and hence the catalytic activity depends not only on the basicity of the amine but also on steric factors. Dialkylanilines, *e.g.*, do not form hydrogen-bonded alcohol-amine complexes and do not catalyze the reaction, while pyridine, of approximately equal basicity, does form a complex and also accelerates the reaction. Based on kinetic data, combined with ir studies, a reaction mechanism is proposed which properly accounts for the effect of solvents and amines on the reaction rate. It is proposed that the rate-determining step in the urethane reaction is the rearrangement of the alcohol-isocyanate complex to the urethane. The kinetic description of the reaction centers in the calculation of the concentration of the alcohol-isocyanate complex in the reaction mixture. Such calculations are shown to reasonably portray the urethane reaction over the whole range of reactant concentrations.

Introduction

The rate of the uncatalyzed urethane reaction is strongly affected by the reaction medium. For example, in 0.15 *M* solution, the reaction between 1-butanol and phenylisocyanate proceeds about 500 times faster in heptane than in dioxane. Since the solvent plays such a large role, it is not surprising that changes of the concentration of the reactants have a more or less pronounced effect on the rate constant, depending on the type of solvent in which the reaction is run. Nevertheless, it is presently believed that the alcohol has a catalyzing effect on the rate of the urethane formation.¹ This alcohol catalysis goes back to the work of Baker,² who explained the concentration dependence of the rate constant by a mechanism where the isocyanate forms first an activated complex with one molecule of alcohol which then reacts with a second alcohol molecule to form the product. The dependence of k_0 , expressed as a second-order rate constant, on the alcohol concentration is given by Baker as

$$k_0 = k_1 k_3 (\text{ROH}) / [k_2 + k_3 (\text{ROH})] \quad (1)$$

An analogous expression, where the alcohol in the numerator is replaced by the base, has been given by Baker for base catalysis. It is derived from a similar mechanism where an intermediate base-isocyanate complex replaces the alcohol-isocyanate complex.

Obviously, k_0 is not a true second-order constant, but in spite of this, it has become conventional to report kinetic data in form of second-order constants in the literature,¹ and most investigators obtained their data from second-order plots.²⁻⁵ Today, Baker's mechanism

is probably the most widely accepted one, although Ephraim, *et al.*⁴ and notably Robertson and Stutchbury³ showed that the kinetic data obtained in other solvents than the dibutyl ether and benzene, used by Baker, were not compatible with the above mechanism.

Ephraim and coworkers⁴ pointed out the strong influence of the nature of the solvent on the rate of the reaction. The effect on the rate was correlated with the dielectric constant of the solvent, while deviations from second-order kinetics were attributed to hydrogen bonding between alcohol and solvent molecules. The kinetic expression presented by Ephraim

$$\begin{aligned} -\frac{d(\text{RNCO})}{dt} = & k_1(\text{RNCO})(\text{ROH})^2 + \\ & k_2(\text{solvent})(\text{RNCO})(\text{ROH}) + \\ & k_3(\text{ROCONHR})(\text{ROH})(\text{RNCO}) \quad (2) \end{aligned}$$

is difficult to apply because it contains the concentration of the monomeric alcohol species, while the second-order plots are based on the total alcohol concentration. The concentration of the monomeric alcohol is unknown and should be expressed as a function of the

(1) J. H. Saunders and K. C. Frisch, "Polyurethanes, Chemistry and Technology," Part I, Interscience Publishers, Inc., New York, N. Y., 1962, p 138.

(2) J. H. Baker and J. Gaunt, *J. Chem. Soc.*, 9, 19 (1949).

(3) W. G. P. Robertson and J. E. Stutchbury, *ibid.*, 4000 (1964).

(4) S. Ephraim, A. E. Woodward, and R. B. Mesrobian, *J. Am. Chem. Soc.*, 80, 1326 (1958).

(5) E. Dyer, H. A. Taylor, S. J. Mason, and J. Samson, *ibid.*, 71, 4106 (1949).

total alcohol concentration, since its concentration in the reaction mixture is only a small fraction of the total alcohol. Robertson and Stutchbury³ reported that neither Baker's mechanism nor the above equation agreed with their experimental results.

Although many investigators^{3,4,6,7} felt that hydrogen bonding was responsible for deviations from predicted behavior, none has spent much effort to prove this premise or to derive kinetic expressions which include hydrogen bonding between the alcohol and the solvent.

Baker, *et al.*,⁸ the only group who studied this interaction in di-*n*-butyl ether and benzene solutions, concluded that "the main factor for the increased reaction velocity in benzene is the presence of monomeric alcohol molecules which have a much greater facility to attack the intermediate (alcohol-isocyanate) complex, than have the alcohol-ether solvated or associated (alcohol) molecules, exclusively present in the di-*n*-butyl ether." This explanation, although quite convincing at a first glance, does not hold up with other solvents. For example, a 0.15 *M* solution of alcohol in nitrobenzene shows a very high concentration of the monomeric form, yet the rate of the urethane reaction in this solvent is slightly slower than in the dibutyl ether, where practically no monomeric alcohol is detectable.

The present paper is an attempt to shed more light on the role of hydrogen bonding, as well as to explain the complex kinetics of the urethane reaction by taking this interaction into account.

Experimental Section

Materials. All solvents used in kinetic runs were first checked for reactivity toward phenyl isocyanate in a blank run. Only if they showed none or less than 0.2% consumption of the isocyanate over a period of 24 hr at 25.5° were they used for kinetic determinations. Some of the solvents, which failed this test even after the purification described below, were refluxed with toluene diisocyanate and a small amount of ferric acetylacetonate catalyst for 24 hr, and subsequently distilled twice from a column. This treatment was found to be particularly necessary for the purification of butyl acetate, which contains copious amounts of butyl alcohol. 1,2-Dichloroethane, chloroform, carbon tetrachloride, ethyl acetate, *n*-heptane, acetonitrile, benzene, and toluene were spectroquality grade, purchased from Matheson Coleman and Bell Co., and were used without further purification. All the remaining solvents, with the exception of diethylene glycol dimethyl ether were reagent grade chemicals. Dibutyl ether, dioxane, diethylene glycol dimethyl ether, and xylene were refluxed over sodium until the latter became shiny and then fractionated. Dibutyl ether (bp 141.5°), dioxane, (bp 101°) diethylene glycol dimethyl ether (bp 162°), and the fraction of xylene boiling between 138 and 140° were used. Methyl ethyl ketone was

stored over anhydrous Na₂SO₄ and distilled, bp 79–80°. Nitrobenzene, bp 90° at 12.9 mm, was redistilled prior to use. Butyl *N*-phenylcarbamate was prepared from stoichiometric quantities of 1-butanol and phenyl isocyanate. The product was twice recrystallized from hot heptane, mp 60.5°. Phenyl isocyanate was purified according to Baker,² and butyl isocyanate was purified as described previously.⁹

Procedure. All reactions were run in a thermostat controlled to ±0.05° by a Tecam Tempunit (La Pine Scientific Co.). The fast reactions (50% completion in less than 30 min) were run in 250-ml iodine flasks in approximately 25-ml portions containing all ingredients except the isocyanate. The reaction was begun by addition with an automatic pipet of 2 ml of the isocyanate and stopped after the desired time interval by the addition of 5 ml of dibutylamine. Vigorous stirring (with a magnetic stirring bar) kept the maximum exotherm below 0.5°. Each flask yielded one point of the conversion-time curve. Liberal application of silicon grease on the ground-glass stopper of the iodine flask prevented moisture from entering the reaction vessel during the kinetic runs—which is the greatest potential source of error. For these reactions, reproducibility was generally within ±2%. The very fast reactions, such as undiluted phenyl isocyanate-butanol (total volume of reaction mixture about 3.5 ml) and phenyl isocyanate in excess butanol were run in approximately 250-ml stainless steel vessels to provide better dissipation of heat.

The slower reactions were run in a 1-l. flask with generally 275 ml of total reaction mixture. After certain time intervals, aliquots were withdrawn and transferred to erlenmeyer flasks containing a measured amount of dibutylamine dissolved in benzene.

The unreacted isocyanate was determined by back titrating the excess dibutylamine with 1 *N* HCl using a mixed indicator (0.060 % bromocresol green and 0.040 % methyl red in methanol) with a sharp color change at pH 5.1. Usually 50–100 ml of methanol was added to the reaction mixture prior to titration in order to maintain a homogeneous solution during titration.

The infrared spectra shown in the figures were obtained in a Beckman IR9 spectrophotometer, using sodium chloride cells. This instrument was also used to determine the rate of the urethane reaction in excess isocyanate, using the increase of the carbonyl band at 1743 cm⁻¹ to follow the course of the reaction. It was also used to double check the rates of the reaction at low concentrations (0.15 *M*). The agreement between the two methods was within 10% or better.

(6) M. Sato, *J. Org. Chem.*, **27**, 819 (1962).

(7) J. W. Baker and J. Gaunt, *J. Chem. Soc.*, **28** (1949).

(8) J. W. Baker, M. M. Davies, and J. Gaunt, *ibid.*, **24** (1949).

(9) R. S. Bruenner and A. E. Oberth, *J. Org. Chem.*, **31**, 887 (1966).

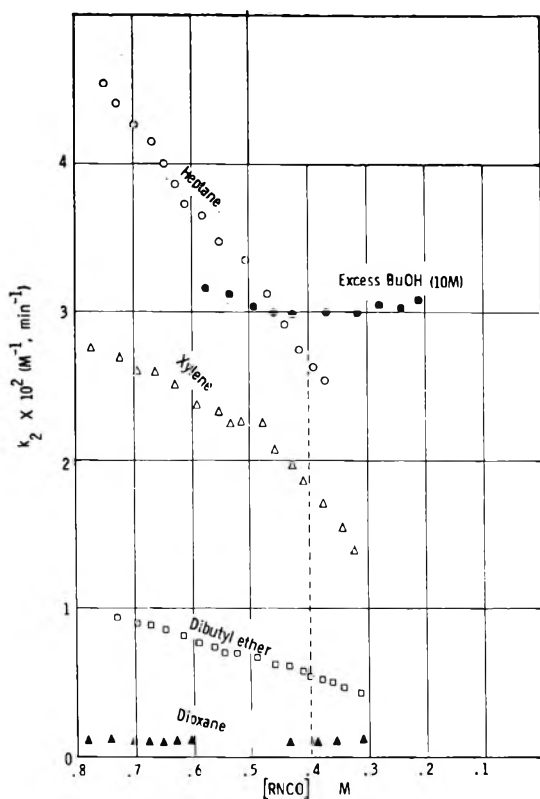


Figure 1. Trend of k_2 values with conversion in some solvents: $T = 25.5^\circ$, and initial concentration, $\text{PhNCO} = \text{BuOH} = 0.8 M$.

Evaluation of Test Data

The order of the uncatalyzed urethane reaction appears to depend on the solvent (see Figure 1). Furthermore, the magnitude of the rate constant depends on the concentration of the reactants, as was already shown by Baker² (*cf.* Table I). Nevertheless, it has become customary in the literature to report velocity data in terms of an "apparent second-order constant." In order to obtain meaningful data, we established the experimental rate at any time of the reaction by drawing a conversion-time curve. The rate of the reaction at a given time is simply the slope of the curve at that time normalized to units of concentration and time. The slope of the curve was established with the aid of a mirror device. The apparent second-order constant was obtained by dividing the experimentally determined rate, $r = du/dt$ by the product of the concentrations of the reactants at that instant of conversion, or $k_2 = (du/dt)/[(\text{ROH})(\text{RNCO})]$. The thus established k_2 values were plotted against conversion, as shown in Figure 1. Extrapolation to zero conversion (zero time) yields the initial rate constant. This procedure is perhaps less accurate than a second-order plot and also requires somewhat more work, but it gives the experimental rate constants, which are unbiased by any presupposed mechanism. All the rate constants listed were obtained this way. The precision of the k_2

Table I: Apparent Second-Order Rate Constant for the Butanol-Phenyl Isocyanate Reaction in Various Solvents at 25°

Solvent	Dielectric constant at 25°	BuOH-PhNCO, M	$-10^3 k_2, M^{-1} \text{min}^{-1}$	
			Initial	At 50% conversion
Cyclohexane	2.02	0.15	39	...
<i>n</i> -Heptane	1.93	0.15	39	...
		0.35	40	33
		0.80	44	28
Carbon tetrachloride	2.24	0.15	18	...
		0.80	39	28
<i>m</i> -Xylene	2.37	0.15	11	...
		0.80	26	19
Toluene	2.38	0.15	9.2	...
		0.80	25	22
Chlorobenzene	5.71	0.15	8.0	...
Benzene	2.28	0.15	5.8	...
		0.80	22	18
Chloroform	4.81	0.15	2.9	...
		0.80	18	16
1,2-Dichloroethane	10.65	0.15	2.7	...
		0.80	17.4	11
Dibutyl ether	3.08	0.15	2.1	...
		0.25	3.7	3.2
		0.50	6.5	4.7
		0.80	9.5	5.8
		1.00	11.5	6.5
		1.20	13.5	7.0
Nitrobenzene	36.1	0.15	1.8	...
Methyl ethyl ketone	18.4	0.15	0.33	...
		0.80	1.85	1.1
Butyl acetate	5.01	0.15	0.26	...
		0.80	2.5	2.0
Ethyl acetate	6.4	0.15	0.18	...
		0.80	2.4	1.6
Tetrahydrofuran	8.20	0.15	0.17	...
Acetonitrile	38.8	0.15	0.15	...
		0.80	1.3	1.25
Dioxane	2.21	0.15	0.08	...
		0.80	1.0	0.95
Diethylene glycol dimethyl ether	...	0.80	0.79	0.70

values, as estimated from repeat experiments, is $\pm 10\%$.

Results

The effect of different solvents on the butanol-phenyl isocyanate reaction is shown in Table I. The data have been arranged in order of decreasing rate constants. For the reactions run at higher concentrations than $0.15 M$, the apparent second order-rate constant at 50% conversion is given also. In all reactions the second-order constant decreased with conversion. This decrease is most pronounced in the inert solvents, while in very dilute solutions in strongly retarding solvents second order appears to be followed. The exceptions reported by Ephraim,⁴ *i.e.*, a noted increase of the rate constant with conversion, for the urethane reaction in butyl acetate and dioxane were probably caused by impurities. In the case of butyl acetate, the "auto-

catalysis" was probably the result of residual butanol in the solvent, since the effect vanished after the solvent had been refluxed with toluene diisocyanate, as described in the Experimental Section. The dioxane apparently decomposed slowly in the presence of the reactants, which may have had an effect on the reaction. This decomposition was indicated by a strong yellowing of the reaction mixture, which was absent in other solvents. At higher concentrations of the reactants, where the reactions proceed fast, the decomposition of dioxane is not as noticeable and k_2 decreases also with conversion. In general, it may be stated that the decrease of the rate constant during reaction is most pronounced in inert solvents where the reaction is fastest, while k_2 is nearly constant in the most retarding solvents (see Figure 1). The magnitude of the effect depends also on the initial concentration of the reactants, decreasing with dilution of the reaction mixture.

Table I shows the large effect of the concentration of the reactants on the rate constant. Again, there is a strong influence stemming from the nature of the solvent. In the most inert solvents such as heptane, k_2 changes little with dilution, and its magnitude is comparable to that of the excess butanol-phenyl isocyanate reaction (Table II), while in the more interfering solvents, k_2 decreases sharply with dilution. Replacement of part of an inert solvent by an interfering solvent will lower the rate constant as shown in Figure 2. Comparison of the effect of the addition of butyl-N-phenyl carbamate on the rate constant of the

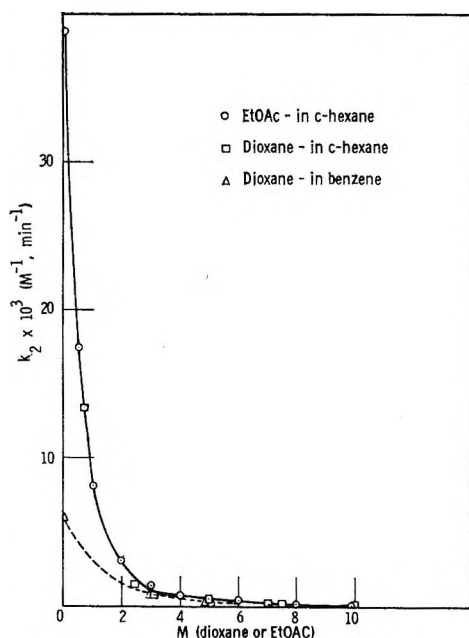


Figure 2. Retardation of rate for alcohol-isocyanate reaction by increasing concentrations of hydrogen-bonding solvents (ethyl acetate, dioxane) in hydrocarbons (cyclohexane, benzene); concentration of *n*-butanol and phenyl isocyanate = 0.15 *M* each; and temperature = 25.5°.

butanol-phenyl isocyanate reaction in two different solvents indicates acceleration in the more interfering di-*n*-butyl ether and retardation in the comparatively inert benzene (Tables III and IV). Thus at least for the butanol-phenyl isocyanate reaction, there is no indication of autocatalysis. This explains the generally observed decrease of the rate constant with increasing conversion, since the reactants are replaced by the interfering urethane.

Table II: Apparent Second-Order Rate Constant for the Undilute Butanol-Phenyl Isocyanate Reaction at 25°

BuOH, <i>M</i>	PhNCO, <i>M</i>	$10^3 k_2, M^{-1} \text{ min}^{-1}$	
		Initial	50% Conversion
0.15	9.12	6.2	6.8
10.9	0.15	50	...
5.0	5.0	40	21

Table III: Effect of Some Additives on the k_2 Values at 50% Conversion of the BuOH-PhNCO Reaction (both 0.8 *M*) in Benzene at 25.5°

Additive	Concentration of additive, <i>M</i>	$10^3 k_2, M^{-1} \text{ min}^{-1}$ 50% conversion
None	...	1.8
Butyl N-phenylcarbamate	1.6	1.7
Dibutyl ether	1.6	1.3
Methyl ethyl ketone	0.8	1.6
	1.6	1.3
Acetonitrile	1.6	0.9
Dioxane	1.6	0.8
Diethylene glycol dimethyl ether	1.6	0.5

Table IV: Effect of the Addition of Butyl N-Phenylcarbamate and an Equal Volume of Benzene on k_2 of the Reaction between BuOH and PhNCO (both 0.5 *M*) in Dibutyl Ether at 25.5°

Additive	Concentration, <i>M</i>	$10^3 k_2, M^{-1} \text{ min}^{-1}$
None	...	4.7
$C_6H_5NHCOOC_4H_9$	0.5	5.5
Benzene	1.24	5.8

In most solvents, the k_2 value decreases with dilution of the alcohol concentration. However, in inert solvents like the alkanes, the initial k_2 value increases with dilution. Table V compares the effect of dilution on the initial apparent second-order constant for some representative solvents. Some of such data are also plotted in Figure 3.

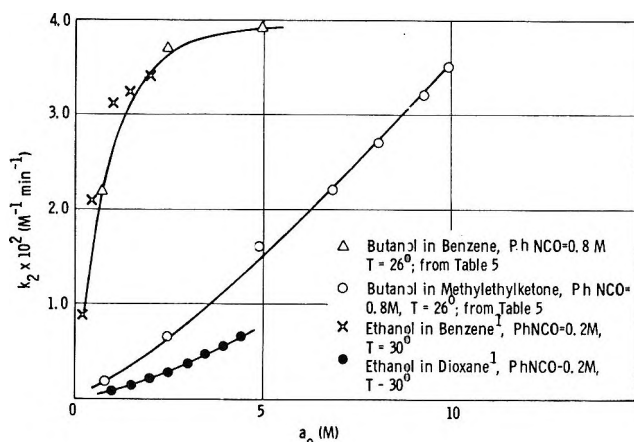


Figure 3. k_2 values vs. initial alcohol concentration in some solvents. [1, Data by courtesy of W. G. P. Robertson and J. E. Stutchbury, and *J. Chem. Soc.*, 4000 (1964)].

Table V: Dependence of Initial k_2 Value on the Alcohol Concentration of the BuOH-PhNCO Reaction in Some Solvents^a

BuOH, M	$10^3 k_2, M^{-1} \text{min}^{-1}$		
	Methyl ethyl ketone	C ₆ H ₆	Heptane
10 (no solvent)	3.5	3.5	3.5
9.3	3.2
8.1	2.7
6.9	2.2
5	1.6	3.9	...
2.5	0.66	3.7	3.9
0.8	0.18	2.2	4.7
0.5	6.3
0.2	7.0

^a Temperature 25.5°; PhNCO = 0.8 M.

The data of Table I show only a moderate correlation with the dielectric constant of the solvent. Some of the most interfering solvents, such as ethyl acetate, dioxane, methyl ethyl ketone, and esters, possess a rather low dielectric constant. It, therefore, was of interest to investigate whether the influence of the solvents on the rate constant would not more closely correlate with the state of association of the alcohol in the respective solvent. The infrared absorption in the region from 3700 to 3200 cm^{-1} gives information about the state of association of the alcohol in the reactant solution.¹⁰ Infrared spectra were obtained for 0.15 M solutions of butanol in all the solvents listed in Table I. Based on these spectra, the solvents can be roughly divided into three groups.

In the first group, which comprises all the inert solvents (alkanes, CCl_4), the absorption attributed to the polymeric form (self-associated alcohol, degree of association > 2) predominates. The absorption spectrum shown for butanol in cyclohexane in Figure 4

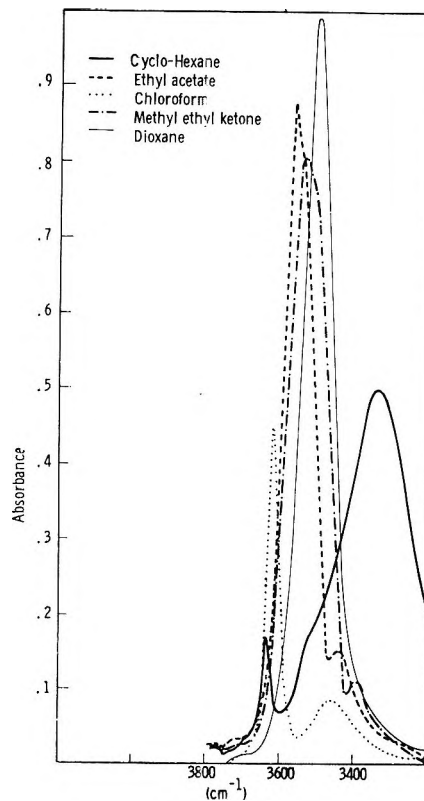


Figure 4. Infrared absorption spectra of 1-butanol (0.15 M) in various solvents: $T = 26^\circ$ and $d = 0.4$ mm.

(broad band, maximum about 3350 cm^{-1}) may serve as an example for this group. In these solvents, as well as in the undilute excess BuOH mixture, the urethane reaction proceeds fastest. In the second group of solvents, the alcohol shows predominantly the monomeric band. Benzene, chloroform, and nitrobenzene are examples (see Figures 4 and 5). The monomeric form of the alcohol exhibits a sharp narrow band whose maximum ranges from 3650 cm^{-1} to 3590 cm^{-1} .¹⁰ Increasing solvent interaction in this class of solvents is revealed by an increasing intensity of the monomeric band with a simultaneous slight shift toward lower frequencies, while the polymeric absorption decreases. Mecke¹¹ has used this behavior to arrange solvents according to their "proton-attracting power." The same order, which has been given by Mecke, is also found in Table I, only that here the solvents have been arranged according to their effects on the rate of the urethane reaction. An example of this change of the spectrum of butanol in three solvents differing in their hydrogen bonding power is shown in Figure 5. The rate of the urethane reaction, therefore, appears to be a sensitive means to detect small differences in the hydrogen bonding power of solvents. For example, dilute solutions of the reactants in such solvents as xylene,

(10) L. J. Bellamy, "The Infra-Red Spectra of Complex Molecules," John Wiley and Sons, Inc., New York, N. Y., 1959, p 96.

(11) R. Mecke, *Discussions Faraday Soc.*, 9, 161 (1950).

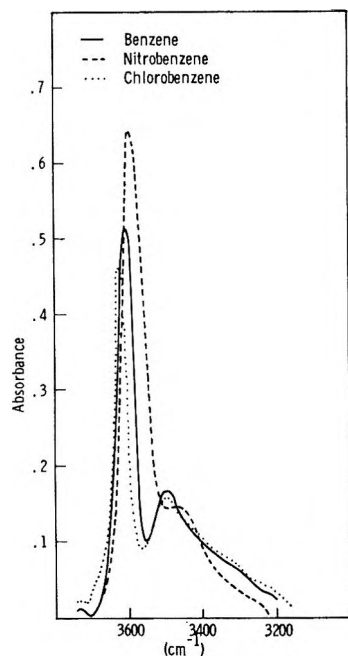


Figure 5. Absorption of 1-butanol (0.15 *M*) in benzene, nitrobenzene, and chlorobenzene: $T = 27^\circ$ and $d = 0.4$ mm.

toluene, or benzene show quite marked differences in the magnitude of the rate constant, while the absorption spectra of alcohol in these solvents are nearly the same.

If butanol is diluted by dioxane, an altogether different spectroscopic behavior is observed. There is little evidence of a monomeric alcoholic species; instead, the broad absorption band of the polymer peaking at around 3350 cm^{-1} is gradually shifted toward 3500 cm^{-1} , simultaneously increasing in sharpness. When this stage is reached, further dilution does not alter the absorption spectrum. The new absorption band at 3500 cm^{-1} is attributed to single-bridge compounds, *i.e.*, the alcohol-solvent complex. Ethers, ketones, nitriles, and carboxylic acid esters, unless they possess very large hydrocarbon radicals or are otherwise sterically hindered, have this type of absorption behavior and constitute group 3 of this classification. Some representative spectra are shown in Figure 4. In these solvents, the rate of the urethane reaction is slowest.

Contemplation of Figures 6 and 7 reveals the greater affinity between butanol and dioxane than between butanol and benzene. This is evident from the preponderance of the alcohol-dioxane complex absorption at comparatively low dioxane concentrations. Therefore, one may conclude that dioxane possesses a higher hydrogen-bonding power than the other two solvents. Similar tests were also conducted with other solvent mixtures and gave the order shown in Table I. It should be noted that this order is on an equal volume basis.

The inflection at 3500 cm^{-1} shown in the cyclohexane

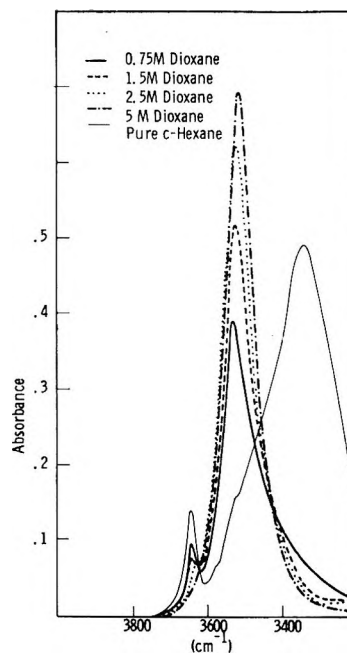


Figure 6. Absorption spectra of 1-butanol in cyclohexane-dioxane mixtures: $T = 27^\circ$ and $d = 0.4$ mm.

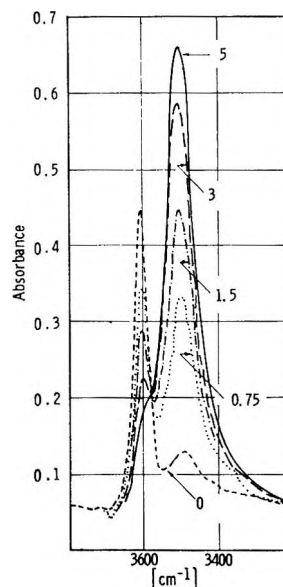


Figure 7. Absorption of butanol (0.15 *M*) in benzene-dioxane mixtures: numbers refer to molarity of dioxane, $T = 26^\circ$, and $d = 0.4$ mm.

spectrum and also the low-intensity absorption bands around 3500 cm^{-1} of the benzene-alcohol solutions may be due to an alcohol-alcohol dimer, which absorbs at this frequency.¹²

According to its effect on the butanol spectrum (Figure 8), phenyl isocyanate may be grouped with solvents like nitrobenzene (group 2), as far as its hydrogen-bonding power is concerned. Thus it appears that in excess phenyl isocyanate, the alcohol is essentially

(12) L. P. Kuhn, *J. Am. Chem. Soc.*, **74**, 2492 (1952).

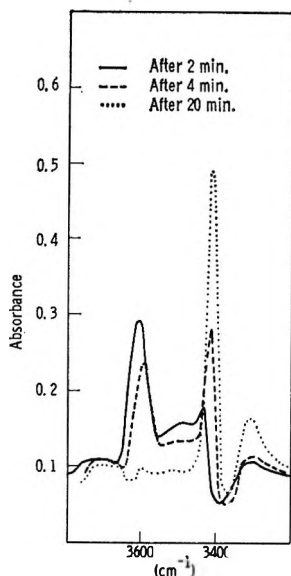


Figure 8. Absorption of 1-butanol (0.15 M) in phenylisocyanate as a function of time: $T = 27^\circ$ and $d = 0.4$ mm.

monomeric, while in the mixture containing the excess butanol as the solvent, the alcohol must be practically completely self-associated. Since the isocyanate is only moderately hydrogen bonding with the alcohol, the undilute 1:1 mixture of the reactants will, at the beginning of the reaction, contain predominantly the polymeric species and reacts accordingly fast. During the reaction, the formed urethane (band at 3400 cm^{-1} , belonging to the N-H stretch, Figure 8) associates with the alcohol, so that the rate constant rapidly decreases to reach $2.1 \times 10^{-2}\text{ M}^{-1}\text{ min}^{-1}$ at 50% conversion. A similarly steep decrease of the rate constant during the reaction is also encountered in all inert solvents for the same reason. In excess alcohol, k_2 remains essentially constant (pseudo-first order).

The absorption spectrum of phenyl isocyanate was not found to be affected significantly in any of the solvents. No shift of the NCO absorption band at 2250 cm^{-1} was detected, even in pure pyridine. If the isocyanate is dissolved in such bases, the spectrum has to be taken immediately, since homopolymerization occurs on standing. Thus it must be concluded that if the isocyanate forms a complex with any of these compounds, its concentration will be very small. The complexes between isocyanates and bases reported by Pestemer and Lauerer¹³ cannot be considered in this connection since their formation takes considerable time (minutes to hours), whereas base catalysis does not have an induction period.

On the other hand, amines and alcohols form very strong hydrogen-bonded complexes, for which Figures 9, 10, and 11 may serve as examples. Figures 9 and 11 show that the amine-alcohol complex forms even in such strongly hydrogen-bonding solvents as dioxane, whereby, of course, the concentration of the amine-alcohol complex is greater in inert solvents than in the

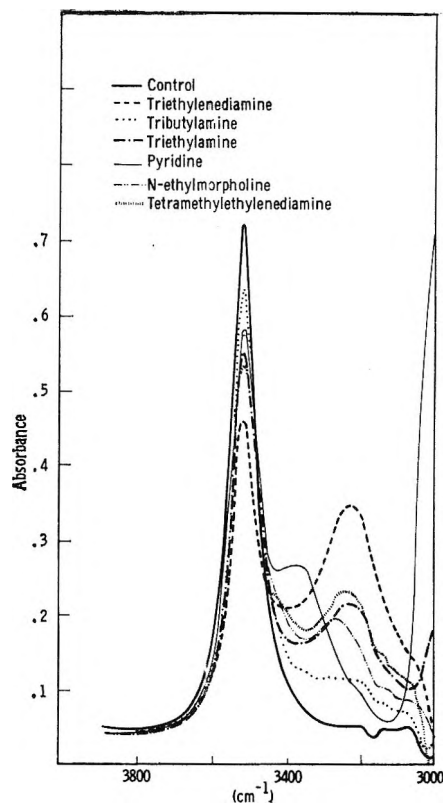


Figure 9. Infrared absorption spectra of various amine-1-butanol-dioxane combinations: butanol, 0.15 M ; amine, 1 N ; *p*-dioxane, 5 M in cyclohexane; $T = 27^\circ$ and $d = 0.4$ mm.

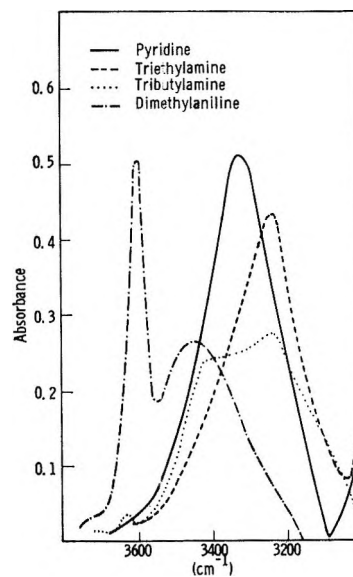


Figure 10. Absorption of 1-butanol, 0.15 M , in various amines: $T = 27^\circ$ and $d = 0.4$ mm.

latter (Figure 11). It is important to note that the amine-alcohol complexes absorb at lower frequencies than the alcohol polymer. In this respect, they differ from the alcohol-solvent complexes.

(13) M. Pestemer and D. Lauerer, *Angew. Chem.*, **72**, 612 (1960).

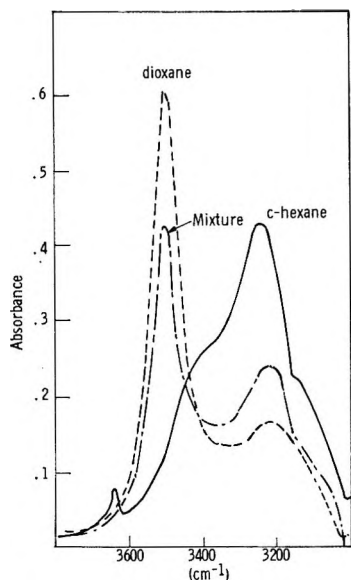


Figure 11. Absorption of 0.15 *M* BuOH and 1 *M* NEt₃ in dioxane, cyclohexane, and a dioxane-cyclohexane mixture (33 mole % dioxane): *T* = 27° and *d* = 0.4 mm.

The rate data of Table VI show no direct correlation of the catalytic activity of the amine with its basicity. For example, triethylenediamine is the strongest base catalyst so far uncovered.¹⁴ Its base dissociation constant, however, is only 0.01 of the less active triethylamine (Table VI). Similarly, dimethylaniline, having no catalytic activity,¹⁵ has about the same basicity as pyridine, which is a moderate catalyst. Burkus¹⁶ has pointed out the superior catalytic activity of amines with bridge-head nitrogen atoms and the decrease of catalytic power if methyl groups on the amine nitrogen are replaced by larger alkyl radicals. Thus tributylamine appears to be more sterically hindered toward amine-alcohol complex formation than triethylamine or tetramethylethylene diamine (Figure 9), and the intensity of the amine-alcohol band appears to correlate well with the catalytic activity of the amine. This becomes evident if one compares the rate data of Table VI with the amine-alcohol band of Figure 9. Figure 10 shows the absorption of butanol in the undiluted amine. It is clearly seen that diethyl aniline does not form an amine-alcohol complex like pyridine, and it appears that steric factors are as important as the basicity of an amine with respect to its catalytic as well as complexing ability.

Amine catalysis greatly reduces the solvent effect for which Table VI also shows examples. This is further evidence for the reactivity of the amine-alcohol complex which is formed also in the most strongly hydrogen-bonding solvents like dioxane (compare Figure 11). In summary, it may be stated that the magnitude of the shift toward lower frequencies, as well as the intensity of the amine-alcohol absorption band, establishes a good criterion for the catalytic activity of an amine.

Table VI: Base Catalysis of the Phenyl Isocyanate Reaction with (a) 1-Butanol, Both 0.15 *M* in Cyclohexane Containing 33 mol % Dioxane at 31°, Catalyst Concentration, 0.05 *M*; (b) Methanol, Both 0.24 *M* in Dibutyl Ether at 20°, Catalyst Concentration, 0.03 *M*

Base	<i>pK_b</i> ^{26°}	$10^2k_2, M^{-1} \text{min}^{-1}$	
		a	b
Uncatalyzed	...	0.59	0.17 ^c
N,N-Dimethylaniline	9.0	0.61	0.20 ^c
Pyridine	8.64	3.0	1.88 ^c
N-Ethylmorpholine	6.49	5.5	...
Tributylamine	4.07	6.5	9.11
Triethylamine	3.25	22	22.9 ^e
N,N,N',N'-Tetramethyl- ethylenediamine	...	28	...
Triethylenediamine	5.40	240	205
Triethylamine	3.25	18 ^a	6.76 ^{c,e}
Triethylamine	3.25	25 ^b	27.6 ^{d,e}

^a In dioxane. ^b In cyclohexane. ^c 0.01 *M* NR₃. ^d = 0.01 *M* NR₃ in benzene. ^e Data from ref 15 by courtesy of John R. Baker and *J. Chem. Soc.*

Discussion

Most investigators^{2-5,7,8} who studied the urethane reaction in dilute solution stated that it followed second order. It is easily seen that this is so because, except for the most inert solvents (which have not been investigated previously), the alcohol exists practically entirely in the form of the alcohol-solvent complex or in the "monomeric" form, depending on the type of solvent used. We may write

$$\frac{dM}{dt} = k_2(\text{ROH-solvent})(\text{RNCO}) \quad (3)$$

The difficulty, however, arises when rate constants from reaction mixtures having different initial reactant concentrations are compared. Again, excepting the most inert solvents, it is found that *k*₂ increases with the concentration of the reactants, particularly that of the alcohol. Some plots of the initial second-order constant *vs.* alcohol concentration are shown in Figure 3. The data were obtained from a number of kinetic runs in which the alcohol concentration was varied while the isocyanate concentration was kept constant. It appears as if the curve for ethanol in dioxane flattens with increasing dilution and approaches a finite value, which could be interpreted as the true second-order constant for the ethyl alcohol-dioxane complex. Thus it is conceivable that at low enough concentration, the true second-order constant for the reaction between isocyanate and the respective solvent-alcohol complex could be determined. In this connection, it may be stated that the monomeric alcohol in the following dis-

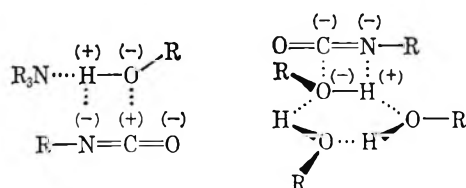
(14) A. Farkas and K. G. Flynn, *J. Am. Chem. Soc.*, **82**, 642 (1960).

(15) J. W. Baker and J. B. Holdsworth, *J. Chem. Soc.*, 713 (1947).

(16) J. Burkus, *J. Org. Chem.*, **26**, 779 (1961).

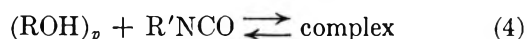
cussion is considered to be just another alcohol-solvent complex in which the O-H stretch vibration is less affected by hydrogen bonding, as distinguished from the single-bridge dimers formed in solvents having strong acceptor atoms. Unfortunately, the determination of k_2 becomes increasingly difficult with further dilution, because side reactions of the isocyanate with other active hydrogen compounds start to interfere measurably. Also, at high dilutions, catalyzing impurities, such as moisture, begin to play a major role.

The increase of the rate constant at the higher reactant concentrations is attributed to the appearance of the more reactive alcohol polymer, whose concentration will depend primarily on the concentration of the alcohol and the nature of the solvent. The high reactivity of the polymeric alcohol as well as the amine-alcohol complex can be explained by the polarization (weakening) of the O-H bond of the alcohol molecule, which would facilitate the attack by the C atom of the isocyanate group. The activated complexes may perhaps be visualized as



According to Badger and Bauer,¹⁷ the polarization is directly related to the shift of the O-H stretch band to lower frequencies. Thus the comparatively low reactivity of the monomeric alcohol, the alcohol-solvent complex, and the alcohol dimer would be due to the low degree of polarization of the O-H bond, which is manifest from their spectra. It must be noted that Baker² also had considered catalysis through the complex $RO^- \cdots H^+NR_3$. However, this concept was rejected because dialkylanilines do not exhibit catalytic activity, while pyridine of comparable basicity is a catalyst. He assumed erroneously that both compounds should form the alcohol-amine complex, since protonation of the amine nitrogen atom should not depend on steric factors. In fact, the dependence of the catalytic activity on the structure of the amine has been held as a strong argument against this mechanism by later investigators, notably Burkus¹⁶ and Farkas and Mills,¹⁸ because, like Baker, they considered complete ionization of the amine-alcohol complex. Sutton¹⁹ has shown that not even in the amine-phenol complex has complete charge separation been reached. In a recent paper, Farkas and Strohm²⁰ have revised the older theory and have shown that complex formation between the alcohol and amine can well account for the catalytic behavior of the base. Thus the experimental results presented in this paper may be considered as further evidence for the mechanism presented by Farkas and Strohm.

In the following, a mechanism is presented which, based on the high reactivity of the polymeric alcohol, accounts well for the concentration dependence of k_2 in the various solvents (Figures 12 and 3), and the other effects described in this paper. The reaction is thought to proceed *via* the alcohol polymer-isocyanate intermediate, depicted above, whose rearrangement to the urethane is the rate-determining step. This latter assumption is almost a necessity, because the equilibrium yielding the intermediate, like all the other hydrogen bonded alcohol-solvent complexes, is established instantaneously upon mixing. We may write



and



The rate of the uncatalyzed reaction is then given by

$$\frac{du}{dt} = k(\text{complex}) \quad (6)$$

Solvation of the alcohol by any of the components of the reaction mixture will lower the concentration of the alcohol polymer and hence slow down the reaction. Consequently, a quantitative description requires knowledge of the alcohol polymer concentration.

We may write the equation containing all the alcoholic species²¹ in solution

$$a_0 = a_i + a_u + a_s + a_1 + 2a_2 + 3a_3 + 4a_4 \quad (7)$$

where a_i , a_u , and a_s are the concentrations of alcohol-isocyanate complex, alcohol-urethane complex, and alcohol-solvent complex, respectively, and a_1 , a_2 , a_3 , and a_4 denote the concentration of the monomeric, dimeric, trimeric, and tetrameric alcohol. In the usual kinetic runs, the concentration of the isocyanate is very small and a_i is, therefore, neglected in the following calculation. A further simplification is achieved if only the initial stages of the reaction are considered so that the alcohol urethane complex drops out.

The concentrations of the other quantities contained in eq 4 are obtained from the simultaneous equilibria: $a_1 + s \rightleftharpoons a_s$, $a_2 + s \rightleftharpoons a_s + a_1$, $a_3 + s \rightleftharpoons a_s + a_2$, and $a_4 + s \rightleftharpoons a_s + a_3$, where s is the concentration of the solvent in solution. Considering also that $s = s_0 - a_s$ the four equilibria are

(17) R. M. Badger and S. H. Bauer, *J. Chem. Phys.*, **5**, 839 (1937).

(18) A. Farkas and G. A. Mills in "Advances in Catalysis," Vol. XIII, Academic Press Inc., New York, N. Y., 1962, p 393.

(19) J. R. Hulett, J. A. Pegg, and L. E. Sutton, *J. Chem. Soc.*, 3901 (1955).

(20) A. Farkas and P. F. Strohm, *Ind. Eng. Chem. Fundamentals*, **4**, 37 (1965).

(21) Degrees of polymerization of greater than 4 are not reported in the literature. Compare, *e.g.*, G. C. Pimentel and A. L. McClellan, "The Hydrogen Bond," W. H. Freeman and Co., San Francisco, Calif., 1960.

$$K_1 = \frac{a_s}{a_1(s_0 - a_s)}$$

$$K_2 = \frac{a_s a_1}{a_2(s_0 - a_s)}$$

$$K_3 = \frac{a_s a_2}{a_3(s_0 - a_s)}$$

and

$$K_4 = \frac{a_s a_3}{a_4(s_0 - a_s)}$$

Rearranging and substituting into eq 7 leads to eq 8, in which the only variable is the monomeric alcohol concentration.

$$a_0 - \frac{a_1 K_1 s_0}{1 + a_1 K_1} - a_1 - 2 \left(\frac{K_1}{K_2} \right) a_1^2 - 3 \left(\frac{K_1}{K_2} \right)^2 \left(\frac{K_2}{K_3} \right) a_1^3 - 4 \left(\frac{K_1}{K_2} \right)^3 \left(\frac{K_2}{K_3} \right)^2 \left(\frac{K_3}{K_4} \right) a_1^4 = 0 \quad (8)$$

The concentration of trimer is then

$$a_3 = \left(\frac{K_1}{K_2} \right)^2 \left(\frac{K_2}{K_3} \right) a_1^3$$

and that of the tetramer

$$a_4 = \left(\frac{K_1}{K_2} \right)^3 \left(\frac{K_2}{K_3} \right)^2 \left(\frac{K_3}{K_4} \right) a_1^4$$

If the equilibrium constants are known, eq 8 can be solved by introducing values for a_1 and calculating a_0 . A sample calculation readily shows that the concentration of the alcohol polymer (*i.e.*, the concentration of all species having a degree of association >2) is little affected by the term for a_4 , so that for practical purposes the concentration of the trimer as obtained from eq 8 represents that of all polymeric species.

The main difficulty in applying eq 8 is not only a lack of knowledge of the appropriate complex constants but also considerable discordance between the reported values.²¹ For example, the constant for polymeric association of ethanol is given to be as $11 M^{-1}$ by Ens and Murray,²² while a value of $0.64 M^{-1}$ is reported by Grunwald and Coburn.²³ The latter report a value of $1.7 M^{-1}$ for the association constant between ethanol and ethyl acetate, while Coggeshall²⁴ gives a value of $0.3 M^{-1}$ for the complex formation constant between benzyl alcohol and methyl ethyl ketone.

Equation 8 has been solved by adopting values for the individual equilibrium constants K_1 , K_2 , and K_3 . The results for a series of such calculations are shown in Figure 12. The values for k_2 were obtained by setting the rate of the reaction proportional to the concentration of the trimer, which is permissible at low concentrations of isocyanate. The k_2 value at $a_0 = 10$, the highest alcohol concentration possible in the BuOH

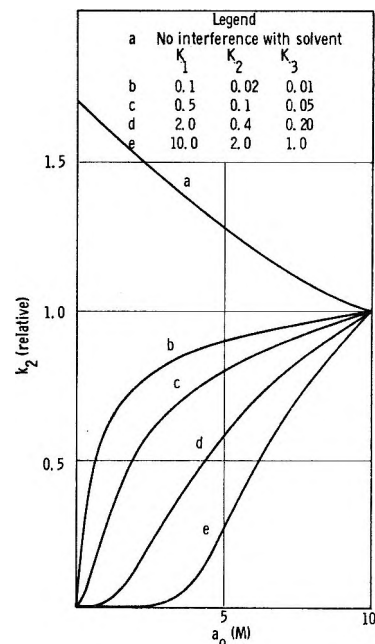


Figure 12. Relative pseudo-second-order rate constants vs. the initial alcohol concentration.

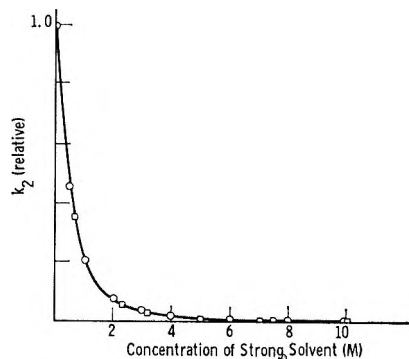


Figure 13. Comparison of calculated and experimental k_2 values as a function of the replacement of an inert solvent by a strong solvent: $C_{PhNCO} = C_{BuOH} = 0.15 M$. Calculated values are represented by curve; experimental points, by the symbols. The latter are taken from Figure 2 and have the same meaning and absolute values.

system, is arbitrarily set equal to 1.0; thus $k_{2(rel)} = (10a_3)/(2.75a_0)$.

In Figure 13, the agreement between theoretical and experimental data is shown for the experiments depicted in Figure 2. Using the same values as those for curve d in Figure 12, eq 8 is solved for s_0 at constant $a_0 = 0.15 M$.

The rising k_2 values with decreasing alcohol concentration (Table V and Figure 12) in inert solvents are obtained if $K_i > K_s$. K_i is the equilibrium constant

(22) A. Ens and F. E. Murray, *Can. J. Chem.*, **35**, 170 (1957).

(23) E. Grunwald and W. C. Coburn, *J. Am. Chem. Soc.*, **80**, 1322 (1958).

(24) R. A. Coggeshall and E. L. Saier, *ibid.*, **73**, 5414 (1951); **69**, 1620 (1947).

for the alcohol-isocyanate complex. Curve a of Figure 12 was calculated by using an estimated value of $0.3 M^{-1}$ for K_i in the analytical form of eq 4. Comparison of Figures 3 and 12 as well as Figures 2 and 13 shows that by proper choice of the alcohol-solvent complex constants reasonable fits with the experimental data are obtained over the entire range of (ROH) concentrations. Moreover, the proposed mechanism predicts the rise of the k_2 values with dilution in inert solvents as well as the other observations presented in the Results section. It should be noted that the assumed equilibrium constants are well within the range of reported values.²¹

Base catalysis offers a comparatively uncomplicated system. The amine-alcohol complex forms readily and its concentration is only moderately affected by the nature of the solvent. Moreover, in dilute solutions the contribution to the rate of the reaction by the amine-alcohol complex predominates, so that any other species can be neglected. Farkas and Strohm²⁰ have presented rate expressions based on the alcohol-base complex. In the following treatment, a slightly different approach is presented which, in addition, accounts for the effect of solvents on the rate. At low base concentrations, the solvent effect is still quite pronounced.

In dilute solution, we have essentially the following two simultaneous equilibria: $a + s \rightleftharpoons a_s$ and $a + b \rightleftharpoons a_b$, where b , a_b and a are the concentrations of the base, the alcohol-base complex, and the alcohol, respectively; in addition a third equilibrium between a_b and the isocyanate has to be considered, $a_b + i \rightleftharpoons a_{bi}$, since such a step must precede the reaction as discussed before. The concentration of the alcohol-base-isocyanate complex, a_{bi} is probably very small, so that we can calculate the concentration of a_b from the first

two equilibria. With the simplification that in dilute solution $s_0 - s \approx s_0$ and $a_0 - (a_s + a_b) \approx a_0 - a_s$, a_b is found to be

$$a_0 b K_b / (K_b a_0 + K_s s_0 + 1)$$

In analogy to the uncatalyzed reaction, the rearrangement of the alcohol-base-isocyanate intermediate, a_{bi} , is considered rate determining. Its concentration is obtained from the equilibrium $a_b + i \rightleftharpoons a_{bi}$. Considering that in dilute solution $a_b \gg a_{bi}$ and also $i_0 \gg a_{bi}$, $a_{bi} \approx K_i' i_0 a_b$, where K_i' is the constant for the alcohol-base-isocyanate equilibrium. Hence, the second-order rate constant for the base catalyzed reaction, k_b is given by

$$k_b = \frac{k' a_{bi}}{a_0 i_0} = \frac{b k' K_i' K_b}{K_b a_0 + K_s s_0 + 1} \quad (9)$$

where k' is the rate constant for the rearrangement of the alcohol-base-isocyanate complex.

Equation 9 is, in most aspects, mathematically equivalent to the one given by Baker,² *i.e.*, $k_2 = k_1 k_3 b / (k_2 + k_3 a_0)$, except that it contains in addition the equilibrium constants K_b and K_s which account for the effects of the nature of alcohol and solvent. It differs from the equations presented by Farkas and Strohm²⁰ by the inclusion of the solvent interaction term.

We hope to have shown that hydrogen bonding could offer a uniform explanation for the rather complicated urethane reaction. An exact mathematical representation will have to wait until more information is available about the underlying equilibria.

Acknowledgment. The authors wish to express their gratitude to J. F. Humphreys, who helped much in the experimental work.

Thermodynamic Data from Fluorescence Spectra. II. Hydrophobic

Bond Formation in Binary Complexes¹

by Donald K. Kunimitsu,² A. Young Woody,
Evelyn R. Stimson, and Harold A. Scheraga³

Department of Chemistry, Cornell University, Ithaca, New York 14850 (Received July 19, 1967)

Association constants for the formation of complexes between some phenolic compounds and sodium monocarboxylic acid salts have been determined at several temperatures by the method of fluorescence quenching. Some discussion is provided to support the validity of attributing deviations from Stern-Volmer kinetics, *in these systems*, to association. Assuming that complexes involving formate contain only a hydrogen bond, but that complexes involving higher homologs of formate contain *both* a hydrogen and a hydrophobic bond, subtraction of the thermodynamic parameters for hydrogen bonding from those for association in the higher homologs yields the thermodynamic parameters for the formation of *pairwise* hydrophobic bonds. These experimental values agree with those predicted from theory.

Introduction

This is a continuation of previous work⁴ designed to provide experimental verification⁵⁻⁷ of theoretically predicted values⁸ of the thermodynamic parameters for the formation of *pairwise* hydrophobic bonds. As used previously,⁴ the method of fluorescence quenching is applied here to determine the equilibrium constants for the association of phenolic compounds with carboxylate compounds. The complex is assumed to involve both a hydrogen bond between the phenolic OH group and the carboxylate ion group and also a *pairwise* hydrophobic bond between the nonpolar parts of the phenolic and carboxylate compounds. As the nonpolar parts vary in a homologous series, the hydrogen bond is assumed to be identical in all of the complexes studied. Thus, a subtraction of the free energy of hydrogen-bond formation from the free energy of association should provide a measure of the free energy of formation of the pairwise hydrophobic bond; in a similar manner, the enthalpy and entropy of formation of the hydrophobic bonds may be determined. The experimental quantities are then compared with theoretical values.⁸ Some of the problems involved in the interpretation of fluorescence quenching data, and the calculation of association constants from them, are discussed.

Experimental Section

Materials. Phenol, 3,5-xyleneol, butyric acid, and isobutyric acid were Baker grade products from J. T. Baker and Co., New York, N. Y., *p*-cresol (redistilled) was purchased from the Matheson Co., East Rutherford, N. J., and used without further purification.

4-*n*-Propyl phenol was a product of Aldrich Co., Milwaukee, Wis., and was redistilled once under vacuum immediately before use. The sodium salts of all the compounds used were the best grades available commercially. Sodium butyrate and sodium isobutyrate were prepared from the corresponding acids; the acids were redistilled twice in the presence of potassium permanganate and their concentrations were determined by titration. D₂O (99.7%) was acquired from the U. S. Atomic Energy Commission, Aiken, S. C., and was bottled by the Cornell University department of chemistry. Deionized water was used throughout.

Fluorescence and Ultraviolet Difference Spectra Measurements. Fluorescence quenching data and ultraviolet difference spectra were obtained by the methods described previously.⁴ The concentration of fluorescent solute (*e.g.*, phenol) employed in the fluorescence quenching studies was 2.0×10^{-4} M. The difference

(1) This work was supported by a research grant (HE-01662) from the National Heart Institute, National Institutes of Health, Public Health Service, and by a research grant (GB-4766) from the National Science Foundation.

(2) Postdoctoral Fellow of the National Institute of General Medical Sciences, National Institutes of Health, 1965-1966.

(3) To whom requests for reprints should be addressed.

(4) A. Y. Moon, D. C. Poland, and H. A. Scheraga, *J. Phys. Chem.*, **69**, 2960 (1965).

(5) E. E. Schrier, M. Pottle, and H. A. Scheraga, *J. Am. Chem. Soc.*, **86**, 3444 (1964).

(6) H. Schneider, G. C. Kresheck, and H. A. Scheraga, *J. Phys. Chem.*, **69**, 1310 (1965).

(7) M. E. Friedman and H. A. Scheraga, *ibid.*, **69**, 3795 (1965).

(8) G. Nemethy and H. A. Scheraga, *ibid.*, **66**, 1773 (1962); **67**, 2888 (1963).

spectra studies were carried out at a higher concentration of phenol ($6.4 \times 10^{-4} M$).

Viscosity Measurements. Viscosity measurements were made with a Cannon-Ubbelohde semimicro dilution viscosimeter, with flow times for water in excess of 200 sec. Kinetic-energy corrections were not made, and viscosities were computed simply as products of flow time and density, relative to the same product measured with water. The temperature was controlled to better than $\pm 0.1^\circ$. Densities of the mixed electrolytes were calculated from the densities of the individual electrolytes,⁹ essentially by a method outlined by Kawahara and Tanford.¹⁰ The ratio of the density of a given solution to that of water was calculated at either 20 or 25° and was assumed to hold over the temperature range of 10–45°.

Treatment of Fluorescence Data

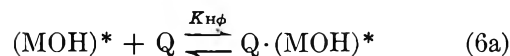
Mechanism of Fluorescence Quenching. If MOH refers to a fluorescent phenolic solute in a solvent S, and Q to the various added fluorescence quenchers, then, using parentheses to represent concentrations, we may write Scheme I for excitation by light of frequency ν (with an asterisk to denote excited species), for fluorescence at a frequency ν' , and for fluorescence quenching; the definitions of the rate constants are apparent from their use in eq 1–10.

Scheme I

Process		Rate or equilibrium expression	
Absorption	$\text{MOH} + h\nu \rightarrow (\text{MOH})^*$	$k_A(\text{MOH})$	(1)
Emission	$(\text{MOH})^* \rightarrow \text{MOH} + h\nu'$	$k_f(\text{MOH})^*$	(2)
Quenching	$(\text{MOH})^* + \text{Q} \rightarrow \text{MOH} + \text{Q} + \text{heat}$	$k_i(\text{MOH})^*(\text{Q})$	(3)
Deactivation by solvent and by internal conversion processes	$(\text{MOH})^* + \text{S} \rightarrow \text{MOH} + \text{S} + \text{heat}$	$k_i(\text{MOH})^*(\text{S})$	(4)
Association involving phenolic-OH group	$\text{MOH} + \text{Q} \rightleftharpoons \text{MOH} \cdot \text{Q}$	K_{assoc}	(5)
Association not involving phenolic-OH group	$\text{MOH} + \text{Q} \rightleftharpoons \text{Q} \cdot \text{MOH}$	$K_{\text{H}\phi}$	(6)
Absorption	$\text{Q} \cdot \text{MOH} + h\nu \rightarrow \text{Q} \cdot (\text{MOH})^*$	$k_A(\text{Q} \cdot \text{MOH})$	(7)
Emission	$\text{Q} \cdot (\text{MOH})^* \rightarrow \text{Q} \cdot (\text{MOH}) + h\nu'$	$k_f(\text{Q} \cdot (\text{MOH})^*)$	(8)
Quenching	$\text{Q} \cdot (\text{MOH})^* + \text{Q} \rightarrow \text{Q} \cdot (\text{MOH}) + \text{Q} + \text{heat}$	$k_2(\text{Q} \cdot (\text{MOH})^*)(\text{Q})$	(9)
Deactivation by solvent and by internal conversion processes	$\text{Q} \cdot (\text{MOH})^* + \text{S} \rightarrow \text{Q} \cdot (\text{MOH}) + \text{S} + \text{heat}$	$k_i(\text{Q} \cdot (\text{MOH})^*)(\text{S})$	(10)

In the previous treatment,⁴ we allowed only for the species $\text{MOH} \cdot \text{Q}$, which is postulated to involve an $\text{OH} \cdots \text{OOC}$ hydrogen bond, with an additional hydrophobic bond between the nonpolar parts of MOH and Q; the hydrogen bond of such a complex accounts for the instantaneous de-excitation of excited phenol.¹¹ The above scheme differs from the previous one⁴ in that we have allowed for the species $\text{Q} \cdot \text{MOH}$, a complex involving only hydrophobic bonding between the nonpolar parts of MOH and Q, but no hydrogen bonding of the phenolic OH group; this complex is postulated to be capable of being excited and fluorescing. Here, k_1 is

assumed to differ from k_2 because of repulsion between the carboxylate ion groups of Q and of the $\text{Q} \cdot (\text{MOH})^*$ complex. Also, we make the reasonable approximation that the excited species, $\text{Q} \cdot (\text{MOH})^*$, is in equilibrium as follows



It should be emphasized that $K_{\text{H}\phi}$ is very small compared to K_{assoc} ; hence, the concentration of $\text{Q} \cdot \text{MOH}$ will be much smaller than that of $\text{MOH} \cdot \text{Q}$. Equation 6 is nevertheless introduced here, since the concentration of $\text{Q} \cdot \text{MOH}$, though small, is not negligible. Thus, the $K_{\text{H}\phi}$ of eq 6 represents a small correction to be made in the experimental data and is not the quantity to be determined in this investigation. Instead, the equilibrium constant for pairwise hydrophobic bond formation, to be determined here by the fluorescence quenching method, is a component of K_{assoc} ; it is, therefore, K_{assoc} which will be obtained from the experimental data.

For steady illumination and no irreversible photochemical reactions, and assuming (a) that steady-state concentrations of $(\text{MOH})^*$ and $\text{Q} \cdot (\text{MOH})^*$ are achieved, and (b) that S is large and constant so that it appears in k_i , eq 11 may be derived.

$$\frac{\phi_0}{\phi} = \frac{I_0}{I} = \frac{k_f + k_i}{k_f + k_{i,0}} + \frac{A(\text{Q}) + B(\text{Q})^2 + C(\text{Q})^3}{[1 + K_{\text{H}\phi}(\text{Q})]^2} \quad (11)$$

where I_0 and ϕ_0 are the intensity of fluorescent light and

(9) International Critical Tables, Vol. 3, McGraw-Hill Book Co., New York, N. Y., 1928, p 51 ff.

(10) K. Kawahara and C. Tanford, *J. Biol. Chem.*, **241**, 3228 (1966).

(11) The quenching of phenol fluorescence is assumed to occur by a base-catalyzed dissociation of the proton of the aromatic hydroxyl group. For the experimental basis of this mechanism, see (a) A. White, *Biochem. J.*, **71**, 217 (1960); (b) G. Weber and K. Rosenheck, *Biopolymers, Symposia*, **1**, 333 (1964); and (c) J. Feitelson, *J. Phys. Chem.*, **68**, 391 (1964).

quantum yield, respectively, of emission from (MOH)* in the absence of Q, *i.e.*

$$\phi_0 = \frac{k_f}{k_f + k_{i,0}} \quad (11a)$$

and I and ϕ are the intensity of fluorescent light and the quantum yield, respectively, of emission from (MOH)* and Q·(MOH)*, *i.e.*, in the presence of Q. The expression for ϕ can be obtained by dividing ϕ_0 of eq 11a by ϕ_0/ϕ of eq 11. The constants of eq 11 are defined as follows

$$A = k_q + 2K_{H\phi} + K_{\text{assoc}} \quad (11b)$$

$$B = k_q'K_{H\phi} + K_{H\phi}^2 + k_qK_{H\phi} + K_{\text{assoc}}K_{H\phi} + k_qK_{\text{assoc}} \quad (11c)$$

$$C = k_q'K_{H\phi}^2 + k_q'K_{\text{assoc}}K_{H\phi} \quad (11d)$$

$$k_q = k_1/(k_f + k_{i,0}) \quad (11e)$$

$$k_q' = k_2/(k_f + k_{i,0}) \quad (11f)$$

$k_{i,0}$ is the rate constant for solvent quenching and other internal conversion processes which result in the de-excitation of (MOH)* in the absence of Q. In general, $k_{i,0} = k_i$ only if the viscosity (among other things) of the solution of MOH is the same as that of the solution of MOH + Q.

It is possible to determine the various parameters of eq 11 from the ratio I_0/I in a manner to be discussed below. However, it is of interest at this point to note two limiting cases of eq 11, if $k_{i,0} = k_i$. These are: (1) for $K_{H\phi} = 0$, eq 11 reduces to eq 8 of our previous paper,⁴ which was used to account for positive deviations from the Stern-Volmer equation; and (2) for $K_{H\phi} = K_{\text{assoc}} = 0$, eq 11 reduces to the Stern-Volmer equation.

Problems in Interpreting Fluorescence Quenching Data. Since $K_{\text{assoc}} < 1$ for the systems studied here, it was necessary to use relatively high concentrations of quencher (0.4–1.0 M) in order to obtain precise values of K_{assoc} . This introduced three problems: (1) the addition of quencher increased the viscosity of the solution; hence, $k_{i,0}$ had to be corrected (by a method outlined in the next section) to the viscosity of the solution containing quencher; (2) the addition of quencher affects the activity coefficients; nevertheless, concentrations have been used here instead of activities for reasons stated in the paragraph following eq 3 of our previous paper;⁴ and (3) in attributing positive deviations from Stern-Volmer kinetics to K_{assoc} , it is necessary to rule out an alternative mechanism,¹² *viz.*, if the possibility of (fast) diffusion-controlled rates exists, there may be deviations from the stationary concentrations assumed in the derivation of eq 11; these deviations can become important at short excited-state lifetimes or, equivalently, at higher quencher concentrations. The theory for such a mechanism involving

diffusion-controlled reactions has been developed;^{13,14} there exists, at present, at least one application of this theory,¹⁵ providing a satisfactory explanation of departures from Stern-Volmer kinetics which had originally been attributed to association.¹⁶ We will show that this effect is negligible in our systems; hence, eq 11 may be applied directly to interpret our data.

Viscosity Correction. In order to correct $k_{i,0}$ to the viscosity, η , of the solution containing quencher, we assume that k_f is independent of viscosity and temperature. Hence, according to eq 11a, the dependence of $k_{i,0}$ on viscosity is given by the dependence of ϕ_0 on viscosity. Thus, we require the dependence of I_0 (which is proportional to ϕ_0) on viscosity *in the absence of quencher*. From the dependence of I_0 on η , we can then compute $k_{i,0}$ at the value of η , for the solution containing quencher, when using eq 11.

The value of $k_{i,0}$ for phenol in water at 25° was obtained as follows. The value of ϕ_0 is 0.22 for phenol under these conditions,^{11b} and the value of $(k_f + k_{i,0})$, which is the reciprocal of the lifetime of the excited state, was taken as 1.33×10^8 , as calculated by Feitelson for tyrosine from its absorption spectrum.^{11c, 17} Hence, both k_f and $k_{i,0}$ could be obtained, from eq 11a, for phenol in water at 25°.

With k_f assumed constant, I_0 (and hence $k_{i,0}$) was measured for phenol as a function of viscosity at 25°. The viscosity was varied over the required range by adding D₂O to the phenol solution, assuming no additional quenching by D₂O, to obtain I_0 at low viscosities.¹⁸ Ethanol (EtOH) was added to H₂O to attain higher viscosities. However, since there is a small amount of quenching by ethanol, it was corrected for by assuming that the ratio

$$\frac{I_0 \text{ (in D}_2\text{O-H}_2\text{O)}}{I \text{ (in EtOH-H}_2\text{O)}} - 1$$

(EtOH)

is the same at all viscosities.

In order to evaluate $k_{i,0}$ for phenol as a function of viscosity at temperatures other than 25°, we require values of ϕ_0 of phenol at these other temperatures and viscosities. Similarly, we require ϕ_0 for 3,5-xyleneol,

(12) We are indebted to R. M. Noyes for pointing this out to us.

(13) R. M. Noyes, *Progr. Reaction Kinetics*, **1**, 129 (1961).

(14) A. Weller, *ibid.*, **1**, 187 (1961).

(15) W. R. Ware and J. S. Novros, *J. Phys. Chem.*, **70**, 3246 (1966).

(16) E. J. Bowen and W. S. Metcalf, *Proc. Roy. Soc. (London)*, **A206**, 437 (1951).

(17) While the use of $(k_f + k_{i,0})$ for tyrosine may introduce some error in k_1 and k_2 for the other phenolic compounds (since k_q and k_q' are experimental quantities, yielding k_1 and k_2 from eq 11e and 11f), it will not affect the calculated value of K_{assoc} very much, since the viscosity corrections appear in the *ratios* of the quantum yields (see eq 11).

(18) The viscosities of H₂O–D₂O mixtures at various temperatures are given by R. C. Hardy and R. L. Cottingham, *J. Res. Natl. Bur. Std.*, **42**, 573 (1949).

p-cresol, and 4-*n*-propyl phenol as a function of viscosity at various temperatures in order to obtain $k_{i,0}$ for these phenolic compounds as a function of viscosity and temperature. Since there are no significant differences in the wavelengths of absorption ($270 \pm 5 \text{ m}\mu$) and emission ($305 \pm 5 \text{ m}\mu$) at 25° for all of the phenolic compounds used in this study, and since these wavelengths do not shift by more than $5 \text{ m}\mu$ over the temperature range $10\text{--}45^\circ$, the quantum yields of interest were obtained by the comparative method described by Parker and Rees.¹⁹ In this method, it is assumed that, for a given spectrofluorimeter, the integrated area, A , under the fluorescence emission curve is proportional to the total intensity of fluorescent light, I_0 , emitted by the fluorescer. Now, I_0 is proportional to the product $I_{\text{ex}}\phi_0 Ecd$, where I_{ex} is the intensity of the exciting light, E is the molar extinction coefficient, c is the concentration, and d is the optical path length. Therefore, assuming the proportionality constants to be equal, it can be seen that, for a comparison of fluorescence from two solutions at the same intensity of the exciting light, I_0/A is the same for the two solutions. Hence, using subscripts 1 and 2 to represent the two solutions, $(\phi_0)_1/(\phi_0)_2 = (A_1/A_2)(E_2c_2/E_1c_1)$. In order to avoid the necessity of correcting the observed emission spectra for variation in the intensity of the xenon lamp with the wavelength of excitation, the wavelength of the exciting light was maintained constant at $270 \text{ m}\mu$ for all of the phenolic compounds used in this study. While the sensitivity of the photomultiplier tube varies with the wavelength of light, the similarity in the emission spectrum of the reference compound (phenol) to all the other phenolic compounds allowed us to compare the integrated areas directly without the necessity of first correcting the observed emission curves. The reference value^{11b} of $\phi_0 = 0.22$ for phenol in water at 25° was adopted.

In order to obtain the dependence of ϕ_0 on η for 3,5-xyleneol, *p*-cresol, and 4-*n*-propyl phenol, the same method used for phenol was employed. With the approximation that k_f is independent of η and T , and the assumption that $(k_f + k_{i,0}) = 1.33 \times 10^8$ for all the phenolic compounds at 25° , it was possible to evaluate $k_{i,0}$ as a function of η and T from the corresponding data for the dependence of ϕ_0 on η and T .

Departure from Stationary Concentrations. Consider next the possibility that the alternative mechanism of diffusion-controlled rates may be the cause of the deviations from Stern–Volmer kinetics or, at least, may be making a significant contribution, along with K_{assoc} , to such deviations. Since we do not have data on the lifetimes of the excited states, we must consider other factors to decide on this question.

First of all, the fact that similar values of K_{assoc} for phenol and acetate were obtained by both the fluorescence quenching technique (neglecting this alternative mechanism) and the method of ultraviolet difference

spectra⁴ suggests that association is the main origin of the departures from Stern–Volmer kinetics.

Secondly, in using the fluorescence quenching data to evaluate K_{assoc} (assuming that the alternative mechanism is not operative), we carry out a subtraction of free energies, *i.e.*, we subtract out the free energy of hydrogen-bond formation to obtain the free energy of hydrophobic-bond formation. This subtraction will largely eliminate effects from this alternative mechanism. Nevertheless, we shall not rely on this subtraction, but will estimate the effect of the alternative mechanism and show that it is negligible.

For this estimation, we use Noyes' theory²⁰ for the case where the quenching reaction is intermediate between a diffusion-controlled and an activation-controlled one; we assume that this may be the situation for the reaction between phenol and acetate.^{11c} Defining $[(I_0/I) - (k_f + k_i)/(k_f + k_{i,0})]/(Q)$ as k_{ex} (with the viscosity correction already introduced), Noyes writes the following equation to express the departure from Stern–Volmer kinetics^{20a}

$$k_{\text{ex}} = k_{\text{ex}}^0 + U(Q) \quad (12)$$

where

$$U = \pi^{1/2}KJ + 4(\pi - 1)K^2 \quad (13)$$

$$K = [1000(k_f + k_i)/4\pi DN]^{3/2}(N/1000)^{1/2}J^2 \quad (14)$$

and k_{ex}^0 is the value of k_{ex} at $(Q) = 0$. The quantity K describes the competition of fluorescence with the rate of the establishment of the steady-state concentration gradient and is related to fundamental parameters of collision theory; D is the coefficient of relative diffusion, N is Avogadro's number, and J is the collisional quenching constant when an equilibrium distribution is applicable. According to eq 28 of ref 20a

$$k_{\text{ex}}^0 = J + 2\pi^{1/2}K \quad (15)$$

In order to show that this alternative mechanism is not applicable here, we shall compute U of eq 13 and show that it is too small to account for the large deviations from Stern–Volmer kinetics in our systems.

For the phenol–acetate system at 25° ($k_f + k_i$) was taken as 1.33×10^8 . The intercept, k_{ex}^0 from our experimental plot of k_{ex} vs. (Q) is 5.70 M^{-1} . Neglecting K in eq 15 (see below for justification), $J = k_{\text{ex}}^0 = 5.70$. Using this value of J , and $D = 2.0 \times 10^{-5} \text{ cm}^2/\text{sec}$, K is found to be 0.02 from eq 14 (justifying the neglect of K in eq 15). With these values of J and K , eq 13 yields a value of 0.21 M^{-2} for U . As will be shown in the Results, the observed value of U for this system is 2.5 (the product of k_q and K_{assoc} of Table I). Hence, we conclude that this alternative mechanism is

(19) A. Parker and W. T. Rees, *Analyst*, **85**, 587 (1960).

(20) (a) R. M. Noyes, *J. Am. Chem. Soc.*, **79**, 551 (1957); (b) R. M. Noyes, *J. Phys. Chem.*, **65**, 763 (1961).

Table I: Temperature Dependence of the Association and Collisional Quenching Constants for the Reaction between Phenol and Some Bases^a

Base	Temp, °C	Ionic strength	K_{assoc} , M^{-1} ^b	k_q , M^{-1} ^c
Sodium formate	10	0.40	0.27	3.37
	15	0.40	0.25	3.49
	18	0.40	0.24	3.99
	25	0.40	0.24	4.35
	30	0.40	0.24	4.64
	35	0.40	0.23	5.05
	40	0.40	0.22	5.16
	45	0.40	0.24	5.47
Sodium acetate	10	0.40	0.47	4.35
	15	0.40	0.45	4.69
	18	0.40	0.41	5.15
	25	0.40	0.44	5.69
	35	0.40	0.41	6.53
	40	0.40	0.42	6.69
Sodium propionate	10	0.40	0.43	4.49
	18	0.40	0.43	5.20
	25	0.40	0.42	5.77
	35	0.40	0.41	6.65
	40	0.40	0.40	6.80
Sodium isobutyrate	10	0.40	0.32	3.57
	15	0.40	0.33	4.10
	18	0.40	0.34	4.40
	25	0.40	0.33	5.11
	30	0.40	0.32	5.66
	35	0.40	0.34	6.02
	40	0.40	0.34	6.47
45	0.40	0.33	6.86	
Sodium butyrate	10	0.40	0.41	3.96
	15	0.40	0.44	4.44
	18	0.40	0.45	4.74
	25	0.40	0.45	5.50
	30	0.40	0.45	6.23
	35	0.40	0.44	6.73
	40	0.40	0.45	7.12
	45	0.40	0.44	7.39
Sodium glycinate	25	1.00	0.05	1.48
Sodium chloroacetate ^g	25	1.00	0.12	4.15
Sodium bicarbonate	25	1.00	0.08	4.28
Sodium fluoride	25	0.50	0.15	3.62
Sodium tartrate	25	1.50	0.42 ± 0.05^d	3.73^e
Sodium succinate	25	1.50	1.01 ± 0.20^d	6.65^e
Sodium malonate	25	1.50	0.56 ± 0.10^d	6.09^e
Sodium citrate	25	3.00	Not known ^f	8.79^e
Sodium monohydrogen phosphate	25	1.50	Not known ^f	9.00^e

^a Calculated with eq 16. ^b Probable error = $\pm 4\%$, determined as the probable errors of the slope and intercept, and based on a minimum of eight points in the Stern-Volmer plot. ^c Probable error = $\pm 2\%$. ^d For these data, the cubic term of eq 11 is *not* negligible. Hence, these values were obtained from ultraviolet difference spectra instead of from fluorescence quenching. ^e Estimated from the intercept (with the assumption that $K_{\text{assoc}} = 1.0$, the value found for sodium succinate). ^f No data available, since ultraviolet difference spectra measurements were not made.

not operative in this system, and that association is the origin of the departure from Stern-Volmer kinetics, in agreement with the conclusions from ultraviolet spectra studies.⁴ Taken together with the subtraction procedure already mentioned, we may neglect this alternative mechanism. Had we been interested in the parameters for *hydrogen* bonding, a correction for this small alternative effect would have had to be made.

Results

As already pointed out, $K_{\text{H}\phi} < K_{\text{assoc}}$, and processes such as eq 6 take place only to a small, but not negligible extent. Thus, such processes had to be included in eq 11 to obtain precise values of the parameters. Nevertheless, it is instructive to consider the data first from the point of view that $K_{\text{H}\phi} \sim 0$ in order to see the first-order effects; processes such as eq 6 will be included in a later section.

The experimental data are (Q) and k_{ex} , the latter being defined in connection with eq 12 (with the viscosity correction of $k_{i,0}$ included). The evaluation of K_{assoc} from these experimental data is based on eq 11, and the assumptions introduced therein.

Equation 11 with $K_{\text{H}\phi} \sim 0$. If we assume that $K_{\text{H}\phi} \sim 0$, then eq 11 becomes

$$k_{\text{ex}} = (k_q + K_{\text{assoc}}) + k_q K_{\text{assoc}}(Q) \quad (16)$$

i.e., eq 8 of ref 4. A plot of k_{ex} vs. (Q) yields a straight line, from which we conclude that C of eq 11d is small; this is consistent with our assumption that $K_{\text{H}\phi}$ is small. From the slopes and intercepts of such linear plots, we obtain k_q and K_{assoc} . These results are shown in Table I for phenol and in Table II for the other fluorescent compounds. The values of k_q and K_{assoc} are lower for the phenolic compounds of Table II than for phenol (Table I). The reason may lie in the lower ground state pK_a and the excited state pK_a (*i.e.*, pK_a^*) of phenol (pK_a 10.0)^{21a} compared to those of the other compounds: 3,5-xyleneol ($pK_a = 10.20$),^{21a} *p*-cresol ($pK_a = 10.17$),^{21a} and 4-*n*-propyl phenol ($pK_a = 10.34$).^{21b} Since such differences in pK_a will influence the strength of the intermolecular hydrogen bond, they will affect K_{assoc} . They will also affect k_q since this reaction is base catalyzed (see also below).

Since we have shown that the alternative mechanism of diffusion-controlled rates is inapplicable in our systems, it is of interest here to demonstrate that the quantity k_1 (and, presumably, also k_2) represents an intermediate situation between a diffusion-controlled and an activation-controlled reaction. For this purpose we shall present two different arguments, one based on Brønsted catalysis and the other on the in-

(21) (a) D. Chen and K. J. Laidler, *Trans. Faraday Soc.*, **58**, 480 (1962); (b) P. Demerseman, J. Lechartier, R. Reynard, A. Cheutin, R. Bover, and P. Rumpf, *Bull. Soc. Chim. Fr.*, **11**, 2559 (1963).

Table II: Temperature Dependence of the Association and Collisional Quenching Constants for the Reaction between 3,5-Xylenol, *p*-Cresol, and 4-*n*-Propyl Phenol and Some Bases^a

Base	Temp, °C	Ionic strength	$K_{\text{assoc}}, M^{-1} b$	$k_q, M^{-1} c$
3,5-Xylenol				
Sodium formate	10	1.00	0.15	2.38
	18	1.00	0.14	2.60
	25	1.00	0.15	2.70
	35	1.00	0.16	2.63
	45	1.00	0.15	2.51
Sodium acetate	10	1.00	0.25	3.23
	15	1.00	0.26	3.45
	18	1.00	0.25	3.60
	25	1.00	0.26	3.73
	35	1.00	0.27	3.58
Sodium propionate	10	1.00	0.20	3.27
	15	1.00	0.20	3.54
	18	1.00	0.20	3.67
	25	1.00	0.22	3.78
	30	1.00	0.22	3.61
Sodium isobutyrate	10	1.00	0.15	3.09
	18	1.00	0.15	3.46
	25	1.00	0.18	3.59
	30	1.00	0.15	3.72
	40	1.00	0.18	3.57
Sodium butyrate	10	1.00	0.20	3.52
	15	1.00	0.21	3.70
	20	1.00	0.22	3.88
	25	1.00	0.22	4.02
	30	1.00	0.21	4.03
<i>p</i>-Cresol				
Sodium formate	25	1.00	0.17	2.60
Sodium acetate	25	1.00	0.29	3.38
Sodium propionate	25	1.00	0.26	3.36
Sodium isobutyrate	25	1.00	0.21	3.48
Sodium butyrate	25	1.00	0.31	3.29
4-<i>n</i>-Propyl Phenol				
Sodium formate	25	1.00	0.15	2.42
Sodium acetate	25	1.00	0.25	3.50
Sodium propionate	25	1.00	0.26	3.39
Sodium isobutyrate	25	1.00	0.19	3.61
Sodium butyrate	25	1.00	0.22	3.85

^a Calculated with eq 16. ^b Probable error = $\pm 4\%$, determined as the probable errors of the slope and intercept, and based on a minimum of eight points in the Stern-Volmer plot. ^c Probable error = $\pm 2\%$.

$$k_1 = G_B(1/K_a)^\beta \quad (17)$$

which, if applicable (*i.e.*, if $\beta \neq 0$), would imply that k_1 is activation controlled, *viz.*, that k_1 depends on the acid-dissociation constant, K_a , of the quencher; G_B and β are constants. We shall demonstrate that $\beta \neq 0$ in our systems. Taking logarithms, eq 17 becomes

$$\log k_1 = \log G_B + \beta pK_a \quad (18)$$

The k_1 data for phenol (from Table I) are plotted according to eq 18 in Figure 1, from which it can be seen that $\beta = 0.13$. Since this demonstrates the base-catalyzed nature of the quenching of phenol fluorescence, we conclude that the large values of k_1 (which might suggest a diffusion-controlled process) reflect also the influence of base catalysis. This observation had also been made by Feitelson^{11c} to account for the quenching of tyrosine fluorescence by similar bases. We thus conclude that eq 11, based on K_{assoc} (rather than on a diffusion-controlled mechanism) is applicable to our data.

This conclusion is strengthened by showing that k_1 is independent of η at constant temperature (see Figure 2). If the reaction were diffusion controlled, then k_1 should depend on η according to the Debye equation²³

$$k_1 = 8RT/3000\eta \quad (19)$$

It can be seen from Figure 2 (in which k_1 is regarded as a function of T/η and normalized to the value at lowest η) that k_1 does not follow the Debye equation (dashed curve) but is independent of η . Besides showing that the reaction is not diffusion controlled, these data demonstrate the validity of the viscosity correction, since the points in Figure 2 represented by triangles were obtained from solutions in which the viscosity was the same in the presence and absence of quencher, whereas those represented by circles were obtained from solutions in which the viscosity differed (with the viscosity correction being applied). In addition, the data of Figure 2 show that our assumption, that k_q and k_q' are independent of viscosity, is valid.

It was found experimentally that K_{assoc} depends on ionic strength (Figure 3). The ionic strength was varied by addition of NaCl, and the data of Figure 3 are represented as

$$\Delta F^\circ_\mu \equiv [(\Delta F^\circ_{\text{assoc}})_{\mu=0} - (\Delta F^\circ_{\text{assoc}})_\mu] \text{ vs. ionic strength } \mu$$

The dependence on ionic strength increases with increasing size of the nonpolar side chain, reflecting the greater influence of ionic strength on hydrophobic bonding than on hydrogen bonding. In a later section,

fluence of viscosity on diffusion. The Brønsted relation²² is

(22) R. P. Bell, "Acid-Base Catalysis," Oxford University Press, London, 1941, p 83.

(23) P. Debye, *Trans. Electrochem. Soc.*, **82**, 265 (1942).

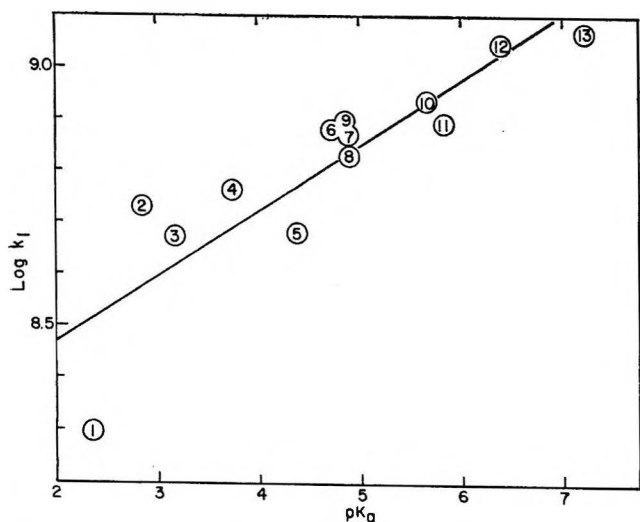


Figure 1. Plot of eq 18 for the quenching of phenol fluorescence by some bases in the form of the sodium salt: (1) glycinate, (2) chloroacetate, (3) fluoride, (4) bicarbonate, (5) formate, (6) tartrate, (7) acetate, (8) butyrate, (9) isobutyrate, (10) propionate, (11) succinate, (12) malonate, (13) citrate, and (14) monohydrogen phosphate. (Temp = 25°). The ionic strengths are variable and are listed in Table I.

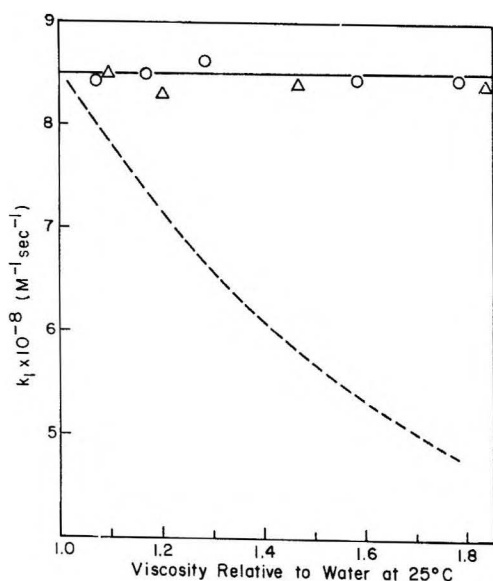


Figure 2. Dependence of k_f on viscosity at 25°, the latter being varied by addition of sucrose (with a correction being made for the *small* amount of quenching by sucrose). The curve is the expected one (eq 19) if the process were diffusion controlled. The points are experimental [phenol concn = $2.0 \times 10^{-4} M$, sodium acetate concn = 0.20 M, pH 6.8, ionic strength = 0.20]: O, solutions (with and without quencher) of different viscosity, with the viscosity correction applied; and Δ, solutions (with and without quencher) both contained sucrose and, therefore, were of the same viscosity.

the values of K_{assoc} of Tables I and II will be corrected for ionic strength, *i.e.*, extrapolated to zero ionic strength.

Since the pK_a 's of the quenchers differ, it is necessary to normalize the data to a common pK_a for a given

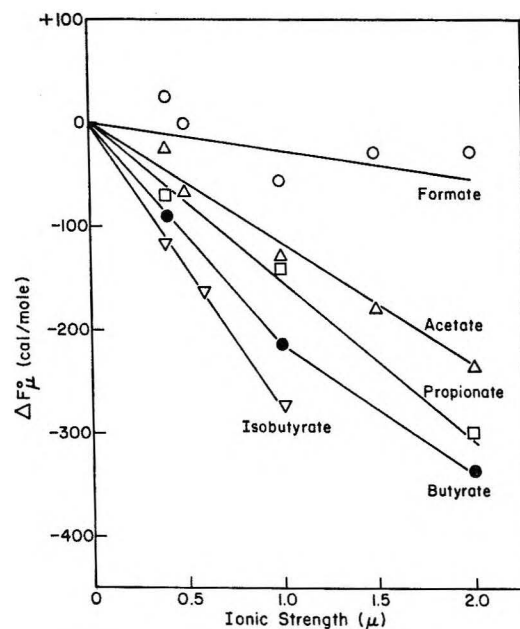


Figure 3. Dependence of standard free energy of association between phenol and some carboxylates at 25° on ionic strength.

fluorescing compound. For this purpose, we consider next the dependence of the free energy of formation of a hydrogen bond on the pK_a 's of the carboxyl groups involved. Except for formic acid, whose $pK_a = 3.75$, all the other monocarboxylic acids used here have a $pK_a = 4.75 \pm 0.15$. Thus, the strength of a hydrogen bond involving formate must be corrected to what it would be if the pK_a of formic acid were 4.75. This correction is important, since we will later assume that the hydrogen bonds between, say, phenol and *any* monocarboxylate are of comparable strength; thus the thermodynamic parameters for formation of such a hydrogen bond can be subtracted from those for the over-all association in order to obtain those for the formation of a hydrophobic bond. For this purpose, we examine a variety of acids to obtain a large enough range of pK_a to examine the dependence of K_{assoc} on pK_a . Even though several bases (*e.g.*, F^- , HCO_3^- , etc.) are listed in Table I, they are not suitable for this purpose, because they are not structurally similar to the carboxylate ion. Hence, only the carboxylate compounds of Table I, which would not contribute a hydrophobic bond, were used; these are: formate, tartrate, and malonate, whose pK_a 's cover the range of interest (3.75, 4.35, and 5.70, respectively). As pointed out in Table I, the values of K_{assoc} for tartrate and malonate were determined by ultraviolet difference spectra. Dividing the values of K_{assoc} for tartrate and malonate by 2 (because the compounds contain two carboxyl groups), we find that the dependence of K_{assoc} on pK_a is such that the observed free energy of association of phenol and formate would have been 150 cal/mol *more negative* if the pK_a of formic acid were

4.75. The value of -150 cal/mol was also used to correct $\Delta F_{\text{assoc}}^0$ for formate with the other phenolic compounds.

Equation 11 with $K_{\text{H}\phi} \neq 0$. While the data of Tables I and II indicate, for the most part, that K_{assoc} increases with increasing size of the nonpolar parts of the molecules, there is a second-order effect which must be introduced in order to obtain a more precise set of parameters. For this purpose, eq 6 (and related equations) were incorporated, and we consider now the complete eq 11, under the conditions that $K_{\text{H}\phi} \neq 0$.

In order to use eq 11 under these conditions, we are faced with the dilemma that we require a knowledge of $K_{\text{H}\phi}$, the quantity we wish to determine, in order to evaluate K_{assoc} from the quenching data. However, since eq 6 introduces only a second-order effect, we may use theoretical values of $K_{\text{H}\phi}$ in the correction term, and then deduce an experimental value of $K_{\text{H}\phi}$ from the experimental value of K_{assoc} . With an assumed value of $K_{\text{H}\phi}$, k_{ex} is redefined as k_{ex}' as follows

$$k_{\text{ex}}' = \frac{I_0}{I} [1 + K_{\text{H}\phi}(\text{Q})]^2 - \frac{k_t + k_i}{k_t + k_{i,0}} \quad (\text{Q}) \quad (20)$$

the prime in k_{ex}' serving to emphasize that it contains $K_{\text{H}\phi}$. As before, the viscosity correction on $k_{i,0}$ is made. Equation 11 then becomes

$$k_{\text{ex}}' = A + B(\text{Q}) + C(\text{Q})^2 \quad (21)$$

Since all the plots of k_{ex}' vs. (Q) are linear (for the monocarboxylic acids), we again conclude that C is very small, since $k_q'K_{\text{H}\phi}$ is very small. The parameters A and B were evaluated from the intercept and slope of eq 21 (with $C \sim 0$). Equations 11b and 11c were then used to obtain k_q and K_{assoc} , with $K_{\text{H}\phi}$ taken from theory and k_q' taken smaller than k_q (specifically, $k_q' = k_q/2$). If k_q' were larger, then the C term of eq 11d would have been observable. From a comparison of K_{assoc} and k_q , with and without the assumption that $K_{\text{H}\phi} = 0$, in Table IV, it can be seen that the introduction of a nonzero value of $K_{\text{H}\phi}$ makes only a very small difference in k_q , and, depending on the size of the nonpolar group, has a measurable effect on K_{assoc} . With $K_{\text{H}\phi} \neq 0$, the K_{assoc} data for the homologous series of monocarboxylic acids vary systematically with the size of the nonpolar group.

In order to obtain $K_{\text{H}\phi}$ for this correction, we use the Nemethy-Scheraga theory⁸ to obtain $\Delta F_{\text{H}\phi}^0$. This correction is introduced *only* for the complex $\text{Q} \cdot (\text{MOH})$. The theoretical values for the complex $(\text{MOH}) \cdot \text{Q}$ are also presented in Table III for later comparison with experimental values in Table V. In the complex, $\text{Q} \cdot (\text{MOH})$ we assume a full-strength hydrophobic bond, but a weaker one in the complex $(\text{MOH}) \cdot \text{Q}$, since the latter is constrained by a hydrogen bond. These differences are reflected in the theoretical values adopted for ΔY^s and Z_{R} , parameters which appear in the

theory.⁸ The values of $\Delta F_{\text{H}\phi}^0$ for both types of hydrophobic bond have a temperature dependence of the form⁸

$$\Delta F_{\text{H}\phi}^0 = a + bT + cT^2 \quad (22)$$

Equation 11 of ref 8 (with the omission of the $\Sigma \Delta F_{\text{rot}}$ term^{5,6}) was used to compute $\Delta F_{\text{H}\phi}^0$. The values of ΔY^s , the number of water molecules which lose contact with hydrocarbon residues, and Z_{R} , the number of hydrocarbon-hydrocarbon contacts made, upon formation of the hydrophobic bond, were estimated with the help of Courtauld's space-filling models. The small differences in a , b , and c between $(\text{MOH}) \cdot \text{Q}$ and $\text{Q} \cdot (\text{MOH})$, for cases where ΔY^s and Z_{R} are the same, arise from different interaction energies between aliphatic and aromatic groups.⁸ The values of a , b , and c were obtained by fitting the computed value of $\Delta F_{\text{H}\phi}^0$ at three temperatures (10, 25, and 45°), according to eq 22. $\Delta H_{\text{H}\phi}^0$ and $\Delta S_{\text{H}\phi}^0$ were obtained from the following equations

$$\Delta H_{\text{H}\phi}^0 = a - cT^2 \quad (23)$$

$$\Delta S_{\text{H}\phi}^0 = -b - 2cT \quad (24)$$

The theoretical data used to obtain $K_{\text{H}\phi}$ for use in eq 11 (and for later comparison with experimental data) are summarized in Table III. These data must be augmented, in the case of the $\text{Q} \cdot (\text{MOH})$ complex by the term $-T\Delta S_{\text{B}}^0$, where ΔS_{B}^0 is the loss of translational entropy on formation of the complex. We have taken $\Delta S_{\text{B}}^0 = -10$ eu, for reasons cited by Schrier, *et al.*;²⁴ this value is consistent with those observed for the dimerization of some small molecules.^{5,25} The value of -10 eu was used for phenol and assumed to hold for *p*-cresol and 4-*n*-propyl phenol; a value of -8.5 eu was used for 3,5-xyleneol, since the entropy of formation of the xyleneol-formate complex is 1.5 eu less than that of the phenol-formate complex. The data for $\Delta F_{\text{H}\phi}^0$ do not have to be augmented, in the case of the $(\text{MOH}) \cdot \text{Q}$ complex, by this translational entropy because it appears in the hydrogen-bonding terms and cancels when the effect of hydrogen bonding is subtracted. However, we must compute the fraction α of $(\text{MOH}) \cdot \text{Q}$ complexes ($M_{\text{H,H}\phi}$) which have *both* a hydrogen and a hydrophobic bond, and the fraction $(1 - \alpha)$ of complexes (M_{H}) in which only a hydrogen bond appears. We assume that

$$\frac{\alpha}{1 - \alpha} = \exp(-\Delta F_{\text{H}\phi}^0/RT) \quad (25)$$

when $\Delta F_{\text{H}\phi}^0$ appears in Table III. Because of the

(24) E. E. Schrier, R. T. Ingwall, and H. A. Scheraga, *J. Phys. Chem.*, **69**, 298 (1965).

(25) J. A. Schellman, *Compt. Rend. Trav. Lab. Carlsberg*, **29**, 223 (1955); I. M. Klotz and J. D. Franzen, *J. Am. Chem. Soc.*, **84**, 3461 (1962); D. R. Cartwright and C. B. Monk, *J. Chem. Soc.*, 2500 (1955).

Table III: Theoretical Parameters Describing the Strengths of Pairwise Hydrophobic Bonds Formed between Various Nonpolar Residues

Bonding groups	ΔY^a	Z_{II}	Coefficients for eq 22			ΔF°_{25} , cal/ mol	ΔH°_{25} , cal/ mol	ΔS°_{25} , eu
			a	b	c			
A. For Complex (MOH)·Q								
Phenol-acetate ^a	2	1	1830	-12.7	0.018	-349	232	1.9
-propionate ^a	4	1	3899	-25.3	0.036	-426	702	3.8
-isobutyrate ^a	5	1	4938	-31.6	0.045	-465	942	4.7
-butyrate ^a	5	2	4668	-31.6	0.045	-735	672	4.7
Xylenol-acetate	3	1	2590	-17.1	0.023	-472	548	3.4
-propionate	4	1	3505	-22.8	0.031	-580	752	4.5
-isobutyrate	5	1	4423	-28.5	0.038	-687	1048	5.8
-butyrate	5	2	4334	-29.1	0.040	-786	782	5.3
B. For Complex Q·(MOH)								
Phenol-acetate	2	1	1830	-12.7	0.018	-349	232	1.9
-propionate	4	2	3628	-25.3	0.036	-696	431	3.8
-isobutyrate	6	2	5698	-37.9	0.054	-774	903	5.6
-butyrate	6	3	5428	-37.9	0.054	-1044	633	5.6
Xylenol-acetate	3	1	2847	-18.9	0.027	-387	449	2.8
-propionate	5	2	4325	-29.1	0.040	-786	773	5.2
-isobutyrate	6	2	5449	-36.1	0.050	-860	1009	6.3
-butyrate	6	3	5239	-36.1	0.050	-1070	799	6.3
<i>p</i> -Cresol-acetate	2	1	1830	-12.7	0.018	-349	232	1.9
-propionate	4	2	3628	-25.3	0.036	-696	431	3.8
-isobutyrate	5	2	4668	-31.6	0.045	-735	672	4.7
-butyrate	6	3	5428	-37.9	0.054	-1044	633	5.6
4- <i>n</i> -Propyl phenol-acetate	2	1	1661	-11.3	0.015	-365	329	2.3
-propionate	4	2	3355	-22.8	0.031	-730	602	4.5
-isobutyrate	5	2	4264	-28.5	0.038	-837	889	5.8
-butyrate	6	3	5018	-34.1	0.046	-1095	933	6.8

^a Assumed to be applicable to *p*-cresol-carboxylates and 4-*n*-propyl phenol-carboxylates also.

freedom in the complex $M_{H,H\phi}$, we have neglected an entropy contribution for the reaction $M_{II} \rightarrow M_{H,H\phi}$.

Using the $\Delta F^{\circ}_{H\phi}$ values of Table III, together with ΔS°_B , we can compute a correction term $K_{H\phi}'$, where the prime indicates that the ΔS°_B term has been added. These values of $K_{H\phi}'$ are listed in Table IV together with the uncorrected values of K_{assoc} (from Tables I and II). Substituting these values of $K_{H\phi}'$ for $K_{H\phi}$ in eq 20, we recompute k_{ex}' and evaluate A and B of eq 21, from which we obtain refined values $k_q^{R'}$ and $k_{assoc}^{R'}$ (from eq 11b and 11c). The value of $(\Delta F^{\circ}_{assoc})^0$ was corrected to zero ionic strength by addition of the term ΔF°_μ (obtained from Figure 3, assuming that the data of Figure 3 hold for all the phenolic compounds), and the resulting refined data expressed as K_{assoc}^R (see Table IV). It can be seen from Table IV that the corrected values K_{assoc}^R differ somewhat from the uncorrected values K_{assoc} .

The values of α obtained from eq 25 are listed in Table IV. Multiplication of K_{assoc}^R by α , and conversion to the corresponding standard free energy $\Delta F^{\circ}_{\alpha K}$, gives the standard free energy of formation of a complex having both a hydrogen and a hydrophobic bond.

The values of $\Delta F^{\circ}_{\alpha K}$ for formate were corrected for the lower basicity of formate, by addition of -150 cal/mol, as described earlier. Finally, from a van't Hoff plot of the temperature dependence of the uncorrected values of K_{assoc} (from Tables I and II), the values of ΔH°_{assoc} listed in Table IV were obtained; the data were not accurate enough to discern any variation of ΔH°_{assoc} with temperature.

Discussion

In order to obtain the experimental values of $\Delta F^{\circ}_{H\phi}$ for the formation of the hydrophobic bond in the (MOH)·Q complex, we subtract the values of $\Delta F^{\circ}_{\alpha K}$ (of Table IV) for the hydrogen bond (assumed to be those for the complex involving formate) from those for the higher homologs, *i.e.*

$$\Delta F^{\circ}_{H\phi} = (\Delta F^{\circ}_{\alpha K})_{\text{higher homolog}} - (\Delta F^{\circ}_{\alpha K})_{\text{formate}} \quad (26)$$

This subtraction procedure assumes additivity of the effects of hydrogen and hydrophobic bonding, and serves to minimize errors arising from the Noyes mechanism and errors in ΔS°_B . A similar subtraction provides $\Delta H^{\circ}_{H\phi}$ and $\Delta S^{\circ}_{H\phi}$. These experimental data

Table IV: Evaluation of $\Delta F^{\circ}_{H\phi}$ at 25°

Base	(K_{assoc}) ^a	($K_{H\phi}$) ^b	($K_{\text{assoc}}R'$) ^c	(k_qR') ^c	ΔF°_{μ} , cal/ mol	K_{assoc}^R	α	$\Delta F^{\circ}_{\alpha K}$	$\Delta H^{\circ}_{\text{assoc}}$, cal/mol
Phenol									
Formate	0.24	...	0.24	4.35	...	0.24	0.50	1111 ^d	-700 ± 170 ^{e,f}
Acetate	0.44	0.012	0.44	5.70	-30	0.46	0.64	737	-600 ± 280
Propionate	0.42	0.021	0.45	5.73	-45	0.49	0.67	660	-520 ± 160
Isobutyrate	0.33	0.025	0.36	5.08	-120	0.44	0.69	697	160 ± 110
Butyrate	0.45	0.039	0.52	5.42	-80	0.60	0.77	462	240 ± 70
3,5-Xylenol									
Formate	0.15	...	0.15	2.70	...	0.15	0.50	1353 ^d	0 ± 270
Acetate	0.26	0.027	0.29	3.68	-85	0.34	0.69	874	470 ± 110
Propionate	0.22	0.053	0.28	3.74	-130	0.35	0.73	801	880 ± 120
Isobutyrate	0.18	0.060	0.26	3.49	-245	0.43	0.76	660	980 ± 320
Butyrate	0.22	0.086	0.34	3.86	-190	0.47	0.79	592	350 ± 130
p-Cresol									
Formate	0.17	...	0.17	2.60	...	0.17	0.50	1283 ^d	Not determined
Acetate	0.29	0.012	0.29	3.39	-85	0.34	0.64	901	Not determined
Propionate	0.26	0.021	0.29	3.33	-130	0.36	0.67	849	Not determined
Isobutyrate	0.21	0.023	0.24	3.44	-245	0.36	0.69	825	Not determined
Butyrate	0.31	0.039	0.38	3.20	-190	0.52	0.77	545	Not determined
4-n-Propyl Phenol									
Formate	0.15	...	0.15	2.42	...	0.15	0.50	1353 ^d	Not determined
Acetate	0.25	0.012	0.25	3.50	-85	0.29	0.64	988	Not determined
Propionate	0.26	0.023	0.29	3.34	-130	0.36	0.67	849	Not determined
Isobutyrate	0.19	0.027	0.22	3.56	-245	0.34	0.69	874	Not determined
Butyrate	0.22	0.042	0.28	3.50	-190	0.39	0.77	717	Not determined

^a Uncorrected values taken from Tables I and II. ^b Calculated for the complex Q·(MOH) from the data in Table III, together with the ΔS°_B term. ^c Calculated with eq 20 and 21. ^d Standard free-energy change corrected for lower basicity of formate as described in text. ^e Probable error. ^f The values of $\Delta H^{\circ}_{\text{assoc}}$ were calculated from least-squares lines through the log K_{assoc} vs. $1/T$ data of Tables I and II.

Table V: Thermodynamic Parameters for Pairwise Hydrophobic Bond Formation between the Nonpolar Side Chains of Sodium Carboxylates and Phenolic Compounds at 25°

System	Experimental data ^a			Theoretical data ^a		
	ΔF° , cal/mol	ΔH° , cal/mol	ΔS° , eu	ΔF° , cal/mol	ΔH° , cal/mol	ΔS° , eu
Phenol-acetate	-374 ^b	100 ± 450 ^b	2.1 ± 1.8 ^b	-349	230	1.9
-propionate	-451	180 ± 330	2.6 ± 1.4	-426	700	3.8
-isobutyrate	-414	860 ± 280	4.8 ± 1.3	-465	940	4.7
-butyrate	-649	940 ± 240	5.8 ± 1.1	-735	670	4.7
Xylenol-acetate	-479	470 ± 380	3.6 ± 1.7	-472	550	3.4
-propionate	-552	880 ± 390	5.2 ± 1.7	-580	750	4.5
-isobutyrate	-693	980 ± 590	6.1 ± 2.3	-687	1050	5.8
-butyrate	-761	350 ± 400	4.2 ± 1.6	-786	780	5.3
p-Cresol-acetate	-382	Not determined		-349	230	1.9
-propionate	-434	Not determined		-426	700	3.8
-isobutyrate	-458	Not determined		-465	940	4.7
-butyrate	-738	Not determined		-735	670	4.7
4-n-Propyl phenol-acetate	-365	Not determined		-349	230	1.9
-propionate	-504	Not determined		-426	700	3.8
-isobutyrate	-479	Not determined		-465	940	4.7
-butyrate	-636	Not determined		-735	670	4.7

^a Calculated for the complex (MOH)·Q from the data in Table III. ^b Probable error. The probable error in ΔF° is ±100 cal/mol.

are shown in Table V, together with theoretical values computed for the complex $(\text{MOH}) \cdot \text{Q}$ from the data in Table III. The magnitudes, and trends with size of nonpolar group, of the experimental free energies agree very well with theoretical values.²⁶ For the enthalpy (and, therefore, the entropy), the experimental trends are in accord with theory, but the absolute values of the experimental data do not agree as well as do the free energies.²⁶ Considering the experimental diffi-

culties and correction terms involved, these experimental data provide verification of the theoretical values for *pairwise* hydrophobic bonds computed by Nemethy and Scheraga.⁸

(26) The values of $\Delta H^\circ_{\text{assoc}}$ of Table IV were obtained by a least-squares calculation, as indicated in footnote *f* of Table IV. Even so, the relative errors in $\Delta H^\circ_{\text{assoc}}$ are quite large. The ΔF data are much more reliable. This is reflected in the comparison of theoretical and experimental data in Table V.

The Electrical Conductivity of 0.10 M Potassium Chloride

Water-Alcohol Solutions under Hydrostatic Pressure

by R. A. Horne, D. S. Johnson, and R. P. Young

Arthur D. Little, Incorporated, Cambridge, Massachusetts (Received July 20, 1967)

The electrical conductivities of 0.10 M KCl in $\text{CH}_3\text{OH}-\text{H}_2\text{O}$, $\text{C}_2\text{H}_5\text{OH}-\text{H}_2\text{O}$, and $n\text{-C}_3\text{H}_7\text{OH}-\text{H}_2\text{O}$ solutions have been measured as a function of temperature, pressure, and solvent composition over the ranges 0–20°, 1 atm–4500 kg/cm², and 0.0–0.4 mole fraction of alcohol. The presence of the second solvent tends to make the solution more "normal" by decreasing the structure of the bulk medium and the local structure near the ions. The order of effectiveness, $n\text{-C}_3\text{H}_7\text{OH} > \text{C}_2\text{H}_5\text{OH} > \text{CH}_3\text{OH}$, indicates that the more dissimilar the second solvent is from water, the more "normal," *i.e.*, the less structured, the mixed solvent.

Introduction

The subject of the structure of liquid water is a highly controversial one. In this paper we will adopt a "mixture" rather than a continuum model, in particular the flickering cluster model of Frank and Wen.¹ Qualitatively speaking, this model seems to us to be the most reasonable of the many theories advanced although attempts to apply it quantitatively have not always been successful. According to this model, liquid water consists of relatively open H-bonded aggregates or "clusters," which are constantly forming and disappearing with thermal fluctuations of the microregions in the liquid, immersed in a more dense matrix of "free" or unaggregated water molecules.^{1–3}

We are fortunate inasmuch as we shall not be obliged to commit ourselves to such difficult questions as the fraction of H-bonded water, the structural details of the clusters, or whether or not the "free" water is indeed free, rotatable, monomeric water. As the temperature is increased, the water clusters are believed to fragment and dissolve,² but in going from 0 to 100°, while different theories give widely different values, they do seem to be in fairly general agreement that the decrease in the fraction of H bonding is

relatively slight, that is to say, there is an appreciable fraction of H bonding even at the boiling temperature. On the other hand, the application of hydrostatic pressure appears to be very effective at destroying water structure—indeed, viscosity data indicate that the high specific volume structured regions in liquid water have completely disappeared at a pressure of about 1000 kg/cm².⁴ The addition of an electrolyte affects both the water structure immediately adjacent to the ions and the more remote water as well, and may either increase or decrease the apparent amount of water structure depending on the nature of the ions.^{1,3,5}

(1) H. S. Frank and W. Y. Wen, *Discussions Faraday Soc.*, **24**, 133 (1957).

(2) G. Nemethy and H. A. Scheraga, *J. Chem. Phys.*, **36**, 3382 (1962).

(3) A great many models for liquid water have been proposed. For reviews, see (a) J. L. Kavanau, "Water and Water-Solute Interactions," Holden-Day, Inc., San Francisco, Calif., 1964; (b) O. Y. Samoilov, "Structure of Aqueous Electrolytic Solutions and the Hydration of Ions," Consultants Bureau, New York, N. Y., 1965; (c) R. A. Horne, *Survey Progr. Chem.*, in press, 1968. For the case against mixture models, see M. Falk and T. A. Ford, *Can. J. Chem.*, **44**, 1699 (1966).

(4) R. A. Horne and D. S. Johnson, *J. Phys. Chem.*, **70**, 2182 (1966).

(5) R. W. Gurney, "Ionic Processes in Solution," McGraw-Hill Book Co., Inc., New York, N. Y., 1953, Chapter 9.

Varying the temperature or pressure also affects the local water structure of the hydration atmospheres of ions in aqueous solutions.^{3,6} Increased temperature results in the loss of the more weakly bound outer regions of an ion's hydration atmosphere while leaving the innermost, tightly bound, electrostricted region intact, whereas increased pressure is capable of completely destroying the hydration atmosphere of an ion in aqueous solution. The presence of hydrophobic molecules or groups, or of an interface, is also capable of perturbing the local water structure.⁷ In the present studies we have added still another water-structure-perturbing factor to the combined influence of temperature, pressure, and electrolyte concentration, namely a second solvent. In this respect, because they contain both a hydrophobic hydrocarbon group and a hydrophilic hydroxyl group, alcohols are of particular interest. Fortunately, the structure of water-alcohol mixtures has been reviewed recently by Franks and Ives.⁸

In the past, although possible legitimate questions can be raised concerning its rigorous meaning, we have found the Arrhenius activation energy E_a of transport processes⁹ to be highly dependent upon and thus very useful in interpreting structural changes in aqueous electrolyte solutions,¹⁰ and this practice will be continued here. E_a of "normal" electrical conductivity exhibits a minimum between 1000 and 2000 kg/cm²,¹¹ and the behavior of E_a of viscous flow signals profound changes in this same pressure range.⁴

The structure of liquid alcohols is probably much simpler than that of water. They associate much less strongly, and, rather than forming large clusters, they form polymeric H-bonded chains which rarely contain more than 5 to 7 molecules for sterically hindered alcohols.⁸ The addition of alcohols to water raises the temperature of maximum density of the solutions.¹² This behavior and that from nmr¹³ and dielectric¹⁴ studies all suggest that alcohols tend to stabilize water structure, but this, as we shall see, is in contrast to the present results which lead to the conclusion that the addition of an alcohol tends to break up the structured regions in liquid water thus making the liquid more "normal," *i.e.*, unassociated.

Experimental Section

The apparatus and experimental procedures for measuring the electrical conductivity of solutions under hydrostatic pressure were described earlier.¹⁵ A capillary type of conductivity cell was used. Ordinarily, this cell contains a solution-hydraulic fluid interface. In the present experiments initial erratic results were attributed to the extraction of the alcoholic component of the solution by the hydraulic fluid, but this behavior was eliminated by using a Union Carbide L-45 silicone and/or rubber diaphragm barrier. The alcohols used were Mallinckrodt CP anhydrous

methanol, Rossville anhydrous ethanol, and Fisher Certified 1-propanol.

Results and Discussion

1. *The System 0.10 M KCl in CH₃OH-H₂O.* Figure 1 shows the temperature dependence of the specific conductance of 0.10 M KCl at 1 atm for 0.00, 0.05, 0.10, 0.15, 0.20, and 0.25 mole fraction of methanol. In order to compare present values with conductivities quoted in the literature, the information contained in Figure 1 is replotted in Figure 2 where conductivities read from Figure 1 are plotted *vs.* mole fraction of methanol. Extrapolation of the present results to 25° yields values in poor agreement with those reported by Agarwala and Manderville¹⁶ and Thomas and Manderville¹⁷ (these two papers are not in good agreement with one another despite their common author) but in good agreement with Garzon y Carmona.¹⁸ The present results at 5 and 10° are also in agreement with the older work. Unfortunately, more recent work¹⁹⁻²¹ on the conductivity of KCl solutions in CH₃OH-H₂O has been confined to concentration, solvent composition, or temperature ranges that makes comparisons with the present results difficult.

The dependence of conductance on solvent composition is apparently very complex. The Walden product *vs.* solvent composition curves exhibit maxima;⁸ hence there must be factors other than viscosity playing important roles in the ion-transport processes. Plots of the equivalent conductance *vs.* the square root of the electrolyte concentration exhibit maxima and minima^{16,17} not observed in the case of pure water. Amis²² has advanced a hypothesis of preferential

(6) R. A. Horne, *Advan. High Pressure Res.*, in press.

(7) R. A. Horne, A. F. Day, R. P. Young, and N. T. Yu, "Interfacial Water Structure," Arthur D. Little, Inc., Technical Report No. 23, Sept 30, 1966; Office of Naval Research Contract Nonr-4424(00).

(8) F. Franks and D. J. G. Ives, *Quart. Rev. (London)*, **20**, 1 (1966).

(9) S. Glasstone, J. K. Laidler, and H. Eyring, "The Theory of Rate Processes," McGraw-Hill Book Co., Inc., New York, N. Y., 1941, Chapters IX, X.

(10) R. A. Horne, R. A. Courant, and D. S. Johnson, *Electrochim. Acta*, **11**, 987 (1966).

(11) R. A. Horne, B. R. Myers, and G. R. Frysinger, *J. Chem. Phys.*, **39**, 2666 (1963).

(12) A. G. Mitchell and W. F. K. Wynne-Jones, *Discussions Faraday Soc.*, **15**, 161 (1953).

(13) I. V. Matyash and V. I. Yashichev, *Zh. Strukt. Khim.*, **5**, 13 (1964).

(14) P. S. Yastremostii and O. Y. Samoilov, *ibid.*, **4**, 844 (1963).

(15) R. A. Horne and G. R. Frysinger, *J. Geophys. Res.*, **68**, 1967 (1963).

(16) R. N. Agarwala and D. C. Manderville, *J. Indian Chem. Soc.*, **12**, 699 (1935).

(17) M. K. Thomas and D. C. Manderville, *Proc. Indian Chem. Soc.*, **6A**, 312 (1937).

(18) A. Garzon y Carmona, *Rev. Real. Acad. Cien. Exact., Fis. Nat Madrid*, **8**, 70 (1909).

(19) H. I. Schiff and A. R. Gordon, *J. Chem. Phys.*, **16**, 336 (1948).

(20) N. G. Foster and E. S. Amis, *Z. Physik. Chem.*, **3**, 365 (1955).

(21) S. Petrucci, *Acta Chem. Scand.*, **16**, 760 (1962).

(22) E. S. Amis, *J. Phys. Chem.*, **60**, 428 (1956).

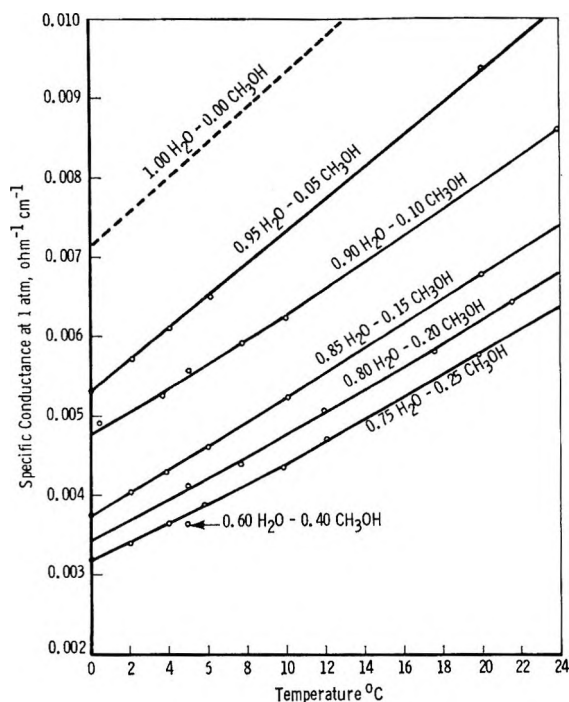


Figure 1. Temperature dependence of the specific conductance of 0.10 *M* KCl at 1 atm for various compositions of water-methanol as solvent.

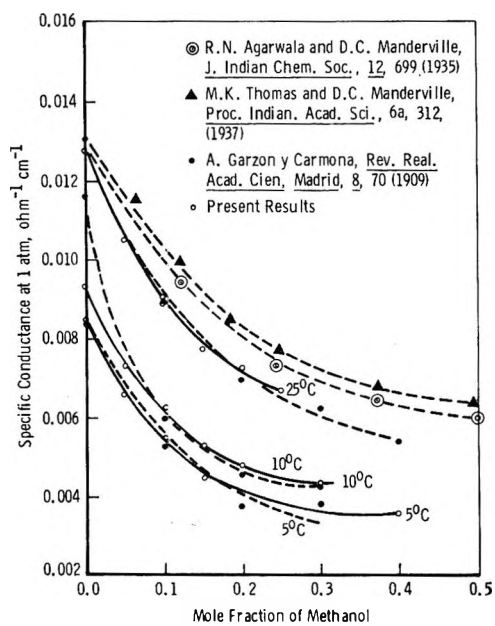


Figure 2. Solvent composition dependence of the specific conductance of 0.10 *M* KCl solutions at 1 atm in water-methanol.

solvation, and on the basis of the observed deviation from Walden's rule he concludes that the K^+ and Cl^- cling tenaciously to the higher dielectric constant solvent component and that CH_3OH 's do not substitute for H_2O 's in the innermost solvation sheath until the alcohol component reaches 30–40 wt %.

KCl is a strong electrolyte in water; however, the

question arises whether or not there might be association between K^+ and Cl^- in the lower dielectric constant medium of the mixed solvents. According to Franks and Ives,⁸ the Walden product for KCl in CH_3OH-H_2O mixtures exhibits a maximum between 0.1 and 0.2 mole fraction of methanol and then falls steeply with increasing methanol concentration just as one might expect if there is increasing association of K^+ and Cl^- . However, the present data would appear to indicate that association is not a problem. At 25° in going from 0.0 to 0.4 mole fraction of methanol, the twofold decrease in conductance (Figure 2) is just what one would expect from the twofold increase in viscosity; similarly in ethanol-water mixtures there is about a threefold decrease in conductance (extrapolated) corresponding to the threefold increase in viscosity. Furthermore, owing to electrostriction, the dissociation of partially dissociated electrolytes increases with increasing pressure;⁶ this phenomenon has been studied in particular detail in the case of $MgSO_4$;²³ hence, if KCl were weakly dissociated in the mixed media, $\kappa_P/\kappa_{1 \text{ atm}}$ should increase more rapidly with pressure than in pure water which is contrary to what is observed; it actually increases less rapidly. However, in applying this criterion it should be cautioned that a weak ion

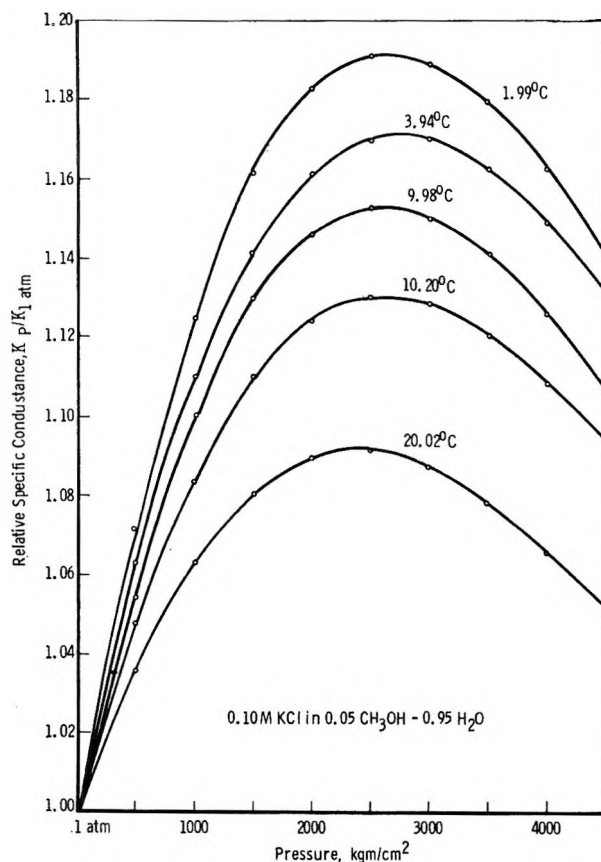


Figure 3. The relative conductance of 0.10 *M* KCl in 0.05 mole fraction of methanol under hydrostatic pressure.

(23) F. H. Fisher, *J. Phys. Chem.*, **66**, 1607 (1962).

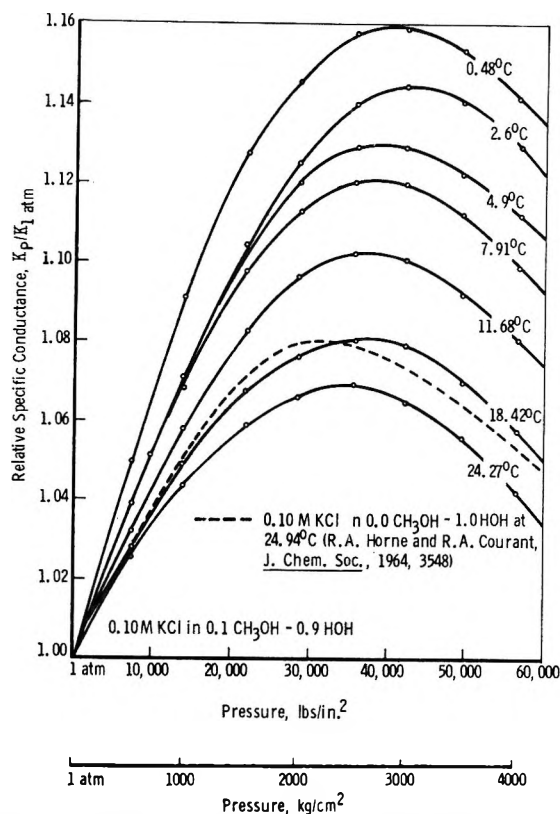


Figure 4. The relative conductance of 0.10 *M* KCl in 0.10 mole fraction of methanol under hydrostatic pressure.

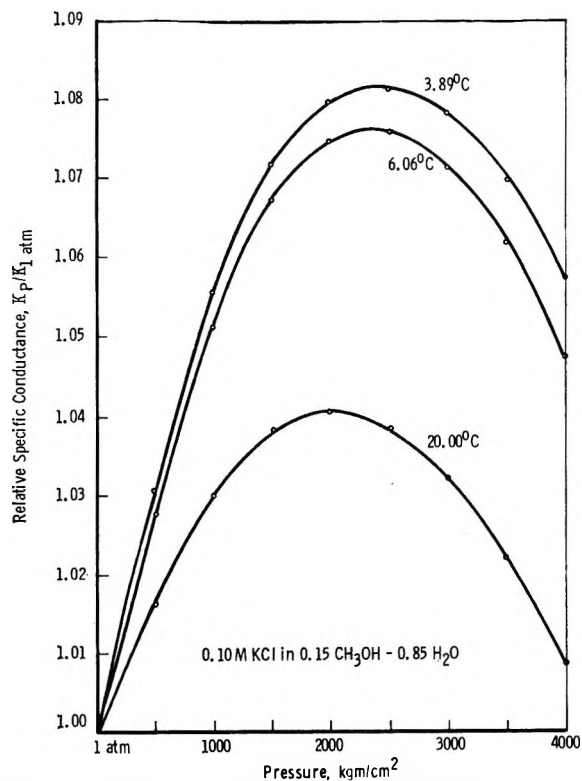


Figure 5. The relative conductance of 0.10 *M* KCl in 0.15 mole fraction of methanol under hydrostatic pressure.

pair in contrast to a strong, large volume change association may dissociate ever so slightly with increasing pressure.²⁴ In summary, then, the available

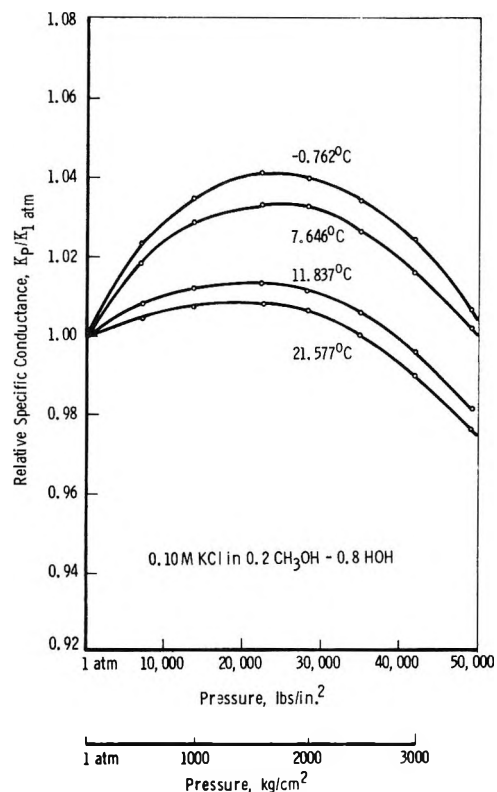


Figure 6. The relative conductance of 0.10 *M* KCl in 0.20 mole fraction of methanol under hydrostatic pressure.

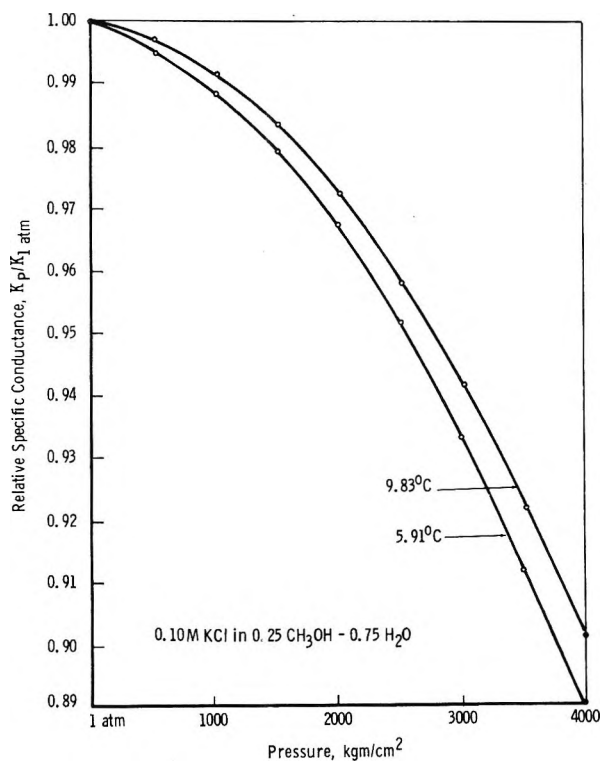


Figure 7. The relative conductance of 0.10 *M* KCl in 0.25 mole fraction of methanol under hydrostatic pressure.

(24) R. A. Horne, B. R. Myers, and G. R. Frysinger, *Inorg. Chem.*, **3**, 452 (1964).

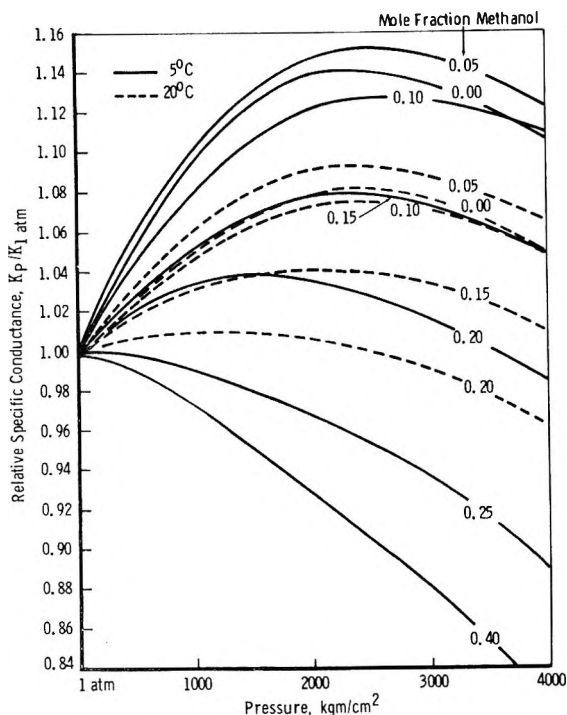


Figure 8. The effect of pressure on the relative specific conductance of 0.10 *M* KCl in CH₃OH-H₂O solutions.

evidence appears to point to the conclusion that ion association is not a complicating factor in the mixed solvent composition ranges of the present experiments.

At 24.35° the present conductance *vs.* pressure curve for water alone as solvent (not shown) over the range 1 atm-1000 kg/cm² is in good agreement with that published earlier by Horne and Courant,²⁵ the greatest difference between the two curves being at the maximum (at about 2000 kg/cm²) where the present results are about 0.38% higher. The effects of pressure on the relative specific conductances, $\kappa_P/\kappa_{1 \text{ atm}}$, for 0.10 *M* KCl in CH₃OH-H₂O mixtures are shown in Figures 3-7. The salient features of these curves are summarized in Figure 8 where $\kappa_P/\kappa_{1 \text{ atm}}$ at 5 and 20° is plotted *vs.* *P* for various mole fractions of methanol, including 0.4 mole fraction. Inspection of Figure 8 suggests that in a general way the influence of the addition of a second solvent is the same as increasing the temperature, namely, in the sense of breaking up the structured regions and making the solution more "normal" and reducing the height of the maxima in the pressure dependence of conductivity. This is not necessarily incompatible with the conclusion cited earlier that the addition of alcohols tends to stabilize water structure. A little bit of the foreign solvent may stabilize water structure, but larger amounts destroy it. The maxima in the methanolic mole fraction dependence of $(\kappa_P/\kappa_{1 \text{ atm}})_{\text{max}}$ (Figure 9) may be evidence of this, and more detailed examination of the structural contribution to change in the temperature of maximum density of water in the presence of alcohols⁸ points to this

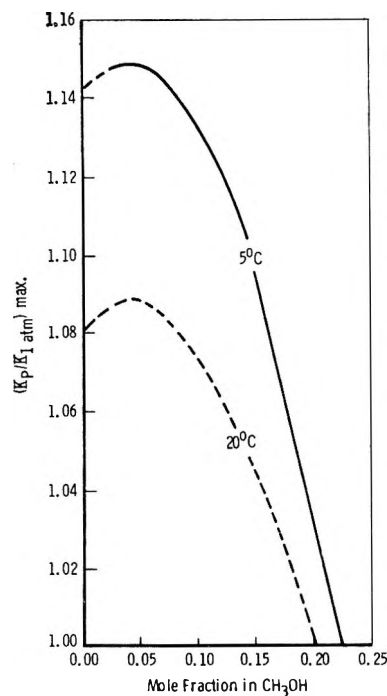


Figure 9. The dependence of the value of the maximum relative conductance on solvent composition.

same conclusion. Methanol is predominantly substitutionally dissolved in water. Thus, while small quantities can get "lost" in the clusters or in cages, larger quantities disrupt them. Then too we must remember that the anomalous maxima in conductance *vs.* *P* in aqueous solutions arise also in part from the pressure dehydration of the ions.⁶ If the presence of the second solvent destroys the outer and/or stabilizes the inner hydration atmospheres of ions, then the conduction behavior of the solution would be expected to be more "normal" in the sense that Stokes' law is more exactly applicable.

Further qualitative features of Figure 8 and the other figures which should be noticed are the decrease in the pressure at which $(\kappa_P/\kappa_{1 \text{ atm}})_{\text{max}}$ occurs with increasing mole fraction of methanol, the decrease in $(\kappa_P/\kappa_{1 \text{ atm}})$ at a given pressure, say 2000 kg/cm², with increasing temperature or mole fraction of methanol, and the lessening of this temperature effect with increased mole fraction of methanol.

Activation energies of the conduction process, E_a , were calculated by the integrated form of the Arrhenius equation

$$E_a = (\log \kappa_2 - \log \kappa_1) 4.576 T_2 T_1 / \Delta T \quad (1)$$

for 2° intervals. The minimum observed in E_a *vs.* *P* for strong 1:1 electrolytes¹¹ persists in the mixed solvent (Figure 10). However, as the mole fraction of methanol is increased, the minimum shifts to lower pressures, and by the time a mole fraction of 0.30 has

(25) R. A. Horne and R. A. Courant, *J. Chem. Soc.*, 3548 (1964).

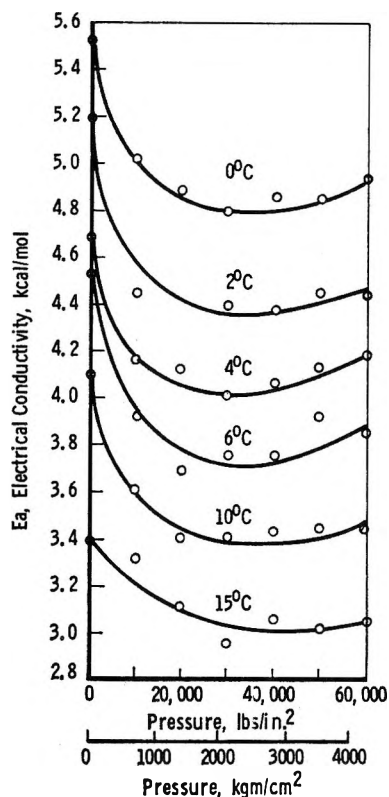


Figure 10. Pressure dependence of the Arrhenius activation energy of conductance in 0.2 mole fraction of methanol.

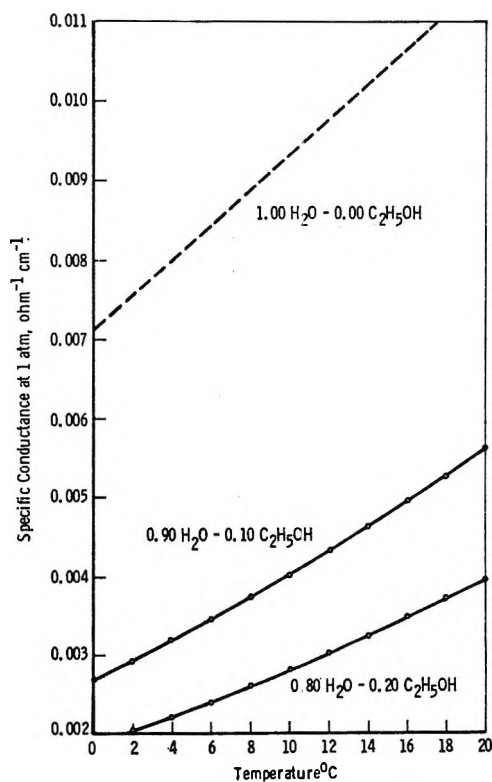


Figure 11. Temperature dependence of the specific conductance of 0.10 M KCl at 1 atm for various compositions of water-ethanol as solvent.

been reached, it has entirely disappeared for temperatures above 1°, so that E_a increases with increasing P .

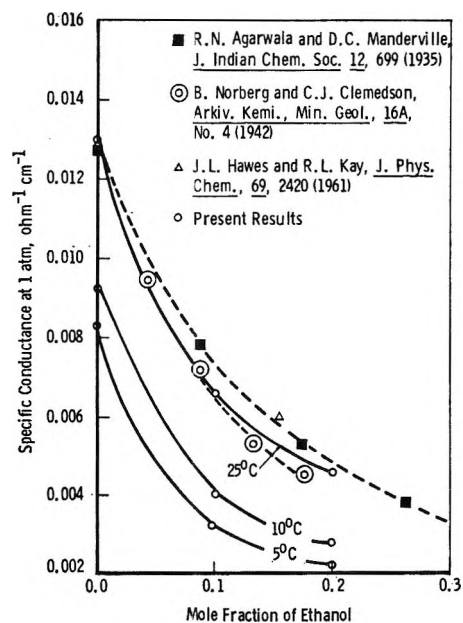


Figure 12. Solvent composition dependence of the specific conductance of 0.10 M KCl solutions at 1 atm in water-ethanol.

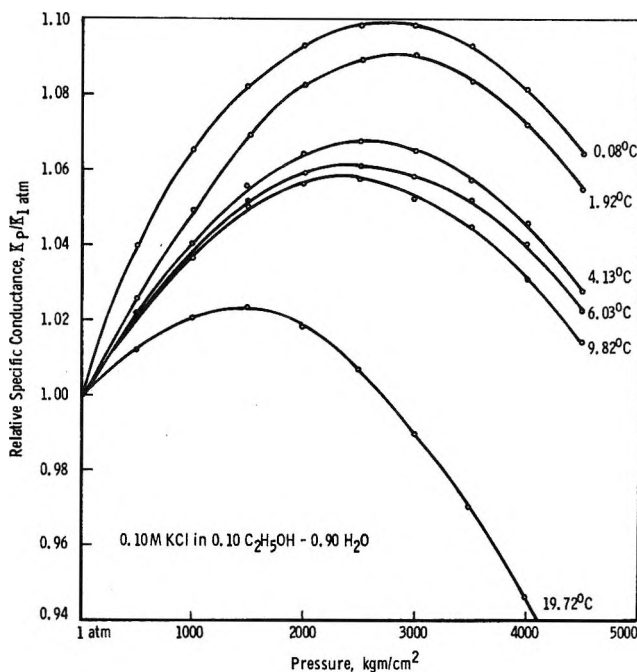


Figure 13. The relative conductance of 0.10 M KCl in 0.10 mole fraction of ethanol under hydrostatic pressure.

Below 1°, however, even in 0.30 mole fraction of methanol, a shallow minimum is still evident. Plots of E_a vs. mole fraction of methanol (not shown) tended to be very erratic for unclear reasons. Despite these difficulties, a trend did emerge indicating that, as one might have expected, E_a generally increases with increasing mole fraction of methanol. E_a vs. mole fraction may exhibit a maximum, but the scatter was so great that this cannot be said with any degree of certitude. The increased difficulty of the transport process

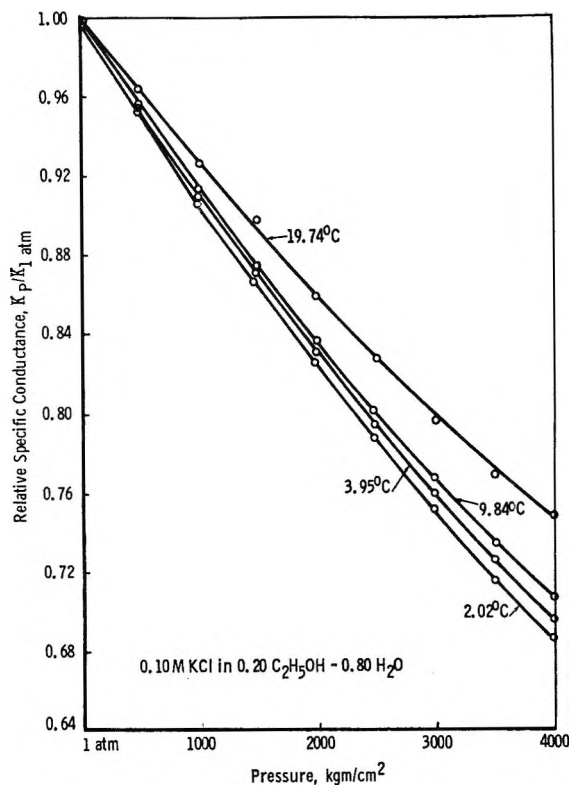


Figure 14. The relative conductance of 0.10 *M* KCl in 0.20 mole fraction of ethanol under hydrostatic pressure.

as reflected in the increased E_a need not imply solvent structure enhancement. For example, E_a in pure water decreases with increasing LiCl concentration although this electrolyte is a structure maker.²⁶

2. *The System 0.10 M KCl in C₂H₅OH-H₂O.* The specific conductances of 0.10 *M* KCl solutions in 0.0, 0.1, and 0.2 mole fraction of methanol at 1 atm are shown in Figures 11 and 12. The latter also contains values reported in the literature for the sake of comparison. The present results extrapolated to 25° yield values somewhat lower than those reported by Agarwala and Manderville¹⁶ for 0.10 *M* solutions and Hawes and Kay²⁷ for a 0.013 *M* solution but in good agreement with Norberg and Clemenson²⁸ below 0.1 mole fraction and somewhat higher above. Figures 13 and 14 show the relative conductance, $\kappa_P/\kappa_{1 \text{ atm}}$, of 0.10 *M* KCl solutions in 0.10 and 0.20 mole fraction of ethanol, respectively, under hydrostatic pressures. Comparison with Figures 4 and 6 clearly indicates that ethanol is more effective at reducing both $(\kappa_P/\kappa_{1 \text{ atm}})_{\text{max}}$ and the pressure at which it occurs. In fact, in 0.20 mole fraction of ethanol the maximum has disappeared entirely at all temperatures examined and the specific conductance decreases with increasing pressure just as one might expect if the solvent were a "normal" unassociated liquid. Similarly, the minimum in E_a vs. P , which, for methanol-water systems, disappeared only at the higher mole fractions, in the case of ethanol-water systems has entirely disappeared at all temperatures

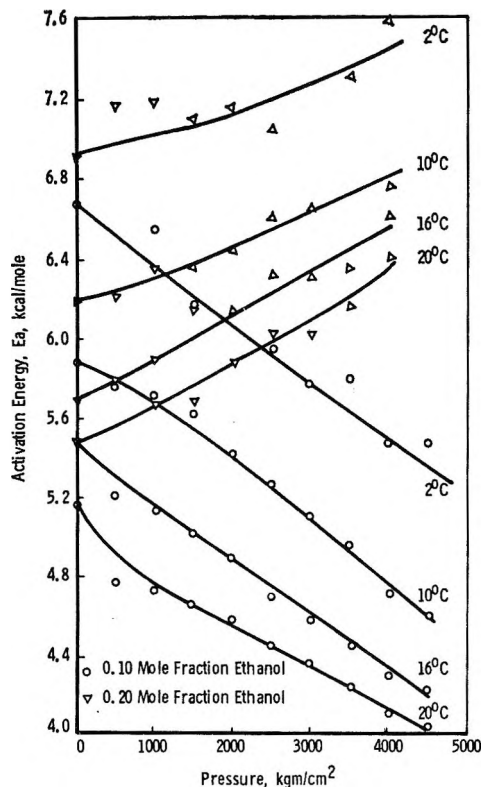


Figure 15. Pressure dependence of the Arrhenius activation energy of conductance in ethanol-water.

so that at a mole fraction of only 0.20, E_a increases steadily with increasing pressure (Figure 15). An unexpected feature is the decrease in E_a with increasing pressure at 0.10 mole fraction of ethanol with no evidence of a minimum such as was observed in the case of methanol. Despite these marked differences in behavior of E_a vs. P , E_a vs. T (not shown) decreases with increasing T over the range 5–20° with the same slope, about 0.07 kcal/mole deg at both 0.10 and 0.20 mole fraction of ethanol and at all pressures up to 4000 kg/cm². At 1 atm, E_a is between 0.1 and 0.2 kcal/mole greater in 0.20 than in 0.10 mole fraction of ethanol (Figure 15).

3. *The System 0.10 M KCl in n-C₃H₇OH-H₂O.* The specific conductances of 0.10 *M* KCl solutions in water-1-propanol are shown in Figure 16 as a function of temperature and replotted in Figure 17 in order to show the dependence on the mole fraction of the non-aqueous constituent of the solvent. Figures 18, 19, 20, and 21 show the dependence of the conductance relative to its 1-atm value as a function of pressure for various mole fractions of 1-propanol. The same phenomena noted in the case of ethanol such as the disappearance of the maximum in $\kappa_P/\kappa_{1 \text{ atm}}$ vs. P are now even more marked and occur at a lower mole fraction

(26) R. A. Horne and D. S. Johnson, *J. Chem. Phys.*, **45**, 21 (1966).

(27) J. L. Hawes and R. L. Kay, *J. Phys. Chem.*, **69**, 2420 (1965).

(28) N. Norberg and C. J. Clemenson, *Arkiv Kemi Min. Geol.*, **16A**, No. 4 (1942).

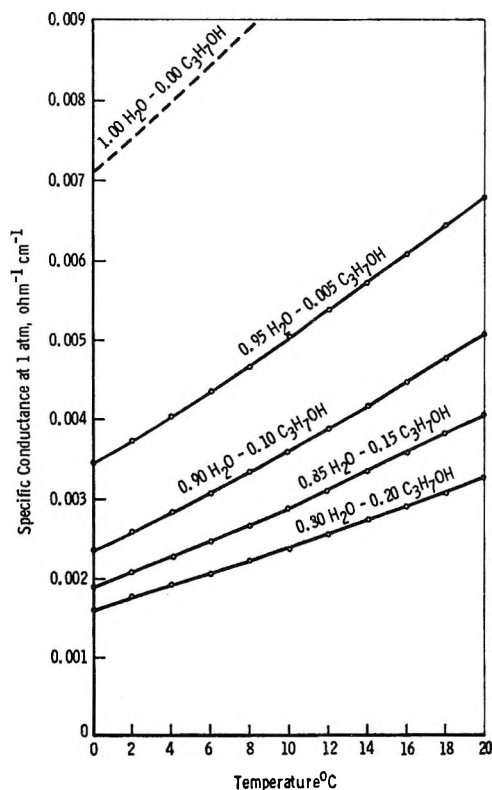


Figure 16. Temperature dependence of the specific conductance of 0.10 M KCl at 1 atm for various compositions of water-1-propanol as solvent.

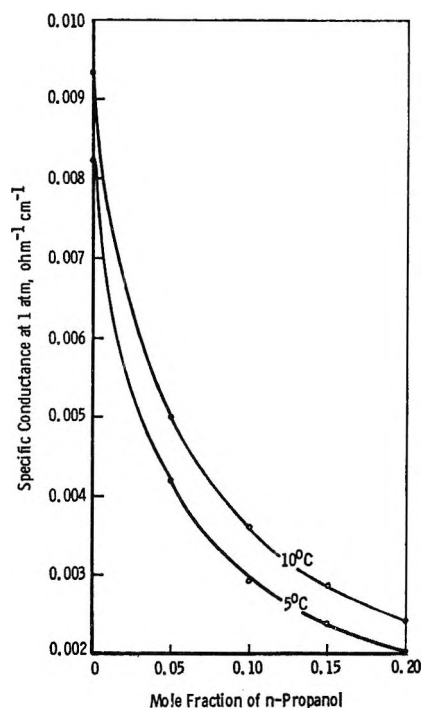


Figure 17. Solvent composition dependence of the specific conductance of 0.10 M KCl solutions at 1 atm in water-1-propanol.

of the alcoholic solvent constituent. In fact, the mole fraction of the alcohol must now be reduced to 0.05 in order for the maxima to appear (Figure 18). At tem-

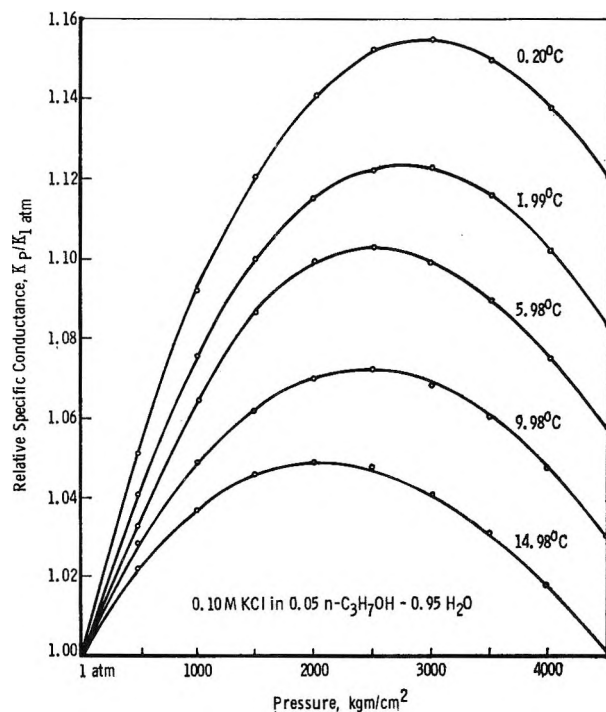


Figure 18. The relative conductance of 0.10 M KCl in 0.05 mole fraction of 1-propanol under hydrostatic pressure.

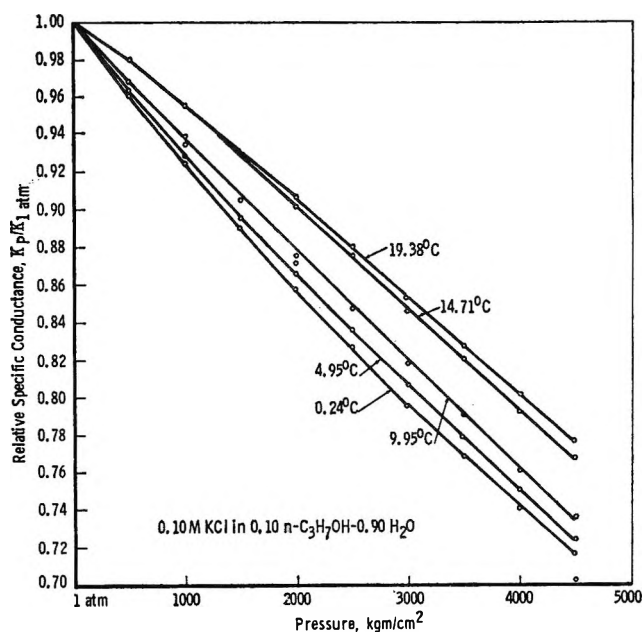


Figure 19. The relative conductance of 0.10 M KCl in 0.10 mole fraction of 1-propanol under hydrostatic pressure.

peratures and concentrations where maxima appear, that is to say conditions such that $\kappa_P/\kappa_{1 \text{ atm}} > 1$, $\kappa_P/\kappa_{1 \text{ atm}}$ increases with decreasing temperature, but in the absence of maxima where $\kappa_P/\kappa_{1 \text{ atm}}$ is always < 1 , $\kappa_P/\kappa_{1 \text{ atm}}$ decreases with decreasing temperature. E_a vs. P for the $C_3H_7OH-H_2O$ system (not shown) resembles the corresponding curves for the CH_3OH-H_2O system: for 0.05 mole fraction of $n-C_3H_7OH$ a shallow minimum occurs at about 3000 kg/cm², but for all higher mole fractions

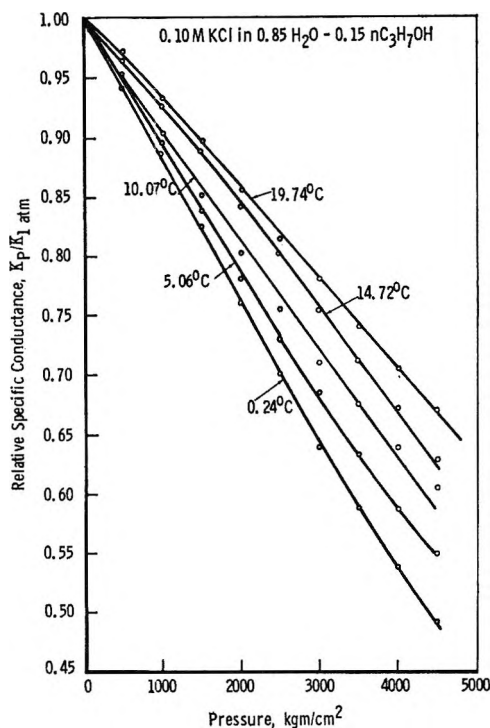


Figure 20. The relative conductance of 0.10 *M* KCl in 0.15 mole fraction of 1-propanol under hydrostatic pressure.

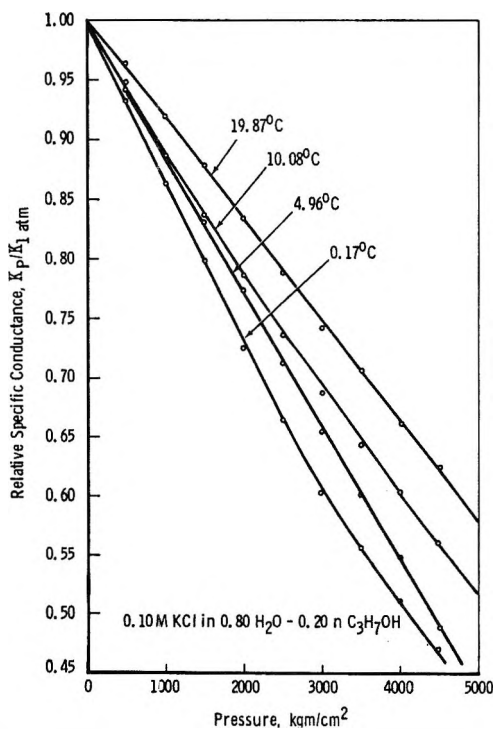


Figure 21. The relative conductance of 0.10 *M* KCl in 0.20 mole fraction of 1-propanol under hydrostatic pressure.

E_a increases with increasing hydrostatic pressure. As in the case of methanol, E_a vs. mole fraction (not shown) generally increases, but there appears to be a maximum whose height increases with increasing pressure and whose position shifts to higher mole fractions with increasing pressure.

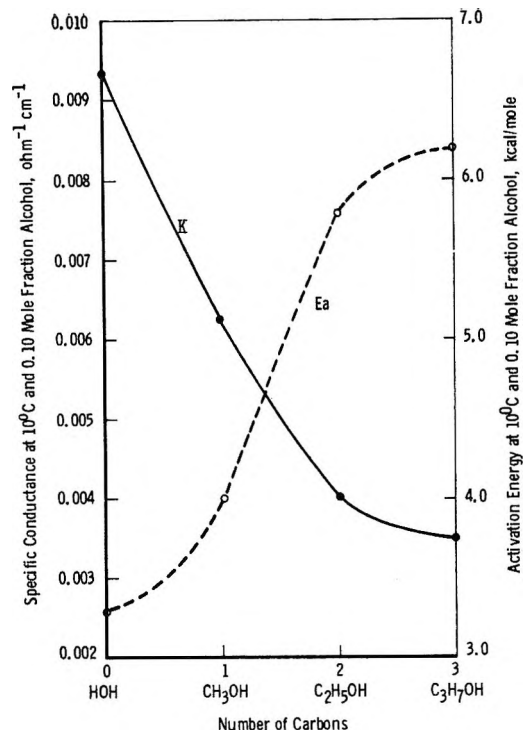


Figure 22. Comparison of the effects of different alcohols on the specific conductance and activation energy of conductance at 1 atm.

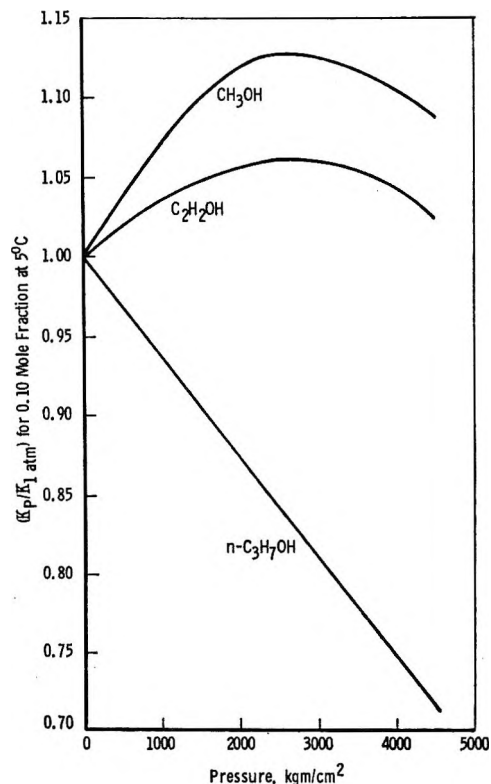


Figure 23. The effect of different alcohols on the relative specific conductance of aqueous 0.10 *M* KCl solutions under hydrostatic pressure.

4. *Comparison of the Three Mixed-Solvent Systems and Summary.* The addition of a series of second solvents of increasing dissimilarity to water in terms of the

increasing importance of their hydrophobic portion impedes ion transport resulting in a decrease in conductivity and an increase in the required activation energy (Figure 22). While it may not be possible to assign quantitative values of the relative importance of the several factors responsible for this impedance of the transport process, they can be identified as (1) increasing viscosity, (2) possible changes in solvent structure, and (3) changes in the composition of the total solvation atmospheres of the ions. In the light of the pressure dependence of conductivity (Figure 23), the more dissimilar to water the second solvent added, the more "normal" the solutions become in the sense that the anomalous maximum in $\kappa_P/\kappa_{1 \text{ atm}}$ vs. P becomes diminished in magnitude, displaced to smaller pressures, and, in the presence of a structure-breaking influence such as increased temperature, tends to disappear altogether. From this we conclude that the addition of a solvent dissimilar to water tends to destroy the structure of water, and/or the presence of an alien second solvent stabilizes the apparent radii of ions in solution. The second alien solvent, then, like increased temperature or increased pressure, is a water-structure breaker. The order of effectiveness of the second solvent in inducing "normalcy" is $n\text{-C}_3\text{H}_7\text{OH} > \text{C}_2\text{H}_5\text{OH} > \text{CH}_3\text{OH}$. The structural contributions to elevation of the temperature of maximum density of

water exhibit their maxima for the several alcohols at low mole fractions (less than 0.04), and the basis of this phenomenon is apparently quite complex.⁸ It is thus premature to take the foregoing conclusion based on much larger mole fractions as being incompatible with the apparent enhancement of water structure as evidenced by the elevation of the temperature of maximum density.

Stabilization of the apparent radii of the ions can come about in two ways. Preferential solvation by the high dielectric constant component might stabilize the innermost, strongly bound, electrostricted hydration sheath, thereby protecting the ions from further pressure dehydration. Alternatively, but less likely, the second solvent may sufficiently disrupt the hydration atmosphere of the ions so that there is no hydration sheath left to be destroyed by the application of pressure.

The Walden products of the alkali halides in $\text{CH}_3\text{OH}-\text{H}_2\text{O}$ and $\text{C}_2\text{H}_5\text{OH}-\text{H}_2\text{O}$, as mentioned earlier, exhibit maxima below 0.2 mole fraction,⁸ but again interpretation is confounded by the inability to separate the effects of the second solvent on the structure of the bulk media from the effects on the local solvent structure near the ions.

Acknowledgment. This work was supported in part by the Office of Naval Research.

The Rate of Oxidation of Nitrite Ions in Dilute Solutions of Sodium Nitrite in Molten Lithium Perchlorate¹

by David W. James

Department of Chemistry, University of Queensland, Brisbane, Australia (Received July 24, 1967)

In dilute solutions of sodium nitrite in molten lithium perchlorate at 245–301°, nitrite ions are oxidized to nitrate ions while perchlorate ions are reduced to chloride ions in a pseudo-first-order homogeneous reaction. The first-order rate constant is $3.51 \times 10^{-4} \text{ sec}^{-1}$ at 274°, and the activation energy is 31.5 kcal/mol. There is no buildup of chlorate ions during the course of the reaction. The reaction is unaffected by gaseous nitrogen or substantial additions of water, LiOH (5 mol %), or LiNO₃ (10 mol %) and by gaseous oxygen. The evidence suggests the possibility that the rate-determining step involves a direct oxygen transfer between a nitrite and a perchlorate ion.

Introduction

There is very little quantitative information about reaction rates in ionic liquids and even less information about reaction mechanisms. The singular presence of ionic species, the interaction of which is not diluted by a nonionic solvent, gives these systems their unique character. Thus it has been found that when molten nitrates are used as solvents in acid–base reactions, the nitrate ion enters actively into the reaction mechanism with the formation of NO₂⁺ and NO₂.² On the other hand, in systems containing bromate ions, the participation of nitrate ions was suppressed with the formation of BrO₂⁺ and Br₂.³ It is not uncommon for such reactions to be quite fast. In many instances, the rate is probably determined by the diffusion of reacting species. Thus the chemical behavior of many molten salt systems is successfully rationalized by the assumption that thermodynamic equilibrium is attained very rapidly. On the other hand, it is also well known that molten salt reactions which involve oxo ions may be rather slow, as, for example, the decomposition of molten alkali metal nitrates a few hundred degrees above their melting points.

In the present paper, we report quantitative data on a slow reaction between oxo anions in an ionic melt. Small amounts of NO₂⁻ in the form of NaNO₂ were added to molten LiClO₄ and the NO₂⁻ anions were oxidized to NO₃⁻, while the solvent ClO₄⁻ anions were simultaneously reduced to Cl⁻. The reaction isotherm was measured spectrophotometrically by determining the change with time of the absorption intensity of NO₂⁻ and NO₃⁻ bands.

Experimental Section

Lithium perchlorate of 99.5% purity (reagent grade) was recrystallized twice from water and dried under a

current of dry nitrogen, while the temperature was slowly raised to 270°. The molten salt was maintained at this temperature for several hours with dry nitrogen bubbling through it. Then the salt was filtered through a fine Pyrex filter and sealed in a Pyrex tube under a reduced pressure of dry nitrogen. The dry, solidified material was subsequently handled in a controlled-atmosphere box. The chlorate content of this material was 0.004 mol %.

Reagent grade sodium nitrite was recrystallized from water, dried under reduced pressure at 100° for 48 hr, and stored in a desiccator.

Lithium nitrite⁴ was recrystallized twice from water and dried at 50° under reduced pressure. This produced the monohydrate.

Lithium hydroxide, lithium nitrate, and sodium nitrate were recrystallized from water and dried by heating to their melting points under vacuum.

Reaction isotherms were determined by measuring the ultraviolet spectra of the solution as functions of time. Lithium perchlorate is essentially transparent to 190 mμ, while nitrite, nitrate, and chloride ions have absorption bands at longer wavelengths in the ultraviolet. The nitrite ion dissolved in molten lithium perchlorate has an absorption maximum at 330 mμ, while the nitrate ion has a maximum of 286 mμ. Either of these bands may be monitored to follow the course of the reaction.

The nitrate peak occurs at a wavelength where nitrite

(1) Part of this research was sponsored by the U. S. Atomic Energy Commission under contract with the Union Carbide Corp.

(2) F. R. Duke and S. Yamamoto, *J. Am. Chem. Soc.*, **81**, 6378 (1959); F. R. Duke and M. L. Iverson, *ibid.*, **80**, 5061 (1958); *Anal. Chem.*, **31**, 1283 (1959).

(3) F. R. Duke and J. Schlegal, *J. Phys. Chem.*, **67**, 2487 (1963).

(4) Dr. D. Gruen, Argonne National Laboratory, is thanked for the gift of LiNO₂·H₂O.

absorbs somewhat, while the nitrite maximum has little or no significant contribution from the nitrate band at the concentrations we studied. The chloride ion has an intense absorption in the region 180–200 $m\mu$, but our measurements were made beyond the effective zero of the tail of this band. The chlorate ion spectrum was determined and found to have a weak band (~ 0.1) at a wavelength of 286 $m\mu$.⁶ However, since this ion was present only in trace concentrations, this band did not contribute to the measured absorbance.

The reaction vessel was a standard 1-cm square absorption cell made of fused silica. The absorption was continuously monitored at a fixed wavelength with a Cary Model 11 spectrophotometer. The furnace and absorption cells used have been described previously.⁶ Absorption measurements were made against air as a reference. Losses due to solvent absorption and internal reflections were measured before addition of nitrite and subtracted from subsequent measurements.

A sample of LiClO_4 was weighed into the absorption cell in the drybox and transferred, under an atmosphere of dry nitrogen, to the preheated spectrophotometer cell compartment. The salt was allowed to melt and come to equilibrium at the temperature of the measurement. Then all air bubbles that formed during melting were removed by vigorous stirring. The absorption of cell with solvent was determined over a small wavelength interval in the neighborhood of 330 $m\mu$. Then an addition of dry NaNO_2 to give a concentration between 0.05 and 0.3 mol % was made, and the mixture was stirred for several minutes. Stirring was carried out manually and also by bubbling with dry nitrogen gas, both methods giving identical results. It was not possible to stir continuously during spectrophotometric measurements. Therefore the reaction mixture was stirred for 30 sec at 15-min intervals and allowed to equilibrate. The absorption of 330 $m\mu$ was followed continuously (including mixing periods). The temperature fluctuation during the addition and mixing procedure was estimated to be no more than 2–3°. The increase in concentration of chloride and chlorate ions was determined for a selection of samples after the reaction was complete.

The furnace temperature was controlled by a Leeds and Northrup Speedomax G/DAT controller, and the optical cell inside the furnace was located within a silver block which acted as a heat reservoir. The temperature of this block did not vary by more than 0.5° during 24 hr.

A second series of measurements was made to examine the effect on the reaction of changing some of the chemical variables. These reactions were carried out in Pyrex tubes heated in an aluminium-block tube furnace controlled by a Thermoelectric Model 80410 proportional controller. The reaction was allowed to proceed for a fixed time, after which the tube was

chilled to solidify the reaction medium. The increase in chloride ion content of the medium was determined by one of three methods. In most cases, a titration with mercuric nitrate using diphenylcarbazone as indicator was used.⁷ However, samples that contained an excess of nitrite, and also some other samples, were analyzed either by Volhard titrations with silver nitrate or by gravimetric precipitation as silver chloride.⁸

Results and Discussion

There was a brief initial period during which the reaction rate showed irregular behavior. This normally lasted from 10 to 20 min, and for the whole of the subsequent time, the reaction isotherm was simple and regular. The reaction was studied at five temperatures from 245 to 301°. At each temperature, several determinations of the reaction isotherm were made to obtain the final kinetic parameters. Results for duplicate runs agreed to within experimental uncertainty.

At all temperatures, the nitrite concentration followed a first-order rate of decrease that was independent of the initial nitrite concentration for the dilute solutions studied (0.05–0.30 mol %). The collected data from all determinations are given in Table I. When an Arrhenius plot is made of these data, it is found that all, except the lowest temperature datum point, fit a straight line. The lowest temperature determination was ignored in the Arrhenius plot, because difficulty was

Table I: First-Order Rate Constants

Temp, °C	Concn of NaNO_2 , mol %	10^4k , sec^{-1}
245	0.28	0.404 ± 0.1
260	0.1–0.3	1.79 ± 0.05
274	0.15–0.3	3.51 ± 0.05
290	0.2–0.3	9.61 ± 0.05
301	0.2–0.3	13.10 ± 0.05

encountered in measurements within 10° of the melting point of LiClO_4 , so it was considered that large errors might be associated with the data at 245°. The activation energy and frequency factor derived from the remainder of the data are 31.5 kcal and $8.91 \times 10^8 \text{ sec}^{-1}$, respectively.

Since the reaction involves an oxygen transfer of some sort from perchlorate to nitrite, a material balance provides some information on the reaction. It is known

(5) Dr. W. G. Williams is thanked for the gift of a sample of anhydrous LiClO_4 .

(6) C. R. Boston and G. P. Smith, *J. Phys. Chem.*, **62**, 409 (1958).

(7) F. E. Clark, *Anal. Chem.*, **22**, 553 (1950); I. Roberts, *Ind. Eng. Chem. Anal. Ed.*, **8**, 365 (1936); G. B. Smith, *Anal. Chim. Acta*, **7**, 330 (1952).

(8) A. I. Vogel, "Quantitative Inorganic Analysis," 2nd ed, Longmans, Green and Co., London, 1957, pp 251, 258.

that the decomposition of sodium perchlorate in fused hydroxide takes place in two steps; the first step leads to formation of sodium chlorate and is about 18 times as fast as the second step which is the decomposition of chlorate to chloride.⁹ If a similar reaction path were followed in the present reaction, chlorate ion would be the dominant reduced species with small amounts of chloride ion. Analysis of reaction mixtures from several kinetic determinations showed no increase in chlorate concentration over that initially present in the lithium perchlorate (0.004 mol %).

If an over-all reaction obeying the equation



is postulated, then a final concentration of chloride ion equal to one-fourth of the initial nitrite concentration should be formed. The results of several determinations of terminal chloride concentration are presented in Table II, which shows that complete reduction of the perchlorate ion takes place. The terminal concentration of nitrate ion was checked spectrophotometrically (interference from other ions was negligible) and found to agree closely with the concentration of sodium nitrite originally added.

Table II: Stoichiometry of Over-all Reaction

Wt of NaNO ₂ , g	Concn of NaNO ₂ , mol %	Temp, °C	Wt of Cl ⁻ measd, g-ions × 10 ³	Wt of Cl ⁻ calcd, g-ions × 10 ³
0.0282	0.08	280	3.58 ± 0.15	3.58
0.0206	0.07	280	2.44 ± 0.15	2.59
0.0157	0.04	275	1.77 ± 0.1	1.97

Seward and Otto⁹ found considerable dependence of the perchlorate decomposition rate on the nature of the cation. The cations in our melts are predominantly Li⁺ with a small concentration of Na⁺ from the NaNO₂ added. Nevertheless, an attempt was made to carry out the reaction with lithium as the only cationic species. Anhydrous lithium nitrite is unstable and so the monohydrated salt was used. It was not possible to obtain consistent reaction isotherms at any temperature in the range studied (245–301°).

The reaction isotherms were the same when either silica or Pyrex vessels were used as containers. Furthermore, when finely ground silica or Pyrex was added in amounts sufficient to increase the surface area by at least an order of magnitude, the change in the rate constant measured at 270° was less than experimental uncertainty. These measurements indicate that the reaction is homogeneous.

The effect of adding a number of chemicals in varying concentrations was carried out in order to elucidate the reaction mechanism with the results given in Table III.

The concentration of water added was quite uncertain as the lithium perchlorate dehydrates at the temperatures used. The addition of lithium hydroxide and nitrate demonstrates that the reaction is independent of minor concentrations of hydroxyl and nitrate ions (in contrast to the findings of Seward and Otto for related systems⁹). Presence of dissolved oxygen gas or larger cations however had a pronounced retarding effect, the effect of oxygen persisting even after the melt was well scrubbed by bubbling with dry nitrogen. It may be noted that an increase in glass surface did not alter the measured rate in the presence of dissolved oxygen, showing that the retardation was independent of surface area. The pronounced retardation of the reaction noted when significant concentrations of NaNO₃ were added must be attributed to the presence of Na⁺ ions in the melt, as no retardation was noted with LiNO₃. We therefore conclude that the strong polarizing power of the lithium ion (compared with the sodium ion) probably plays an important role in the reaction mechanism.

Although the data presented here do not identify the reaction path or permit an unambiguous specification of the rate-controlling step, they are in better accord with certain possible rate-controlling steps than others. The reaction, as shown in eq 1, goes all the way to chloride, so that four oxygens are transferred for each perchlorate consumed. The reaction is very efficient; virtually all oxygens end up in nitrate ions rather than oxygen gas. Possible intermediates include ClO₃⁻, ClO₂⁻, and ClO⁻. There is no buildup of ClO₃⁻, so that if this particular intermediate is formed, it is consumed very rapidly compared with the rate-controlling step. Furthermore, the analysis of quenched-reaction mixtures indicates that Cl⁻ builds up about as fast as NO₂⁻ reacts, so that it would appear that the reaction of other intermediates is not rate controlling either. We are led to suppose that the rate-determining step is an oxygen transfer between ClO₄⁻ and NO₂⁻.

This rate-determining oxygen transfer may take place by direct nitrite-perchlorate contact or by diffusion. The latter alternative corresponds to decomposition of the perchlorate. There are two considerations which suggest that perchlorate decomposition is not rate controlling. First, the oxidation of the dissolved nitrite was definitely faster than the decomposition of lithium perchlorate in the absence of nitrite. Second, the rate of decomposition of perchlorate in molten NaOH is reported⁹ to be 10⁴ times as fast as the same reaction in pure NaClO₄ or KClO₄, whereas we found that additions of 5 mol % LiOH to LiClO₄ had no appreciable effect on the rate of oxidation of dissolved nitrite. When lithium is the only cationic species, anion contact is inevitable, and, thus, it is considered

(9) R. P. Seward and H. W. Otto, *J. Phys. Chem.*, **65**, 2078 (1961).

Table III: Effect of Added Reagents on Rate Constant^a

Added chemical	Concn, mol %	Temp, °C	Rate constant × 10 ⁴ , sec ⁻¹	Comment
H ₂ O	8-40	265, 275	2.3, 3.5	Water added before fusion
N ₂	...	265-300	2.3-13.1	Nitrogen gas bubbled through melt
O ₂	...	265	0.7	Oxygen bubbled for 10 min before and after nitrite addition
		275	0.85	
O ₂ + N ₂	...	275	0.85	Oxygen as above followed by nitrogen bubbling for 10 min
LiOH	5	270	2.9	Salts added to the LiClO ₄ before fusion
LiNO ₃	10	270	2.9	
NaNO ₃	10	270	0.3	
	20	270	0.08	

^a Rate constant estimated by determination of chloride concentration in quenched reaction.

that oxygen transfer probably involves an anion-anion contact pair.

No details of subsequent steps in the reaction can be verified. It is known however that LiClO₃ is extremely unstable above 170°,¹⁰ and, hence, a rapid decomposition of the chlorate ion is assumed. The resultant atomic oxygen could either form molecular oxygen or diffuse through the melt and react with nitrite ions. Stoichiometric considerations and the absence of evolved oxygen support the latter proposal.

Although the above mechanism is plausible and describes the experimental isotherms reasonably well, it does not explain why the reaction is retarded by larger cations, is unaffected by anions, water, or nitrogen, and is retarded by molecular oxygen. On a size basis, the larger cations would be expected to hinder anion-anion contact more effectively than the lithium ion. It is unlikely however that the sodium ion is large enough to produce the observed retardation on this basis. The small size of the lithium ion confers a high polarizing power which may act on either or both of the anions. It is known that the perchlorate ion is difficult to polarize and the lithium ion will tend to "solvate" itself with polarizable species either ionic or dipolar.¹¹ The nitrite ion being very unsymmetrical is very readily polarized. Hence whereas the lithium ion has a relatively minor effect on the perchlorate ion, the nitrite ion is strongly polarized, and, as shown by

the instability of lithium nitrite, this polarization decreases the potential energy of the ion. The active complex may then be seen as the lithium-nitrite ion pair and the problem of the kinetics resolves itself into a consideration of the probability of a suitably orientated collision. The determination of the symmetry of this ion pair and the nature of the Li⁺-O₂N interaction are far from simple and will be the subject of a separate communication.

On the basis of the active participation of Li⁺ in the reaction mechanism, the retarding effect of sodium ions is understood as predominantly due to a reduction in the average polarization of the nitrite ions.

The effect of dissolved oxygen gas is of obvious importance to the reaction mechanism. The effect is evidently quite complex, however, since the oxygen is not removed by prolonged scrubbing with nitrogen and more work is necessary before the action of dissolved oxygen can be adequately described.

Acknowledgments. Dr. G. P. Smith and Dr. J. H. O'Donnell are thanked for helpful discussion during the preparation of this paper. Mr. J. Burnett and Mr. D. Clegg are thanked for assistance in some of the analytical determinations.

(10) D. G. Williams, private communication.

(11) D. W. James, W. H. Leong, and R. C. Marshall, unpublished work.

Reactions of the Hydrated Electron in Alkaline Solution

by Nathan Klein,^{1a,b} Conrad N. Trumbore,^{1b} James E. Fanning, Jr.,^{1a} and John W. Warner^{1a}

U. S. Army Nuclear Defense Laboratory, Edgewood Arsenal, Maryland, and University of Delaware, Newark, Delaware (Received July 27, 1967)

An investigation of chemical reactions taking place in aqueous solutions during and immediately after an X-radiation pulse was carried out. Equipment with resolving time in the nanosecond range was assembled to measure optical absorption as a function of time using 6328-Å light. The hydrated electron, e_{aq}^- , was produced in solutions of Na_2CO_3 , $Ba(OH)_2$, H_2SO_4 , and $HClO_4$ by a 3-krad, 50-nsec X-ray pulse from an electron accelerator. No evidence for nonhomogeneous distribution of e_{aq}^- was obtained in the time frame investigated. In air-free alkaline solution, an extremely rapid decay of the e_{aq}^- absorption was observed. This decay is observed for approximately 0.5 μ sec after an X-ray pulse. The very fast disappearance is quenched when the solutions contain an excess of structure-breaking ions over structure makers. It is postulated that the observed decay is due to reaction of e_{aq}^- with H_2O^* .

Introduction

X and γ radiation transfer energy to aqueous solutions primarily by the Compton process when the photon energy is between 0.03 and 20 MeV. The Compton electron transfers energy by interaction with the system, approximately 100 eV being transferred per interaction.^{2a} This energy is deposited in small, roughly spherical regions commonly called "spurs" in which several ionizations and excitations occur. It has been estimated^{2b} that the spur has an initial diameter of 20 Å. The ions and radicals in the vicinity of the spur then diffuse into the surrounding medium and estimates based on mobility of the reactive species indicate³ that a homogeneous distribution exists within 10^{-8} sec after the spur is created.

The species usually considered as produced in the vicinity of the spur are H, OH, H_2 , H_2O_2 , e_{aq}^- , H^+ , and OH^- . Of these, the hydrated electron, e_{aq}^- , has a significant absorption spectrum in the visible region,⁴ which provides a convenient means for observing its reactions. The recent availability of electron accelerators that produce large radiation pulses of several nanoseconds duration together with intense light sources and very fast detection equipment have made possible the investigation of the reactions of e_{aq}^- in time frames where the nonhomogeneous distribution of the reacting species might still exist in the vicinity of the spur.

In this work, large X-ray pulses were the short-duration radiation source and a laser was the intense light source which made possible a direct measurement of the upper limit of the lifetime of the spur through observing absorbing transient species during the radiation pulse.

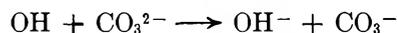
Experimental Details and Treatment of Data

The experimental array was essentially identical with that described previously.⁵ Equipment response

time was measured using a Kerr light shutter and was found to be less than 5 nsec, which is in complete agreement with calculated root-mean-square response time.

The pH range 2–12 was covered using $HClO_4$, H_2SO_4 , $Ba(OH)_2$, and Na_2CO_3 . Some of the $Ba(OH)_2$ solutions contained KBr ranging in concentrations from 3×10^{-4} to 3×10^{-2} M. All reagents were analytical grade and were used without further purification. The water was quadruply distilled, and all solutions used were deaerated by repeated shaking in an argon atmosphere. Dose was measured using manganese-activated LiF thermoluminescent dosimeters.⁶

Photographs of the oscilloscope display were enlarged and read to obtain e_{aq}^- concentration as a function of time. Absolute concentration measurements could not be made with the Na_2CO_3 solutions because of the presence of the CO_3^- radical ion, produced by the reaction



CO_3^- absorbs light at 6328 Å but is sufficiently long-lived⁷ that its decay could be ignored over the time intervals considered without introducing any significant error. Relative e_{aq}^- measurements in Na_2CO_3 were made, and decay rates are in complete agreement with data obtained using $Ba(OH)_2$ where the problem of a second absorbing species at 6328 Å did not exist.

(1) (a) Edgewood Arsenal, Md. (b) University of Delaware, Newark, Del.

(2) (a) E. C. Pollard, *Advan. Biol. Med. Phys.*, **3**, 153 (1953); (b) A. H. Samuel and J. L. Magee, *J. Chem. Phys.*, **21**, 1080 (1953).

(3) (a) A. Kupperman, *J. Chem. Educ.*, **36**, 279 (1959); (b) A. Kupperman, "Actions Chimiques et Biologiques des Radiations," Vol. 5, M. Haissinsky, Ed., Masson et Cie, Paris, 1961.

(4) J. W. Boag and E. J. Hart, *Nature*, **197**, 45 (1963); (b) E. J. Hart and J. W. Boag, *J. Am. Chem. Soc.*, **84**, 4090 (1962); (c) J. P. Keene, *Nature*, **197**, 47 (1963).

(5) N. Klein and J. W. Warner, *Trans. Am. Nucl. Soc.*, **9**, 83 (1966).

(6) E. Tochilin and N. Goldstein, *Health Phys.*, **12**, 1705 (1966).

(7) G. E. Adams and J. W. Boag, *Proc. Chem. Soc.*, 112 (1964).

Table I: Reactions and Rate Constants Used in Computations^a

Reaction	Rate constants ($\times 10^9$)							
	1.5	2.5	4.0	5.0	6.0	9.0	12.0	
$\text{OH} + \text{Br}^- \rightarrow \text{OH}^- + \text{Br}$	6	4.5	2.6	1.2	1.2	1.2	18×10^{-2}	
$\text{Br} + \text{Br}^- \rightarrow \text{Br}_2^-$	50	50	50	50	50	50	50	
$2\text{Br}_2^- \rightarrow \text{Br}_2 + 2\text{Br}^-$	2.4	2.4	1.5	1.67	1.67	1.8	5	
$e_{\text{aq}}^- + \text{Br}_2^- \rightarrow 2\text{Br}$	13	13	13	13	13	13	13	
$\text{OH} + \text{H}_2\text{O}_2 \rightarrow \text{H}_2\text{O} + \text{HO}_2$	45×10^{-3}	45×10^{-3}	45×10^{-3}	45×10^{-3}	45×10^{-3}	45×10^{-3}	45×10^{-3}	
$e_{\text{aq}}^- + \text{H}_2\text{O} \rightarrow \text{H} + \text{OH}^-$	16×10^{-9}	16×10^{-9}	16×10^{-9}	16×10^{-9}	16×10^{-9}	16×10^{-9}	16×10^{-9}	
$2e_{\text{aq}}^- \rightarrow \text{H}_2 + 2\text{OH}^-$	$\leq .5$	4.5	4.5	4.5	4.5	4.5	5.5	
$e_{\text{aq}}^- + \text{H} \rightarrow \text{H}_2 + \text{OH}^-$	25	25	25	25	25	25	25	
$e_{\text{aq}}^- + \text{OH} \rightarrow \text{OH}^-$	30	30	30	30	30	30	30	
$e_{\text{aq}}^- + \text{H}^+ \rightarrow \text{H}$	21	21	23	23	23	23	23	
$e_{\text{aq}}^- + \text{H}_2\text{O}_2 \rightarrow \text{OH} + \text{OH}^-$	13	13	13	13	13	13	13	
$e_{\text{aq}}^- + \text{O}_2 \rightarrow \text{O}_2^-$	20	20	20	20	20	20	20	
$2\text{H} \rightarrow \text{H}_2$	15	10	10	10	10	10	10	
$\text{H} + \text{OH} \rightarrow \text{H}_2\text{O}$	7	7	7	7	7	7	7	
$2\text{OH} \rightarrow \text{H}_2\text{O}_2$	5.2	5.2	5.2	5.2	5.2	5.2	5.2	
$e_{\text{aq}}^- + \text{O}_2^- \rightarrow \text{O}_2^{2-}$	20	20	20	20	20	20	20	
$\text{H} + \text{O}_2 \rightarrow \text{HO}_2$	15	20	30	30	30	30	30	
$\text{H}^+ + \text{OH}^- \rightarrow \text{H}_2\text{O}$	143	143	143	143	143	143	143	
$\text{H} + \text{OH}^- \rightarrow e_{\text{aq}}^- + \text{H}_2\text{O}$	2×10^{-2}	2×10^{-2}	2×10^{-2}	2×10^{-2}	2×10^{-2}	2×10^{-2}	2×10^{-2}	
$\text{H} + \text{H}_2\text{O}_2 \rightarrow \text{OH} + \text{H}_2\text{O}$	9×10^{-2}	9×10^{-2}	9×10^{-2}	9×10^{-2}	9×10^{-2}	9×10^{-2}	9×10^{-2}	
$\text{OH} + \text{H}_2 \rightarrow \text{H} + \text{H}_2\text{O}$	45×10^{-3}	45×10^{-3}	45×10^{-3}	7×10^{-2}	7×10^{-2}	45×10^{-3}	7×10^{-2}	
$2\text{HO}_2 \rightarrow \text{H}_2\text{O}_2 + \text{O}_2$	24×10^{-4}	22×10^{-4}	88×10^{-4}	15×10^{-3}	15×10^{-3}	15×10^{-3}	15×10^{-3}	
$\text{H}_2\text{O} \rightarrow \text{H}^+ + \text{OH}^-$	26×10^{-16}	26×10^{-16}	26×10^{-15}					
$\text{H} + \text{O}_2^- \rightarrow \text{HO}_2^-$	20	20	20	20	20	20	20	
$e_{\text{aq}}^- + \text{Br}_2 \rightarrow \text{Br}_2^-$	13	13	13	13	13	13	13	

^a The rate constants used are taken from ref 8.

The transient species, produced by the ionizing radiation, react with each other and with solute to give a sufficiently complex sequence of simultaneous chemical reactions as to make simple kinetic treatment of the data virtually impossible. However, all of the reactions that were expected to take place in the systems being investigated and their rate constants were known, and a computer program, assuming homogeneous kinetics, was prepared. The reactions and rate constants used are listed in Table I.⁸ The computer program is available on request. The concentration of the various transients as a function of time during and after a typical radiation pulse was calculated and compared with the experimental results obtained.

Results and Discussion

Typical oscilloscope traces obtained from irradiation of $\text{Ba}(\text{OH})_2$ solutions at pH 9.1 are shown in Figure 1. The two traces have been superimposed to facilitate comparison. It is obvious that the presence of $3 \times 10^{-4} M$ KBr substantially decreases the rate of decay of the absorbing species. Data obtained from these traces are plotted in Figure 2 together with the calculated values.

The yield of e_{aq}^- was determined from oscilloscope traces taken at sweep speeds of 10 and 20 nsec/cm so that little or no decay of the transient was observed on the trace. Since the radiation pulse was 50 nsec in duration, correction is required for decay of the e_{aq}^-

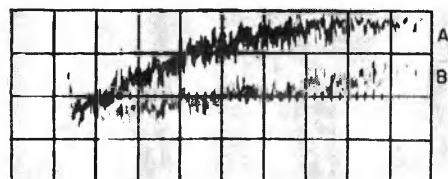


Figure 1. Concentration of e_{aq}^- as a function of time: horizontal, 200 nsec/div; vertical, 25% T/div. A, O_2 -free $\text{Ba}(\text{OH})_2$, pH 9.1, $\text{KBr} = 0$. B, O_2 -free $\text{Ba}(\text{OH})_2$, pH 9.1, $\text{KBr} = 3 \times 10^{-4} M$.

signal during the irradiation. This correction was obtained by calculation using an idealized pulse. Table II lists maximum e_{aq}^- concentration obtainable as a function of pH from such a calculation.

Table II: Maximum e_{aq}^- Concentration during a Radiation Pulse

pH	Max $[e_{\text{aq}}^-]$, μM
2.5	3.62
4.0	8.03
5.0	8.51
6.0	8.56
9.0	8.57
12.0	8.67

(8) L. M. Dorfman and M. S. Matheson, *Progr. Reaction Kinetics*, 3, 237 (1965).

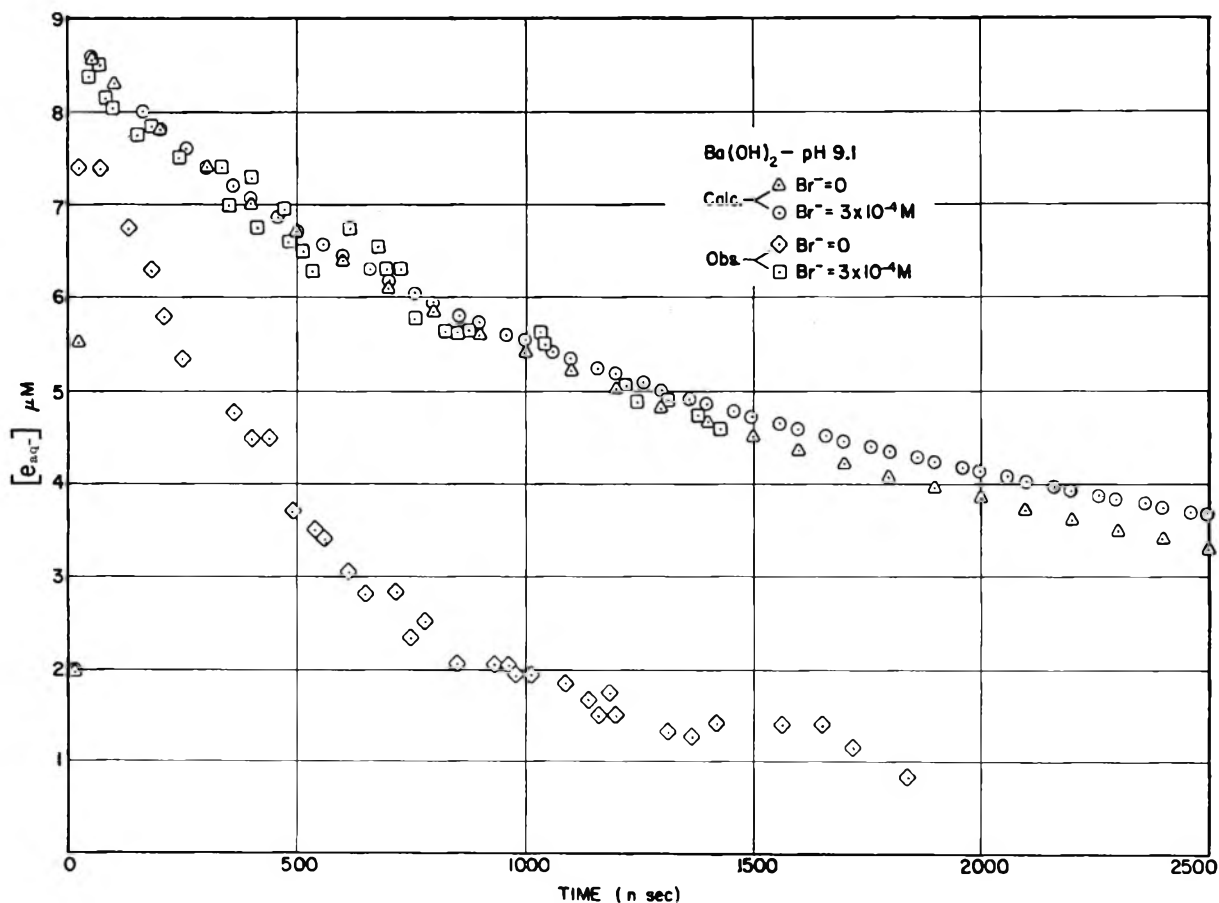


Figure 2. Plots of e_{aq}^- as a function of time.

The data from Table II provide correction factors for determination of $G_{e_{aq}^-}$ (molecules/100 eV absorbed). It was found that $G_{e_{aq}^-}$ was independent of pH between 4 and 12 after correction for decay and was independent of Br^- concentration. The value obtained was 2.76 ± 0.17 .

Evaluation of the data was undertaken by comparison of the calculated e_{aq}^- concentration with that actually observed. Calculations indicate that the decay of e_{aq}^- should appear to be kinetically first order in acidic solution. Results at pH 2 are presented in Figure 3. The agreement between the observed and computed values indicates that the observations are adequately explained by the computations. Essentially similar results were obtained in air-free $HClO_4$ solutions at pH 4.2.

In the case of neutral or basic solutions, the computations predicted that the reciprocal of e_{aq}^- concentration would be a linear function of time up to approximately 500 nsec. For a simple chemical reaction, data presentation in this form would indicate a second-order reaction with both species present in equal concentration. The slope of lines obtained would be the second-order rate constant for the reaction. Such considerations are not valid for the problem under discussion here owing to the very complex reaction

scheme. However, an intercomparison of the "rate constants" is instructive in that it points out the differences between the calculated and observed data. A compilation of "rate constants" is presented in Table III.

Table III: Second-Order "Rate Constants" Obtained by Pulse Radiolysis

Solution	pH	KBr	$k, M^{-1} \text{sec}^{-1}$	
			Calcd	Obsd
$Ba(OH)_2$	12.1	0	5.3×10^{10}	4.0×10^{11}
		3×10^{-4}	4.1×10^{10}	1.8×10^{11}
		3×10^{-3}	3.3×10^{10}	1.4×10^{11}
		3×10^{-2}	2.4×10^{10}	...
Na_2CO_3	10.6	0	6.5×10^{10}	3.2×10^{11}
$Ba(OH)_2$	9.1	0	7.3×10^{10}	3.2×10^{11}
		3×10^{-4}	5.7×10^{10}	6.3×10^{10}
		3×10^{-3}	4.1×10^{10}	4.6×10^{10}
		3×10^{-2}	4.1×10^{10}	3.4×10^{10}
Na_2CO_3	8.3	0	8.2×10^{10}	3.2×10^{10}
$HClO_4$	6.0	0	9.0×10^{10}	7.2×10^{10}
		3×10^{-4}	8.3×10^{10}	...
		3×10^{-3}	6.0×10^{10}	5.5×10^{10}
		3×10^{-2}	5.5×10^{10}	4.0×10^{10}

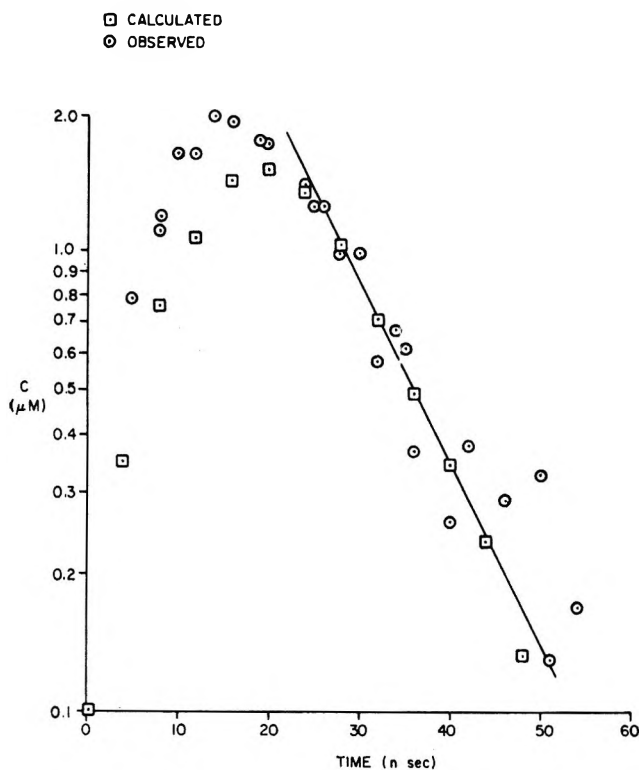


Figure 3. First-order kinetics test: air-free H_2SO_4 , pH 2.0.

If it is assumed that the "rate constants" are precise to $\pm 20\%$, then the calculated and experimental data are essentially in agreement at pH 6. At pH between 8.3 and 10.6, the observed rate of decay appears independent of pH and in substantial disagreement with the calculated values. The addition of KBr at pH 9.1 results in a decrease in the rate of decay of e_{aq}^- to where calculated and observed results are in agreement. At pH 12.1 the observed decay rate exceeds the calculated rate for all concentrations where data are available although the addition of KBr appears to decrease the decay rate significantly.

The above computations of e_{aq}^- were based on a homogeneous distribution of all reacting species in solution. The fairly good agreement between calculation and observation at pH 6.0 and at pH 9.1 for solutions containing KBr would seem to indicate that spurs were no longer present as significant concentration gradient regions within the resolving time of the equipment used. The 5-nsec response time quoted for the equipment is based on a 10–90% of full scale response to a signal of infinite slope. Usable response time for a more slowly changing signal is considerably faster and would be conservatively estimated at about 1 nsec. One must then conclude that spurs, if they indeed exist, have completely disappeared into the surrounding medium in less than 10^{-9} sec. If the assumption of homogeneity is valid in acidic solution and in solutions containing as little as $3 \times 10^{-4} M$ KBr at pH 9.1, there would be little basis to question it at pH 8.3 or 9.1 in the absence of KBr, and an explanation

of the difference between the computed decay and the exceedingly rapid decay observed immediately after an X-ray pulse need not be based on diffusion kinetic models.

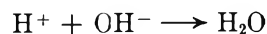
In all cases, the observed rate of decay after the first 500 nsec agreed with the calculated value, indicating that the collection of reactions and rate constants used in the computation adequately accounts for all of the reactions of the transient species other than the exceedingly fast reactions under discussion.

Thomas and Bensasson⁹ report the observation of a fast decay of e_{aq}^- following a radiation pulse. They attribute this decay to a nonhomogeneous distribution of e_{aq}^- in contrast to the results reported herein. However, more recent work¹⁰ indicates no significant nonhomogeneous decay of e_{aq}^- in times longer than 0.5 nsec.

To achieve a calculated rate of decay comparable to those observed experimentally, one or more reactions with rate constants exceeding $10^{11} M^{-1} \text{sec}^{-1}$ must be included in the set of chemical reactions taking place. However, such rate constants are not readily obtained since for a system consisting of an ion and a neutral species where reaction takes place on every encounter, *i.e.*, activation energy approaches zero, the rate constant is given by

$$k = \frac{4\pi N D_{AB} r_{AB}}{1000} \quad (1)$$

where N is Avogadro's number, D_{AB} is the sum of the diffusion coefficients of A and B, and r_{AB} is the sum of the radii of A and B. For small molecules, $D_{AB} \approx 10^{-5} \text{cm}^2 \text{sec}^{-1}$ and $r_{AB} \approx 10^{-8} \text{cm}$. For e_{aq}^- , the diffusion constant¹¹ is $4.7 \times 10^{-5} \text{cm}^2 \text{sec}^{-1}$, and the radius of charge distribution has been calculated¹² as 2.5–3.0 Å. Comparable values have been determined for the other transients present in the solutions. Values for rate constants based on D_{AB} and r_{AB} for small molecules are in the range $1-4 \times 10^{10} M^{-1} \text{sec}^{-1}$. It would, therefore, appear that the requirement for reactions with rate constants exceeding $10^{11} M^{-1} \text{sec}^{-1}$ results in a situation somewhat like that of the neutralization reaction



where the rate constant determined¹³ is $1.43 \times 10^{11} M^{-1} \text{sec}^{-1}$. In this case the propagation of charge through the highly hydrogen-bonded medium accounts for the extremely rapid reaction rate.

(9) J. K. Thomas and R. V. Bensasson, *J. Chem. Phys.*, **46**, 4147 (1967).

(10) J. W. Hunt and J. K. Thomas, *Radiation Res.*, **32**, 149 (1967).

(11) K. Schmidt and W. Buck, *Science*, **151**, 70 (1966).

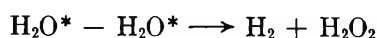
(12) J. Jortner, *Radiation Res. Suppl.*, **4**, 139 (1964).

(13) (a) M. Eigen and L. DeMaeyer, *Z. Elektrochem.*, **59**, 986 (1955); (b) G. Ertl and H. Gerisher, *ibid.*, **66**, 560 (1962).

Consideration of the structure of liquid water might provide a basis for increasing D_{AB} and/or r_{AB} . It has been known for some time¹⁴ that liquid water retains some of the tetrahedrally directed hydrogen bonding found in the crystal structure of ice. X-Ray scattering studies indicate¹⁵ that the average number of nearest neighbors in water is between four and six with an average distance between centers of 2.92 Å. A high concentration of molecules is found at 4.75–4.90 Å which would be expected for a tetrahedral arrangement.

Numerous attempts have been made to describe liquid water in terms of its relationship to the structure of ice. Samoilov⁶ proposed that liquid water was essentially an expanded ice structure with sufficient space between the tetrahedrally coordinated water molecules to accommodate nonassociated molecules. This model was expanded on by Forslind¹⁷ and explains reasonably well many of the properties of water. A second model of liquid water was proposed by Frank and Wen in 1957.¹⁸ This proposal is based on the proposition that hydrogen-bond formation is essentially a cooperative phenomenon; that is, the existence of a pair of hydrogen-bonded atoms promotes the formation of additional hydrogen bonds in its vicinity. As a result, there are produced short-lived, ice-like "flickering clusters" of varying size consisting of highly hydrogen-bonded molecules surrounded by nonhydrogen-bonded molecules. If the dielectric relaxation time in water consisted of cluster formation and cluster dissolution, then the relaxation half-life would be the mean lifetime of the cluster, *i.e.*, 10^{-10} to 10^{-11} sec.¹⁹ This would indicate that the clusters would appear to be extremely mobile in the water. This model was developed theoretically in considerable detail by Némethy and Scheraga²⁰ and calculated values of free energy, enthalpy, and entropy agree quite well with experimental values. The model predicts that an average cluster at 20° contains 57 water molecules. Seventy per cent of the water molecules would be cluster members. The flickering cluster model makes possible an adequate explanation of the apparent increase in ice-like character associated with solutions of nonpolar solutes. Although the model does not adequately explain all of the observed properties of water, it seems good enough to warrant reasonably wide-spread acceptance at this time.

Electronically excited water, H_2O^* , has been postulated as a primary species in water radiolysis. It has been suggested²¹ that H_2O^* may react to produce part of the observed H_2 and H_2O_2 yield



The existence of H_2O^* as a significant primary chemical species was more recently suggested by Dainton and Peterson²² and either H_2O^* or isolated radical pairs ($H + OH$) were suggested²³ as an explanation for an observed increase in e_{aq}^- and OH yield in strongly

alkaline solution. Scavenger studies²⁴ using N_2O as an e_{aq}^- scavenger have led to the conclusion that another species, possibly H_2O^* , is present in solution and may be the precursor of e_{aq}^- . Recent investigation²⁵ of H_2 yield indicates that either H_2O^* or the recombination of H_3O with OH results in the intraspur H_2 yield. A suggested lifetime of H_2O^* was given as 10^{-9} to 10^{-10} sec. The requirement²⁴ that H_2O^* be highly delocalized causes the reasonable supposition that the excitation energy be spread over a water cluster. If the excitation energy does not significantly change the properties of the cluster, then the species H_2O^* is essentially characterized with regard to size and mobility.

The concept of "flickering clusters" cannot be used to explain the interaction of ions with water. An ion, when introduced into water, interferes with the tetrahedral structure of the "iceberg"²⁶ by causing orientation of water dipoles around itself. The nature of the ion tends to determine the extent of the effect on the water structure, the effect being roughly proportional to the polarizing power of the ion (charge divided by radius). Very small or highly charged ions tend to orient water molecules strongly in their vicinity and, in fact, increase the structuring of the water in the vicinity of the ions. Large ions tend to have the opposite effect. Having disrupted the icebergs in the water, they do not possess sufficient polarizability to produce significant orientation about themselves—the over-all effect being that of "structure breaking." Ions such as H_3O^+ , Na^+ , Ba^{2+} , OH^- , and F^- increase the viscosity of water and exhibit effects not only on the water molecules in their immediate vicinity but also show long-range structuring effects. In contrast, ions such as

(14) W. K. Röntgen, *Ann. Physik. Chem.*, **45**, 91 (1892).

(15) (a) G. S. Brady and W. J. Romanov, *J. Chem. Phys.*, **32**, 306 (1960); (b) M. D. Danford and H. A. Levy, *J. Am. Chem. Soc.*, **84**, 3965 (1962).

(16) O. Ya. Samoilov, *Zh. Fiz. Khim.*, **20**, 12 (1946).

(17) E. Forslind, *Acta Polytechn.*, **115**, 9 (1952).

(18) H. S. Frank and W. Y. Wen, *Discussions Faraday Soc.*, **24**, 133 (1957).

(19) C. H. Collie, J. B. Hasted, and D. M. Ritson, *Proc. Phys. Soc.*, **60**, 145 (1948).

(20) (a) G. Némethy and H. A. Scheraga, *J. Chem. Phys.*, **36**, 3382 (1962); (b) *J. Phys. Chem.*, **66**, 1773 (1962).

(21) (a) H. A. Dewhurst, A. H. Samuel, and J. L. Magee, *Radiation Res.*, **1**, 62 (1964); (b) P. Kelly, T. Rigg, and J. Weiss, *Nature*, **173**, 1130 (1954).

(22) F. S. Dainton and D. B. Peterson, *Proc. Roy. Soc. (London)*, **A267**, 443 (1962).

(23) F. S. Dainton and S. R. Logan, *Trans. Faraday Soc.*, **61**, 715 (1965).

(24) F. S. Dainton, A. R. Gibbs, and D. Smithies, *ibid.*, **62**, 3170 (1966).

(25) T. J. Sworski in "Solvated Electron," American Chemical Society, Washington, D. C., 1965.

(26) (a) J. O'M. Bockris, *Quart. Rev. (London)*, **3**, 179 (1949); (b) O. Ya. Samoilov, "Structure of Aqueous Electrolyte Solutions and Ion Hydration," *Izdatel'stvo Akademii Nauk SSSR, Moscow*, 1957; (c) L. J. Kavanau, "Water and Solute-Water Interactions," Holden-Day, San Francisco, Calif., 1964.

K^+ , Br^- , and ClO_4^- are structure breaking. Comparing the polarizability of e_{aq}^- with that of F^- would suggest that e_{aq}^- is a more powerful "structure maker" than is F^- . One would expect very extensive structuring in solutions containing e_{aq}^- since F^- is known to be a very efficient structure maker. This effect would increase the diffusion coefficient of H_2O^* since the mobility of the species is dependent on the ease of orientation of the water dipoles. Furthermore, if it is proposed that H_2O^* reacts with e_{aq}^- , then the structuring effect of e_{aq}^- would greatly increase the reaction radius. The increase in both D_{AB} and r_{AB} in eq 1 would mean that a diffusion-limited rate constant for the reaction of e_{aq}^- with H_2O^* could exceed $10^{11} M^{-1} sec^{-1}$.

Consideration of the experimental data indicates that the observed decay of e_{aq}^- is adequately explained by previously studied reactions in acidic solution and in

$Ba(OH)_2$ at pH 9.1 when $3 \times 10^{-4} M$ or more KBr is present. Each of these solutions contains an excess of structure-breaking ions over structure makers. In the cases where the experimentally observed decay of e_{aq}^- does not agree with the calculated values, an excess of structure-making ions is present.

It should be emphasized that the work reported discusses only the disappearance of the optical absorption due to e_{aq}^- . The reason for the disappearance, whether it be due to chemical reaction or simply the removal of some of the waters of hydration brought about by promotion of the species to an excited state, is not considered.

Acknowledgment. The authors gratefully acknowledge the technical assistance of Thomas L. Smith, U. S. Army Nuclear Defense Laboratory, and stimulating discussions with Professor R. H. Wood, University of Delaware.

Implications and Use of Spectral Shifts in Polymerization Studies of Metal Ions

by Jack I. Morrow and Joel Levy

*Department of Chemistry, The City College of The City University of New York, New York, New York 10031
(Received July 28, 1967)*

For polymers which conform to Sillén's hypothesis of cores and links, a method was developed to determine both the value of l in the links $(OH)_lM$ and the degree of polymerization (average number of monomers present in all species). It is based upon the spectral shift caused by hydrolysis and polymerization of the metal ion, which in this study was Cr(III). As the a value (moles of added OH^- per mole of Cr(III)) was increased, the wavelength of the first maximum in the visible region shifted from 408 to 422 $m\mu$. The degree of polymerization in the wavelength span from 410 to 415 $m\mu$ changed from 1.20 to 1.62. The value of l in the links was shown to be 2.

The ultimate object in most polymerization studies is the identification of species present. Acidity measurements, molecular weight determinations, and equilibrium centrifugation are among the most commonly employed techniques used in achieving this object.

Accompanying the polymerization there is usually a red spectral shift when bridging occurs through hydroxo or oxo groups, and the peak originates from d-d splitting. Thus, red-purple solutions of monomeric Cr(III) solutions turn green when polymerization occurs to an appreciable extent.¹ Dimerization of Fe(III) solutions is accompanied by a color change from yellow to red.²

The wavelength of the principal charge-transfer band is also sensitive to polymerization.^{3,4} The direction of the shift, however, would depend upon the direction of electron transfer.

With regard to the treatment developed in this paper, the direction of the shift is not important. Of importance is that the position of maximum absorbance must change monotonically as the degree of polymerization increases.

The implications and use of spectral shifts in polymerization studies, unfortunately, have not been developed, and it is to this that we turn our attention.

Consider a series of solutions of a given metal ion, M^{2+} , at a total metal concentration, T_M . To each

(1) C. L. Rollinson in "Chemistry of the Coordination Compounds," J. Bailar, Ed., Reinhold Publishing Corp., New York, N. Y., 1964.

(2) H. Schugar, C. Walling, R. B. Jones, and H. B. Gray, *J. Amer. Chem. Soc.*, **89**, 3712 (1967).

(3) C. Altman and E. L. King, *ibid.*, **71**, 425 (1961).

(4) C. Berecki-Biedermann, Proceedings of the 7th International Conference on Coordination Chemistry, Stockholm, 1962, p 161.

solution in this series a different amount of hydroxide is added, allowing us to obtain solutions of various a values, where $a = T_{\text{OH}}/T_{\text{M}}$ (moles of OH^- added per mole M^{z+}). Spectral analysis would then show that as a increases, the position of maximum absorbance, λ_{max} , changes owing to increasing polymerization.⁵ If this procedure was followed using solutions of different T_{M} values, it would be observed that λ_{max} is a function of both T_{M} and a . In order to obtain solutions having the same λ_{max} (isolambda solutions) for different T_{M} values, their a values must of necessity be different. The mathematical argument given below indicates that isolambda solutions should have a similar fractional distribution of species.

Let C_1, C_2, C_3 , etc. be the concentrations of the various species in equilibrium for a given T_{M} , and a_1, a_2, a_3 , etc., their molar absorptivities. The fractional concentration of the i th species is $C_i^* = C_i/T_{\text{M}}$. In applying Beer's law, a 1-cm cell length is assumed.

The measured absorbance, A , at any wavelength is $A = a_1C_1 + a_2C_2 + a_3C_3 + \dots$ or $A = T_{\text{M}}C_1^*a_1 + T_{\text{M}}C_2^*a_2 + T_{\text{M}}C_3^*a_3 + \dots$. At λ_{max} only

$$\frac{\partial A}{\partial \lambda} = 0 = T_{\text{M}}C_1^* \frac{\partial a_1}{\partial \lambda} + T_{\text{M}}C_2^* \frac{\partial a_2}{\partial \lambda} + T_{\text{M}}C_3^* \frac{\partial a_3}{\partial \lambda} + \dots$$

The last equation may be more conveniently written in the form of a summation,

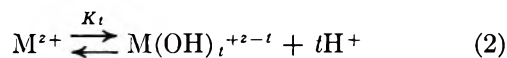
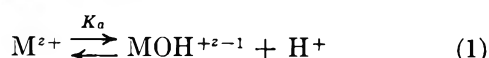
$$\sum_{i=1}^i C_i^* \frac{\partial a_i}{\partial \lambda} = 0$$

The values of $\partial a_i/\partial \lambda$, like a_i , are independent of C_i^* and are fixed for a given wavelength. As they are slopes, they may have positive, negative, and zero values. It must be noted that these fractional concentrations of species are related to one another through their equilibrium constants. It will be shown in the Theory that the limiting C_i^* values for isolambda solutions, as $1/[\text{H}^+]$ approaches zero, yields information concerning both the extent of polymerization and the nature of the polymers formed.

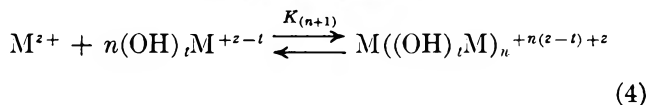
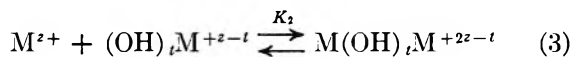
The use of Cr(III) solutions in this study was dictated both by the availability of the spectra of several polymeric species and by the fact that the composition of these polymers⁶ is in accord with Sillén's hypothesis of cores and links.^{7,8} The hypothesis states that the predominant species are members of a homologous series (which does not necessarily include all possibilities). The polymers $\text{M}[(\text{OH})_t\text{M}]_n$ are composed of the core, M , added to the links, $(\text{OH})_t\text{M}$. For $\text{Cr}(\text{ClO}_4)_3$ solutions, the value of t is 2.^{6,9}

General Theory

The reactions occurring are written to illustrate and conform to Sillén's hypothesis.



The value of t in reaction 2 is most frequently 2 or 3.



Reaction 4 is the over-all reaction involving n links, thereby yielding the $n + 1$ polymer. The minimum value of n is 1, corresponding to dimer formation (eq 3). In subsequent equations, the charges of the species while not indicated are understood.

The equilibrium constants for the several reactions are

$$K_a = \frac{[\text{MOH}][\text{H}^+]}{[\text{M}]} \quad (5)$$

$$K_t = \frac{[\text{M}(\text{OH})_t][\text{H}^+]^t}{[\text{M}]} \quad (6)$$

and for the $n + 1$ polymeric species

$$K_{n+1} = \frac{[\text{M}((\text{OH})_t\text{M})_n]}{[\text{M}][(\text{OH})_t\text{M}]^n} \quad (7)$$

The material balance equations are for total metal

$$T_{\text{M}} = [\text{M}] + [\text{MOH}] + [\text{M}(\text{OH})_t] + 2[\text{M}(\text{OH})_t\text{M}] + \dots + (n + 1)[\text{M}((\text{OH})_t\text{M})_n] \quad (8)$$

for total hydrogen ion

$$T_{\text{OH}} + [\text{H}^+] - [\text{OH}^-] = [\text{MOH}] + t[\text{M}(\text{OH})_t] + t[\text{M}(\text{OH})_t\text{M}] + \dots + nt[\text{M}((\text{OH})_t\text{M})_n] \quad (9)$$

and for total concentration of all species

$$\sum C_i = [\text{M}] + [\text{MOH}] + [\text{M}(\text{OH})_t] + [\text{M}(\text{OH})_t\text{M}] + \dots + [\text{M}((\text{OH})_t\text{M})_n] \quad (10)$$

By combining eq 5, 6, and 7 with each of the material balance equations, the latter equations may be written as

$$T_{\text{M}} = [\text{M}] \left\{ 1 + \frac{K_a}{[\text{H}^+]} + \frac{K_t}{[\text{H}^+]^t} + \sum_{n=1}^n (n + 1) K_{(n+1)} K_t^n \left(\frac{[\text{M}]}{[\text{H}^+]^t} \right)^n \right\} \quad (11)$$

(5) An excellent discussion on the relationship between a values and polymerization is given by L. Pokras, *J. Chem. Educ.*, **33**, 223 (1956).

(6) G. Thomson, AEC Accession, No. 35255, Report No. UCRL-11410, University of California, Berkeley, Calif., 1964.

(7) L. G. Sillén, *Acta Chem. Scand.*, **8**, 299, 318 (1954).

(8) S. Hietanen, and L. G. Sillén, **8**, 1607 (1954).

(9) R. W. Kolaczowski and R. A. Plane, *Inorg. Chem.*, **3**, 322 (1964).

$$T_{\text{OH}} + [\text{H}^+] - [\text{OH}^-] = [\text{M}] \left\{ \frac{K_a}{[\text{H}^+]} + \frac{tK_t}{[\text{H}^+]^t} + \sum_{n=1}^n n t K_{(n+1)} K_t^n \left(\frac{[\text{M}]}{[\text{H}^+]^t} \right)^n \right\} \quad (12)$$

In applying eq 12 to the Cr(III) study, $[\text{OH}^-]$ was neglected, since measured pH values were in the range 2-4.

$$\sum C_i = [\text{M}] \left\{ 1 + \frac{K_a}{[\text{H}^+]} + \frac{K_t}{[\text{H}^+]^t} + \sum_{n=1}^n K_{(n+1)} K_t^n \left(\frac{[\text{M}]}{[\text{H}^+]^t} \right)^n \right\} \quad (13)$$

When equilibrium is attained, the concentration of each polymeric species (and of course the monomer) relative to that of the monomer is fixed by the ratio $[\text{M}]/[\text{H}^+]^t$. This is not so with the monomeric hydroxides, whose concentrations relative to the monomer are determined only by $[\text{H}^+]$.

The basic assumption of this method is that isolambda solutions have the same value of $[\text{M}]/[\text{H}^+]^t$ ($= [\text{M}(\text{OH})_t]/K_t$). This means adherence to "core plus links" behavior, and the plausible assumption that λ_{max} must change monotonically with increasing n .

For isolambda solutions presumably having a fixed value of $[\text{M}]/[\text{H}^+]^t$, eq 13 may be written as

$$\sum C_i = [\text{M}] \left\{ R + \frac{K_a}{[\text{H}^+]} + \frac{K_t}{[\text{H}^+]^t} \right\} \quad (14)$$

where

$$R = 1 + \sum_{n=1}^n K_{(n+1)} K_t^n \left(\frac{[\text{M}]}{[\text{H}^+]^t} \right)^n \quad (14a)$$

The degree of polymerization, DP , may now be defined as

$$DP = \frac{T_M}{\sum C_i} = \frac{T_M}{[\text{M}] \left\{ R + \frac{K_a}{[\text{H}^+]} + \frac{K_t}{[\text{H}^+]^t} \right\}} = \frac{1}{[\text{M}]^* \left\{ R + \frac{K_a}{[\text{H}^+]} + \frac{K_t}{[\text{H}^+]^t} \right\}} \quad (15)$$

Many metal ions, including Cr (III), have well-separated hydrolysis constants, thereby allowing eq 15 to be simplified to

$$DP = \frac{1}{[\text{M}]^* \left\{ R + \frac{K_a}{[\text{H}^+]} \right\}} \quad (16)$$

For Cr(III) ion, $K_a = 1.5 \times 10^{-4}$ ^{10,11} and K_t (where $t = 2$) $\approx 1.5 \times 10^{-11}$ ¹⁰. Under the experimental conditions, the measured pH values were less than 4; therefore, $K_a[\text{H}^+] \gg K_t$, and the simplification introduces no measurable error. Ions having hydrolysis constants not so well separated might require the use of the more rigorously derived equation.

The reciprocal of eq 16 yields

$$\frac{1}{DP} = [\text{M}]^* R + \frac{[\text{M}]^* K_a}{[\text{H}^+]} \quad (17)$$

If isolambda solutions have similar $[\text{M}]^*$ values, then a plot of $1/DP$ vs. $K_a/[\text{H}^+]$ should be linear, with a slope of $[\text{M}]^*$ and an intercept of $[\text{M}]^* R$.

In terms of experimentally measurable quantities, with the exception of $[\text{MOH}]$, the DP may be written as

$$DP = \frac{T_M}{\sum C_i} = \frac{T_M}{T_M - \frac{T_{\text{OH}} + [\text{H}^+]}{t} + \frac{[\text{MOH}]}{t}} \quad (18)$$

To allow comparison of terms in eq 18 with those of eq 16, eq 18 may be written as

$$DP = \frac{1}{[\text{M}]^* \left\{ \left(\frac{tT_M - T_{\text{OH}} - [\text{H}^+]}{tT_M[\text{M}]^*} - \frac{t-1}{t} \frac{K_a}{[\text{H}^+]} \right) + \frac{K_a}{[\text{H}^+]} \right\}} \quad (19)$$

therefore, R of eq 16 is

$$R = \frac{tT_M - T_{\text{OH}} - [\text{H}^+]}{tT_M[\text{M}]^*} - \frac{t-1}{t} \frac{K_a}{[\text{H}^+]}$$

Although the value of $[\text{M}]^*$ is unknown, a decrease in $\{tT_M - T_{\text{OH}} - [\text{H}^+]\}/tT_M$ with increasing $[\text{H}^+]$ should be observed to counterbalance the decrease of $[(t-1)/t]K_a/[\text{H}^+]$, thereby maintaining R constant for isolambda solutions. Careful scrutiny of eq 11 reveals that $[\text{M}]^*$ for isolambda solutions should also vary slightly with $[\text{H}^+]$, but becomes constant as $K_a/[\text{H}^+]$ approaches zero. This is seen in eq 20, obtained by rearrangement of eq 11

$$[\text{M}]^* = \frac{[\text{M}]}{T_M} = \frac{1}{1 + \frac{K_a}{[\text{H}^+]} + \sum_{n=1}^n (n+1) K_{(n+1)} K_t^n \left(\frac{[\text{M}]}{[\text{H}^+]^t} \right)^n} \quad (20)$$

As $K_a/[\text{H}^+]$ approaches zero, the limiting value of $[\text{M}]^*$ for isolambda solutions is obtained.

$$[\text{M}]^* = \frac{1}{1 + \sum_{n=1}^n (n+1) K_{(n+1)} K_t^n \left(\frac{[\text{M}]}{[\text{H}^+]^t} \right)^n}$$

Equation 20 indicates that a proportionality exists between $[\text{M}]$ and T_M for isolambda solutions at high $[\text{H}^+]$. We, therefore, may write

(10) J. E. Earley and R. D. Cannon in "Transition Metal Chemistry, A Series of Advances," Vol. 1, R. L. Carlin, Ed., Marcel Dekker Inc., New York, N. Y., 1965.

(11) C. Postmus and E. L. King, *J. Phys. Chem.*, **59**, 1208 (1955).

$$\frac{[M]}{[H^+]^t} \propto \frac{T_M}{[H^+]^t} = \text{constant}$$

or

$$-\log T_M = t\text{pH} + \log(\text{constant}) \quad (21)$$

A plot of $-\log T_M$ vs. pH should be approximately linear with a constant limiting slope of t at lower pH values.

Once the value of t is determined, the degree of polymerization may be calculated using eq 18, but neglecting the $[\text{MOH}]/t$ term. This should not produce any error in the $(DP)_0$ values obtained by extrapolation of the data to $K_a/[\text{H}^+] = 0$ (eq 17), since $[\text{MOH}]$ becomes effectively zero at high $[\text{H}^+]$.

Experimental Section

Sulfate-free $\text{Cr}(\text{ClO}_4)_3$, >99.95% pure, obtained from K & K Laboratories, Inc., was used. Solutions of $\text{Cr}(\text{ClO}_4)_3$ were analyzed by comparing their absorbancies to those on a Beer's-law curve and were prepared by reducing acidified $\text{K}_2\text{Cr}_2\text{O}_7$ solutions with H_2O_2 and driving off the excess H_2O_2 . A Beckman Model DU spectrophotometer was used for these measurements. A Beer's-law curve was also run on acidified $\text{Cr}(\text{ClO}_4)_3$ solutions. It was observed that freshly prepared solutions did not obey Beer's law, having a wide scattering of points. After the solutions stood for 2 weeks, depolymerization of $\text{Cr}(\text{ClO}_4)_3$ occurred and these same solutions obeyed Beer's law. The a value of each solution was set using a Na_2CO_3 -free NaOH solution. Hydrogen ion concentrations were measured using an L & N pH meter. The spectra of all solutions, with the exception of those used for standardization, were obtained using a Cary 14 recording spectrophotometer. In preparing the chromium solutions of various a values, the reactants were mixed rapidly using a constant method of addition. Homogeneity was attained within 2-3 sec after addition. Schwartzbach¹² has recently used fast-flow apparatus to obtain complete mixing within several milliseconds, thereby allowing him to study the very rapid formation of monomeric hydroxo complexes uncomplicated by the formation of polynuclear species. We prepared a limited number of solutions using the Aminco-Chance rapid-mixing apparatus (time of mixing ≈ 0.02 sec) and observed no significant difference in results between the rapid mixing and the addition method.

All solutions were maintained at a temperature of 25.0° until the pH in each solution was constant. It was assumed that equilibrium had been attained when the pH remained constant (within ± 0.01 pH unit for 2 weeks). The ionic strength was held constant using NaClO_4 at $\mu = 1.0$ in all solutions.

Results and Discussion

It was observed that as a increased for a given T_M value, the maximum in the visible spectrum of $\text{Cr}(\text{III})$

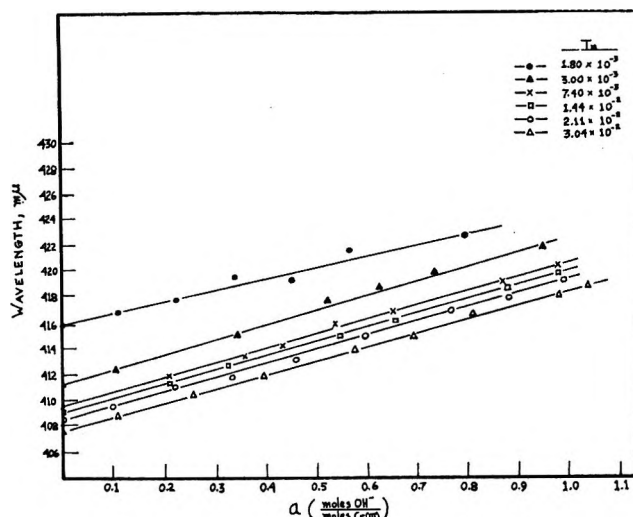


Figure 1. Variation of the wavelength maximum with increasing a value for several different total metal concentrations.

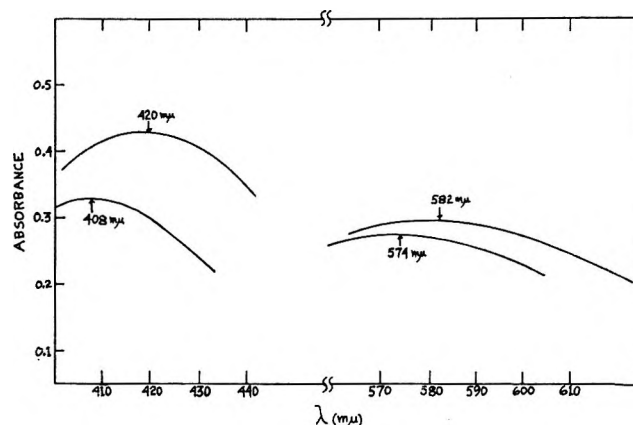


Figure 2. Variation of λ_{max} for both peaks in visible region: upper spectrum has $a = 1.0$; lower spectrum has $a = 0.0$. The total metal concentrations for both spectra are the same, $T_M = 2.11 \times 10^{-2} M$.

ion shifted toward the red (Figure 1). It should be noted that chromium has two peaks in the visible region, one in the vicinity of $408 \text{ m}\mu$ and the other around $575 \text{ m}\mu$. Both peaks showed a red shift, (Figure 2), with the shift of the former peak being larger than that of the latter peak. The $408\text{-m}\mu$ peak was also the sharper of the two and so was used in this study.

The experimentally measurable quantities, T_M , T_{OH} , and $[\text{H}^+]$, were used in eq 19 and 21 and results compared only for solutions exhibiting the same λ_{max} value, since, as was shown earlier, isolambda solutions most likely have a constant value of $[\text{M}]/[\text{H}^+]^t$. In many instances, the values of T_M , T_{OH} , and $[\text{H}^+]$ used were obtained by interpolation of our data in the following manner. Isolambda lines were drawn through

(12) G. Geier, J. Littler, and G. Schwartzbach, *Helv. Chim. Acta*, 45, 260 (1962).

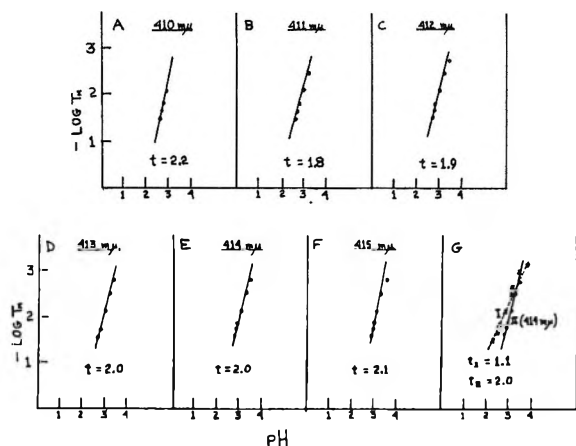


Figure 3. Determination of t from the limiting slope at low pH values.

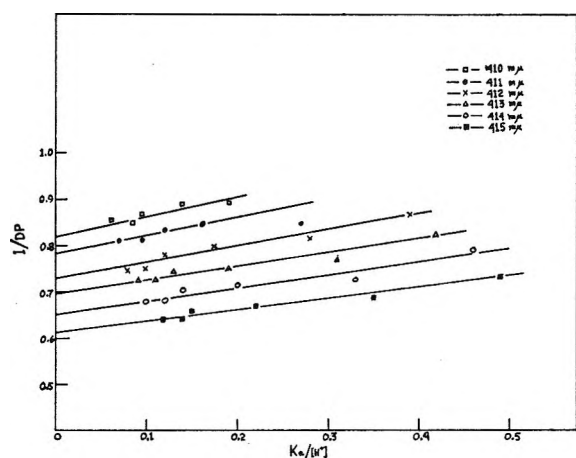


Figure 4. Variation of $1/DP$ with $K_a/[H^+]$. Extrapolation to $K_a/[H^+] = 0$ yields $1/(DP)_0$.

the lines in Figure 1 at wavelengths of 410, 411, 412, 413, 414, and 415 μ . From this, the a values required to give the wavelength maxima above were obtained. Graphs of T_M vs. a were also prepared, since there was a slight dilution factor which was taken into account even though it was small. A graph of pH vs. a was also prepared so that $[H^+]$ could be calculated.

Determination of t . Equation 21 predicts an approximately linear relationship between $-\log T_M$ and pH with a limiting slope of t at lower pH values. The results for the six isolambda series of solutions are shown in Figure 3 (A-F). Figure 3G serves as a comparison between the 414 μ (t_{II}) isolambda series and the series of solutions (t_I) to which no hydroxide was added, $a = 0$. These solutions do not exhibit the same λ_{max} as is evident from Figure 1.

The values of t for the isolambda solutions are in good agreement with each other and with the reported value.^{6,9} The value of t_I in Figure 3G is considerably different from the other six values and is well outside of experimental error.

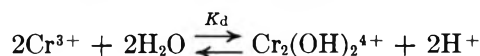
Degree of Polymerization. DP values for iso-

lambda solutions were calculated using eq 18; their reciprocals were plotted against $K_a/[H^+]$ (Figure 4). The plot is linear and positive in slope as required by eq 17. A value of 1.5×10^{-4} for K_a was used.¹¹ Table I lists the $(DP)_0$ values obtained by extrapolation to $K_a/[H^+] = 0$. The third column of this table contains DP values calculated from the work of Thomson,⁶ by using our spectra and her molar absorptivities for monomer, dimer, and trimer which she had separated using ion exchange. The two methods yield comparable results. The last two columns contain the $[M]^*$ (slopes) and R values for the several isolambda series of solutions.

Table I

λ , $m\mu$	$(DP)_0$	DP (G. T.)	$[M]^*$	R
410	1.20	1.12	0.40	2.1
411	1.25	1.20	0.37	2.1
412	1.35	1.25	0.34	2.2
413	1.43	1.38	0.30	2.3
414	1.54	1.46	0.27	2.4
415	1.62	1.55	0.25	2.5

In partially hydrolyzed solutions $[Cr_2(OH)_2^{4+}] \gg [Cr(OH)^{2+}]$,¹³⁻¹⁶ the equilibrium constant,¹⁰ K_{22} , for this "true" dimerization, $2Cr(OH)^{2+} \rightleftharpoons Cr_2(OH)_2^{4+}$, is $K_{22} = 10^4$. This permits the $[M]^*$ values in Table I to be tested for correctness by calculating the equilibrium constant, K_d , for the dimerization



(assuming the only two chromium species present are monomer and dimer) and comparing this value to that obtained from the product of $K_a^2 K_{22}$ ($=K_d$), where $K_a = 1.5 \times 10^{-4}$ and $K_{22} = 10^4$. The following relationships were employed

$$[Cr^{3+}] = [M]^* T_M \quad (\text{see eq 20})$$

$$[Cr_2(OH)_2^{4+}] = \frac{1}{2}(T_M - [Cr^{3+}]) = \frac{1}{2}T_M(1 - [M]^*)$$

and

$$K_d = \frac{[Cr_2(OH)_2^{4+}][H^+]^2}{[Cr^{3+}]^2} = \frac{(1 - [M]^*)[H^+]^2}{2[M]^* T_M}$$

Values of K_d were calculated for each of the 415 μ isolambda solutions using $[M]^* = 0.25$, and for each of the 410- μ isolambda solutions using $[M]^* = 0.40$. The 415- μ series yielded a value of $K_d = 3.6 \times 10^{-4}$

(13) J. Faucherre and R. Schaal, *Compt. Rend.*, **225**, 118 (1947).

(14) R. Schaal and J. Faucherre, *Bull. Soc. Chim. France*, 927 (1947).

(15) P. Souchay, *ibid.*, 143 (1948).

(16) J. Faucherre, *ibid.*, 253 (1954).

$\pm 0.3 \times 10^{-4}$; the 410 $m\mu$ series yielded a value of $K_d = 3.3 \times 10^{-4} \pm 0.3 \times 10^{-4}$. These are in excellent agreement with each other and with the value of $K_d = 2.3 \times 10^{-4}$ ($= K_d^2 K_{22}$).

The R values listed in Table I may also be tested for correctness by comparing them with the values obtained using eq 14a

$$R = 1 + \sum_{n=1}^{\infty} K_{(n+1)} K_t^n \left(\frac{[M]}{[H^+]^t} \right)^n$$

Assuming only dimer formation, that is, $n = 1$, this may be written as

$$R = 1 + K_d \left(\frac{[M]}{[H^+]^2} \right) = 1 + \left\{ 2.3 \times 10^{-4} \left(\frac{[M]}{[H^+]^2} \right) \right\}$$

where $K_d = K_2 K_t$.

The 415- $m\mu$ series gave an average value of $R = 2.1$; the 410- $m\mu$ series, $R = 1.8$. The only significance attached to these results is their demonstration of internal consistency.

Conclusion

A method for determining the stoichiometry of the links for polymers conforming to Sillén's hypothesis was devised and tested and found to yield good results for the particular metal ion, Cr(III), studied. Degrees of polymerization, defined as $DP = T_M / \Sigma C_t$, were also calculated and were in agreement with results obtained using a different method.

This method should be useful in determining whether a homologous series is formed; for if it is not formed,

the t values for all isolambda solutions should not be in agreement.

For those who might desire to use this method, some words of caution resulting from our observations should be noted. First, as degree of polymerization increases corresponding to higher λ_{max} values, the peaks tend to broaden, as might be expected. This broadening makes it increasingly more difficult to obtain accurate values of λ_{max} . For this reason we reported results for isolambda solutions up to 415 $m\mu$, although λ_{max} values up to 422 $m\mu$ were observed.

Second, increased accuracy and reliability in determining both the t value and the $(DP)_0$ values can be obtained by extending the range of T_M values covered to include the highest values (absorbance) measurable. This is predictable from the theoretical treatment, since as the T_M value increases, for isolambda solutions, the pH decreases (eq 21), and hence the importance of [MOH] in the many equations in which it appears is lessened.

The last limitation and precaution imposed upon this method is that no ligands, other than water and its conjugate base, capable of complexing can be present. For this reason, the method is probably limited to studies of metal ion perchlorates and nitrates.

Acknowledgment. The authors gratefully acknowledge the support of this research by the National Science Foundation Undergraduate Research Participation Program and the City College Faculty Research Committee. Discussions with Professors F. Condon and M. Green are also gratefully acknowledged.

Theoretical Relations among Rate Constants, Barriers, and Brønsted Slopes of Chemical Reactions¹

by R. A. Marcus

Noyes Chemical Laboratory, University of Illinois, Urbana, Illinois 61801 (Received August 10, 1967)

A simple relation, $\Delta F^* = \lambda(1 + \Delta/\lambda)^2/4$, derived originally for weak-overlap electron transfers, is explored in a slightly modified version for reactions with considerable resonance splitting, such as atom transfers, proton transfers, and strong-overlap electron transfers. A useful additivity property, $\lambda_{12} = (\lambda_{11} + \lambda_{22})/2$, permits barriers ΔF^* for cross-reactions to be computed from those of exchange reactions, $\lambda_{ii}/4$. Some 45 barriers, calculated from some ten others, agreed with BEBO results, within a few kilocalories per mole. The agreement is analyzed and more general models for which it might occur are considered. A functional relationship between barrier and a degree-of-reaction parameter is devised to avoid commitment to too specific a model. An example where breakdown should occur is also given. Experimental data, as well as quantum mechanical calculations of barriers, will permit further tests. Corollaries of the relation include: (1) a classification of reaction barriers in terms of intrinsic (λ_{ii}) and extrinsic ($\Delta F^{0'}$) contributions, (2) a rate-constant relation $k_{12} \cong (k_{11}k_{22}K_{12}f_{12})^{1/2}$ and modifications thereof, (3) a calculation of the local Brønsted slope α from the intercept of the ΔF^* vs. ΔF^0 plot, $\alpha = (1 + \Delta/\lambda)/2$, (4) a relation between k_H/k_D vs. $\Delta F^{0'}$ plots and local α 's, and (5) other relations among rate constants. Throughout, ΔF^* and $\Delta F^{0'}$ refer to an elementary step.

Introduction

A simple relation has been derived for the free-energy barrier and rate constant of weak-overlap electron-transfer reactions^{2,3}

$$k = Z \exp(-\Delta F^*/RT) \quad (1)$$

$$\Delta F^* = w^r + \lambda(1 + \Delta F_R^{0'}/\lambda)^2/4 \quad (2)$$

where Z is a bimolecular collision frequency in solution ($\cong 10^{11}$ l./mol sec), $\Delta F_R^{0'}$ denotes $\Delta F^{0'} + w^p - w^r$, $\Delta F^{0'}$ is the "standard" free energy of the reaction for the prevailing medium and temperature, w^r (or w^p) is the work required to bring the reactants (or products) together to the mean separation distance in the activated complex, and λ for a cross-reaction is the mean of that for two electron-exchange reactions⁴

$$\lambda_{12} = (\lambda_{11} + \lambda_{22})/2 \quad (3)$$

As a consequence of eq 1–3 one finds^{2c,5}

$$k_{12} \cong (k_{11}k_{22}K_{12}f_{12})^{1/2} \quad (4)$$

where k_{12} and K_{12} are the rate constant and equilibrium constant of the cross-reaction, k_{11} and k_{22} are the rate constants of the electron-exchange reaction of the two different redox systems, and $\ln f_{12}$, which equals $-\Delta F_R^{0'}/2\lambda RT$, is given by eq 5.

$$\ln f_{12} \cong (\ln K_{12})^2/4 \ln(k_{11}k_{22}/Z^2) \quad (5)$$

Equation 4 has been applied in the literature to weak-overlap electron transfers.⁶ Recently, as a conjecture, it was applied to a few examples of atom-transfer reactions.⁷ Equations 1 and 2 have been similarly used to calculate Brønsted slopes in atom- and proton-transfer reactions.⁸ In each case, the results were

(1) Acknowledgment is made to the donors of the Petroleum Research Fund, administered by the American Chemical Society, and to the National Science Foundation for their support of this research.

(2) (a) *J. Chem. Phys.*, **24**, 966 (1956); (b) *Discussions Faraday Soc.*, **29**, 21 (1960); (c) R. A. Marcus, *J. Phys. Chem.*, **67**, 853, 2889 (1963); (d) *Ann. Rev. Phys. Chem.*, **15**, 155 (1964); (e) *J. Chem. Phys.*, **44**, 679 (1965); (f) a review of this work and of that of other investigators (e.g., Levich and Dogonadze, Hush) is given in ref 2d. A factor of κ_p , omitted in eq 1, is about unity for an adiabatic reaction and is not relevant for the present purposes.

(3) When the reaction is partially or completely diffusion controlled, k is only one contribution to the observed rate constant. E.g., when the diffusion step is followed by an irreversible reaction step, $k_{\text{obsd}}^{-1} = k^{-1} + k_{\text{diff}}^{-1}$. Compare R. A. Marcus, *Proc. Exchange Reactions Symp., Upton, N. Y.*, **1** (1965); and R. A. Marcus, *Discussions Faraday Soc.*, **29**, 129 (1960).

(4) The cross-reaction is $A_1^{\text{ox}} - A_2^{\text{red}} \rightarrow A_1^{\text{red}} + A_2^{\text{ox}}$, where A_1^{ox} and A_1^{red} differ only in their redox state. The exchange reactions are $A_1^{\text{ox}} + A_1^{\text{red}} \rightarrow A_1^{\text{red}} + A_1^{\text{ox}}$ and $A_2^{\text{ox}} + A_2^{\text{red}} \rightarrow A_2^{\text{red}} + A_2^{\text{ox}}$.

(5) The work terms are omitted in eq 4. When they are included and $f_{12} \cong 1$, the right side of eq 4 has an additional factor $\exp[-(w_{12}^r + w_{12}^p - w_{11}^r - w_{22}^r)/2RT]$. (Note that $w_{ii}^r = w_{ii}^p$.) When f_{12} is not close to unity, the appropriate correction of eq 4 is made using eq 2.

(6) N. Sutin, *Ann. Rev. Phys. Chem.*, **17**, 119 (1966).

(7) (a) N. Sutin, *ibid.*, **17**, 154 (1966); (b) N. Sutin, *Proc. Exchange Reactions Symp., Upton, N. Y.*, **7** (1965); (c) A. Haim and N. Sutin, *J. Am. Chem. Soc.*, **88**, 434 (1966).

(8) A. O. Cohen and R. A. Marcus, unpublished data.

encouraging, but more extensive application is needed.

A semi-empirical, bond energy–bond order (BEBO) method has been used to calculate activation energies of gas-phase atom transfers.⁹ The potential energy form of eq 2, slightly modified in a way expected for atom transfers, permitted¹⁰ the calculation of potential-energy barriers for some 45 cross-reactions from those of 10 exchange reactions, with a reasonable agreement of about 2 kcal/mol. (There were 90 cross-reactions, but only 45 were independent.) The results are given in Appendix I.

In the present paper these equations are discussed for “strong-overlap” reactions, such as atom transfers, proton transfers, and strong-overlap electron transfers, and various consequences are noted. In some respects, the present discussion is a quantitative treatment of the common notion in the literature¹¹ that the Brønsted slope reflects the extent to which the activated complex resembles the reaction products (*e.g.*, our eq 31). The definitions or physical meanings of principal symbols are given in the Glossary.

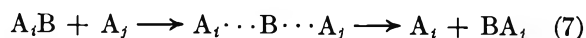
A Modification of Eq 2

Because of an expected difference in potential-energy surfaces, discussed in Appendix II, any applicability of eq 2 to gas-phase atom-transfer reactions is expected to be limited to $|\Delta F_R^{0'}| \leq \lambda$. Outside that interval, eq 6 is to be used. The same remarks apply to reactions in solution (Appendix II) if most of the reorganization comes from the bonds being broken and formed, rather than from all the other coordinates.¹²

$$\begin{aligned} \Delta F^* &\cong w^r \quad (-\Delta F_R^{0'} \geq \lambda) \\ \Delta F^* &\cong \Delta F^{0'} + w^p \quad (\Delta F_R^{0'} \geq \lambda) \end{aligned} \quad (6)$$

The λ in eq 2 and 6 is seen from eq 2 to equal approximately $4\Delta F_0^*$, where ΔF_0^* is the value of ΔF^* at $\Delta F^{0'} = 0$.

The following potential-energy counterparts (for gas-phase reactions) of eq 2 and 6 were used to calculate the energy barriers for gas-phase atom transfers mentioned earlier. (The work terms, w^r and w^p , usually coulombic, are absent now.) Let E_{ij} be the potential energy barrier of the atom transfer (7)



and let ΔE^0 be the net potential-energy change when $i = 1$ and $j = 2$. Then

$$E_{12} = E(1 + \Delta E^0/4E)^2 \quad (\Delta E^0 \leq 4E) \quad (8a)$$

$$E_{12} = 0 \quad (\Delta E^0 \geq 4E) \quad (8b)$$

$$E_{12} = \Delta E^0 \quad (\Delta E^0 \geq 4E_1)$$

In (8a) and (8b)

$$E = (E_{11} + E_{22})/2 \quad (8c)$$

Outline of Treatment

Before proceeding with detailed derivations, aspects of the paper are first reviewed. In weak-overlap electron-transfer reactions, it may be recalled, reactants experience work terms w^r , which are of coulombic and, in some cases,^{2c} “hydrophobic–hydrophilic” origin (solvent structural effects). These reactants also experience a readjustment of bond lengths, of bond angles when appropriate, and of orientations of solvent molecules outside the reactants’ coordination shells. Typically, the need for making these readjustments, more than w^r , constitutes the principal barrier to reaction. They occur because the system not only has to undergo electron transfer, but also has to eventually adopt values of these coordinates which are appropriate to the reaction products.

In the present paper, the arguments are extended to reactions in which bonds are broken and formed. Initially, a very simple bond energy–bond order model for gas-phase reactions (eq 9), is considered and eq 12 is derived. The main purpose of using eq 12 is to provide a simple, plausible vehicle for considering atom transfers and for comparing with eq 8, not for making a detailed calculation for these reactions. More elaborate quantum-mechanical calculations of E_{12} , E_{11} , and E_{22} would be useful for testing eq 8 or for testing eq 20, a result derived from eq 12.

For some purposes, it is not necessary to employ an equation which contains the specific assumptions present in eq 12 or 8. A more general, functional equation (16) is therefore introduced to generalize a portion of the subsequent treatment. Equation 16 includes eq 8 and 12 as special cases and, like them, relates barriers of cross-reactions to exchange reactions and serves also as a basis for a discussion of Brønsted slopes.

A comparison of these equations is then given. At low $\Delta E^0/4E$, they are found to give exactly the same first-order term for the barrier, and the latter term is found to contain no intrinsic asymmetry. When eq 8 and a symmetrized eq 12 are compared at arbitrary $\Delta E^0/4E$, they are found to give fairly similar results.

Reactions in solution are considered next. The coordinates of the reactants and solvent molecules in such systems can be roughly grouped as follows: (1) several bond distances, for bonds undergoing rupture or formation, and (2) coordinates describing more minor

(9) C. Parr and H. S. Johnston, *J. Am. Chem. Soc.*, **85**, 2544 (1963).

(10) I am indebted to Mrs. Audrey Cohen for these calculations. The mean-square deviation was 1.5 kcal/mol.

(11) (a) *E.g.*, J. E. Leffler and E. Grunwald, “Rates and Equilibria of Organic Reactions,” John Wiley and Sons, Inc., New York, N. Y., 1963, p 157; (b) see also R. P. Bell, “The Proton in Chemistry,” Cornell University Press, Ithaca, N. Y., 1959, Chapter 10; J. O. Edwards, “Inorganic Reaction Mechanisms,” W. A. Benjamin, Inc., New York, N. Y., 1964, Chapter 3.

(12) We note that eq 6 and 2 form a continuous function for ΔF^* for all values of $\Delta F_R^{0'}$. Also, in each case in eq 6 the rate constant or that of the reverse reaction is now essentially diffusion controlled in solution, and one calculates k_{obsd} accordingly.³

adjustments in bond lengths and angles in reactants, of which the solvent may be one, and orientations of solvent molecules. A simple treatment of group 1 could parallel the one used to obtain eq 8 and, simultaneously, group 2 could be treated by the method used to obtain eq 2. The details of the latter would differ somewhat from that for weak-overlap electron transfers,¹³ and so the contribution of group 2 coordinates to intrinsic terms g_i in eq 21 would differ. However, the basic approach could be made rather similar. A discussion of steric and statistical factors is also given. (They were absent in weak-overlap electron transfers.)

Equation 4 relating rate constants of cross-reactions to those of exchange reactions is next examined, and the implications of the preceding results are given. The discussion suggests that eq 4 comes through fairly intact, particularly at low $\Delta_i^{\ddagger 0}/4\Delta F_0^*$. In several subsequent sections, the meaning and magnitude of the Brønsted slope are considered, as is its relation to a kinetic isotope effect. The various findings are then summarized and, in a concluding section, the classification of activation free energies into intrinsic and extrinsic contributions is noted.

One Model for Atom Transfers

In the BEBO method,¹⁴ the energy of the A_iB bond in a gas-phase reaction (7) is written empirically as $-V_i n_i^{p_i}$, where n_i is the instantaneous bond order of A_iB , V_i is the A_iB bond energy when $n_i = 1$, and p_i is a quantity determined from bond energy-bond order relations in the literature; p_i is quite close to unity. Thus, E_t , the potential energy of formation of the system from the initial configuration is eq 9 when $n_1 = 1$ and $n_2 = 0$ initially.

$$E_t = (-V_1 n_1^{p_1} - V_2 n_2^{p_2}) + V_1 \quad (9)$$

In the cited model of the gas-phase reaction, it is then assumed that the total bond order $n_1 + n_2$ is constant along the reaction path; it is unity in the present case. By setting $dE_t/dn_2 = 0$ at the energy maximum along the reaction path, the activation energy is calculated from empirically known V_i 's and p_i 's.

To later compare eq 8 with \mathcal{E} , we first note that the former depends on only three quantities, E_{11} , E_{22} , and ΔE^0 , while the latter depends on four, V_1 , V_2 , p_1 , and p_2 . We may remove this difference as follows. Since $p_i \cong 1$, a Taylor's expansion of eq 9 can be made and powers of $(p_i - 1)$ higher than the first neglected. The instantaneous bond energy of A_iB is then

$$-V_i n_i^{p_i} \cong -V_i [n_i + (p_i - 1) n_i \ln n_i] \quad (10)$$

Maximization of eq 9 using eq 10 yields $n_i = 1/2$ for an exchange reaction.¹⁵ One finds

$$E_{11} = V_1(p_1 - 1) \ln 2 \quad (11)$$

$$E_t = n_2 \Delta E^0 - E_{11} \frac{n_1 \ln n_1}{\ln 2} - E_{22} \frac{n_2 \ln n_2}{\ln 2} \quad (12)$$

Since $n_1 + n_2$ equals unity, and since n_2 is determined from $dE_t/dn_2 = 0$, one sees E_t now depends only on three properties, E_{11} , E_{22} , and ΔE^0 .

It is useful to introduce E , the symmetric combination of E_{11} and E_{22} given by eq 8c, and an antisymmetric combination ϵ defined by

$$\epsilon = (E_{11} - E_{22}) / (E_{11} + E_{22}) \quad (13)$$

The terms intrinsic asymmetry, measured by ϵ , and extrinsic asymmetry, measured by $\Delta E^0/4E$, will be employed throughout this paper.

In the region of small intrinsic and extrinsic asymmetry eq 12 can be expanded about the symmetric condition $n_2 = 1/2$, and powers of $(n_2 - 1/2)$ higher than the second neglected. Maximization of E_t with respect to n_2 yields

$$E_t = E + 1/2 \Delta E^0 + (2x^\pm E / \ln 2) + \dots \quad (14)$$

where $x^\pm (= n_2^\pm - 1/2)$ is

$$x^\pm = \{-\Delta E^0 + 2\epsilon E [1 - (1/\ln 2)]\} (\ln 2) / 4E \quad (15)$$

A More General Equation

Equations 8 and 12 are special cases of a more general one

$$E_t = n \Delta E^0 + 1/2 E_{11} g_1(n) + 1/2 E_{22} g_2(1 - n) \quad (16)$$

$$dE_t/dn = 0 \quad (n = n^\pm)$$

where n is some degree-of-reaction parameter, being zero initially, unity finally, and n^\pm for the activated complex. E_{11} and E_{22} retain their earlier definitions. The term $g_i(n)$ is any function^{16,17} of n , normalized so that $g(1/2) = 1$.

In the region of small intrinsic and extrinsic asymmetry, eq 16 may be expanded in powers of $n = 1/2$ and terms beyond the second power neglected. One obtains eq 17

(13) In this reaction, there is a relatively abrupt charge transfer, namely near a value of the reaction coordinate defining the intersection of reactants' and products' potential-energy surfaces. In the case of proton or strong-overlap electron transfers, the change of charge distribution is expected to occur more gradually, i.e., over a wider interval along the reaction coordinate.

(14) For simplicity, the method discussed is the one originally used in H. S. Johnston, *Advan. Chem. Phys.*, **3**, 131 (1960).

(15) While $(p_i - 1) \ln 2$ varies widely from bond to bond, it averages around 0.05 to 0.1, so that the energy barrier (11) of an atom-exchange reaction might be about 5-10% of the bond energy, a reasonable figure. In a few cases $p_i - 1$ was negative, so the maximum occurred at the end points and one sets $E_{ii} = 0$ instead of eq 11.

(16) In this notation, the n and $1 - n$ in the last two terms of eq 16 are the arguments of the functions g_i , rather than multiplying factors.

(17) (a) Equation 8a follows from eq 16 by setting $g_i(n) = 4n(1 - n)$ in the interval $(0 < n < 1)$ and so outside of the infinitesimal regions around $n = 0$ and $n = 1$. In those regions, one could choose the g_i to approach zero extremely rapidly and, thereby, approximate eq 8b as closely as desired. The details of this choice of g_i are unimportant for our purposes, but a study of the g_i in footnote 17b is revealing; (b) to obtain eq 12, one sets $n = n_2$, $g_1(n) = g_2(n) = -2(1 - n) \ln(1 - n) / \ln 2$.

$$E_t = E + \frac{1}{2}\Delta E^0 - \frac{x^{\pm 2}}{4} [E_{11}g_1'' + E_{22}g_2''] \quad (17)$$

where $x^{\pm} (= n^{\pm} - 1/2)$ is

$$x^{\pm} = 2[-\Delta E^0 - \frac{1}{2}(E_{11}g_1' - E_{22}g_2')]/(E_{11}g_1'' + E_{22}g_2'') \quad (18)$$

The primes denote derivatives evaluated at $n = 1/2$.

Relation among Eq 8, 12, and 16

It has already been noted that eq 8 and 12 are special cases of eq 16. Unlike eq 8, eq 12 and 16 do have an intrinsic asymmetry term. However, a rather striking result can be proven when the intrinsic and the extrinsic asymmetry ($\Delta E^0/4E$) are both small: the intrinsic asymmetry makes no contribution to the first-order term in those equations for E_t . For example, in eq 14 and 17, the first-order term is $E + \frac{1}{2}\Delta E^0$, the same as it is in eq 8. It contains no intrinsic asymmetry, ϵ . Thus, all three equations agree at low $\Delta E^0/4E$. (A consequence of this absence of ϵ is noted under Remarks in eq 4.)

We next consider the relation between eq 8 and 12 at any value of $\Delta E^0/4E$. In both equations, E_t becomes 0 or ΔE^0 , accordingly, as $\Delta E^0/4E$ becomes very negative or very positive. For other $\Delta E^0/4E$, eq 8 is most easily compared with eq 19, the symmetrized form of eq 12, since 8 contains no intrinsic asymmetry.

$$E_t = n\Delta E^0 - E[n \ln n + (1-n) \ln(1-n)]/\ln 2 \quad (19)$$

The value of n which solves $dE_t/dn = 0$ is found and inserted into eq 19. Manipulation yields¹⁸

$$E_t = E + \frac{1}{2}\Delta E^0 + (\frac{1}{2}\Delta E^0/y) \ln \cosh y \quad (20)$$

where $y = (\Delta E^0/2E) \ln 2$. The $\Delta E^0/16E$ term in eq 8a can be written for comparison, as $\frac{1}{2}\Delta E^0 y/4 \ln 2$.

When y tends to $\pm\infty$, $\ln \cosh y$ tends to $\pm y - \ln 2$. Thereby, E_t in eq 20 tends to 0 or ΔE^0 , according as ΔE^0 tends to $-\infty$ or to $+\infty$, respectively, in agreement with eq 8b. When $\Delta E^0 = 2E$, which is midway between the extremes of small $\Delta E^0/4E$ and of $\Delta E^0/4E \sim 1$, $(1/y) \ln \cosh y$ is about $1/3$, while $y/4 \ln 2$ is $1/4$. The difference of eq 8a and 20 is, therefore, $\frac{1}{24}\Delta E^0$, which is small.

E , defined by eq 8c, is sometimes of the order of 10 kcal/mole, so that a ΔE^0 of about $2E$ is then about 20 kcal/mole.

Reactions in Solution

Two quite different gas-phase models of a reaction obeyed eq 16, one being BEBO and the other (see Appendix II) having a pair of intersecting potential energy parabolas. In the free-energy analog of eq 16, to be used for reactions in solution, E_t , ΔE^0 , and E_{ii} are replaced by their analogs at a mean separation distance, R , in the activated complex, $\Delta F^* - w^r$, $\Delta F_R^{0'}$, and $\Delta F_{ii}^* - w_{ii}$

$$\Delta F^* - w^r = n\Delta F_R^{0'} + \frac{1}{2}(\Delta F_{11}^* - w_{11})g_1(n) + \frac{1}{2}(\Delta F_{22}^* - w_{22})g_2(1-n) \quad (21)$$

$$\partial \Delta F^* / \partial n = 0 \quad (n = n^{\pm})$$

where $w_{ii} = w_{ii}^r = w_{ii}^p$ and $\Delta F_R^{0'} = \Delta F^{0'} + w^p - w^r$.

The quadratic expression (2) can in fact be written as in eq 21, with $g_1(n) = g_2(n) = 4n(1-n)$ and $\Delta F_{ii}^* - w_{ii} = \lambda_{ii}/4$. In Appendix III the results of ref 2e are used to show that weak-overlap electron transfers in solution obey eq 21, even before some approximations present in eq 2 are introduced.

As noted earlier, the nuclear coordinates in electron-transfer reactions are of two types: (a) vibrational coordinates (bond lengths and angles) in reactants, including those of any solvent molecules in the coordination shell, and (b) orientational coordinates of solvent molecules outside the coordination shell. For the former, a quadratic potential-energy function is appropriate. For the latter, it is not. Instead, the statistical mechanical equivalent of dielectric unsaturation for partial saturation was introduced into the free-energy expression for the solvent system.^{2e,19} The free energy of the solvent then became a quadratic function of fluctuations in solvent polarization, just as the harmonic potential energy for vibrational coordinates is a quadratic function of fluctuations in those coordinates. The total of the two contributions to ΔF^* leads, as noted in Appendix III, to eq 21.

In the case of an atom, proton, or strong-overlap electron transfer reaction in solution, it was noted that there are: (a) bonds being broken or formed, including any involving addition or removal of a solvent molecule to or from a reactant; (b) vibrational coordinates undergoing smaller changes; and (c) orientations of solvent molecules changing their distribution because of a change in charge distribution in the reactants. The first group might be treated as in eq 12 or 16, the second as in the preceding paragraph, and the third by the statistical mechanical dielectric unsaturation method noted there. The final result for the latter two contributions would differ somewhat from that found for weak-overlap electron transfers, because the change in charge distribution as the system moves along the reaction coordinate is now less abrupt. However, since quite different models led to eq 16, there is little doubt that a reasonable theory consistent with eq 21 can be formulated.

Steric and Statistical Factors

In atom or proton transfers, steric and statistical factors may contribute to the rate constant in a manner which depends on details of the potential-energy surface.

(18) *E.g.*, one finds $(\Delta E^0 \ln 2)/E = \ln [n/(1-n)]$. Thus, $n = \exp(2y)/[1 + \exp(2y)] = \exp(y)/2 \cosh y$ and $1-n = \exp(-y)/2 \cosh y$. Substitution in eq 19 yields eq 20.

(19) R. A. Marcus, *J. Chem. Phys.*, **38**, 1858 (1963); **39**, 1734 (1963).

Several models can be considered in such a way as to permit the preceding formalism to be utilized intact, as for example the following. (1) The reactants come together, requiring the coulombic or other work term, w^r . They reorient, with a steric and statistical factor of S^r and s^r , respectively.²⁰ (2) The system undergoes the pertinent changes of bond lengths and solvation and so reaction occurs. (3) The products separate, the relevant terms for the reverse process being w^p , S^p , and s^p .

The free-energy change in steps 1 and 3 is $w^r - RT \ln S^r s^r$ and $w^p - RT \ln S^p s^p$, respectively, and we write

$$W^r = w^r - RT \ln S^r s^r \quad (22)$$

The over-all "standard" free energy of reaction in steps 1-3 is $\Delta F^{0'}$, so that in step 2 is $\Delta F_R^{0'} = \Delta F^{0'} + W^p - W^r$. The configurational free-energy barrier to form the activated complex is $^{1/4}\lambda(1 + \Delta F_R^{0'}/\lambda)^2$ when $|\Delta F_R^{0'}/\lambda| \leq 1$, according to the arguments which led to eq 2; λ has the additivity in eq 3.

The "translational" contribution²¹ to the free energy of activation ΔF^\ddagger is $-kT \ln (hZ/kT)$, where Z is the collision number of uncharged species in solution ($\sim 10^{11}$ l./mol sec). Thus from $k_{\text{rate}} = (kT/h) \exp(-\Delta F^\ddagger/RT)$, one again obtains eq 1-3, where now the w^r and w^p are replaced by W^r and W^p . *E.g.*

$$\Delta F^* = W^r + \frac{\lambda}{4} (1 + \Delta F_R^{0'}/\lambda)^2 \quad (23)$$

$|\Delta F_R^{0'}/\lambda| \leq 1$, where $\Delta F_R^{0'} = \Delta F^{0'} + W^p - W^r$ now.

Remarks on Eq 4

In this section, a modification of eq 4 based on the free-energy analog of eq 20 is first given. We also consider a case where eq 4 could break down.

The free-energy analog of eq 20 yields eq 4, but with

$$f_{12} = K_{12}^{(1/y \ln c \cosh y)} \quad (24a)$$

where

$$y = (\ln K_{12})(\ln 2)/\ln (k_{11}k_{22}/Z^2) \quad (24b)$$

For comparison, eq 5 can be rewritten as

$$f_{12} = K_{12}^{y/4 \ln 2} \quad (25)$$

When, as in a previous section, $\Delta E^0/2E \sim 1$ and so $y = \ln 2$, and when $K_{12} = 10^{-12}$, the $f_{12}^{1/2}$'s in eq 24a and 25 differ only by a factor of 3.

The breakdown of eq 4 can be investigated by examining the breakdown of the first-order term in eq 8a, $E + 1/2\Delta E^0$, because of the related theoretical origin of both equations. Equation 4 rests on the dependence of all terms in the energy change on any degree-of-reaction variable n . Even a natural asymmetry in the potential-energy surface did not affect this equation in the region of small $\Delta E^0/4E$, because of a compensation.

Correspondingly, some breakdown will occur in these equations when an important term in the free-energy barrier does not vary with n . For example, in the case of eq 16, let a fraction c of the ΔE^0 occur before the principal reorganization. Then E_t is zero initially, and is given by eq 16, subsequently, with $n\Delta E^0$ replaced by $c\Delta E^0 + (1 - c)n\Delta E^0$. Manipulation as before leads to

$$E_t = E + 1/2(1 + c)\Delta E^0 - \frac{x^{\ddagger 2}}{2} Eg''^{(1/2)} + \dots \quad (26)$$

where x^\ddagger is given by eq 18, with ΔE^0 replaced by $(1 - c)\Delta E^0$, and where we have let $g_1(n) = g_2(n)$ for simplicity of illustration.

From eq 26, or really from its free-energy counterpart, one finds

$$k_{12} \cong (k_{11}k_{22}K_{12}^{1+c})^{1/2} \quad (27)$$

When c is small, $K_{12}^{c/2}$ becomes a second-order term. *E.g.*, if $c = 0.1$ and $K_{12} = 10^{10}$, $K_{12}^{c/2} \cong 3$.

When steric and statistical effects are included, eq 4 becomes

$$k_{12} \cong (k_{11}k_{22}K_{12}f_{12})^{1/2}(\zeta_{12}^2/\zeta_{11}\zeta_{22})^{1/2} \quad (28)$$

where ζ for a reaction is

$$\zeta = (S^r s^r S^p s^p)^{1/2} \quad (29)$$

and f_{12} is

$$\ln f_{12} = (\ln K_{12})^2/4 \ln (k_{11}k_{22}/\zeta_{11}\zeta_{22}Z^2) \quad (30)$$

(Similarly, eq 24b can be corrected for the ζ 's by dividing $k_{11}k_{22}$ by $\zeta_{11}\zeta_{22}$.)

Meaning of the Brønsted Slope

The Brønsted slope, α , is $\partial\Delta F^*/\partial\Delta F^{0'}$ and, according to eq 21, equals $n + (\partial\Delta F^*/\partial n)_{\Delta F^{0'}}(\partial n/\partial\Delta F^{0'})$, evaluated at $n = n^\ddagger$. Since $(\partial\Delta F^*/\partial n)_{\Delta F^{0'}}$ vanishes at $n = n^\ddagger$, we obtain

$$\alpha = n^\ddagger \quad (31)$$

For the BEBO model described earlier for a gas-phase reaction, n^\ddagger , and hence α , is the bond order of the bond being formed. For weak-overlap transfers

(20) S^r can be expressed in terms of a ratio of a vibrational partition function of the activated complex to the rotational-vibrational one of the reactants. s^r can be expressed several ways, one being intuitive and all of which give a similar answer. Compare ref 11a, p 133. See also R. A. Marcus, *J. Chem. Phys.*, **43**, 1601 (1965), eq 17; E. W. Schlag and G. L. Haller, *ibid.*, **42**, 584 (1965); D. M. Bishop and K. J. Laidler, *ibid.*, **42**, 1688 (1965).

(21) Of the six translational degrees of freedom of the two reactants (masses m_1, m_2), five coordinates become three translations and two principal rotations of the activated complex, and a sixth may mix with other coordinates to yield the reaction coordinate and others. The partition function ratio of the five coordinates of the activated complex to the six of the reactants is $[2\pi(m_1 + m_2)kT]^{5/2}(8\pi^2IkT)/\sigma(2\pi m_1kT2\pi m_2kT)^{3/2}(h^6/h^6)$, where I is the relevant principal moment of inertia, written suggestively as μR^2 , σ is a symmetry number ($\sigma = 1$ or 2 according as the reactants are unlike or like), and $\mu = m_1m_2/(m_1 + m_2)$. This ratio equals hZ/kT , where Z is defined as $(8\pi kT/\mu)^{1/2}R^2/\sigma$ and equals about 10^{11} l./mol sec.

in solution, discussed in Appendix III and involving no bond ruptures, the distribution of coordinates in the activated complex is determined by a potential-energy function $(1 - n^\ddagger) U^r + n^\ddagger U^p$; *i.e.*, n^\ddagger and, thereby, α represents the products' contribution to this function. For an atom or proton transfer or strong-overlap electron-transfer solution, if some method, such as that briefly touched on in a preceding section, were employed to calculate the terms in eq 21, n^\ddagger and hence, α would characterize the product-like character of both types of coordinates.

As exemplified by the equations of the following section, and in accordance with the usual notion, the Brønsted plot should be curved when $\Delta F^{0'}$ is varied over a sufficiently wide range. For any compound the α and, hence, the n^\ddagger equals the instantaneous slope of this plot at the given $\Delta F^{0'}$ for this compound.

Magnitude of the Brønsted Slope

Since α is $\partial \Delta F^* / \partial \Delta F^{0'}$, eq 2 yields

$$\alpha = 1/2(1 + \Delta F_R^{0'} / \lambda) \quad (32)$$

when $|\Delta F_R^{0'}| \leq \lambda$. If ΔF_0^* denotes the intercept at $\Delta F^{0'} = 0$ of a plot of ΔF^* vs. $\Delta F^{0'}$, then

$$\Delta F_0^* = w^r + \frac{\lambda}{4} [1 + (w^p - w^r) / \lambda]^2 \cong \frac{w^r + w^p}{2} + \frac{\lambda}{4} \quad (33)$$

since $\lambda \gg (w^p - w^r)$. Thus²²

$$\alpha \cong (1 + \Delta F_R^{0'} / 4\Delta F_0^*) / 2 \quad (34)$$

When statistical and steric factors are included, eq 34 again follows, but with w^r and w^p in $\Delta F_R^{0'}$ and ΔF_0^* replaced by W^r and W^p .

For a reaction whose functional dependence of ΔF^* on $\Delta F^{0'}$ is given instead by eq 20 (with E_f and ΔE^0 replaced by ΔF^* and $\Delta F_R^{0'}$, etc.) α would be

$$\alpha = (1 + \tanh y) / 2 \quad (35)$$

where $y = (\Delta F_R^{0'} / 2\Delta F_0^*) \ln 2$. When $\Delta F_R^{0'} / \Delta F_0^*$ is 2, this α is 0.8, while that obtained from eq 34 is 0.75.

Comparisons of experimental plots of ΔF^* vs. $\Delta F^{0'}$ with these equations are appropriate when λ is constant for all points in the plot.

Kinetic Isotopic Effect k_H/k_D and Brønsted Slope

A maximum in plots of k_H/k_D vs. pK^s has sometimes been reported. A useful simple explanation has been given,²³ based on little isotopic effect on ΔpK and on the reaction's forward or reverse step becoming fast (diffusion controlled) at either extremity of the plot.²³ With the aid of eq 2, we can formulate the suggestion in quantitative terms. We consider, then, reactions for which there is little isotopic effect on $\Delta F^{0'}$ (and W^r or W^p). The barrier difference for hydrogen and deuterium isotopes is then found from eq 2 to be ²⁴

$$\Delta F_H^* - \Delta F_D^* \cong 1/4(\lambda_H - \lambda_D) \left[1 - \left(\frac{\Delta F_R^{0'}}{\lambda_H} \right)^2 \right] \quad (36)$$

when $|\Delta F_R^{0'}| \leq \lambda_H$. We have used the fact that $\lambda_H \lambda_D \cong \lambda_H^2$. The barrier difference is seen to pass through a maximum. Since $\alpha - 1/2$ is $\Delta F_R^{0'} / 2\lambda_H$, the last factor in eq 36 is $[1 - 4(\alpha - 1/2)^2]$.

Summary of Findings for Cross-Relation and for Brønsted Slope

We summarize our findings regarding eq 4. (1) Except as noted in Appendix II, the application of eq 4 to atom or proton transfers is probably limited to $|\Delta F^{0'} / 4\Delta F_0^*| < 1$, a normally minor limitation. (2) Several models, including the BEBO one and a generalization thereof, lead to eq 4 in the vicinity of small $\Delta F^{0'} / 4\Delta F_0^*$. Intrinsic asymmetry does not alter this equation when $\Delta F^{0'} / 4\Delta F_0^*$ is small. (3) The difference of the BEBO and quadratic approximations, eq 20 and 8, is rather small where we have tested it. (4) Since eq 4 rests ultimately upon a continuous dependence of the main configurational free-energy change on some reaction parameter, the equation will break down when some appreciable fraction of the total free-energy change becomes independent of n , to the extent given by eq 27. (5) When steric and statistical effects occur, several models can be considered, one of which replaces eq 4 by 28. (6) Any effects which are specific only for the cross-reaction or only for one of the exchange reactions are excluded in eq 16, and so tend to cause eq 4 to break down.

The Brønsted slope, α is expected to be 0.5, when $\Delta F^{0'} = 0$. However, deviations would occur (a) if $c \neq 0$ in eq 27, *i.e.*, if an appreciable fraction of the free-energy change were independent of the reaction parameter n , or (b) if $g_i' \neq 0$ in eq 18 and, at the same time, the asymmetry ϵ is large. Equation 34 is a simple, approximate expression for α for any $\Delta F^{0'}$ for which $|\Delta F^{0'} / 4\Delta F_0^*| < 1$. It yielded a value (0.75) close to that obtained (0.8) from a quite different model (eq 35) even when $\Delta F^{0'} / \Delta F_0^*$ had the fairly large value of 2. An interpretation of α for a certain class of models, those for which eq 21 is applicable, is given by eq 31 and the associated discussion.

Remark on Intrinsic Barriers

Reaction barriers have been considered here in terms of intrinsic (λ_{it}) and thermodynamic ($\Delta F^{0'}$) contributions, as well as of steric (ζ) and statistical ones. Some test of the intrinsic-extrinsic separation can be made with data on Brønsted slopes and with the cross-relation, *e.g.*, with tests of eq 4 and 34.

(22) In writing eq 34, $1/2(w^r + w^p)$ was neglected relative to ΔF_0^* , since it is normally much smaller. To avoid this approximation, the ΔF_0^* in eq 34 can be replaced by $\Delta F_0^* - 1/2(w^r + w^p)$.

(23) E. S. Lewis and C. H. Funderburk, *J. Am. Chem. Soc.*, **89**, 2322 (1967); eq 33 shows that the diffusion-control aspect is incidental, rather than necessary.

(24) All zero-point effects have been included in the λ 's.

Table I: Comparison of BEBO Calculations with Eq 8

A _i	A _j										D _{A,H}
	F	HO	H	CF ₃	Cl	CH ₃	Et	Me ₂ CH	Me ₃ C	Br	
F	6										140
HO	0.3 (0)	4									115
H	2 (0)	6 (4)	10								109
CF ₃	3 (0.2)	7 (5)	12 (11)	13							107
Cl	0.3 (0)	0.3 (0)	5 (4)	8 (6)	0						106
CH ₃	3 (0.1)	6 (5)	11 (10)	12 (12)	7 (6)	13					105
Et	2 (0)	4 (2)	8 (7)	9 (9)	4 (3)	10 (10)	12				100
Me ₂ CH	2 (0)	4 (2)	8 (6)	9 (8)	3 (3)	9 (9)	11 (11)	12			98
Me ₃ C	2 (0)	3 (1)	6 (5)	7 (7)	2 (1)	7 (7)	9 (9)	10 (10)	12		93
Br	0 (0)	0.4 (0)	2 (0)	3 (1)	0 (0)	3 (1)	4 (2)	4 (3)	5 (5)	0	90

In interpretations of Brønsted slopes, λ has been assumed constant as a conjecture for a reaction series when the substituent is not part of the reaction site.^{6,8} When a similar assumption is valid for other reactions, such as those involved in the Hammett $\sigma\rho$ relation, there is an interesting consequence. In the region of $\alpha = 1/2$, σ and ρ then depend only on variations in $\Delta F^{0'}$. For other α 's they depend on variations in $\Delta F^{0'}$ ($1 + \Delta F^{0'}/2\lambda$) at constant λ . Then, with λ estimated from the data, discussions of substituent effects reduce purely to a discussion of effects on $\Delta F^{0'}$ and so fall within a broader class of problems concerning the effect of substituents on thermodynamic properties.

Appendix I. Comparison of BEBO Calculations and Eq 8

Equation 8 relates the barriers of cross-reactions [$i \neq j$ in eq 7], to exchange reactions [$i = j$ in eq 7]. Table I gives a comparison with calculations made for a BEBO model more complicated than eq 9. The reactions in this table are hydrogen-atom transfers, *i.e.*, B in eq 7 is H now. The diagonal elements in Table I provide the values of the exchange barriers E_{ii} . Values of ΔE^0 are obtained by subtracting the dissociation energies of the A_iH used in the BEBO calculations, D_{A_iH} , given in the last column. Use of eq 8 then permits the nondiagonal elements of the table to be computed. They are given in parentheses. For brevity, only values below the diagonal are given. Those above the diagonal refer to the reverse reaction and are not independent of the former.

The values based on eq 8 are seen to be close to the BEBO ones. The two sets of results show about the same agreement with the experimental data.

Appendix II. Potential Energy Surfaces in Reactions

If the potential energy of a reaction along the reaction coordinate involves a pair of intersecting parabolas, eq 8a is obtained. In this case, the predominant motion along the reaction coordinate is a vibrational or pseudo-vibrational one. In the case of a weak-overlap electron transfer in solution, numerous coordinates are involved and this plot is a profile of the potential energy along a reaction coordinate in many dimensional configuration space (*e.g.*, Figure 1 of ref 2b). The reaction coordinate is expected to be associated in part with vibrational motion of the ligands and dielectric relaxation of the solvent polarization.²⁶

In a gas-phase atom transfer, the reaction coordinate involves a concerted motion of a compressing of one bond and a stretching of the other. Here, using the usual potential contour diagrams, one can plot the potential energy along the reactants' valley, up to the saddle point, and down to the products' valley. Here, the curve, potential energy *vs.* reaction coordinate, is initially constant, then rises to a maximum, like an Eckart barrier, and then falls to another constant value.²⁵ One can no longer, therefore, obtain the "inverted chemical effect"^{2b} possible with eq 2 at large $|\Delta F^{0'}/\lambda|$, and so the added equation (6) is imposed.

When the bond rupture-bond formation in atom or proton transfers in solution is the principal contributor to the reaction coordinate, as one would expect, the remarks of the last paragraph apply here as well. However, when most of the reorganization is associated

(25) *E.g.*, I. Amdur and G. G. Hammes, "Chemical Kinetics: Principles and Selected Topics," McGraw-Hill Book Co., New York, N. Y., 1966, p 47.

with coordinates not involved in bond rupture or formation, eq 6 would no longer be applicable. The "inverted chemical effect" could again occur, and the unrestricted eq 2 would again be relevant.

Appendix III. Weak-Overlap Electron Transfers and the Free Energy Analog of Eq 16

We denote by ΔF_R^* the configurational contribution to ΔF^* at any separation distance, *i.e.*

$$\Delta F_R^* = \Delta F^* - w^r \quad (\text{A1})$$

Similarly, for formation of activated complex from products at a separation distance R , we write

$$\Delta F_R^{*p} = \Delta F^{*p} - w^p \quad (\text{A2})$$

In ref 2b and 2e, it was noted (i) that the distribution of activated complex configurations for weak-overlap reactions was centered at the intersection of two potential energy functions U^r and U^p in many dimensional configuration space, (ii) that the distribution can be expressed in terms of an equivalent equilibrium distribution for which the configurations are distributed in accordance²⁶ with the function $f^* = A \exp\{-(1-n)U^r + nU^p/kT\}$, where A is a normalizing constant, and (iii) that f^* is unchanged when the symbols (r , p , and n) are changed to (p , r , and $1-n$), respectively.

ΔF_R^* can be written as $(1-n)\Delta F_R^* + n\Delta F_R^{*p} + n\Delta F_R^{0'}$, since $\Delta F_R^{0'}$ equals $\Delta F_R^* - \Delta F_R^{*p}$. There is now a useful symmetry property. Because of property iii, examination of an expression for ΔF_R^* shows at once that when (r , p , and n) is replaced by (p , r , and $1-n$), respectively, ΔF_R^* goes over to ΔF_R^{*p} , ΔF_R^{*p} goes over to ΔF_R^* , and, thus, $(1-n)\Delta F_R^* + n\Delta F_R^{*p}$ remains unchanged. This result is used later to obtain eq A4.

We shall first show that $\partial\Delta F_R^*/\partial n = 0$. From the definition of F_R^* , *i.e.*, $\langle U^r \rangle + kT(\ln f^*)$, [eq 35, ref 2e], where $\langle \rangle$ denotes average with respect to f^* , and from the equation reflecting the centered distribution, $\langle U^r \rangle = \langle U^p \rangle$ [eq A1, ref 2e], one finds that $\partial F_R^*/\partial n = 0$. Thus, $\partial\Delta F_R^*/\partial n = 0$, and part of eq 21 has been derived.

We next derive eq A4.

If, for the moment, we regard the ions as far apart, the distribution function f^* can be factored into two parts, one for each ion and its environment. So can that of the initial reactants. Thereby, the expression $(1-n)\Delta F_R^* + n\Delta F_R^{*p}$ can also be written as the sum of two functions, $f_{11}(r, p, n)$ and $f_{22}(r, p, n)$, one for each reactant. Thus, we may write

$$\Delta F_R^* = n\Delta F_R^{0'} + f_{11}(A_1^{\text{ox}}, A_1^{\text{red}}, n) + f_{22}(A_2^{\text{red}}, A_2^{\text{ox}}, n) \quad (\text{A3})$$

since the reactants are A_1^{ox} and A_2^{red} . In virtue of the symmetry property proven earlier, the last term also equals $f_{22}(A_2^{\text{ox}}, A_2^{\text{red}}, 1-n)$. For brevity, we denote

this term by $f_{22}(1-n)$ and the term before it in eq A3 by $f_{11}(n)$

$$\Delta F_R^* = n\Delta F_R^{0'} + f_{11}(n) + f_{22}(1-n) \quad (\text{A4})$$

We consider now the case where the ions are close together in the activated complex rather than separated. Their vibrational contributions to U^r and U^p are largely additive, so this contribution to the distribution function f^* factors as before. The solvent-polarization contributions from the two ions are not independent. However, as noted on p 693 of ref 2e, deviation from an *apparent* additivity can be estimated to be small. Thus, eq A3 applies even for interacting cases.

For an exchange reaction, $f_{22}(n) = f_{11}(n)$. For these systems, according to the analysis, $\kappa = 1/2$. (There is no double maximum for barrier *vs.* reaction coordinate in this treatment.) Thus, for an exchange we have

$$\Delta F_{ii}^* = 2f_{ii}(1/2) \quad (\text{A5})$$

If we denote $f_{ii}(n)/f_{ii}(1/2)$ by $g_i(n)$, the free energy analog of eq 16 follows.

In summary, there are two basic ingredients to this free energy analog of eq 16: (1) a dependence of ΔF^* on a parameter n , and (2) an additivity, which is partly apparent and partly actual, of intrinsic barrier for the changes of configuration around each center, A_1 and A_2 , *i.e.*, for the changes that would occur if $\Delta F_R^{0'}$ were zero.

Glossary of Principal Symbols

Symbols	Physical Meaning or Definition
ΔF^*	Gibbs free energy barrier to reaction, related to rate constant k by 1.
ΔF^\ddagger	Gibbs free energy of activation ($= \Delta F^* - RT \ln kT/hZ$; compare footnote 21).
$\lambda/4$	Intrinsic contribution to the barrier for electron transfers. It equals the average of the reorganizational barriers ($\lambda_{11}/4$, $\lambda_{22}/4$) of two exchange reactions, as in eq 3.
$\Delta F^{0'}$	Gibbs "standard" free energy of reaction for the prevailing medium and temperature. It differs slightly from the standard free energy change, which refers to STP and to infinite dilution.
K_{12}	Equilibrium "constant," given by $\exp(-\Delta F^{0'}/RT)$.
$\Delta F_R^{0'}$	"Standard" free energy of reaction at a typical separation distance R for the prevailing medium and temperature

(26) We have replaced the $-m$, in ref 2 by n , to conform with present notation.

	$(\Delta F_R^{0'} = \Delta F^{0'} + w^p - w^r$ in eq 2 and $= \Delta F^{0'} + W^p - W^r$ in eq 23).	E_t	Potential energy in atom transfer (7) relative to initial potential energy.
w^r, w^p	w^r is work required to bring reactants together to mean separation distance R ; w^p is the similar quantity for the products.	ϵ	Intrinsic asymmetry defined by eq 13.
f_{12}	Defined by eq 5. Compare also eq 25.	x^\ddagger	$n_2^\ddagger - 1/2$ in eq 14 or $n^\ddagger - 1/2$ in eq 18.
k_{12}, k_{11}, k_{22}	Rate constants of the cross-reaction (k_{12}) and of the exchange reactions (k_{11}, k_{22}).	g_1, g_2	Intrinsic barrier terms in eq 16.
ΔF_0^*	Value of ΔF^* extrapolated, in a ΔF^* <i>vs.</i> $\Delta F^{0'}$ plot, to $\Delta F^{0'} = 0$.	n	Degree-of-reaction parameter in eq 16.
E_{12}	Potential-energy barrier of a gas-phase cross-reaction (7).	n^\ddagger	Value of n at barrier maximum.
E_{11}, E_{22}	Potential-energy barriers of gaseous ex- change reactions (7) (with $i = j$).	g_i', g_i''	dg_i/dn and d^2g_i/dn^2 at barrier maximum.
E	Average barrier for the two exchange reactions, as in eq 8c.	$\Delta F_{11}^*, \Delta F_{22}^*$	Free-energy barriers in two exchange re- actions.
ΔE^0	Potential-energy change in the reaction.	w_{11}, w_{22}	Work terms in two exchange reactions ($w_{ii}^r = w_{ii}^p$).
V_1, V_2	Bond energies of A_1B and A_2B single bonds.	S^r, S^p	Steric factors for forward and reverse reactions.
n_1, n_2	Bond orders of A_1B and A_2B .	s^r, s^p	Statistical factors for forward and reverse reactions.
p_1, p_2	Exponents in bond energy <i>vs.</i> bond order plots.	W^r, W^p	Contributions to ΔF^* before (W^r) and after ($-W^p$) the rearrangements, de- fined in eq 22.
		y, c, ζ	See eq 24b, paragraph before eq 26, and 29, respectively.
		α	Brønsted slope. For its variation with $\Delta F^{0'}$, see eq 34 or 35.

The Effect of Solutes and Temperature on the Structure of Water

by O. D. Bonner and G. B. Woolsey

Department of Chemistry, University of South Carolina, Columbia, South Carolina 29208 (Received August 14, 1967)

The spectrum of liquid water has been observed over the range 600–1800 $m\mu$ by a differential method in which water at 25° is compared either with an aqueous solution at the same temperature or water at an elevated temperature. Five overtones have been observed, which may be identified with the same ones occurring in the vapor phase, and are believed to be due to the presence of nonbonded liquid water. The band at 958 $m\mu$ was chosen for quantitative studies, and solvation numbers have been calculated for a series of simple electrolytes and also for several organic solutes. The numbers obtained for electrolytes differ only slightly from those which appear as parameters in certain equations, but the sequence for the alkali halides is not the same. Water-structure enhancement by organic solutes is experimentally confirmed. Temperatures studies show that the concentration of monomeric water increases approximately linearly with temperature and doubles over the range from 25 to 80°. The strength of the hydrogen bond, based upon this temperature dependence of the monomer concentration, is estimated to be 2.67 kcal/mol. A combination of these data with those from the literature yields a calculated value of the concentration of nonbonded water at 25° of 3.5 mol/l. or about 6%.

Introduction

The structure of water has been the subject of numerous investigations and of much controversy for many years. Various techniques, such as infrared and Raman spectroscopy, nmr, X-ray diffraction, and dielectric relaxation measurements, have been used in these studies, which have also been extended to aqueous

solutions. An extensive bibliography on water structure will not be presented in this paper, since excellent ones are available in Kavanau's monograph and in the book published by Pimentel and McClellan.¹ Some of

(1) (a) J. L. Kavanau, "Water and Solute-Water Interactions," Holden-Day, San Francisco, Calif., 1964; (b) "The Hydrogen Bond," G. C. Pimentel and A. L. McClellan, W. H. Freeman and Co., San Francisco, Calif., 1960.

the models which are most successful in relating the structure of water to its properties are due to Forslind,² Frank,³ and Claussen.⁴

The degree of association of water has been the subject of much speculation, and evidence has been cited for both a mixture model and a continuum model.⁵ In the first instance, water is postulated to consist of an equilibrium mixture of molecular species with different numbers of hydrogen bonds per molecule. The continuum model describes water as an essentially complete hydrogen-bonded system. Choppin and co-workers^{6,7} have, for example, investigated the near-infrared spectrum of water and have stated that "a ready explanation for the bands is found in their assignment to water molecules having different degrees of polymerization." Falk and Ford,⁵ on the other hand, have examined the spectra of HDO in the same region and state that the spectra "are incompatible with the existence in water of any discrete molecular species differing in the extent of hydrogen bonding."

Although water molecules are known to be continuously making and breaking hydrogen bonds, infrared spectra represent an average structure, in that species having lifetimes of the order of 10^{-13} sec may be detected and this experimental technique was used in the studies which are being reported.

Experimental Section

All spectra were recorded using a Cary Model-14M spectrophotometer. The spectra in Figure 1 were recorded with water or aqueous solution in a 2-cm cell and with an empty cell in the reference beam. All other absorbances were measured using a differential technique which was developed for the observation of charge-transfer complexes between N-methylacetamide and aromatic acceptors. For each measurement, water at 25° was used in one of the matched cells as a reference, and aqueous solutions or water at another temperature was placed in the other cell. Cells of 10 cm length were used for the spectral region 900–1000 $m\mu$ and, because of the increasingly stronger absorbance, progressively shorter cells were used for measurements further into the infrared region. This technique has the advantage of compensating to a great extent for the underlying absorption of water, which is not directly due to the monomer overtones which are of interest, and emphasizes the differences in water structure caused by a change in temperature or the presence of a solute. In contrast with direct measurements, such as those in Figure 1, the observed bands are sharp and do not shift with temperature or with the concentration of solute.

Results and Discussion

A. Vibrational Bands. The positions of the fundamental vibrational bands of water vapor and their overtones have been accurately determined.³ These

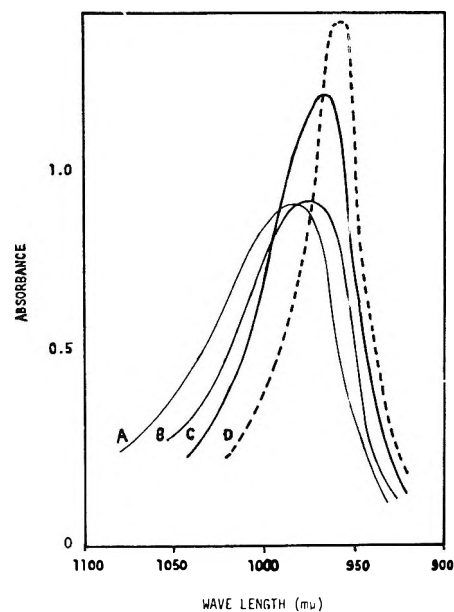


Figure 1. Shifts in the absorbance maxima of water with temperature and added electrolyte: (a) saturated $MgCl_2$, peak at 986 $m\mu$; (B) water at 25°, peak at 977 $m\mu$; (C) water at 80°, peak at 965 $m\mu$; and (D) postulated curve for liquid monomeric water, peak at 958 $m\mu$.

bands are known to arise from the three vibrational modes of monomeric water. The spectrum of liquid water is considerably complicated, however, by hydrogen bonding which broadens the bands and shifts them to longer wavelengths. This shift is accentuated as the temperature of the liquid water is lowered and is related to the increased hydrogen bonding. Waggener and coworkers⁹ have recorded the spectra of liquid water over the range of temperature from 2 to 250°. It may be noted that as the temperature is raised, the bands become sharper and shift toward the blue, so as to approach a constant wavelength asymptotically. In the case of the 201 overtone, this value is approximately 960 $m\mu$ and it is about 1150 $m\mu$ for the 111 overtone. There is certainly some hydrogen bonding in liquid water at 250°, but since the wavelengths of the bands do not shift appreciably with temperature above 200°, this probably represents the positions of the 201 and 111 overtones of liquid monomeric water and the shift from the vapor-phase values of 942 and

- (2) E. Forslind, *Acta Polytech.*, **115**, 9 (1952).
- (3) H. S. Frank and A. S. Quist, *J. Chem. Phys.*, **34**, 604 (1961).
- (4) W. F. Claussen, *ibid.*, **19**, 259, 662, 1425 (1951).
- (5) M. Falk and T. A. Ford, *Can. J. Chem.*, **44**, 1699 (1966).
- (6) K. Buijs and G. R. Choppin, *J. Chem. Phys.*, **39**, 2035 (1963).
- (7) G. R. Choppin and K. Buijs, *ibid.*, **39**, 2042 (1963).
- (8) G. Herzberg, "Molecular Spectra and Molecular Structure. II. Infrared and Raman Spectra of Polyatomic Molecular," D. Van Nostrand Co., Inc., Princeton, N. J., 1959, p 281.
- (9) W. C. Waggener, A. J. Weinberger, and R. W. Stoughton, Annual Progress Report ORNL-3832, UC-4-Chemistry, Oak Ridge, Tenn., May 1965, pp 76-81.

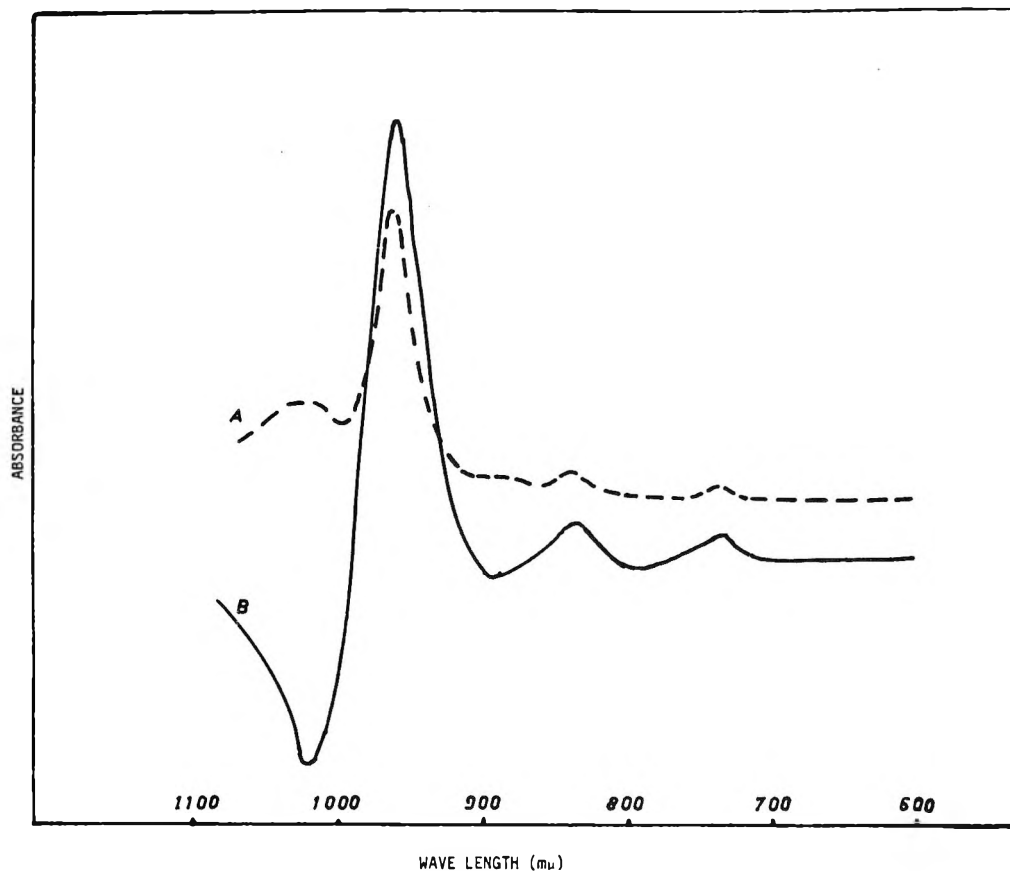


Figure 2. Absorbance of water: (A) water vs. 5 *m* LiCl solution in 10-cm cells; (B) water at 25° vs. water at 58° in 10-cm cells.

1136 $m\mu$ may be ascribed to the proximity of nearest neighbors in the liquid.¹⁰

It has been observed that the presence of electrolyte shifts the water bands toward the red in a manner similar to hydrogen bonding. The spectra in Figure 1 were recorded to obtain quantitative shifts for the 201 overtone, which might be useful in the interpretation of the subsequent data. Curve A for a saturated solution of $MgCl_2$, in which it may be assumed that essentially all water molecules are polarized by Mg^{2+} ion, has a peak at the longest wavelength (986 $m\mu$). A similar curve was obtained for a saturated solution of $LaCl_3$. The band maximum is shifted to 977 $m\mu$ for pure water at the same temperature. It appears at shorter wavelengths and increases in intensity as the temperature is increased. Curve D represents a postulated curve for liquid monomeric water. The position of this band and its intensity are estimated from the data⁹ on liquid water at 250°. Similar families of curves are experimentally obtainable for the other overtones of water.

In other studies, vibrational bands have been observed at five different wavelengths by the differential technique, described above, when solutions of LiCl are compared with pure water at 25°. The bands are sharp and their position is unchanged when electrolytes

other than LiCl are used. They also occur in the same position when pure water samples at two different temperatures are compared (Figures 2 and 3). These results are consistent with the vacant-lattice-point model,² depicting water as primarily a hydrogen-bonded structure with a small fraction of interstitial monomeric molecules. One might consider all of the experimentally observed spectra to be combinations of curves A and D of Figure 1, which represent the hydrogen bonded and monomeric forms, respectively. Any shift in equilibrium caused by the addition of electrolyte or a change in temperature would result in a maximum change in absorbance at the wavelengths of monomeric-water overtones, since these have much larger molar absorbances. Table I lists the positions of these vibrational bands in liquid water and also the positions of bands which have been observed in the vapor phase.⁸

It is apparent that these band positions in the liquid phase do not correspond with those of Choppin,⁶ which were obtained by the mathematical resolution of the water spectrum. It is believed that this differential method is more accurate in compensating for the absorbance caused by the shoulders of bands, which have

(10) Reference 8, p 534.

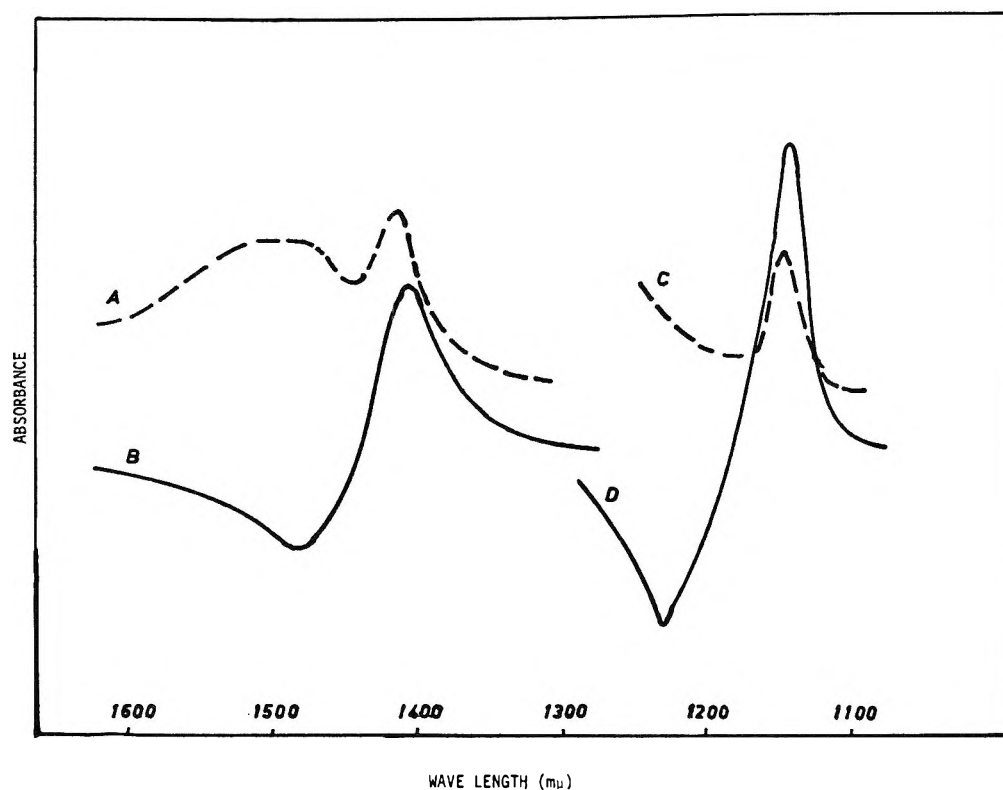


Figure 3. Absorbance of water: (A) water vs. 5 *m* LiCl solution in 1-mm cells; (B) water at 25° vs. water at 58° in 1-mm cells; (C) water vs. 5 *m* LiCl solution in 2-cm cells; and (D) water at 25° vs. water at 58° in 2-cm cells.

Table I: Vibrational Bands of Water

Band position, $m\mu$		Band assignment
Vapor	Liquid	
723	734	$3\nu_1 + \nu_3$
823	832	$2\nu_1 + \nu_2 + \nu_3$
942	958	$2\nu_1 + \nu_3$
1136	1148	$\nu_1 + \nu_2 + \nu_3$
1379	1405	$\nu_1 + \nu_3$

been shifted by hydrogen bonding or by polarization, due to the presence of an electrolyte, and more nearly represents the position of the band due to monomeric water in the liquid state. The correspondence of the values for the 201 and 111 overtones with the high temperature values of Waggener⁹ and the uniformity of the shift for all overtones in the liquid is further substantiation of the experimental method.

It is interesting to note (Figures 2 and 3) that when water at a higher temperature is compared with water at 25°, there is an absorption minimum which lies just to the red side of the bands listed in Table I. On the other hand, when water at 25° is compared with a solution of any electrolyte, there are broad absorption maxima which lie at approximately the same position. This might be expected, since electrolytes will decrease the concentration of all water and thus pure water would have more hydrogen-bonded water as well as

more water monomer than solutions. In water at 58°, however, the concentration of the monomer species has been increased at the expense of the hydrogen-bonded water. The fact that the absorption minima in this curve at 1030 and 1235 $m\mu$ are reasonably sharp may substantiate, to some extent, the evidence presented by Choppin^{6,7} for water molecules containing one hydrogen bond, since the concentration of this specie should decrease as the temperature is elevated and the observed shift from the position of nonbonded band is reasonable.

B. Solvation of Simple Electrolytes. Estimates of the extent of solvation of simple electrolytes in aqueous solutions are available. These have been primarily based on measurements of various properties of their aqueous solutions, such as conductance, heat of mixing, and activity coefficients. Stokes and Robinson¹¹ have calculated hydration numbers, which are parameters occurring in an extended Debye-Hückel type of equation. Glueckauf¹² arrives at another set of numbers which are slightly smaller, by using a modified expression.

In contrast with solvation numbers, which are calculated so that certain observed properties of these solutions will fit a semitheoretical expression, it is

(11) R. H. Stokes and R. A. Robinson, *J. Am. Chem. Soc.*, **70**, 1870 (1948).

(12) E. Glueckauf, *Trans. Faraday Soc.*, **51**, 1235 (1955).

possible to make a more direct measurement of the extent of solute-solvent interaction as a function of electrolyte concentration from observations of the intensities of the bands listed in Table I.¹³ Three of the bands (958, 1148, and 1405 $m\mu$) have intensities sufficiently large for quantitative measurements, and preliminary studies indicated that the concentration dependence of the intensities of these bands were identical when pure water at 25° was compared with solutions of either LiCl, KCl, or KI; *i.e.*, the ratios of the intensities of all three bands were the same when solutions of different concentrations were compared. The band at 958 $m\mu$ was chosen for all of the quantitative measurements, since there is less interference from other overtones which occur when organic solutes are used. Band intensities were determined for a number of electrolytes at concentrations ranging from 0.4 to 5.0 *m*, with water serving as the reference. Concentration-dependent bands similar to that of Figure 2A were obtained for all electrolytes. The data were converted to molar absorbances to yield a series of numbers representing the effectiveness per mole of these electrolytes in reducing the concentration of the species giving rise to the 958- $m\mu$ band. This number tended to decrease for a given electrolyte as the concentration increased, indicating that each ion was polarizing a smaller number of water molecules. These numbers, which are reproducible with a deviation of not more than 3%, represent the relative solvations of the ions. It was desired to estimate absolute solvation numbers, and absorbances of saturated solutions of LiCl, MgCl₂, and LaCl₃ were, therefore, measured with water as a standard. It is felt that since these electrolytes are very highly solvated, it is probable that saturated solutions which contain comparable numbers of ions and water molecules will polarize all water in the solution. It was further recognized that even in the dilute solutions the concentration of water is not 55.5 mol/l., since a portion of the volume is occupied by the solute, and the following procedure was used to correct the absorbances of all solutions. The simplest assumption is that the absorbance at 958 $m\mu$ may be represented as a sum of that due to the monomeric species (band D, Figure 1) and a second species whose concentration is proportional only to the volume fraction of water (band A, Figure 1).¹⁴ The absorbance in the pure reference water is

$$A_r = k_1[\text{H}_2\text{O}] + k_2[\text{X}] \quad (1)$$

where k_1 and k_2 are the molar absorbances, $[\text{H}_2\text{O}]$ is the concentration of monomer, and $[\text{X}]$ is the concentration of the other absorbing species. When saturated LiCl, MgCl₂, or LaCl₃ is used, the absorbance is

$$A = k_2f[\text{X}] \quad (2)$$

where f is the volume fraction of water in the solution. The term $k_1[\text{H}_2\text{O}]$ disappears, since all monomer is

presumed to have been removed. The observed absorbance in the differential experiment using the double-beam instrument is

$$A_{\text{obsd}} = A_r - A = k_1[\text{H}_2\text{O}] + k_2[1 - f][\text{X}] \quad (3)$$

Data for the three saturated salt solutions having quite different volume fractions of water yield three equations for the solution of the two unknowns. A fourth equation results when one measures the absorption of pure water at 958 $m\mu$ vs. air. The solution of the four equations for the two unknowns give values of 0.55 for $k_1[\text{H}_2\text{O}]$ and 0.75 for $k_2[\text{X}]$ in pure water, with an average deviation of $\pm 2\%$. This remarkable agreement is highly suggestive of the validity of the assumptions which have been made. These data indicate that monomeric water molecules account for 42% of the absorbance of the liquid at 25°, even though they represent only a small fraction of the total water. The value for $k_2[\text{X}]$ was then used in the solution of eq 3 for the more dilute solutions. The solvation numbers listed in Table II are the fractions of monomeric water molecules removed by a mole of electrolyte multiplied by 55.5 mol of water per 1000 g, *i.e.*

$$\{k_1[\text{H}_2\text{O}]\}_{\text{soln}}/\{k_1[\text{H}_2\text{O}]\}_{\text{pure H}_2\text{O}} \times 55.5 \quad (4)$$

Table II: Table of Spectroscopic Solvation Numbers

Electrolyte	Solvation number	Electrolyte	Solvation number
HCl	9.0		
LiCl	5.2	KBr	1.4
NaCl	2.1	KI	0.8
KCl	2.3	KNO ₃	~0
CsCl	4.6	MgCl ₂	11.5
NH ₄ Cl	3.0	CaCl ₂	8.2
NaBr	0.7	BaCl ₂	5.0
NaI	0.6	LaCl ₃	16.8

These numbers are those obtained by extrapolation of the molar absorbance to infinite dilution so that the equilibrium concentration of the species present in water will not be shifted by the presence of electrolyte and thus the decrease in concentration of water monomer will be proportional to the total decrease in the fraction of water unaffected by ionic solvation.

Inspection of these solvation numbers shows them to be of the same order of magnitude as those appearing

(13) It may be noted that Durst and Taylor have used the water band between 980 and 1020 $m\mu$ to estimate the solvation of chromic salts: R. A. Durst and J. K. Taylor, *J. Res. Natl. Bur. Std.*, **68A**, 625 (1964).

(14) The second species is obviously the polarized and/or hydrogen-bonded water. Since only a small fraction of liquid water is monomeric, the above assumption is valid. Water spectra in Figure 1 and ref 9, as well as the subsequent calculations, verify that the molar absorbance of polarized and hydrogen-bonded water, k_2 , at this wavelength is quite small compared with that of monomeric water, k_1 , since this is far out on the shoulder of the band.

as parameters in various equations,^{11,12} although there are significant differences in the trends which are exhibited. The alkali metal chlorides are observed to decrease in solvation from LiCl to NaCl and then to increase again to CsCl. This phenomenon is confirmed by the greater solvation of KBr than NaBr and KI than NaI. This is not in agreement with the order in usual tables of hydration numbers,¹⁵ which are calculated from measurements of colligative properties. It is believed, however, that the usual hydration numbers represent both ion-solvent interaction and ion-ion interactions such as ion pairing, etc. Solvation as measured spectroscopically is, on the other hand, believed to represent only ion-solvent interactions. This solvation can be accomplished in either of two fashions. A small ion such as Li⁺ or a highly charged ion such as Mg²⁺ or La³⁺ can polarize large numbers of water molecules and thus decrease the absorption at 958 m μ . A larger ion such as Cs⁺ can increase the hydrogen bonding around the ion by reinforcing the structure in a similar fashion to organic solutes. These findings are in qualitative agreement with those of Bergqvist and Forslind,¹⁶ who report that nmr shifts for solutions of Rb⁺ and Cs⁺ indicate a *stabilizing* effect on the water lattice. It is also interesting that the larger NH₄⁺ ion is observed to be more highly solvated than the K⁺ ion, even though the activity coefficients of NH₄Cl and KCl are quite similar. This appears to substantiate the separation of ion-solvent and ion-ion interactions by the spectroscopic technique.

C. Solvation of Organic Solutes. The solvation of organic nonelectrolytes as well as that of large organic ions such as the tetraalkylammonium ions must be considered as a different phenomenon from the solvation of lithium chloride. The tetraalkylammonium salts, for example, form crystalline hydrates, and X-ray diffraction patterns indicate that the hydrocarbon tails are found to be located in clathrate cages.¹⁷ Aqueous solutions of these salts have osmotic and activity coefficients which are indicative of extensive ion pairing, in spite of the shielding of the positive charge of the cation by the organic groups. Diamond¹⁸ has introduced the concept of water-structure enforced ion pairing to explain these results. This concept is based upon the assumption that hydrophobic ions tighten the water structure around them and force the oppositely charged ions even closer together. A similar phenomenon has been observed for nonelectrolytes when inert gases or hydrocarbons are dissolved in water. Frank¹⁹ has interpreted the entropy decrease on solution as being due to a tightening of the water structure around the solute.

The enhancement of the water structure by organic solutes, such as the above mentioned examples, should be experimentally observable by the same technique which was used in the case of the simple electrolytes. The term solvation as used for these solutes, however,

is related to the increase in solvent hydrogen bonding per mole, rather than to the polarization of the solvent. Solvation numbers of four typical organic solutes have been measured (Table III) in the same manner as for the simple electrolytes. The 958-m μ bands were again similar to those of Figure 2A, although there was interference in some instances in the observation of the 1148- and 1405-m μ bands. Three of these solvation

Table III: Solvation Numbers of Organic Solutes

Solute	Solvation number
Sucrose	21.0
Dextrose	10.0
Urea	2.5
(CH ₃) ₄ NCl	13.8

numbers are quite large when compared with those of simple 1-1 electrolytes. It is of interest that the nonelectrolytes, dextrose and sucrose, which have osmotic coefficients greater than unity, are also solvated to a much greater extent than urea, for which the osmotic coefficient decreases rapidly from unity with increasing concentration. There is further correlation of solvation numbers and osmotic coefficients in that the quantity ($\phi - 1$) is about twice as large for sucrose solutions as for dextrose solutions of the same concentration.

D. Effect of Temperature on the Structure of Water and the Strength of the Hydrogen Bonds. Intensities of the 958-m μ band have been measured as a function of temperature over the range from 25 to 85°, with water at 25° being used as a reference in each instance. The absorbances are shown in Figure 4. This plot indicates that the absorbance increases almost linearly with increasing temperature. The value of $k_1[\text{H}_2\text{O}]$, which is proportional to the concentration of monomeric water increases by a factor of 2 over the temperature at 25 to 80°.

It may be shown that these data also yield values for the strengths of the hydrogen bonds which are quite reasonable. If one makes the simplest approximation of the existence of two species in water, a monomer and a hydrogen-bonded polymer,²⁰ and

(15) H. S. Harned and B. B. Owen, "The Physical Chemistry of Electrolytic Solutions," Reinhold Publishing Corp., New York, N. Y., 1957, p 525.

(16) M. S. Bergqvist and E. Forslind, *Acta Chem. Scand.*, **16**, 2069 (1962).

(17) P. T. Buerskens and G. A. Jeffrey, *J. Chem. Phys.*, **40**, 906 (1964).

(18) R. M. Diamond, *J. Phys. Chem.*, **67**, 2513 (1963).

(19) H. S. Frank and M. W. Evans, *J. Chem. Phys.*, **13**, 507 (1945).

(20) This assumption is identical with that which was assumed earlier in the calculation of solvation numbers and is essentially an interpretation of the data using the vacant-lattice-point model (ref 2).

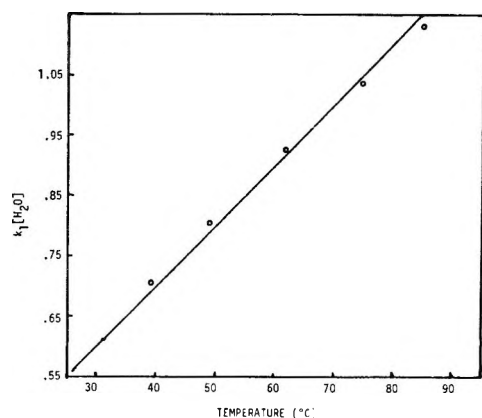


Figure 4. Concentration of monomeric water as a function of temperature.

further assumes that the first monomer molecule to be freed, as the temperature is elevated, is one which is held by only one bond, one may write the equilibrium expression



or

$$K = \frac{\alpha_{\text{H}_2\text{O}}}{\alpha_{(\text{H}_2\text{O})B}} \quad (6)$$

where $(\text{H}_2\text{O})B$ represents a molecule of hydrogen-bonded water. The resulting van't Hoff equation

$$\frac{d \ln K}{dT} = \frac{d \ln \alpha_{\text{H}_2\text{O}}}{dT} - \frac{d \ln \alpha_{(\text{H}_2\text{O})B}}{dT} = \frac{\Delta H}{RT^2} \quad (7)$$

may be easily solved since, because of the small fraction of water existing as a monomer, the term involving $(\text{H}_2\text{O})B$ is relatively unaffected by the formation of one molecule of free water. The integrated expression is then

$$\ln \frac{K_2}{K_1} = \ln \frac{\alpha_{\text{H}_2\text{O}(2)}}{\alpha_{\text{H}_2\text{O}(1)}} = \frac{\Delta H}{R} \left[\frac{T_2 - T_1}{T_1 T_2} \right] \quad (8)$$

One may now calculate a value of $\Delta H = 2.67$ kcal, based upon the evidence that the concentration of water monomer, and thus the activity, approximately doubles over the temperature range from 25 to 80°. This value may be compared with 2.8 kcal, as calculated by Walrafen,²¹ and 3.41 kcal, as calculated by Scatchard.²²

E. Concentration of Monomeric Water at 25°. Although the above data yield relative values for the degree of association of water as a function of temperature, they give no indication of the absolute concentration of nonbonded water. Molar absorptivities, unfortunately, cannot be determined, since the concentration of the absorbing species in the liquid giving rise to the 958-m μ band are unknown at any temperature. It is possible, however, that an approximate answer can be obtained from the data of Waggener, *et al.*⁹ These data indicate that the absorbance of the liquid at 25° is approximately 7.4 times that of the vapor at 250°. From the calculations which were made in an earlier section of this paper, it is known that 42% of the absorbance of the liquid at 25° is due to water monomer. If one assumes that all of the absorbance in the vapor is due to monomer and that the molar absorptivities of this species are the same²³ at 25 and 250°, the concentration of nonhydrogen-bonded water at 25° may be calculated to be 3.5 mol/l., or about 6%. This may be compared with the calculated value of 19.3% interstitial water molecules at 20° using the vacant-lattice-point model.²⁴ The lower experimental value could result for a distortion of the hydrogen bonds in the matrix water with the consequent decrease in the number of vacant lattice sites.

(21) G. E. Walrafen, *J. Chem. Phys.*, **44**, 1546 (1966).

(22) G. Scatchard, G. M. Kavanaugh, and L. B. Ticknor, *J. Am. Chem. Soc.*, **74**, 3715 (1952).

(23) It is realized that this assumption may introduce an error of the order of 10%.

(24) Reference 1a, p 12.

Relationship between the DTA Peak and the Maximum Reaction Rate

by K. Akita

Department of Fuel Technology, The Faculty of Engineering, University of Tokyo, Bunkyo-ku, Tokyo, Japan

and M. Kase

Fire Research Institute, Ministry of Home Affairs, Mitaka, Tokyo, Japan (Received August 18, 1967)

A theory of differential thermal analysis for first- and n th-order reactions was developed. Linearized basic equations were solved by means of the Laplace transformation and Green's function, and by approximating the solutions; it was found that the peak of the DTA curve agrees with the maximum rate of reaction, provided the appropriate experimental conditions are chosen. Discussions of this conclusion are given, comparing it with a few theories presented heretofore.

Theories of DTA and TGA for analysis of reaction kinetics have been developed by many investigators. Kissinger¹ presented a semitheoretical method which can determine the activation energy and the reaction order from experimental DTA curves, and Borchardt and Daniels² suggested a graphical analysis based on the heat balance in the sample material. Reed, Weber, and Gottfried³ gave a precise analysis for stirred systems and pointed out that the peak of the DTA curve is not always in agreement with the maximum reaction rate, unlike Kissinger's conclusion. These theories are useful for quantitative analysis of DTA curves, but considered from the theoretical aspect, they seem to be unsatisfactory: the first theory does not contain the exact solution of the differential equation and the latter two theories should be applied to stirred systems only. The authors tried to analyze approximately the DTA curve for the first-order reaction in a previous paper⁴ on the pyrolysis of cellulose, and they suggested that Kissinger's result is satisfactory for our experimental conditions if a small vessel is used.

In the present paper, the basic equations of DTA for the infinite cylindrical sample with first- and n th-order reactions were solved strictly by the Laplace transformation and Green's function method, under a boundary condition that the surface temperature of the cylinder rises linearly with time. Then the relation between the DTA peak and maximum reaction rate was discussed quantitatively on the basis of these solutions.

Basic Equations of DTA

Assuming that the reaction vessel can be regarded as an infinite cylinder, that the effects of temperature and material consumption upon the thermal constants of the sample material are negligible, and that the weight loss of the reactant is small, as compared with the total weight of sample (this assumption may be attained by mixing some standard material into the reactant), the basic equations for standard and sample cells are expressed by

$$\frac{\partial T_1}{\partial t} = \kappa_1 \left(\frac{\partial^2 T_1}{\partial r^2} + \frac{1}{r} \frac{\partial T_1}{\partial r} \right) \quad (1)$$

$$\frac{\partial T_2}{\partial t} = \kappa_2 \left(\frac{\partial^2 T_2}{\partial r^2} + \frac{1}{r} \frac{\partial T_2}{\partial r} \right) + \frac{Qw_0}{c_2w_2} \frac{d}{dt} \left(\frac{w}{w_0} \right) \quad (2)$$

where T_1 and T_2 are the temperatures in the standard and sample cell, respectively, r is the radial coordinate, t is the time, κ_1 and κ_2 are the mean thermal diffusivities of materials packed in each cell, Q is the heat of reaction per weight, c_2 is the mean specific heat of the sample cell, w_2 is the total weight of sample cell, w_0 is the initial weight of reactant, and $d(w/w_0)/dt$ is the reaction rate of the reactant.

Initial and boundary conditions are given commonly by

$$(T)_{t=0} = T_0 \quad (3)$$

$$(T)_{r=a} = T_0 + \phi t \quad (4)$$

where a is the radius, having the same value in both cells, ϕ is the constant heating rate, and T_0 is the initial temperature. The boundary condition (4) was obtained by neglecting the thermal effect of the small gap existing between packed materials and the cell walls; this assumption will be reasonable for the usual systems of DTA.

Solution for a First-Order Reaction

Provided that the reaction is first order and that the temperature dependence of the rate is given by the Arrhenius equation, the heat-source term in eq 2 becomes

$$\frac{Qw_0}{c_2w_2} \frac{d}{dt} \left(\frac{w}{w_0} \right) = \frac{Qw_0}{c_2w_2} \left(1 - \frac{w}{w_0} \right) k_0 \exp \left(-\frac{E}{RT_2} \right) \quad (5)$$

(1) H. E. Kissinger, *Anal. Chem.*, **29**, 1702 (1957).

(2) H. J. Borchardt and F. Daniels, *J. Amer. Chem. Soc.*, **79**, 41 (1957).

(3) R. L. Reed, L. Weber, and B. S. Gottfried, *Ind. Eng. Chem., Fundamentals*, **4**, 38 (1965).

(4) K. Akita and M. Kase, *J. Polym. Sci.*, **5**, 833 (1967).

where k_0 is the preexponential factor, E is the activation energy for the reaction, and R is the gas constant.

In general the temperature change in the sample cell is negligibly small compared with the heating temperature, and the surface-temperature rise up to the DTA peak is much smaller than the initial temperature, defined as the temperature at which the DTA curve just starts to deviate from the base line, that is

$$T_0 \gg \phi t \gg |T_2 - (T_0 + \phi t)| \tag{a}$$

Then eq 5 can be approximated as

$$\frac{d}{dt} \left(\frac{w}{w_0} \right) \simeq \frac{w_0 - w}{w_0} k_0 \exp\left(-\frac{E}{RT_0}\right) \exp\left(\frac{E\phi}{RT_0^2} t\right) \tag{6}$$

Integrating eq 6 and making the substitution $A \equiv k_0 \exp(-E/RT_0)$ and $\alpha \equiv E\phi/RT_0^2$, we get

$$\left(1 - \frac{w}{w_0}\right) \simeq \exp\left(\frac{A}{\alpha}\right) \exp\left\{-\frac{A}{\alpha} \exp(\alpha t)\right\} \tag{7}$$

By using eq 6 and 7, eq 2 may be rewritten as

$$\frac{\partial T_2}{\partial t} = \kappa_2 \left(\frac{\partial^2 T_2}{\partial r^2} + \frac{1}{r} \frac{\partial T_2}{\partial r} \right) + \delta_1 \exp(\alpha t) \exp\left\{-\frac{A}{\alpha} \exp(\alpha t)\right\} \tag{8}$$

where

$$\delta_1 \equiv \frac{Qw_0}{c_2 w_2} A \exp\left(\frac{A}{\alpha}\right) \tag{9}$$

To solve this equation under conditions 3 and 4, we make the transformation

$$T_2 = \theta_2(r, t) + T_0 - \frac{\delta_1}{A} \exp\left\{-\frac{A}{\alpha} \exp(\alpha t)\right\} + \frac{\delta_1}{A} \exp\left(-\frac{A}{\alpha}\right) \tag{10}$$

We obtain

$$\frac{\partial \theta_2}{\partial t} = \kappa_2 \left(\frac{\partial^2 \theta_2}{\partial r^2} + \frac{1}{r} \frac{\partial \theta_2}{\partial r} \right) \tag{11}$$

$$(\theta_2)_{t=0} = 0 \tag{12}$$

$$(\theta_2)_{r=a} = \phi t +$$

$$\frac{\delta_1}{A} \exp\left\{-\frac{A}{\alpha} \exp(\alpha t)\right\} - \frac{\delta_1}{A} \exp\left(-\frac{A}{\alpha}\right) \tag{13}$$

Furthermore, since the two exponential terms of the right-hand side of eq 13 are expressed, respectively, by

$$\frac{\delta_1}{A} \exp\left\{-\frac{A}{\alpha} \exp(\alpha t)\right\} = \frac{\delta_1}{A} \sum_{l=0}^{\infty} \frac{(-1)^l}{l!} \left(\frac{A}{\alpha}\right)^l \exp(l\alpha t) = \sum_{l=0}^{\infty} P_1(l) \exp(l\alpha t) \tag{14}$$

$$\frac{\delta_1}{A} \exp\left(-\frac{A}{\alpha}\right) = \frac{\delta_1}{A} \sum_{l=0}^{\infty} \frac{(-1)^l}{l!} \left(\frac{A}{\alpha}\right)^l = \sum_{l=0}^{\infty} P_1(l) \tag{15}$$

where

$$P_1(l) \equiv \frac{\delta_1}{A} \frac{(-1)^l}{l!} \left(\frac{A}{\alpha}\right)^l \tag{16}$$

Equations 13 and 10 can be rewritten as

$$(\theta_2)_{r=a} = \phi t + \sum_{l=0}^{\infty} P_1(l) \{ \exp(l\alpha t) - 1 \} \tag{17}$$

$$T_2(r, t) = \theta_2(r, t) + T_0 - \sum_{l=0}^{\infty} P_1(l) \{ \exp(l\alpha t) - 1 \} \tag{18}$$

Thus the problem will be arrived at by solving eq 11 under the conditions of eq 12 and 17.

A. *Solution by the Laplace Transformation.* Making the Laplace transformation of eq 11, and using eq 12, we get

$$s\bar{\theta}_2 = \kappa_2 \left(\frac{\partial^2 \bar{\theta}_2}{\partial r^2} + \frac{1}{r} \frac{\partial \bar{\theta}_2}{\partial r} \right) \tag{19}$$

where $\bar{\theta}_2(s, r)$ denotes the image function of the Laplace transformation. The boundary condition, eq 17, becomes

$$(\bar{\theta}_2)_{r=a} = \frac{\phi}{s^2} + \sum_{l=0}^{\infty} P_1(l) \left(\frac{1}{s - l\alpha} - \frac{1}{s} \right) \tag{20}$$

As $\bar{\theta}_2$ is finite at $r = 0$, the solution of eq 19 is

$$\bar{\theta}_2 = \frac{J_0(ir\sqrt{s/\kappa_2})}{J_0(ia\sqrt{s/\kappa_2})} \left\{ \frac{\phi}{s^2} + \sum_{l=0}^{\infty} P_1(l) \left(\frac{1}{s - l\alpha} - \frac{1}{s} \right) \right\} \tag{21}$$

Then by using the inversion theorem and the known relations on the Bessel function

$$\sum_{h=1}^{\infty} \frac{J_0\left(\frac{r}{a}\lambda_h\right)}{\lambda_h^3 J_1(\lambda_h)} = \frac{a^2 - r^2}{8a^2} \tag{22}$$

$$\sum_{h=1}^{\infty} \frac{J_0\left(\frac{r}{a}\lambda_h\right)}{\lambda_h J_1(\lambda_h)} = \frac{1}{2} \tag{23}$$

we obtain

$$\theta_2 = \phi t - \frac{2a^2\phi}{\kappa_2} \sum_{h=1}^{\infty} \frac{J_0\left(\frac{r}{a}\lambda_h\right)}{\lambda_h^3 J_1(\lambda_h)} \left\{ 1 - \exp\left(-\frac{\kappa_2\lambda_h^2}{a^2} t\right) \right\} - 2 \sum_{l=0}^{\infty} P_1(l) \sum_{h=1}^{\infty} \frac{J_0\left(\frac{r}{a}\lambda_h\right)}{\lambda_h J_1(\lambda_h)} \left[\left\{ 1 - \exp(l\alpha t) \frac{J_0(ir\sqrt{l\alpha/\kappa_2})}{J_0(ia\sqrt{l\alpha/\kappa_2})} \right\} - \exp\left(-\frac{\kappa_2\lambda_h^2}{a^2} t\right) \left\{ 1 - \frac{1}{1 + (laa^2/\kappa_2\lambda_h^2)} \right\} \right] \tag{24}$$

where J_0 and J_1 mean the Bessel function of zero and the first order, respectively, and λ_h is the h th root of

$$J_0(ia\sqrt{s/\kappa_2}) = 0 \tag{25}$$

Turning the variable θ_2 to T_2 by eq 18, the solution becomes

$$T_2(r, t) = T_0 + \phi t - \frac{2a^2\phi}{\kappa_2} \sum_{h=1}^{\infty} \frac{J_0\left(\frac{r}{a}\lambda_h\right)}{\lambda_h^3 J_1(\lambda_h)} \times \left\{ 1 - \exp\left(-\frac{\kappa_2\lambda_h^2}{a^2}t\right) \right\} - 2 \sum_{l=0}^{\infty} \sum_{h=1}^{\infty} P_1(l) \frac{J_0\left(\frac{r}{a}\lambda_h\right)}{\lambda_h J_1(\lambda_h)} \times \left[\exp(l\alpha t) \left\{ 1 - \frac{J_0(ir\sqrt{l\alpha/\kappa_2})}{J_0(ia\sqrt{l\alpha/\kappa_2})} \right\} - \exp\left(-\frac{\kappa_2\lambda_h^2}{a^2}t\right) \left\{ 1 - \frac{1}{1 + \frac{l\alpha a^2}{\kappa_2\lambda_h^2}} \right\} \right] \quad (26)$$

Since the Fourier-Bessel's expansion of $[J_0(ir\sqrt{l\alpha/\kappa_2})/J_0(ia\sqrt{l\alpha/\kappa_2})]$ is given by

$$\frac{J_0(ir\sqrt{l\alpha/\kappa_2})}{J_0(ia\sqrt{l\alpha/\kappa_2})} = \sum_{h=1}^{\infty} \frac{2}{1 + (l\alpha a^2/\kappa_2\lambda_h^2)} \frac{J_0\left(\frac{r}{a}\lambda_h\right)}{\lambda_h J_1(\lambda_h)} \quad (27)$$

using eq 27, the final solution can be written as

$$T_2(r, t) = T_0 + \phi t - \frac{2a^2\phi}{\kappa_2} \sum_{h=1}^{\infty} \frac{J_0\left(\frac{r}{a}\lambda_h\right)}{\lambda_h^3 J_1(\lambda_h)} \times \left\{ 1 - \exp\left(-\frac{\kappa_2\lambda_h^2}{a^2}t\right) \right\} - 2 \sum_{l=0}^{\infty} \sum_{h=1}^{\infty} P_1(l) \frac{J_0\left(\frac{r}{a}\lambda_h\right)}{\lambda_h J_1(\lambda_h)} \times \left\{ \exp(l\alpha t) - \exp\left(-\frac{\kappa_2\lambda_h^2}{a^2}t\right) \right\} \left(1 - \frac{1}{1 + \frac{l\alpha a^2}{\kappa_2\lambda_h^2}} \right) \quad (28)$$

This equation satisfies the initial and boundary conditions and shows the temperature profile in the sample cell for the case of a first-order reaction.

By inserting $Q = 0$ or $P_1(l) = 0$ into eq 28, the solution for the standard cell becomes

$$T_1(r, t) = T_0 + \phi t - \frac{2a^2\phi}{\kappa_2} \sum_{h=1}^{\infty} \frac{J_0\left(\frac{r}{a}\lambda_h\right)}{\lambda_h^3 J_1(\lambda_h)} \times \left\{ 1 - \exp\left(-\frac{\kappa_2\lambda_h^2}{a^2}t\right) \right\} \quad (29)$$

Thus the temperature difference, ΔT , between the sample and the standard cell can be obtained from $T_2 - T_1$.

B. Solution by the Green's Function Method. In this case, Green's function, or the temperature u at r and t due to the unit instantaneous cylindrical surface source at radius r' and time τ , is given by⁵

$$u(r, t) = \frac{1}{\pi a^2} \sum_{h=1}^{\infty} \frac{J_0\left(\frac{r}{a}\lambda_h\right) J_0\left(\frac{r'}{a}\lambda_h\right)}{J_1^2(\lambda_h)} \times \exp\left\{-\frac{\kappa_2\lambda_h^2}{a^2}(t - \tau)\right\} \quad (30)$$

The solution of eq 11 under the conditions of eq 12 and 17 can be expressed by

$$\theta_2(r', t) = \kappa_2 \int_0^t 2\pi a \left[\phi\tau + \sum_{l=0}^{\infty} P_1(l) \times \left\{ \exp(l\alpha\tau) - 1 \right\} \right] \left(\frac{\partial u}{\partial r} \right) d\tau$$

$$= \phi t - \frac{2a^2\phi}{\kappa_2} \sum_{h=1}^{\infty} \frac{J_0\left(\frac{r'}{a}\lambda_h\right)}{\lambda_h^3 J_1(\lambda_h)} \times \left\{ 1 - \exp\left(-\frac{\kappa_2\lambda_h^2}{a^2}t\right) \right\} - 2 \sum_{l=0}^{\infty} \sum_{h=1}^{\infty} P_1(l) \frac{J_0\left(\frac{r'}{a}\lambda_h\right)}{\lambda_h J_1(\lambda_h)} \times \left\{ \exp(l\alpha t) - \exp\left(-\frac{\kappa_2\lambda_h^2}{a^2}t\right) \right\} \left(1 - \frac{1}{1 + \frac{l\alpha a^2}{\kappa_2\lambda_h^2}} \right) \quad (31)$$

Replacing the variable r with r' , and using eq 18, this equation can be rewritten in the same form as eq 28. Therefore, the solution obtained here does not depend on the mathematical procedures.

C. Approximated Solution. If an assumption

$$(l\alpha a^2/\kappa_2\lambda_h^2) \ll 1 \quad (b)$$

is accepted, the following approximation will be natural.

$$1 - \frac{1}{1 + \frac{l\alpha a^2}{\kappa_2\lambda_h^2}} \approx \frac{l\alpha a^2}{\kappa_2\lambda_h^2} \quad (32)$$

Substituting eq 32 into eq 28, and using eq 22 and 23, we get

$$T_2(r, t) = T_0 + \phi t - \frac{2a^2\phi}{\kappa_2} \sum_{h=1}^{\infty} \frac{J_0\left(\frac{r}{a}\lambda_h\right)}{\lambda_h^3 J_1(\lambda_h)} \times \left\{ 1 - \exp\left(-\frac{\kappa_2\lambda_h^2}{a^2}t\right) \right\} - \frac{2a^2}{\kappa_2} \sum_{l=0}^{\infty} P_1(l) l\alpha \exp(l\alpha t) \times \sum_{h=1}^{\infty} \frac{J_0\left(\frac{r}{a}\lambda_h\right)}{\lambda_h^3 J_1(\lambda_h)} \left\{ 1 - \exp\left(-\frac{\kappa_2\lambda_h^2}{a^2}t\right) \right\} \quad (33)$$

(5) H. S. Carslaw and J. C. Jaeger, "Conduction of Heat in Solids," 2nd ed, Clarendon Press, Oxford, 1959.

However, since the heat-source term in eq 2 is given by

$$\frac{Qw_0}{c_2w_2} \frac{d(w)}{dt} = \delta_1 \exp(\alpha t) \exp\left\{-\frac{A}{\alpha} \exp(\alpha t)\right\} = \delta_1 \sum_{l=0}^{\infty} \frac{(-1)^l \left(\frac{A}{\alpha}\right)^l}{l!} \exp\{(l+1)\alpha t\} \quad (34)$$

then

$$-\sum_{l=0}^{\infty} P_1(l) l \alpha \exp(l\alpha t) = -\sum_{l=0}^{\infty} \frac{\delta_1 (-1)^l \left(\frac{A}{\alpha}\right)^l}{A l!} l \alpha \exp(l\alpha t) = \delta_1 \sum_{l'=1}^{\infty} \frac{(-1)^{l'} \left(\frac{A}{\alpha}\right)^{l'}}{(l'-1)!} \exp(l'\alpha t) \times \left(\frac{A}{\alpha}\right)^{l'} \exp\{(l'+1)\alpha t\} = \frac{Qw_0}{c_2w_2} \frac{d(w)}{dt} \quad (35)$$

By inserting eq 35 into eq 33, we obtain

$$T_2(r, t) = T_0 + \phi t - \frac{2a^2}{\kappa_2} \left\{ \phi - \frac{Qw_0}{c_2w_2} \frac{d(w)}{dt} \right\} \times \sum_{h=1}^{\infty} \frac{J_0\left(\frac{r}{a} \lambda_h\right)}{\lambda_h^3 J_1(\lambda_h)} \left\{ 1 - \exp\left(-\frac{\kappa_2 \lambda_h^2}{\alpha^2} t\right) \right\} \quad (36)$$

Thus the temperature difference between the sample and the standard cells (DTA curve) is expressed as

$$\Delta T = T_2 - T_1 \simeq 2a^2 \phi \sum_{h=1}^{\infty} \frac{J_0\left(\frac{r}{a} \lambda_h\right)}{\lambda_h^3 J_1(\lambda_h)} \times \left[\frac{1}{\kappa_1} \left\{ 1 - \exp\left(-\frac{\kappa_1 \lambda_h^2}{a^2} t\right) \right\} - \frac{1}{\kappa_2} \left\{ 1 - \exp\left(-\frac{\kappa_2 \lambda_h^2}{a^2} t\right) \right\} \right] + 2a^2 \frac{Qw_0}{c_2w_2} \frac{d(w)}{dt} \sum_{h=1}^{\infty} \frac{J_0\left(\frac{r}{a} \lambda_h\right)}{\lambda_h^3 J_1(\lambda_h)} \times \frac{1}{\kappa_2} \left\{ 1 - \exp\left(-\frac{\kappa_2 \lambda_h^2}{a^2} t\right) \right\} \quad (37)$$

In eq 37, the first term of the right-hand side of the equation shows the shift of the base line due to the difference of thermal properties in both cells, and the second term corresponds to the displacement of the DTA curve due to the heat source. Moreover, excluding the initial short period, the assumption

$$\exp(-\kappa_i \lambda_h^2 t / a_i) \ll 1 \quad (i = 1, 2) \quad (c)$$

must be satisfied, and eq 37 can be approximated as

$$\Delta T \approx 2a^2 \sum_{h=1}^{\infty} \frac{J_0\left(\frac{r}{a} \lambda_h\right)}{\lambda_h^3 J_1(\lambda_h)} \left\{ \left(\frac{1}{\kappa_1} - \frac{1}{\kappa_2} \right) \phi + \frac{1}{\kappa_2} \frac{Qw_0}{c_2w_2} \frac{d(w)}{dt} \right\} = \frac{a^2 - r^2}{4} \left\{ \left(\frac{1}{\kappa_1} - \frac{1}{\kappa_2} \right) \phi + \frac{1}{\kappa_2} \frac{Qw_0}{c_2w_2} \frac{d(w)}{dt} \right\} \quad (38)$$

Differentiating eq 38, we get

$$\frac{d}{dt}(\Delta T) \simeq \frac{a^2 - r^2}{4\kappa_2} \frac{Qw_0}{c_2w_2} \frac{d^2(w)}{dt^2} \quad (39)$$

Equation 38 means that the temperature difference in DTA has a linear correlation with the reaction rate, and eq 39 shows that the peak of DTA curve just coincides with the inflection point of the TGA curve. This result once again seems to support the theory of Kissinger¹ rather than the one of Reed, *et al.*³ These equations are in agreement with the result obtained by using Stokes' method in our previous paper.⁴

Solution for the n th-Order Reaction

For the n th-order reaction, the heat-source term in eq 2 is given by

$$\frac{Qw_0}{c_2w_2} \frac{d(w)}{dt} = \frac{Qw_0}{c_2w_2} \left(1 - \frac{w}{w_0}\right)^n k_0 \exp\left(-\frac{E}{RT_2}\right) \quad (40)$$

$n \neq 1$ and $n > 0$. As with the first-order reaction, assuming the relation $T_0 \gg \phi t \gg |T - (T_0 + \phi t)|$, we get

$$\frac{d(w)}{dt} \simeq A \exp(\alpha t) \left(1 - \frac{w}{w_0}\right)^n \quad (41)$$

Integrating eq 41

$$\left(1 - \frac{w}{w_0}\right)^n = \left[1 - (1-n) \frac{A}{\alpha} \{ \exp(\alpha t) - 1 \} \right]^{n/(1-n)} \quad (42)$$

By inserting eq 42 into eq 41, and by putting

$$X \equiv \frac{1}{1-n} \frac{\alpha}{A} + 1 \quad (43)$$

$$\delta_n \equiv \frac{Qw_0}{c_2w_2} A \left\{ 1 + \frac{A}{\alpha} (1-n) \right\}^{n/(1-n)} \quad (44)$$

we obtain

$$\frac{Qw_0}{c_2w_2} \frac{d(w)}{dt} = \delta_n \exp(\alpha t) \left\{ 1 - \frac{1}{X} \exp(\alpha t) \right\}^{n/(1-n)} \quad (45)$$

Accordingly, the basic equation for the n th-order reaction becomes

$$\frac{\partial T_2}{\partial t} = \kappa_2 \left(\frac{\partial^2 T_2}{\partial r^2} + \frac{1}{r} \frac{\partial T_2}{\partial r} \right) + \delta_n \exp(\alpha t) \left\{ 1 - \frac{1}{X} \exp(\alpha t) \right\}^{n/(1-n)} \quad (46)$$

To solve this equation under the conditions of eq 3 and 4, we make the transformation

$$T_2 = \theta_2(r, t) + T_0 - \delta_n \frac{X}{\alpha} (1-n) \times \left[\left\{ 1 - \frac{1}{X} \exp(\alpha t) \right\}^{1/(1-n)} - \left(1 - \frac{1}{X} \right)^{1/(1-n)} \right] \quad (47)$$

and we get

$$\frac{\partial \theta_2}{\partial t} = \kappa_2 \left(\frac{\partial^2 \theta_2}{\partial r^2} + \frac{1}{r} \frac{\partial \theta_2}{\partial r} \right) \quad (48)$$

$$(\theta_2)_{t=0} = 0 \quad (49)$$

$$(\theta_2)_{r=a} = \phi t + \delta_n \frac{X}{\alpha} (1-n) \times \left[\left\{ 1 - \frac{1}{X} \exp(\alpha t) \right\}^{1/(1-n)} - \left(1 - \frac{1}{X} \right)^{1/(1-n)} \right] \quad (50)$$

Equations 48-50 are the set of equations to be solved for this case.

Using the assumption

$$\left| 1 - \frac{1}{X} \exp(\alpha t) \right| < 1 \quad (d)$$

the two terms, $\left\{ 1 - [1/X \exp(\alpha t)]^{1/(1-n)} \right\}$ and $\left(1 - 1/X \right)^{1/(1-n)}$ into eq 50 can be expressed, respectively, by

$$\left\{ 1 - \frac{1}{X} \exp(\alpha t) \right\}^{1/(1-n)} = \sum_{l=0}^{\infty} \frac{(-1)^l}{l!} \frac{\Gamma\left(\frac{2-n}{1-n}\right)}{\Gamma\left(\frac{2-n}{1-n} - l\right)} \frac{1}{X^l} \exp(l\alpha t) \quad (51)$$

$$\left(1 - \frac{1}{X} \right)^{1/(1-n)} = \sum_{l=0}^{\infty} \frac{(-1)^l}{l!} \frac{\Gamma\left(\frac{2-n}{1-n}\right)}{\Gamma\left(\frac{2-n}{1-n} - l\right)} \frac{1}{X^l} \quad (52)$$

Hence by substituting

$$P_n(l) \equiv \delta_n \frac{X}{\alpha} (1-n) \frac{(-1)^l}{l!} \frac{\Gamma\left(\frac{2-n}{1-n}\right)}{\Gamma\left(\frac{2-n}{1-n} - l\right)} \frac{1}{X^l} \quad (53)$$

the boundary condition (50) is simplified as

$$(\theta_2)_{r=a} = \phi t + \sum_{l=0}^{\infty} P_n(l) \{ \exp(l\alpha t) - 1 \} \quad (54)$$

Equation 54 is the same as eq 17 for the first-order reaction, except that $P_n(l)$ is used instead of $P_1(l)$. The final solution for the n th-order reaction can be given by eq 28, in which $P_1(l)$ is replaced by $P_n(l)$, and the consequent equations, 36, 37, 38, and 39, become common for every order of reaction.

If the following assumptions: (a) $T_0 \gg \phi t \gg |T_0 - (T_0 + \phi t)|$ for the heat-source term of the basic equation, (b) $(l\alpha a^2 / \kappa_2 \lambda_n^2) \ll 1$ for the properties of the sample material, the cell size, and the heating conditions, (c) $\exp\{-\kappa_i \lambda_n^2 t / a^2\} \ll 1$ ($i = 1, 2$) for the initial transient period, and (d) $|(1/X) \exp(\alpha t)| < 1$ for the limit of reaction order are accepted, we can easily arrive at the conclusion that the peak of the DTA curve coincides with the maximum rate of reaction

regardless of the reaction order. When the above assumptions are dissatisfied, the two will not coincide substantially with each other.

Considerations of the Assumptions

To discuss the relation between the DTA peak and the maximum reaction rate on the basis of the present theory, it is necessary to know whether or not the four assumptions, a-d, are satisfied for the experimental conditions of DTA. Of these, assumption a can be easily accepted, for the reason already mentioned, and for the usual conditions, assumption c will be fully satisfied, except for an initial short period required for stabilizing the base line of the DTA curve.

Considering the time interval up to the time t_m corresponding to the maximum rate of reaction, one finds that assumption d is satisfied within the limit on the reaction order of $0 < n < 2$. If equations 6 and 7 or 41 and 42 are inserted into the equation of the maximum rate condition

$$\left[\frac{d}{dt} \left\{ \frac{d}{dt} \left(\frac{w}{w_0} \right) \right\} \right]_m = 0 \quad (55)$$

and the equation is rearranged, a general expression of t_m for arbitrary n becomes

$$\alpha t_m = \ln \left\{ \frac{\alpha}{A} + (1-n) \right\} \quad (56)$$

By using eq 56, assumption d can be rewritten as

$$|(1-n)\chi| < 1 \quad (57)$$

where

$$\chi \equiv \exp(\alpha t) / \exp(\alpha t_m) \quad (58)$$

Obviously this result is reasonable for usual pyrolysis reactions.

In discussing assumption b, it is sufficient to use only λ_1 as the root of eq 25, because $1/\lambda_n^2$ is always smaller than $1/\lambda_1^2$ for arbitrary h . Also, since l is combined with the parameter χ in eq 58 by the relation

$$\left\{ 1 - (1-n)\chi \right\}^{1/(1-n)} = \sum_{l=0}^{\infty} \frac{(-1)^l}{l!} \times \frac{\Gamma\left(\frac{2-n}{1-n}\right)}{\Gamma\left(\frac{2-n}{1-n} - l\right)} \chi^l \quad (59)$$

where $n \neq 1$

$$\exp(-\chi) = \sum_{l=0}^{\infty} \frac{(-1)^l}{l!} \chi^l \quad (60)$$

where $n = 1$, we can estimate a required value of l by eq 59 or 60. In other words, the series contained in these equations are asymptotic under condition 57, and the error committed in truncating the residue, except for the first l terms in the series, can be made small

Table I: Dependence of $\left\{ \sum_{l=0}^{\infty} f(l) - \sum_{l=0}^l f(l) \right\} / \sum_{l=0}^l f(l)$ on n and l at $\chi = 1^a$

n	1	2	3	4	5	6	7	8	9	10
0.1	1.000	0.354	0.182	0.110	0.071	0.049	0.035	0.025		
0.2	1.000	0.253	0.103	0.051	0.028	0.015	0.008			
0.3	1.000	0.162	0.051	0.020	0.010	0.006				
0.4	1.000	0.079	0.018	0.005	0.000					
0.5	1.000	0.000								
0.6	1.000	-0.076	-0.004	-0.000						
0.7	1.000	-0.149	0.004	0.000						
0.8	1.000	-0.221	0.023	-0.001	0.000					
0.9	1.000	-0.291	0.054	-0.007	0.000					
1.0	1.000	-0.359	0.094	-0.019	0.003					
1.1	1.000	-0.427	0.141	-0.041	0.011					
1.2	1.000	-0.493	0.204	-0.075	0.025	-0.008				
1.3	1.000	-0.559	0.271	-0.123	0.050	-0.022				
1.4	1.000	-0.623	0.351	-0.185	0.094	-0.046				
1.5	1.000	-0.688	0.437	-0.261	0.176	-0.086	0.067	-0.021		
1.6	1.000	-0.751	0.533	-0.366	0.245	-0.162	0.106	-0.068	0.044	
1.7	1.000	-0.814	0.637	-0.487	0.367	-0.274	0.202	-0.149	0.109	-0.079
1.8	1.000	-0.876	0.750	-0.633	0.529	-0.439	0.363	-0.299	0.245	-0.201
1.9	1.000	-0.938	0.871	-0.803	0.737	-0.674	0.616	-0.562	0.511	-0.465

^a Where

$$\sum_{l=0}^{\infty} f(l) = \{1 - (1 - n)\chi\}^{1/(1-n)} = \sum_{l=0}^{\infty} \frac{(-1)^l}{l!} \frac{\Gamma\left(\frac{2-n}{1-n}\right)}{\Gamma\left(\frac{2-n}{1-n} - l\right)} \chi^l \quad (n \neq 1)$$

$$\sum_{l=0}^{\infty} f(l) = e^{-\chi} = \sum_{l=0}^{\infty} \frac{(-1)^l}{l!} \chi^l \quad (n = 1)$$

enough with the increase of l . The number of terms, l , required to replace equations 59 or 60 by the finite series, within a certain accuracy, can be determined. The result obtained for χ corresponding to the maximum rate is given in Table I. From this table it is found that $l = 5$ ensures sufficient accuracy for $0.2 < n < 1.3$, but beyond the range of n , l increases rapidly as n comes close to the limits $n = 0$ and $n = 2$.

For practical use, the dependences of $\gamma \equiv l\alpha a^2 / \kappa_2 \lambda_h^2$, in assumption b, on a^2 / κ_2 and α were calculated by the use of λ_1 and l , obtained here, and are shown in Figures 1-3. The dependence of α on ϕ and E/T_0^2 is shown in Figure 4.

Discussion

Reed, *et al.*,³ pointed out in their paper that the peak of the DTA curve for stirred systems should disagree with the maximum rate of reaction. This suggestion is substantially reasonable as can be understood from the present theory, and in that sense, we have no objection. However, it is also true that the main problem in this field is not the existence of discrepancy between the two positions; it is the extent of discrepancy for actual DTA curves, and hence, in this study, the criterion of coincidence was examined numerically. The results, as mentioned above, gave an opposite

conclusion: the discrepancy can be rather negligible under usual experimental conditions, such as the small cell, the slow heating rate, and the moderate reaction rate of sample materials.

As is well known, Kissinger¹ claimed a coincidence between the DTA peak and maximum reaction rate on the basis of his speculative consideration. Our conclusion is more similar to his, but the contents are quite different, since he does not use an exact solution in his theory.

It is fairly difficult to determine strictly the limits of the parameters affecting the discrepancy between the above two positions because the kinetic and thermal constants of sample materials are not widely known and an allowable error for coincidence cannot be defined unconditionally. However, if the accuracy of coincidence is given, we may make a rough estimate of the limits for any experiments through the present theory. In the case of a first-order pyrolysis of a solid sample, such as cellulose, having an activation energy larger than 50 kcal/mol and a preexponential factor near 10^{19} min^{-1} , assuming an accuracy of 5% and a cell size of 0.3 cm, the upper limit of the heating rate required for the coincidence becomes about 0.5 deg/min. This result was anticipated by the authors in a previous paper.⁴ In the case of inorganic powders, as in ceramic

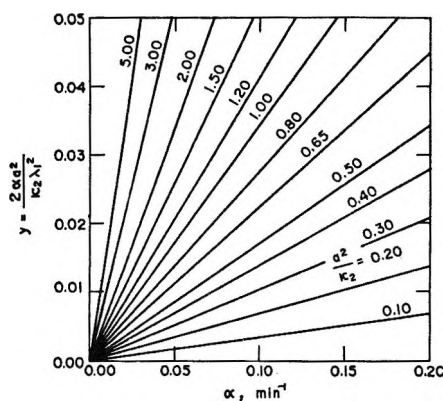


Figure 1. Diagram illustrating the limit of parameters for coincidence between the DTA peak and maximum reaction rate ($n = 0.5$).

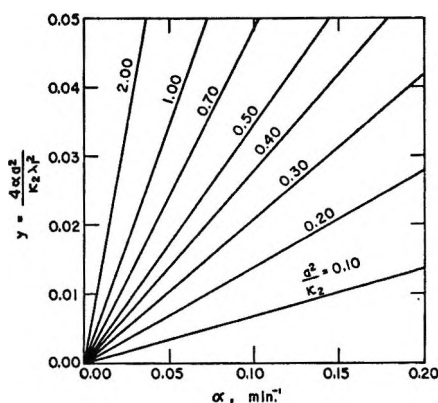


Figure 2. Diagram illustrating the limit of parameters for coincidence between the DTA peak and maximum reaction rate ($n = 1.0$).

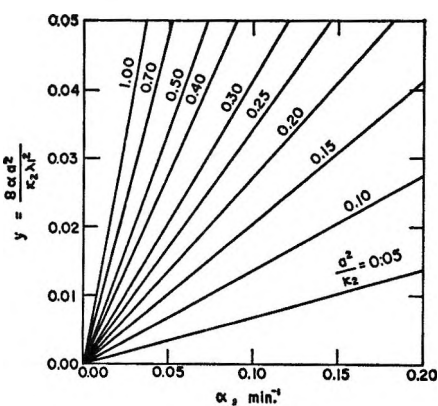


Figure 3. Diagram illustrating the limit of parameters for coincidence between the DTA peak and maximum reaction rate ($n = 1.5$).

products, having a reaction order of about one-half, the critical heating rate required for coincidence with an accuracy of 5% becomes about 10 deg/min, almost, for a cell diameter of 0.4 cm because of a small α , due to the high threshold temperature of reaction, and a rather large κ_2 . Although this critical value usually decreases with an increase in the cell size and in the accuracy, since the experiments for these materials are mostly

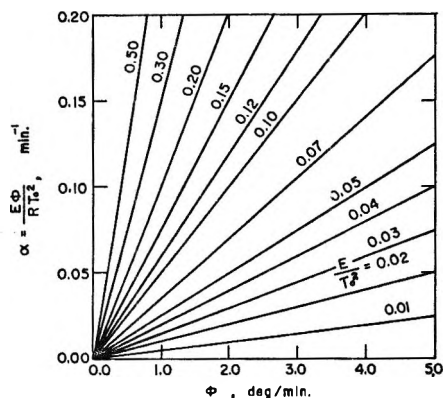


Figure 4. Dependence of α on ϕ and E/T_c^2 .

carried out at such conditions, it appears that the discrepancy is out of the question unless an especially large heating rate and cell size are used.

By inserting eq 55 into the equation obtained from differentiating eq 37, it is easily understood that when this discrepancy occurs, the position of the maximum rate moves toward a lower temperature region of the peak point of the DTA curve. This result is in agreement with the suggestion by Reed, *et al.*, and shows that the DTA peak cannot precede the inflection point of the TGA curve in any experiments involving unstirred systems. Thus if an inverse correlation between the two positions is obtained, the experimental results will be regarded as unreliable.

According to this theory, the shift of base line of the DTA curve is expressed by the first term of the right-hand side of eq 37 or eq 38. Since the thermal diffusivities are assumed constant in our theory, we cannot give a further discussion on the base-line problem of DTA. Provided that the thermal diffusivities of the sample and standard cells are nearly equal, as adopted by many investigators, it will be understood from these equations that no shift of the base line appears.

If the displacement of the DTA curve is shown by eq 38, the displacement ΔT keeps a linear relation to the reaction rate $d(w/w_0)/dt$ depending on the reaction order (n), the heating rate (ϕ), the activation energy (E), and the other parameters in the form of eq 34 and 45. In Figures 5 and 6, the variations of ΔT with n and ϕ for the kinetic parameters selected arbitrarily are shown for references. In particular, if the displacement $(\Delta T)_p$ at the peak is needed, we can use the following equations obtained from eq 34, 45, and 56.

$$(\Delta T)_p = \delta_n \left\{ \frac{\alpha}{A} + (1 - n) \right\} \times \left[1 - \frac{1}{X} \left\{ \frac{\alpha}{A} + (1 - n) \right\} \right]^{n/(1-n)} \quad (61)$$

where $n \neq 1$

$$(\Delta T)_p = \frac{\delta_1 \alpha}{e A} \quad (62)$$

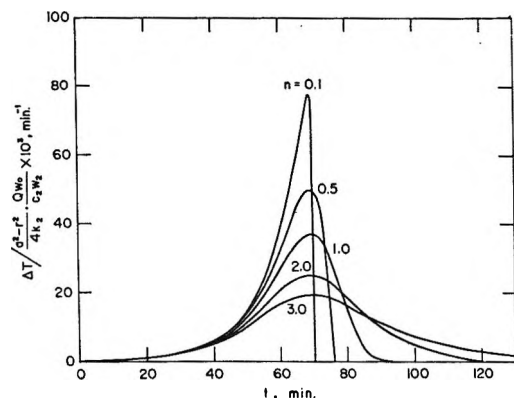


Figure 5. Variation of ΔT with n ; $A = 10^{-4} \text{ min}^{-1}$ and $\alpha = 10^{-1} \text{ min}^{-1}$.

where $n = 1$. Since the temperature profile in the sample cell is expressed approximately by a cubic parabola, as known from eq 38, it can be easily understood that the maximum temperature exists in the center of the cell regardless of any other parameters.

Summary

The basic equations of DTA including the temperature profile in the cells were solved strictly by means of the Laplace transformation and Green's function. These solutions give almost the same result as was gotten from Stokes' method in a previous paper, except for a few approximations. From these results, it was concluded that the peak of the DTA curve and the inflection point of the TGA curve agree with each other within certain limits of the experimental conditions,

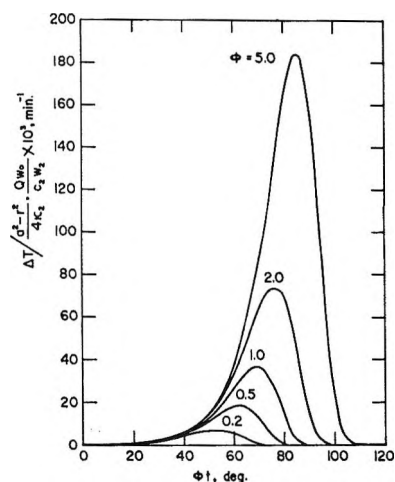


Figure 6. Variation of ΔT with ϕ ; $A = 10^{-4} \text{ min}^{-1}$ and $E/RT_0^2 = 10^{-1} \text{ deg}^{-1}$.

such as the heating rate, the cell size, and the kinetic properties of the sample material. Some diagrams which can be used for a judgment of the coincidence were also given.

The main restrictions of this theory are that the experimental conditions are approximated by the original assumptions: use of an infinite cylindrical cell and neglect of the change of thermal properties of the sample material due to chemical reaction.

Acknowledgment. We are grateful to Dr. P. H. Thomas for his suggestion at the course of development of our theory.

SCFMO Calculations of Heteroatomic Systems with the Variable- β Approximation. III. Electronic Spectra of Anions of Hydroxyaromatics¹

by Kichisuke Nishimoto and Leslie S. Forster

Department of Chemistry, University of Arizona, Tucson, Arizona (Received August 21, 1967)

The singlet transition energies of the anions of phenol, α - and β -naphthol, and the quinolinols have been computed. Good agreement with experiment is obtained with $I_0 = 27.83$ eV and $\gamma_{00} = 19.43$ eV, when $+5/3$ is assigned as the core charge for oxygen.

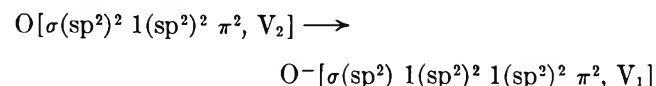
Introduction

The SCFMO method in the Pariser-Parr-Pople approximation has proven to be very useful in computing singlet transition energies. A particular parameterization (the variable- β approximation) has been applied, with considerable success, to a wide variety of neutral molecules containing nitrogen and oxygen atoms.^{2,3} Extension of the method to ionized species has proven to be troublesome. The central problem in any semiempirical method is the parameter choice. We now describe a suitable parameterization for the anions of hydroxy-substituted molecules, phenol, α - and β -naphthol, and the quinolinols.

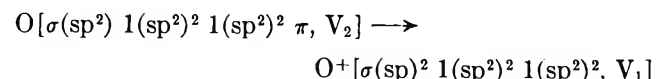
Method

With the exception of the parameters associated with O^- , the method was identical with that previously described.^{2,3} The Nishimoto-Mataga integrals were used throughout. Three approaches to the anion parameterization were explored.

Model I. The removal of the proton is assumed to leave the valence state essentially undisturbed. Thus $ROH \rightarrow RO^-$ is represented by

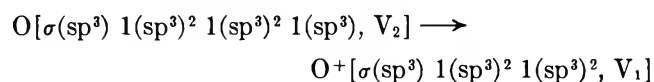


The two electrons are then successively removed and the valence-state ionization energy corresponds to



This is analogous in every respect to the situation encountered when a carbonyl group donates one π electron to the conjugated system and the normal carbonyl parameters are used, $I_0 = 17.7$ and $\gamma_{00} = 15.23$ eV.² The core charge is $+1$.

Model II. In this approach, the removal of the proton from OH is accompanied by rehybridization to $O^-[\sigma(sp^3) 1(sp^3)^2 1(sp^3)^2 1(sp^3)^2, V_1]$. The valence-state ionization energy is then computed for



The appropriate quantities are $I_0 = 24.39$ and $\gamma_{00} = 18.28$ eV.⁴ Again the core charge is assumed to be $+1$.

It can be seen (Table I) that the phenolate spectrum is not well reproduced by Model I. Model II is considerably better for phenolate, but not very satisfactory for the naphtholates (Table II). Two bands of moderate intensity (3.58 and 4.40 eV) appear in the β -naphtholate spectrum.⁵ In α -naphtholate, the higher energy transition becomes a shoulder on the lower energy band. Model II is conspicuously deficient in reproducing this behavior.

Model III. In this model the effect of changing the ROH core ($O^2+[\sigma(sp^2)\sigma(sp^2) 1(sp^2)^2, V_2]$) to RO^- is assumed to correspond to reducing Z_{eff} by 0.35 (Slater's rules). The core charge is then $+5/3$ and the parameters are calculated by the weighted averages

$$I_0 = \frac{2 \times 32.9 + 17.7}{3} = 27.83 \text{ eV}$$

$$\gamma_{00} = \frac{2 \times 21.53 + 15.23}{3} = 19.43 \text{ eV}$$

$$a_0 = 0.741$$

It is evident that this model yields the best results of the three schemes.

The spectra of the anions of phenol and α - and β -naphthol resemble the spectra of the corresponding amines, aniline, and the naphthylamines.⁶ The C-N bond orders in the amines are about 0.4. The model

(1) Supported by the U. S. Public Health Service, Grant No. GM-13218.

(2) K. Nishimoto and L. S. Forster, *Theor. Chim. Acta*, **4**, 155 (1966).

(3) K. Nishimoto and L. S. Forster, *J. Phys. Chem.*, **71**, 409 (1967).

(4) J. Hinze and H. H. Jaffé, *J. Am. Chem. Soc.*, **84**, 540 (1962).

(5) G. W. Ewing and E. A. Steck, *ibid.*, **68**, 2181 (1946).

(6) H. Baba and S. Suzuki, *Bull. Chem. Soc. Japan*, **34**, 76, 82 (1961).

Table I: Data for the Phenolate Ion

	Transition energies, eV, and intensities, f			Polarizations ^b	Exptl ^a	
	Model I	Model II	Model III		Energy	$10^{-4}\epsilon_{\max}$
	3.90 (0.146)	4.56 (0.127)	4.48 (0.082)	x	4.32	0.32
	4.99 (0.514)	5.48 (0.262)	5.55 (0.307)	y	5.30	1.1
	6.32 (0.079)	6.71 (0.633)	6.61 (0.660)	x		
	6.73 (0.881)	6.86 (1.118)	6.77 (1.073)	y		
-----Charge densities-----						
q_1	0.858	0.789	0.913			
q_2	1.120	1.076	1.082			
q_3	1.039	1.042	1.009			
q_4	1.164	1.125	1.074			
q_7	1.660	1.849	1.830			
-----Bond orders-----						
P_{12}	0.517	0.583	0.599			
P_{23}	0.712	0.692	0.682			
P_{34}	0.632	0.648	0.657			
P_{17}	0.615	0.601	0.427			
-----Energy of highest occupied orbital, eV-----						
	-3.97	-5.06	-7.61			

^a American Petroleum Institute Research Project 44. ^b The y axis coincides with the C-O direction.

Table II: Transition Energies, eV and Intensities, f for the Naphtholate Ions

	α -Naphtholate						β -Naphtholate								
	Model II		Model III		θ , deg	Exptl ^a		Model II		Model III		θ , deg	Exptl ^a		
	Energy	f	Energy	f		Energy	$10^{-4}\epsilon_{\max}$	Energy	f	Energy	f		Energy	$10^{-4}\epsilon_{\max}$	
1L_1	3.52	(0.204)	3.80	(0.228)	60	3.73	0.76	1L_1	3.38	(0.178)	3.65	(0.123)	125	3.59	0.30
1L_2	3.83	(0.130)	3.84	(0.080)	133			1L_2	3.99	(0.041)	4.19	(0.096)	145	4.40	0.62
	5.00	(0.582)	5.05	(0.570)	1	5.04	2.6		5.03	(0.123)	5.09	(0.209)	39		
	5.28	(0.197)	5.34	(0.156)	130				5.11	(0.160)	5.26	(1.553)	15	5.20	5.8
	5.66	(0.071)	5.58	(0.021)	138				5.43	(0.501)	5.42	(0.046)	141		
	5.95	(0.632)	5.77	(0.923)	0				6.02	(0.259)	5.90	(0.595)	128		
-----Energy of highest occupied orbital, eV-----															
	-4.83		-7.22						-5.08		-7.41				

^a American Petroleum Institute Project 44. ^b Measured from the long axis toward the oxygen atom.

III parameterization yields approximately the same value for the C-O bond order in phenolate.

Results and Discussion

Phenolate. The ${}^1L_{a,b}$ benzene transition energies are progressively lowered in energy by OH and O⁻ substitution (Figure 1). The 1E_u degeneracy is removed but the splitting is probably insufficient to detect spectrally. The ionization potential of phenol should be reduced about 1.7 eV (model III) by removal of the proton.

Although the benzene spectrum is strongly affected by the O⁻ substituent, little departure from hexagonal symmetry is predicted.

α -Naphtholate. There is configuration mixing between $6 \rightarrow 7$, $6 \rightarrow 8$, and $5 \rightarrow 7$, as in α -naphthol,⁷ but this mixing is so marked that the 1L_a and 1L_b designations are no longer useful,³ and the transitions are labeled 1L_1 and 1L_2 in order of increasing energy. The 1L_1 and 1L_2 transitions are predicted to be at nearly equal energies. The weak 1L_1 would then be obscured by the stronger 1L_2 . This is consistent with the observation of one broad absorption band.⁵ The computed polarizations are 1L_1 (60°) and 1L_2 (133°), the angle being measured from the long molecular axis toward

(7) L. S. Forster and K. Nishimoto, *J. Am. Chem. Soc.*, **87**, 1459 (1965).

Table III: Transition Energies, eV, and Intensities, f , of Quinolinalates Calculated with Model III

2-OH			3-OH			4-OH			5-OH			6-OH			7-OH			8-OH												
Energy	f	θ , deg	Energy	f	θ , deg	Energy	f	θ , deg	Energy	f	θ , deg	Energy	f	θ , deg	Energy	f	θ , deg	Energy	f	θ , deg	Energy	f	θ , deg	Energy	f	θ , deg	Energy	f	θ , deg	
Exptl ^a			Exptl ^a			Exptl ^a			Exptl ^a			Exptl ^a			Exptl ^a			Exptl ^a												
Energy	f	θ , deg	Energy	f	θ , deg	Energy	f	θ , deg	Energy	f	θ , deg	Energy	f	θ , deg	Energy	f	θ , deg	Energy	f	θ , deg	Energy	f	θ , deg	Energy	f	θ , deg	Energy	f	θ , deg	
¹ L ₁	3.82	(0.193)	151	3.76	1.1	¹ L ₁	3.66	(0.207)	37	3.54	6.0	¹ L ₁	4.03	(0.006)	77	3.94	1.7	¹ L ₁	3.54	(0.195)	35	3.33	6.3	¹ L ₁	3.53	(0.180)	107	3.44	3.2	
¹ L ₂	4.54	(0.067)	110	4.59		¹ L ₂	4.31	(0.069)	55	4.59		¹ L ₂	4.09	(0.297)	104	4.48		¹ L ₂	4.13	(0.018)	67	4.48		¹ L ₂	3.84	(0.023)	18	3.68		
	5.21	(0.461)	0				5.13	(0.268)	132				5.28	(0.848)	2	5.44			5.09	(1.190)	157	5.17			4.93	(0.971)	158	4.96		
	5.45	(1.206)	29	5.41			5.24	(0.970)	165	4.96			5.44	(0.038)	9	5.55	(0.070)			5.36	(0.148)	171				5.33	(0.174)	59		
	5.82	(0.390)	94				5.50	(0.470)	151				5.55	(0.070)	52	5.66	(0.753)			5.52	(0.355)	6				5.70	(0.059)	42		
	5.96	(0.490)	163				5.89	(0.680)	28				5.66	(0.753)	10	6.15	(0.573)			6.14	(0.873)	57				6.05	(0.354)	151		
	6.16	(0.006)	44				6.08	(0.077)	56				6.15	(0.573)	96					6.21	(0.331)	124				6.35	(0.974)	86		

^a With the exception of 2- and 4-quinolinalates, the experimental values were taken from ref 5. These were confirmed and extended to include the 2- and 4- derivatives by K. Kimura.

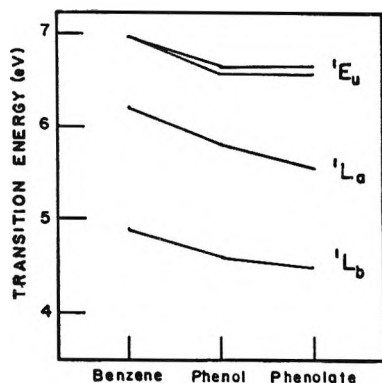


Figure 1. Variation in transition energies with structure.

the oxygen atom. The combination of $5 \rightarrow 7$ and $6 \rightarrow 8$ that leads to the 1B_b transition in naphthalene contributes strongly to two states (5.35 and 5.77 eV) in α -naphtholate. The spectrum of α -naphthylamine does exhibit two strong bands in this region.⁶

The ionization potential, computed from the energy of the highest occupied orbital (corrected by adding 1.3 eV²), is 6.28 eV. This species should be a good electron donor in solution.

From the molecular diagram (Figure 2), it can be seen that most of the 0.17 unit of charge that has migrated into the ring system is concentrated in the ring to which the substituent is attached.

β -Naphtholate. As indicated above, two moderately strong transitions are expected at wavelengths greater than 2500 Å. The failure of the usual variable β parameterization (assuming either +1 or +2 core) in this computation provided the impetus for the proposal of the fractional charge model. The configuration mixing in α - and β -naphtholate is nearly the same, in contrast to the situation in the neutral species.⁷ The 1L_1 and 1L_2 transitions are polarized at 125 and 145°, respectively. The calculated and observed intensity ratios for 1L_1 and 1L_2 are inverted, but all other calculations yield much smaller intensities for 1L_2 . The 1L_1 transition is polarized nearly perpendicular to the C–O bond axis, as is the corresponding transition in β -naphthol and β -naphthylamine. Experimental information about the polarizations is lacking.

Quinolinolates. The spectra of the anions of hy-

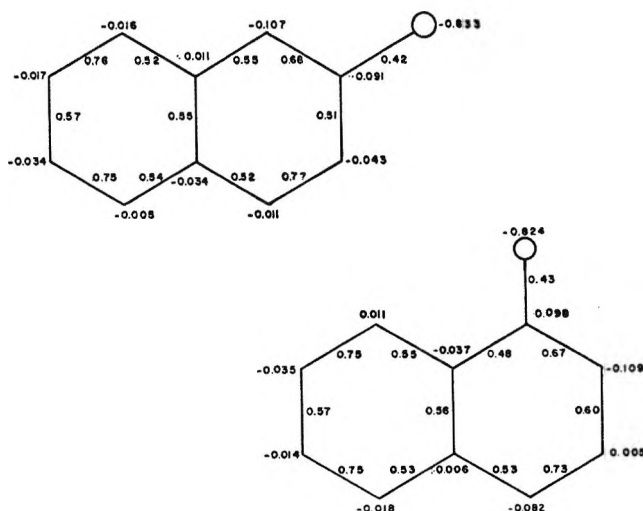


Figure 2. Molecular diagrams for α - and β -naphtholate ions, model III.

droxy-substituted quinolines provide a good test for the parameterization. The calculations follow the observed substitutional shifts quite well (Table III). Noteworthy is the corroboration that 1L_a and 1L_b are nearly degenerate in the 4-OH derivative, but not in the 5- and 8-quinolinolates (the validity of the Platt symbols is restored by the *aza* substitution). The calculated intensity ratios for the two lowest states of the anions derived from β -naphtholate are not satisfactory. Nevertheless, the applicability of the fractional charge model to the calculation of singlet transition energies has been established.

With the exception of the near degeneracy in 4-quinolate, the 1L_a states are lower than 1L_b , a reversal of the order in quinoline. A similar inversion was obtained in the quinolinol calculations.⁸ The marked lowering in 1L_a compared to quinoline is largely due to the reduction in the energy difference between the highest occupied and lowest empty orbitals. The effect of the O⁻ substituent on 1L_a can be treated as a simple perturbation, and a Hückel scheme may be used for approximate calculations. The substituent effect 1L_b is more complicated; both the configuration energies and the interconfiguration matrix elements are altered by substitution. The references to 1L_a in this paragraph are applicable to the 1L_1 transitions and the remarks about 1L_b are pertinent to 1L_2 .

A Potentiometric Study of Acid-Base Equilibria in 1,1,3,3-Tetramethylguanidine

by Joseph A. Caruso and Alexander I. Popov

Department of Chemistry, Michigan State University, East Lansing, Michigan 48823
(Received August 23, 1967)

Acid dissociation constants of four 5-substituted tetrazoles, perchloric acid, *m*-chlorobenzoic acid, and phenol were determined in 1,1,3,3-tetramethylguanidine by potentiometric techniques. A hydrogen indicator electrode and a mercury-mercury(II) chloride reference electrode were used. Perchloric acid is the strongest acid with $pK_a = 3.11$ and phenol is the weakest with $pK_a = 7.54$. The pK_a values obtained by the potentiometric method are in good agreement with the values obtained from electrical conductance measurements.

Introduction

The usefulness of nonaqueous solvents in the study of acid-base equilibria (particularly in the Brønsted-Lowry sense) is clearly illustrated by the large number of analytical techniques that utilize either pure nonaqueous solvents or their mixtures for a wide variety of titrations of substances that, for one reason or another, cannot be analyzed in aqueous solutions.

With few exceptions, the development of the theory of acid-base equilibria in nonaqueous solvents, however, has not kept pace with the practical applications. Acidic solvents, such as acetic acid and sulfuric acid, have been studied very intensively and the nature of acid-base equilibria in these solvents has been elucidated particularly by the classical investigations of Kolthoff and Bruckenstein in acetic acid solutions¹ and by Gillespie and his coworkers² in sulfuric acid. On the other hand, acid-base equilibria in basic solvents seem to have been studied less completely, although of course, there are significant publications on such solvents as pyridine,³⁻⁶ ethylenediamine,⁷⁻¹² and ammonia.¹³⁻¹⁵

Recently, we reported an electrical conductance study on 5-substituted tetrazoles in a strongly basic solvent, 1,1,3,3-tetramethylguanidine (hereafter abbreviated as TMG).¹⁶ In order to establish a useful electrode system in TMG, as well as to verify the results of the electrical-conductance study, a potentiometric study of acid-base equilibria in TMG was initiated.

Since tetramethylguanidine has a relatively low dielectric constant of 11.00,¹⁶ it is to be expected that ionic equilibria in this solvent would be substantially influenced by ion pairing. It has been shown by Kolthoff and Bruckenstein¹ that in such cases the over-all dissociation of a weak acid HX will proceed in two steps $HX \rightleftharpoons H^+X^- \rightleftharpoons H^+ + X^-$, resulting in the over-all dissociation constant, K_{HX} , which is given by the expression

$$K_{HX} = \frac{a_{H^+}a_{X^-}}{a_{HX} + a_{H^+X^-}} \quad (1)$$

where the terms have their usual meanings. The mass balance relationship may be written as

$$(C_{HX})_t = [H^+] + [H^+X^-] + [HX] \quad (2)$$

where $(C_{HX})_t$ is the total analytical concentration of the acid HX and the terms in brackets represent the equilibrium concentrations of the respective species. If we assume that the activity coefficients of uncharged species equal unity, that $a_{H^+} = a_{X^-}$, and that $a_{H^+} = [H^+]$, it then follows that

- (1) I. M. Kolthoff and S. Bruckenstein in I. M. Kolthoff and P. J. Elving, "Acid-Base Equilibria in Nonaqueous Solvents. Treatise on Analytical Chemistry," Part I, Vol. I, The Interscience Encyclopedia Company, Inc., New York, N. Y., 1959, Chapter XIII, and references cited therein.
- (2) R. J. Gillespie and E. A. Robinson in "Non-Aqueous Solvent Systems," T. C. Waddington, Ed., Academic Press, Inc., New York, N. Y., 1965, Chapter 4.
- (3) P. Walden, L. F. Audrieth, and E. J. Birr, *Z. Physik. Chem.*, **A160**, 337 (1932).
- (4) W. A. Luder and C. A. Kraus, *J. Am. Chem. Soc.*, **69**, 2481 (1947).
- (5) D. S. Burgess and C. A. Kraus, *ibid.*, **70**, 706 (1948).
- (6) R. Gopal and M. M. Hussain, *J. Indian Chem. Soc.*, **40**, 981 (1963).
- (7) M. L. Moss, J. S. Elliot, and R. T. Hall, *Anal. Chem.*, **20**, 784 (1948).
- (8) M. Katz and P. A. Glenn, *ibid.*, **24**, 1157 (1952).
- (9) A. J. Martin, *ibid.*, **29**, 79 (1957).
- (10) B. B. Hibbard and F. C. Schmidt, *J. Am. Chem. Soc.*, **77**, 225 (1955).
- (11) J. Peacock, F. C. Schmidt, R. E. Davis, and W. B. Schaap, *ibid.*, **77**, 5829 (1955).
- (12) L. M. Mukherjee and S. Bruckenstein, *J. Phys. Chem.*, **66**, 2228 (1962).
- (13) V. A. Pleskov and A. Monosson, *Z. Physik. Chem.*, **156**, 176 (1931).
- (14) G. W. Watt, J. L. Hall, and G. R. Choppin, *J. Phys. Chem.*, **57**, 567 (1953).
- (15) J. L. Hawes and R. L. Kay, *ibid.*, **69**, 2420 (1965).
- (16) J. A. Caruso, P. G. Sears, and A. I. Popov, *ibid.*, **71**, 1756 (1967).

$$K_{\text{HX}} = \frac{a_{\text{H}^+}{}^2}{(C_{\text{HX}})_t - a_{\text{H}^+}} \quad (3)$$

Solving eq 3 for a_{H^+} , we get

$$a_{\text{H}^+} = (K_{\text{HX}}[(C_{\text{HX}})_t - a_{\text{H}^+}]^{1/2}) \quad (4)$$

Potentiometric studies of acids in TMG were carried out by means of the galvanic cell

Ref electrode || $\text{HX}(C_{\text{HX}})_t$ (TMG) | H_2 (1 atm), Pt

The reference electrode consisted of a mercury-mercury(II) couple, which was composed of a mercury layer in contact with a saturated solution of mercury(II) chloride in TMG. The emf generated by this cell is given by the equation

$$E_{\text{HX}} = E'_{\text{H}} + 0.0592 \log a_{\text{H}^+} \quad (5)$$

where

$$E'_{\text{H}} = E^0_{\text{H}^+/\text{H}_2} + E_{\text{lj}} + E_{\text{ref}} \quad (6)$$

Substituting eq 4 into eq 5 yields

$$E_{\text{HX}} = E'_{\text{H}} + 0.0296 \log K_{\text{HX}} + 0.0296 \log [(C_{\text{HX}})_t - a_{\text{H}^+}] \quad (7)$$

It is seen that a plot of E_{HX} vs. $\log [(C_{\text{HX}})_t - a_{\text{H}^+}]$ should give a straight line with slope of 0.0296 and intercept of $E'_{\text{H}} + 0.0296 \log K_{\text{HX}}$. If K_{HX} of an acid is known from independent measurements, the value of E'_{H} may be calculated (assuming that the liquid-junction potential remains constant). Essentially the same technique is then used in an iterative process to calculate K_{HX} values for other substances. As the first approximation, we can write $[(C_{\text{HX}})_t - a_{\text{H}^+}] = (C_{\text{HX}})_t$. The emf values are then plotted vs. $\log (C_{\text{HX}})_t$ and a value of K_{HX} obtained. From this value of K_{HX} a first value of a_{H^+} is calculated and E_{HX} is plotted vs. $\log [(C_{\text{HX}})_t - a_{\text{H}^+}]$, from which a new value of K_{HX} is obtained. The process is repeated until the consecutive K_{HX} values converge within an acceptable tolerance. This method usually requires four or five iterative steps and is easily handled by a digital computer.

In a similar potentiometric study using ethylenediamine as solvent, Bruckenstein and Mukherjee¹² have postulated the following conjugate ion equilibrium



where

$$K_{\text{HX}_2^-} = \frac{a_{\text{HX}_2^-}}{(a_{\text{X}^-})(a_{\text{HX}})} \quad (9)$$

In the cases where the conjugate ion equilibrium is present, a plot of E_{HX} vs. $\log (C_{\text{HX}})_t$ yields two linear portions, one of slope 0.0296 representing the two-step ionization and dissociation equilibria, and one of slope

0.0592 representing equilibrium 8, shown above. At the point of intersection of the two linear segments they obtain the relationship

$$K_{\text{HX}_2^-} = \frac{1}{(C_{\text{HX}})_t'} \quad (10)$$

where $(C_{\text{HX}})_t'$ gives the concentration of the acid at the point of intersection.

Experimental Part

Reagents. The solvent purification and the preparation and purification of the 5-substituted tetrazoles have been previously described.¹⁶ Perchloric acid and mercury (both Baker Analyzed reagent grade), as well as Fisher Certified Reagent mercury(II) chloride were used without further purification. Matheson Co., Inc. prepurified hydrogen was passed through a flow meter to assure constant delivery to the hydrogen-electrode half cell. It was then passed through a column of Ascarite and a column of Drierite before use. Phenol, obtained from Eastman Chemical Co., was purified by vacuum distillation in a micro distillation apparatus; *m*-chlorobenzoic acid was purified by recrystallizing from a water-ethanol mixture.

Apparatus. The emf readings were taken on a Beckman expanded-scale pH meter. The 0–200-mV full scale was extended by recalibrating against the output of a Biddle-Gray portable potentiometer Model 605014. Readings were good to 0.2 mV. The cell used in the emf measurements was similar to one previously described.¹⁷

Procedures. Solutions of various acids in TMG were prepared by the usual volumetric technique, but the manipulations were carried out in a drybox under a dry nitrogen atmosphere.

It was found that a mercury-mercury(II) electrode had a steady and reproducible potential when used in conjunction with a hydrogen electrode. A saturated solution of mercury(II) chloride was prepared by suspending 2.00 g of dry salt in 100 ml of solvent and stirring the mixture for 2 hr. The solutions appeared to be stable for at least 24 hr. After the solution had been aged for several days, however, a black deposit was formed on the bottom of the flask. In order to avoid a possible source of error, fresh saturated solutions of mercury(II) chloride were prepared just prior to use.

Attempts to prepare a calomel reference electrode in TMG were unsuccessful, since addition of calomel to TMG instantly produced a black precipitate. The reference-electrode half cell was prepared with a 1-cm layer of mercury and a platinum contact inserted into the mercury. Saturated mercury(II) chloride solution was then added to the reference-electrode compartment.

(17) J. A. Caruso, G. Jones, and A. I. Popov, *Anal. Chim. Acta*, **40**, 49 (1968).

Sixteen-gauge platinum wires 1 to 1.5 in. in length were sealed into soft glass tubes and coated with platinum black by electrolysis in a previously described solution¹⁶ for 5 min at 10 mA. The electrodes were then charged with hydrogen by cathodizing in a dilute sulfuric acid solution. As the measurements were taken, electrodes were interchanged to compare their response. Fresh electrodes were used when readings became erratic or when readings did not agree to within ± 0.5 mV between fresh and previously used electrodes. Immediately before use, the platinum electrodes were washed with distilled water, rinsed in acetone, and air dried.

A gas dispersion tube was inserted into the hydrogen-electrode half cell and the half cell purged with hydrogen for 5 min. The reference-electrode compartment was then filled with saturated mercury(II) chloride solution. Finally, the hydrogen-electrode compartment was filled with the solution to be studied. The bridging compartment was also filled with the same solution to minimize errors due to diffusion. A current of hydrogen was allowed to stream through the solution for at least 20 min. The readings were taken when changes in potential were about 2 mV or less over a 20–30-min recording interval. This behavior may be due to the hydrogen electrode coming slowly into equilibrium with the solution. It was found that when the system was thermostated in a constant-temperature bath at 25°, the accuracy of the measurements did not improve. Reproducible measurements could be obtained in a water thermostat only after 40–45 min. All reported measurements, therefore, were taken in an unthermostated cell at room temperature of *ca.* 24°. The reported emf values are the mean value of the best four readings and have average deviations of ± 0.5 – ± 1.0 mV. The hydrogen partial-pressure correction to the observed emf was ignored, since it would be less than experimental error.

Results and Discussion

Over-all dissociation constants of 5-methyltetrazole, 5-benzyltetrazole, 5-phenyltetrazole, 5-*p*-chlorobenzyltetrazole, perchloric, and *m*-chlorobenzoic acids, and phenol were determined potentiometrically by the procedure described above. Unfortunately, in a number of cases, limited solubilities of acids in TMG precluded their study. For example, attempts have been made to study the dissociation of acetic acid, hydrochloric acid, and hydrobromic acid in TMG, but the experiments could not be carried out due to the low solubility of these acids in TMG.

The value for E°_{H} was calculated from the K_{HX} value for 5-benzyltetrazole obtained from electrical conductance measurements.¹⁶ The emf data were fitted by the method of least squares to yield a straight line with slope of 0.0288 (± 0.0012) and an intercept of -0.8021 (± 0.0015) V, where the numbers in parenthe-

ses represent the respective standard deviations. Recalling that the intercept = $E^{\circ}_{\text{H}} + 0.0296 \log K_{\text{HX}}$, the value of E°_{H} was calculated to be -0.6657 V. This value for E°_{H} was used in conjunction with the emf data to calculate the over-all acidity constants for the other systems. The data were analyzed by the use of a FORTRAN computer program run on a Control Data Corp. Model-3600 computer and the results are given in Table I. It is seen that there is good agreement between the potentiometric and conductometric methods, and that the experimental slopes agree well with the theoretical slope of 0.0296. The behavior of all substances listed, except phenol, is characteristic of weakly acidic substances in the concentration range of *ca.* 0.002–0.03 *M*. The same behavior was found for the conductance measurements which were done at < 0.001 *M*.¹⁶ The potentiometric method has led to $\text{p}K_{\text{HX}}$ values for systems which could not be readily studied conductometrically, *i.e.*, phenol and *m*-chlorobenzoic acid. In the case of tetrazoles, the inductive nature of the substituent groups is reflected in their $\text{p}K_{\text{HX}}$ values. Perchloric acid, the strongest acid studied ($\text{p}K_{\text{HX}} = 3.11$), does not differ greatly in acid strength from the rest of the substances with the exception of phenol. Even in the latter case, the leveling effect of the solvent is clearly noted considering that aqueous phenol has a $\text{p}K_{\text{a}} = 10$, while aqueous perchloric acid is completely dissociated. The $\text{p}K_{\text{HX}}$ value of perchloric acid also compares favorably with the value of 3.28 for picric acid as measured conductometrically.¹⁶ This is not surprising, however, since both are strong acids in aqueous solution and it would be expected that they exhibit similar acidic character in a strongly basic solvent such as TMG. The linearity of some typical E_{HX} vs. $\log [(C_{\text{HX}})_t - a_{\text{H}^+}]$ plots is shown in Figure 1. Measurements at low concentration (< 0.001 *M*) for hydrogen bromide solutions in TMG indicated that a $\text{p}K_{\text{HX}}$ value of *ca.* 4 might be expected. Mukherjee found that hydrogen bromide had a $\text{p}K_{\text{HX}}$ value of 3.28 in ethylenediamine.¹⁸

The importance of the iterative process in evaluating the data may be illustrated by comparing the following data for perchloric acid. The original plot of E_{HX} vs. $\log (C_{\text{HX}})_t$ yielded a slope of 0.0349, an intercept of -0.7537 V, and a $\text{p}K_{\text{HX}}$ value of 2.98, whereas in the final iterative step, for which E_{HX} was plotted vs. $\log [(C_{\text{HX}})_t - a_{\text{H}^+}]$, a slope of 0.0305, an intercept of -0.7579 V, and a $\text{p}K_{\text{HX}}$ value of 3.11 were obtained.

The $\text{p}K_{\text{HX}}$ value of phenol of 7.54 indicates that it behaves as a stronger acid in TMG than in ethylenediamine, for which the corresponding value is 8.23.¹⁸ This behavior would be expected, in as much as TMG is a considerably stronger aqueous base than ethylene-

(18) M. L. Mukherjee, Ph.D. Thesis, University of Minnesota, Minneapolis, Minn., 1961.

Table I: Results of Potentiometric Studies in TMG^{a,b}

Substance	Intercept	Slope	pK_{HX}^{emf}	$pK_{HX}^{cond^{18}}$
5-BzTz (ref)	-0.8021 (0.0015)	0.0288 (0.0012)	...	4.61
5-MeTz	-0.8019 (0.0015)	0.0280 (0.0007)	4.60	4.60
5- <i>p</i> -ClBzTz	-0.7921 (0.0085)	0.0298 (0.0033)	4.28	4.34
5-PhTz	-0.7881 (0.0036)	0.0288 (0.0016)	4.13	4.24
<i>m</i> -Chlorobenzoic acid	-0.8076 (0.0076)	0.0303 (0.0034)	4.80	...
Phenol	-0.8887 (0.0073)	0.0282 (0.0038)	7.54	...
HClO ₄	-0.7580 (0.0044)	0.0305 (0.0019)	3.11	...

^a Numbers in parentheses represent the respective standard deviations. ^b Bz = benzyl, Me = methyl, Ph = phenyl, and Tz = tetrazole.

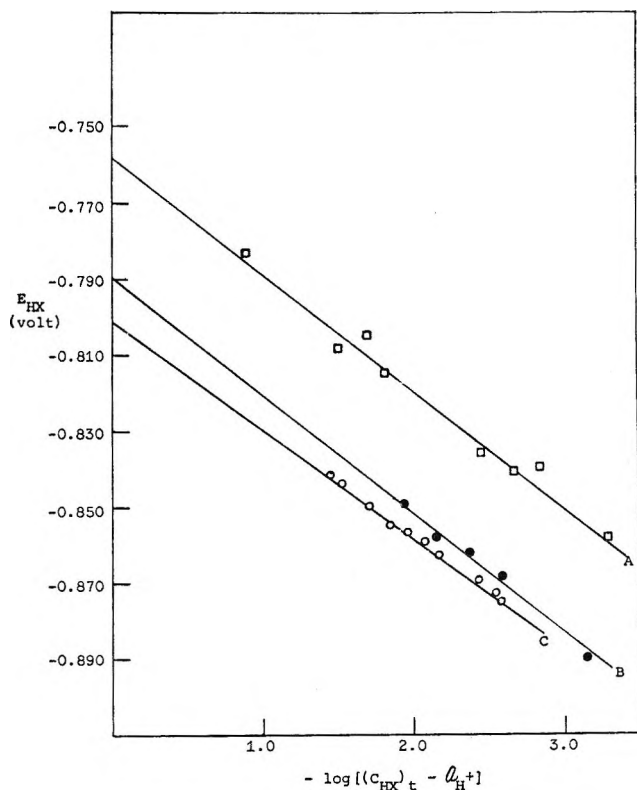


Figure 1. E_{HX} vs. $\log (CHX)_t - a_{H^+}$ for TMG solutions of: A, HClO₄; B, 5-*p*-chlorobenzyltetrazole; and C, 5-methyltetrazole.

diamine (aqueous $pK_a = 0.4$, as opposed to an aqueous $pK_a = 4.15$,¹⁸ respectively).

The data illustrated in Figure 2 indicate that the conjugate ion, HX_2^- , may be one of the species present in the more concentrated phenol-TMG solutions. It would appear that the discussion given by Bruckenstein¹² regarding phenolic ions of the HX_2^- type would also be pertinent in this work, since he points out that ions of this type have been previously reported on the basis of photometric, potentiometric, and conducto-

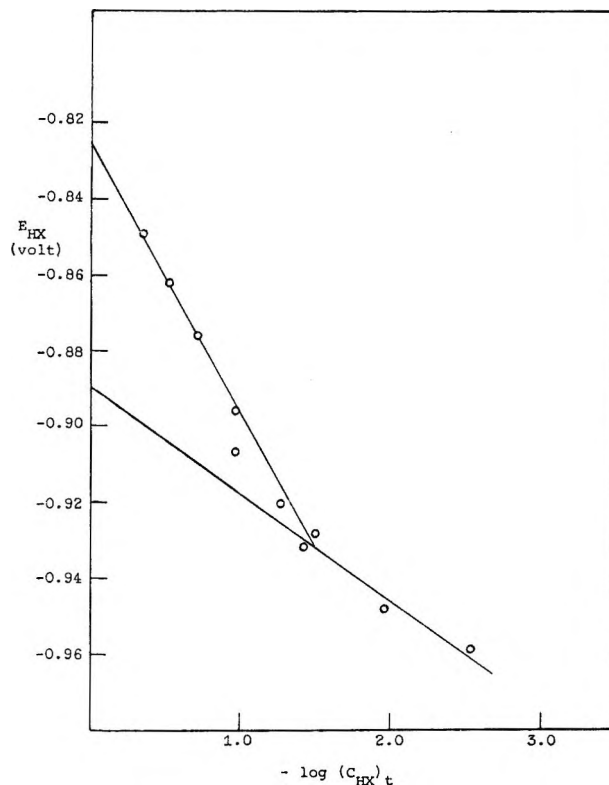


Figure 2. E_{HX} vs. $\log (CHX)_t$ for phenol solutions in TMG.

metric information. He indicates that this would probably be a hydrogen-bonded species. The value for $pK_{HX_2^-}$ was found from the data shown in Figure 2 to be 1.52 ($K_{HX_2^-} = 34.2$). A formation constant of 34.2 may be somewhat higher than would be expected, since it would seem likely that the anion, X^- , might preferentially hydrogen bond to the solvent rather than to the parent acid, HX.

Acknowledgment. The authors gratefully acknowledge the support of this work by Research Grant MH-07825 from the Institute of Mental Health, U. S. Public Health Service.

The Solid-State Radiation Chemistry of Selected Transition

Metal Chelates of Glycine and Alanine¹

by W. Carl Gottschall, Jr.,² and Bert M. Tolbert

University of Colorado, Department of Chemistry, Boulder, Colorado 80502 (Received August 23, 1967)

The radiation chemistry of selected transition metal chelates of glycine and alanine has been investigated in the solid state. Ammonia was released in greatest yield upon dissolution of the cesium-137 γ -irradiated samples and CO₂ was the chief gaseous product measured from the crystalline samples. Reliability of the CO₂ determinations after dissolution made this product the best basis of comparison between the chelates and their parent amino acid. $G(\text{CO}_2)$ values were: glycine, 1.02; cadmium diglycinate monohydrate, 0.21; zinc diglycinate monohydrate, 0.28; cobalt triglycinate dihydrate, 0.32; nickel diglycinate dihydrate, 0.34; copper diglycinate monohydrate, 0.45; alanine, 0.89; nickel alaninate dihydrate, 0.21; zinc alaninate monohydrate, 0.53; and copper alaninate monohydrate, 0.99. $G(\text{NH}_3)$ values were: glycine, 4.3; alanine, 3.3; copper diglycinate monohydrate, 1.0; and cadmium diglycinate monohydrate, 0.8. Qualitative and quantitative similarities between the chelates and their parent amino acid indicate similar decomposition mechanisms in agreement with the scheme proposed earlier by Tolbert.

Introduction

The protection or enhanced sensitivity afforded an organic moiety by the presence of a transition metal ion is of obvious concern to radiation chemists. From mean lethal-dose data and tabulations of copper content in living organisms, Schubert³ has postulated a direct relationship—with increasing copper content, the organism exhibits greater stability toward radiation effects. On a less controversial scale, other authors have studied the effect of inorganic ions on the radiolysis of organic⁴⁻⁶ and biochemical⁷ compounds in aqueous solution. Anbar and Rona,⁸ in fact, reported that cupric and thallos ions enhanced decomposition of glycine, as evidenced by ammonia production, with nickel having no effect. Willix and Garrison,⁹ on the other hand, report decreasing decomposition with increasing cupric concentration. In an effort to resolve these apparent conflicts and to discern meaningful relations between radiation decomposition and the presence of various metallic ions, the study of simple amino acid chelates in the solid state was undertaken.

Experimental Section

(a) *Materials.* The best grade commercial glycine and alanine from the California Corp. for Biochemical Research were recrystallized twice—first from glacial acetic acid and then from ethanol-water. An aliquot of labeled amino acid 1-¹⁴C from Nuclear Chicago Corp. (calculated to yield amino acid of specific activity such that the chelate formed from it would have a specific activity of approximately 0.1 $\mu\text{curie}/\text{mg}$) was pipetted into the solution immediately prior to the preparations. Procedures used for each of the specific chelates differed but slightly from the literature preparations.¹⁰⁻¹⁵ Crystals obtained were recrystallized and dried in a vacuum desiccator over MgClO₄. Spe-

cific activity of each chelate was checked by combustion in a modified Pregl furnace, followed by assay of the ¹⁴CO₂ with a Cary vibrating reed electrometer. Sample analyses agreed with calculations as indicated below: *Anal.* Calcd for copper diglycinate monohydrate: C, 20.92; H, 4.39; N, 12.20; Cu, 27.66. Found: C, 21.38; H, 4.42; N, 12.23; Cu, 27.82. Calcd for cadmium diglycinate monohydrate: C, 17.25; H, 3.62; N, 10.06. Found C, 17.32; H, 3.66; N, 10.24.

(b) *Apparatus.* The irradiations were performed in the University of Colorado cesium-137 γ source. The source was calibrated at $2.78 \pm 0.02 \times 10^{19}$ eV/g hr by a Fricke dosimeter at 22°, using $G(\text{Fe}^{3+}) = 15.6$.

The mass spectra were run on a Consolidated Electro-dynamics Corp. mass spectrometer Type 21-103 C.

(1) Supported in part by Contract AT(11-1)-690 from the United States Atomic Energy Commission.

(2) Department of Chemistry, University of Denver, Denver, Colo. 80210.

(3) J. Schubert, *Nature*, **200**, (4904); 376 (1963).

(4) J. Baxendale and D. Smithies, *J. Chem. Phys.*, **23**, 604 (1955).

(5) J. Baxendale and D. Smithies, *J. Chem. Soc.*, 779 (1959).

(6) A. Sugimori and G. Tsuchihashi, *Bull. Chem. Soc. Japan*, **33**, 713 (1960).

(7) J. Butler and A. Robins, *Radiation Res.*, **19**, 582 (1963).

(8) M. Anbar and P. Rona, *Proc. Chem. Soc.*, 244 (1963).

(9) R. L. Willix and W. M. Garrison, *J. Phys. Chem.*, **69**, 1579 (1965).

(10) W. C. Gottschall, Jr., Ph.D. Thesis, University of Colorado, Boulder, Colo., 1964.

(11) E. Aberhalden and E. Schnitzler, *Z. Physik. Chem.*, **163**, 94 (1927).

(12) I. Fedorov and T. Balakaeva, *Russ. J. Inorg. Chem.*, **5**, 737 (1960).

(13) A. Stosick, *J. Am. Chem. Soc.*, **67**, 365 (1945).

(14) J. Dubsky and A. Rabas, *Spisy Vydavane Prirodovedeckou Fak. Masary. Univ.*, **123**, 3 (1930); *Chem. Abstr.*, **25**, 2655 (1931).

(15) H. Ley and H. Winkler, *Ber.*, **42**, 3894 (1909).

Sample tubes were broken directly in the gas sampling system.

The gas chromatograph used was a Perkin-Elmer vapor fractometer Model 154. A simple device was constructed of Tygon tubing and brass connectors to permit breakage of the irradiated sample tubes directly in the carrier stream.

(c) *Procedure.* The procedures used have been detailed elsewhere¹⁶ and essentially consisted of $^{14}\text{CO}_2$ assay with a vibrating reed electrometer and ionization chambers. The NH_3 was determined by the Conway microdiffusion method¹⁷ with the Russell colorimetric procedure¹⁸ results read on a Beckman spectrophotometer at 628 $\text{m}\mu$. Dry analyses for H_2 and other products were determined *via* gas chromatography and mass spectrometry. Specific gravities were determined by the flotation method of Bernal and Crowfoot.¹⁹

Results

Figures 1-4 show the mole per cents of CO_2 produced from the irradiated chelates as a function of dose. The curves are linear to good approximations with small deviations at the highest doses on some probably indicating a decrease in the original material present. Difficulties due to contamination by radiation products are unavoidable but minimized by utilizing the line slope at the lowest doses to determine the G values. Table I lists the $G(\text{NH}_3)$ values for several of the chelates and parent amino acid.

Table I: Initial $G(\text{NH}_3)$ Values on Dissolving Irradiated Solid Compounds

Compound	$G(\text{NH}_3)$
Glycine	4.3
Alanine	3.3
$\text{Cu}(\text{Gly})_2 \cdot \text{H}_2\text{O}$	1.0
$\text{Cd}(\text{Gly})_2 \cdot \text{H}_2\text{O}$	0.8

Other products were not quantitatively determined, but qualitatively resembled those of the parent amino acid.¹⁶ Quantitative similarities were observed wherever checked.

All yields and G values in this paper were determined *via* wet techniques, *i.e.*, analysis after dissolution. This should be stressed, since dry results from gas chromatography or mass spectrometry of the irradiated samples consistently gave much lower quantitative yields.¹⁰ Extensive trapping or adsorption of gaseous radiation products has been demonstrated²⁰ and this study confirms these results, as well as indicating that much of the NH_3 yield may result from hydrolysis of truly primary products, perhaps imines.

Discussion

The preceding results indicate that the presence of some transition metal ions in a biochemical complex do

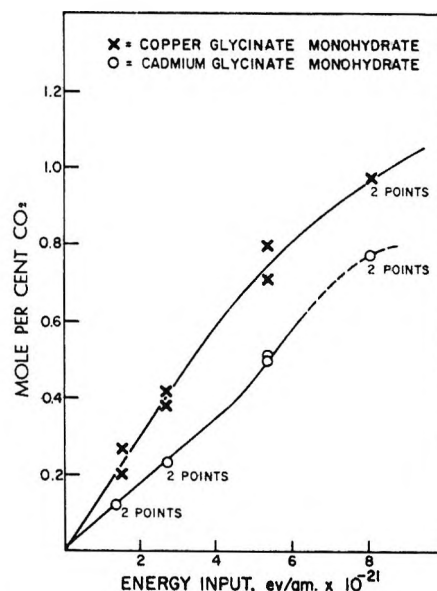


Figure 1.

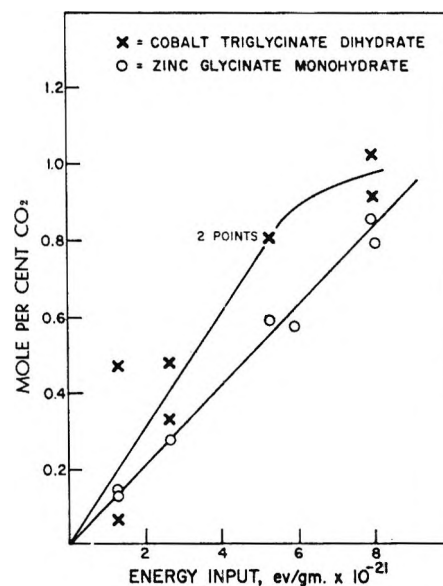


Figure 2.

indeed cause increased radiation stability. In no case was the protection an order of magnitude and the similarity, both quantitatively and qualitatively, to the decomposition pattern of the parent amino acids indicates a close parallel in their decomposition mechanisms. The mechanistic scheme proposed earlier¹⁶ hence seems applicable.

(16) W. C. Gottschall and B. M. Tolbert, submitted for publication in *J. Phys. Chem.*

(17) E. Conway, "Microdiffusion Analysis and Volumetric Error," Crosby Lockwood and Son Ltd., London, 1957.

(18) J. Russell, *J. Biol. Chem.*, **156**, 457 (1945).

(19) J. Bernal and D. Crowfoot, *Nature*, **134**, 809 (1934).

(20) J. Cunningham and H. Heal, *Trans. Faraday Soc.*, **54**, 1356 (1958).

Table II: Decarboxylation $G(\text{CO}_2)$ Values for Glycine and Alanine Chelates with Comparative Values for Physical Properties

Compound	Initial G corrected for e^- density	Metal ⁽²¹⁾ ion's 1st ion pair, eV	Metal ⁽²¹⁾ ion's 2nd ion pair, eV	Metal ⁽²¹⁾ ion's covalent radius, Å	Metal ⁽²¹⁾ ion's ionic radius, Å	Density, g/cm ³	Relative free space ⁽²²⁾
Cd(Gly) ₂ · H ₂ O	0.21	8.96	16.84	1.413	0.97	2.32	169
Zn(Gly) ₂ · H ₂ O	0.28	9.36	17.89	1.249	0.74	1.84	175
Co(Gly) ₂ · 2H ₂ O	0.32	7.81	17.3	1.157	0.4	1.82	161
Ni(Gly) ₂ · 2H ₂ O	0.34	7.61	18.2	1.149	0.69	1.84	167
Cu(Gly) ₂ · H ₂ O	0.45	7.68	20.34	1.173	0.70	1.83	174
Ni(Ala) ₂ · 2H ₂ O	0.21	7.61	18.2	1.149	0.69		
Zn(Ala) ₂ · H ₂ O	0.53	9.36	17.89	1.249	0.74		
Cu(Ala) ₂ · H ₂ O	0.99	7.68	20.34	1.173	0.70	1.74	207

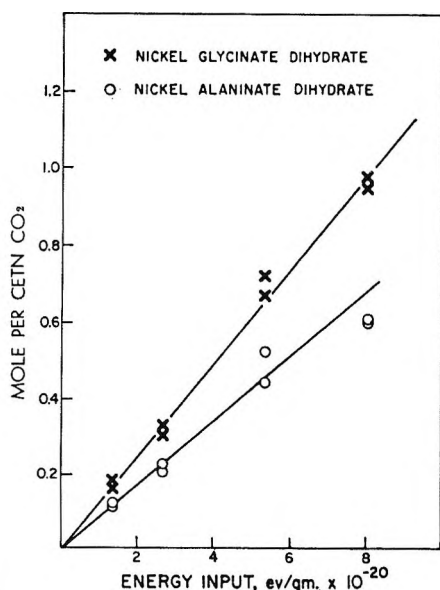


Figure 3.

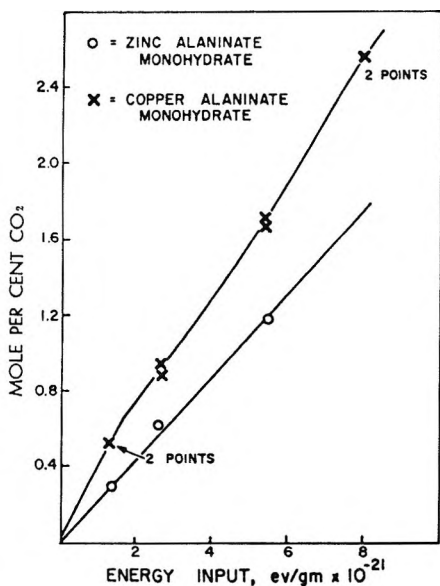


Figure 4.

Correlation of these results with various physical parameters proved fruitless with one exception. Table

II⁽²¹⁾ is a compilation of these parameters. Most are self-explanatory. The "free space"⁽²²⁾ values are the crystal volume per ion pair less the calculated cation and anion volumes, this quantity to the exponential $2/3$ based on Cunningham's diffusion-theory model. This model successfully predicted decomposition values of selected nitrates. Later work on other nitrates and on the rates of NO_3^- decomposition and NO_2^- formation failed to confirm this theory.⁽²³⁾ Our results have shown no correlation with free space.

The one successful correlation found for the glycine chelates in this study, log stability constants *vs.* G values, is illustrated in Figure 5. If one postulates an important primary radiation effect to be ejection of an oxygen electron, this series logically follows. A recent

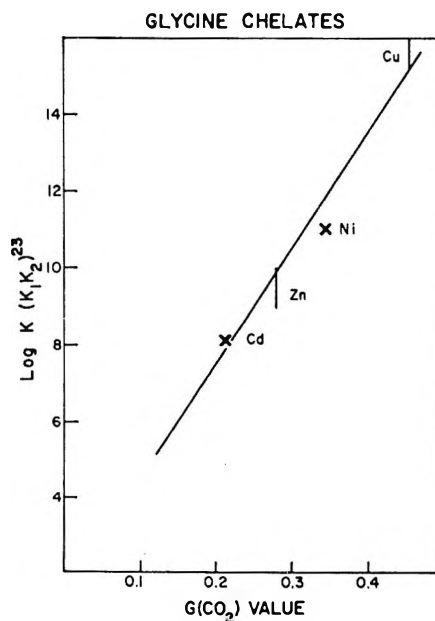


Figure 5.

(21) "Handbook of Chemistry and Physics," 36th ed, Chemical Rubber Publishing Co., Cleveland, Ohio, 1954-1955.

(22) J. Cunningham, *J. Phys. Chem.*, **65**, 628 (1961).

(23) C. Hochanadel, *Rad. Res.*, **15**, 546 (1961).

epr study by Sinclair and Hanna²⁴ confirms this concept. They find the initial fragment in irradiated L-alanine at 80° K has an unpaired electron localized mainly on the carboxy group. All evidence points to similar octahedral coordination for the transition metal ions in the solid-state chelates,²⁵⁻²⁹ thus eliminating any special geometric energy considerations or widely differing entropy effects. The generally observed increase in N:→metal bond strengths, Cu > Ni > Zn > Cd, parallels this stability constant order moreover, and hence one would assume variations in electron density on the oxygen atom still to exist but be less pronounced than, say, the variations among the alkali metal salts. In fact, the observed $G(\text{CO}_2)$ variation is lower than that observed for these salts¹⁶ and, hence, this theory seems capable of explaining both series. Application to the alanine chelates indicates a discrepancy, however, with zinc apparently out of line. A possible explanation is a different crystal structure for the zinc complex, since zinc normally exhibits tetrahedral coordination, whereas nickel and copper usually are found in octahedral or

square-planar coordination. The crystal structure would obviously be expected to exert great influence on radiation chemistry of crystalline compounds and, of course, γ radiation can deposit sufficient energy to disrupt any electron and break any bond. Other ligand series are currently being investigated to further check the validity of the proposed mechanism.

Acknowledgments. W. C. G. wish to acknowledge support from a University of Colorado Fellowship, a Du Pont Teaching Fellowship, and an NIH Predoctoral Fellowship in successive years during which the research was performed.

(24) J. W. Sinclair and M. W. Hanna, *J. Phys. Chem.*, **71**, 84 (1967).

(25) M. Calvin and A. Martell, "Chemistry of the Metal Chelate Compounds," Prentice-Hall, New York, N. Y., 1952.

(26) D. Sen, S. Mizushima, C. Curran, and J. Quagliano, *J. Am. Chem. Soc.*, **77**, 211 (1955).

(27) A. Saraceno, I. Nakagawa, S. Mizushima, C. Curran, and J. Quagliano, *ibid.*, **80**, 5018 (1958).

(28) D. Sweeny, C. Curran, and J. Quagliano, *ibid.*, **77**, 5508 (1955).

(29) K. Tomita and I. Nitta, *Bull. Chem. Soc. Japan*, **34**, 286 (1961).

Properties of Organic-Water Mixtures. VI. Activity Coefficients of

Sodium Chloride in Saturated Water-Pyridine Mixtures at 5 and 25°¹

by Richard J. Raridon, Willis H. Baldwin, and Kurt A. Kraus

Oak Ridge National Laboratory, Oak Ridge, Tennessee 37831 (Received August 23, 1967)

The solubility of NaCl in mixtures of pyridine and water was determined at 5 and 25° by packed-column techniques. Miscibility limits of pyridine and water in saturated NaCl solutions were established as a function of temperature. The pyridine-water system, saturated with NaCl, was found to have a lower consolute temperature of 11° with a broad minimum from 20 to 40 wt % pyridine. From the solubility data, activity coefficient ratios, Γ^* , of NaCl were computed. The values of Γ^* at 5°, where the system is completely miscible, and at 25°, where a miscibility gap from 6 to 63 wt % pyridine is present, did not differ appreciably. Comparison is made of activity coefficient ratios with salt rejection by hyperfiltration membranes containing poly(4-vinylpyridine).

As part of the study of water desalination by hyperfiltration (separation of salts from water by filtration through suitable membranes under pressure) thermodynamic and transport data for a variety of organic-water mixtures have been measured. Previous papers^{2,3} dealt with the comparison of activity coefficients of several salts, including NaCl, in water-organic mixtures at saturation. Several of these solvent systems showed miscibility gaps with salts present. When using model

solution systems for predicting properties of membranes, one wonders about the direct applicability of

(1) (a) Research sponsored by The Office of Saline Water, U. S. Department of the Interior under a Union Carbide Corp. contract with the U. S. Atomic Energy Commission; (b) previous paper in series: A. E. Marcinkowsky, H. O. Phillips, and K. A. Kraus, *J. Phys. Chem.*, **69**, 3968 (1965).

(2) K. A. Kraus, R. J. Raridon, and W. H. Baldwin, *J. Am. Chem. Soc.*, **86**, 2571 (1964).

(3) C. F. Coleman, *J. Phys. Chem.*, **69**, 1377 (1965).

the values of the activity coefficients, γ_{\pm}^* , of salts obtained in homogeneous systems to these intrinsically two-phase systems. Estimation of γ_{\pm}^* for partially miscible systems and suitable interpolations seem satisfactory if one can assume that the presence of a miscibility gap has little influence on the activity coefficients of the salt, although, of course, activities of the water and organic components can be very different for miscible and immiscible systems.

The present paper deals with a test of this assumption with the pyridine–water system. There is a large miscibility gap in this system at 25° when saturated with NaCl. However, at low temperatures (<11°), the pyridine–water system saturated with NaCl is completely miscible and activity coefficients can be measured by the solubility method in the same solvent system but under conditions of both miscibility and immiscibility.

Experimental Section

1. *Method.* The solubilities were measured using the packed-column techniques previously described.^{2,4} These techniques are particularly well suited for measurements at other than ambient temperatures. Analyses were by titration with silver nitrate, using chromate as indicator, except for measurements at pyridine contents of 95% or greater where a Buchler–Cotlove chloridometer was used to obtain the desired accuracy. It was necessary to evaporate the pyridine from the collected samples because of interference with the titration.

For the miscibility studies, weighed amounts of pyridine and water were added to a 5-ml flask. Sufficient NaCl was added to saturate the mixture. The flask was placed in a water bath and the mixture agitated with a magnetic stirrer. The temperature was gradually changed and visual observation was used to determine the maximum temperature for miscibility in the presence of solid NaCl.

2. *Materials.* Reagent grade NaCl was used, with a stated maximum impurity of 0.025%. It was dried for 24 hr at 400° to remove traces of moisture. The pyridine was purified by standard distillation techniques. It was analyzed by Karl Fischer titration and was found to contain 0.07% water.

Results and Discussion

1. *Miscibility Limits.* Pyridine and water, which are miscible in all proportions, are salted out by NaCl.⁵ In the present study, we found that the miscibility gap at 25° extends from ca. 6 wt % pyridine to ca. 63 wt % pyridine when saturated with NaCl. The gap is smaller at lower temperatures and disappears entirely below ca. 11°. Measurements of maximum temperature for miscibility at saturation with NaCl were made at selected pyridine–water compositions in the presence of solid NaCl. Readings made as the temperature was

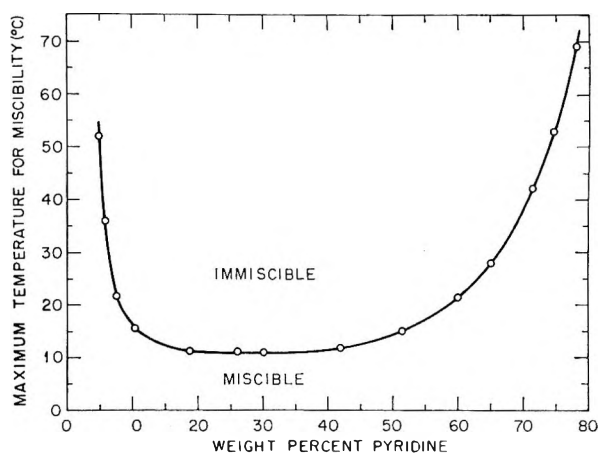


Figure 1. Effect of temperature on the miscibility of pyridine–water mixtures saturated with NaCl.

increased and then decreased, generally agreed to within 0.5°. The results are shown in Figure 1. The miscibility curve is asymmetrical, with a broad minimum extending from 20 to 40 wt % pyridine, at which the maximum miscibility temperature is 11°. The curve rises rapidly at high water contents, with the maximum miscibility temperature being over 100° at 4.5 wt % pyridine. There is a gradual increase in maximum temperature with increasing pyridine content between 40 and 65 wt % pyridine, beyond which there is a rapid rise in the maximum temperature.

2. *Solubility of NaCl.* The solubility of NaCl was measured at 5° over the entire range of pyridine–water compositions and at 25° in the organic-rich end of the phase diagram (above 63 wt % pyridine). The results are given in Table I. The solubilities at 5° are somewhat lower (at the same solvent composition) than those at 25°, except at 95 wt % pyridine, where the solubility of NaCl at 5° seems slightly higher than at 25°.

Table I: Solubility of NaCl in Pyridine–Water Mixtures at 5 and 25°

Wt % pyridine	Solubility in mixed solvent, g/kg		Activity coefficient ratios, Γ^*	
	5°	25°	5°	25°
0.0	357	360	1.00	1.00
25.0	225	...	1.19	...
50.0	113	...	1.58	...
65.0	50.5	53.2	2.47	2.37
75.0	18.3	20.6	4.88	4.37
85.0	3.43	3.95	15.6	13.6
90.0	1.13	1.14	31.6	31.6
95.0	0.18	0.15	99	120
99.9		<0.001		

(4) K. A. Kraus, H. O. Phillips, and F. Nelson, "Radioisotopes in the Physical Sciences and Industry, Sept 1960," Vol. III, IAEA, Vienna, 1962.

(5) P. M. Ginnings, B. Webb, and E. Hinohara, *J. Am. Chem. Soc.*, 55, 4898 (1933).

3. *Activity Coefficients of NaCl.* The results at different temperatures can be compared in terms of an activity coefficient ratio, $\Gamma^* = \gamma_{\pm}^*/\gamma_{\pm}$ where the activity coefficient in the mixed solvent, γ_{\pm}^* , is computed on the same basis as that in water (γ_{\pm}), namely, by using the same standard state as in water and expressing concentrations in moles per kilogram of water. Γ^* thus measures the relative selectivity of the medium for salt and water; it is a useful quantity for evaluation of model solutions for hyperfiltration membranes.⁶

If s_{aq} is the solubility in pure water and s_o is the solubility in the water-organic mixture, both expressed in moles per kilogram of solvent, and f_w is the fractional water content of the pyridine-water mixture (kilogram of water per kilogram of solvent), Γ^* is given by

$$\Gamma^* \equiv \gamma_{\pm}^*/\gamma_{\pm} = s_{aq}f_w/s_o \quad (1)$$

Γ^* is approximately the same as γ_{\pm}^* for NaCl since, by coincidence, at saturation $\gamma_{\pm NaCl} \approx 1$.

Values of Γ^* obtained in the present study are listed in Table I. The variation of Γ^* with temperature is less than the variation of solubility, since NaCl is slightly less soluble at the lower temperature. The miscibility gap at 25° seems to have no substantial effect on the activity coefficient ratios in the miscible region of the solvent system at 25°.

Although activity coefficients are evaluated here at saturation (activity $a_{NaCl} = 38.4$) rather than infinite dilution, correlation with dielectric constants ϵ seems of interest. Dielectric constants of pyridine-water mixtures were measured (see Table II) at 25° with a cell and bridge arrangement essentially identical with that used by Fuoss and coworkers.⁷ Values of ϵ for the mixtures at 5° were calculated assuming a linear variation of $\log \epsilon$ with temperature, as is the case with water and pure pyridine over this temperature range.⁸ For pyridine, $d \log \epsilon/dT = -0.00182$ and for water $d \log \epsilon/dT = -0.00204$; for intermediate compositions the slopes were assumed to vary linearly with water content.

Table II: Dielectric Constants of Pyridine-Water Mixtures

Wt % pyridine	Dielectric constant	
	25°	5° ^b
0	78.5	86.2 ^a
25	64.0	70.1
50	49.5	54.1
65	40.4 ^a	44.1
75	33.9	37.0
85	26.4 ^a	28.8
90	22.3	24.3
95	18.0 ^a	19.6
100	13.2	14.4 ^a

^a Interpolated values. ^b Values for mixtures calculated from 25° values by extrapolation using temperature coefficients given in text.

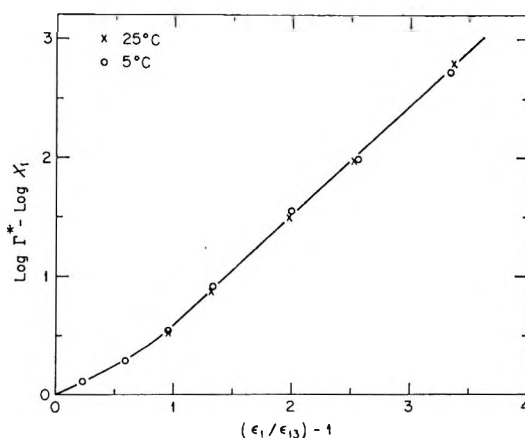


Figure 2. Activity coefficients of NaCl at saturation in pyridine-water mixtures.

In Figure 2, $\log \Gamma^* - \log X_1$ (X_1 is the mole fraction of water in the mixture) is plotted vs. $(\epsilon_1/\epsilon_{13}) - 1$, where ϵ_1 and ϵ_{13} are the dielectric constants of water and of the water-pyridine mixture, respectively. The plot is linear, except for a slight curvature near the origin. Qualitatively a linear variation of $(\log \Gamma^* - \log X_1)$ with $((\epsilon_1/\epsilon_{13}) - 1)$ is perhaps expected. Lanier⁹ used a similar plot, suggested by Scatchard,¹⁰ to compare activity coefficients (at infinite dilution of salt) in different water-organic systems. Lanier employed an emf method to measure NaCl activities as a function of concentration and then extrapolated to get γ_{\pm}^* at infinite dilution. He found that the quantity $(\log \gamma_{\pm}^* - \log X_1)$ vs. the same reciprocal function of the dielectric constant (ρ in ref 9 corresponds to ϵ_{13}/ϵ_1) gives plots that are roughly linear, but with different slopes for different water-organic mixtures. Apparently similar linear variations hold at saturation. The curvature near the origin occurs at high water contents and high solubilities where, in addition to the Debye-Hückel function, terms linear in concentration become increasingly important for representing activity coefficients.

4. *Some Implications for Hyperfiltration.* In hyperfiltration (removal of salts from solution by pressure filtration through suitable membranes) limiting salt rejection R_{∞} at sufficiently high fluxes of water is related to a distribution coefficient D^* at the entrance interface by⁶

$$1 - R_{\infty} = \beta D^* \quad (2)$$

(6) J. S. Johnson, L. Dresner, and K. A. Kraus in "Principles of Desalination," K. S. Spiegel, Ed., Academic Press Inc., New York, N. Y., 1966.

(7) J. E. Lind, Jr., and R. M. Fuoss, *J. Phys. Chem.*, **65**, 999 (1961).

(8) F. Buckley and A. A. Maryott, "Tables of Dielectric Dispersion Data for Pure Liquids and Dilute Solutions," National Bureau of Standards Circular No. 589, U. S. Government Printing Office, Washington, D. C., 1958.

(9) R. D. Lanier, *J. Phys. Chem.*, **69**, 3992 (1965).

(10) G. Scatchard, *ibid.*, **68**, 1056 (1964).

Here β is a coupling coefficient which is presumed to be usually between 0 and 1. Thus, a low value of D^* is equivalent to good limiting salt rejection and for $\beta = 1$, $R_\infty = 1 - D^*$. The distribution coefficient (for uncharged membranes) in turn is related to the activity coefficient ratio by $D^* = 1/\Gamma^*$. Present observations support the view that the miscibility gap, which by necessity exists in a membrane-water system, does not seriously affect prediction of D^* from the values of Γ^* obtained from a suitable model water-organic system. Hence one predicts that pyridine-containing membranes should have good salt-rejecting properties at sufficiently low water content and dielectric constant. Predicted asymptotic rejections R_∞ for $\beta = 1$ for a "pyridine membrane" are given as a function of f_w in Figure 3 and as a function of $(\epsilon_1/\epsilon_{13}) - 1$ in Figure 4. We presume that the dielectric constant variable is more directly applicable to membranes which, in general, will also contain other groups. Since for neutral membranes $\beta \leq 1$, the values of R_∞ given should be lower limits. Also, at a given water content Γ^* and hence R_∞ are usually less at saturation than at lower activities a .

We have attempted to prepare hyperfiltration membranes from various pyridine derivatives but with only limited success. Membranes prepared by grafting poly(4-vinylpyridine) to cellulose membranes (Schleicher and Schuell 06, 07, and 08) yielded salt rejections of 20–45% (0.5 M NaCl) and fluxes of 1–4 gal/day ft² at 1500–2000 psi pressure.

In attempts to cast poly(4-vinylpyridine) from various solvents, a membrane prepared from a methanol-glycerol solvent mixture (0.5 g of polymer in 5 ml of methanol and 1 ml of glycerol) gave 70% salt rejection (0.5 M NaCl); flux was only 1.5 gal/day ft² at 2500 psi pressure. However, considering the thickness of this neutral membrane (43 μ , measured wet), its flux seems high. A cellulose acetate membrane of the same thickness should have a flux of 0.14 gal/day ft² if Reid and Breton's permeability data¹¹ are used.¹²

The water content of this membrane was 48.8%, as determined by "wet" and dry weighings. Using the values of Γ^* for pyridine (Figure 3) at this composition, one predicts that $(1 - R_\infty) \leq 0.62$ or $R_\infty \geq 0.38$. As already mentioned, there are several reasons why one expects R_{obsd} to be larger than the computed limiting value of R_∞ . (Effects which might cause R_{obsd} to be less than R_∞ are concentration polarization and too low a pressure to reach R_∞ . We presume that these effects should be negligible here.) The observed rejection was obtained at $M = 0.5$, rather than at saturation; D^* should be less (or Γ^* larger) at $M = 0.5$ than at saturation.⁹ The calculations refer to pyridine; a substituted pyridine (e.g., methylpyridine) with a presumably lower dielectric constant and hence probably higher values of Γ^* should be a better model. Finally, the calculations assume $\beta = 1$; values of $\beta < 1$ for this system are not

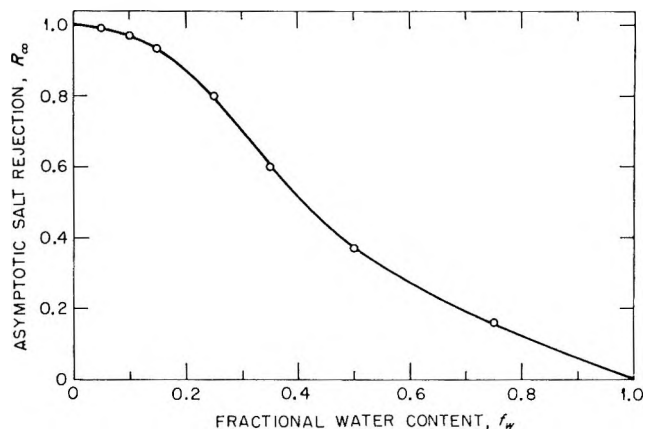


Figure 3. Computed salt rejection for pyridine system (saturated NaCl, $\beta = 1$).

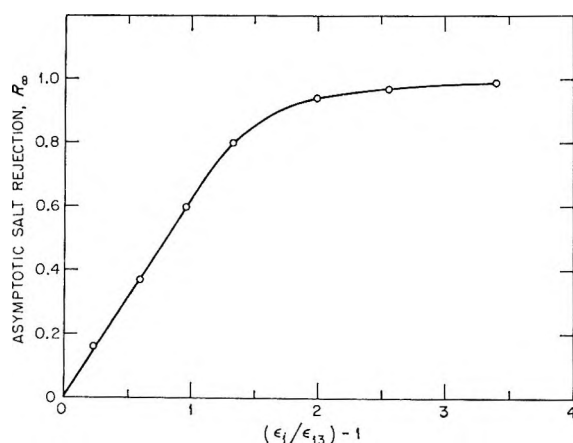


Figure 4. Computed salt rejection for pyridine system (saturated NaCl, $\beta = 1$).

unexpected. We thus consider the agreement between computed and observed rejections satisfactory and conclude that this membrane probably was reasonably homogeneous and free of pinholes.

Use of the dynamic technique¹³ gave poly(4-vinylpyridine) membranes with somewhat better rejections and fluxes. Thus chloride rejection of 90% was observed with sea water at fluxes of 3 gal/day ft² at 1500 psi pressure. Presumably, this membrane had a somewhat lower water content and was much thinner than the cast membrane. Hopefully, still thinner membranes will eventually be prepared which permit fuller exploitation of the attractive intrinsic salt-rejecting properties of these pyridine-based materials.

Acknowledgment. We are greatly indebted to J. S.

(11) C. E. Reid and E. J. Breton, *J. Appl. Polymer Sci.*, **1**, 133 (1959).

(12) R. J. Raridon, L. Dresner, and K. A. Kraus, *Desalination*, **1**, 210 (1966).

(13) K. A. Kraus, A. J. Shor, and J. S. Johnson, Proceedings of the Second European Symposium on Fresh Water from the Sea, Athens, 1967; *Desalination*, **2**, 243 (1967).

Johnson for permission to quote the hyperfiltration results and for many helpful discussions. We are

also indebted to M. D. Danford, C. G. Westmoreland, J. Curny, and Neva Harrison for technical assistance.

Detailed Studies of a One-Electron, Two-Photon Ionization in a Rigid Organic Solution at 77°K^{1,2}

by K. D. Cadogan and A. C. Albrecht

Department of Chemistry, Cornell University, Ithaca, New York 14850 (Received August 24, 1967)

A quantitative spectrophotometric study is made of the photoionization of N,N,N',N'-tetramethyl-*p*-phenylenediamine (TMPD) in 3-methylpentane (3MP) rigid solution at 77°K. Some extension is also made to an ether-isopentane-ethanol (EPA) rigid solution. The ionization is shown to proceed by a biphotonic mechanism with the metastable triplet state as the second photon-absorbing intermediate. It is further shown by polarization measurements that ionization of the triplet state occurs by direct excitation into the continuum or near continuum. Quantitative estimations are obtained and wavelength dependence is determined for the quantum efficiencies of both one-photon steps.

I. Introduction

For some time now it has been known that it is possible to photoeject electrons from organic molecules in rigid solutions with light energy far below the gaseous ionization potential. The mechanism of this photoionization has been the subject of much recent study. Photoconductivity studies³ produced early evidence for the involvement of two photons in the photoionization of organic molecules in the condensed phase. The system most studied in this photoconductivity work has been N,N,N',N'-tetramethyl-*p*-phenylenediamine (TMPD) in 3-methylpentane (3MP) at 77°K, which can be readily photoionized to give the monocation Wurster's blue (WB) and a "free" electron. Since then, several other biphotonic phenomena in similar systems have been observed and these will be specified below. In a preliminary report,⁴ we have presented spectrophotometric evidence supporting a biphotonic mechanism for photoionization of the TMPD-3MP system. The photoconductivity study³ naturally focuses on the mobile charge carriers (electrons), while this spectrophotometric work focuses on the other photoionization product, the stable, immobile cation (WB). The technique employed is to monitor the cation photoproduct spectroscopically while it is being formed, which is an elaboration of the initial spectrophotometric study made on this system in which the biphotonic mechanism was not discovered.⁵

The preliminary report⁴ has strongly implicated the lowest excited triplet state as a photoactive intermediate in the two-photon ionization process. The results of several quite distinct experimental studies taken together provide the evidence of triplet state involvement. These results include the observation that (1) the observed lifetime of the photochemical intermediate matches the phosphorescence lifetime; (2) the addition of O₂ quenches both the long-lived phosphorescence of TMPD, as well as the initial rate of formation of WB; (3) the wavelength dependence for creating the photochemical intermediate is the same as that for exciting phosphorescence; (4) ultraviolet excitation induces phosphorescence lifetime shortening, suggesting that there is an excitation-induced destruction of the triplet state; and (5) polarization of the second photon step, which is defined as the photoionization of the intermediate state, matches the polarization of triplet-triplet (T-T) absorption over a con-

(1) Supported by Public Health Research Grant A-3415 from the National Institute of Arthritis and Metabolic Diseases.

(2) Taken in part from the Ph.D. Thesis of K. D. Cadogan, Cornell University, Ithaca, N. Y., 1966.

(3) G. E. Johnson, Thesis, Cornell University, Ithaca, N. Y., 1965; G. E. Johnson and A. C. Albrecht, *J. Chem. Phys.*, **44**, 3162, 3179 (1966).

(4) K. D. Cadogan and A. C. Albrecht, *ibid.*, **43**, 2550 (1965).

(5) W. C. Meyer and A. C. Albrecht, *J. Phys. Chem.*, **66**, 1168 (1962).

siderable wavelength region. In what follows, the details of this spectrophotometric work will be presented with a partial extension to another system. Details of the photoionization are thereby elucidated and estimates are obtained for the efficiencies and energy requirements for each of the consecutive one-photon steps.

II. Experimental Section

A. Materials. Aniline (AN) (Mallinckrodt, purified) was vacuum distilled over zinc dust. *N,N,N',N'*-Tetramethyl-*p*-phenylenediamine (TMPD) (from TMPD-2HCl, Eastman Kodak Co.) was sublimed from the prepared base⁶ then zone refined. White crystals resulted.

The solvent 3-methylpentane (3MP) (Phillips petroleum, pure grade) was purified as described elsewhere.⁵ EPA (by volume: 5 parts diethyl ether, 5 parts isopentane, and 2 parts ethanol) (Hartman-Leddon Co., Philadelphia, Pa.) was used without further purification.

B. Apparatus and Procedure. Rectangular Pyrex or fused-quartz cells with 1×1 cm cross-sectional dimensions were used to contain the samples under study. Solution concentrations varied from 0.5×10^{-3} to 3×10^{-3} *M*. Cooling to liquid nitrogen temperature was accomplished either by simply immersing the cell in liquid nitrogen, or by attaching copper plates to the cell and immersing the copper in liquid nitrogen inside a partially unsilvered quartz dewar. This latter method eliminated the interference of liquid nitrogen bubbles and schlieren in the optical measurements. (For further details see, ref 2.)

Figure 1 is a schematic diagram of the apparatus used to study photoionization rates. A General Electric A-H6 mercury lamp in conjunction with a Bausch and Lomb 500-mm focal length grating monochromator, having a dispersion of $33 \text{ \AA}/\text{mm}$, provided ultraviolet (primary) excitation. (Excitation within the absorption bands of the solute will be called *primary* excitation.) The monochromator was positioned to make the exit slit horizontal. Both entrance and exit slits were usually set at 1-mm width. An image 0.5 cm wide and 1 mm high was focused on the cell, which was mounted so that it could be raised or lowered independently of the dewar. Because the photoionized sections of the sample were so thin, studies on previously unexposed sections of the rigid solution could be made at 2-mm intervals along the cell. As many as 20 individual studies could thereby be made on the same frozen sample. A second monitoring light beam was introduced by reflection off a thin quartz plate into the same optical path as the primary beam and focused at the same spot on the cell. This monitoring source consisted of a 110-W tungsten lamp stabilized by a constant-voltage transformer and focused through an Aminco grating monochromator (250-mm focal length,

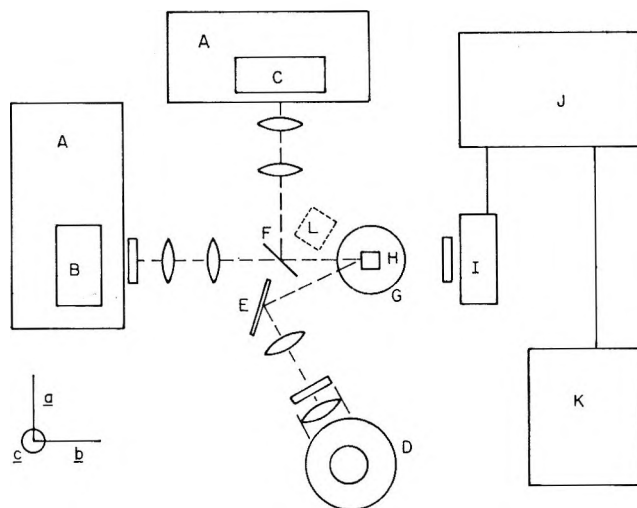


Figure 1. Schematic diagram of apparatus: A, monochromator; B, Hg lamp; C, tungsten lamp; D, Xe-Hg lamp; E, mirror; F, thin quartz plate; G, quartz dewar; H, sample cell; I, photomultiplier tube; J, Photovolt photometer (Model 520-M); K, Varian G-14 recorder; and L, additional photomultiplier.

$66\text{-\AA}/\text{mm}$ dispersion), which was also positioned to provide a horizontal slit image. Slit widths were set close to 1 mm and the focused image on the cell was typically 0.3 cm wide and 0.5 mm high. Care was taken so that the primary beam always completely overlapped the monitoring beam while passing through the cell. The rate of cation production was determined by measuring the change in optical density with the monitoring light at the $634\text{-m}\mu$ absorption peak of Wurster's blue (WB).

The detector was an RCA-1P21 photomultiplier tube attached to a Photovolt photometer (Series 520-M). The output of the photometer was fed into a Varian G-14 recorder with a counter voltage introduced to reduce the input signal to the recorder. In this way, only 20% of the photometer output could be displayed as a full-scale deflection on the recorder chart, and an intensity change as small as 0.2% in the monitoring light or, consequently, a 0.001 unit change in optical density, was detectable.

A Corning glass filter (2424) in front of the phototube served to keep out TMPD luminescence and a Corning filter (9863) in the primary-excitation beam removed any unwanted light from that source.

A typical experimental rate study is shown in Figure 2. Ignoring the initial rise in optical density (OD) which is due to triplet-triplet (T-T) absorption, it was observed that the OD increased linearly with time up to at least a 0.04-unit change, but the rate of change would eventually approach zero after prolonged excitation (1 hr or longer). To avoid complicated analysis, rate measurements were confined to the linear region. Even so, over this period at least two separate rate

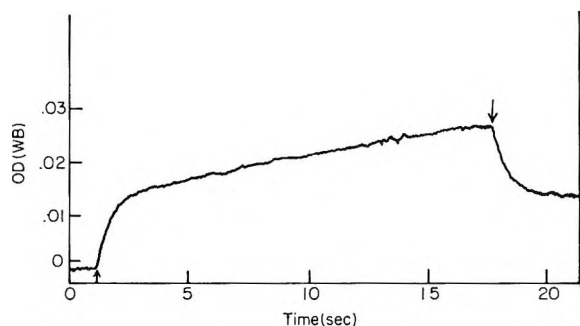


Figure 2. A typical experimental study of photoionization rate in a $1.1 \times 10^{-3} M$ rigid solution of TMPD in 3MP at 77°K exciting at $335 m\mu$ (\uparrow , light on; \downarrow , light off). The optical density is measured at $634 m\mu$. The initial rise in optical density, as well as the decay, when the excitation is cut off, is due to the buildup and collapse of the transient (triplet) state. The essentially linear increase in optical density over this time scale represents the buildup of stable cation (WB).

measurements could be made without repositioning the sample.

Since visible light can stimulate charge recombination in photoionized rigid solutions of TMPD,⁶ causing a decrease in WB concentration, it was checked and found that the weak red monitoring beam had no effect on the cation concentration.

The photoionization rate as a function of wavelength was determined at 5- $m\mu$ intervals, exposing a new section of the sample for each measurement. On any one frozen sample, a range of 50 $m\mu$ could be covered while still allowing two separate measurements at most wavelengths to essay reproducibility. Occasionally, initial slopes for two different wavelengths were measured without changing the positioning, in order to check the uniformity of the rigid solution. The average precision of initial slopes determined by these reproducibility checks was $\pm 6\%$.

The light-intensity dependence of the photoionization rate was determined by varying the light intensity with neutral density filters over a range of almost one order of magnitude. The relative primary-light intensities at different wavelengths were determined by using an integrating screen, which consisted of an aqueous solution of esculin (1 g/l.).⁷ Absolute-intensity measurements were made using a ferrioxalate actinometer.⁸

For double-beam excitation, a method similar to that used in the photoconductivity work was employed. The additional source of excitation introduced (see Figure 1) was an Hanovia 2500-W xenon-mercury short-arc lamp intercepted by Corning filters (3850) and (5850) plus an $NiSO_4$ solution. This filter combination cuts off all light below $360 m\mu$ and passes a band peaking around $380 m\mu$. This second source of excitation is called the *secondary* beam and does not directly excite the solute. When used alone, a negligible amount of photoionization occurs, but when employed in conjunction with the primary excitation, it dra-

matically enhances the rate of ionization. Wavelength- and intensity-dependence studies of the ionization rate were repeated with this additional beam flooding the sample. As much as a 200-fold secondary-beam enhancement over primary excitation alone was observed when the primary light was sufficiently weak. In any case, at least a tenfold enhancement was always maintained. To accomplish this it was necessary, at times, to reduce primary-light intensities with neutral density filters in the regions of strongest A-H6 lamp output. As a check, a few two-beam measurements were also made with the secondary source focused at a right angle to the primary beam.

The influence of oxygen on the photoionization was determined by studying a rigid solution with essentially three different, rather cleanly separated layers of oxygen concentration. This was accomplished simply by freezing the sample slowly from the bottom up while bubbling first helium and then oxygen through the still fluid portion. Photoionization rates as well as the steady-state phosphorescence intensity were measured in each layer. This intensity should reflect oxygen levels inversely, since oxygen quenches TMPD phosphorescence.

Rate studies were also made with polarized excitation beams. The monitoring beam was already accidentally almost completely polarized along one laboratory axis (*c*), largely because of reflection off the quartz plate; however, experiments were also done with the polarization rotated 90° . The intensity of the monitoring light for the unfavorable polarization was quite weak, but still suitable. Double Glan prisms were used to polarize each of the two excitation beams and a polaroid sheet effected polarization of the monitoring beam. For these experiments, the secondary beam was focused at right angles to the primary beam (along the *a* laboratory axis).

The above details apply to work with the TMPD-3MP system. Some changes were necessary in order to study the photoionization of aniline (AN) in EPA. The tungsten monitoring lamp was replaced by a compact Hanovia 150-W xenon arc lamp which was used to monitor at $420 m\mu$. This is, where the photoproduct, which is assumed to be the cation, has a maximum in its visible absorption band. Unfortunately the phosphorescence band of AN is in this same wavelength region. The resulting serious interference, due to phosphorescence, was eliminated by bucking with a signal from a second phototube positioned (see Figure 1) to pick up only sample phosphorescence. Photoionization proceeded much more slowly in the AN-EPA system, and the xenon lamp was somewhat less stable than the

(6) W. M. McClain and A. C. Albrecht, *J. Chem. Phys.*, **43**, 465 (1965).

(7) E. J. Bowen, *Proc. Roy. Soc. (London)*, **A154**, 349 (1936).

(8) C. G. Hatchard and C. A. Parker, *ibid.*, **A235**, 518 (1956).

tungsten lamp, but rate studies could still be made with reasonable reproducibility.

When secondary excitation was required, a band just outside of the first absorption band of AN was isolated with Corning filters (4303, 5850, 9788, and 9863).

III. Results and Discussion

The presentation of the results with discussion is divided into three main parts. In part A, the kinetic studies are presented showing the biphotonic nature of the ionization. The intermediate-state lifetime is also determined. The results are discussed within the simplest possible kinetic scheme. In part B, three additional experiments are presented which bear on the ionization mechanism. Finally, part C outlines our efforts to make quantitative statements concerning the efficiencies of each of the two-photon steps. It must be emphasized that the identification of the triplet state as the photochemical intermediate follows because of the simple kinetic scheme employed. This scheme is not unique, and more complicated models, involving additional intermediate states, are possible which allow the photochemical intermediate to be distinct from the triplet state and which, at the same time, can assimilate all of the present results. However, until additional evidence demands otherwise, we choose to analyze the data within the framework of the simple kinetic scheme and, as will be seen, this forces the identification of the triplet state as the photochemical intermediate.

A. Kinetic Studies. 1. Two-Photon Ionization and Kinetic Scheme. Typical results of the primary light intensity dependence studies are illustrated in Figure 3. The biphotonic nature of the ionization is clearly established by the nearly exact quadratic dependence of the photoionization rate on light intensity. The two-photon ionization mechanism being proposed is based on the triplet-state intermediate and is indicated schematically in Figure 4. In this scheme, $D(S_0)$ is the unexcited donor solute molecule, S_1 and T_1 are the thermally equilibrated lowest excited singlet and triplet states, respectively, of the solute, while P is the one-electron-ionized product (consisting of the electron and the cation). The highly excited state or group of states from which ionization can result through some radiationless steps is symbolized by χ .

Utilizing this scheme, the initial rate of cation production, S_1 , is derived in Appendix A-1 giving

$$S_1 \equiv \frac{dA}{dt} = \frac{\epsilon_P}{2} \tau_p \phi_i \epsilon_T \phi_{IC} I_0^2 (1 - e^{-2\epsilon_D C_D l}) \quad (1)$$

Here A is the optical density (absorbance) of the sample at the monitoring wavelength; ϵ_D and ϵ_T are the molar extinction coefficients in appropriate units of species D and T , respectively, at the wavelength of excitation; ϵ_P is the extinction coefficient of the product at the monitoring wavelength; ϕ_{IC} and ϕ_i are the quantum

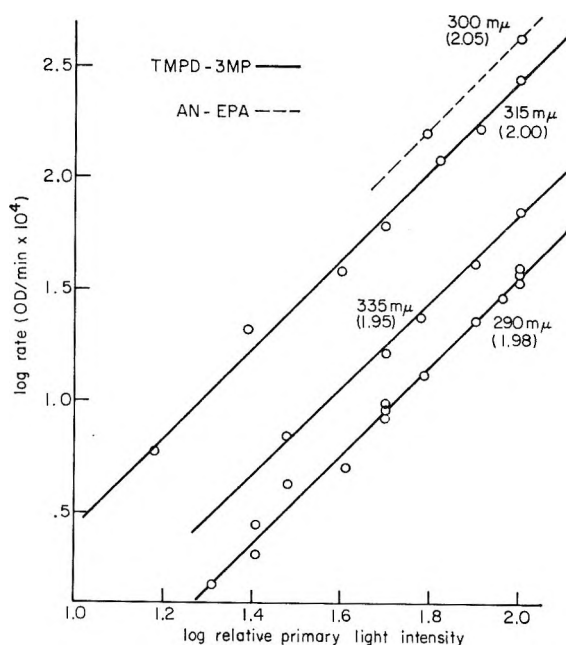


Figure 3. Log of photoionization rate vs. log of relative primary light intensity at different wavelengths. The slope of each plot appears in parentheses.

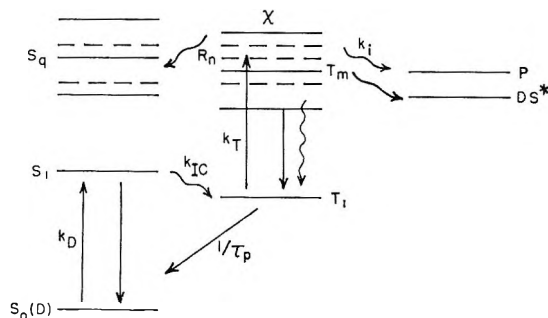


Figure 4. Schematic diagram of the proposed two-photon ionization mechanism. The dashed lines indicate Rydberg near-continuum levels (R) which are likely precursors to the fully ionized product, P . Radiative decay is indicated by \rightarrow , and radiationless decay by $\sim\sim\sim$. The decay from the excited triplet manifold has four distinct paths: return to the lowest triplet state, transfer to the excited singlet manifold, ionization with the formation of P , or energy transfer to the solvent giving an excited solvent and ground-state solute (or a possible solvent-solute complex) indicated by (DS^*).

efficiencies for intersystem crossing from the singlet manifold and ionization from the state χ , respectively; τ_p is the phosphorescence (triplet) lifetime during primary excitation (which is negligibly different from the dark lifetime); C_D is the initial concentration of D ; l is the cell length; and I_0 is the incident primary-light intensity. In the derivation of eq 1, it is assumed that species D is negligibly depleted and that the photo-products are not competitive for light absorption. This assumption is reasonable in this study because rate measurements are confined to the linear region of the optical density rise and conversion to the triplet state is kept well under 5% (see Table V below). It is al-

so assumed that the long-lived photochemical intermediate (T_1) has equilibrated, a condition assured because rate measurements are made after the lowest triplet state has reached steady state. Equation 1 predicts the observed quadratic dependence of the rate S_1 on primary-light intensity.

When, in addition to the primary light, the secondary source of excitation is included, the initial rate becomes

$$S_2 \equiv \frac{dA}{dt} = \epsilon_T \tau_p' \phi_i' \epsilon_T' \phi_{IC} I_0' I_0 (1 - e^{-\epsilon_D C_D t}) \quad (2)$$

by a derivation sketched in Appendix A-2. Here ϵ_T' is the average triplet extinction coefficient for the band of secondary light, τ_p' is the phosphorescence lifetime during secondary illumination, ϕ_i' is the average ionization efficiency induced by secondary excitation, and I_0' is the incident secondary-light intensity. It is assumed that I' is constant over the cell width (no absorption by solute) and that the secondary source is sufficiently intense and energetic to supersede the primary source in the photochemical excitation of the triplet intermediate. (See below for evidence.)

Equation 2 predicts a linear dependence of the ionization rate on both the primary- and secondary-light intensity. The linear dependence on primary-light intensity is verified by the results in Figure 5. The dependence of S_2 on the secondary beam was checked in a rough way by reducing I_0' by 50% with a neutral density filter. The intensity exponent for I_0' determined in this way varied from 0.7 to 1.0, in essential agreement with eq 2.

2. *Intermediate-State Lifetime.* By measuring the lifetime (τ_I) of the photochemical intermediate, direct proof (within the simple kinetic scheme) that it is the lowest triplet state would be obtained if it can be shown that $\tau_I = \tau_p$ (as we have already assumed above). Two related techniques were employed to measure τ_I directly, utilizing alternating one- and two-beam excitation.

When the cation production is followed while the sample is being exposed to periodically interrupted primary excitation, a chart trace, such as illustrated in Figure 6, is obtained. The cation optical density rise during the excitation periods is obscured by the superimposed triplet-triplet (T-T) absorption.

However, when the dark periods are made long enough to allow the T-T absorption to disappear, the underlying optical density due to cation absorption can be measured. An average rate of cation production (\bar{S}_1) can be determined by dividing the observed increase in the stable (nontransient) optical density per excitation period by the periodic exposure time.

By a simple analysis worked out in Appendix B-1, $(\bar{S}_1)_\rho$ can be derived as a function of τ_I , the exposure time per cycle (ρ), and the steady-state slope S_1 , measured with uninterrupted excitation, giving

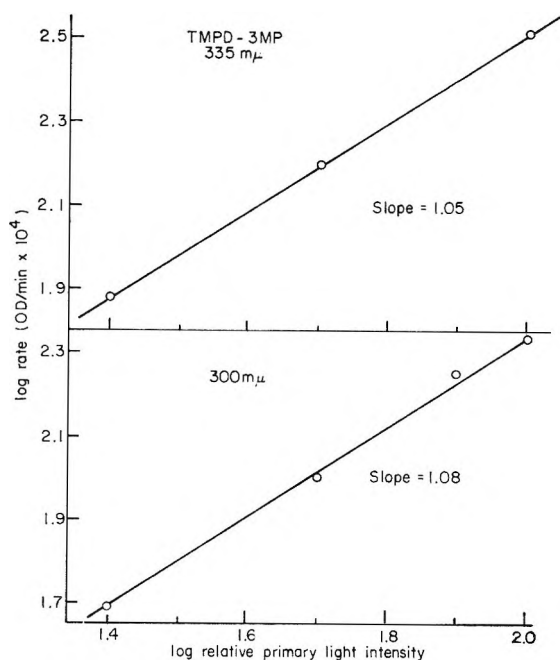


Figure 5. Primary light intensity dependence of photoionization rate under secondary-beam excitation.

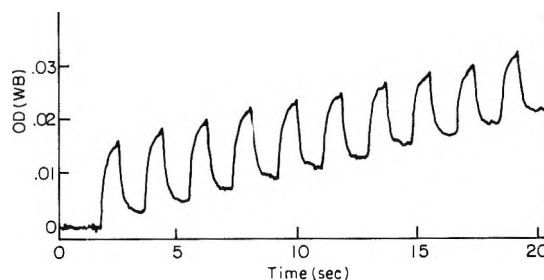


Figure 6. A typical experimental study of photoionization rate for periodically interrupted excitation at 300 $m\mu$ of a $1.1 \times 10^{-3} M$ rigid solution of TMPD in 3MP. The periodic fast rise and decay is due to triplet-triplet absorption following the periodic excitation.

$$F(\tau_I, \rho) = \tau_I(1 - e^{-\rho/\tau_I}) = \rho \left(1 - \frac{(\bar{S}_1)_\rho}{S_1}\right) \quad (3)$$

For a given ρ , τ_I can be determined from a graph of $F(\tau_I)$ vs. τ_I . The values of τ_I obtained for the TMPD-3MP system are listed in Table I and, given the estimated experimental error, they are in excellent agreement with the phosphorescence lifetime for TMPD.

An alternate method for measuring τ_I involves exposing the solution to secondary excitation during the dark periods of primary excitation. In this case of alternating two-beam excitation, the average rate of cation production is composed of two contributions

$$(\bar{S}) = \frac{\rho}{\rho + \delta} (\bar{S}_1)_\rho + \frac{\delta}{\rho + \delta} (\bar{S}_2)_\delta \quad (4)$$

where $(\bar{S}_2)_\delta$ is the contribution from secondary excita-

Table I: Results of Experimental Measurements of Intermediate-State Lifetime in TMPD-3MP Rigid Medium

λ , m μ	τ_I , ^a sec		ρ , sec	δ , sec	τ_p , sec
	One beam	Two beam			
335	2.5 \pm 0.6	2.5 \pm 0.5	15.3	44.7	2.35
290	2.8 \pm ?		15.3	44.7	
335	2.1 \pm 0.3		12.2	17.8	

^a The maximum range of error is estimated by taking the extreme values obtained.

tion during the dark periods (δ) of primary excitation. After first determining $(\bar{S}_1)_p$ by blocking the second beam, $(\bar{S}_2)_\delta$ can be determined through eq 4. As shown in Appendix B-2, the function $F(\rho, \tau_I)$ can be evaluated in this case as

$$F(\rho, \tau_I) = \tau_I(1 - e^{-\rho/\tau_I}) = \frac{\delta(\bar{S}_2)_\delta}{\bar{S}_2} \quad (5)$$

and for a given ρ and δ , the value of τ_I can again be obtained. The average value of τ_I obtained in this manner is included in column 3 of Table I and, again, good agreement with τ_p is obtained.

B. Three Further Studies. Three additional investigations, very different in nature, have been completed which provide helpful insight into the ionization mechanism. The studies deal with: (1) oxygen effects on the initial rate, (2) radiatively induced lifetime shortening of the intermediate state, and (3) kinetic studies using polarized light to determine the degree of anisotropy of the second photon act. The results are discussed in turn.

1. Oxygen Quenching. Oxygen quenches the phosphorescence of TMPD in rigid solutions and should therefore similarly quench the rate of photoionization, if indeed the rate depends linearly on the lowest triplet-state concentration. The results of the oxygen quenching studies definitely bear this out. A plot of the initial ionization rate (S_1) vs. the steady-state phosphorescence intensity (I_p), obtained by measuring both quantities at various positions along a rigid solution with an oxygen-concentration gradient should extrapolate linearly through the origin. A typical result of such a plot is displayed in Figure 7 which clearly reveals the direct proportionality of S_1 and I_p . It should be noted that (Figure 7) the rate measurements in the region of highest oxygen concentration consistently fell above the extrapolated line to an extent beyond experimental error. Why this was so is not yet understood.

It is certain, however, that oxygen plays a more complex role in these systems than merely that of quenching triplet states. Oxygen is also an effective electron trap, and the photoproduced cation is much less stable if oxygen is removed from solution.⁶ It is essential to limit

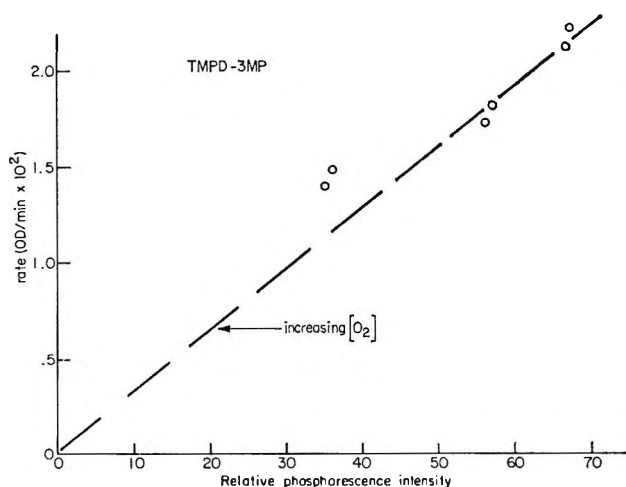


Figure 7. Initial rate of photoionization vs. relative steady-state phosphorescence intensity in a solution with an oxygen concentration gradient.

observations to initial rates if the influence of oxygen on the primary photochemical processes is to be studied. In several experiments on He-O₂ double-layered samples, the rate of WB production under monochromatic excitation was followed well beyond the initial rate region. It was observed (Figure 8) that only in the initial period of excitation was the rate of photoionization in the O₂-free portion significantly faster than in the O₂-saturated portion. These observations may explain why the rate of WB formation previously appeared to be independent of the oxygen concentration,⁵ since previous measurements were not confined to the initial rates.

The phenomenon of oxygen quenching in rigid solutions is also of interest in itself, because, although an oxygen concentration of approximately 5×10^{-3} M is sufficient to quench the phosphorescence by 50%, it was found to have no significant effect on the lifetime τ_p . Thus the possibility of significant quenching by slowly diffusing oxygen molecules seems to be ruled out (as any consideration of viscosity would suggest) and apparently the quenching oxygen molecules must be somewhat permanently bound close enough to the affected solute molecules to bring about almost immediate decay of the triplet state. This can only be true at such low concentration of O₂ and TMPD if in the fluid solution oxygen tends to complex with TMPD.

2. Radiation Effects on Triplet Lifetimes. Since the reciprocal of the triplet-state lifetime is just the sum over all unimolecular (or pseudo-unimolecular) decay constants, the triplet-state lifetime during the primary excitation is written as

$$\tau_p = \frac{1}{\epsilon_T I [\phi_i + \phi_\chi] + (1/\tau_p^0)} \quad (6)$$

where τ_p^0 is the dark lifetime, the quantum efficiency for ionization from the states χ is given by ϕ_i , while ϕ_χ

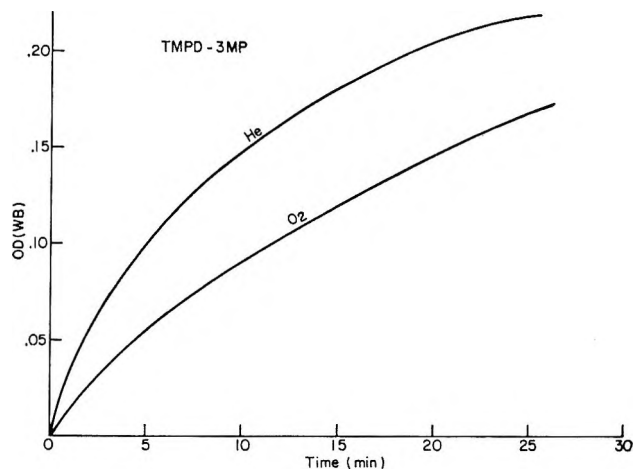


Figure 8. Photoionization study over an extended period of time in a double-layered He-O₂ saturated TMPD-3MP rigid solution ($1.2 \times 10^{-3} M$).

represents the efficiency for all other excitation-induced triplet depopulation processes that do not lead to stable cation formation. For the case of double-beam excitation, in which the secondary light dominates the triplet excitation processes, the lifetime becomes

$$\tau_p' = \frac{1}{\epsilon_T' I_0' (\phi_i' + \phi_x') + (1/\tau_p^0)} \quad (7)$$

where the primes indicate the presence of secondary excitation.

Equations 6 and 7 predict that the lifetime of the triplet state can be reduced during excitation if either ϕ_i or ϕ_x is nonzero. Successful attempts were made to observe such a lifetime shortening in τ_p and also in the lifetime of the optical density of triplet absorption (τ_{A_T}). This constitutes additional proof that the triplet state is being directly ionized by the radiation. Both the TMPD-3MP solution and the aniline-EPA solution were studied and τ_p was measured in the presence of secondary excitation and primary excitation. The effect of secondary excitation on τ_{A_T} was also measured for the TMPD solution and, of course, the effect should be and was identical with that observed for τ_p .

Typical results obtained by measuring the decay of τ_p and τ_{A_T} during exposure to secondary excitation are shown in Table II. It can be seen that a reduction from the dark lifetimes by as much as 20% could be effected. The possibility that the observed shortening is due to warming of the solute by the secondary light can be easily discarded because the solvents do not absorb in the region of the secondary band. (The infrared is filtered out.) Also a study already made⁹ has proved that intense visible light (with a solvent filter) has no effect on the rigidity of 3MP by noting that the orientation of WB is unaltered by prolonged exposure.

Table II: Typical Excitation-Induced Lifetime-Shortening Results for Phosphorescence and T-T Absorption (sec)

	τ_p^0 (dark)	τ_p' (secondary excitation)	τ_p^0 (dark)	τ_p (primary excitation)
TMPD (phos)	2.47	2.15	2.40	2.29
A _T	2.48	2.20		
AN (phos)	4.50	3.63	4.41	4.04

The effect of primary excitation on τ_p was determined by observing decay rates after a 60% transmitting neutral density filter was placed in the primary beam. Typical results obtained for both the aniline and the TMPD solutions are included in Table II.

Because of this radiatively induced lifetime shortening, the rate of triplet-state depopulation *via* excitation can be calculated from the observed reduction in τ_p and can be compared with the ionization rate. The frequency of triplet-state depopulation due to secondary excitation is, from eq 7

$$\frac{1}{\tau_p'} - \frac{1}{\tau_p^0} = \epsilon_T' [\phi_i' + \phi_x'] I_0' \quad (7')$$

It is shown in Appendix A that

$$S_2 = \epsilon_P \phi_i' \epsilon_T' I_0' \int_0^l C_T(x) dx$$

where $C_T(x)$ is the triplet concentration at a distance x inside the sample, and since $\int_0^l C_T(x) dx = A_T(\lambda)/\epsilon_T(\lambda)$, where λ is any wavelength in the triplet absorption bands, it follows that

$$\phi_i' \epsilon_T' I_0' = \frac{S_2}{\epsilon_P} \frac{\epsilon_T(\lambda)}{A_T(\lambda)} \quad (8)$$

In order to evaluate the ionization rate coefficient ($\phi_i' \epsilon_T' I_0'$) from eq 8, it is necessary to know the extinction coefficient ϵ_T' or at least the ratio of ϵ_T'/ϵ_P . There is some reason to believe that at the visible absorption peaks of WB and TMPD triplet states, the above ratio is close to unity. Justification for this belief will be discussed below, where estimated values of the extinction coefficient ratios are given. The frequency of ionization (8) can be compared now, with the frequency of depopulation (7') by measuring S_2 , A_T , and τ_p' under the same conditions, and they should agree if $\phi_x' = 0$. This was carried out for the case of irradiated TMPD solutions with the results shown in Table III.

For single-beam excitations the quantities to be compared are $(1/\tau_p) - (1/\tau_p^0)$ and $S_1 \epsilon_T'/\epsilon_P A_T$. The results for both TMPD and aniline irradiation are also included in Table III. In every case, the agreement is good

(9) A. C. Albrecht, unpublished work.

Table III: Ionization Rate Coefficients Compared with Rates Determined from Excitation-Induced Phosphorescence Lifetime Shortening in TMPD-3 MP and AN-EPA Rigid Media (sec⁻¹)

	$\frac{1}{\tau_p} - \frac{1}{\tau_p^0}$	$\frac{S_1 \epsilon_T^{*a}}{\epsilon_P A_T}$	$\frac{1}{\tau_p'} - \frac{1}{\tau_p^0}$	$\frac{S_2^* \epsilon_T^a}{\epsilon_P A_T}$
TMPD	0.025 ± 0.005 (315 mμ)	0.008 ± 0.001	0.068 ± 0.008 (335 mμ)	0.032 ± 0.003
Aniline	0.019 ± 0.002 (300 mμ)	0.007 ± 0.002		

^a The asterisk indicates that the assumption $\epsilon_T(610 \text{ m}\mu)/\epsilon_P(634 \text{ m}\mu) = 0.79$ is made.

enough between the values of both functions to support the interpretation offered to explain the phenomenon of radiation-induced lifetime shortening. Looking more closely at the results, the rate determined from the measured lifetime reduction is consistently larger than the ionization rate. If this discrepancy can be believed (which depends primarily on the accuracy of the value assigned to the ratio ϵ_T/ϵ_P), it indicates that other decay paths, besides ionization, are effectively competing with the decay to the lowest triplet state; that is, $\phi_\chi \neq 0$. At least two possible alternate processes are intersystem crossing from the highly excited triplet χ state into the singlet manifold and energy transfer to a solvent molecule. Intersystem crossing from upper levels is not commonly seen, although not much is known in this regard for levels near the ionization continuum. On the other hand, energy transfer to the solvent actually is quite likely, since a number of benzene derivatives have been shown to photosensitize solvent radical formation and it has also been found, by esr measurements,¹⁰ that TMPD photosensitizes solvent radical formation in rigid solutions. This is especially conspicuous in 3MP and isopentane mixtures. The mechanism generally proposed for photosensitized reactions in rigid solutions involves energy transfer from a highly excited triplet state to a solvent molecule. The polarization results presented below, however, make very clear that the solute triplet which may transfer its energy to the solvent is not the usual N-V triplet, but rather a near-continuum triplet. Another observation in the TMPD-3MP system may further indicate that such an energy transfer is occurring. Under steady illumination the equilibrium TMPD phosphorescence (I_p) diminishes slowly: too slowly to interfere with the kinetic studies, but faster than can be accounted for either by depletion of the solute or by attenuation of the exciting light due to screening by the photoproduct. Any such depletion or screening should also be detected as a decline of TMPD fluorescence which, in fact, decreases much more slowly than the phosphorescence. I_p has been observed to decrease under steady illumination in systems (for one, naphthalene in methylocyclohexane) where no solute photoproducts were detected and it has been explained by assuming that solvent radicals formed by solute-solvent

energy transfer were quenching solute triplet states.¹¹

3. Polarization of Intermediate-State Absorption. The polarization of the transition $T \rightarrow \chi$ resulting in ionization can be investigated by ionizing oriented samples of T with polarized secondary excitation. Oriented triplet states can be created in solid solutions by polarized primary excitation at wavelengths where the solute absorbs along a preferred molecular axis. It is known¹² that TMPD absorbs primarily along its short in-plane axis at 335 mμ, while at 280 mμ it absorbs along its long in-plane axis. When primary light at one of these two selective wavelengths is polarized along the *c* laboratory axis (see Figure 1), the secondary photons incident along the *a* laboratory axis will see oriented triplet intermediates. Anisotropy in the photochemically active $T \rightarrow \chi$ transitions will be revealed by a dependence of the photoionization rate on whether the secondary light is polarized along the *b* or *c* laboratory axis. The results of such a study are tabulated in Table IV, which shows that the rate (S_2) was observed to be independent of the polarization of secondary light. This indicates that the photoionization of the intermediate state occurs isotropically in the region of second-beam activity. More generally, it is found that the excitation-induced lifetime shortening of the phosphorescence (2.50–2.18 sec in the case studied) is also independent of the polarization of the second beam. The second observation indicates that *all near-wv radiative routes for depopulating the triplet state are isotropic*—not only the photoionizing route.

In order to determine whether the polarized secondary light intensity was in any way biased in favor of either *c*- or *b*-axis polarization, control measurements were made by exciting with *a*-axis-polarized primary light. For simple geometric reasons, the oriented triplets resulting from *a*-axis-polarized primary excitation will appear completely randomized to the secondary photons (when viewing along *a*). Thus, independently of the absorption characteristics of the triplet intermediate, no dependence of photoionization

(10) P. M. Johnson, Ph.D. Thesis, Cornell University, Ithaca, N. Y., 1967.

(11) S. Siegel and K. Eisenthal, *J. Chem. Phys.*, **42**, 2494 (1965).

(12) A. H. Kalantar and A. C. Albrecht, *Ber. Bunsenges. Physik. Chem.*, **68**, 361 (1964).

Table IV: The Dependence of the Photoionization Rate on the Relative Polarizations of Primary and Secondary Excitation in a TMPD-3MP Rigid Solution

Monitoring-beam polarization (634 m μ) ^a	Primary wavelength and polarization ^a	Secondary-beam polarization ^a	S _p ^b
335 m μ			
$\leftrightarrow a$	$\uparrow c$	$\uparrow c$	0.0079
$\leftrightarrow a$	$\uparrow c$	$\leftrightarrow b$	0.0074
280 m μ			
$\uparrow c$	$\uparrow c$	$\uparrow c$	0.0049
$\uparrow c$	$\uparrow c$	$\leftrightarrow b$	0.0052
$\leftrightarrow a$	$\uparrow c$	$\leftrightarrow b$	0.0021
$\leftrightarrow a$	$\uparrow c$	$\uparrow c$	0.0022
335 m μ ^c			
$\uparrow c$	$\leftrightarrow a$	$\uparrow c$	0.0072
$\uparrow c$	$\leftrightarrow a$	$\leftrightarrow b$	0.0072

^a See Figure 1 for coordinate system used. However, here the secondary beam is incident along *a*. ^b In units of optical density of WB at 634 m μ /sec. ^c Control (see text).

rates on second beam-polarization should be observed. The results of this blank measurement are also contained in Table IV and it can be seen that no correction for secondary-beam bias is necessary.

A further check on the reliability of the polarization studies can be made by varying the direction of polarization of the monitoring beam. (See column I of Table IV.) It has previously been determined¹³ that WB absorbs along its long in-plane axis in its visible absorption band and that, therefore, the optical density ratio (A_{\parallel}/A_{\perp}) observed when the monitoring light is polarized parallel (A_{\parallel}) (*c* direction) and perpendicular (A_{\perp}) (*a* direction) to the 280-m μ exciting light should theoretically be 3.0. Since the ratio A_{\parallel}/A_{\perp} is equivalent to a ratio of rate slopes, from Table IV (taking averages) the ratio is $505/215 = 2.35$, in good agreement with ratios usually observed.¹² This is also an indication of the anisotropic orientation of the photo-selected triplet states.

Thus, from these polarization studies, it can be concluded that the photochemical intermediate absorbs isotropically, at least when averaged over the near-uv band of secondary excitation.

This isotropic behavior of the photoionization from the intermediate state finds its parallel in polarized absorption studies of the oriented triplet state.¹⁴ Here the visible absorption band is quite anisotropic. However, as soon as the blue and near-ultraviolet region is reached—where the second photon is active—the triplet absorption becomes isotropic. This isotropy is on a much finer energy scale (~ 5 -m μ band width) than is this second-beam photochemistry (~ 40 -m μ band

width). This detailed isotropic behavior over a considerable wavelength region certainly precludes accidental overlapping of a small number of differently polarized bands. Instead it raises the distinct possibility that one is exciting into a continuum or near continuum of states with several polarizations possible within a small energy interval. These states may be derived from the high-energy Rydberg states near the ionization continuum of the isolated molecule. The coincidence of the isotropic behavior in triplet-state absorption and in the second-photon step of the photoionization offers still more evidence for the triplet state as the intermediate state.

C. Some Quantitative Aspects: Quantum Efficiencies of Each of the Two Steps. 1. The First-Photon Step. The radiative excitation in the first-photon step is taken to be excitation into the excited singlet states with a known efficiency determined by the absorption spectrum. The efficiency of the over-all first-photon step rests, in addition, on the efficiency of conversion from the excited singlet state to the photochemical intermediate. This latter efficiency will be designated as ϕ_{IC} . The wavelength dependence of ϕ_{IC} can be determined from photoionization measurements using eq 2, where the product $\epsilon_p \tau_p' \phi_T' \epsilon_T' I_0'$ is independent of primary excitation. It is already known^{3,5} from phosphorescence measurements that for TMPD the intersystem crossing efficiency to the triplet state is constant over the entire absorption region of interest as would be expected. If the lowest triplet state is the intermediate state in the photoionization, then ϕ_{IC} determined from eq 2 should also show no wavelength dependence. The results displayed in Figure 9 confirm this.

The absolute value of ϕ_{IC} has not been measured in TMPD. If one knew the triplet-state extinction coefficient, its concentration could be fixed and ϕ_{IC} determined.

Normally an independent determination of C_T is quite difficult. However for TMPD there is good reason to believe that one can arrive at a good estimate of the oscillator strength of the visible T-T band. In TMPD the visible T-T absorption band is remarkably similar in energy, structure, and polarization to the visible band of WB.¹⁴ For these and other reasons,¹⁴ it can be speculated that the oscillator strength for these two bands should be about the same. If it is assumed that the oscillator strengths are identical, then it has been determined that

$$\epsilon_T(610 \text{ m}\mu) = 0.79 \epsilon_P(634 \text{ m}\mu) \quad (9)$$

at the respective visible absorption peaks of the two bands. Now if the concentration of triplet states is

(13) A. C. Albrecht and W. T. Simpson, *J. Am. Chem. Soc.*, **77**, 4454 (1955).

(14) K. D. Cadogan and A. C. Albrecht, submitted for publication.

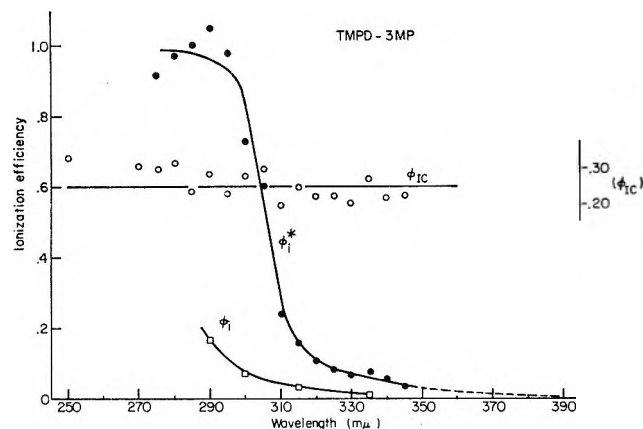


Figure 9. Wavelength dependence of intersystem crossing efficiency, ϕ_{IC} , and wavelength dependence of ionization efficiency, ϕ_i and ϕ_i^* , as defined in text, in the TMPD-3MP system.

integrated over the depth of the cell, eq A-4 of Appendix A becomes (after using Beer's law for $I(x)$)

$$\bar{C}_T = \int_0^l C_T(x) dx = \phi_{IC} \tau_p I_0 (1 - e^{-\epsilon_D C_D l}) = \frac{A_T(\lambda)}{\epsilon_T(\lambda)} \quad (10)$$

where λ is the monitoring wavelength and where \bar{C}_T is the total moles of triplet TMPD produced under steady-state illumination per square centimeter. Equation 10 with eq 9 can be used to evaluate ϕ_{IC} and the value determined at 300 m μ is included in Table V, as well as an estimated value of \bar{C}_T (converted to mole per liter) at the intensity of excitation used in the determination. The values of $\phi_{IC}(\lambda)$ in Figure 9 were put on an absolute scale by matching with the estimated value in Table V.

Table V: Quantitative Estimates of Intersystem Crossing and Ionization Quantum Efficiencies in TMPD-3MP Rigid Solution

C_D , M	I_0^a (300 m μ), photons/ cm ² sec	ϵ_T^b (610 m μ)	\bar{C}_T/l , M	ϕ_{IC} (300 m μ)	ϕ_i (300 m μ)
1.1×10^{-3}	5.05×10^{16}	1.1×10^4	5×10^{-6}	0.27	0.11

^a This I_0 was higher than that used in most of the experiments, and the monochromator slits were open 2 mm. ^b Molar, decadic extinction coefficient based on that of WB (see eq 9 in text).

2. *The Second-Photon Step.* The parameter pertaining to the second-photon step is ϕ_i the absolute efficiency for ionizing the intermediate state. The relative wavelength dependence of ϕ_i can be determined throughout the range of primary excitation from eq 1, taking the product $\epsilon_P \tau_P \phi_{IC}$ to be wavelength independent, provided that $\epsilon_T(\lambda)$ is known throughout the range of primary excitation. The T-T absorption

bands have been determined, in at least a preliminary way, across the region of primary excitation revealing strong, structured bands¹⁴ and the approximate shape of $\phi_i(\lambda)$ that results is illustrated in Figure 9. However, additional thought must be given to the meaning of $\phi_i(\lambda)$. A question always posed in photochemical studies must be asked: Is the photoreactive absorption band identical with or hidden beneath the observed absorption band?

The strong T-T absorption at wavelengths <340 m μ responsible for the observed ϵ_T is undoubtedly due mostly to N-V transitions in the triplet manifold. Now it can be asked whether these N-V transitions or underlying continuum transitions are responsible for ionization in the region of primary excitation. The latter alternative must be chosen for the following reasons. As already mentioned, TMPD in its lowest triplet state absorbs isotropically in the very near ultraviolet.¹⁴ Given the basic anisotropy of the molecular state, this has given rise to the suggestion that one is dealing with transitions into a continuum or near continuum of states. It has also been shown that this near-ultraviolet continuum absorption initiates photoionization (this is the onset of second-photon activity.) It can be inferred from the following additional information that direct absorption into the continuum continues to be the important prerequisite for photoionization at higher energies also (where measurements are complicated by the presence of TMPD absorption). It is known that the anisotropy of photoproducted WB follows in detail the anisotropy of TMPD fluorescence across the entire first absorption band of TMPD.¹⁵ The generation of WB and the excitation of fluorescence share the first-photon step—namely, excitation of TMPD into its first excited singlet state. The second-photon step is required only for making WB. Because of the identical behavior of the two polarized photoselection experiments, it must follow that the second-photon step in the ionization is isotropic in the wavelength region corresponding to TMPD absorption—as well as at the lower energies (very near ultraviolet) studied directly here. In light of this important information (which was also discovered for *p*-phenylenediamine¹²), it must be concluded that the second transition resulting in ionization must be completely isotropic from its low-energy threshold to at least 280 m μ . Now there is a strong T-T absorption band¹⁴ which peaks near 300 m μ . Although a direct measure of its anisotropy was not achieved, one expects this transition to be anisotropic for the following reasons. This ultraviolet T-T absorption seems to represent one or two intense transitions to states, which are evidently easily coupled with the lowest triplet state. Each such state

(15) A. H. Kalantar and A. C. Albrecht, *J. Phys. Chem.*, **66**, 2279 (1962).

should be responsive to the molecular symmetry and a transition to it should be polarized. N-V transitions are in this category and the near-ultraviolet transitions of WB—very similar to these T-T transitions—are known to be anisotropic.¹³ If indeed these ultraviolet bands are anisotropic much as is the visible T-T band (but not the near-ultraviolet T-T absorption), it must follow that these conspicuous ultraviolet T-T transitions do not lead to any significant ionization. Rather an underlying, isotropic continuum band is responsible for photoionization.

If this conclusion is correct, then $\phi_i(\lambda)$, determined from eq 1, does not represent the efficiency of ionization from the *photochemically active* transitions. Let this latter efficiency be called $\phi_i^*(\lambda)$. In order to estimate the efficiency $\phi_i^*(\lambda)$ for the ionizing transition, it will be assumed that $\epsilon_T^*(\lambda)$, the extinction coefficient for the continuum transitions, is constant across the region of primary excitation and equal to its value around 380 m μ (estimated as 1.8×10^3 , ref 14). This simply corresponds to extrapolating its monotonous behavior from the very near ultraviolet into the near ultraviolet. Now $\phi_i^*(\lambda)$ can be determined by rescaling $\phi_i(\lambda)$ as follows

$$\phi_i^*(\lambda) = \phi_i(\lambda) \frac{\epsilon_T(\lambda)}{\epsilon_T^*(\lambda)} = \frac{S_1(\lambda)}{I_0^2(\lambda)(1 - e^{-2\epsilon_D C_D^l})} \frac{1}{K} \quad (11)$$

where $K \equiv (\epsilon_P/2)\tau_p\phi_{IC}\epsilon_T^*$ is constant with respect to wavelength. The resulting curve for $\phi_i^*(\lambda)$ is included in Figure 9. The quantitative scale for ϕ_i and ϕ_i^* in Figure 9 was achieved as follows. By combining eq 1 and 10, one obtains

$$\phi_i(\lambda) = \frac{2S_1(\lambda)(1 - e^{-\epsilon_D C_D^l})}{I_0(\lambda)(1 - e^{-2\epsilon_D C_D^l})\epsilon_T(\lambda)} \frac{\epsilon_T(\lambda')}{A_T(\lambda')\epsilon_P} \quad (12)$$

where λ' is the monitoring wavelength. The ratio $\epsilon_T(\lambda')/\epsilon_T(\lambda)$ can be determined from the T-T spectrum in ref 14 and is equal to 0.88 when λ equals 300 m μ and λ' equals 610 m μ . In principle, no assumptions about the absolute value of ϵ_T are necessary to evaluate ϕ_i , and its estimated value at 300 m μ , determined in the same experiment in which ϕ_{IC} was estimated, is included in Table V.

Now eq 11 can be used to approximate $\phi_i^*(300 \text{ m}\mu)$. Using values for $\epsilon_T^*(300 \text{ m}\mu)$ and $\epsilon_T(300 \text{ m}\mu)$ of 1.8×10^3 (by extrapolation from 380 m μ) and 17.4×10^3 , respectively, it is calculated that $\phi_i^*(300 \text{ m}\mu)$ equals 1.0. This is in interesting agreement with the fact that ϕ_i^* reaches a plateau at 300 m μ . Therefore $\phi_i^*(\lambda)$ was plotted in Figure 9 on an absolute scale with a maximum at unity (ignoring the value at 270 m μ , where the measurements were least accurate in any case).

The $\phi_i^*(\lambda)$ curve in Figure 9 can be compared with the gaseous ionization efficiency curve obtained for N,N-dimethylaniline in the vacuum ultraviolet.¹⁶

There is an interesting similarity in that the vacuum ultraviolet efficiency first levels off about 1.1 eV above the ionization threshold as does $\phi_i^*(\lambda)$ for TMPD. However, the gaseous ionization efficiency is still well below unity, since at higher energies it rises sharply to new levels. The second and third step-ups in the gaseous ionization efficiency curve were interpreted as being associated with the removal of a π electron from the lower occupied benzene orbitals. These subsequent step-ups in efficiency cannot be seen in the rigid solutions if ϕ_i^* reaches unity as quickly as it apparently does.

It must be emphasized that these quantitative results rest on at least two assumptions. First, a scaling of T-T absorption to an extinction coefficient basis was made by a comparison with the visible oscillator strength of WB.¹⁴ Second, the continuum T-T extinction coefficient, which is seen¹⁴ to be constant over the very near ultraviolet, was arbitrarily continued as the same constant down to $\sim 270 \text{ m}\mu$. These assumptions lead to the quantitative and physically reasonable scaling found in Figure 9. The shape of ϕ_i^* and its saturation in the vicinity of unity would seem to give some confidence to the procedures used. This behavior of ϕ_i^* also reinforces the view that the ionizing states, χ , are continuum or near-continuum states as required by the polarization results.

IV. Conclusions

The accumulated evidence presented above leaves little doubt that, at least for the TMPD-3MP systems, photoionization involves a two-photon mechanism with the solute lowest triplet state as the major photoactive intermediate. In addition, it has been shown that there is very good reason to believe that the second-photon absorption act causes ionization by promoting an electron directly into the ionization continuum. It follows that the threshold for ionization of the lowest triplet state of TMPD in 3MP at 77°K is 3.1 eV (the onset of second-photon activity). Since the triplet state is 2.8 eV above the ground state, the threshold for ionization of TMPD is 5.9 eV in this system. This may be compared with the gaseous ionization potential measured by indirect means to be 6.6¹⁷ or 6.7 eV.¹⁸

It is probable that photoionization in rigid solutions quite generally involves a two-photon mechanism, although this was only further verified for an AN-EPA system in this work. It has been shown¹⁹ that thermoluminescence from a number of aromatic hydrocarbon solutions in 3MP at 77°K depends quadrati-

(16) M. E. Akopyan, F. I. Vilesov, and A. N. Terenin, *Dokl. Akad. Nauk SSSR*, **140**, 1037 (1961); also F. I. Vilesov and M. E. Akopyan, *ibid.*, **158**, 1386 (1964).

(17) G. Briegleb and J. Czekalla, *Z. Elektrochem.*, **63**, 6 (1959).

(18) R. Foster, *Nature*, **183**, 1253 (1959).

(19) W. A. Gibbons, G. Porter, and M. I. Savadatti, *ibid.*, **206**, 1355 (1965).

cally on the exciting-light intensity. This was explained by postulating that the underlying photochemical process is a two-photon photoionization. It has also been determined²⁰ that the photoionization of 3,4-benzpyrene in boric acid glass depends quadratically on excitation intensity. If the excitation energy is high enough, there should be no need to involve an intermediate step and a single sufficiently energetic photon should be able to ionize the solute. The direct transition from ground state to ionization continuum should not be much weaker than the triplet-continuum transition discussed here. In fact, in the work just cited, ref 20, the intensity dependence was reported to become linear when the photon energy exceeded the threshold of double photon ionization of 3,4-benzpyrene by an amount approximately equal to the energy of the lowest triplet state.

Photoionization is not confined to the rigid phase. It has been demonstrated²¹ that fluid solutions of aromatic amines in *n*-hexane can be photoionized with an intense flash as evidenced by a transient increase in the sample conductivity, and more recently it has also been shown²² by conductivity measurements that a biphotonic mechanism is involved in the photoionization of liquid solutions of TMPD-3MP, although the nature of the intermediate state was not established.

Other biphotonic phenomena in similar systems have been observed. Principally through esr techniques various photosensitized reactions in rigid organic solutions have been studied.²³⁻²⁹ These reactions have been shown to proceed generally by a two-photon mechanism with strong evidence presented in several systems identifying the lowest triplet state of the photosensitizer as the second photon absorbing intermediate.

An important generalization from the present work is the suggestion that even photosensitization (as opposed to ionization) may proceed through Rydberg-like near-continuum states, rather than well-defined excited triplet states of the solute molecule. This point emerged from the observation that triplet-state lifetime shortening, when studied with polarized light, is *isotropic* and that a large part of the lifetime shortening is due to processes (like sensitization) other than ionization. It may even be that sensitization proceeds *via* charge-pair recombination states following partial ionization.

It is becoming quite evident that the lowest solute triplet state, because it is conveniently long lived, is often involved in two-photon reactions. However, this cannot automatically be assumed. A case in point seemed to be the photoconductivity results mentioned in the introduction. In this same laboratory, it was demonstrated that the production of mobile electrons in the same TMPD-3MP system involves a two-photon process in which the triplet state was definitely ruled out as the intermediate. The results presented in this paper may at first seem to be in direct contradiction

to these photoconductivity results. This seeming contradiction was a major reason that such detailed studies were undertaken to identify the triplet state as the intermediate in cation production. However, recent photoconductivity experiments³⁰ have revealed that the triplet state is indeed implicated in photocurrent generation. It turns out that photoconductivity measurements are complicated by the fact that electrons, once ejected, can fall into a variety of solvent traps which are in turn photoionized (one photon) and contribute to the observed photocurrent (the photocurrent is, in a sense, triphotonic). It becomes difficult to distinguish between possible metastable filled solvent traps and metastable true intermediates in the primary biphotonic process. It is hoped that the new photoconductivity work, soon to be published, will partially resolve the curiously conflicting pictures which have emerged when studying cation production on the one hand (present work) and "free" electron generation on the other (photoconductivity work).

The major challenge posed by the present study is to identify more closely the two-photon-excited solute-solvent states responsible for electron emission as well as for sensitization processes. It may turn out that states closely related to the near-ionization-continuum Rydberg levels of the isolated molecule are of primary importance. In the language of the solute-solvent system, these states may well be closely related to very energetic solute-solvent charge-transfer states.

Appendix A: Kinetics Analysis

1. *Derivation of Eq 1.* Using the two-photon model sketched in Figure 4, the rate coefficients for the two photoexcitation steps are

$$k_D(x, t) = \epsilon_D I(x, t)$$

and

$$k_T(x, t) = \epsilon_T I(x, t)$$

where $I(x, t)$ is the primary-beam photon flux at a distance (x) inside the sample from the surface of incidence

(20) J. P. Ray and T. D. S. Hamilton, *Nature*, **206**, 1040 (1965).

(21) U. Krog, H. Ruppel, and H. T. Witt, *Ber. Bunsenges. Physik. Chem.*, **67**, 795 (1963).

(22) H. S. Pilloff and A. C. Albrecht, *Nature*, **212**, 499 (1966).

(23) B. Smaller, *ibid.*, **195**, 593 (1963).

(24) V. E. Kholmogorov, E. V. Baranov, and A. N. Terenin, *Dokl. Akad. Nauk SSSR*, **149**, 142 (1963); **152**, 1399 (1963).

(25) Kh. Bagdasaryan, Z. A. Sinitsyna, and V. I. Muromtsev, *ibid.*, **152**, 349 (1963); **153**, 374 (1963); also Kh. Bagdasaryan and Z. A. Sinitsyna, *ibid.*, **160**, 625 (1965).

(26) V. G. Vinogradova, B. N. Shelimov, N. V. Fok, and V. V. Voevodskii, *ibid.*, **154**, 188 (1964).

(27) For a recent complete review of this topic see the session on biphotonic processes, The Eighth International Symposium on Free Radicals, Novosibirsk, U. S. S. R., Session V, July, 1967.

(28) P. Douzon and M. Ptak, *J. Chim. Phys.*, **61**, 1681 (1964).

(29) Y. U. Kozlov and D. N. Shigorin, *Dokl. Akad. Nauk SSSR*, **161**, 871 (1965).

(30) K. D. Cadogan and A. C. Albrecht, submitted for publication.

after t sec of excitation and ϵ_D and ϵ_T are the extinction coefficients as already defined in the text. Now, most generally, $I(x, t)$ is by Beer's law

$$I(x, t) = I_0(t)e\left[-\int_0^x \sum_j C_j(x, t)\epsilon_j dx\right]$$

C_j represents the concentration of the j th species and the summation includes the unexcited solute concentration as well as all photoproducts. However, it is assumed in this analysis that species D is negligibly depleted and that the photoproducts are not competitive for light absorption, *i.e.*

$$\epsilon_D C_D \gg \sum_j' C_j(x, t)\epsilon_j$$

where the primed summation is over all photoproducts, *i.e.*, cation and triplet state. Thus $I(x, t)$ can be simplified to

$$I(x, t) \cong I(x, 0) = I_0 e^{-C_D \epsilon_D x} \quad (\text{A-1})$$

where I_0 is the incident primary-light intensity.

Assuming the mechanism outlined in Figure 4, the initial rate of cation production is

$$\frac{dC_P(x)}{dt} = k_i C_\chi(x) \quad (\text{A-2})$$

ignoring higher order recombination terms. The states χ can be presumed to have a lifetime (τ_χ) short enough to be almost immediately in equilibrium, therefore their concentration is

$$C_\chi(x, t) = \epsilon_T C_T(x, t) I(x) \tau_\chi \quad (\text{A-3})$$

where $C_T(x, t)$ is the concentration of the solute triplet-state intermediate. Also, since rate measurements are made after initial times long enough to allow the lowest triplet state to reach steady state

$$\begin{aligned} C_T(x, t) = C_T(x) &= \phi_{IC} k_D(x) C_D \tau_p \\ &= \phi_{IC} \epsilon_D C_D I(x) \tau_p \end{aligned} \quad (\text{A-4})$$

where ϕ_{IC} is the efficiency for intersystem crossing and τ_p is the phosphorescence lifetime during primary excitation.

In order to express the ionization rate in terms of the observed rate of optical density (A) change, the cation concentration must be integrated over the depth of the cell

$$\frac{dA}{dt} = \gamma \epsilon_P \int_0^l \frac{dC_P(x)}{dt} dx \quad (\text{A-5})$$

or, by combining eq A-2, A-3, A-4, and A-5

$$\frac{dA}{dt} = \gamma \epsilon_P \phi_i \epsilon_D C_D \phi_{IC} \epsilon_T \tau_p \int_0^l I^2(x) dx \quad (\text{A-6})$$

$\phi_i \equiv k_i \tau_\chi$ is the quantum efficiency for ionization from the state χ and ϵ_P is the isotropic or average extinction coefficient of the cation at the monitoring wavelength.

γ is an anisotropy correction factor which is needed because neither the photoreactant nor the photoproduct absorbs isotropically and photochemistry (with polarized or unpolarized light) produces an oriented sample in rigid media. The analysis necessary to determine γ has already been worked out¹³ and will be discussed for present conditions in Appendix C and it will be found that for the present study $\gamma \cong 1$. Since τ_p is experimentally determined to be within 5% of the dark lifetime (τ_p^0), it is assumed constant and removed from under the integration sign. Utilizing eq A-1 and integrating (with C_D constant) gives

$$S_1 \equiv \frac{dA}{dt} = \frac{\epsilon_P}{2} \tau_p \phi_i \epsilon_T \phi_{IC} I_0^2 (1 - e^{-2\epsilon_D C_D l}) \quad (\text{A-7})$$

2. *Derivation of Equation 2.* When the secondary source of excitation is included, the rate constant for triplet-state excitation becomes

$$k_T(x) = \epsilon_T I(x) + \epsilon_T' I'$$

where (primes indicating secondary excitation) I' is the secondary photon flux and ϵ_T' is the average triplet extinction coefficient for the band of secondary light. Since there is essentially no solute absorption by secondary light, I' is constant over the cell and can be replaced by I_0' , the incident flux. If the secondary source of excitation light is sufficiently intense and energetic to supersede the primary beam in the photochemical excitation of the triplet intermediate, *i.e.*, if

$$\epsilon_T' I_0' \gg \epsilon_T I(x)$$

where $0 \leq x \leq l$, then k_T can be approximated as

$$k_T = \epsilon_T' I_0'$$

Now for the case of two-beam excitation, in analogy with the development of eq A-7

$$S_2 \equiv \frac{dA}{dt} = \gamma' \epsilon_P \phi_i' \epsilon_T' I_0' \int_0^l C_T(x) dx \quad (\text{A-8})$$

$$= \gamma' \epsilon_P \phi_i' \epsilon_T' \tau_p' \epsilon_D C_D \phi_{IC} I_0' \int_0^l I(x) dx$$

where τ_p' is the phosphorescence lifetime during secondary excitation, and ϕ_i' is the average efficiency for ionization from the state(s) χ produced by secondary excitation. The same anisotropy correction factor can be used as in the single-beam experiments, since it is shown (see text) that only the primary absorption act determines photoproduct orientation (that is, the second photon is absorbed isotropically). Thus $\gamma' = \gamma \cong 1$ (see Appendix C). Integrating eq A-8, since eq A-1 is still a good approximation, gives

$$S_2 = \epsilon_P \tau_p' \phi_i' \epsilon_T' \phi_{IC} I_0' I_0 (1 - e^{-\epsilon_D C_D l}) \quad (\text{A-9})$$

Appendix B: Kinetics in Intermittent Photochemistry

1. *One-Beam Excitation.* When the cation pro-

duction is followed while the sample is being exposed to periodically interrupted excitation, a chart trace, such as illustrated in Figure 6, is obtained. The cation optical density rise during the excitation periods is obscured by the superimposed triplet-triplet (T-T) absorption. However, when the dark periods are made long enough to allow the T-T absorption to disappear, the underlying optical density due to cation absorption can be measured. An average rate of cation production (\bar{S}_1) can be measured by dividing the observed increase in nontransient optical density per excitation period by the periodic-exposure time.

After t sec of excitation, the concentration of the intermediate state will be

$$C_T(x, t) = \bar{C}_T(x)(1 - e^{-t/\tau_1}) \quad (\text{B-1})$$

$[C_T(x, 0) = 0]$ where $\bar{C}_T(x)$ is the steady-state concentration at a distance x from the front surface. Over ρ sec of excitation, the average concentration of T will be

$$\overline{[C_T(x, \rho)]} = \frac{\int_0^\rho C_T(x, t) dt}{\int_0^\rho dt} = \frac{\bar{C}_T(x)}{\rho} [\rho - \tau_1(1 - e^{-\rho/\tau_1})] \quad (\text{B-2})$$

and the average rate of cation production will be

$$\left(\frac{dC_P(x)}{dt}\right)_\rho = \xi(x) \overline{[C_T(x, \rho)]}$$

where $\xi(x) = \phi_1 \epsilon_T I(x)$, or, by incorporating eq B-2

$$\left(\frac{dC_P(x)}{dt}\right)_\rho = \frac{\xi(x) \bar{C}_T(x)}{\rho} [\rho - \tau_1(1 - e^{-\rho/\tau_1})] \quad (\text{B-3})$$

$\xi(x) \bar{C}_T(x)$ is the steady-state rate of cation production. Thus, expressing the rate in terms of optical density change, eq B-3 can be written

$$(\bar{S}_1)_\rho = \frac{S_1 [\rho - \tau_1(1 - e^{-\rho/\tau_1})]}{\rho} \quad (\text{B-4})$$

where S_1 is the steady-state slope defined as in eq 1 of the text (*i.e.*, $S_1 = \lim (\bar{S}_1)_\rho$ as $\rho \rightarrow \infty$). If after ρ sec of exposure, the primary-excitation light is interrupted for δ sec, C_T will decay to

$$C_T(x, \delta) = C_T(x, \rho) e^{-\delta/\tau_1}$$

If δ is sufficiently large to allow essentially complete decay

$$C_T(x, \delta) \simeq 0 \quad (\text{B-5})$$

then repetition of the ρ -sec excitation period will result in the same average slope for the OD change as during the initial exposure. Therefore, by repeating the cycle

of excitation and interruption a sufficient number of times, $(\bar{S}_1)_\rho$ can be accurately measured.

Now τ_1 can be determined from eq B-4, which can be written as

$$F(\rho, \tau_1) \equiv \tau_1(1 - e^{-\rho/\tau_1}) = \rho \left(1 - \frac{(\bar{S}_1)_\rho}{S_1}\right) \quad (\text{B-6})$$

For a given ρ , τ_1 can be determined from a graph of F vs. τ_1 . The assumption that $C_T(\delta) = 0$ is not absolutely essential but greatly simplifies the analysis. If the dark time δ were not long enough, then the average concentration of T during the exposure period would depend on the number of cycles completed, and thus the OD would not increase linearly with the number of excitation-interruption cycles making (\bar{S}_1) more difficult to determine. The actual experimental dark times (δ) were as high as 45 sec, which is long enough for eq B-5 to be an accurate approximation for a τ_1 as high as 15 sec. If τ_1 were much longer than that, the cation OD would not increase linearly as experimentally observed (see Figure 6).

2. Two-Beam Excitation. This alternate method involves exposing the solution to secondary excitation during the dark periods of primary excitation. If after ρ sec, of primary excitation, the intermediate state is allowed to decay while exposed to secondary excitation, then the decay law will be

$$C_T(x, t) = C_T(x, \rho) e^{-t/\tau_1'} \quad (\text{B-7})$$

where τ_1' is the intermediate-state lifetime during secondary excitation. The average concentration of T during a δ -sec decay is therefore

$$\overline{C_T(x)_\delta} = \frac{\int_0^\delta C_T(x, t) dt}{\int_0^\delta dt} = \frac{\tau_1'}{\delta} C_T(x, \rho) (1 - e^{-\delta/\tau_1'}) \cong \frac{\tau_1'}{\delta} C_T(x, \rho) \quad (\text{B-8})$$

It is still assumed that $e^{-\delta/\tau_1'} \cong 0$ and here at $t = 0$, $C_T(x) = C_T(x, \rho)$. Thus, during the dark periods of primary excitation the average rate of cation production is

$$\left(\frac{dC_P(x)}{dt}\right)_\delta = \xi' \overline{C_T(x)_\delta} \quad (\text{B-9})$$

where

$$\xi' = \phi_1' \epsilon_T' I_0'$$

Substituting eq B-8 and B-1 gives

$$\left(\frac{dC_P(x)}{dt}\right)_\delta = \frac{\xi' \tau_1'}{\delta} \bar{C}_T(x) (1 - e^{-\rho/\tau_1}) \quad (\text{B-10})$$

The steady-state concentration of T during double-beam excitation is

$$(\bar{C}_T(x))' = \bar{C}_T(x) \frac{\tau_I'}{\tau_I}$$

Making this substitution in eq B-10 gives

$$\left(\frac{dC_P(x)}{dt}\right)_\delta = \frac{\xi' \tau_I}{\delta} (\bar{C}_T(x))' (1 - e^{-\rho/\tau_I}) \quad (\text{B-11})$$

Now $\xi'(\bar{C}_T(x))'$ is the steady-state rate of cation production (S_2) for double-beam excitation so, in terms of optical density change, eq B-11 becomes

$$(\bar{S}_2)_\delta = \frac{S_2 \tau_I}{\delta} (1 - e^{-\rho/\tau_I}) \quad (\text{B-12})$$

The observed rate during alternating two-beam excitation is, in this case, composed of two contributions

$$(\bar{S}) = \eta(\bar{S}_1)_\rho + \nu(\bar{S}_2)_\delta$$

where

$$\eta = \frac{\rho}{\rho + \delta}$$

and

$$\nu = \frac{\delta}{\rho + \delta}$$

After first determining $(\bar{S}_1)_\rho$ by blocking the second beam, $(\bar{S}_2)_\delta$ can be determined as $(\bar{S}_2)_\delta = [(\bar{S}) - \eta(\bar{S}_1)_\rho]/\nu$. By rearranging eq B-12, the function $F(\rho, \tau_I)$ can again be evaluated

$$F(\rho, \tau_I) \equiv \tau_I (1 - e^{-\rho/\tau_I}) = \frac{\delta(\bar{S}_2)_\delta}{S_2} \quad (\text{B-13})$$

And for a given ρ and δ , the value of τ_I can again be obtained from a curve of this function.

Appendix C: Optical Density Correction Due to Anisotropy of Absorption

In rigid solutions, if the fixed photoreactant absorbs anisotropically, an oriented photoproduct will result whether the excitation beam is polarized or not. This introduces a somewhat subtle complication into the interpretation of measured optical densities. The optical density observed for a given concentration of photoproducts will depend on the polarization of excitation and monitoring light and on the anisotropy of parent and daughter molecular absorption. For the case of single-photon-created photoproducts, this dependence has been explicitly determined.¹³ If the photochemical light is incident along the *b* laboratory axis and polarized a fraction *p* along the *a* axis and a fraction $1 - p$ along the *c* axis, it has been shown¹³ that optical density measurements of the photoproduct made with light polarized along the *a*, *b*, and *c* axes show the proportionalities

$$OD^a \propto A = (1 - p)B + p[3(r_x q_x + r_y q_y + r_z q_z) + q_x(r_y + r_z) + q_y(r_x + r_z) + q_z(r_x + r_y)]$$

$$OD^b \propto B = r_x q_x + r_y q_y + r_z q_z + 2[q_x(r_y + r_z) + q_y(r_x + r_z) + q_z(r_x + r_y)]$$

$$OD^c \propto C = pB + (1 - p)[3(r_x q_x + r_y q_y + r_z q_z) + q_x(r_x + r_z) + q_y(r_x + r_z) + q_z(r_y + r_z)]$$

$$r_x + r_y + r_z = 1$$

$$q_x + q_y + q_z = 1$$

Here r_x, r_y, r_z and q_x, q_y, q_z are the fractional apparent extinction coefficients for the three molecular axes of the photoreactant and photoproduct, respectively, at given wavelengths of excitation and monitoring. These relations were first utilized in correcting photochemical rate measurements in the initial study made on the TMPD-3MP solutions.⁵

When two tandem photons are involved in the generation of the photoproduct, the above already complicated relations will in general become much more complicated. Fortunately in this present study the second photon is absorbed isotropically (in the ionization process) so that the above equations will still apply.

The optical density can be written as

$$OD^a = kA$$

$$OD^c = kC$$

where *k*, the proportionality constant, is not related to any anisotropy. If the monitoring beam is polarized a fraction ω along *c* and a fraction $1 - \omega$ along *a*, then the observed optical density (OD) will be, to the first approximation

$$OD \cong \omega(OD^c) + (1 - \omega)OD^a = k[\omega C + (1 - \omega)A]$$

This is a very good approximation for present purposes because

$$OD \leq 0.04$$

Now it has already been shown⁵ that *k* is related to the isotropic or average (fluid solution) extinction coefficient (ϵ) and the concentration ($C(x)$) of the photoproduct as

$$k = \frac{3}{5}\epsilon \int_0^l C(x) dx$$

thus

$$OD = \frac{3}{5}[\omega C + (1 - \omega)A] \int_0^l C(x) dx$$

Therefore, the anisotropy correction factor necessary in relating OD to the total moles of photoproduct is

$$\gamma = \frac{3}{5}[\omega C + (1 - \omega)A]$$

In the visible band, where the cation is monitored $q_z = 1, q_x = q_y = 0$, and for TMPD absorption $r_x = 0, r_y = 1 - r_z, i.e.$

$$A = 2 - r_z - p + 3r_z p$$

$$C = p - 3pr_z + 2r_z + 1$$

The parameter r_z (which is known for the near-ultraviolet band of TMPD³¹) changes with exciting wavelength. Consequently γ is wavelength dependent.

For the photoionization studies in this report the

approximate values of the polarization parameters were $p = 3/5$ and $\omega = 0.95$, so that, in this case, γ can vary at most from 0.95 to 1.10 as r_z varies from 0 to 1. Thus in *this* case the correction is small, and in the results reported it is assumed that $\gamma = 1$.

(31) A. C. Albrecht, *J. Am. Chem. Soc.*, **82**, 3813 (1960).

Nuclear Magnetic Resonance and Ultraviolet Spectroscopy of Phenylmagnesium Bromide, Phenyllithium, and Pyridine¹

by Gideon Fraenkel, David G. Adams, and Ronald R. Dean

Evans Chemical Laboratory, The Ohio State University, Columbus, Ohio 43210 (Received August 24, 1967)

Nuclear magnetic resonance spectra have been obtained for phenyllithium, phenylmagnesium bromide, and pyridine. Analysis of the spectra by a combination of deuterium substitution and computer techniques reveals that the nmr parameters for these compounds are quite similar. The coupling constants for the organometallic reagents are all of the same sign, and hydrogens *ortho* to the carbon-metal bond are considerably deshielded with respect to benzene. These results are explained on the basis that phenyl anion and pyridine are isoelectronic and, to the degree that the carbon-metal bonds are ionic, the same effects should account for the shifts in all three compounds. By analogy to the published discussion on shifts in pyridine, it is suggested that paramagnetic terms are mainly responsible for shifts in the organometallic reagents and π -electron density changes are not important. In fact, the shifts around C_6H_5Li and C_6H_5MgBr follow the order expected from the point anisotropy approximation. Noting that mixing of the ground with the $n \rightarrow \pi^*$ excited state in pyridine is mainly responsible for paramagnetic shifts, it is suggested that similar electronic transitions might be available to C_6H_5Li and C_6H_5MgBr . In fact, long tails indicative of such weak absorption is tentatively assigned $\sigma_{C-M} \rightarrow \pi^*$. The similarities in the nmr and uv spectra of the above three compounds together with the way the nmr parameters change among the reagents leads to the conclusion that the magnitude of the downfield shift for the *ortho* hydrogens in ArM is a qualitative measure of the ionic character of the carbon-metal bond.

The study of carbanions is complicated by the fact that most of them come as the negative or partially negative part of an organometallic compound. Among the questions which concern the physical properties and behavior of these compounds are: (1) carbanion-inversion phenomena,^{2,3} (2) the ionic character of the



carbon-metal bonds,⁴ and (3) the mean lifetime of the carbon-metal bonds between exchanges.^{5,6} The organometallic compounds most likely to contain carbanions are those of sodium or other alkali elements with higher atomic weights. Unfortunately, most of these are insoluble in or react with all solvents which have so far been tested and are, therefore, not susceptible to spectroscopic investigation.

Organolithium and -magnesium compounds dissolve

in a wide variety of solvents and behave chemically like carbanionic species;⁷ it would be expected that

(1) Presented in part at the 147th National Meeting of the American Chemical Society, Philadelphia, Pa., April 1964, Abstracts, p N41; D. G. Adams, Ph.D. Thesis, The Ohio State University, Columbus, Ohio, 1964.

(2) G. M. Whitesides, F. Kaplan, and J. D. Roberts, *J. Am. Chem. Soc.*, **85**, 2167 (1963); G. M. Whitesides, M. Witanowsky, and J. D. Roberts, *ibid.*, **87**, 2854 (1965); G. M. Whitesides and J. D. Roberts, *ibid.*, **87**, 4878 (1965); M. Witanowski and J. D. Roberts, *ibid.*, **88**, 737 (1966).

(3) G. Fraenkel, D. T. Dix, and D. G. Adams, *Tetrahedron Letters*, 3155 (1964); G. Fraenkel and D. T. Dix, *J. Am. Chem. Soc.*, **88**, 979 (1966).

(4) G. Fraenkel, D. G. Adams, and J. Williams, *Tetrahedron Letters*, 767 (1963).

(5) D. F. Evans and M. S. Khan, *Chem. Commun.*, 67 (1966).

(6) H. O. House, R. A. Latham, and G. M. Whitesides, *J. Org. Chem.*, **32**, 2481 (1967).

(7) M. S. Kharasch and O. Reinmuth, "Grignard Reactions of Nonmetallic Substances," Prentice-Hall Inc., New York, N. Y., 1954; G. E. Coates, "Organometallic Compounds," 2nd ed, John Wiley and Sons, Inc., New York, N. Y., 1960.

these materials might reflect useful information about carbanions in their physical properties.

This paper concerns aspects of the electronic structure of the phenyl anion which have been uncovered with nmr spectroscopy.¹ It will be shown that the results for phenyllithium and phenylmagnesium bromide bear close resemblance to those for pyridine, which is isoelectronic with the phenyl anion.

While the present work was being written, certain aspects of it were published by other groups, working independently. These are Ladd's analysis of the nmr spectra of phenyllithium, diphenylmagnesium, and diphenylzinc,⁸ some coupling constants for phenyllithium,⁹ and the analysis of the nmr spectrum of pyridine due to Merry and Goldstein, and Castellano, *et al.*¹⁰ These findings complement our results and strengthen the conclusions.

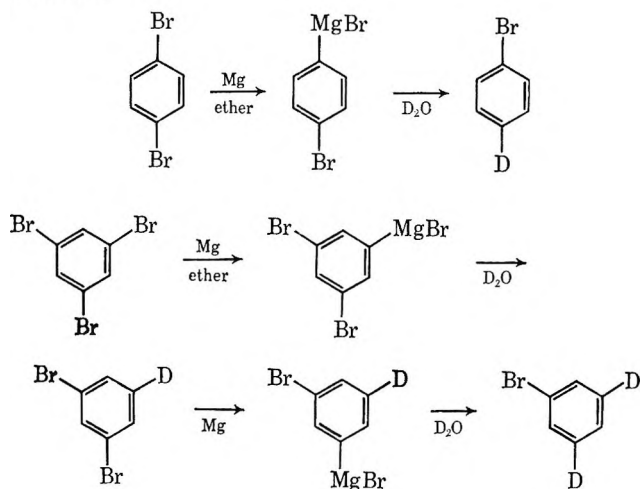
In other physicochemical studies, much work has been done on the infrared spectroscopy of organometallic compounds. Lanpher¹¹ found a band in the ir spectra of phenyllithium, phenylsodium, and phenylpotassium whose energy was linear with the square of the electronegativity of the corresponding metal. In the infrared spectroscopy of organolithium compounds Rodionov, Kocheshkov, and their colleagues found evidence for bridged bonds¹² and resolved dissociated species from larger aggregates¹² as well as one etherate from another.¹³ West and Glaze have reported on the Li⁶-Li⁷ isotope effects in the ir spectra of organolithium compounds.¹⁴ Magnetic susceptibility measurements indicate phenyllithium to be ionic.¹⁵ Various authors have reported on the aggregation of organomagnesium¹⁶ and -lithium compounds.¹⁷ Under different conditions, phenyllithium and phenylmagnesium bromide consist of mixtures of monomers and dimers. In the solid state, diphenylmagnesium dietherate and phenylmagnesium bromide dietherate are monomeric.¹⁸

Recently, Evans and Khan reported the preparation of pentafluorophenylmagnesium bromide. At low temperatures, they were able to resolve the fluorine resonance of the Grignard reagent from that of the diarylmagnesium compound. Raising the temperature increased the exchange rate among all species and averaged their shifts.⁵

Results and Discussion

The syntheses of deuterated bromobenzenes are illustrated in Scheme I. *p*-Dibromobenzene was converted to the mono-Grignard reagent. The latter was hydrolyzed with D₂O to give 4-deuteriobromobenzene. By two such reaction sequences, 1,3,5-tribromobenzene was transformed to 3,5-dideuteriobromobenzene. Grignard reagents were prepared from the two deuterated bromides and from bromobenzene; see the Experimental Section. These bromides were also converted to the corresponding organolithium compounds by reaction

Scheme I



with lithium metal¹⁹ and by halogen-lithium exchange reactions.²⁰

The nmr spectra of *p*-deuteriophenyllithium and *p*-deuteriophenylmagnesium bromide are illustrated in Figures 1 and 2 with expanded reproductions of the downfield multiplets. The single absorption at τ 2.74 is due to deuteriobenzene. These spectra are AA'BB' systems,²¹ the upfield portions of which are broadened by coupling of the deuterium to the hydrogens *ortho* to it. Hence, the downfield multiplets are assigned to hydrogens *ortho* to the carbon-metal bond. These latter multiplets were analyzed with Pople's method²¹ and the fit of the nmr parameters with the observed spectra was improved with the aid of computer programs

- (8) J. A. Ladd, *Spectrochim. Acta*, **22**, 1157 (1966).
 (9) S. Castellano and C. Sun, *J. Am. Chem. Soc.*, **88**, 4742 (1966).
 (10) J. B. Merry and J. H. Goldstein, *ibid.*, **88**, 5563 (1966); C. Castellano, C. Sun, and K. Kostelnik, *J. Chem. Phys.*, **46**, 327 (1967).
 (11) E. J. Lampher, *J. Org. Chem.*, **21**, 830 (1956).
 (12) A. N. Rodionov, D. Shigorin, T. V. Talalaeva, and K. Kocheshkov, *Izv. Akad. Nauk SSSR Otd. Khim. Nauk*, 120 (1958).
 (13) A. N. Rodionov, D. N. Shigorin, E. N. Gur'yanova, and K. A. Kocheshkov, *Dokl. Akad. Nauk SSSR*, **125**, 562 (1959); **123**, 113 (1958); **128**, 728 (1959); A. N. Rodionov, D. N. Shigorin, and K. A. Kocheshkov, *ibid.*, **136**, 269 (1961); T. V. Talalaeva, A. N. Rodionov, and K. A. Kocheshkov, *Izv. Akad. Nauk SSSR Otd. Khim. Nauk*, 1990 (1961).
 (14) R. West and W. H. Glaze, *J. Am. Chem. Soc.*, **83**, 3580 (1961).
 (15) I. B. Golovanov and A. K. Piskunov, *Zh. Fiz. Khim.*, **38**, 2063 (1965).
 (16) E. C. Ashby and M. B. Smith, *J. Am. Chem. Soc.*, **86**, 4363 (1964). This paper contains numerous references to previous molecular weight studies.
 (17) (a) T. V. Talalaeva, A. N. Rodionov, and K. A. Kocheshkov, *Dokl. Akad. Nauk SSSR*, **154**, 174 (1964); (b) R. Waake, 151st National Meeting of the American Chemical Society, New York, N. Y., Sept 1966.
 (18) G. Stucky and R. E. Rundle, *J. Am. Chem. Soc.*, **86**, 4829 (1964).
 (19) H. Gilman and R. Jones, "Organic Reactions," Vol. VI, John Wiley and Sons, Inc., New York, N. Y., 1951, p 353.
 (20) H. Gilman, W. Langham, and F. W. Moore, *J. Am. Chem. Soc.*, **62**, 2327 (1940).
 (21) Terminology of J. A. Pople, W. G. Schneider, and H. J. Bernstein, "High Resolution Nuclear Magnetic Resonance," McGraw-Hill Book Co., Inc., New York, N. Y., 1959, Chapter 6.

Table I: Nmr Parameters Obtained from 1 M Solutions of Aromatic Compounds

	τ_o^a	τ_m	τ_p	$J_{2,3}^b$	$J_{2,4}$	$J_{2,5}$	$J_{2,6}$	$J_{3,4}$	$J_{3,5}$
Pyridine	1.450	2.813	2.414	4.82	1.77	0.96	-0.14	7.64	1.24
C ₆ H ₅ Li	1.976	2.975	3.042	6.52	1.62	0.84	0.65	7.20	1.17
C ₆ H ₅ Li ^d	2.007	2.978	3.058	6.85	1.53	0.51	0.72	7.76	1.65
C ₆ H ₅ Li-4-d	1.975	2.975		6.50		0.84	0.68		1.20
C ₆ H ₅ MgBr	2.362	2.982	3.025	6.98	1.65	0.98	0.95	7.47	1.40
(C ₆ H ₅) ₂ Mg ^d	2.307	2.969	3.046	6.80	1.62	0.70	0.63	7.76	1.34
C ₆ H ₅ MgBr-4-d	2.361	2.982		7.00		0.96	0.92		1.39
C ₆ H ₅ MgBr-3,5-d ₂	2.360		3.023		1.63				
Benzene	2.743		2.743						
Covalently substituted benzene ^c	...	1.6-3.3	...	7.5-9.0	2.0-3.0	0.3-0.6	2.0-3.0	7.5-9.0	2.0-3.0

^a $\tau \pm 0.001$. ^b ± 0.02 Hz. ^c See ref 29. ^d Reference 10, concentration not given.

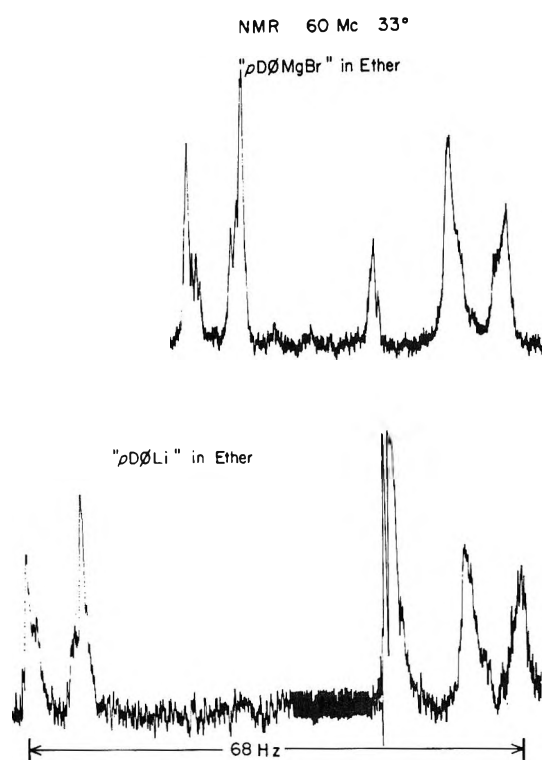


Figure 1. Nmr spectrum, 60 Hz: top, 4-deuteriophenylmagnesium bromide; bottom, 4-deuteriophenyllithium.

NMREN and NMRIT.²² The results of this calculation are listed in Table I. The shift of the *para* hydrogen in phenylmagnesium bromide was obtained from the spectrum of 3,5-dideuteriophenylmagnesium bromide. The latter gave a first-order spectrum and yielded the *ortho-para* coupling constant $J_{2,4}$ under conditions where deuterium was decoupled.

Spectra for phenyllithium and phenylmagnesium bromide are illustrated in Figure 3. The low-field absorptions are due to *ortho* hydrogens, while the other multiplet represents the *meta* and *para* hydrogens. Using the parameters from the two deuterated compounds, together with several sets of reasonable values

for the missing ones, theoretical AA'BB'C spectra were computed²³ and compared to the experimental spectrum of phenylmagnesium bromide. Using the theoretical spectrum most similar to the observed one, transitions were assigned to the experimental lines and energy levels calculated with NMREN. Prior to this calculation, at least two cycles were checked manually with the energy sum rule.²³ Finally, the nmr parameters were iterated to fit the observed spectrum to give the results listed in Table I, stick diagram Figure 4A.

In the above analysis, the possibility still existed that deuterium might change the chemical shifts of hydrogens relative to the undeuterated reagents. In fact, the proton shifts for all three Grignard reagents are identical within experimental error and no isotope effect was observed.

Diphenylmagnesium in ether gave nmr parameters almost identical with those of phenylmagnesium bromide. Analysis of the nmr spectrum of phenyllithium was accomplished as described above for the Grignard reagent, Table I, Figure 4b. These shifts for phenyllithium and phenylmagnesium bromide are very similar to those Ladd obtained for phenyllithium and diphenylmagnesium,⁸ respectively. However, the coupling constants differ by as much as 0.2 Hz.²⁴

To date, the signs of H-H coupling constants in aromatic compounds have been reported as positive.²⁵⁻²⁸ Since the present examples are strongly coupled systems, changing the sign of one or more coupling constants should alter the appearance of the spectra. That this is the case is evident in Figures 5

(22) J. D. Swalen, International Business Machines Corp., San Jose, Calif.

(23) J. D. Swalen and C. A. Reilly, *J. Chem. Phys.*, **37**, 21 (1962).

(24) Note that Ladd's analyses were accomplished by a combination of decoupling and computer techniques.

(25) S. Clough, *Mol. Phys.*, **2**, 349 (1959).

(26) R. Freeman, N. S. Bhacca, and C. A. Reilly, *J. Chem. Phys.*, **38**, 293 (1963).

(27) J. S. Martin and B. P. Dailey, *ibid.*, **37**, 2594 (1962).

(28) T. Schaefer, *Can. J. Chem.*, **40**, 1678 (1962).

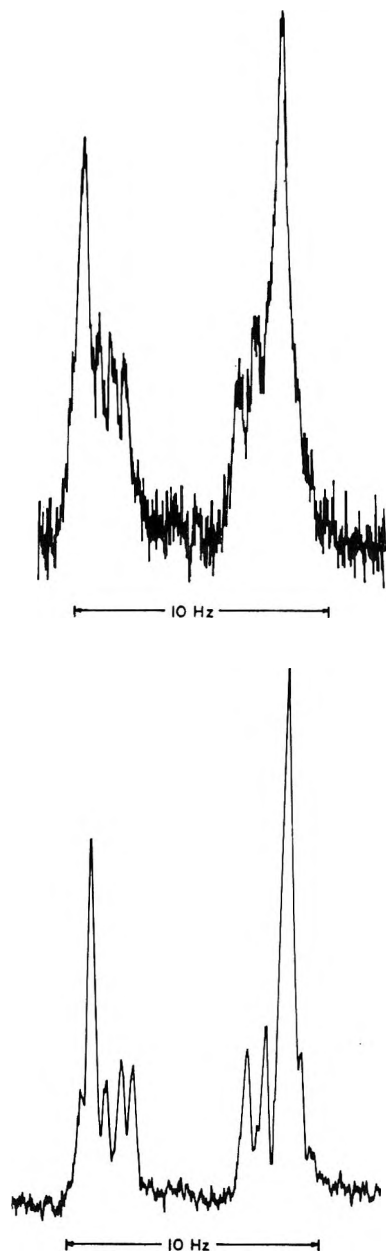


Figure 2. Nmr spectrum, 60 Hz: top, low-field multiplet in Figure 1, top; bottom, low-field multiplet in Figure 1, bottom.

and 6, which depict stick diagrams for theoretical spectra of phenylmagnesium bromide where the signs of the smaller coupling constants have been changed one at a time. These diagrams are quite different from the final iterated solution, Figure 4a. Also, allowing any combination of two or three of the small coupling constants to be negative causes the theoretical spectra to look quite different. It is thus assumed that all the coupling constants in phenylmagnesium bromide are of the same sign. This conclusion also applies to phenyllithium.

The nmr spectrum of pyridine has been discussed by several authors.^{29,30} An analysis of the 40-Hz spectrum of neat pyridine based on results obtained with

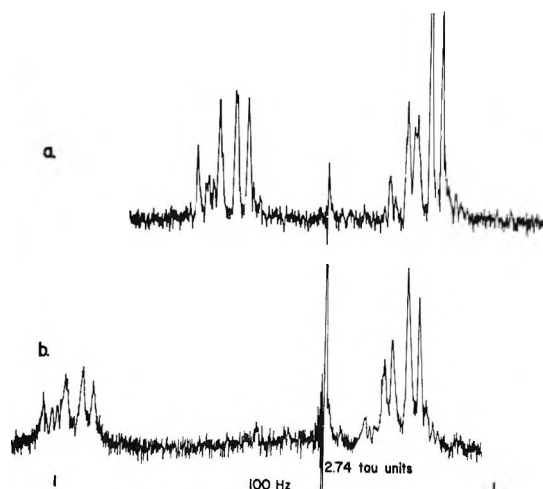


Figure 3. Nmr spectra of (a) phenylmagnesium bromide and (b) phenyllithium.

deuterated pyridines was reported by Schneider, Bernstein, and Pople.³¹ Using their parameters, we have assigned the 60-Hz spectrum of pyridine in ether and analyzed it with the aid of computer programs NMREN and NMRIT,^{22,23} Table I. The principle difference between this and the previous analysis³¹ is the very small value of $J_{2,6}$ noticed also by the Kowalewskis in their study of substituted pyridines.³² Very similar results have been recently published by Merry and Goldstein for neat pyridine and pyridine in water, pH 9.¹⁰

The nmr parameters for the organometallic reagents and pyridine are compared to typical values for covalently substituted benzenes in Table I. Each organometallic preparation yielded a single spectrum whose lines were of normal width (0.15–0.3 Hz). Mixtures of phenylmagnesium bromide and phenyllithium gave single spectra whose parameters lay between those of the two pure reagents. Hence, under our conditions, exchange among species is fast on the nmr time scale. However, in the pentafluorophenylmagnesium system carbon–magnesium exchange rates have been measured with the nmr line-shape technique.⁵

It is seen in Table I that the values for the lithium and magnesium reagents lie between those for pyridine and the typical substituted benzenes. Actually, the C_6H_5MgBr and C_6H_5Li parameters are more similar to those of pyridine than to the last class of compounds in Table I. This is especially noticeable among the coupling constants. For instance, while in ordinary substituted benzenes, the values of $J_{2,4}$, $J_{2,5}$, $J_{2,6}$, and $J_{3,5}$ all lie between 2 and 3 Hz, among the organo-

(29) H. J. Bernstein and W. G. Schneider, *J. Chem. Phys.*, **24**, 469 (1956).

(30) E. B. Baker, *ibid.*, **23**, 1981 (1955).

(31) W. G. Schneider, H. J. Bernstein, and J. A. Pople, *Ann. N. Y. Acad. Sci.*, **70**, 806 (1958).

(32) V. J. Kowalewski and D. G. de Kowalewski, *J. Chem. Phys.*, **36**, 266 (1962).

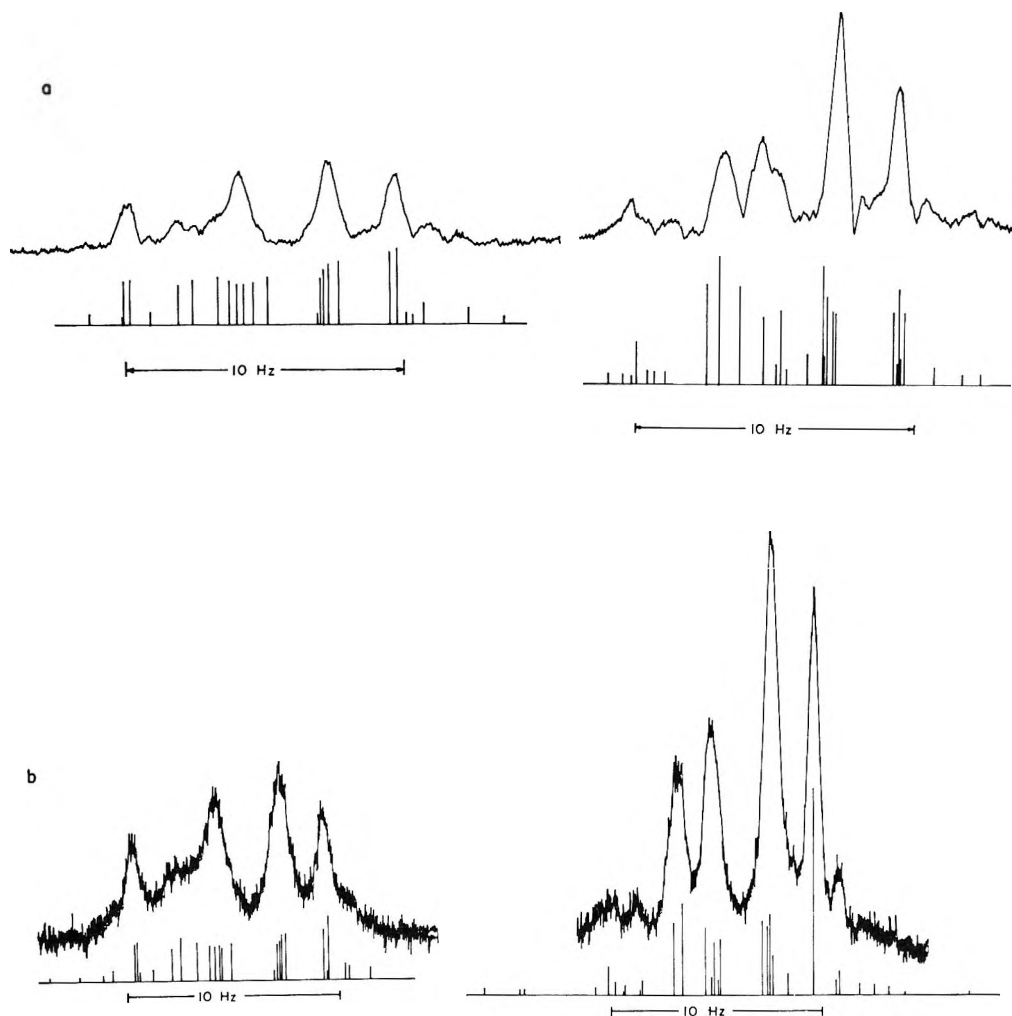


Figure 4. Theoretical and experimental nmr spectra of (a) phenylmagnesium bromide and (b) phenyllithium: *ortho* multiplets at left; *meta* and *para* absorption at right.

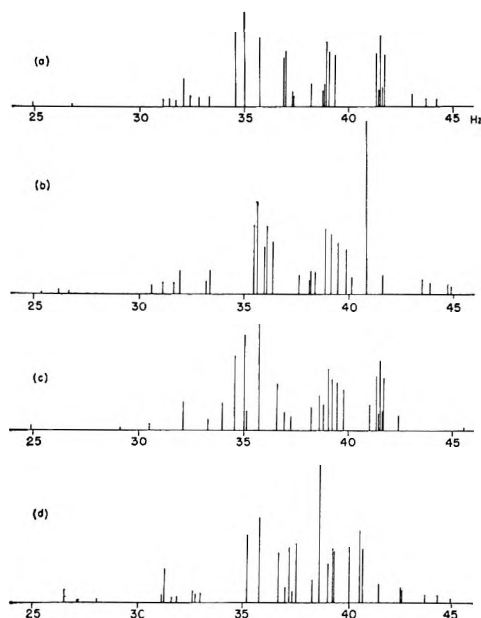


Figure 5. Theoretical nmr spectra for phenylmagnesium bromide (*meta* and *para* hydrogen) with the following negative coupling constants: (a) $J_{2,6}$, (b) $J_{2,5}$, (c) $J_{3,5}$, and (d) $J_{2,4}$. Other parameters are listed in Table I or assumed from symmetry.

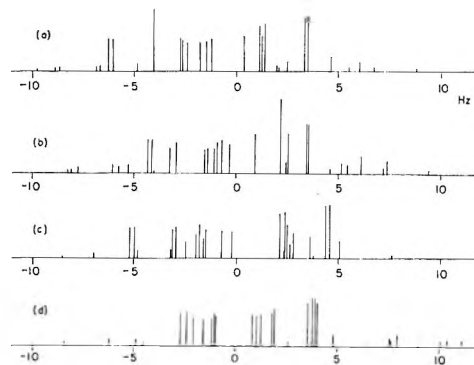


Figure 6. Theoretical nmr spectra for phenylmagnesium bromide (*ortho* hydrogens) with the following negative coupling constants: (a) $J_{2,6}$, (b) $J_{2,5}$, (c) $J_{3,5}$, and (d) $J_{2,4}$. Other parameters are listed in Table I or assumed from symmetry.

metallic reagents and pyridine they fall within the ranges 1.6–1.8, 0.8–1.0, 0.0–1.0, and 1.2–1.4 Hz, respectively. Furthermore, the organometallic compounds are all deshielded with respect to benzene at the *ortho* hydrogens. This low-field shift is remarkable, in view of the fact that the opposite effect occurs in

aliphatic Grignard reagents and organolithium compounds.^{4,33,34}

The following discussion concerns the downfield shift for the *ortho* hydrogens in phenylmagnesium bromide and phenyllithium. The screening constant of a nucleus in a large molecule is very difficult to calculate because the diamagnetic and paramagnetic terms, which are both large,^{35,36} tend to cancel each other.

Still, there are systems where contributions to the chemical shifts from different effects have been isolated and identified. For hydrogens in aromatic compounds, the main contributions to the shifts are ring currents,³⁷⁻⁴¹ the effect of charge,⁴²⁻⁴⁴ paramagnetic shifts,^{38,45} and solvent effects.⁴⁶⁻⁴⁸ These effects will be examined to account for the anomalous shift of the *ortho* hydrogens in our organometallic reagents and pyridine compared to hydrogens in benzene. (1) Solvent effects in this case probably chiefly arise from specific chemical interactions in the organometallic aggregates. These will not be considered now. (2) The ring current³⁸⁻⁴¹ presumably is affected only in a minor way by substitution of a metal for hydrogen. (3) Negative charge at C₁ should produce a large upfield shift⁴² at the *ortho* hydrogens and smaller upfield shifts at more distant hydrogens, since the effects are most likely transmitted by the inductive effect. Actually, the *meta* and *para* hydrogens are slightly shielded, though this need not be due to charge; see below. (4) If the ionic carbon-metal bond may be regarded as a dipole, the latter will have only a minor influence on the chemical shifts of the ring hydrogens. Fraenkel and Kim⁴⁹ have observed this effect in nmr spectra of aniline oxides and BL₃ adducts of anilines. (5) The paramagnetic contribution to the chemical shift^{38,45} would appear to be partly responsible for the effects observed here. Employing the point-dipole approximation,^{50,51} we consider point anisotropies for different atoms around the rings. Compared to benzene, these will be most altered by the egregious change in the anisotropy of the carbon atom undergoing substitution by metal.

Pyridine is isoelectronic with phenyl anion. These two species should have similar electronic structures. The nmr parameters for the aryl organometallic compounds and pyridine are also similar. To the extent that the carbon-metal bonds are partially ionic, it is instructive to mention the origins of proton shifts in pyridine. This subject has been discussed by several investigators.^{10,29-32,52-54} The prevailing conclusion is that the contributions due to π -electron densities and paramagnetic terms mainly account for the observed shifts.⁵⁵

The contribution of a paramagnetic term to shifts in pyridine is most evident from the fact that the α -proton shift is too low to be accounted for by electron density effects alone. Paramagnetic shifts in pyridine come

from magnetic mixing of the ground and nearest electronic excited states,⁵² the principle low-lying excited state being $n \rightarrow \pi^*$. According to Pople's treatment,³⁸ the paramagnetic shift δ_{para} should be inversely proportional to the lowest electronic excitation energy, ΔE

$$\delta_{\text{para}} \propto \frac{1}{\Delta E} \quad (2)$$

It seems reasonable that similar considerations to those discussed to account for shifts in pyridine should also apply to the arylorganometallic reagents. However, here variations in the π -electron densities should be relatively small, since there is no conjugative mechanism to delocalize the charge associated with C₁. Hence, π -electron density shifts with respect to benzene should be fairly uniform.

To summarize the above discussion, chemical shifts in phenylmagnesium bromide and phenyllithium due to different π -electron densities and the inductive effect of charges associated with the C-M bond are expected to be small. It is tentatively suggested that paramagnetic shifts are mainly responsible for the results reported here. Although this cannot be proved exactly, there are two considerations which lend weight to the above suggestion; these are now outlined below.

(33) G. Fraenkel, D. G. Adams, and J. Williams, *Tetrahedron Letters*, 767 (1963).

(34) D. F. Evans and J. P. Maher, *J. Chem. Soc.*, 5125 (1962); H. Roos and W. Zeil, *Ber. Bunsenges. Physik. Chem.*, 67, 28 (1963).

(35) N. F. Ramsay, *Phys. Rev.*, 78, 699 (1950).

(36) N. F. Ramsay, *ibid.*, 86, 243 (1952).

(37) J. A. Pople, *Proc. Roy. Soc. (London)*, A239, 541 (1957).

(38) J. A. Pople, *ibid.*, A239, 550 (1957).

(39) G. E. Johnson and F. M. Bovey, *J. Chem. Phys.*, 29, 1012 (1958).

(40) N. Jonathan, S. Gordon, and B. P. Dailey, *ibid.*, 36, 2443 (1962).

(41) J. S. Waugh and R. W. Fessenden, *J. Am. Chem. Soc.*, 79, 846 (1957).

(42) G. Fraenkel, R. E. Carter, A. D. McLachlan, and J. H. Richards, *ibid.*, 82, 5846 (1960), and references cited therein; J. I. Musher, *J. Chem. Phys.*, 37, 34 (1960).

(43) A. D. Buckingham, *Can. J. Chem.*, 38, 300 (1960).

(44) B. P. Dailey and J. S. Martin, *J. Chem. Phys.*, 39, 1722 (1963).

(45) J. D. Das and R. Bersohn, *Phys. Rev.*, 104, 476 (1956).

(46) A. D. Buckingham, T. Shaeffer, and W. G. Schneider, *J. Chem. Phys.*, 32, 1227 (1960).

(47) R. J. Abraham, *Mol. Phys.*, 4, 309 (1961).

(48) A. A. Bothner-By, *J. Mol. Spectry.*, 5, 52 (1960).

(49) G. Fraenkel and J. P. Kim, *J. Am. Chem. Soc.*, 88, 4203 (1966).

(50) H. M. McConnell, *J. Chem. Phys.*, 27, 226 (1957).

(51) A. A. Bothner-By and C. Naar-Colin, *J. Am. Chem. Soc.*, 80, 1728 (1958).

(52) V. M. S. Gil and J. N. Murrell, *Trans. Faraday Soc.*, 60, 248 (1964).

(53) J. A. Elvidge and L. M. Jackman, *J. Chem. Soc.*, 859 (1961).

(54) B. P. Dailey and J. K. Wu, *J. Chem. Phys.*, 41, 3307 (1964).

(55) These two contributions have been calculated using SCF wave functions. The results closely reproduce observed ¹H and ¹³C shifts in pyridine. For pyridinium ion, π -electron densities are mainly responsible for the observed shifts: G. Fraenkel and T. Tokuhira, unpublished results.

Anisotropy Approximation. Let us assume that the *para* hydrogen in phenyllithium is sufficiently distant from C₁ that inductive contributions to its shift are not important. The shift $\delta(H_p)$ relative to benzene should be mainly paramagnetic. Using McConnell's point-anisotropy approximation,⁵⁰ eq 3, to assign a

$$\Delta\sigma = \frac{\Delta\chi}{3R^3}(1 - 3\cos^2\theta) \quad (3)$$

value to $\Delta\chi$ and the parameters in Figure 7, the *meta* and *ortho* shifts are nearly identical with those observed: calculated, +0.22 and -0.85 ppm; observed, +0.232 and -0.767 ppm, for *meta* and *ortho* hydrogens, respectively. A similar treatment for phenylmagnesium bromide gives +0.21 and -0.79 ppm compared to the observed values of +0.24 (*meta*) and -0.34 (*ortho*) ppm, respectively. Although the close agreement of the values for phenyllithium must be fortuitous, both treatments do give the correct order for the shifts around the reagents.

Ultraviolet Spectra. In pyridine, the low-lying excited state mainly responsible for the paramagnetic shifts is $n \rightarrow \pi^*$.⁵² If the analogies between C₆H₅M and pyridine are correct, a transition corresponding to $n \rightarrow \pi^*$ in pyridine should be available to the organometallic compounds also. Such an excitation may be written $\sigma_{C-M} \rightarrow \tau^*$, recognizing that the C-M bond must be partially covalent. Accordingly, we have obtained uv spectra of specially purified samples of phenylmagnesium bromide and phenyllithium, Figure 8. In both spectra, the absorption tails off slowly toward 300-350 m μ .⁵⁶ Waake and Doran⁵⁷ have also reported uv data for phenyllithium. By analogy to the results for pyridine, we suggest that the high-wavelength tails in these uv spectra involve $\sigma_{C-M} \rightarrow \pi^*$ excitation.

Ordinarily, $n \rightarrow \pi^*$ excitation energies in pyridine and aromatic diazines increase with the strength of hydrogen bonding at nitrogen.⁵⁸ At the same time, the paramagnetic contributions to the various proton shifts should decrease.

Applying the above argument to the organometallic compounds, as M in C₆H₅M- becomes more electropositive, the ionic character of the carbon-metal bond should increase, $\Delta E(\sigma_{C-M} \rightarrow \pi^*)$ decrease, and δ_o decrease (become more negative). Such a trend is evident among the *ortho* proton shifts which decrease along the series (C₆H₅)₂Zn > C₆H₅MgBr \sim (C₆H₅)₂Mg > C₆H₅Li.^{8,59} Although absorption bands for the proposed $\sigma_{C-M} \rightarrow \pi^*$ transition could not be resolved, it is qualitatively seen that the value for C₆H₅Li is lower than that for C₆H₅MgBr.

Following the above argument, it is speculated that coordination of different solvents with M in ArM would be expected to alter $\Delta E(\sigma_{C-M} \rightarrow \pi^*)$ and thus also the *ortho* shift. The principal solvent effect on these shifts should take place *via* specific chemical interactions.

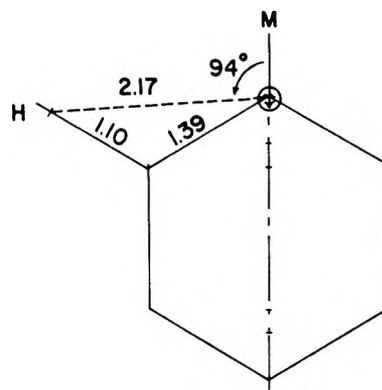


Figure 7. Geometry in C₆H₅M...

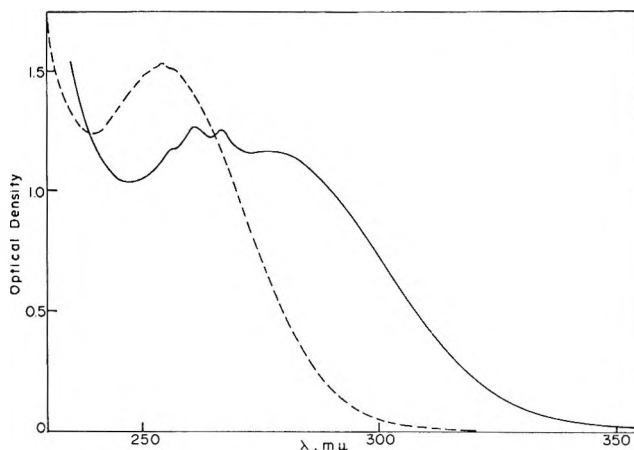


Figure 8. Uv spectra: —, phenyllithium, 0.25 M in ether (path = 0.05 mm); ---, phenylmagnesium bromide, 0.09 M in ether (path 0.1 mm.).

Taken together, the spectral similarities—chemical shifts, coupling constants, and uv data—presented here for C₆H₅MgBr, C₆H₅Li, and pyridine strongly imply that paramagnetic terms are the most important contributions to the *ortho* shifts in the organometallic reagents.

Proceeding down the series of organometallic compounds as M becomes more electropositive, $J_{2,3}$, $J_{2,6}$, and $J_{3,5}$ all decrease and the most conspicuous effect is the decrease in δ_o . The lowest value for this latter shift should occur for free phenyl anion, so far not reported.

(56) For phenyllithium, λ and ϵ are, respectively, 261, 1000 and 330, 40; for phenylmagnesium bromide, λ and ϵ are, respectively, 255, 630 and 290, 63. These results were reproducible. On hydrolysis of these reagents, there was obtained only the weak uv absorption due to the expected concentration of benzene.

(57) R. Waake and M. A. Doran, *J. Am. Chem. Soc.*, **85**, 1651 (1963).

(58) M. Kasha and G. J. Brealey, *ibid.*, **77**, 4462 (1955).

(59) The *ortho* hydrogens in compounds such as C₆H₅SiCl₃ and (C₆H₅)₂SnCl₂ are also deshielded while the shifts of the other hydrogens are not much different from benzene: J. C. Maire and F. Hemmert, *Bull. Soc. Chim. Fr.*, 2785 (1963). Since coupling constants have not been reported for these compounds, it is not clear whether the arguments presented in the paper apply here also.

The main conclusion derived from this work is that the downfield shift of the *ortho* hydrogens in ArM is a qualitative measure of the ionic character of the carbon-metal bond.

Experimental Section

Chemicals. The following chemicals were obtained: bromobenzene, Matheson Coleman and Bell; butyllithium, Foote Mineral Co.; lithium wire, Lithium Corp. of America; deuterium oxide, Columbia Chemical Co.; and sublimed magnesium, Dow Chemical Co. Diethyl ether was distilled from methylmagnesium bromide.

Magnesium. Sublimed magnesium was milled to fine shavings, care being taken to avoid contamination by iron. The metal shavings were washed with benzene, then with three portions of diethyl ether (CP). The ether was removed in a stream of dry helium and the magnesium stored over anhydrous magnesium sulfate.

4-Deuteriobromobenzene. Magnesium turnings (2.9 g; 0.12 mol) were placed in a three-neck 500-cm³ flask fitted with addition funnel, mechanical stirrer, and reflux condenser with drying tube. Diethyl ether (100 ml) was distilled into the flask from a solution of methylmagnesium bromide in ether. *p*-Dibromobenzene (23.6 g; 0.1 mol) was dissolved in an additional 100 ml of anhydrous ethyl ether and transferred to the addition funnel under helium. Ethylene dibromide (0.5 g; 0.003 mol) was added to the magnesium-ether mixture to initiate reaction. Stirring was begun and the dihalide-ether mixture admitted at a rate sufficient to cause continuous reflux of ether. After addition was complete, the mixture was refluxed 30 min to ensure reaction of any bromobenzene formed by hydrolysis of *p*-bromophenylmagnesium bromide. Deuterium oxide (10 g; 0.5 mol) was added dropwise, followed by 100 ml of 10% ammonium chloride solution, added rapidly. The ether layer was separated, dried over anhydrous magnesium sulfate, and the ether removed by distillation. The product, 4-deuteriobromobenzene, was distilled under reduced pressure, bp 74.0–74.5° (40 mm), 75% yield.

3,5-Dideuteriobromobenzene. *sym*-Tribromobenzene⁶⁰ (31.5 g; 0.1 mol) was treated with magnesium (3.8 g; 0.15 mol) in the same manner as the previous preparation and hydrolyzed with deuterium oxide (12 g; 0.6 mol). The product, 3,5-dideuteriobromobenzene was separated from bromobenzene by vapor chromatography in a 45% yield. The entire yield of 3,5-dibromodeuteriobenzene (10.6 g; 0.045 mol) was treated with magnesium (1.2 g; 0.05 mol) in the same manner as above and hydrolyzed with deuterium oxide (3.8 g; 0.18 mol). The product, 3,5-dideuteriobromobenzene, was separated as above, 80% yield and 36% over-all.

Syringes. The syringes used for addition of the bromides were ordinary hypodermic syringes (Multifit) with a locking needle; the syringe used for extractions

of samples of Grignard reagents was a 1-cm³ gastight syringe (Hamilton). All syringes were oven dried at 90° and stored over phosphorus pentoxide. Just before use, the syringes were flushed with dry helium.

Instrumentation. Two nmr spectrometers were employed in this study: a Varian HR-60 high-resolution nmr spectrometer equipped with a Hewlett-Packard wide-range audiooscillator, Hewlett-Packard Model 522D digital counter, and an NMR Specialties heteronuclear decoupler; and a Varian A-60 high-resolution nmr spectrometer. The A-60 was used for the majority of spectra not requiring decoupling.

Grignard Reagents. The reaction vessel was a cylinder 25-mm o.d. × 90 mm. An 8-mm o.d. side arm equipped with a Teflon straight-bore stopcock served as the inlet for helides. The outer arm of the stopcock was protected with a serum cap. The top of the vessel was attached *via* a condenser to the receiver side of an ether still. The glassware described above, excluding the still, was dried with flaming in a current of helium. A small Teflon-covered magnet and magnesium turnings in 100% excess were placed in the vessel and the system was connected to the ether still. Ether, 15 ml, was distilled into the vessel in an atmosphere of helium. Then, 0.1 ml of the aromatic halide was injected into the vessel through the side arm. Reaction usually set in within a few minutes, accompanied by ebullition, cloudiness, and/or color formation. The remaining halide was added at the rate of about 1 mm/min and the mixture was then heated for 30 min and stirred for 5 hr to complete the reaction.

The nmr tube was dried with a flow of dry helium through a 10-in. 18-gauge hypodermic needle inserted in the tube with simultaneous warming in a Bunsen flame. After removal of the flame, the flow of helium was continued until the tube cooled to room temperature, when the needle was withdrawn and the tube closed with a serum cap. Before use, the 1-cm³ gastight syringe for sample withdrawal was flushed several times with helium. The syringe was fitted with the 10-in. needle used for drying the nmr tube and was inserted through the serum cap and stopcock on the reaction vessel. After filling the syringe, the needle was withdrawn from the reaction vessel and quickly inserted through the serum cap on the nmr tube. The tube was filled to a depth of 1 in. and cooled in Dry Ice, and the upper end was quickly sealed off.

A 1.00-ml aliquot was withdrawn from the reaction vessel for acidimetric titration, using methyl red as the indicator. After titration, the mixture was extracted with 1 ml of carbon tetrachloride. The organic phase was separated, dried over anhydrous potassium carbonate, and analyzed by vapor chromatography and nmr spectroscopy.

(60) Undergraduate preparation, The Ohio State University, Columbus, Ohio.

The only impurity present in these Grignard preparations was benzene or one of the deuterated benzenes. Yields of 96–98% were obtained in these reactions.

Phenyllithium. The reaction vessel consisted of a round-bottomed flask equipped with an 8-mm o.d. side arm, a ball joint which led, *via* a condenser, to an ether still and a second side arm at the bottom, 15-mm o.d., which contained a glass frit. Both side arms were protected on the outside with Teflon straight-bore stopcocks and serum caps.

Lithium wire (2.3 equiv) was dipped into anhydrous ethanol and the coating scraped off under petroleum ether. The wire was cut into 1-mm lengths and dropped into the reaction vessel in a stream of helium. Ether was distilled in and decanted through the frit to remove soluble impurities. Ether (10–15 ml) was again distilled in and the mixture cooled to -25° with acetone–Dry Ice. A small amount (1 mmol) of bromobenzene was added, and reaction began within 15 min, evidenced by the lithium wire turning black, then white, with formation of a white precipitate. The

remainder of the halide (9 mmol) was added over a period of 30 min, during which time the reaction mixture was permitted to warm to 10° .

The mixture was then stirred 1 hr at room temperature to complete reaction. Phenyllithium was obtained in 98% yield, the principal impurity being benzene.

Phenyllithium was also prepared by the halogen-metal exchange reaction by mixing equivalent quantities of bromobenzene and butyllithium in ether at 0° . The nmr spectra for the two different preparations were nearly identical.

Purification of Reagents. Phenyllithium and phenylmagnesium bromide were purified by crystallization from ether on the vacuum line.⁶¹

Acknowledgment. This research was supported by the Petroleum Research Fund, Administered by the American Chemical Society, and by the Air Force Office of Scientific Research, Grant No. AF-AFOSR-251-63.

(61) S. Kobayashi, M.S. Thesis, The Ohio State University, Columbus, Ohio, 1965.

Nuclear Magnetic Resonance and Ultraviolet Spectroscopy of Substituted Aromatic Organometallic Compounds of Lithium, Magnesium, and Calcium

by Gideon Fraenkel, Shlomo Dayagi, and Sadao Kobayashi

Evans Chemical Laboratory, The Ohio State University, Columbus, Ohio 43210 (Received August 24, 1967)

Nmr and uv spectra have been obtained for a variety of aromatic organometallic reagents of lithium, magnesium, and calcium, including two bifunctional reagents. *m*-Dilithiobenzene is reported for the first time. The nmr parameters for these compounds depend little on solvent or concentration and are much more similar to those of the corresponding heterocycles than to values for covalently substituted benzenes. In particular, $J_{2,6}$ lies in the region 0.8–1.0 Hz and the shift of hydrogen *ortho* to the carbon–metal bond is unusually low, decreasing with metal electronegativity. Among these analyses, the coupling constants are found to be all of the same sign. Low concentrations, 0.001 *M*, of organometallic compounds are oxidized by the peroxide impurities in the solvents. However, reproducible uv spectra have been obtained for several ArM compounds in higher concentrations, 0.04–0.2 *M*. These spectra consist of (1) strong absorption around 260 $m\mu$ ($\epsilon \simeq 1200$) assigned to $\pi \rightarrow \pi^*$ excitation, (2) weak absorption which tails off toward 350 $m\mu$, attributed to $\sigma_{C-M} \rightarrow \pi^*$ analogous to $n \rightarrow \pi^*$ in pyridine, and (3) a shoulder ($\epsilon \simeq 1000$) which moves to higher wavelengths with increasing solvent polarity. The latter is assigned to a transition in which the ionic character of the carbon–metal bond increases. The close resemblance of the nmr and uv data for ArM compounds and pyridines leads to the conclusion that magnetic mixing of the ground and the nearest excited electronic states, $\sigma_{C-M} \rightarrow \pi^*$, is responsible for C–M bond anisotropy and thus deshielding the *ortho* hydrogens in ArM. Other effects—inductive, π density, and ring-current variations—need not be considered. This postulate for paramagnetic shifts is supported by the dependence of the *ortho* shifts on metal electronegativities and the observation that the ring shifts vary around the rings qualitatively according to the trend predicted by the geometrical factor in the point-anisotropy approximation.

Introduction

Aromatic organometallic compounds of magnesium and lithium exhibit carbanionic character in their chemical properties¹ and it might be expected that these materials would reflect useful information about carbanions in their physical properties. In fact, the conclusions from infrared spectroscopy^{2–7} and magnetic susceptibility measurements⁸ support the postulate of partially ionic carbon–metal bonds.

Recent nmr⁹ and uv^{9,10} studies of phenyllithium, phenylmagnesium bromide, and pyridine reveal that there is a surprising similarity among the nmr parameters for these materials, compared to values for ordinary covalently substituted benzenes,¹¹ in particular, the low values of $J_{2,6}$ and τ_o . It was suggested that since phenyl anion (I) and pyridine (II) are isoelectronic



I



II

these species should have similar electronic structures. To the extent that the carbon–metal bonds in phenyllithium and phenylmagnesium bromide are ionic, proton shifts in these materials should have similar origins to those in pyridine.

The currently accepted explanation for the α shift in pyridines is that they are of paramagnetic origin

due to the low-lying $n \rightarrow \pi^*$ excited state.¹² Therefore, on the basis of the nmr data, similar effects should operate also in the phenylorganometallic compounds. Furthermore, there should be a low-energy electronic excitation, analogous to $n \rightarrow \pi^*$ in pyridine, available to ArM compounds.

In this paper, we have further explored the similarities in electronic structure among pyridines and a

(1) M. S. Kharasch and O. Reinmuth, "Grignard Reactions of Non-metallic Substances," Prentice-Hall, Inc., New York, N. Y., 1954; G. E. Coates, "Organometallic Compounds," 2nd ed, John Wiley and Sons, Inc., New York, N. Y., 1960.

(2) E. J. Lanpher, *J. Org. Chem.*, **21**, 830 (1956).

(3) A. N. Rodionov, D. Shigorin, T. V. Talalaeva, and K. Kocheshkov, *Izv. Akad. Nauk SSSR Otd. Khim. Nauk*, **120** (1958).

(4) A. N. Rodionov, D. N. Shigorin, E. N. Gur'yanova, and K. A. Kocheshkov, *Dokl. Akad. Nauk SSSR*, **125**, 562 (1959); **123**, 113 (1958); **128**, 728 (1959).

(5) A. N. Rodionov, D. N. Shigorin, and K. A. Kocheshkov, *ibid.*, **136**, 369 (1961).

(6) T. V. Talalaeva, A. N. Rodionov, and K. A. Kocheshkov, *Izv. Akad. Nauk SSSR Otd. Khim. Nauk*, 1990 (1961).

(7) R. West and W. H. Glaze, *J. Am. Chem. Soc.*, **83**, 3580 (1961).

(8) I. B. Golovanov and A. K. Piskunov, *Zh. Fiz. Khim.*, **38**, 2063 (1965).

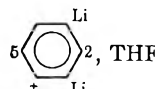
(9) J. A. Ladd, *Spectrochim. Acta*, **22**, 1157 (1966).

(10) G. Fraenkel and D. G. Adams, Abstracts, 147th National Meeting of the American Chemical Society, Philadelphia, Pa., April 1964; G. Fraenkel, D. G. Adams, and R. R. Dean, *J. Phys. Chem.*, **72**, 944 (1968).

(11) J. S. Martin and B. P. Dailey, *J. Chem. Phys.*, **37**, 2594 (1962).

(12) V. M. S. Gil and J. N. Murrell, *Trans. Faraday Soc.*, **60**, 248 (1964).

Table I: Nmr Parameters for Aromatic Lithium and Magnesium Compounds

Species, solvent	Concn, <i>M</i>	τ_0^a	τ_m	$J_{2,3}^b$	$J_{2,6}$	$J_{3,5}$	$J_{2,5}$
<i>p</i> -Tolylmagnesium bromide, ether	0.76	2.515	3.143	7.14	0.91	2.31	0.62
<i>p</i> -Tolylmagnesium bromide, THF	0.44	2.584	3.298	7.33	0.73	1.72	0.48
<i>p</i> -Tollyllithium, ether	0.50	2.090	3.080	7.04	0.63	1.68	0.57
<i>p</i> -Tolylcalcium iodide, THF	0.50	1.755	3.040	7.00	<i>c</i>	<i>c</i>	<i>c</i>
<i>p</i> -Anisylmagnesium bromide, ether	0.58	2.596	3.340	7.69	1.13	2.62	0.51
<i>p</i> -Anisylmagnesium bromide, THF	0.68	2.505	3.395	7.60	1.09	2.59	0.53
<i>p</i> -Anisyllithium, ether	0.50	2.030	3.200	7.42	1.11	2.50	0.45
<i>p</i> -Dimethylaminophenyllithium, ether	0.50	2.093	3.313	7.58	1.14	2.58	0.61
Mesityllithium, THF	0.50		3.489				
1,4-Bis(bromomagnesium)benzene, THF	0.50	2.300					
<i>p</i> -Chlorophenylmagnesium bromide, ether	0.50	2.461	2.907	7.07	1.70	1.70	0.56
<i>p</i> -Chlorophenyllithium, ether	0.50	2.545	2.744	8.10	2.20	2.20	0.73
		τ_3	τ_4	τ_5	$J_{3,4}$	$J_{4,5}$	
 $\text{C}_6\text{H}_4\text{Li}_2$, THF	0.50	0.396	2.383	3.325	<0.5	6.50	

^a Numbering is from C₁-M. ^b ±0.08 Hz. ^c Could not be resolved.

variety of aromatic organometallic compounds with nmr and uv studies. Evidence is presented for carbon-metal bond anisotropies together with low-lying electronic excited states of the $n \rightarrow \pi^*$ and charge-transfer types.

Results and Discussion

Aromatic halides were converted to the corresponding organolithium reagents with butyllithium¹³ and, in certain cases, lithium metal.¹⁴ Grignard reagents were prepared by standard procedures. When necessary, these materials were purified by precipitation or crystallization techniques; see Experimental Section. Possible contamination of these samples by hydrolysis coupling or oxidation products could not be detected in their nmr spectra. These spectra are attributed entirely to the organometallic reagent and solvent. All samples were analyzed by a combination of titration and reaction with benzophenone.

Of the organometallic compounds which are so far unreported, *m*-dilithiobenzene, *p*-dilithiobenzene, and 9,10-dilithio-1,2,3,4,5,6,7,8-octahydroanthracene were

prepared from the bromides by halogen-lithium exchange.¹³ The last two compounds were too insoluble to use in this investigation.

Nmr spectra were obtained for a variety of organomagnesium and lithium reagents listed in Table I. The nmr spectra of the reagents discussed here changed little with temperature. Di-*p*-tolylmagnesium in ether or THF gave the same results from -20 to +80° as did *p*-tolyllithium from -25 to +30°. At higher temperatures, *p*-tolyllithium slowly reacted with ether as evidenced by the appearance of a sharp line at τ 4.11 due to ethylene.

Above 30°, the *p*-tolyllithium solution in THF developed a single line for ethylene together with the absorption illustrated in Figure 1. This spectrum is very similar to the nmr spectrum of vinyl acetate.¹⁵

(13) H. Gilman, W. Langham, and F. W. Moore, *J. Am. Chem. Soc.*, **62**, 2327 (1940).

(14) H. Gilman and R. Jones, "Organic Reactions," Vol. VI, John Wiley and Sons, Inc., New York, N. Y., 1951, p 353.

(15) N. S. Bhacca, L. F. Johnson, and J. R. Shoolery, "Varian Nmr Spectra Catalog," Vol. 1, Varian Associates Palo Alto, Calif., 1962, no. 65.

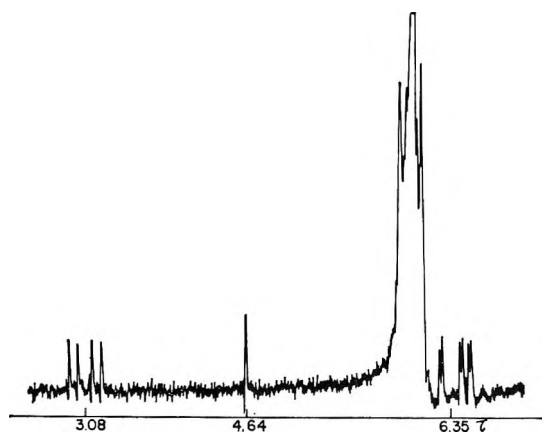
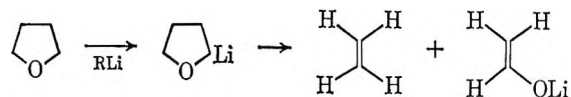


Figure 1. Nmr spectrum of reaction product of organolithium compounds with THF.

These results are best accommodated by the following scheme which involves α deprotonation followed by



fragmentation to ethylene and the enolate salt of acetaldehyde. Both ethylene and acetaldehyde were identified in the hydrolysate from this experiment. The above cleavage reaction is common to many organolithium compounds in tetrahydrofuran.¹⁶

The *para*-substituted reagents all give rise to single A_2B_2 spectra. Since these multiplets are symmetrical, the ring proton shifts cannot be assigned *a priori*; they were inferred on the basis of known effects of substituents on aromatic hydrogen shifts.^{11,18} Also, in the case of *p*-methyl and -methoxy reagents, there is some broadening in the nmr absorption for hydrogens *ortho* to these substituents owing to long-range coupling.

The AA'BB' systems were first analyzed by standard procedures described in the literature.¹⁷ The remaining reagents gave rise to almost first-order spectra. All analyses were completed by computer iteration¹⁹ of the derived nmr parameters until the theoretical spectra matched the experimental ones. This was accomplished with the aid of programs NMRIT and NMREN.¹⁹

Each preparation studied in this work gave rise to a single nmr spectrum. The individual lines which could be resolved were 0.1–0.2 Hz wide at half-height. Although under our conditions many of the reagents were known to consist of several species,^{20,21} no evidence was found for slow exchange among chemically shifted species down to -60° .²²

For most of the reagents reported here, the shifts depend only to a small extent on concentration within the range 0.2–1.0 *M*, Table II. However, in the case of *p*-anisylmagnesium bromide in ether, there is a definite and parallel increase for both τ_o and τ_m with concentration. The variation in $\tau_m - \tau_o$ is very much less than that of the individual shifts.

Table II: Dependence of Chemical Shifts in Aromatic Organometallic Compounds on Concentration

Concn, <i>M</i>	τ_o	τ_m
<i>p</i> -Tolylmagnesium bromide in diethyl ether		
1.042	2.517	3.141
0.764	2.515	3.143
0.666	2.515	3.143
0.312	2.521	3.155
0.248	2.511	3.143
0.192	2.517	3.153
<i>p</i> -Tolylmagnesium bromide in tetrahydrofuran		
0.876	2.596	3.301
0.493	2.583	3.299
0.275	2.591	3.303
0.223	2.581	3.291
0.138	2.610	3.320
<i>p</i> -Anisylmagnesium bromide in diethyl ether		
2.180	2.510	3.338
1.300	2.498	3.336
0.575	2.473	3.340
0.440	2.490	3.344
0.127	2.460	3.314
<i>p</i> -Anisylmagnesium bromide in tetrahydrofuran		
1.093	2.514	3.400
0.679	2.505	3.395
0.549	2.521	3.411
0.429	2.514	3.402
0.271	2.509	3.399
0.138	2.504	3.392
<i>p</i> -Tolylmagnesium bromide in ether		
1.140	2.098	3.086
1.090	2.081	3.063
0.778	2.106	3.090
0.569	2.080	3.076
0.196	2.137	3.109
0.139	2.137	3.113
0.090	2.183	3.133
0.049	2.175	3.135

The nmr spectrum of *p*-tolylmagnesium bromide was investigated within the concentration range 0.2–0.6 *M* using tetrahydrofuran, 70:30 triethylamine–ether, and glyme as solvents. The results with all these media were remarkably similar.

(16) A. Rembaum, S.-P. Siao, and N. Indictor, *J. Polymer Sci.*, **56**, 517 (1962).

(17) Terminology of J. A. Pople, W. G. Schneider, and H. J. Bernstein, "High Resolution Nuclear Magnetic Resonance," McGraw-Hill Book Co., Inc., New York, N. Y., 1959, Chapter 6.

(18) (a) P. Diehl, *Helv. Chim. Acta*, **44**, 829 (1961); (b) J. C. Corio and B. P. Dailey, *J. Am. Chem. Soc.*, **78**, 3043 (1956); (c) H. Spiesscke and W. G. Schneider, *J. Chem. Phys.*, **35**, 731 (1961); (d) W. Smith, *J. Mol. Spectry.*, **12**, 146 (1964).

(19) J. D. Swalen, International Business Machines Corp., San Jose, Calif.

(20) E. C. Ashby and M. B. Smith, *J. Am. Chem. Soc.*, **86**, 4363 (1964).

(21) T. V. Talalaeva, A. N. Rodionov, and K. A. Kocheshkov, *Dokl. Akad. Nauk SSSR*, **154**, 174 (1964).

(22) It is also possible that shifts among species were degenerate.

Table III: Uv Spectral Data for Metal Phenolates, Ar(OM)_n

Ar	M	Solvent	λ_{\max} , m μ	Lit.							
				M	Solvent	λ_{\max} , m μ	Log ϵ				
Phenyl	Li	Ether	287	Na ^a	CH ₃ OH	289.5	3.68				
						237.5	4.25				
<i>p</i> -Tolyl	Li	Ether	{ 295 242 222	Na ^b	C ₂ H ₅ OH	309	3.49				
								<i>p</i> -Tolyl	Li	THF	{ 293 249

^a T. W. Campbell and G. M. Coppinger, *J. Am. Chem. Soc.*, **73**, 2708 (1951). ^b G. A. Wiley and J. Meinwald, *J. Org. Chem.*, **23**, 166 (1958).

Di-*p*-tolylmagnesium, 0.5 *M*, gave an nmr spectrum very similar to that of *p*-tolylmagnesium bromide, 1.0 *M*. Furthermore, a 1:1 mixture of di-*p*-tolylmagnesium with diethylmagnesium, which may be assumed to yield a distribution of these two compounds with ethyl-*p*-tolylmagnesium, gave an aromatic spectrum no different from di-*p*-tolylmagnesium. Evidently, the ring currents in di-*p*-tolylmagnesium do not affect the chemical shifts of the neighboring rings.

The AA'BB' systems discussed here are very sensitive to the sign chosen for the smaller coupling constants. On the basis of these analyses, it is concluded that, at least among the organometallic reagents which gave A₂B₂ spectra, all the coupling constants are of the same sign. Most likely, this conclusion also applies to all the reagents in Table I.

The coupling constants for the aromatic organometallic reagents are quite different from those for ordinary covalently substituted benzenes. Thus for the ArM compounds, $J_{2,6}$, $J_{2,5}$, and $J_{2,3}$ are 0.6–1.1, 0.5–0.6, and 7.0–7.5 Hz, respectively; among ordinary covalently substituted benzenes, we find values around 2.0–3.0, 0.3–0.5, and 8.0–9.0 Hz. Castellano and Sun have shown that coupling constants of *ortho* with other hydrogens in a series of monosubstituted benzenes increase with the substituent electronegativity.²³ Pyridine properly belongs to the electropositive limit of such a series. A qualitative survey of the presently available data on such compounds^{11,18,23,24} reveals that, proceeding down the substituent electronegativity scale to pyridine,¹⁰ $J_{2,3}$, $J_{2,6}$, and $J_{2,4}$ decrease while $J_{2,5}$ increases. The coupling constants for the aromatic organometallic reagents are far more similar to those of pyridine²⁵ than to values for more covalently substituted benzenes.

It is also interesting that among the present and previous results^{9,10} the *para* substituent in ArM has some influence on coupling constants. $J_{2,6}$ increases with the electronegativity of the substituent in the order $H \simeq CH_3 < CH_3O \simeq (CH_3)_2N$.

The resemblance among coupling constants for aromatic organometallic reagents to those in the pyridines¹⁰ persists also among the *ortho* ring hydrogen shifts in these materials. Hydrogens *ortho* to the carbon-metal bond are always deshielded with respect to benzene, in one case, H₂ in *m*-dilithiobenzene, by as much as 2.3 ppm. The magnitude of this deshielding increases with decreasing metal electronegativity.

In summary, we find that the nmr parameters for arylorganometallics are more similar to those for the corresponding heterocycles than to values for covalently substituted benzenes. This is most evident in the low values for the *ortho* shifts and the relatively large sizes of $J_{2,5}$.

To explore further the electronic similarities among ArM compounds and pyridines, we obtained uv spectra for several aromatic organometallic compounds.

Low concentrations, 0.001 *M*, in ether or THF of both the aromatic magnesium and lithium compounds gave uv spectra which were identical with those for the corresponding phenoxides. Examples are listed in Table III. This assignment was confirmed with uv spectra of lithium and magnesium phenoxides. Prominent in these spectra is a band at about 295 m μ ($\epsilon \simeq 3000$). Evidently, even though the solvents used in this work were distilled from organometallic reagents, there was still enough peroxide present to oxidize low concentrations of ArM.

Problems due to peroxide impurities in the solvents were eliminated by using more concentrated solutions of ArM reagents, 0.04–0.2 *M*, in conjunction with a short-path uv cell; see the Experimental Section. Organometallic reagents which were purified by crystal-

(23) S. Castellano and C. Sun, *J. Am. Chem. Soc.*, **88**, 4741 (1966).

(24) D. M. Grant, R. C. Hirst, and H. S. Gutowsky, *J. Chem. Phys.*, **38**, 470 (1963); P. F. Cox, *J. Am. Chem. Soc.*, **85**, 380 (1963); B. Dischler, *Z. Naturforsch.*, **209**, 888 (1965).

(25) W. G. Schneider, H. J. Bernstein, and J. A. Pople, *Ann. N. Y. Acad. Sci.*, **70**, 806 (1958); V. J. Kowalewski and D. G. de Kowalewski, *J. Chem. Phys.*, **36**, 266 (1962); J. B. Merry and J. M. Goldstein, *J. Am. Chem. Soc.*, **88**, 5563 (1966).

lization or precipitation gave reproducible uv spectra. Uv spectral analysis of the hydrolysates revealed only weak absorption due to the expected quantity of hydrocarbon.

In the spectral region for which we report uv data, Li^+ , Mg^{2+} , and Br^- were found to be essentially transparent. As indicated in Table IV, the data for *p*-tolyllithium in ether follow Beer's law to a rough approximation. It is also interesting that the optical density of 0.1 *M* diphenylmagnesium in ether is almost exactly twice that of 0.1 *M* phenylmagnesium bromide.

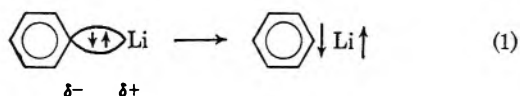
Table IV: Effect of Concentration on the Uv Absorption of *p*-Tolyllithium

$\lambda_{\text{max.}}$ $m\mu$	Concn, <i>M</i>		
	0.0217	0.0804	0.2350
261.5	ϵ^a	1390	1400
267.5		1470	1530
272.0		1340	1430

^a Apparent extinction coefficient.

Tables V and VI list uv data for a number of ArM compounds, and Figures 2-5 illustrate several examples of these spectra. Their principal features are: (1) strong absorption in the region around 260 $m\mu$ (ϵ 1000-3000); (2) a long tail stretching toward 350 $m\mu$; and (3) a solvent-dependent shoulder, not always discerned.

Assuming that the analogies we have suggested among ArM compounds and pyridines hold, one might expect uv absorption due to $\pi \rightarrow \pi^*$, some transition analogous to $n \rightarrow \pi^*$ in pyridine, and possibly charge transfer from carbon to metal²⁶



We now assign the strong 260- $m\mu$ region absorption to $\pi \rightarrow \pi^*$ ²⁷ excitation by analogy to the allowed ${}^1\text{B}_1\text{-A}_1$ transition in pyridine. The weak low-energy absorption in the tails of these spectra is analogous to the forbidden weak band due to $n \rightarrow \pi^*$ in pyridine.^{27,28} Such a transition for the ArM compounds is now written $\sigma_{\text{C-M}} \rightarrow \pi^*$, to the extent that the carbon-metal bonds may be partially covalent.

The $\sigma_{\text{C-M}} \rightarrow \pi^*$ transition should be subject to a blue shift analogous to that observed for $n \rightarrow \pi^*$ in pyridine and the diazines with progressively stronger hydrogen-bonding media.²⁸ It might be expected that ΔE ($\sigma_{\text{C-M}} \rightarrow \pi^*$) would increase with the covalent character of the carbon-metal bond. Such a trend is seen qualitatively, since there is less tailing at higher wavelengths in the magnesium compounds than in the lithium compounds.

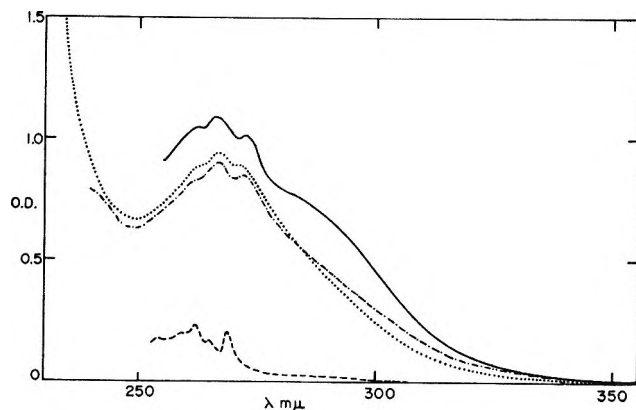


Figure 2. Uv spectra of *p*-tolyllithium (cell path = 0.05 mm): —, 0.15 *M* triethylamine-ether (85:15); ····, 0.10 *M* pentane-ether (85:15); - · - ·, 0.12 *M* ether; - - - -, hydrolysate of first solution.

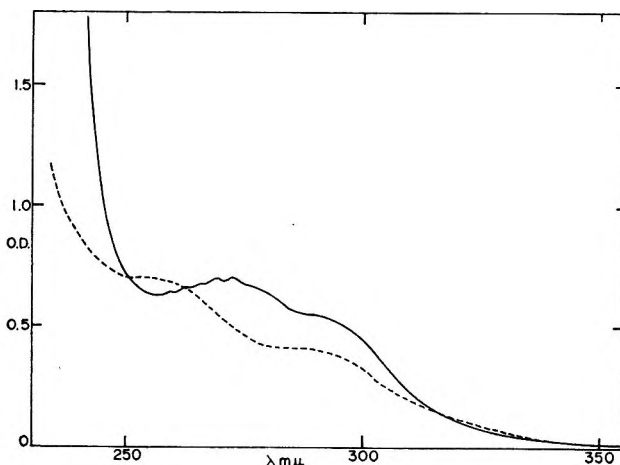


Figure 3. Uv spectra in ether: —, mesityllithium (0.045 *M*), path = 2 mm; - - - -, *m*-dilithiobenzene (0.1 *M*), path = 0.05 mm.

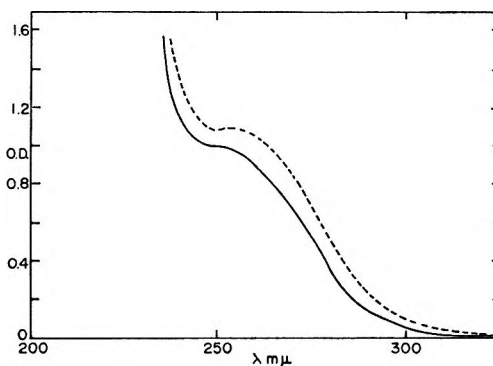


Figure 4. Uv spectra in THF (path = 0.1 mm): - - - -, 1,4-bis(bromomagnesio)benzene (0.06 *M*); —, *p*-tolylmagnesium bromide (0.07 *M*).

(26) Singlet state.

(27) H. P. Stephenson, *J. Chem. Phys.*, **22**, 1077 (1954).

(28) M. Kasha and G. J. Brealey, *J. Am. Chem. Soc.*, **77**, 4452 (1955).

Table V: Uv Data on Aryllithium Compounds

Ar	Solvent	Concn, <i>M</i>	λ_{\max} , $m\mu$	ϵ^a	Hydroly- sate uv (ref)
Phenyl ¹⁰	Ether	0.252	256 ^b	928	<i>c</i>
			261	1,000	
			267	996	
<i>p</i> -Tolyl	Ether	0.235	267	1,530	<i>d</i>
			272	1,430	
<i>p</i> -Tolyl	Pentane, 15% ether	0.104	267	1,820	<i>d</i>
			271	1,720	
<i>p</i> -Tolyl	Triethylamine, 15% ether	0.145	266	1,505	<i>d</i>
			273	1,400	
			285 ^b	1,000	
<i>p</i> -Anisyl	Ether	0.098	271	2,340	<i>e</i>
			275	2,350	
<i>p</i> -Dimethylamino- phenyl	Ether	0.0132	252	14,000	<i>f</i>
			257 ^b	12,600	
Mesityl	Ether	0.045	269	1,000	<i>g</i>
			294 ^b	590	
<i>m</i> -Phenylene	Ether	0.100	255 ^b	1,400	<i>c</i>
			288 ^b	820	

^a Apparent extinction coefficient. ^b Shoulder. ^c T. W. Campbell, S. Linden, S. Godshalk, and W. G. Young, *J. Am. Chem. Soc.*, **69**, 880 (1947). ^d E. A. Fehnel and M. Carmack, *ibid.*, **71**, 84 (1949). ^e J. J. Dearden and W. F. Forbes, *Can. J. Chem.*, **37**, 1305 (1959). ^f F. Walba and G. E. K. Branch, *J. Am. Chem. Soc.*, **73**, 3341 (1951). ^g E. A. Fehnel and M. Carmack, *ibid.*, **71**, 2932 (1949).

Table VI: Uv Data on Aromatic Grignard Reagents RMgBr in Tetrahydrofuran

R	Concn, <i>M</i>	λ_{\max} , $m\mu$	ϵ^a
Phenyl ¹⁰	0.09	255	1680
<i>p</i> -Phenylene	0.06	255	1840
<i>p</i> -Tolyl	0.07	250	1410
<i>p</i> -Anisyl	0.07	277	1720

^a Apparent ϵ .

Finally, in certain spectra there is a shoulder whose position depends on the nature of the solvent. For instance, a well-defined shoulder is observed at 285 $m\mu$ for *p*-tolyllithium in 85:15 triethylamine-ether. This is barely discernible when the solvent is pure ether and cannot be observed when the solvent is 85:15 pentane-ether. This progression is accompanied by an increase in the apparent extinction coefficient of the main band. Hence, it is likely that the absorption band responsible for the shoulder²⁹ undergoes a bathochromic shift with increasing solvent polarity. Such behavior indicates the operation of a transition whose excited state is more polar than the ground state. The simplest such process would involve increasing the ionic character of the carbon-metal bond in the photoexcited state. Note that partial photoioniza-

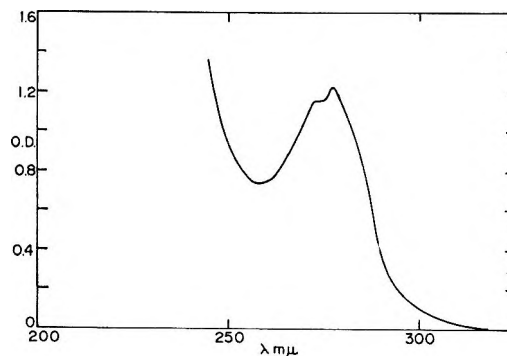
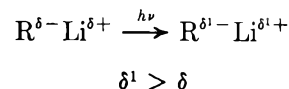


Figure 5. Uv spectrum in THF of *p*-anisylmagnesium bromide (0.07 *M*), cell path = 0.1 mm.

tion³⁰ of ligands is a well-recognized process³¹ in inorganic systems.



Uv evidence has been presented above for $\pi \rightarrow \pi^*$,

(29) Mesityllithium and *m*-dilithiobenzene behave in a similar fashion: S. Dayagi, unpublished observations.

(30) Conclusions from recent photochemical studies on organomagnesium and organolithium compounds support this suggestion: W. Breitigam, M.S. Thesis, The Ohio State University, Columbus, Ohio, 1967.

(31) J. G. Calvert and J. N. Pitts, "Photochemistry," John Wiley and Sons, Inc., New York, N. Y., 1966, p 269.

$\sigma_{C-M} \rightarrow \pi^*$, and a partial carbon-metal photoionization excitation in arylorganometallic compounds. Also, it was shown how similar the nmr parameters are among ArM compounds and pyridines. All these data support the suggestion that the two sets of compounds have similar electronic structures.

In the previous paper,¹⁰ we have examined the origins of the hydrogen shifts in arylmetallic compounds. It was shown that the effects on the shifts due to changes in the ring current³² and π -electron densities³³ were not important. The influence of the electric field due to the carbon-metal bond dipole was discounted.³⁴ Finally, on the basis of the analogies with pyridine it was concluded that paramagnetic³⁵⁻³⁷ terms dominate especially the *ortho*-proton shifts in phenyllithium and phenylmagnesium bromide. Note, however, that whereas in pyridine π -electron density and paramagnetic terms are mainly responsible for the proton shifts, in ArM there is no conjugative mechanism to produce large variations in the π -electron densities around the rings.

Paramagnetic shifts in pyridine arise from magnetic mixing of the ground and nearest excited electronic states ($n \rightarrow \pi^*$).¹² Since perturbation theory is used to calculate these shifts, the paramagnetic term is always inversely proportional to the mean electronic excitation energy, taken to be $\Delta E(n \rightarrow \pi^*)$ in this case.

$$\delta_{\text{para}} \propto \frac{1}{\Delta E} \quad (2)$$

The following discussion concerns the suggestion that effects similar to those discussed for shifts in pyridine take place in the ArM compounds also.

As described above, our uv evidence indicates that the lowest electronically excited state in ArM compounds is very similar to that in pyridine. Furthermore, this weak absorption assigned to $\sigma_{C-M} \rightarrow \pi^*$ appears to shift to lower wavelengths with increasing electronegativity of the substituent metal. An increase in $\Delta E(\sigma_{C-M} \rightarrow \pi^*)$ should be accompanied by a decrease in magnitude of the paramagnetic shift. This is actually observed for the *ortho* shifts in the reagents studied in this work and elsewhere.^{9,10}

The effect of different solvents on the ring shifts in ArM compounds would be expected to operate *via* changes in the coordination of metal to solvent. This would alter the ionic character of the carbon-metal bond, $\Delta E(\sigma_{C-M} \rightarrow \pi^*)$ and hence also the paramagnetic shift. Effects due to solvents in this work are found to be quite small.

In McConnell's point-anisotropy approximation³⁸ for paramagnetic shifts, there is a geometrical factor of $(1 - 3 \cos^2 \theta)/R^3$. The latter is *linear* with the shifts observed for phenyllithium.¹⁰ Among the magnesium compounds, such a treatment gives only qualitative agreement.

With regard to substituent effects on the ring shifts in the ArM reagents, the evidence is that, in most cases, the effect of the substituent is constant and independent of the nature of the metal.

Ring hydrogen shifts in a large number of substituted benzenes are given accurately by a linear combination of empirically derived contributions from the different substituents.^{11,18} This correlation holds even though the shifts from different substituents are due to several effects. A similar relationship pertains to hydrogen shifts in γ -substituted picolines.³⁹ To test whether this correlation also applies to metals as substituents, we have calculated shifts from substituent constants for the ArM reagents studied here. The shifts, with respect to benzene around phenyllithium and phenylmagnesium bromide were used as the metal-substituent constants, Table VII. All others were obtained from the literature.¹⁸ The results of this comparison are listed in Table VIII. It is seen that the correlation applies very poorly to the last three examples. The largest deviations take place in the lithium compounds when the substituent is Cl, $N(\text{CH}_3)_2$, or OCH_3 . Where the deviation for the calculated *ortho* shift is large, *p*-chlorophenyllithium, it may be speculated on the basis of the preceding arguments that here the carbon-lithium bond is only as ionic as the C-Mg bond in the corresponding Grignard reagent. In those cases where the deviation in the calculated *meta* shift is large, this may reflect some interaction between M in ArM with the substituent on a neighboring ArM fragment.

Table VII: Ring Shifts in $\text{C}_6\text{H}_5\text{Li}$ and $\text{C}_6\text{H}_5\text{MgBr}$ ^a

	δ_o^b	δ_m	δ_p
$\text{C}_6\text{H}_5\text{Li}$	-0.767	+0.232	+0.299
$\text{C}_6\text{H}_5\text{MgBr}$	-0.381	+0.239	+0.282

^a References 9 and 10. ^b Shifts with respect to benzene, ppm.

Finally, it should be pointed out that the data presented here do not provide information on the struc-

(32) (a) J. A. Pople, *Proc. Roy. Soc. (London)*, **A239**, 541 (1957); (b) J. A. Pople, *ibid.*, **A239**, 550 (1957); (c) G. E. Johnson and F. M. Bovey, *J. Chem. Phys.*, **29**, 1012 (1958); (d) N. Jonathan, S. Gordon, and B. P. Dailey, *ibid.*, **36**, 2443 (1962); (e) J. S. Waugh and R. W. Fessenden, *J. Am. Chem. Soc.*, **79**, 846 (1957).

(33) (a) G. Fraenkel, R. E. Carter, A. D. McLachlan, and J. H. Richards, *J. Am. Chem. Soc.*, **82**, 5846 (1960), and references cited therein; (b) J. I. Musher, *J. Chem. Phys.*, **37**, 34 (1961); (c) A. D. Buckingham, *Can. J. Chem.*, **38**, 300 (1960); (d) B. P. Dailey and J. S. Martin, *J. Chem. Phys.*, **39**, 1722 (1963).

(34) G. Fraenkel and J. P. Kim, *J. Am. Chem. Soc.*, **88**, 4203 (1966).

(35) Reference 32a, p 544.

(36) Reference 33d, p 1725.

(37) J. D. Das and R. Bersohn, *Phys. Rev.*, **104**, 476 (1956).

(38) H. M. McConnell, *J. Chem. Phys.*, **27**, 226 (1957); A. A. Bothner-By and C. Naar-Colin, *J. Am. Chem. Soc.*, **80**, 1728 (1958).

(39) T. K. Wu and B. P. Dailey, *J. Chem. Phys.*, **41**, 3307 (1964).

tures of these ArM aggregates in solution and the role of bridged bonding. These questions have been omitted from the discussion.

Table VIII: Shifts in ArM (0.5 M) Obtained from Substituent Constants and Deviations from Observed Values

Species, solvent	Calcd		Obsd - calcd shifts	
	τ_o	τ_m	<i>ortho</i>	<i>meta</i>
<i>p</i> -Tolylmagnesium bromide, ether	2.502	3.152	+0.013	-0.090
<i>p</i> -Anisylmagnesium bromide, ether	2.502	3.340	+0.094	-0.062
<i>p</i> -Chlorophenylmagnesium bromide, ether	2.422	2.922	+0.039	-0.015
<i>p</i> -Tolyl lithium, ether	2.116	3.145	-0.026	-0.065
<i>p</i> -Anisyl lithium, ether	2.116	3.425	-0.086	-0.225
<i>p</i> -Dimethylamino-phenyllithium, ether	2.176	3.765	-0.083	-0.452
<i>p</i> -Chlorophenyllithium, ether	2.036	2.915	+0.509	-0.171

Experimental Section

Gases. Nitrogen, helium, and argon were dried and deoxygenated with an ether solution of methylmagnesium bromide.

Inorganic Halides. Magnesium bromide and lithium bromide were prepared from ethylene dibromide with excess metal in ether. The bromides were purified by successive precipitations from ether solution with pentane.

Organic Compounds. Unless otherwise stated, the organic compounds used in this research were of commercial origin. The halides, if solid, were crystallized and dried *in vacuo*. Liquids were dried over P_2O_5 and then distilled under nitrogen. 9,10-Dibromo-1,2,3,4,5,6,7,8-octahydroanthracene was kindly donated by Professor M. P. Cava.

Solvents. Commercial diethyl ether was distilled from methylmagnesium bromide. Tetrahydrofuran and triethylamine was dried over calcium hydride overnight and then distilled from lithium aluminum hydride under nitrogen.

Grignard Reagents. These were prepared as previously described.¹⁰

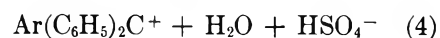
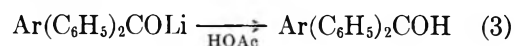
The solutions were analyzed by acidimetric titration using methyl orange as the indicator, and magnesium was determined with EDTA using Eriochrome Black Tin an ammonia buffer. Starting materials and impurities formed in these reactions were determined by a combination of vapor-phase chromatography and nmr spectroscopy.

Nmr Spectroscopy. All nmr spectra were obtained with the Varian A-60 nmr spectrometer, care being taken to optimize the resolution and avoid saturation.

Otherwise, the instrumental settings were unexceptional.

Organolithium Compounds. The aromatic lithium compounds were prepared by the reaction of the corresponding bromo compound with *n*-butyllithium.¹³ The following operations were conducted in a drybox under nitrogen. A solution of 0.002 mol of the aromatic bromide in 2 ml of deoxygenated pentane was syringed into a vial protected by a straight-bore stopcock and serum cap. An equivalent amount of *n*-butyllithium, 2 M , in hexane was added to the above solution and the reaction mixture allowed to stand at room temperature for 6 hr. Within 2 hr, the organolithium compound precipitated out. After 6 hr, the precipitate was washed with pentane and dissolved in the desired solvent for uv, nmr, and chemical analysis. In this way, the following organolithium compounds were prepared in nearly quantitative (95%) yield: *p*-dilithiobenzene, *m*-dilithiobenzene, mesityllithium, *p*-dimethylaminophenyllithium, *p*-anisyllithium, phenyllithium, and *p*-tolyllithium. In certain cases, phenyllithium and *p*-tolyllithium, the reagents were crystallized from ether. However, this procedure gave results identical with the first one.

Chemical Analysis of the Organolithium Compounds. Organolithium solution (1 ml) was syringed into a solution of 0.2 g of benzophenone in 2 ml of dry ether in a 25-ml volumetric flask. After standing 1 day at room temperature, glacial acetic acid was added up to the 25-ml mark. Then, 1 ml of this solution was diluted with 96% sulfuric acid to about 10^{-5} M in contained aromatic compounds. By this method, benzophenone reacts with the organolithium compound to give the triarylcarbinol and the latter is converted to the cation in strong acid (see reactions 3 and 4). The visible



spectra of the sulfuric acid solutions were determined and the concentration of triaryl cation was calculated using the extinction coefficients listed in the literature; see Table IX. In this way, the concentration of the organolithium compound was obtained. The yields for reaction of $ArLi$ with benzophenone are assumed to be nearly quantitative.

The dilithio compounds and mesityllithium do not react quantitatively with benzophenone; their concentrations were determined by acidimetric titration and by uv analysis of the hydrolysis products.

Both methods of analysis showed the organolithium compounds used in this work to be at least 98% pure. The level of impurities in the solutions was below our experimental error.

Table IX: Visible Absorption Spectra in $\text{Ar}(\text{C}_6\text{H}_5)_2\text{C}^+$ in H_2SO_4

Ar	$\lambda_{\text{max.}}$ $\mu\mu$		Lit. ϵ	Ref
	This work	Lit.		
Phenyl	405	408	36,400	a
	431	431	37,400	a
<i>p</i> -Tolyl	450	450	45,700	b, c
<i>p</i> -Anisyl	472	470	46,800	b
<i>p</i> -Dimethylamino-phenyl	445	446	33,100	d

^a V. Gold and B. W. V. Hawes, *J. Chem. Soc.*, 2102 (1951).

^b N. C. Deno, J. J. Jaruzelski, and A. Schriesheim, *J. Org. Chem.*, **19**, 155 (1954). ^c N. C. Deno, J. J. Jaruzelski, and A. Schriesheim, *J. Am. Chem. Soc.*, **77**, 3044 (1955). ^d G. Branch and H. Walba, *ibid.*, **76**, 1564 (1953).

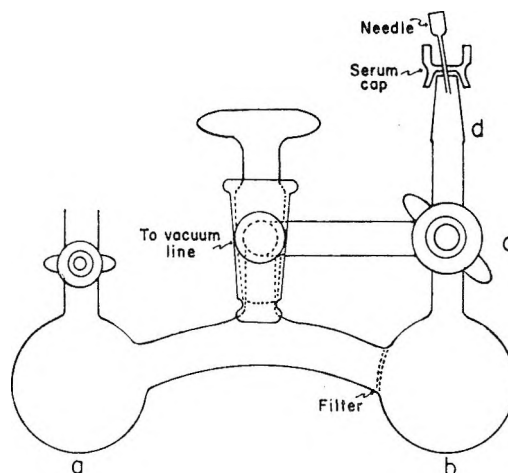


Figure 6. Apparatus for purification of organometallic reagents.

p-Tolylcalcium Iodide. The apparatus for Grignard preparations was used. Diethyl ether (40 ml) was distilled from lithium aluminum hydride into the reaction vessel under an atmosphere of argon. Calcium powder (Ethyl Corp.)⁴⁰ (0.14 mol, 0.56 g) was added together with a small amount of magnesium to catalyze the reaction.⁴¹ Freshly distilled *p*-iodotoluene (0.07 mol, 14.7 g) was added over a period of 2 hr at 0° with stirring. Reaction was evident from the appearance of a purple color and the precipitation of calcium iodide. Stirring was maintained for 2 additional hr. The reaction mixture was then filtered and samples removed for chemical and nmr analysis. This sample was 1.0 M in *p*-tolylcalcium iodide.

Purification of Organomagnesium Compounds by Crystallization. The apparatus in Figure 6 was flamed out in a current of dry argon. Grignard solution was syringed into side d through the straight-bore stopcock, c. First, the system was attached to the vacuum line and the contents pumped out and degassed. By tilting the apparatus, the solution was filtered into side b. Cooling with Dry Ice-acetone effected crystallization. The mother liquor was filtered into side a, and the crystals were washed with pentane, distilled over the vacuum line. Finally, the crystals were dissolved in ether, the apparatus was filled with argon, and samples of solution were removed with a syringe.

Purification of Organomagnesium Reagents by Precipitation. A volumetric flask, 50 ml, was covered with a serum cap and flushed with dry nitrogen using two needles: one for introduction of and the other for exit of gas. After the solution sample, 10 ml, was transferred to the volumetric flask with a syringe, the flask was put in a drybox under a nitrogen atmosphere.

Hexane, 10 ml, distilled from lithium aluminum hydride under a helium gas stream was added to the

sample in the drybox with a syringe. A white precipitate was formed immediately, if the Grignard reagent concentration was over 0.3 M.

After standing for 2 hr, the supernatant solution was removed with a syringe, carefully, to avoid sucking out the precipitate. Then, new hexane was injected into the sample and it was washed several times in this way. The white precipitate in the flask was washed with a small amount of ether, 0.5 ml, and the washings were removed to take out the remaining hexane, two times. The appropriate volume of ether was injected to dissolve the remaining white crystals on the walls and the solution was utilized for the uv and nmr sample.

Uv Spectroscopy. The Cary-14 recording spectrophotometer was used.

Uv Sample. The uv cell manufactured by the Limit Research Corp. consists of two quartz plates, separated by a Teflon spacer, 0.1 mm, the entirety being clamped between stainless steel plates. Two Luer syringe joints were attached to the cell for filling purposes. The cell was flushed with dry nitrogen for over 2 hr. The sample, 0.4 ml, was taken up into a syringe equipped with a stopcock, transferred to a drybox under a nitrogen atmosphere, and injected into the cell. The syringe joints on the cell were then closed with Teflon stoppers, and the uv spectrum was obtained. The rest of the sample, 2 ml, was removed from the drybox and hydrolyzed with air-free water.

Acknowledgment. This research was supported by the Air Force office of Scientific Research, Grant No. AF-AFOSR-251-63, and the National Institutes of Health, Grant No. GM. 08686-05.

(40) We thank the Ethyl Corp., New York, N. Y., for a generous gift of calcium powder.

(41) C. Glacet, *Bull. Soc. Chim.*, **5**, 895 (1938); Bryce-Smith, *J. Chem. Soc.*, 577 (1963).

Vibrational Intensities. XVIII. Infrared Band Shapes for Some Liquid Methyl Iodide Bands

by C. E. Favelukes, A. A. Clifford, and Bryce Crawford, Jr.

Molecular Spectroscopy Laboratory, Department of Chemistry, University of Minnesota, Minneapolis, Minnesota 55455
(Received August 28, 1967)

The optical constants for the 522- and 884-cm⁻¹ bands of pure liquid methyl iodide were measured using an attenuated total reflection technique. Evidence from the band shapes for partial rotation of the molecules in the liquid phase is discussed by comparing the band shapes with the Van Vleck and Weisskopf band shape and also by means of time-correlation functions.

The infrared absorption bands of the methyl halides in solution have been studied in a number of laboratories.¹⁻³ The perpendicular bands show unusually large band widths and in some cases unusual band shapes, whereas the parallel bands were found to be fairly normal in both respects. The difference has been explained by assuming that, in liquids, rotation of the methyl halide molecules about the symmetry axis is comparatively weakly hindered by collisions.

The attenuated total reflection (ATR) techniques developed in this laboratory⁴⁻⁶ have made it seem worthwhile to restudy this problem, particularly with respect to band shapes. This technique can give results of good accuracy (with known dispersions), especially at the edges of the band: one is not plagued by the usual base-line errors. We therefore could calculate more confidently moments and time-correlation functions using the appropriate integral equations.^{7,8} Also, having values for the dispersions of the optical constants enabled us to complete the important task of propagating errors through the integral transforms, thus possibly avoiding futile interpretation of artifacts of the calculations. A drawback to using our single-reflection ATR technique is that it gives best results for fairly strong bands. For this reason we were obliged to work with pure methyl halides to obtain the best results, whereas the greatest band-shape effects have been previously observed in nonpolar solvents.³

Because it is the least polar of the methyl halides, as well as having convenient physical properties, methyl iodide was chosen for study. In particular, two fundamentals, one the perpendicular e fundamental at 884 cm⁻¹, and the other the a₁ parallel fundamental at 522 cm⁻¹, were chosen as they are sufficiently isolated from other bands. The optical constants for these two bands are shown in Tables I and II and were obtained using the latest modifications of our ATR methods.⁴⁻⁶ The optical constants, n and n_k , at each frequency were obtained from the best fit to four reflectivities, two at each of the angles given in the tables. The resolution of

the instrument was between 1 and 2 cm⁻¹ in both regions and the temperature was about 27°. The data were finally checked using the Kramers-Kronig transform, as described previously,⁶ and agreed well within the stated dispersions. The integrated intensities of the two bands, defined as $\Gamma = (4\pi/C_m) \int n_k d\nu$, are shown in Table III.

Comparison with Van Vleck and Weisskopf Band Shapes

The data were first compared to Van Vleck and Weisskopf⁹ band shapes, after correcting for dielectric effects by transforming to the local susceptibility, $\hat{C} = C' + iC''$, using the Lorentz-Lorenz field.¹⁰ The four Van Vleck and Weisskopf parameters for each band were obtained using unweighted least-squares refinement. These are shown in Table III, using the notation of ref 10. The experimental and calculated values of the local susceptibility are compared in Figure 1. As can be seen from this figure, agreement between the observed and calculated data for the 522-cm⁻¹ a₁ band is satisfactory and is largely within experimental error. For the 884-cm⁻¹ e band, the agreement is poorer. In particular, there is, comparatively, more intensity on the wings of the band than would be pre-

(1) W. J. Jones and N. Shepperd, *Trans. Faraday Soc.*, **56**, 625 (1960).

(2) W. K. Class and A. D. E. Pullin, *ibid.*, **59**, 25 (1963).

(3) M. D. Bulanin and M. V. Tonkov, *Opt. Spectry.*, **16**, 234 (1964).

(4) A. C. Gilby, J. Burr, Jr., and B. Crawford, Jr., *J. Phys. Chem.*, **70**, 1520 (1966).

(5) A. C. Gilby, J. Burr, Jr., W. Krueger, and B. Crawford, Jr., *ibid.*, **70**, 1525 (1966).

(6) W. C. Krueger, A. A. Clifford, and B. Crawford, Jr., *ibid.*, to be published.

(7) R. G. Gordon, *J. Chem. Phys.*, **43**, 1307 (1965); H. Shimizu, *ibid.*, **43**, 2453 (1965).

(8) R. G. Gordon, *ibid.*, **39**, 2788 (1963).

(9) J. H. Van Vleck and V. F. Weisskopf, *Rev. Mod. Phys.*, **17**, 227 (1945).

(10) A. A. Clifford and B. Crawford, Jr., *J. Phys. Chem.*, **70**, 1536 (1966).

Table I: Optical Constants for the 884-cm⁻¹ Band of Liquid Methyl Iodide

ν , cm ⁻¹	n_κ	$\sigma(n_\kappa)$	n	$\sigma(n)$	ν , cm ⁻¹	n_κ	$\sigma(n_\kappa)$	n	$\sigma(n)$
38.7°, 40.2° ^a					39.5°, 44.0° ^a				
1019.7	0.0008	0.0002	1.4975	0.0011	885.9	0.0488	0.0015	1.4947	0.0032
1009.6	0.0012	0.0002	1.4960	0.0014	884.8	0.0499	0.0015	1.4983	0.0032
999.6	0.0014	0.0002	1.4942	0.0015	883.7	0.0500	0.0015	1.5021	0.0031
989.7	0.0019	0.0003	1.4925	0.0016	882.6	0.0498	0.0015	1.5053	0.0030
979.9	0.0023	0.0003	1.4910	0.0016	880.0	0.0464	0.0014	1.5132	0.0028
970.3	0.0033	0.0003	1.4900	0.0016	877.8	0.0419	0.0013	1.5178	0.0026
959.7	0.0046	0.0004	1.4889	0.0016	876.3	0.0383	0.0011	1.5266	0.0025
950.0	0.0056	0.0004	1.4884	0.0016	874.2	0.0340	0.0010	1.5224	0.0023
945.3	0.0063	0.0004	1.4878	0.0016	872.1	0.0299	0.0009	1.5233	0.0022
38.5°, 41.0° ^a					39.5°, 42.0° ^a				
945.3	0.0060	0.0004	1.4890	0.0015	870.1	0.0263	0.0008	1.5235	0.0021
940.1	0.0068	0.0004	1.4886	0.0015	868.0	0.0235	0.0008	1.5232	0.0020
934.9	0.0078	0.0004	1.4874	0.0016	866.0	0.0206	0.0007	1.5227	0.0019
929.8	0.0084	0.0004	1.4870	0.0016	864.0	0.0182	0.0007	1.5221	0.0018
926.0	0.0092	0.0005	1.4863	0.0016	862.0	0.0164	0.0006	1.5212	0.0018
922.3	0.0097	0.0005	1.4856	0.0017	860.0	0.0147	0.0006	1.5204	0.0017
918.1	0.0109	0.0005	1.4846	0.0017	860.0	0.0146	0.0006	1.5209	0.0018
913.9	0.0125	0.0006	1.4834	0.0018	856.1	0.0122	0.0005	1.5193	0.0017
910.3	0.0144	0.0006	1.4821	0.0018	852.2	0.0105	0.0005	1.5180	0.0017
908.0	0.0157	0.0006	1.4812	0.0019	847.9	0.0090	0.0005	1.5165	0.0016
906.2	0.0168	0.0007	1.4806	0.0019	844.2	0.0078	0.0004	1.5156	0.0016
38.0°, 42.0° ^a					39.5°, 41.0° ^a				
906.1	0.0172	0.0006	1.4813	0.0019	840.0	0.0070	0.0004	1.5143	0.0016
903.8	0.0190	0.0007	1.4805	0.0019	839.9	0.0071	0.0005	1.5144	0.0017
902.0	0.0207	0.0007	1.4798	0.0020	835.2	0.0062	0.0004	1.5134	0.0017
899.8	0.0235	0.0007	1.4790	0.0020	830.2	0.0055	0.0004	1.5123	0.0016
898.1	0.0258	0.0008	1.4789	0.0021	825.2	0.0048	0.0004	1.5115	0.0016
895.8	0.0291	0.0009	1.4791	0.0022	819.9	0.0045	0.0004	1.5106	0.0016
894.1	0.0323	0.0010	1.4798	0.0023	810.1	0.0032	0.0003	1.5093	0.0015
891.9	0.0375	0.0011	1.4810	0.0025	39.5°, 40.5° ^a				
890.2	0.0412	0.0013	1.4831	0.0027	810.1	0.0033	0.0003	1.5091	0.0016
888.0	0.0459	0.0014	1.4880	0.0029	799.9	0.0025	0.0003	1.5078	0.0015
885.9	0.0488	0.0016	1.4952	0.0031	790.0	0.0017	0.0002	1.5068	0.0014
					780.2	0.0013	0.0002	1.5058	0.0013
					770.1	0.0009	0.0002	1.5053	0.0012

^a Angles of incidence.

dicted by Van Vleck and Weisskopf's model. Although this effect is not a large one, it is well outside the experimental error and is in accord with previous results for methyl bromide in carbon tetrachloride solutions.¹

Calculation of Time-Correlation Functions

The data were next investigated by means of an alternative approach that is completely independent of any model such as that of Van Vleck and Weisskopf. The time-correlation functions, $\alpha(t)$, were calculated using the equation

$$\alpha(t) = (1/N) \int n_\kappa(\omega) \cos(\omega t) d\omega$$

or rather the sum

$$\alpha(t) = (1/2Nt) \sum_i [n_\kappa(\omega_i) + n_\kappa(\omega_{i+1})] \times [\sin(\omega_{i+1}t) - \sin(\omega_i t)]$$

where ω is the circular frequency measured from the maximum of n_κ and N is a normalization coefficient to adjust $\alpha(0)$ to unity. The natural logarithms of the values of these functions, with their errors, are shown in Figure 2. The calculation of errors presents a problem because of the unknown extent to which the errors in optical constants at different frequencies are correlated. The optical-constant errors at all frequencies are somewhat correlated, and correlation between optical constant errors at frequencies close together is probably fairly strong. It is not possible, however, to assign numerical values to the correlation coefficients. One is therefore compelled to assume that all errors are fully positively correlated. Errors in the time-correlation functions, $\alpha(t)$, were calculated on this basis; *i.e.*, the dispersions $\sigma\{n_\kappa(\omega_i)\}$ simply replaced the value $n_\kappa(\omega_i)$ in the previous sum. The actual dispersions are

Table II: Optical Constants for the 552-cm⁻¹ Band of Liquid Methyl Iodide

ν , cm ⁻¹	n_{κ}	$\sigma(n_{\kappa})$	n	$\sigma(n)$
39.0°, 40.5° ^a				
599.8	0.0010	0.0002	1.4991	0.0014
594.8	0.0010	0.0002	1.4989	0.0013
589.8	0.0011	0.0002	1.4987	0.0014
585.0	0.0014	0.0002	1.4983	0.0014
580.3	0.0013	0.0002	1.4979	0.0014
575.1	0.0015	0.0002	1.4977	0.0014
570.1	0.0015	0.0002	1.4973	0.0014
565.2	0.0014	0.0002	1.4969	0.0014
559.8	0.0020	0.0002	1.4962	0.0014
555.1	0.0023	0.0002	1.4955	0.0014
550.1	0.0025	0.0003	1.4944	0.0013
545.1	0.0031	0.0003	1.4931	0.0014
539.8	0.0045	0.0003	1.4897	0.0016
538.2	0.0049	0.0004	1.4886	0.0016
536.2	0.0057	0.0004	1.4864	0.0017
534.1	0.0069	0.0004	1.4937	0.0017
532.1	0.0088	0.0005	1.4810	0.0017
38.2°, 44.0° ^a				
532.1	0.0092	0.0005	1.4822	0.0017
530.1	0.0129	0.0006	1.4788	0.0018
529.2	0.0155	0.0006	1.4769	0.0018
528.2	0.0188	0.0007	1.4751	0.0019
527.2	0.0233	0.0007	1.4731	0.0020
526.2	0.0293	0.0009	1.4718	0.0022
524.8	0.0405	0.0012	1.4731	0.0026
524.3	0.0442	0.0012	1.4750	0.0027
523.9	0.0478	0.0014	1.4773	0.0028
523.4	0.0506	0.0015	1.4811	0.0030
522.9	0.0521	0.0016	1.4862	0.0031
522.4	0.0527	0.0014	1.4920	0.0032
522.0	0.0523	0.0014	1.4978	0.0033
521.5	0.0511	0.0014	1.5033	0.0034
521.0	0.0491	0.0014	1.5087	0.0035
520.6	0.0463	0.0014	1.5135	0.0036
520.1	0.0435	0.0013	1.5176	0.0037
519.2	0.0378	0.0012	1.5231	0.0038
517.8	0.0310	0.0011	1.5258	0.0037
516.9	0.0276	0.0010	1.5261	0.0037
516.0	0.0247	0.0009	1.5258	0.0036
515.1	0.0222	0.0008	1.5253	0.0036
514.2	0.0196	0.0007	1.5255	0.0035
512.8	0.0163	0.0006	1.5244	0.0034
511.1	0.0127	0.0006	1.5231	0.0033
510.2	0.0115	0.0005	1.5217	0.0033
39.5°, 42.0° ^a				
510.2	0.0122	0.0007	1.5210	0.0018
508.0	0.0087	0.0006	1.5192	0.0017
505.9	0.0067	0.0005	1.5179	0.0016
504.2	0.0059	0.0005	1.5162	0.0016
502.1	0.0052	0.0005	1.5150	0.0015
500.1	0.0045	0.0004	1.5140	0.0015
494.9	0.0028	0.0004	1.5123	0.0014
490.2	0.0022	0.0004	1.5114	0.0013
485.0	0.0017	0.0004	1.5105	0.0013
479.3	0.0015	0.0004	1.5097	0.0012
39.25°, 40.25° ^a				
479.9	0.0007	0.0005	1.5095	0.0015
475.0	0.0005	0.0004	1.5089	0.0015

^a Angles of incidence.**Table III:** Band Constants for the 522- and 884-cm⁻¹ Bands of Liquid Methyl Iodide

Maximum of n_{κ} , cm ⁻¹	Intensity, cm ² /mol	Van Vleck and Weisskopf parameters ^a				
		ν_0 , cm ⁻¹	γ , cm ⁻¹	$10^4 S$	K	β , psec ⁻¹
522	730 ± 60	521.6	5.2	0.61	0.0704	1.06
884	1970 ± 110	(884.2) ^b	(16.0)	(1.02)	(0.0701)	2.5

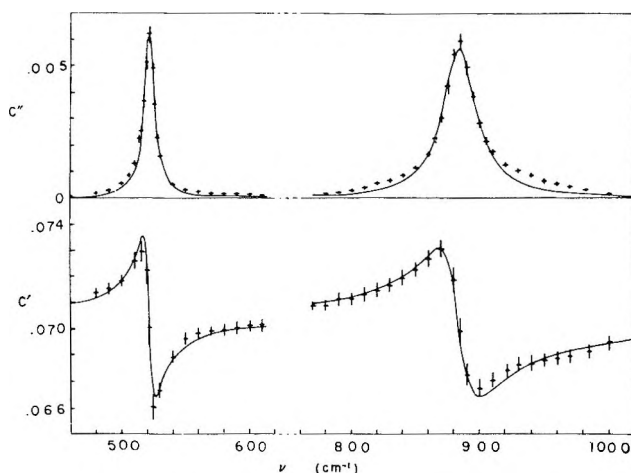
^a See ref 9 for notation. ^b Parentheses indicate that the fit to a Van Vleck and Weisskopf band was poor.

Figure 1. Comparison of experimental (crosses) and calculated (continuous line) local susceptibility for liquid methyl iodide. The heights of the crosses indicate the experimental dispersions.

thus likely to be considerably smaller than shown in Figure 2.

It is also possible to calculate time-correlation functions from the imaginary part of the local susceptibility, C'' . This has been advocated for strong bands in condensed phases¹⁰ as a way of avoiding dielectric effects. And indeed, for the 770-cm⁻¹ chloroform band and the 1510-cm⁻¹ carbon disulfide band of the pure liquids, there is a considerable difference between the time-correlation functions calculated from n_{κ} and C'' . However, for these weaker methyl iodide bands, the time-correlation functions calculated for C'' were essentially the same as those for n_{κ} . We therefore follow the more conventional practice of using functions calculated from n_{κ} .

Interpretation of the Time-Correlation Functions

The time-correlation function, $\alpha(t)$, may be interpreted in various ways. Macroscopically and most simply, it is the decay function for the component of polarization with frequency ν_0 . If we irradiate the sample with light of this frequency for a long enough time, the polarization will vary with the same frequency, following after the imposed field; if then we turn off the imposed field at time $t = 0$, the amplitude of the oscillat-

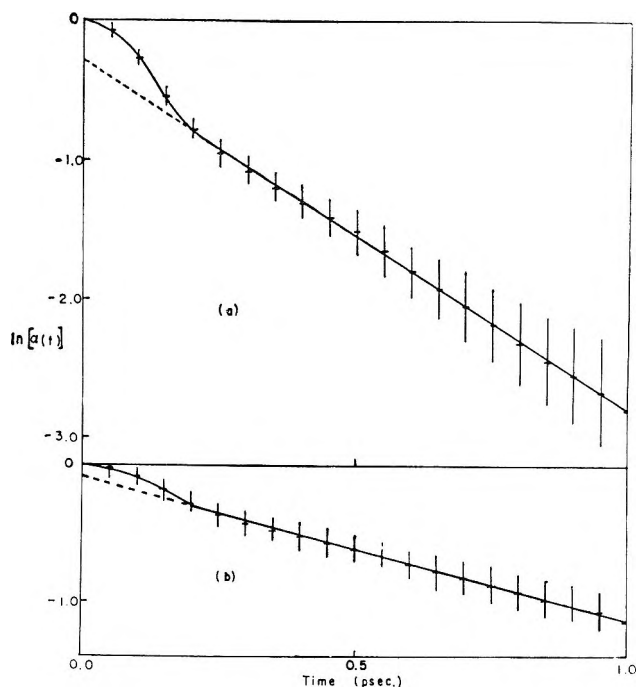


Figure 2. The natural logarithms of the time-correlation functions of (a) the 884-cm^{-1} perpendicular band, and (b) the 522-cm^{-1} parallel band of liquid methyl iodide. The heights of the crosses indicate the experimental dispersions.

ing polarization will decay, and $\alpha(t)$ describes this decaying amplitude.

From a microscopic or molecular viewpoint, a time-correlation function $\alpha(t)$ gives an average value for the cosine of the angle between the transition-moment vector at any time, and the transition moment t sec later.⁷ Thus, these functions describe how the molecules move, on the average, in the liquid. In our case, the two time-correlation functions describe motions about different molecular axes. The transition-moment vector responsible for the 884-cm^{-1} e band is perpendicular to the symmetry axis of the molecule. This vector can move by rotation of the molecule either about the symmetry axis or about a perpendicular axis. The transition-moment vector for the 522-cm^{-1} a_1 band is parallel to the symmetry axis; hence this vector can move only by rotation of the molecule about a perpendicular axis. Therefore Figure 2b, derived from the a_1 band, describes rotation of methyl iodide about the perpendicular axes of the molecule, whereas Figure 2a, derived from the e band, describes motion about both the symmetry axis and a perpendicular axis.

The Lorentzian of the VVW model would predict a pure exponential correlation function; *i.e.*, graphs such as Figure 2 would show a sloping straight line. Deviations from such a straight line in Figure 2 are straightforward reflections of the deviations from the VVW model shown in Figure 1.

Gordon⁷ has described the expected behavior of time-correlation functions at long and short times.

At short times, only a few of the molecules will have received hard collisions; most will be rotating fairly freely. The correlation function will be a superposition of periodic functions. Later on, most molecules will have undergone a number of hard collisions and will be approaching random orientation in an exponential way.

Both our time-correlation functions show this behavior, as can be seen from Figure 2. On the logarithmic scale, the exponential decay at long times appears as a straight line on both graphs. The deviations from the straight lines are the initial inertial rotations. For both functions, the change of behavior occurs after the same period of time, that is approximately 0.2 psec. Thus we can say that after some 0.2 psec, on an average, a methyl iodide molecule, in the pure liquid, receives one or more collisions which largely disrupt its inertial motion.

The value that the correlation function has reached when this change in behavior occurs is different for the two bands. The a_1 data in Figure 2b show a correlation value at this point of 0.75; the e data in Figure 2a show a value of 0.45. Since the e data, as we have discussed, involve the presumably faster rotation about the symmetry axis, it is satisfying that they show the lower correlation at 0.2 psec. Indeed we may push forward to a pictorial overinterpretation of our data: taking Gordon's interpretation literally, we take the arc cosine of 0.75 and say that the a_1 moment vector has moved 41° in 0.2 psec. Since this movement has occurred about two perpendicular axes with equal moments of inertia, we can say that the molecule moves about 30° about each perpendicular axis before disruptive collision occurs. Similarly, from the e data of Figure 2a, we take the arc cosine of 0.45 and find for the e moment vector an angular movement of about 65° . This corresponds to motion about a perpendicular and about the symmetry axis. Since we already know the rotation about the perpendicular axis to be 30° in 0.2 psec, we can calculate that the average angular movement about the symmetry axis is approximately 58° , or twice that about a perpendicular axis. This result, though hardly to be taken literally, is very pleasing from a physical point of view, since the moment of inertia about the symmetry axis ($3.31 \text{ amu } \text{\AA}^2$) is much smaller than the moment of inertia (67.2 amu) about the perpendicular axes.

If we now turn to behavior at long times, the correlation functions are found to have the expected forms $\alpha(t) = \alpha \exp(-\beta t)$. The constants β for the two graphs are given in Table III. That for Figure 2a is smaller, doubtless because it includes a contribution due to rotation about the symmetry axis which involves a lower moment of inertia. However, we shall not here attempt any detailed interpretation of these decay times.

In conclusion, therefore, the differences between the two time-correlation functions and, hence, between the two band widths and shapes, can be explained qualita-

tively at least by the different moments of inertia for the different axes of the methyl iodide molecule.

Calculation of Moments

An attempt was made to calculate moments⁸ from these results. The calculated errors, however, we found to be very large (50–100%). Moreover, these errors did not include a contribution due to the physical necessity of truncating the integrals to reasonable limits.

Approximate calculation showed that this contribution could be greater than the value of the moment itself, in some cases. This line of approach was therefore abandoned.

Acknowledgment. We wish to acknowledge the help of Dr. W. C. Krueger and others in this laboratory and also the National Science Foundation for financial help under Grant GP-3411. C. E. F. wishes to thank the Argentine Government for financial support.

Vapor-Phase Charge-Transfer Complexes. II. The $2I_2 \rightleftharpoons I_4$ System¹

by Milton Tamres, Walter K. Duerksen, and John M. Goodenow

Chemistry Department, University of Michigan, Ann Arbor, Michigan 48104 (Received August 29, 1967)

The $2I_2 \rightleftharpoons I_4$ equilibrium has been investigated in the vapor phase at 110–140° by analysis of the ultraviolet absorption band. The extinction coefficient of I_2 and the product of the extinction coefficient and constant of dimerization of I_4 have been determined as a function of wavelength. The band maxima for I_4 and I_2 , at ~ 2450 and 2700 \AA , respectively, show blue shifts relative to those observed in nonpolar solvents, with the shift for I_4 being much larger. Thermodynamic constants for I_4 formation were not obtained, but it is concluded that ΔE must be quite small.

Introduction

Iodine is known to have a weak absorption in the ultraviolet that fails to obey Beer's law.² The observed dependence of absorbance on concentration has been attributed to a monomer–dimer equilibrium.^{3–6}

Quantitative studies of the spectral and thermodynamic properties of this system have been made in CCl_4 ,^{4,6} and the solvent effect on the system also has been investigated.⁵ Analysis of the data is based on the assumption that the complex is very weak, so that, for the concentrations used at room temperature, the dimer concentration is negligibly small compared to that of monomer. Nevertheless, the dimer species contributes significantly to the total absorption because its extinction coefficient must be several orders of magnitude larger than that for the monomer.⁶ The observation that the enthalpy of dimerization is low, between -1 and -2 kcal/mol ,^{4–6} is in accord with the assumed weak nature of the complex.

Information about the monomer–dimer equilibrium in the vapor phase is very limited. Apparently, the only work in this area is that of Kortum and Friedheim,³ who studied the system qualitatively at 340°. Their absorption curves are those for the composite contribu-

tion of both monomer and dimer, but the study was not carried to the point which allowed separation into contribution from each species.

The present investigation was undertaken for two reasons. First, it was hoped to obtain spectral and thermodynamic properties of the system in the vapor state for comparison with the properties in solution. Second, it was thought essential to establish the extent to which the formation of dimer could interfere in interpreting data on charge-transfer studies in the ultraviolet region where iodine is used as the acceptor. In the latter case, for example, the composite monomer–dimer band maximum at 2670 \AA (for an iodine concentration of $9.238 \times 10^{-4} M$ at 340°)³ is very close to

(1) Taken in part from the Ph.D. Thesis of W. K. Duerksen, University of Michigan, Ann Arbor, Mich., Aug 1967.

(2) J. Groh and S. Papp, *Z. Physik. Chem.* (Frankfurt), **149**, 153 (1930).

(3) V. G. Kortum and G. Friedheim, *Z. Naturforsch.*, **2A**, 20 (1947).

(4) (a) P. A. D. De Maine, *J. Chem. Phys.*, **24**, 1091 (1956); (b) *Can. J. Chem.*, **35**, 573 (1957).

(5) M. M. De Maine, P. A. D. De Maine, and G. E. McAlonie, *J. Mol. Spectry.*, **4**, 271 (1960).

(6) R. M. Keefer and T. L. Allen, *J. Chem. Phys.*, **25**, 1059 (1956).

the maximum of 2680 Å recently reported for the benzene-iodine complex in the vapor phase.⁷

Experimental Section

Apparatus and Procedure. Spectrophotometric measurements were made on samples of iodine vapor of varying concentration. For the higher concentrations, a 10.0-cm cell was used. The cell, cell housing, and temperature control unit have been described elsewhere.⁸ For the lower concentrations, a multireflection unit (White cell) was used, with the mirrors placed outside the 25.0-cm cell to avoid attack by the iodine. Four passes were used to give an effective path length of 100.0 cm. The design of the cell housing and temperature control for the multireflection unit was rather similar to that for the smaller cell.^{1,8b} For both cells, data were taken using a Beckman DU spectrophotometer, Model 2400.

The cells were filled by metering out and transferring the iodine using a Pyrex vacuum line.^{8b} The amount of iodine actually in the cell was determined after the spectrometric measurements were completed. After having cooled to room temperature, the iodine was dissolved in *n*-heptane. An aliquot of the resulting solution was diluted, and the concentration of the second solution was found from a spectrophotometric measurement at the maximum of the visible iodine absorption band (5250 Å).

Reagent. Iodine (Baker Analyzed reagent) was purified by twice subliming it from a finely pulverized mixture with potassium iodide.

Results

In the 10.0-cm cell, spectrophotometric measurements were made on eight samples of iodine vapor at four temperatures and eight wavelengths. One of the samples was measured over a much wider spectral range, and the data obtained at two temperatures are shown in Figure 1. There is an apparent maximum at 2660 Å, which is quite close to that of 2670 Å observed by Kortum and Friedheim³ at 340° for the lowest of their iodine concentrations.

It had been shown^{4,6} that, for the case where dimerization is weak, the apparent extinction coefficient, ϵ_{app} , is expected to be given by an equation of the type

$$\epsilon_{app} \equiv \frac{A}{b[I_2]_0} \simeq \epsilon_{I_2} + K_D \epsilon_{I_4} [I_2]_0 \quad (1)$$

where A is the absorbance, b is the cell path, $[I_2]_0$ is the initial concentration of iodine, ϵ_{I_2} and ϵ_{I_4} are the extinction coefficients of iodine monomer and dimer, respectively, and K_D is the equilibrium constant for dimer formation. The plot of ϵ_{app} vs. $[I_2]_0$ should give a straight line whose intercept is equal to ϵ_{I_2} and whose slope is equal to $K_D \epsilon_{I_4}$. Plots at two temperatures are shown in Figure 2. The intercepts and slopes, determined by the method of least squares, are compiled in

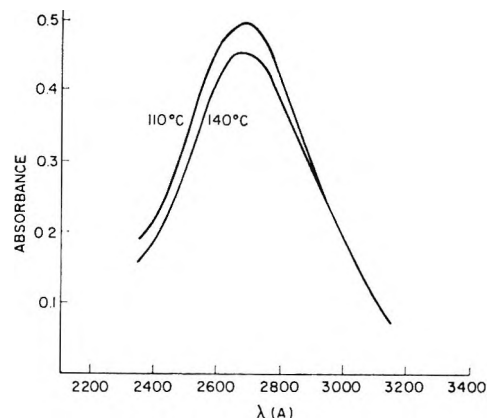


Figure 1. Iodine vapor-phase absorption spectra: $[I_2]_0 = 2.28 \times 10^{-3} M$, cell length = 10.0 cm.

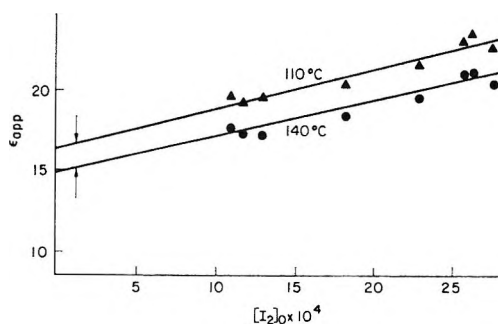


Figure 2. The apparent extinction coefficient, ϵ_{app} in $l. \text{ mole}^{-1} \text{ cm}^{-1}$, vs. initial iodine concentration, $[I_2]_0$ in mol l.^{-1} , at 2640 Å.

Tables I and II, with the probable errors calculated at the 50% confidence level. Within the wavelength region in Table I, it is to be noted that there is a systematic decrease in ϵ_{I_2} with increasing temperature. However, as seen in Table II, no systematic change with temperature is found for the product $K_D \epsilon_{I_4}$.

Table I: The $I_2 \rightleftharpoons I_4$ System. Least-Squares Analysis for Plots of ϵ_{app} vs. $[I_2]_0$: Best Intercepts^a

λ , Å	Temp., °C			
	110	120	130	140
2500	9.6 ± 0.5	9.2 ± 0.6	8.5 ± 0.6	7.1 ± 0.6
2540	12.0 ± 0.5	11.6 ± 0.5	11.0 ± 0.6	9.4 ± 0.6
2580	14.2 ± 0.5	13.9 ± 0.5	13.3 ± 0.6	11.9 ± 0.6
2600	15.3 ± 0.5	15.0 ± 0.5	14.5 ± 0.5	13.1 ± 0.5
2620	16.0 ± 0.5	15.8 ± 0.4	15.0 ± 0.4	13.8 ± 0.4
2640	16.6 ± 0.4	16.5 ± 0.4	15.8 ± 0.4	14.8 ± 0.4
2660	17.1 ± 0.5	16.9 ± 0.4	16.4 ± 0.3	15.6 ± 0.4
2700	17.5 ± 0.4	17.3 ± 0.4	16.8 ± 0.4	15.9 ± 0.4

^a Probable errors calculated at the 50% confidence level.

(7) F. T. Lang and R. L. Strong, *J. Am. Chem. Soc.*, **87**, 2345 (1965).

(8) (a) J. M. Goodenow and M. Tamres, *J. Chem. Phys.*, **43**, 3393 (1965); (b) M. Tamres and J. M. Goodenow, *J. Phys. Chem.*, **71**, 1982 (1967).

Table II: The $I_2 \rightleftharpoons I_4$ System. Least-Squares Analysis for Plots of ϵ_{app} vs. $[I_2]_0$: Best Slopes $\times 10^{-3a}$

λ , \AA	Temp., °C			
	110	120	130	140
2500	2.67 ± 0.25	2.62 ± 0.26	2.68 ± 0.29	2.95 ± 0.30
2540	2.67 ± 0.25	2.62 ± 0.24	2.64 ± 0.26	2.92 ± 0.29
2580	2.70 ± 0.25	2.55 ± 0.26	2.54 ± 0.28	2.74 ± 0.29
2600	2.62 ± 0.23	2.47 ± 0.22	2.39 ± 0.22	2.60 ± 0.23
2620	2.61 ± 0.22	2.38 ± 0.20	2.42 ± 0.19	2.56 ± 0.20
2640	2.50 ± 0.21	2.29 ± 0.19	2.27 ± 0.19	2.39 ± 0.19
2660	2.40 ± 0.23	2.19 ± 0.18	2.13 ± 0.17	2.12 ± 0.18
2700	2.16 ± 0.21	1.95 ± 0.17	1.91 ± 0.18	1.96 ± 0.17

^a Probable errors calculated at the 50% confidence level.

The relative contribution of the I_4 complex is obtained directly from the relation

$$A - \epsilon_{I_2} b [I_2]_0 = K_D \epsilon_{I_4} b [I_2]_0^2 \quad (2)$$

A plot of the left side of equation 2, where ϵ_{I_2} is determined by extrapolation using eq 1, vs. the square of the initial iodine concentration gave a straight line passing through the origin. The I_4 contribution becomes appreciable for iodine vapor above $10^{-3} M$, but at concentrations of the order of $10^{-4} M$, as indicated by the arrows in Figure 2, $\epsilon_{app} \approx \epsilon_{I_2}$, within experimental error limits, and the vapor in this spectral region can be considered to behave essentially as iodine monomer.

By using a path length of 1 m, it is possible to work with iodine concentrations of the order of $10^{-4} M$ and hence obtain ϵ_{I_2} directly. Two such studies were made: (1) four passes through a 25.0-cm multireflection cell of total volume 240 ml, where the I_2 concentration was determined spectrophotometrically (see the Experimental Section), and (2) a 91.3-cm cell of total volume 1.56 l., where the I_2 was weighed directly into a break-seal tube.⁹ Comparison of the various studies of ϵ_{I_2} is shown in Figure 3. The extrapolated values for ϵ_{I_2} as a function of λ are in good agreement with those measured directly, and this gives support to the validity of eq 1. The good agreement also supports the validity of the independent analytical methods used to determine iodine concentration. It was observed,⁹ for an iodine concentration of $3.09 \times 10^{-4} M$, that ϵ_{I_2} decreased with increasing temperature in the region 2440–2880 \AA and increased outside this region on either side, which is indicative of temperature broadening. The extrapolated values for ϵ_{I_2} actually follow this trend (Table I). Similar observations have been reported for the vapor I_2 band in the visible region¹⁰ and for the solution I_2 band in the ultraviolet region.⁶

Discussion

It does not seem possible to separate the product $K_D \epsilon_{I_4}$ into its components in order to compare the effect of solvent on each term. If instead of using the approximation $K_D = [I_4]/[I_2]_0^2$, as was done in deriving

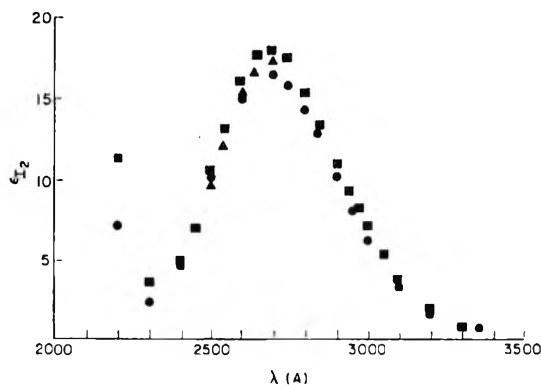


Figure 3. The pure I_2 extinction coefficient (in $l. \text{mol}^{-1} \text{cm}^{-1}$) as a function of wavelength (\AA): \blacktriangle , extrapolated value at 110° from data in 10.0-cm light path; \blacksquare , direct measurement at 100° for $[I_2]_0 = 7.16 \times 10^{-5} M$ in 100.0-cm light path; and \bullet , ref 9 at 101° for $[I_2]_0 = 3.09 \times 10^{-4} M$.

eq 2,^{4,6} one used $K_D = [I_4]/([I_2]_0 - [2I_4])^2$, then eq 2 becomes

$$K_D(\epsilon_{I_4} - 2\epsilon_{I_2})b[I_2]_0^2 = (A - A_0) + 4K_D(A - A_0)[I_2]_0 - \frac{4K_D(A - A_0)^2}{b(\epsilon_{I_4} - 2\epsilon_{I_2})} \quad (3)$$

where $A_0 = \epsilon_{I_2} b [I_2]_0$. On rearranging and considering $\epsilon_{I_4} \gg \epsilon_{I_2}$, this becomes

$$\frac{b[I_2]_0^2}{(A - A_0)} = \frac{1}{K_D \epsilon_{I_4}} + \frac{4[I_2]_0}{\epsilon_{I_4}} - \frac{4(A - A_0)}{b \epsilon_{I_4}^2} \quad (4)$$

In this study, b is large, as is the product $K_D \epsilon_{I_4}$ (Table II). Since $[I_2]_0$ is quite low and, undoubtedly, K_D is small, it follows that

$$\frac{1}{K_D \epsilon_{I_4}} \gg \frac{4[I_2]_0}{\epsilon_{I_4}} \gg \frac{4(A - A_0)}{b \epsilon_{I_4}^2}$$

Dropping the last term in eq 4 results in an expression similar to the Scott¹¹ modification of the Benesi-Hildebrand¹² equation. Person¹³ already has discussed in detail the difficulty of trying to obtain separate values for the equilibrium constant and the extinction coefficient when

$$\frac{1}{K_D \epsilon_{I_4}} \gg \frac{4[I_2]_0}{\epsilon_{I_4}}$$

Separation of the terms in $K_D \epsilon_{I_4}$ could be achieved by using very narrow cells and high iodine concentrations (and assuming unit activity coefficients). These are impractical conditions to attain in the vapor phase. They also are not attainable in solution because of the

(9) This study was done at the University of Chicago, Chicago, Ill.; M. Kroll and M. Tamres, unpublished work.

(10) P. Sulzer and K. Wieland, *Helv. Phys. Acta*, **25**, 653 (1952).

(11) R. L. Scott, *Rec. Trav. Chim.*, **75**, 787 (1956).

(12) H. A. Benesi and J. H. Hildebrand, *J. Am. Chem. Soc.*, **71**, 2703 (1949).

(13) W. B. Person, *ibid.*, **87**, 167 (1965).

limited solubility of iodine. Therefore, the attempt^{4b} to separate terms from data of iodine in CCl_4 at 17° into K_D (2.28 l./mol, which seems high) and ϵ_{I_4} (389 l./mol cm, which seems low) probably is not correct. A better procedure is that of Keefer and Allen,⁶ who estimated that, in CCl_4 , K_D lies between 0.5 and 0.05 l./mol and $\epsilon_{I_4} < 40,000$ l./mol cm. From a general relation of enthalpy and free energy for weak iodine complexes, they calculated, at 25.5° , that $K_D \simeq 0.13$ l./mol and $\epsilon_{I_4} \simeq 16 \times 10^3$ l./mol cm.

It is possible, however, to compare the $K_D\epsilon_{I_4}$ product in the different studies. In the vapor phase, $K_D\epsilon_{I_4}$ at 2500 \AA (around λ_{max}) and 110° is $2.67 \times 10^3 \text{ l.}^2/\text{mol}^2 \text{ cm}$ (Table II), while in CCl_4 solution at 2880 \AA and 25.5° , Keefer and Allen⁶ found a rather comparable value of $2.04 \times 10^3 \text{ l.}^2/\text{mol}^2 \text{ cm}$. De Maine⁴ reports similar figures in CCl_4 , but there is a small dependence of $K_D\epsilon_{I_4}$ on the nature of the solvent.⁵ It should be noted in Table II that, even for the 50% confidence level, the error is of the order of 10%.

In solution, the $K_D\epsilon_{I_4}$ product shows a small but nevertheless systematic temperature dependence which permits evaluation of ΔH , assuming temperature independence of ϵ_{I_4} . The values reported in CCl_4 solution, -1.96 ± 0.15 , -1.52 ± 0.29 , and -1.0 ± 0.2 kcal/mol, respectively,⁴⁻⁶ show that ΔH is low (and also show that experimental variation probably does not permit determination to much better than ± 0.5 kcal/mol). The ΔH 's in several nonpolar hydrocarbon solvents lie in about the same range.⁵ In the absence of specific heat data, it is not possible to estimate the change in ΔH with temperature, but assuming temperature independence in ΔH and similarity in results between vapor and solution, ΔE near 110° would be less negative than the above quoted values by ~ 0.8 kcal/mol. Thus, ΔE may be too small to be determined within the experimental limits of the method, as is suggested by the random variation in $K_D\epsilon_{I_4}$ with temperature (Table II). Another reason for suspecting that ΔE may be quite small is the fact that, for only a slightly higher concentration range, contribution of dimer to the absorption is observed even at 340° .³

The shape of the I_4 band can be obtained by plotting the slopes in eq 1 vs. wavelength, as was done in the solution studies.⁴⁻⁶ In the present case, because of the random temperature variation of the slope, it was thought preferable to use the absorbance data taken on a single iodine sample and subtract out the contribution of monomer at each wavelength. As seen from eq 2, dividing the data in Figure 1 by $b[I_2]_0^2$ and that in Figure 3 by $[I_2]_0$, and subtracting, gives $K_D\epsilon_{I_4}$ as a function of wavelength. The data in Figure 4 used for the calculation were those which correspond to $[I_2]_0 = 7.16 \times 10^{-5} M$ and 100° in a path length of 100.0 cm. This concentration is well below that where any significant I_4 contribution occurs (Figure 2). At this concentration, no temperature dependence of absorption was observed,

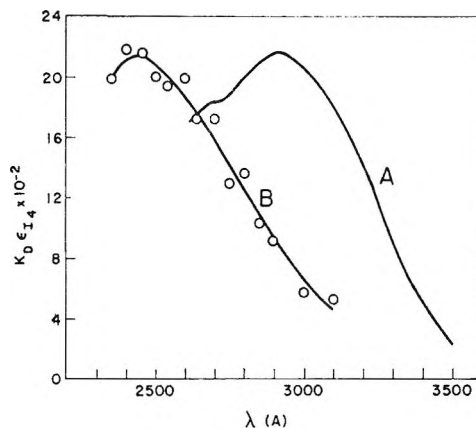


Figure 4. Comparison of the shape of the I_4 absorption band: A, CCl_4 solution at 8° (ref 4); and B, vapor phase at 110° .

within experimental limits, between 100 and 120° , except at low wavelengths (below 2300 \AA).

The shape of the I_4 bands in solution and in the vapor are compared in Figure 4. Because of the different procedure used here to calculate $K_D\epsilon_{I_4}$, as compared to the least-squares method used to calculate the data in Tables I and II, the results in Figure 4 and in Table II are not the same. In the figure, the result for $K_D\epsilon_{I_4}$ at 110° and λ_{max} is only $2.16 \times 10^3 \text{ l.}^2/\text{mol}^2 \text{ cm}$. Considering the error limits, the values obtained by the two procedures cannot be considered to be significantly different from each other or from the solution value.

The band maximum in CCl_4 has been reported at 2880 ⁶ and at 2935 \AA ,^{4,5} and in *n*-hexane it is around 2775 \AA .⁵ In the vapor, the band maximum is approximately 2450 \AA . This is a relatively large blue shift, and is typical of the large effects observed for weak CT complexes.⁷ Caution should be given that the true magnitude of the shift may be in considerable error. It should be noted that there already is some variation in the reported I_4 band maximum in CCl_4 .⁴⁻⁶ This arises because the shape of the band is determined from the absorption data by subtracting the I_2 contribution, and it is sensitive to small variations in ϵ_{I_2} . The same situation applies in the vapor phase, so that the magnitude of the shift may not be reliable to better than 100 \AA .

By contrast, the shift in the band maximum of the iodine monomer is much smaller, from 2800 \AA in CCl_4 solution⁴⁻⁶ to 2700 \AA in the vapor (Figure 3). Maxima for ϵ_{I_2} in hydrocarbon solvents are difficult to obtain because of the onset of contact charge transfer (CT).⁵ At the maximum, ϵ_{I_2} in the vapor phase at 110° is 18 l./mol cm . From the Kortum and Friedheim³ data for iodine vapor at 340° and $[I_2]_0 = 9.238 \times 10^{-4} M$, at which concentration ϵ_{app} and ϵ_{I_2} should not be too different, an upper limit of 14 l./mol cm is set,¹⁴ which is in reasonably good agreement with that of the present study,

(14) L. Mathieson and A. L. G. Rees, *J. Chem. Phys.*, **25**, 753 (1956), estimate a value of $\sim 16 \text{ l./mol cm}$ from these data.

considering the error limits of the methods used and the difference in temperature.

Although the thermodynamics of the equilibrium could not be established, complications in future vapor-phase uv studies of iodine complexes do not seem serious. First, by using iodine concentrations of $\leq 10^{-4} M$, the formation of I_4 can be completely ignored. Second, for larger concentrations, in those cases where the complexes are weak so that the per cent of iodine complexed is small, valid correction of the total ab-

sorbance can be made by subtracting the absorbance curve of iodine of the same concentration as is used in complex formation. For these reasons, the analysis of Lang and Strong⁷ on the benzene-iodine system is valid. Only in the case of high iodine concentration and strong complexation would special consideration be necessary.

Acknowledgment. This work was supported by grants from the National Science Foundation, NSF GP-3691 and GP-6429 Research.

Correlation of Molecular Structure with Fluorescence Spectra in

Rare Earth Chelates. I. Internal Stark Splitting in Tetraethylammonium

Tetrakis(dibenzoylmethido)europate(III)

by Sven Bjorklund,

Department of Physics, The George Washington University, Washington, D. C.

Nicolae Filipescu,

Department of Chemistry, The George Washington University, Washington, D. C.

N. McAvoy, and J. Degnan

Goddard Space Flight Center, NASA, Greenbelt, Maryland (Received August 30, 1967)

The internal Stark splitting in the emission spectrum of tetraethylammonium tetrakis(dibenzoylmethido)europate(III) in microcrystals at 77°K was analyzed in detail treating the ligand field as a perturbation on the free ion levels. The complete equivalence between crystalline field and a molecular (ligand) field in chelates with respect to the splitting of the intra-4f levels allows the use of equivalent operator techniques in the calculation of ligand field parameters. These parameters were derived from the splitting in the 7F_1 and 7F_2 levels of the Eu^{3+} ion without assuming a known molecular geometry, and their values establish the configuration of the emitting species. In addition, the ligand field parameters are used to calculate interatomic distances and bond angles. The method developed for deriving and verifying the geometrical arrangement, interatomic distances, and bond angles from fluorescence spectra proves to be a powerful tool.

Introduction

Narrow-line fluorescence is observed in certain Eu complexes when excited with light absorbed by the organic ligand as a result of intramolecular energy transfer. The absence of broad-line fluorescence characteristic of rare earth ions incorporated in non-homogeneous surroundings (*e.g.*, glasses) indicates the presence of the same environment for all Eu ions similar to that present in doped single crystals.

The present work shows that the splitting of the 7F levels of Eu^{3+} ion observed in the fluorescence spectra of organic chelates can be effectively explained in terms of a first-order perturbation produced by the electrostatic effect of the ligand field on the complexed europium ion. Furthermore, we propose to determine the ligand field parameters in tetrakis- β -ketoenolate chelates from experimental data without assuming any one of the possible octacoordinated models as being

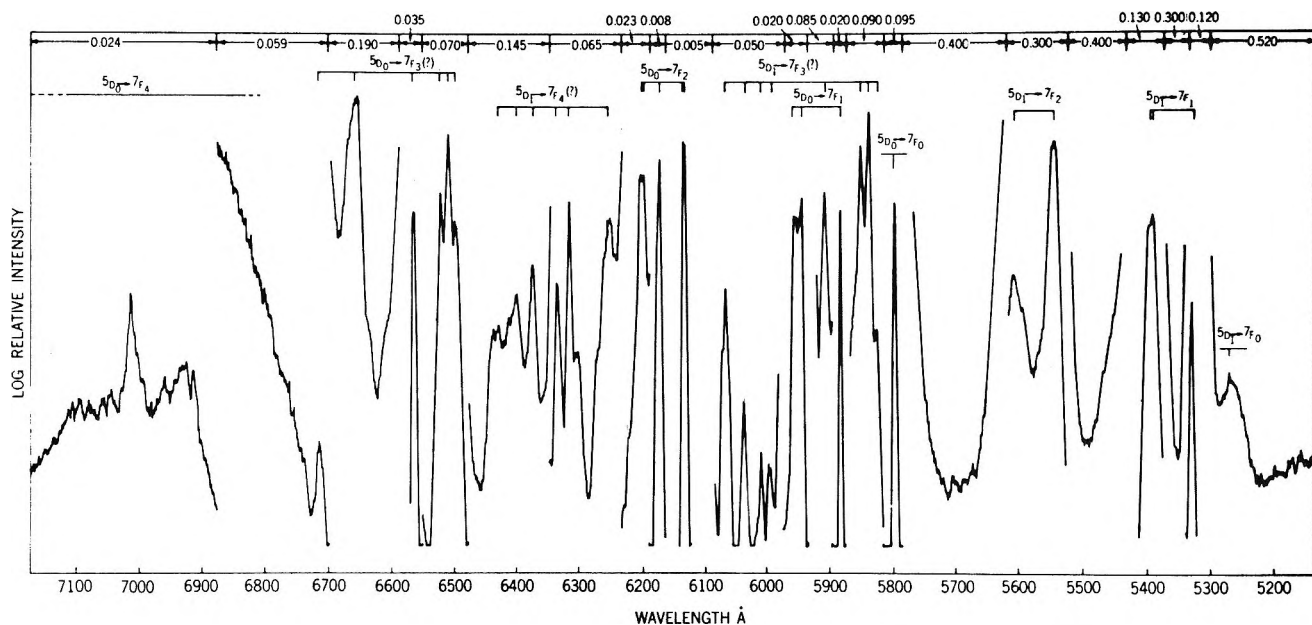


Figure 1. Fluorescence spectrum of microcrystalline EuD_4T at 77°K . Slit widths in millimeters are given at the top.

the emitting species. The only assumption made is that the emitting stereoisomer has C_2 symmetry or higher, a condition which is satisfied by the two dodecahedrons and the two antiprisms configurations required by the use of either d^4sp^3 or d^5p^3 hybrid orbitals of the lanthanide ion in bond formation.¹

Experimental Section

Preparation of Chelates. The tetraethylammonium tetrakis(dibenzoylmethido)europate(III) (EuD_4T) was prepared by adding 8 mmoles of 1 *N* sodium hydroxide to a hot solution of 8 mmoles (1.79 g) of dibenzoylmethane, 8 mmoles (1.68 g) of tetraethylammonium bromide, and 2 mmoles (0.52 g) anhydrous europic chloride in 25 ml of absolute ethanol. The precipitated crystals were filtered, washed repeatedly with water-alcohol mixture, and dried in air. After recrystallization from *o*-dichlorobenzene, the crystals were washed again several times with absolute ethanol and dried under vacuum at 110° . The chelate decomposes at $222\text{--}225^\circ$. The analogous pyrrolidinium chelate of EuD_4 (EuD_4Pyr) was synthesized from dibenzoylmethane, EuCl_3 , and the free base by the usual procedure.¹

Fluorescence Spectrum. The crystals were sealed with nonfluorescent tape between two quartz slides and lowered into a quartz dewar containing liquid nitrogen. Light from a 1000-W water-cooled, high-pressure AH-6 mercury arc was filtered through a Corning CS7-54 filter and directed into a metal box constructed to minimize stray light. The clear bottom part of the dewar was positioned in the box such that the exciting light was focused on the sample. The fluorescence emission was directed into a Cary Model 14 spectrophotometer and detected by a R136 red-sensitive

photomultiplier. The entrance slit to the Cary was adjusted manually for different spectral regions to control the intensity of the light entering the monochromator. Dry air was caused to circulate inside the box to prevent possible frosting on the dewar. The wavelength measurement is estimated to be within 2 \AA . The recorded fluorescence spectra of EuD_4T and EuD_4Pyr are shown in Figures 1 and 2, respectively. (Also see Table I.)

Equivalence of Ligand and Crystal Fields²

Let r, θ, φ be the coordinates of a point in the electric field produced by a charge-distribution of density $\rho(\mathbf{r}')$ originating in the ligand. We can consider $\rho(\mathbf{r}')$ as being the time and space average over the entire ketoenolate structure as represented by both σ bonds frame and delocalized π electrons. The potential is given by

$$V(r, \theta, \varphi) = V(\mathbf{r}) = \int \frac{1}{|\mathbf{r} - \mathbf{r}'|} \rho(\mathbf{r}') d\tau' \quad (1)$$

integrated over the source points with coordinates \mathbf{r}' . In terms of spherical harmonics this is

$$V(r, \theta, \varphi) = 4\pi \sum_{l,m} \frac{r^l Y_l^m(\theta, \varphi)}{2l+1} \int \frac{Y_l^{m*}(\theta', \varphi') \rho(\mathbf{r}') d\tau'}{r'^{l+1}} \quad (2)$$

For a crystal field with point charges q_i at the points \mathbf{r}_i , the charge density $\rho(\mathbf{r}')$ would be given by

(1) (a) C. Brecher, H. Samelson, and A. Lempicki, *J. Chem. Phys.*, **42**, 1081 (1965); (b) H. Bauer, J. Blanc, and D. L. Ross, *J. Am. Chem. Soc.*, **86**, 5125 (1964); (c) L. R. Melby, N. J. Rose, E. Abramson, and J. C. Caris, *ibid.*, **86**, 5117 (1964); (d) L. J. Nugent, M. L. Bhaumik, S. George, and S. M. Lee, *J. Chem. Phys.*, **41**, 1305 (1964).

(2) For a somewhat similar treatment, see J. S. Griffith, "The Theory of Transition Metal Ions," Cambridge University Press, New York, N. Y., 1961, Chapter 8.

$$\rho(\mathbf{r}') = \sum_i q_i \delta(\mathbf{r} - \mathbf{r}_i) \quad (3)$$

$$A_i^m = 4\pi \sum_i \frac{q_i}{(2l+1)r_i^{l+1}} Y_l^m(\theta'_i, \varphi'_i) \quad (5)$$

and the integrals in (2) would reduce to

$$A_i^m = 4\pi \sum_i \frac{q_i Y_l^{m*}(\theta', \varphi') \delta(\mathbf{r} - \mathbf{r}_i) d\tau}{(2l+1)r_i^{l+1}} \quad (4)$$

The equivalent integrals for the ligand field are

$$\alpha_i^m = 4\pi \int \frac{\rho(\mathbf{r}') Y_l^{m*}(\theta', \varphi') d\tau'}{(2l+1)r'^{l+1}} \quad (6)$$

or

Thus the potential produced by the ligand field is given by eq 7, where

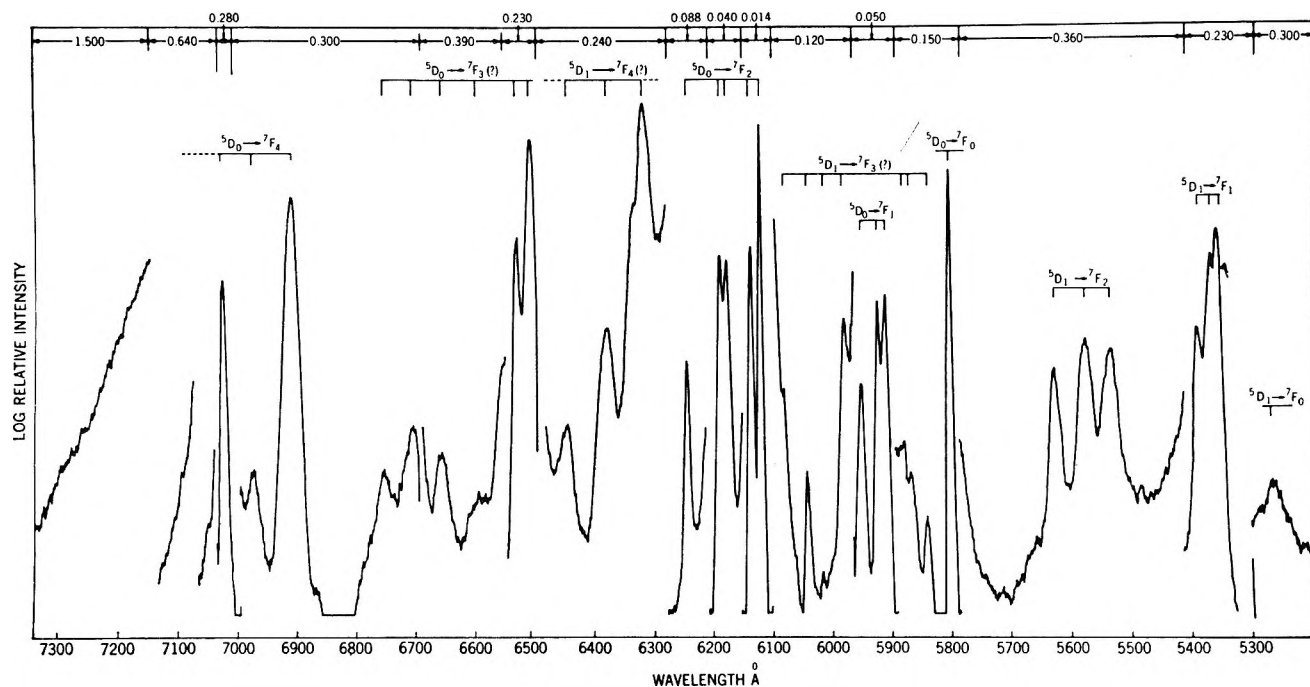


Figure 2. Fluorescence spectrum of microcrystalline EuD₄Pyr at 77°K. Slit widths in millimeters are given at the top.

Table I: Fluorescence Lines in the Emission Spectra of EuD₄T and EuD₄Pyr

Transition	Wave numbers, cm ⁻¹					
	EuD ₄ T			EuD ₄ Pyr		
⁵ D ₀ → ⁷ F ₀	17,248			17,234		
⁵ D ₀ → ⁷ F ₁	17,007			16,926		
	16,819	E ₀ 375 cm ⁻¹ above ⁷ F ₀		16,882	E ₀ 364 cm ⁻¹ above ⁷ F ₀	
	16,792			16,802		
⁵ D ₀ → ⁷ F ₂	16,306			16,333		
	16,298			16,299		
	16,199	E ₀ 1,038 cm ⁻¹ above ⁷ F ₀		16,184	E ₀ 1,036 cm ⁻¹ above ⁷ F ₀	
	16,129			16,157		
	16,119			16,017		
⁵ D ₀ → ⁷ F ₃	15,388	15,330	15,024 (?)	15,365	15,162	14,912
	15,363	15,232 (?)	14,910 (?)	15,313	15,023 (?)	14,811 (?)
⁵ D ₀ → ⁷ F ₄	14,465	14,370 (?)		14,476	14,233	
	14,441 (?)	14,260		14,341		
⁵ D ₁ → ⁷ F ₀	18,982			19,003		
⁵ D ₁ → ⁷ F ₁	18,765	18,547	18,518	18,661	18,636	18,555
⁵ D ₁ → ⁷ F ₂	18,035	17,827		18,074	17,940	17,775
⁵ D ₁ → ⁷ F ₃	17,168	16,923 (?)	16,564 (?)	17,092	17,736	
	17,127	16,677 (?)	16,482 (?)	17,014	16,563 (?)	
	17,092	16,642 (?)		16,973	16,460 (?)	
⁵ D ₁ → ⁷ F ₄ (?)	15,986	15,788	15,534	15,849		
	15,861	15,688	15,536	15,688		
	15,834	15,625		15,519		

$$V(r, \theta, \varphi) = \sum_{l, m} \alpha_l^m r^l Y_l^m(\theta, \varphi) \quad (7)$$

whereas the expression for the potential for a crystal field is

$$V(r, \theta, \varphi) = \sum_{l, m} A_l^m r^l Y_l^m(\theta, \varphi) \quad (8)$$

Consequently, a ligand field has the same potential as a crystal field, in spite of the delocalized electron density associated with the anion–ligand configuration, and will produce the same internal Stark splitting of the energy levels as the equivalent crystal field, provided

$$\alpha_l^m = A_l^m$$

It may well be that to produce the actual field, one needs an infinite number of point charges to get all the parameters α_l^m equal to A_l^m . This, however, is not the point. What one needs in the calculations of internal Stark splitting is not the total field but only a small number of parameters α_l^m , and these can always be found from a small number of point charges. Therefore, one can always find a hypothetical field produced by point charges which will have the same effects on the spectrum as the molecular (ligand) field. In first-order perturbation theory, the energy levels are given by the roots of the secular determinant in terms of the parameters α_l^m and A_l^m , respectively, and both of these will give discrete solutions to the secular equation.

Having established the equivalence between the ligand field and a crystal field, we can employ the operator equivalent methods developed for crystal field problems by Judd³ and Stevens.⁴

Selection of Chelate and Fluorescence Spectra

EuD₄T was specifically selected for analysis in this first paper for three reasons. First, the symmetry of the enolate anion renders the two coordinating oxygen atoms equivalent; second, all possible arrangements of four ligand bridges about the Eu³⁺ ion¹ yield a small number of ligand field parameters α_l^m ; and third, the very bulky tetraethylammonium cation is less likely to influence the symmetry of the ligand field—through penetration into the vicinity of the lanthanide ion—than other primary, secondary, or tertiary ammonium cations. We will assume this type of influence to be negligible for the (C₂H₅)₄N⁺ ion.

The fluorescence spectra of a large number of crystalline europium tetrakis(dibenzoylmethide) chelates with different organic cations were examined in detail to ensure proper identification of the individual transitions. We found that the splitting patterns of the fluorescence transitions in these chelates are remarkably sensitive to the nature of the cation. As an example, the emission spectrum of crystalline EuD₄Pyr at 77°K is illustrated in Figure 2 for comparison with that of EuD₄T in Figure 1. The cation effects in the splitting of the ⁷F levels of Eu³⁺ in octacoordinate chelates will

be discussed in a forthcoming paper. Presently, Figure 2 is shown only to illustrate the identification of the individual transitions and the dependence of the splitting on the organic cation.

For the tetrakis(dibenzoylmethide) chelates the ligand field parameters can be calculated from the fluorescence spectrum by using only transitions from the excited ⁵D₀ state to ⁷F₀, ⁷F₁, and ⁷F₂ levels in the ground multiplet of Eu ion. In less symmetrical systems such as chelates from differently substituted β-diketones, transitions terminating at the ⁷F₃ level may prove to be necessary. However, in this case, the solutions of the secular determinant are so complex that very probably they cannot be correlated to experimental data.

The assignment of the emission lines to the individual ⁵D → ⁷F transitions in Figures 1 and 2 is well verified with the exception of several weaker lines marked by (?) which are only tentatively assigned because of lack of clearly defined structure in the 6700–7500-Å region. Although Blanc and Ross⁵ have suggested the possibility of spurious emission due to surface contamination, we find that the emission lines are reproducible even after recrystallization from different solvents or mechanical pulverization. Other authors¹ propose to explain the extra lines by the presence of two stereoisomers. The relatively few lines in Figures 1 and 2 which were assigned tentatively to ⁵D₁ → ⁷F_{3,4} could presumably originate in another stereoisomer present in very small amounts. The assignment of these few lines is not essential to the discussion of the “predominant species.”

The orbitals available for bonding in the Eu ion are the empty 5d, 6s, and 6p orbitals. The fact that the partially occupied 4f orbitals are not involved in bonding to any great extent is indicated by the discrete structure of both absorption and emission spectra of the chelated ion and their similarity with those of inorganic ionic salts. There are four possibilities for the lanthanide ion to accommodate eight coordinating oxygen atoms^{1,6} (see Figure 3): two dodecahedral arrangements for the use of d⁴sp³ hybrid orbitals (models I and II) and two antiprismatic configurations for d⁴sp³ and d⁵p³ (models III and IV). From the values of the ligand field parameters calculated below from experimental data, we propose to verify the geometry of the emitting stereoisomer.

Perturbation Calculation

Assume that the Hamiltonian can be broken up into two parts $H = H_0 + H'$ where H_0 is the Hamiltonian

(3) (a) B. R. Judd, *Mol. Phys.*, **2**, 407 (1959); (b) B. R. Judd, *Proc. Roy. Soc. (London)*, **A228**, 120 (1955).

(4) K. W. H. Stevens, *Proc. Phys. Soc. (London)*, **65**, 209 (1952).

(5) J. Blanc and D. L. Ross, *J. Chem. Phys.*, **43**, 1286 (1965).

(6) (a) A. F. Wells, “Structural Inorganic Chemistry,” Oxford University Press, New York, N. Y., 1962; (b) G. E. Kimball, *J. Chem. Phys.*, **8**, 188 (1940).

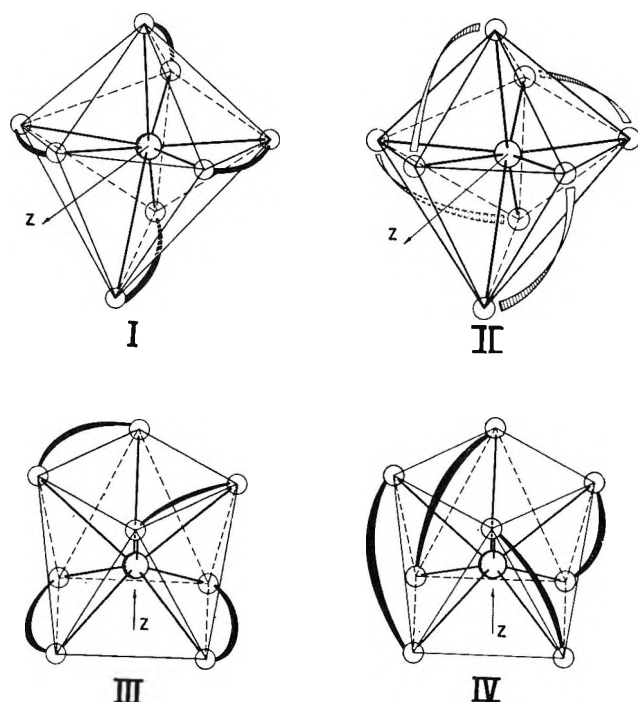


Figure 3.

of the 4f electrons of the free ion and H' is eV with V the electrostatic potential produced by the ligand and given by eq 8. H' is assumed small in comparison with H_0 or $\sum \xi(r_i)l_i \cdot s_i \gg H'$. H_0 is invariant with respect to rotation around the origin, which means that the total angular momentum J of the 4f electrons in the unperturbed ion is a good quantum number and energies of the degenerate levels 7F_J are the eigenvalues of H_0 . We need to calculate the splitting of the 7F_0 , 7F_1 , and 7F_2 levels caused by eV .

The energy levels E can be found from first-order perturbation theory by solving the secular determinants for the 7F_J levels. The secular determinant has the form

$$\text{Det}[\langle M'J|eV|MJ\rangle - E\delta_{M'M}] = 0$$

If one expands the vectors $|MJ\rangle$ and $\langle M'J|$ for f-electron states in terms of spherical harmonics with $l_1 = l_2 = 3$, the matrix elements are proportional to integrals of the product of three spherical harmonics. One of the spherical harmonics originates in the expansion of the potential. Since the integral of the product of three spherical harmonics is proportional to the Clebsch-Gordan coefficient $\langle l_1 0 0 | l_2 0 \rangle$ and these coefficients have to satisfy a triangular condition for l_1 , l_2 , and l , we see that the maximum value for l that will give a contribution to the matrix elements is $l = 6$. Since the Clebsch-Gordan coefficient is zero unless $l_1 + l_2 + l$ is even, only terms with even l contribute.

The first part of the Stevens and Judd method consists of expressing the $r^l Y_l^m$ terms as polynomials in powers of r , x , y , and z . The parameters $\alpha_l^{-|m|}$ and $\alpha_l^{+|m|}$ can be

combined⁷ to yield two new parameters β_l^m and $\beta_l^m(s)$ which have factors of $\cos m\varphi$ and $\sin m\varphi$, respectively. Since for all the models under consideration a proper choice of axis will make the sine term zero, the part of (7) which we will need becomes

$$-|e|V(\mathbf{r}) = \beta_2^0(3z^2 - r^2) + \beta_4^0(35z^2 - 30z^2r^2 + 3r^4) + \beta_2^2(x^2 - y^2) + \beta_4^2(7z^2 - r^2)(x^2 - y^2) + \beta_4^4(x^4 - 6x^2y^2 + y^4) \quad (9)$$

with

$$\begin{aligned} \beta_2^0 &= -|e|\frac{1}{4}\left(\frac{5}{\pi}\right)^{1/2}\alpha_2^0; \quad \beta_4^0 = -|e|\frac{3}{16}\left(\frac{1}{\pi}\right)^{1/2}\alpha_4^0; \\ \beta_2^2 &= -|e|\frac{1}{4}\left(\frac{15}{2\pi}\right)^{1/2}[\alpha_2^{-2} + \alpha_2^2]; \\ \beta_4^2 &= -|e|\frac{3}{8}\left(\frac{5}{2\pi}\right)^{1/2}[\alpha_4^{-2} + \alpha_4^2]; \\ \beta_4^4 &= -|e|\frac{3}{16}\left(\frac{35}{2\pi}\right)^{1/2}[\alpha_4^{-4} + \alpha_4^4] \quad (10) \end{aligned}$$

We will now show that only those parameters β_l^m listed above are needed. All four possible stereoisomers for the tetrakis species have a twofold rotational symmetry. If the axis of symmetry is taken to be the z axis, then

$$e^{im\varphi} = e^{im(\varphi+\pi)} \quad \text{or} \quad e^{im\pi} = 1$$

thus $m = 0, 2, 4, \dots$

For the states ${}^7F_0 - {}^7F_2$, the coefficient of proportionality between the point-charge field and the equivalent angular momentum operators is zero for $l = 6$. Thus, since m and l have to be even, $m \leq l$, and there is no contribution for $l = 6$, one is left with the following parameters contributing to the splitting: β_2^0 , β_4^0 , β_2^2 , β_4^2 , and β_4^4 (the constant β_0^0 has been omitted).

In the dodecahedral configuration I, the eight equal charges are such that $\varphi_1 = \varphi_2 = 0$, $\varphi_3 = \varphi_4 = \pi/2$, $\varphi_5 = \varphi_6 = \pi$, $\varphi_7 = \varphi_8 = 3\pi/2$, and $\theta_1 = \theta_5$, $\theta_3 = \theta_7$, $\theta_1 + \theta_4 = \theta_3 + \theta_6 = \theta_5 + \theta_8 = \theta_7 + \theta_2 = \pi$. The terms Y_2^2 and Y_4^2 add up to zero upon taking into account the relation

$$P_l^m(-x) = (-1)^{m+l}P_l^m(x)$$

thus, only the parameters β_2^0 , β_4^0 , and β_4^4 contribute to the splitting of the 7F_2 level for the dodecahedron I.

The geometry of dodecahedron II is such that all of the five possible parameters β_2^0 , β_4^0 , β_2^2 , β_4^2 , and β_4^4 can be nonzero.

For antiprism III, the equivalent point charges lie at the corners of two parallel rectangles, one rotated around the z axis by $\pi/4$ with respect to the other. The planes of both rectangles are perpendicular to the z

(7) M. T. Hutchings, *Solid State Phys.*, **16**, 254 (1964).

axis. Thus $\varphi_{n+4} = \varphi_n + \pi/4$, $n = 1, 2, 3, 4$, and $\theta_{n-4} + \theta_n = \pi$. β_4^4 is proportional to

$$\sum_{i=1}^8 P_4^4(\cos \theta_i) e^{i4\varphi_i}$$

$$P_4^4 \sim \sin^4 \theta; P_4^4(\cos \theta_n) =$$

$$P_4^4(\cos \theta_{n+4}) e^{i4\varphi_{n+4}} + e^{i4\varphi_n} = e^{i(4\varphi_n + \pi)} + e^{i4\varphi_n} = e^{4i\varphi_n} (1 + e^{i\pi}) = 0 \quad (11)$$

Consequently, for this antiprism β_4^4 is zero. The other parameters can have nonzero values. We are thus left with $\beta_2^0, \beta_4^0, \beta_2^2$, and β_4^2 .

For antiprism IV the equivalent point charges lie at the corners of two parallel squares whose planes are perpendicular to the z axis. For each plane $P_i^m(\cos \theta_i)$ is the same for each charge.

$$\beta_2^2 \sim \sum_{i=1}^4 P_2^2(\cos \theta_1) e^{i2\varphi_i} + \sum_{i=5}^8 P_2^2(\cos \theta_5) e^{i2\varphi_i};$$

$$\sum_{i=1}^4 e^{2i\varphi_i} = e^{2i\varphi_1} + e^{2i(\varphi_1 + (\pi/2))} + e^{2i(\varphi_1 + \pi)} + e^{2i(\varphi_1 + (3\pi/2))} = e^{2i\varphi_1} (1 - 1 + 1 - 1) = 0$$

Thus β_2^2 is zero. In the same way, one can show that β_4^2 is zero. We are thus left with β_2^0, β_4^0 , and β_4^4 .

Substituting the angular momentum operators $J, J_z, J_+,$ and J_- into (9), $-|e|V(r, \theta, \varphi)$ becomes

$$-|e|V(\mathbf{r}) = \alpha_J \langle r^2 \rangle \beta_2^0 [3J_z^2 - J(J+1)] + \beta_J \langle r^4 \rangle \beta_4^0 [35J_z^2 - 30J(J+1)J_z^2 + 25J_z^2 - 6J(J+1) + 3J^2(J+1)^2] + \alpha_J \langle r^2 \rangle \beta_2^2 \frac{1}{2} (J_+^2 + J_-^2) + \beta_J \langle r^4 \rangle \beta_4^2 \frac{1}{4} \{ [7J_z^2 - J(J+1) - 5] \times (J_+^2 + J_-^2) + (J_+^2 + J_-^2) \times [7J_z^2 - J(J+1) - 5] \} + \beta_J \langle r^4 \rangle \beta_4^4 \frac{1}{2} (J_+^4 + J_-^4) \quad (12)$$

where³

$$\alpha_0 = \beta_0 = \beta_1 = 0; \alpha_1 = -\frac{1}{5}; \beta_2 = -\frac{2}{189}; \alpha_2 = -\frac{11}{315}$$

For any geometry having a twofold rotational axis, the secular determinant for the 7F_1 level is

$$\begin{vmatrix} \alpha_1 \langle r^2 \rangle \beta_2^0 - E & 0 & \alpha_1 \langle r^2 \rangle \beta_2^2 \\ 0 & -2\alpha_1 \langle r^2 \rangle \beta_2^0 - E & 0 \\ \alpha_1 \langle r^2 \rangle \beta_2^2 & 0 & \alpha_1 \langle r^2 \rangle \beta_2^0 - E \end{vmatrix} = 0$$

With solutions

$$E_1 = E_0 - 2\alpha_1 \langle r^2 \rangle \beta_2^0$$

$$E_2 = E_0 + \alpha_1 \langle r^2 \rangle \beta_2^0 + \alpha_1 \langle r^2 \rangle \beta_2^2$$

$$E_3 = E_0 + \alpha_1 \langle r^2 \rangle \beta_2^0 - \alpha_1 \langle r^2 \rangle \beta_2^2 \quad (13)$$

The energy levels obtained by solving the secular determinant for 7F_2 are

$$E_1 = E_0 + 6\alpha_2 \langle r^2 \rangle \beta_2^0 + 12\beta_2 \langle r^4 \rangle \beta_4^0 - 12\beta_2 \langle r^4 \rangle \beta_4^4$$

$$E_2 = E_0 - 3\alpha_2 \langle r^2 \rangle \beta_2^0 - 48\beta_2 \langle r^4 \rangle \beta_4^0 - 3\alpha_2 \langle r^2 \rangle \beta_2^2 + 12\beta_2 \langle r^4 \rangle \beta_4^2$$

$$E_3 = E_0 - 3\alpha_2 \langle r^2 \rangle \beta_2^0 - 48\beta_2 \langle r^4 \rangle \beta_4^0 + 3\alpha_2 \langle r^2 \rangle \beta_2^2 - 12\beta_2 \langle r^4 \rangle \beta_4^2$$

$$E_4 = E_0 + \frac{84\beta_2 \langle r^4 \rangle \beta_4^0 + 12\beta_2 \langle r^4 \rangle \beta_4^4 + x}{2}$$

$$E_5 = E_0 + \frac{84\beta_2 \langle r^4 \rangle \beta_4^0 + 12\beta_2 \langle r^4 \rangle \beta_4^4 - x}{2} \quad (14)$$

with

$$x = [(84\beta_2 \langle r^4 \rangle \beta_4^0 + 12\beta_2 \langle r^4 \rangle \beta_4^4)^2 - 24(-\alpha_2 \langle r^2 \rangle \beta_2^0 + 12\beta_2 \langle r^4 \rangle \beta_4^0) \times (6\alpha_2 \langle r^2 \rangle \beta_2^0 + 12\beta_2 \langle r^4 \rangle \beta_4^0 + 12\beta_2 \langle r^4 \rangle \beta_4^4) + 48(\alpha_2 \langle r^2 \rangle \beta_2^2 + 3\beta_2 \langle r^4 \rangle \beta_4^2)^2]^{1/2} \quad (15)$$

Molecular Geometry

Selection of the Model. The energy levels in 7F_2 were fed into an IBM 7094 computer which tested all possible assignments of these levels to the secular equations (14) as outlined below. The parameters $\langle r^2 \rangle \beta_2^0$ and $\langle r^2 \rangle \beta_2^2$ are known from the splitting of the 7F_1 level. The remaining four parameters $\langle r^4 \rangle \beta_4^0, \langle r^4 \rangle \beta_4^2, \langle r^4 \rangle \beta_4^4$, and E_0 are the unknown quantities in the five equations (14). From eq 14 one can see that $E_4 - E_5 = x$ with the expression for x given by eq 15. For each assignment of different experimental energy values to the levels in eq 14 a set of values is obtained for each of the four parameters mentioned above. For each of these sets of values a value for x is obtained from eq 15. That value x is chosen which gives the best agreement with the experimental value of $E_4 - E_5$. In this way, the parameters $\langle r^4 \rangle \beta_i^m$ and a unique assignment of the energy levels are obtained. The values are given in Table II.

The splitting of the 7F_1 is due only to $\langle r^2 \rangle \beta_2^0$ and $\langle r^2 \rangle \beta_2^2$. If $\langle r^2 \rangle \beta_2^2$ is zero, two 7F_1 sublevels would result, one of which is doubly degenerate. In the octacoordinated dodecahedron I, β_2^2 is zero. In addition, $\langle r^4 \rangle \beta_4^4$ should have a definite nonzero value for both dodecahedrons. One can show from the θ and φ dependence of β_4^4 that the only case in which dodecahedron II can have a small β_4^4 is if the equivalent point charges were greatly displaced from the oxygen atoms (more than 20°) and if the two oxygen atoms were non-equivalent. This is very unlikely.

Table II: Energy Levels and Ligand Field Parameters

	Expected spectral data	Predicted by model
Energy Levels		
7F_1	$E_1 = 241 \text{ cm}^{-1}$	$E_1 = 241 \text{ cm}^{-1}$
	$E_2 = 456 \text{ cm}^{-1}$ ^a	$E_2 = 456 \text{ cm}^{-1}$
	$E_3 = 429 \text{ cm}^{-1}$ ^a	$E_3 = 429 \text{ cm}^{-1}$
7F_2	$E_1 = 1119 \text{ cm}^{-1}$	$E_1 = 1122 \text{ cm}^{-1}$
	$E_2 = 942 \text{ cm}^{-1}$ ^a	$E_2 = 940 \text{ cm}^{-1}$
	$E_3 = 950 \text{ cm}^{-1}$ ^a	$E_3 = 952 \text{ cm}^{-1}$
	$E_4 = 1129 \text{ cm}^{-1}$	$E_4 = 1124 \text{ cm}^{-1}$
	$E_5 = 1049 \text{ cm}^{-1}$	$E_5 = 1051 \text{ cm}^{-1}$
Ligand Field Parameters		
$\langle r^2 \rangle \beta_2^0 = -335.85 \text{ cm}^{-1}$	$\langle r^2 \rangle \beta_2^0 = -335.85 \text{ cm}^{-1}$	
$\langle r^2 \rangle \beta_2^2 = \mp 67.50 \text{ cm}^{-1}$	$\langle r^2 \rangle \beta_2^2 = \mp 67.50 \text{ cm}^{-1}$	
$\langle r^4 \rangle \beta_4^0 = -111.46 \text{ cm}^{-1}$	$\langle r^4 \rangle \beta_4^0 = -111.46 \text{ cm}^{-1}$	
$\langle r^4 \rangle \beta_4^2 = \mp 24.18 \text{ cm}^{-1}$	$\langle r^4 \rangle \beta_4^2 = \mp 3.42 \text{ cm}^{-1}$	
$\langle r^4 \rangle \beta_4^4 = -26.16 \text{ cm}^{-1}$	$\langle r^4 \rangle \beta_4^4 = 0 \text{ cm}^{-1}$	

^a E_2 and E_3 can be interchanged without affecting agreement with theory. Only the signs of the β_2^2 and β_4^2 parameters are affected.

Thus, on this basis of the splitting in the 7F_1 and the negligible value of $\langle r^4 \rangle \beta_4^4$ (which is small enough to be of the order of experimental accuracy), both dodecahedrons I and II are ruled out as possible configuration for the emitting species. Furthermore, the parameter $\langle r^2 \rangle \beta_2^2$ is large enough to indicate that antiprism III should be selected as the emitting species since the only remaining alternative, antiprism IV, predicts a zero value for $\langle r^2 \rangle \beta_2^2$ even after considering possible displacement of the point charges along the ligand bridges. The outcome is consistent with the results of Matkovic and Grdenic,⁸ who have determined from diffraction experiments that the tetrakis(acetylacetonato)cerium(IV) has the configuration of antiprism III. Both Eu^{3+} and Ce^{4+} would be expected to use the same bonding orbitals in forming octacoordinated β -diketonate complexes, because their ionic radii are 0.98 and 0.94 Å, respectively, and their electronic configurations are identical except for the number of inner 4f electrons.

Interatomic Distances and Angles. The values of the ligand field parameters listed in Table II can be used to calculate molecular parameters such as interatomic distances, bond angles, and mutual orientations of particles.

The signs on the parameters $\langle r^2 \rangle \beta_2^0$ and $\langle r^4 \rangle \beta_4^0$, when compared with the graphs of the θ functions in Y_2^0 and Y_4^0 , obviously restrict the angle θ from the z axis to a point charge to the range between 55 and 70°.

For antiprism III we also have the following relationship for the ratio of the parameters β_2^0 and β_4^0

$$\frac{\langle r^2 \rangle \beta_2^0}{\langle r^4 \rangle \beta_4^0} = \frac{16R^2(3 \cos \theta - 1)}{35 \cos^4 \theta - 30 \cos^2 \theta + 3} \frac{\langle r^2 \rangle}{\langle r^4 \rangle}$$

where R is the distance to an equivalent point charge

and θ is its angle with respect to the z axis. Solving for R , we obtain

$$R = \left[\frac{\langle r^2 \rangle \beta_2^0 (35 \cos^4 \theta - 30 \cos^2 \theta + 3) \langle r^4 \rangle}{\langle r^4 \rangle \beta_4^0 (16) (3 \cos^2 \theta - 1) \langle r^2 \rangle} \right]^{1/2} \quad (16)$$

Substituting our experimental values for the parameters $\langle r^2 \rangle \beta_2^0$ and $\langle r^4 \rangle \beta_4^0$ and setting $\langle r^4 \rangle$ and $\langle r^2 \rangle$ equal to $1.706 a_0^4$ and $0.834 a_0^2$, respectively (obtained from interpolation of data reported by Freeman and Watson⁹), leaves an expression for R in terms of θ . By definition, R is the distance from the Eu^{3+} ion to an equivalent point charge. We are now going to assume that the point charge is located along the Eu-O bond,¹⁰ so that the angle θ to the point charge is the same as that to the oxygen. Since the $\text{O} \rightarrow \text{Eu}$ bond involves electron donation from the oxygens in the anion to the Eu^{3+} ion, this approximation is a very good one. The value for the angle θ calculated below leads to very satisfactory results for interatomic distances and bond angles which in turn are verified by the recalculated energy levels predicted by the derived molecular geometry.

The distance between the two oxygen atoms in a ketoenolate ring is taken to be 2.81 Å as reported in ref 8. This distance does not change significantly upon changing the complexed ion.^{11,12} The relationship between the Eu-O bond length, $R_{\text{Eu-O}}$, and the O-Eu-O bond angle γ in a chelate ring is

$$R_{\text{Eu-O}}(\gamma) = \frac{2.81}{2 \sin \gamma/2} \quad (17)$$

The geometry of antiprism III allows γ to be expressed in terms of the θ and φ angles of the two oxygens in a given ring. Since both oxygen atoms have the same θ , the expression for γ is

$$\gamma = \cos^{-1} [\sin^2 \theta \cos(\varphi_1 - \varphi_2) + \cos^2 \theta] \quad (18)$$

Furthermore, the ratio of the parameters $\langle r^2 \rangle \beta_2^0$ and $\langle r^2 \rangle \beta_2^2$ yields

$$\frac{\langle r^2 \rangle \beta_2^0}{\langle r^2 \rangle \beta_2^2} = \frac{\sum_{i=1}^8 (3 \cos^2 \theta_i - 1)}{3 \sum_{i=1}^8 (\sin^2 \theta_i \cos 2\varphi_i)}$$

which for an antiprism reduces to

(8) (a) B. Matkovic and D. Grdenic, *Acta Cryst.*, **16**, 456 (1963); (b) *Nature*, **182**, 465 (1958).

(9) A. J. Freeman and R. E. Watson, *Phys. Rev.*, **127**, 2058 (1962).

(10) Such an assumption is not necessary if the splitting in the 7F_2 levels is large enough to determine the value of the $\langle r^2 \rangle \beta_2^2$ parameter with reasonable accuracy. In such a case R and θ can be determined using only the ratios of $\langle r^2 \rangle \beta_2^0$ to $\langle r^2 \rangle \beta_2^2$ and $\langle r^4 \rangle \beta_4^0$ to $\langle r^4 \rangle \beta_4^2$.

(11) See, for example, G. J. Bullen, R. Mason, and P. Pauling, *Nature*, **189**, 291 (1961).

(12) The constancy of the ligand "bite" was also used by W. G. Perkins and G. A. Crosby, *J. Chem. Phys.*, **42**, 407, 2621 (1965), in crystal field calculations on Yb^{3+} and Tm^{3+} tris- β -ketoenolates.

$$\frac{\langle r^2 \rangle \beta_2^0}{\langle r^2 \rangle \beta_2^2} = \frac{8(3 \cos^2 \theta - 1)}{3 \sin^2 \theta \sum_{i=1}^8 \cos 2\varphi_i}$$

Solving for $\sum_{i=1}^8 \cos^2 \varphi_i$ yields

$$\sum_{i=1}^8 \cos^2 \varphi_i = \frac{8(3 \cos^2 \theta - 1)}{3 \sin^2 \theta} \frac{[\langle r^2 \rangle \beta_2^2]}{[\langle r^2 \rangle \beta_2^0]} \quad (19)$$

In antiprism III, however, all of the φ_i 's can be expressed in terms of one of them. Thus, we find that

$$\sum_{i=1}^8 \cos 2\varphi_i = 4(\cos 2\varphi_1 - \sin 2\varphi_1) \quad (20)$$

Substituting eq 20 and the values for $\langle r^2 \rangle \beta_2^0$ and $\langle r^2 \rangle \beta_2^2$ into eq 19 we obtain an expression for φ_1 in terms of θ . Thus γ , as given by eq 18, can be plotted against the angle θ . Furthermore, since $R_{\text{Eu-O}}$ in eq 17 depends on γ only, it too can be plotted against the same angle θ .

The Eu-O distance, $R_{\text{Eu-O}}$, and the distance from the Eu^{3+} ion to the equivalent point charge, R , were plotted against θ in Figure 4. The two $R_{\text{Eu-O}}$ vs. θ graphs in the diagram correspond to the positive and negative values of $\langle r^2 \rangle \beta_2^2$. At the intersection point of the two functions, the equivalent point charge coincides with the oxygen site. If we assume that this is the case, we obtain the values $\theta = 55^\circ 53'$ and $R_{\text{Eu-O}} = 2.40 \text{ \AA}$.

The stereochemistry of octacoordination was theoretically investigated by Kepert,¹³ who showed that a considerable distortion from the hard-sphere model should be expected when coulombic repulsions are taken into consideration. Thus, for the square antiprism the hard-sphere model predicts an angle θ of $59^\circ 15'$, whereas with coulombic interaction the most favorable positions of the ligands are predicted by theory to be at $\theta = 55^\circ 48'$. This is in remarkable agreement with our value. In addition, the Eu-O bond distance of 2.40 \AA obtained from ligand field parameters in the present work is equal to the Ce-O distance in the tetrakis(acetylacetonato)cerium(IV) determined by diffraction experiments.⁸

From eq 19 and 20 we find that the point charges are displaced from the corners of a perfectly square Archimedean antiprism by an angle of only $0^\circ 14'$ in the projection of the xy plane. If the ligand field had a D_{3h} symmetry corresponding to equivalent point charges at the corners of a perfectly square Archimedean antiprism, one would expect two Stark components in 7F_1 and three in 7F_2 levels. Examination of the ${}^5D_0 \rightarrow {}^7F_{1,2}$ lines in Figure 1 shows two 7F_1 levels very close to each other and two pairs of very finely split 7F_2 levels, approaching the two- 7F_1 three- 7F_2 levels pattern. The O-Eu-O angle in a ketoenolate ring is found from eq 18 to be either $71^\circ 20'$ or $71^\circ 59'$ depending on the sign of $\langle r^2 \rangle \beta_2^2$. The same angle in the Ce^{4+} acetylacetonate was found to be $72 \pm 1^\circ$.⁸

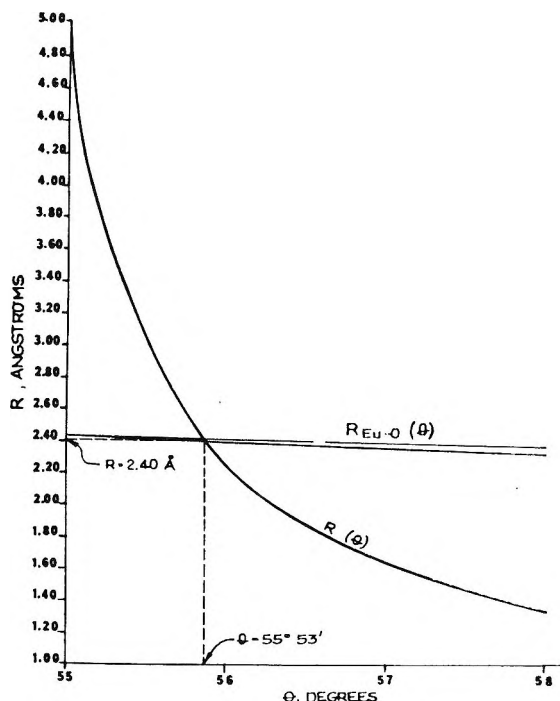


Figure 4. Dependence of $R(\theta)$ and $R_{\text{Eu-O}}(\theta)$ on the angle θ .

The magnitude of the equivalent point charge was calculated from the value of the $\langle r^2 \rangle \beta_2^0$ parameter extracted from spectral data. We substituted our calculated values $\theta = 55^\circ 53'$ and $R = 2.40 \text{ \AA}$, and the interpolated value for $\langle r^2 \rangle$ from ref 9 in the following expression for $\langle r^2 \rangle \beta_2^0$ derived from eq 5 and 10

$$\langle r^2 \rangle \beta_2^0 = -|e| \frac{4\pi q}{5 R^3} \left(\frac{1}{16} \right) \left(\frac{5}{\pi} \right) 8(3 \cos^2 \theta - 1) \langle r^2 \rangle \quad (21)$$

The value $q = -1.54|e|$ obtained from this expression indicates that the equivalent point charge lies closer to the Eu^{3+} ion than the oxygen atom along the Eu-O bond, since q would not be expected to exceed $-0.7|e|$ at the oxygen site.^{12,14} The magnitude of q from eq 21 is strongly dependent on θ and R . Thus, since $R(\theta)$ decreases rapidly with θ in the 55 - 57° region, q takes values from $-60.93|e|$ to $-0.26|e|$ for $\theta = 55^\circ$ and $\theta = 57^\circ$, respectively. Therefore one can restrict the magnitude of θ within approximately a 1° range above the intersection value $55^\circ 53'$. This in turn indicates that the $R_{\text{Eu-O}}$ is between 2.36 and 2.40 \AA . These results are not significantly changed by including second-order corrections such as J -mixing or shielding effects since (1) these were estimated to be of the order of 10 cm^{-1} ³ and (2) in eq 16 we use the square root of the ratio of two experimentally extracted parameters, each being more than an order of magnitude above second-order corrections.

The geometry of the emitting species was verified by

(13) D. L. Kepert, *J. Chem. Soc.*, 4736 (1965).

(14) L. S. Forster, *J. Am. Chem. Soc.*, **86**, 3001 (1964).

the calculation of the expected splitting of the energy levels of the Eu^{3+} ion due to a ligand field produced by an antiprismatic configuration having angles and distances as derived. The new values for $\langle r^l \rangle \beta_l^m$ obtained

from our calculated q , R , θ , and φ_l were substituted into eq 13 and 14 to predict the energy levels listed in Table II next to the experimental values. The agreement is found to be within the experimental accuracy of 2 \AA .

Electrical Phenomena Associated with the Transport of Ions and Ion Pairs in Liquid Ion-Exchange Membranes.

III. Experimental Observations in a Model System¹

by J. L. Walker, Jr., G. Eisenman, and J. P. Sandblom

Department of Physiology, University of Chicago, Chicago, Illinois 60637 (Received August 30, 1967)

An experimental model system, formally equivalent to a liquid ion-exchange membrane having incompletely dissociated sites and counterions, has been devised in order to test the steady-state properties deduced theoretically in a preceding paper.² The membrane model consists of a convection-free column of HCl in 2-propanol contained between AgCl boundaries. Since the AgCl boundaries are reversibly permeable to Cl^- but not to H^+ , Cl^- corresponds to the dissociated counterion, while H^+ is trapped and acts as the dissociated mobile site. The neutral HCl molecules correspond to the associated ion pairs and it has been verified that the concentrations of these species are interrelated through a simple law of mass action. The dissociation constant of HCl and the mobility of H^+ and Cl^- have been measured from conductance and transference number studies, and the mobility of the undissociated HCl species has been measured from the value of the limiting currents at high applied voltages. These parameters suffice to define the theoretically expected instantaneous and steady-state current-voltage characteristics of the system as well as the steady-state concentration and electric-potential profiles within the membrane. The theoretically expected values are compared with those observed experimentally and found to be in satisfactory agreement.

Introduction

In the preceding theoretical paper,² Sandblom, Eisenman, and Walker have extended Conti's and Eisenman's treatment of the steady-state properties of a mobile-site ion-exchange membrane having completely dissociated sites and counterions³ to include the effects of association of these species into electrically neutral pairs. From the extended treatment,² the quantitative behavior of an incompletely dissociated mobile-site membrane is expected to depend on parameters which do not appear in the Conti and Eisenman treatment, such as the degree of dissociation and the mobility of the undissociated species.

Despite certain simplifying assumptions, made chiefly for convenience of exposition, the theoretical

treatment² is sufficiently general to serve as a basis for a rigorous understanding of the properties of the usual liquid ion-exchange membranes⁴⁻⁷ in which sites and counterions are almost certain to be incompletely dissociated. Before using it for such a purpose, however, it

(1) This work was supported by National Science Foundation Grant GB-4039 and USPHS Grant GM-14404-01. It was assisted by USPHS General Research Support Grant FR-5367 and an NIH post-doctoral fellowship to J. L. Walker, Jr.

(2) J. P. Sandblom, G. Eisenman, and J. L. Walker, Jr., *J. Phys. Chem.*, **71**, 3862 (1967).

(3) F. Conti and G. Eisenman, *Biophys. J.*, **6**, 227 (1966).

(4) G. M. Shean and K. Sollner, *Ann. N. Y. Acad. Sci.*, **137**, 759, 763 (1966).

(5) O. D. Bonner and J. Lunney, *J. Phys. Chem.*, **70**, 1140 (1966).

(6) J. W. Ross, *Science*, **155**, 1378 (1967).

(7) G. Eisenman, *Anal. Chem.*, in press.

seemed desirable to test its principal conclusions in a system in which all assumptions were unequivocally satisfied. An experimental system was therefore devised in which all of the simplifying assumptions could be shown unequivocally to be satisfied, and this paper describes the experimentally observed properties of such a system and compares them with those expected from theory.

The principal assumptions of ref 2 are: (a) the mobile sites are *completely* confined to the membrane phase; (b) co-ions are *completely* excluded from the membrane; (c) the membrane interior is convection free; (d) the concentrations of associated and dissociated species are interrelated through an ideal form of the law of mass action; (e) mobilities are constant; and (f) all dissociated species are singly charged. Of these, the most difficult to be certain of in the usual liquid ion-exchange membrane are assumptions a and b, namely the boundary conditions at the membrane-solution interfaces.

While the circumstances for satisfying these assumptions have been discussed,² the chemistry of the usual liquid ion exchangers is sufficiently complex⁷ that we felt it would be desirable to test the theoretical expectations in an experimental system in which assumptions a and b were known to be satisfied⁸ and in which the validity of assumptions c-f could be assessed experimentally.

Such a system has been previously described by Walker and Eisenman, who used it to test the theory of a completely dissociated liquid ion exchange membrane.⁹ For their "membrane" they used a column of dilute aqueous HCl contained between AgCl boundaries. Since the AgCl boundaries are reversibly permeable to Cl⁻ but not to H⁺, Cl⁻ corresponds to the counterion, while H⁺ is trapped and acts as the mobile site. This system is particularly convenient in that fine chlorided silver wires can be used for the direct measurement of the chloride concentration profiles as well as of the electric potential within the interior of the "membrane." The only modification of this system necessary to produce incomplete dissociation of HCl is to replace water by a solvent in which HCl behaves as a weak electrolyte. 2-Propanol was found to be particularly suitable for reasons given below.

The System Studied

The experimental "membrane" is illustrated in Figure 1. In this system, the interior of an incompletely dissociated liquid ion-exchange membrane is represented by a column of dilute HCl in 2-propanol contained between Ag-AgCl boundaries in a length of polyvinyl tubing. The length of the tube corresponds to the thickness of the membrane with the cylindrical geometry chosen to minimize convection. Since the AgCl boundaries are reversibly permeable to Cl⁻ but not to H⁺, H⁺ is trapped within the convection-free

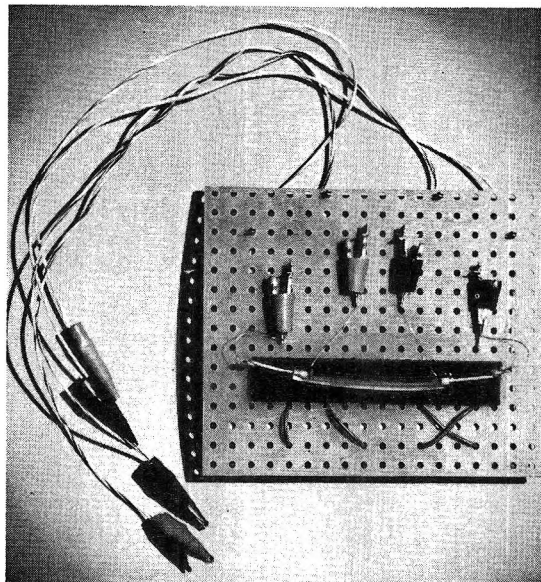


Figure 1. Experimental membrane. Reprinted by permission of *Biophysical Journal*. See ref 9, p 515.

"membrane phase" and acts as a mobile site, while Cl⁻ corresponds to a freely permeable counterion. Although H⁺ and Cl⁻ are completely dissociated when the solvent is water, their dissociation is incomplete in 2-propanol, the concentrations of the species H⁺, Cl⁻, and HCl being interrelated at all points in the system through the law of mass action.

2-Propanol was chosen as the solvent since it was found not to react with the polyvinyl tubing, and because in it the dissociation constant, activity coefficients, and the limiting equivalent conductances of HCl could be measured accurately by classical conductometric procedures.¹⁰⁻¹⁴ Very little triple-ion formation is expected over the concentration range of interest (and none was observed). In addition, we found (*cf.* Figure 2) that AgCl electrodes functioned as reversible electrodes for Cl⁻ in this solvent over an adequate concentration range.

Such a system is simpler than a liquid ion-exchange membrane of comparable degree of dissociation (*e.g.*, a solution of diisooctylphosphoric acid in *n*-amyl alcohol interposed between two aqueous HCl phases) because,

(8) In addition to the difficulties attendant on excluding co-ions completely from a liquid ion-exchange membrane, the sites of such exchangers are only confined to the membrane phase when particular conditions are satisfied as is discussed in ref 2. Moreover, the boundary reactions of a given liquid ion-exchange membrane need to be defined with regard to such complexities as the possibility of oriented surface-active materials at the interfaces as well as of polymer formation.

(9) J. L. Walker, Jr., and G. Eisenman, *Biophys. J.*, 6, 513 (1966).

(10) L. Onsager, *Physik. Z.*, 28, 277 (1927).

(11) R. M. Fuoss and C. A. Krauss, *J. Am. Chem. Soc.*, 55, 476 (1933).

(12) R. M. Fuoss, *ibid.*, 57, 488 (1935).

(13) T. Shedlovsky, *J. Franklin Inst.*, 225, 739 (1938).

(14) R. M. Fuoss and T. Shedlovsky, *J. Am. Chem. Soc.*, 71, 1496 (1949).

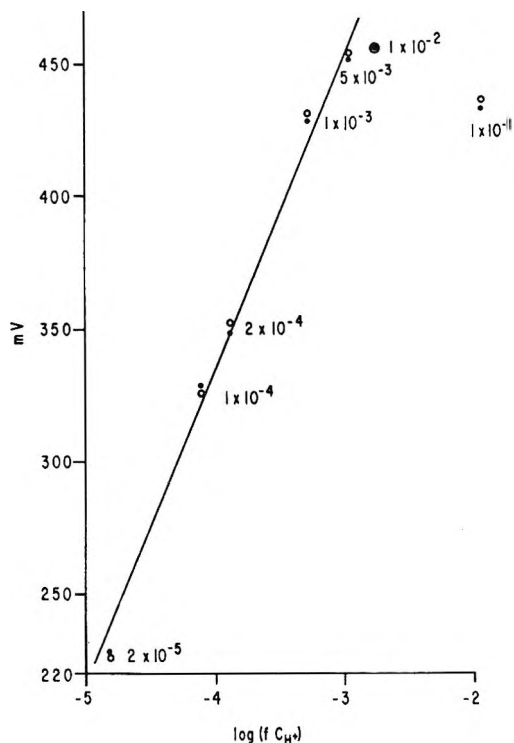


Figure 2. Concentration potentials for HCl in 2-propanol (the concentration for each point is given on the plot; the line is drawn with a slope of 118 mV): open circles, Beckman pH glass electrode; points, Corning pH glass electrode.

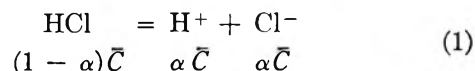
as mentioned above, the AgCl boundaries ensure not only that the H⁺ "sites" remain trapped within the membrane, but also that there are no co-ion species present. In a true liquid ion-exchanger membrane, the situation may be more complicated in that the sites (singly charged diisooctylphosphate anions) are not perfectly trapped within the organic phase (amyl alcohol), since they are partitioned between the alcohol and aqueous phases according to distribution equilibria. Moreover, the exclusion of co-ions (Cl⁻ ions from the aqueous phases) is expected to be complete only when the concentration of the exchanger at the boundary is higher than a certain minimal amount.⁷

The theoretically expected steady-state behavior of this system is completely defined² once values are known for the mobility of hydrogen ion (u_{H}), the mobility of chloride ion (u_{Cl}), the dissociation constant of hydrochloric acid (K), and the mobility of the undissociated HCl molecules (u_{HCl}). The measurement of these parameters is presented in part A of the Results, while in part B their values are used to calculate the behavior of the system expected theoretically for direct comparison with experiment.

Experimental Methods and Results

A. Measurement of the Parameters K , u_{H} , u_{Cl} , u_{HCl} for HCl in 2-Propanol. HCl in alcoholic solutions behaves as a classical weak electrolyte associating

into neutral HCl molecules and possibly into more complex aggregates (*e.g.*, triple ions, H₂Cl₂ dimers).^{12,15} Its chemical behavior in 2-propanol, as well as the value of the dissociation constant for simple ion-pair formation, can be assessed by classical measurements of the ac electrical conductance as a function of HCl concentration.¹⁰⁻¹⁴ Such studies indicate, as will be amplified below, that for a total HCl concentration (\bar{C}) less than 0.01 *M*, the only significant association occurring between H⁺ and Cl⁻ is to form neutral HCl molecules according to the equilibrium



where α is the fraction of HCl dissociated and \bar{C} is the total HCl concentration. $\alpha\bar{C}$ is, therefore, the concentration of H⁺ or Cl⁻ and $(1 - \alpha)\bar{C}$ is the concentration of undissociated HCl. Neglecting activity-coefficient corrections, the dissociation constant is related to these concentrations through

$$K = \frac{\alpha^2 \bar{C}}{1 - \alpha} \quad (2)$$

The Measurement of K . In all the studies presented in this paper, solutions of hydrochloric acid in 2-propyl alcohol were prepared by diluting a standardized aqueous solution of 5.0 *N* HCl (E. H. Sargent Co.) with reagent grade 2-propanol (Mallinckrodt). The 2-propanol was used without drying or further purification. Because of the possibility of serious changes in the dissociation constant resulting from the gain or loss of small quantities of H₂O or HCl from the 2-propanol solutions, the 2-propanol was taken from freshly opened bottles, and the exposure of all solutions to the atmosphere was kept as brief as possible. Because of the initial H₂O content of the 5.0 *N* HCl, all of the 2-propanol solutions contained traces of H₂O (the solution of 10⁻² *N* HCl in 2-propanol contained 0.2% H₂O by volume, while the most dilute solution studied, 2 × 10⁻⁵ *N* HCl in 2-propanol, contained 0.0004% H₂O).

The resistances of these solutions were measured at 50 and 1000 cps with platinized platinum conductivity cells having cell constants of 1.0 and 0.1 cm⁻¹ and using a standard conductivity bridge (Industrial Instruments Co. Model RC-16B2). The conductances measured at these two frequencies were in good agreement with each other and with those from small voltage drops (0.1 V) measured with small applied dc currents in conductivity cells of our own design, using bright silver electrodes (cell constant, 1.0 cm⁻¹).

The equivalent conductance, Λ , of HCl in 2-propanol is plotted in Figure 3 as a function of the square root of \bar{C} , the total molar solution concentration (the open

(15) G. J. Janz and S. S. Danyluk, *Chem. Rev.*, **60**, 209 (1960).

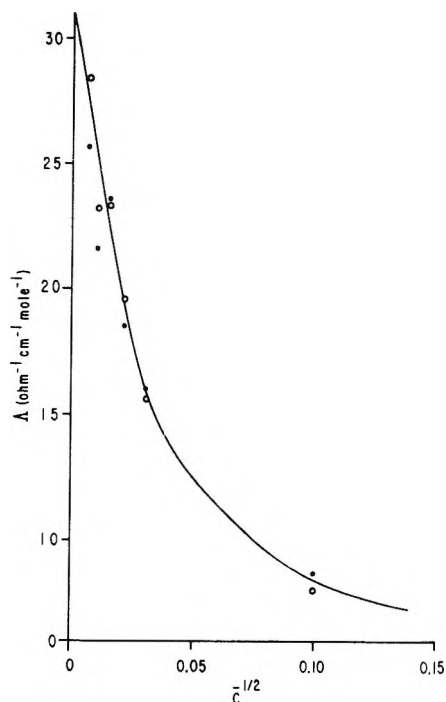


Figure 3. Equivalent conductance of HCl in 2-propanol: open circles, cell constant 1.0; points, cell constant 0.1.

circles were measured with a cell constant of 1.0, the points with a cell constant of 0.1). Extrapolation to zero concentration gives a tentative value for the limiting equivalent conductance, Λ_0 , of $31 \text{ ohm}^{-1} \text{ cm}^{-1} \text{ mol}^{-1}$. Following Fuoss,¹² this tentative value was used, taking the viscosity of 2-propanol as 2.04 cp and the dielectric constant as 18.3, to obtain a plot of $F(z)/\Lambda$ vs. $\Lambda f^2/F(z)$ from which precise values of Λ_0 , and K can be obtained ($F(z)$ is a tabulated function¹² of the equivalent conductance, f the mean activity coefficient of the dissociated species). Such a Fuoss plot is illustrated in Figure 4, where the agreement of the observations with a straight line indicates that no triple-ion formation is occurring. The y intercept is $1/\Lambda_0$, while the slope is $1/(K\Lambda_0^2)$. From Figure 4, Λ_0 is found to be $32 \text{ ohm}^{-1} \text{ cm}^{-1} \text{ mol}^{-1}$ and the dissociation constant, K , is found to be $3.8 \times 10^{-4} \text{ equiv/l.}$

Table I^a

\bar{c} , mol l. ⁻¹	Λ , ohm ⁻¹ cm ⁻¹ mol ⁻¹	f	α
6.25×10^{-5}	28.4	0.881	0.874
1.25×10^{-4}	23.2	0.841	0.793
2.5×10^{-4}	23.4	0.813	0.688
5.0×10^{-4}	19.6	0.741	0.571
1.0×10^{-3}	15.6	0.700	0.451
1.0×10^{-2}	8.0	0.338	0.177

^a $K = 3.8 \times 10^{-4} \text{ mol l.}^{-1}$, $\Lambda_0 = 32 \text{ ohm}^{-1} \text{ cm}^{-1} \text{ mol}^{-1}$, $u_{\text{H}} = 2.48 \times 10^{-9} \text{ mol cm}^2 \text{ sec}^{-1} \text{ J}^{-1}$, $u_{\text{Cl}} = 1.06 \times 10^{-9} \text{ mol cm}^2 \text{ sec}^{-1} \text{ J}^{-1}$.

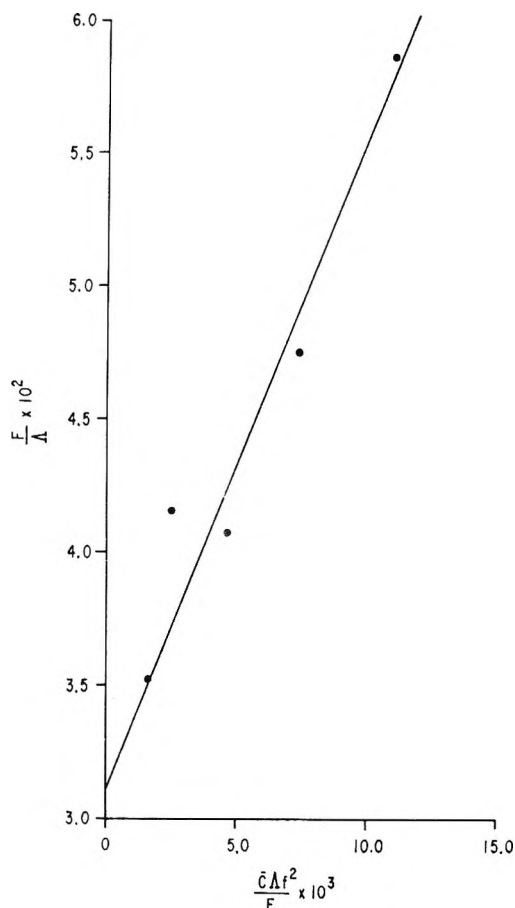


Figure 4. Fuoss plot of equivalent conductance data for HCl in 2-propanol.

These values are given in Table I and are consistent with those observed for HCl in other low molecular weight alcohols.¹⁵

Nonideal Behavior. The Fuoss calculation also yields values for the mean activity coefficient, f , of the dissociated species H^+ and Cl^- as a function of \bar{c} , the total HCl concentration (assuming constant mobilities for all species and ideal behavior for the associated HCl molecules). The logarithm of f is plotted in Figure 5 as a function of the logarithm of the concentration of dissociated species, $C_{\text{H}^+} = C_{\text{Cl}^-} = \alpha\bar{c}$. The fraction dissociated, α , is obtained as part of the Fuoss calculation (see Table I).

It can be seen that f is reasonably close to 1, and, what is more important, is a sufficiently slowly varying function of concentration for the system to be treated as ideal, as was done in the theoretical treatment.² (Ideal behavior is indicated by the horizontal dashed line and the effects of f will be shown in the discussion to be small.)

Before leaving this point, it should be noted that independent measurements of the activity coefficient, in good agreement with the above results, were carried out as a control on the reversibility of Ag-AgCl electrodes in 2-propanol (cf. Figure 2).

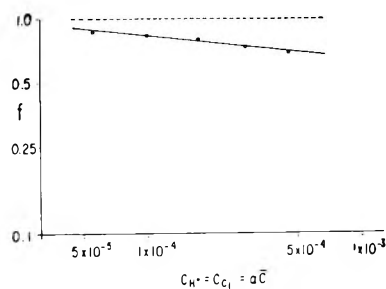


Figure 5. Activity coefficient, f , plotted as a function of the ionic concentration on a logarithmic plot.

Measurement of the Mobilities of H^+ and Cl^- . Provided mobilities are reasonably constant, it is possible to obtain values for u_H and u_{Cl} , the individual mobilities of H^+ and Cl^- , by combining the above measurement of Λ_0 with a measurement of t_H , the transference number of H^+ , recalling that

$$\begin{aligned} t_H \Lambda_0 &= F^2 u_H \\ t_{Cl} \Lambda_0 &= F^2 u_{Cl} \end{aligned} \quad (3)$$

Such a measurement is conveniently made^{16,17} by setting up an HCl concentration cell with a constrained diffusion liquid junction of type A or B



where \bar{C}_1 and \bar{C}_2 refer to two different total concentrations of HCl in 2-propanol. In either of these cells, the potential is directly given by the Planck equation,¹⁸ extended to use activities instead of concentrations. For cell A, it is

$$V = 2t_H \frac{RT}{F} \ln \frac{a_1}{a_2} = 2t_H \frac{RT}{F} \ln \left(\frac{\bar{C}_1}{\bar{C}_2} \frac{\alpha_1 f_1}{\alpha_2 f_2} \right) \quad (4A)$$

while for cell B, it is

$$V = 2t_{Cl} \frac{RT}{F} \ln \left(\frac{\bar{C}_1}{\bar{C}_2} \frac{\alpha_1 f_1}{\alpha_2 f_2} \right) \quad (4B)$$

It should be emphasized that eq 3 and 4 are valid regardless of the degree of dissociation of the system. Setting the activity coefficients f_1 and f_2 equal to unity, eq 4 can be expressed in terms of the conductivities σ_1 and σ_2 ¹⁶

$$V = 2t_H \frac{RT}{F} \ln \frac{\sigma_1}{\sigma_2} \quad (4a)$$

and

$$V = 2t_{Cl} \frac{RT}{F} \ln \frac{\sigma_1}{\sigma_2} \quad (4b)$$

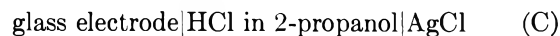
A constrained diffusion junction was formed by interposing an uncharged polyethylene millipore filter (150 μ thick; nominal pore diameter, 1.5 μ) between

two reservoirs filled with different concentrations of HCl. Potential differences were measured (with a Corning Model 12 pH meter) between pairs of Ag–AgCl electrodes, as well as between Corning triple-purpose pH glass electrodes in each of the two reservoirs. (Because of the high impedance of the glass electrodes, the potential difference between the two glass electrodes on each side of the junction was measured with respect to a common Ag–AgCl reference electrode.)

Figure 6 illustrates the potentials observed as a function of \bar{C}_2 for a constant concentration $\bar{C}_1 = 2 \times 10^{-5} N$. The dots plot the difference in potential observed between the two glass electrodes.

The observed points can be seen to fall on a straight line, indicating that t_H and t_{Cl} are reasonably constant. From the slope of 81 mV per log 10 concentration change for the glass electrode, and 35 mV for AgCl electrode, t_H is found to be 0.70, a value somewhat smaller than that in aqueous solution but consistent with that observed in alcohols whose hydrocarbon chain length is similar to 2-propanol.¹⁵ From this value, eq 3 indicates that u_H and u_{Cl} have the values 2.48×10^{-9} and 1.06×10^{-9} mol cm² sec⁻¹ J⁻¹, respectively.

On the Use of AgCl Electrodes to Measure Cl^- Activity in HCl-2-Propanol Solutions. Although there is good reason to expect that AgCl electrodes will be reversible to Cl^- in solutions of HCl in 2-propanol,^{15,16} this behavior will be of sufficient importance in part B when AgCl electrodes are used within the "membrane" for measuring Cl^- concentration profiles, that we felt it desirable to establish this unequivocally under our experimental conditions. As a control that AgCl electrodes prepared in the manner described under Methods indeed measured the activity of Cl^- in 2-propanol, electric potential measurements were carried out on a concentration cell without transference of the type



in which the concentration of HCl in 2-propanol was varied from $2 \times 10^{-5} N$ to $10^{-1} N$. Provided the glass electrode is reversible to H^+ and the AgCl electrode is reversible to Cl^- , the voltage of the cell should vary linearly with the logarithm of the product of the activities of the (dissociated) Cl^- and H^+ ions, yielding a slope of 118.4 mV per tenfold change of the mean H^+ and Cl^- activity at 25°.

The results of such a test are presented in Figure 2 where C_H has been calculated from the total concentration by eq 2, using $K = 3.8 \times 10^{-4}$ and the values of activity coefficients from Figure 5. The filled circles

(16) A. Gemant, "Ions in Hydrocarbons," Interscience Publishers Inc., New York, N. Y., 1962.

(17) H. S. Harned and B. B. Owen, "The Physical Chemistry of Electrolytic Solutions," 3rd ed, Reinhold Publishing Corp., New York, N. Y., 1958, p 478.

(18) M. Planck, *Ann. Physik. Chem.*, **40**, 561 (1890).

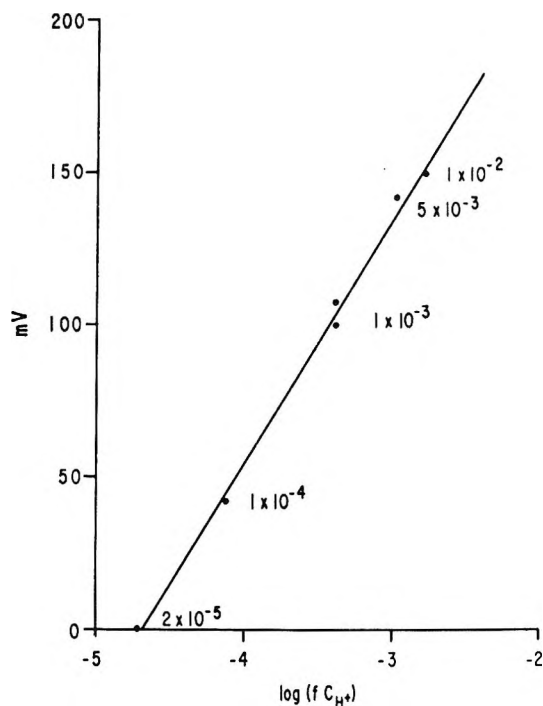


Figure 6. Liquid-junction potentials. The concentrations on side 2 calculated from conductivity measurements by eq 4a and 4b are shown on the plot; side 1 was held constant at $2.0 \times 10^{-5} N$.

represent the data obtained with a Corning triple-purpose pH glass electrode, while the open circles were measured with a Beckman general-purpose pH glass electrode. The observed potentials are seen to be in agreement with theoretical expectations (indicated by the solid line) over the activity range 10^{-5} to $10^{-3} N$ (corresponding to the total concentration range from 2×10^{-5} to $5 \times 10^{-3} N$; total HCl concentrations are indicated by the data points). The deviation observed at higher concentrations (for which the degree of dissociation is less than 0.25) was not studied. Instead, the experiments in part B were designed so that concentrations higher than this were avoided. The range of ideal response to chloride is sufficient to encompass all the concentrations present in our "membrane" in the experiments to be presented in which the total HCl concentration was 0.001 N and most of the data, even when the total HCl concentration was 0.005 N .

It is also possible that the deviation at high concentrations may be related to complex salting-in or salting-out phenomena at the silver chloride electrodes, which would correlate with the discrepancies observed when current-voltage characteristics were carried out at concentrations of $5 \times 10^{-3} N$, for in this case the concentrated end of the chamber can achieve a concentration of slightly more than $10^{-2} N$. For this reason, we consider as more reliable the data obtained with a total concentration of $10^{-3} N$.

The experimentally determined values of K , Λ_0 , u_H , and u_{Cl} at 25° are summarized in Table I, which also presents the values for Λ , f , and α as functions of the total HCl concentrations. It should be noted that in extracting these values, we have implicitly assumed, as is usually done,¹¹⁻¹⁴ that u_H , u_{Cl} , K are concentration independent. Any variation of u_H or u_{Cl} with concentration appears in the value of f . However, the internal consistency of the above results indicates that this is a reasonable physical picture.

The Measurement of the Mobility of the Undissociated HCl Species, u_{HCl} . The only parameter remaining to be measured in order that all of the properties of our system be defined by the theoretical treatment of the preceding paper² is u_{HCl} , the mobility of the undissociated HCl species—a quantity for whose measurement classical methods do not exist. There are a number of ways in which this can be measured, the most convenient being from a measurement of the limiting value of steady-state current for strong applied voltages, as outlined below.

For our system in which H^+ is the trapped site and Cl^- is the counterion, eq 21 of the preceding paper² becomes

$$I_1 = \lim_{v \rightarrow \pm \infty} I = \pm \frac{4FRTu_{Cl}u_{HCl}Q}{d\bar{u}_{HCl}} \quad (5)$$

where

$$Q = \bar{C} + \frac{1}{d} \left(\frac{\bar{u}_{HCl}}{u_{HCl}} - 1 \right) \int_0^d C_H dx \quad (6)$$

and

$$\bar{u}_{HCl} = \frac{2u_H u_{Cl}}{u_H + u_{Cl}} \quad (7)$$

In the above equations I_1 is the limiting current density, d is the thickness of the membrane, and \bar{u}_{HCl} will be recognized as the mean mobility of the dissociated ions. Q depends on the total concentration of HCl, the already measured parameters of the system, and the fraction of saturating current, ϕ . To assess u_{HCl} , the value of Q must be calculated by a method of successive approximations. This is described below, where it is found that Q is a rapidly converging function and consequently can be closely approximated after several approximations. Therefore, it can be seen from eq 5 that the limiting value of the saturating current can be used to calculate the value of u_{HCl} .

If we assume that $\int_0^d C_H dx$ is approximately given by its value at zero current, we can calculate a tentative value of u_{HCl} by noting that in the limit of zero current, eq 6 simplifies to

$$Q = \bar{C} \left[1 + \left(\frac{\bar{u}_{HCl}}{u_{HCl}} - 1 \right) \alpha \right] \quad (6a)$$

Table II^a

10 ⁻³ I/A, A	φ	V _{a,b} ^{obsd} , mV		V _{a,b} ^{obsd} , mV		V _{a,b} ^{off} , mV		C(b) C(a)	
		Before	After	Measd	Theor	Measd	Theor	Measd	Theor
1.03	0.373	0	+0.1	62.0	60.3	17.8	14.5	0.467	0.67
1.6	0.580	+0.7	+0.1	85.8	97.8	22.6	24.4	0.532	0.506
2.0	0.725	+0.3	+0.8	118.4	128.4	31.5	33.4	0.416	0.394
2.3	0.833	-0.3	0	175	157.6	41.8	42.5	0.309	0.306
2.55	0.924	-0.5	+0.7	202	185.9	38.0	53.7	0.347	0.223

^a $\bar{C} = 1.0 \times 10^{-6}$ mol cm⁻³, $I_1 = 2.76 \times 10^{-8}$ A.

where α is calculable directly from \bar{C} and K by eq 2.

Substituting eq 6a in eq 5 as a first approximation gives an explicit expression

$$u_{\text{HCl}} = \frac{\left[\frac{I_1 d}{4RTFu_{\text{H}}\bar{C}} - \alpha \right]}{1 - \alpha} \bar{u}_{\text{HCl}} \quad (5a)$$

for u_{HCl} in terms of the measured value of the limiting current (*i.e.*, of the cross-sectional area $\times I_1$) of 2.76×10^{-8} A. This procedure yields a tentative value for u_{HCl} of 4×10^{-9} cm² mol sec⁻¹ J⁻¹.

With this approximation, we know the range in which the value of u_{HCl} should fall, and we can use eq 6 to calculate Q for values of I from 0 to I_1 in steps of $0.2 \times I_1$, with u_{HCl} varying from 1.0×10^{-9} to 1.0×10^{-8} . For $u_{\text{HCl}} = 2.0, 4.0,$ and 10.0×10^{-9} , Q was found to vary by 0.6, 2.0, and 3.2%, respectively, as I varied from 0 to I_1 . These variations were sufficiently small that it seemed justified, thereafter, to proceed under the assumption that Q was independent of I and to use eq 6a in place of eq 6 to calculate theoretical I - V curves for part B. These results indicate that the tentative value of u_{HCl} , arrived at above, does not differ by more than 2% from the correct value as a result of the simplification introduced by replacing eq 6 by 6a. Thus u_{HCl} is taken to be 4.0×10^{-9} cm² mol sec⁻¹ J⁻¹, a value some *three times larger* than the mean mobility of the dissociated species, \bar{u}_{HCl} .

B. Comparison of Theory and Experiment. The system used as a model for a mobile site membrane has been illustrated in Figure 1. It consists of a length of polyvinyl (Tygon) tubing of nominal $1/16$ in. i.d., which was filled with HCl solution of known concentration. The ends of the tube were plugged with Ag cylinders, of 0.17 cm in diameter, which were used to deliver current. At various distances along the length of the tubing, fine Ag wires (0.018 cm in diameter) were inserted for recording the potential and chloride concentration within the membrane. Guide holes were made through the wall of the tubing at right angles to the lumen with a 7-mil steel wire prior to inserting the Ag wires under a dissecting microscope with an accuracy of ± 0.01 cm, distances being mea-

sured from the center to center of the wires. Silver wire of better than 99.9% purity was used. After all recording electrodes were in place, they were electrolytically chlorided in aqueous 0.1 *N* HCl, using a heavily chlorided silver wire as the cathode. Each recording electrode was chlorided individually by applying 22.5 V for 5 sec, with the cathode first at one end of the tube and then for 5 sec with the cathode at the other end. Immediately after chloriding, the chamber was rinsed with deionized distilled water. Electrodes prepared in this way had a slightly rough, light gray AgCl coat, which was mechanically stable. Any two electrodes so prepared showed a potential difference steady (over the course of an experiment) to within ± 0.75 mV. (*Cf.* the columns of Table II headed $V_{a,b}^{\text{obsd}}$ (Before and After), which give the values of the electrode potential differences in 0.01 *N* HCl in 2-propanol at the beginning and the end of each experiment of the definitive series. These measurements served as controls for the measurement of Cl⁻ concentration during the experiment).

The polarizing electrode plugs were made from silver wire (0.116 cm o.d.) which was melted in a gas flame and shaped into cylinders having a diameter slightly larger than the lumen of the tube, so as to give a tight mechanical seal. The surfaces facing the interior of the tubing were ground flat so as to be normal to the axis of the tubing. Prior to insertion into the tubing for a given experiment, each of these surfaces was chlorided lightly at low current densities in aqueous 2 *N* HCl using a 1-cm length of Tygon tubing as a chloriding chamber and a cathode previously coated with molten AgCl (reagent grade). In order to apply the same amount of AgCl to both plugs, two chloriding chambers were connected in series and both polarizing electrodes were chlorided simultaneously. We found empirically that, since the steady state was attained by 50 hr, it was convenient to chloride for 1 hr using a constant current density 100 times that to be used in the experiment. In this way, we deposited about 100% more chloride than was removed during the experiment. AgCl so deposited formed a smooth, uniform dark brown layer, which was immediately rinsed with deionized distilled water.

A precise calibration of the cross-sectional area was carried out before and after exposure to 2-propanol by measuring the resistance of a known length of tubing containing an aqueous solution of known conductivity with the result that the i.d. was found to be 0.164 cm, in good agreement both with the nominal i.d. (0.159 cm) of the tubing and with a direct optical measurement of 0.16 ± 0.008 cm. No change of diameter was observed, even after a 2-week exposure to 2-propanol. The cross-sectional area of the tubing, A , was therefore taken to be 2.11×10^{-2} cm² for all calculations.

Although it is desirable to keep the system long to minimize convection which would disturb the establishment of steady-state concentration profiles under an applied field, the length of the column was decreased from the 5.0 cm, previously used in aqueous media,⁹ to 1.5 cm in the present experiments, so that a steady-state could be reached in a convenient time. This was necessary because of the considerably lower mobility of H⁺ and Cl⁻ in 2-propanol than in water (Λ_0 was found to be 32 ohm⁻¹ cm⁻¹ equiv⁻¹ in 2-propanol in the present experiment, as opposed to 425 in the previous experiments for aqueous media). Although the present system may, therefore, not have been as convection free as the one previously studied, the increased viscosity from 0.894 cP in H₂O to 2.04 cP in 2-propanol should diminish convective mixing considerably. Reducing the length also required reducing the number of internal probe electrodes to four. The possibility of temperature-induced convection resulting from gradients in temperature introduced into the interior of the membrane by the silver chloride electrodes was minimized, as previously, by placing the entire system in a polyethylene bag which was then immersed in a water bath maintained at $25.0 \pm 0.2^\circ$.

In the experimental setup diagrammed in Figure 7, the recording electrode nearest to one end of the tube was grounded and used as the reference electrode for all potential measurements. The remaining electrodes were connected to the input of a Cary Model 21 vibrating-reed electrometer by way of a high quality, nonshunting single-pole multiposition switch. The output of the electrometer was read directly and also usually monitored by recording on a Rustrak strip-chart recorder with a chart speed of 1 in./hr.

Constant electric current was delivered through the polarizing electrodes from nickel-cadmium batteries (isolated from ground) in series with a calibrated resistor having at least 100 times the maximum resistance of the membrane at any time. The current was monitored, at first continuously and later intermittently, during an experiment by measuring the voltage drop across a second, smaller series resistor of value calibrated to within $\pm 0.05\%$. The batteries were found to deliver very stable currents over long time periods (weeks) with the small currents used for the experiments.

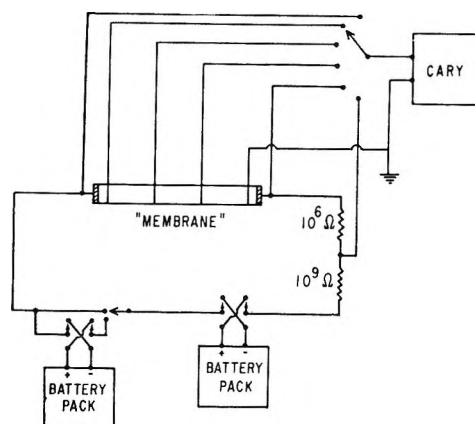


Figure 7. Schematic of the experimental setup for current clamp experiments. For voltage clamp experiments, the battery boxes and the 10^9 resistor were replaced with the voltage clamp circuit.

In addition to the above methods for making voltage measurements under constant applied current, current was measured under constant voltage conditions using a voltage clamp circuit, designed and built by Roland Wyatt, with the same results. The schematic for this instrument is shown in Figure 8.

For measuring instantaneous conductances, a second battery was switched into series with the constant current for delivering brief pulses of constant current, and the instantaneous voltage changes at various points in the membrane were measured with a high-input impedance amplifier (linear dc to 20 kc, designed by Harry Fein¹⁹ and built by Roland Wyatt) in conjunction with a cathode-ray oscilloscope (Tektronix Type 502). The instantaneous voltage change was observed to be time independent from 250 msec to more than 15 sec after the current step was made and was read, as routine, 2 sec after the start of the current pulse.

As a control that the only reaction occurring at the polarizing electrodes was $\text{Ag}^+ + \text{Cl}^- \rightleftharpoons \text{AgCl}$, the conductivity of the membrane was measured at the start and finish of each experiment when the concentration profile was uniform. This procedure also served as check on changes in the proportion of water to 2-propanol during the course of the experiments. The results of the conductance measurements are given in Table III. It can be seen that, though there were changes in conductivity of as much as 20%, they were not systematic. Also, since we observed a decrease in the conductivity of solutions of HCl in 2-propanol when they were allowed to stand for a few days in glass-stoppered flasks, each experiment was set up with a freshly prepared solution.

Experiments were done with two different concentrations of HCl in 2-propanol, $\bar{C} = 0.001$ N for which $\alpha = 0.455$ and $\bar{C} = 0.005$ N for which $\alpha = 0.24$.

(19) H. Fein, *IEEE*, 13 (1964).

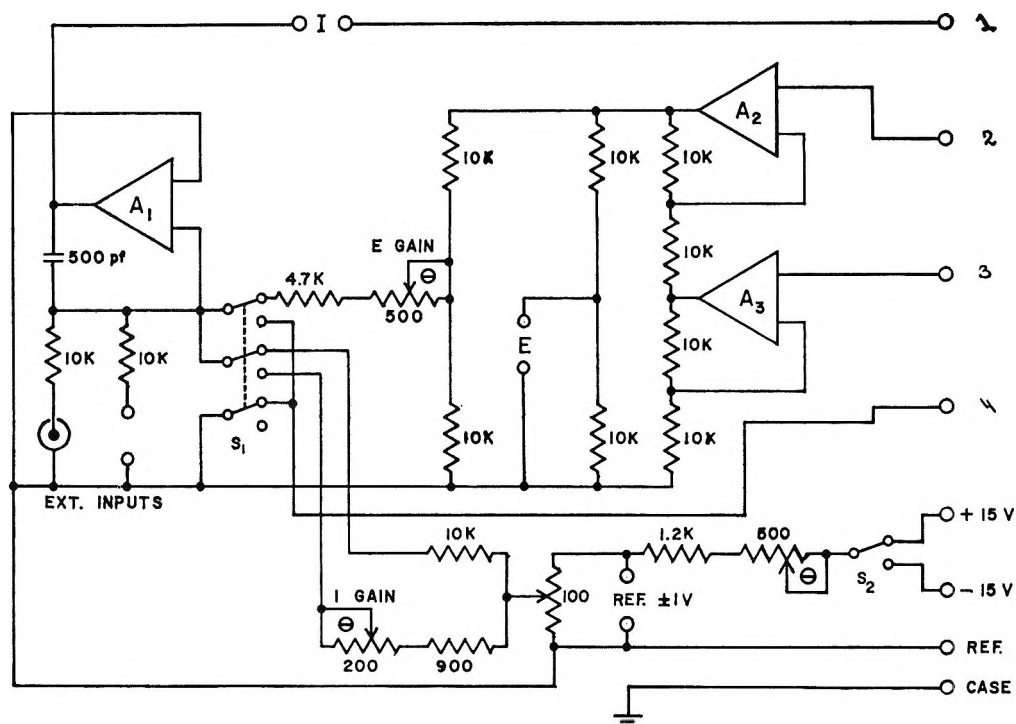


Figure 8. Schematic of the voltage clamp circuit: A_1 , A_2 , and A_3 are Philbrick operational amplifiers P45AU, P25A, and P25A, respectively. Electric current was delivered through the terminals labeled 1 and 4, while the voltage was sensed between terminals 2 and 3.

Table III

ϕ	$10^{-7}G_{inst}, mho$			$10^{-7}G_{inst}^{88}, mho$	
	Before	After	Theor	Measd	Theor
0.373	2.52	2.58	2.40	2.33	2.27
0.580	2.36	2.83	2.40	2.53	2.18
0.725	2.40	2.76	2.40	2.31	2.10
0.833	2.34	2.39	2.40	1.73	2.00
0.924	2.49	2.36	2.40	1.56	1.93

Results

The Potential Observed as a Function of Time for Steps of Applied Constant Current. Even though this paper is restricted to the steady state, it was necessary first to characterize the nonsteady-state behavior of the system to establish the conditions for achieving the steady state. The analysis of the kinetics will be reserved for a later paper, but the time course of a typical experiment is illustrated in Figure 9. In the upper figure, the curves are the potential differences observed during current flow at the indicated times between AgCl electrodes at the indicated points within the membrane (*i.e.*, the AgCl polarizing plugs were at 0 and d , and $V_{0.04d} - V_{0.96d}$ is the potential difference recorded between fine chlorided Ag wires at $0.04d$ and $0.96d$, etc. d was 1.48 cm and a current of 1.6×10^{-8} A was applied between $t = 0$ and $t = 102$ hr). These potential differences reflect both the response of the AgCl electrodes to the change in Cl^- activity and the changes

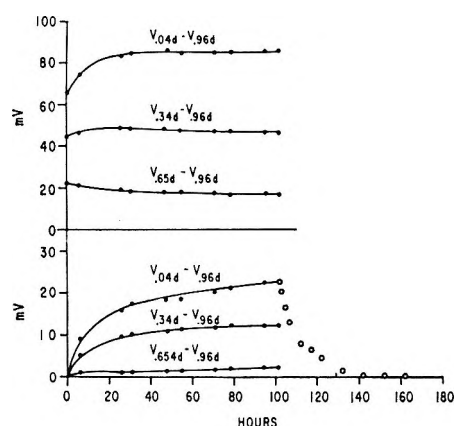


Figure 9. Time course of the current clamp experiment with $\phi = 0.580$ and $\bar{C} = 1.0 \times 10^{-3} N$; upper part: potential between successive pairs of electrodes with current flowing; lower part: points, potential between successive pairs of electrodes with the current off; open circles, return to zero current steady state after the current was turned off.

in IR drop, which occur with time as is expected from the theory² and as will be discussed below.

In the lower figure, the curves are the potential differences observed between the indicated points during brief interruptions of the applied current (*i.e.*, under zero-current conditions) at the indicated times. These potential differences directly reflect the changes in Cl^- activity within the membrane through eq 10.

The open circles subsequent to 102 hr reflect the decay of the concentration polarization which occurs when the applied current is turned off (only the data between the electrodes at $0.04d$ and $0.96d$ are presented).

The Current-Voltage Relationship. Theoretical Expectations. Since we form the boundaries of our membrane with AgCl interfaces instead of aqueous solutions, the activities of the external solution phases, $a'a''$, in the first term in eq 41 of Sandblom, Eisenman, and Walker² must be replaced by the activities of chloride ion in solid silver chloride. The ratio a'/a'' , therefore, becomes unity, and the first term of eq 41 becomes zero so that the current-voltage relationship for our system can be expressed simply in terms of the concentrations of dissociated H^+ or Cl^- just within the membrane, i.e., $C_H(0)$ and $C_H(d)$ for a membrane of thickness d cm. Notice that, formally at least, the silver chloride electrodes are equivalent to our having two external solution phases of constant and equal counterion (i.e., chloride) activities. A secondary electrode reaction such as the production of OH^- would, therefore, correspond to the introduction of another counterion species, while the production of H^+ would correspond to the production or removal of the sites at each of the boundaries (i.e., incomplete site trapping). The voltage observed between the AgCl electrodes at points a and b is simply expressed by eq 8 for any applied current and should not be confused with the electrostatic potential difference between these two points. The electrostatic potential difference is obtained from the observed potential difference by subtracting the quantity $RT/F \ln C_H(a)/C_H(b)$, i.e., the difference in the AgCl electrode potentials due to the difference in chloride activities at these two points.

It can be seen from eq 9 that in the limit of strong applied fields (when $C_H = 0$ at either 0 or d) the current-voltage relationship shows finite limiting currents (I_1), as previously noted by Conti and Eisenman for a completely dissociated system,³ which is of course a limiting case of the more general treatment of Sandblom, Eisenman, and Walker.²

The current-voltage relationship for this particular system can be written most conveniently with the voltage as a function of concentration and then writing the concentration as a function of ϕ , the fraction of limiting current, $\phi = I/I_1$.

$$V_{a,b}^{\text{obsd}} = -\frac{2RT}{F} \times \left\{ \ln \left[\frac{C_H(b)}{C_H(a)} \right] + \frac{u_{HCl}}{u_H K} [C_H(b) - C_H(a)] \right\} \quad (8)$$

$$C_H(x) = -\frac{K\bar{u}_{HCl}}{2u_{HCl}} + \left[\left(\frac{K\bar{u}_{HCl}}{2u_{HCl}} \right)^2 + KQ \left(1 + \phi - 2\phi \frac{x}{d} \right) \right]^{1/2} \quad (9)$$

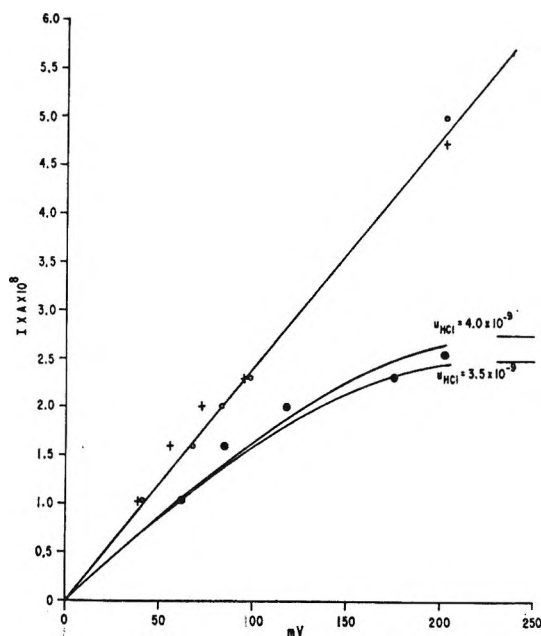


Figure 10. Current-voltage relationship for $\bar{C} = 1.0 \times 10^{-3} N$: straight line, theoretical instantaneous $I-V$; open circles, experimental instantaneous $I-V$ at beginning of experiments; crosses, experimental instantaneous $I-V$ at end of experiments; curved lines, theoretical steady-state $I-V$ curves calculated with the values of u_{HCl} indicated on the right. (limiting currents are shown by the horizontal lines at the right); and filled circles, experimental steady-state $I-V$ points.

In the above equations, $V_{a,b}^{\text{obsd}}$ is the voltage observed between the two points $x = a$ and $x = b$, F is the Faraday (96,500 C equiv⁻¹), R is the gas constant (8.317 J mol⁻¹ K⁻¹), T is the temperature (298.2°K), u_{Cl} is the (absolute) mobility of the chloride ion (1.06×10^{-9} mol cm² J⁻¹ sec⁻¹), u_H is the mobility of the hydrogen ion (2.48×10^{-9} mol cm² J⁻¹ sec⁻¹), u_{HCl} is the mobility of the undissociated HCl (4.0×10^{-9} mol cm² J⁻¹ sec⁻¹), K is the dissociation constant (3.8×10^{-7} mol cm⁻³), and C_H is the concentration of the ionic species in mol cm⁻³. The current density I is related to the electric current actually applied in a given experiment by $I = I(\text{applied})/A$, where A is the cross-sectional area (2.11×10^{-2} cm²).

Experimental Results. Figure 10 compares the observed current-voltage characteristics of the system with those theoretically expected for the ideal system in which activities are assumed equal to concentrations and u_{Cl} , u_H , K , u_{HCl} , and Q are constants. The solid dots are the observed steady-state values between points near the ends of the membrane ($a = 0.04d$, $b = 0.96d$) and the lines are the theoretical predictions for the $I-V$ characteristic between the same points. A theoretical curve has been drawn not only for $u_{HCl} = 4 \times 10^{-9}$ mol cm² J⁻¹ sec⁻¹ but also for $u_{HCl} = 3.5 \times 10^{-9}$ mol cm² J⁻¹ to indicate the extent to which the behavior depends on the particular value of u_{HCl} chosen.

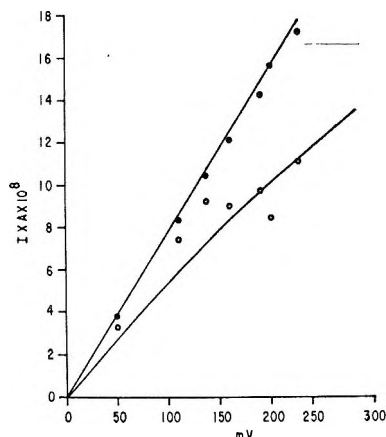


Figure 11. Current-voltage relationship for $\bar{C} = 5.0 \times 10^{-3} N$: straight line, theoretical instantaneous $I-V$; points, experimental instantaneous $I-V$ at beginning of experiments; curved line, theoretical steady-state $I-V$ for $u_{\text{HCl}} = 4.0 \times 10^{-9} \text{ mol cm}^2 \text{ J}^{-1} \text{ sec}^{-1}$ (the horizontal line on the right indicates the limiting current); and open circles, experimental steady-state $I-V$ points.

The open circles are the instantaneous conductances measured at the beginning of the experiment and the crosses are the instantaneous conductances measured at the end of the experiment when the concentration profiles had relaxed to their initial uniform values. For comparison with these values, the straight line is the instantaneous conductance expected for our geometry from the measured value of Λ_{HCl} at $0.001 N$ ($29.5 \text{ ohm}^{-1} \text{ cm}^{-1} \text{ equiv}^{-1}$). The agreement between open circles and dots is not as precise in this system as when the solvent was water,⁹ but was not a systematic effect and, in any event, was sufficiently good not to require introducing any arbitrary corrections in order to compare the experimental $I-V$ curve with that theoretically expected.

The agreement between the theoretically expected $I-V$ relationship and that experimentally observed constitutes our first test of the adequacy of the theory. To test the theory further, we carried out another set of $I-V$ determinations at five times higher HCl concentration and compared the observations with those theoretically expected. The results are plotted in Figure 11. Here the observed steady-state points agree reasonably well with theoretical expectations, although the scatter of the data is considerable. The data of Figures 10 and 11 confirm the theoretical prediction of the effect of changing the degree of dissociation α (*cf.* Figure 6 of Eisenman, Sandblom, and Walker²⁰ and Figure 2 of the preceding paper.² (In the case of $\bar{C} = 0.001 N$, $\alpha = 0.55$, while for $\bar{C} = 0.005 N$, $\alpha = 0.24$.) The difference between the two experiments can best be seen in Figure 12, which compares the theoretical curves for these two experiments on the same voltage and ϕ scales.

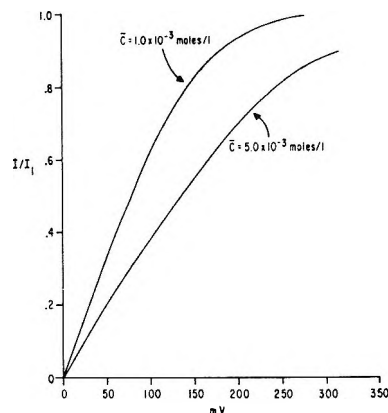


Figure 12. Comparison of the theoretical steady-state $I-V$ curves for the two concentrations of HCl used in the experiments. Note that the ordinate is $I/I_1 = \phi$.

Electric Potential Profile. Theoretical Expectations. The electric potential profile as measured between silver chloride electrodes in the interior can be obtained for the steady state of any applied current or voltage from eq 8 and 9. Once the parameters u_{Cl} , u_{H} , and u_{HCl} are known for the membrane, the potential profile can be solved explicitly through the use of these equations and the results then compared with the observed potential profiles as measured by silver-silver chloride electrodes. It is to be emphasized that the potential profiles referred to here are those expected when recording between silver-silver chloride electrodes and not simply the electrostatic potential in the interior.

Comparison with Experiment. Figure 13 presents a comparison of theory and experiment.

Concentration Profile. Theoretical Expectations. The theoretically expected concentration profile of chloride ion in the steady state is given by the Sandblom, Eisenman, and Walker eq 22 (ref 2), which indicates that it should be increasingly nonlinear with increasing association. This profile is directly measurable through the use of the silver-silver chloride electrodes. The liquid junction potential is given by eq 10, which follows directly from eq 4.

$$V_{a,b}^{\text{off}} = -2t_{\text{H}} \frac{RT}{F} \ln \frac{C_{\text{H}}(b)}{C_{\text{H}}(a)} \quad (10)$$

In this equation, only the dissociated species appear and the neutral species makes no contribution. It is thus possible to use the silver chloride electrodes to measure the chloride ion concentration directly in our system, provided only that there are no other ionic species formed (*i.e.*, triple ions). Evidence has been given above for the lack of substantial triple ion formation.

Comparison with Experiment. Figure 14 compares the experimentally measured steady-state concen-

(20) G. Eisenman, J. P. Sandblom, and J. L. Walker, Jr., *Science*, **155**, 965 (1967).

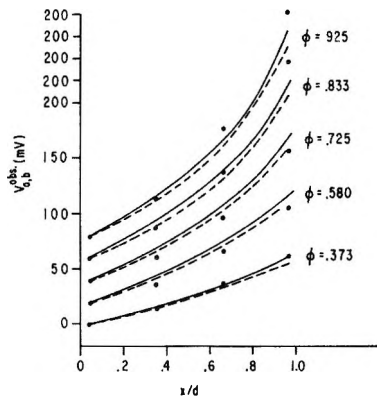


Figure 13. Electric potential profiles: solid lines, calculated from ideal theory with $\bar{C} = 1.0 \times 10^{-3} N$ and $u_{\text{HCl}} = 4.0 \times 10^{-9} \text{ mol cm}^2 \text{ J}^{-1} \text{ sec}^{-1}$, dashed lines, calculated from the nonideal theory; and points, experimental value. The value of ϕ for each experiment is given on the right.

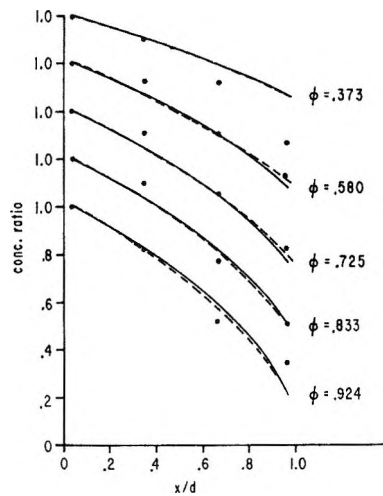


Figure 14. Concentration profiles: solid lines, calculated from ideal theory with $\bar{C} = 1.0 \times 10^{-3} N$ and $u_{\text{HCl}} = 4.0 \times 10^{-9} \text{ mol cm}^2 \text{ J}^{-1} \text{ sec}^{-1}$; dashed lines, calculated from nonideal theory; and points, experimental values. The value of ϕ for each experiment is given on the right.

tration profiles (dots) with the theoretical concentration profiles (lines). The abscissa is the fraction, x/d , of the total distance ($d = 1.48 \text{ cm}$); the ordinate is the ratio of the Cl^- activity at x/d to that at $a/d = 0.04$. The values of the observed concentration ratios were calculated by eq 10 from the potential difference observed between the various AgCl recording electrodes immediately after the current was turned off (*cf.* dashed lines in Figure 3). The theoretical curves were calculated from eq 9 using $u_{\text{HCl}} = 4.0 \times 10^{-9} \text{ cm}^2 \text{ mol sec}^{-1} \text{ J}^{-1}$. In spite of the fact that there is considerable scatter in the points, the observed profiles can be seen to have, at least qualitatively, the proper shape.

The Instantaneous Conductances in Various Steady States. If in the steady state, brief square voltage pulses are applied and the current during the pulse is

measured (or *vice versa*), one obtains a series of points defining a straight line through that particular steady-state I - V point. The slope of that line is the conductance of the system for that particular concentration profile. Because it is a straight line, only two points are needed to define it and, hence, determine the conductance. For every experiment, we have the necessary two points, the steady-state I - V point and the instantaneous off point, which is the step to zero current. From these two points the conductance G_{inst} is found to be

$$G_{\text{inst}} = \frac{I}{V_{a,b}^{\text{obs}} - V_{a,b}^{\text{off}}} = \frac{-I}{\frac{2RT}{F} \left\{ t_{\text{Cl}} \ln \left[\frac{C_{\text{H}}(b)}{C_{\text{H}}(a)} \right] + \frac{u_{\text{HCl}}}{u_{\text{HK}}} [C_{\text{H}}(b) - C_{\text{H}}(a)] \right\}} \quad (11)$$

and the intercept on the ordinate is

$$\text{intercept} = \frac{It_{\text{H}}}{t_{\text{Cl}} + \frac{u_{\text{HCl}}}{u_{\text{HK}}} \left[\frac{C_{\text{H}}(b) - C_{\text{H}}(a)}{\ln \frac{C_{\text{H}}(b)}{C_{\text{H}}(a)}} \right]} \quad (12)$$

From eq 12, it can be seen that for $0 < K$ in the limit of $V_{a,b}^{\text{obs}} \rightarrow \infty$, the intercept on the current axis becomes $I(t_{\text{H}}/t_{\text{Cl}})$, which therefore can be used to calculate the ratio of the site to counterion transference numbers.

In Table II, the theoretical and observed values of G_{inst} for the different steady states are compared.

C. Nonideal Behavior. We can see in Figure 5 that the nonideal behavior of H^+ and Cl^- in 2-propanol can be described by the n -type relationship of Karreman and Eisenman²¹

$$a = pC^n$$

where a is the activity, c the concentration, and p and n are empirical constants. For the concentration range in which we are interested, $p = 0.267$ and $n = 0.923$, when c has the units moles times cubic centimeter. With this definition of the activity for the ionic species (continuing the assumption of ideal behavior for the neutral species), it is possible to modify the previous treatment² to take into account the nonideal behavior of the dissociated species.

In the flux equations (which will not be reproduced here) the concentration in the chemical gradient term is replaced by activity; similarly, in the mass action law the concentration of the dissociated species are replaced by their activities

(21) G. Karreman and G. Eisenman, *Bull. Math. Biophys.*, **24**, 413 (1962).

$$K = \frac{a_{\text{Cl}}a_{\text{H}}}{C_{\text{HCl}}} = \frac{p^2 C_{\text{H}}^{2n}}{C_{\text{HCl}}} = \frac{p^2 \alpha^{2n} C^{2n-1}}{1 - \alpha} \quad (13)$$

where α is still defined as the fraction of dissociation.

Once the activities have been put into these equations, the derivation of the desired results follows Sandblom, Eisenman, and Walker² exactly and, therefore, only the results are presented here. For our particular system, the voltage in terms of concentration is

$$V_{a,b}^{\text{obs}} = -\frac{2nRT}{F} \left\{ \ln \left[\frac{C_{\text{H}}(b)}{C_{\text{H}}(a)} \right] + \frac{p^2 u_{\text{HCl}}}{(2n-1) u_{\text{H}} K} [C_{\text{H}}^{2n-1}(b) - C_{\text{H}}^{2n-1}(a)] \right\} \quad (14)$$

and the concentration as a function of the current density, I , is

$$\frac{p^2 u_{\text{HCl}}}{K \bar{u}_{\text{HCl}}} C_{\text{H}}^{2n}(x) + n C_{\text{H}}(x) - \frac{u_{\text{HCl}}}{\bar{u}_{\text{HCl}}} Q = \frac{I}{2RTFu_{\text{Cl}}} \left(\frac{d}{2} - x \right) \quad (15)$$

where

$$Q = \bar{C} + \frac{1}{d} \left(\frac{n \bar{u}_{\text{HCl}}}{u_{\text{HCl}}} - 1 \right) \int_0^d C_{\text{H}}(x) dx \quad (16)$$

when Q is assumed constant, $C_{\text{H}}(x)$ can be determined graphically for any values of I and x , once all of the other parameters have been assigned values.

The saturating current for the nonideal treatment can be obtained from eq 15 by setting $C_{\text{H}}(x) = 0$ for either $x = 0$ or $x = d$, and then solving for I . The result is

$$I_1 = \frac{4RTFu_{\text{Cl}}Qu_{\text{HCl}}}{d\bar{u}_{\text{HCl}}} \quad (17)$$

which appears to be the same as for the ideal treatment, but is numerically different. The difference arises because the value of Q is different for the two treatments, not only because n appears in eq 16, but also because the integral is evaluated as

$$\frac{1}{d} \int_0^d C_{\text{H}}(x) dx = \alpha \bar{C} \quad (18)$$

where the value of α is 0.455 for the ideal case and 0.525 for the nonideal case. This results from the mass-action law being defined with concentrations in the first case and with activities in the latter case. Due to the difference in the value of Q for the two cases, one is forced to take $u_{\text{HCl}} = 4.5 \times 10^{-9} \text{ cm}^2 \text{ mol sec}^{-1} \text{ J}^{-1}$ for the nonideal treatment in order to have the

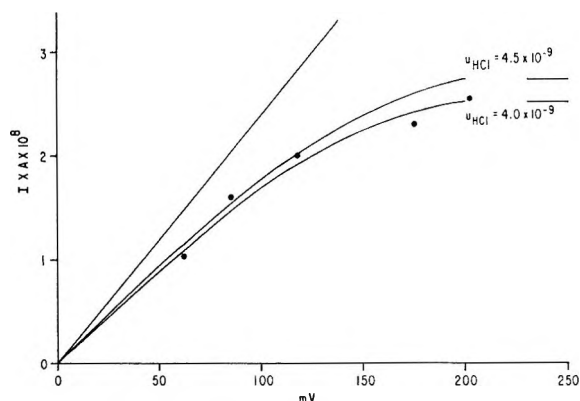


Figure 15. Current-voltage relationship for nonideal treatment with $\bar{C} = 1.0 \times 10^{-3} N$: straight line, theoretical instantaneous I - V ; curves lines, theoretical steady-state I - V calculated from the nonideal theory using the values of u_{HCl} indicated at the right (the horizontal lines on the right are the limiting currents for the two curves); and points, experimental.

same value of I_1 for both cases if $u_{\text{HCl}} = 4.0 \times 10^{-9} \text{ cm}^2 \text{ mol sec}^{-1} \text{ J}^{-1}$ is accepted for the ideal treatment.

Figure 15 shows two theoretical I - V curves calculated from the nonideal treatment for comparison with the ideal Figure 10. The curves are calculated for $\bar{C} = 1.0 \times 10^{-3} N$ with the mobility of the undissociated HCl molecule assumed to be 4.0×10^{-9} and $4.5 \times 10^{-9} \text{ cm}^2 \text{ sec}^{-1} \text{ J}^{-1}$. The calculated curves are to be compared with the experimental data points, which are the same as in Figure 10. The nonideal treatment appears to give a more satisfactory agreement between theory and observation in that the points correspond well to the curve calculated for $u_{\text{HCl}} = 4.0 \times 10^{-9} \text{ cm}^2 \text{ mol sec}^{-1} \text{ J}^{-1}$.

Electric-potential profiles and activity profiles, calculated from the nonideal theory with this value of $u_{\text{HCl}} = 4.0 \times 10^{-9} \text{ cm}^2 \text{ mol sec}^{-1} \text{ J}^{-1}$, are presented in Figures 12 and 13 as dotted curves for comparison with the solid curves calculated for the ideal case. Agreement between theory and observation is satisfactory, as it was with the ideal case. If anything, the ideal curves are in slightly better agreement with the data than the nonideal curves.

Comparing the above results, we conclude that there is no qualitative difference and very little quantitative difference between ideal and nonideal treatments for the present system in which (recalling Figure 5) the mean activity coefficient of the dissociated species remains within the range 0.82 ± 0.1 for the perturbations we have applied. In other systems, activity coefficient effects may not be so insignificant, and the procedure outlined here should be useful in taking them into account.

Nuclear Magnetic Resonance Analyses and Parameters for Some Monohalobenzene Derivatives

by J. E. Loemker,¹ J. M. Read, Jr.,² and J. H. Goldstein

Department of Chemistry, Emory University, Atlanta, Georgia 30322 (Received August 31, 1967)

The nmr spectra of a number of *o*-, *m*-, and *p*-halo-substituted fluorobenzenes have been recorded and precise values of the nmr parameters have been determined by analysis. The H-F couplings have been compared with the corresponding couplings in fluorobenzene and, in addition, correlations between the H-F couplings and substituent electronegativity have been observed. These substituent effects vary in direction and magnitude, depending on the relative positions around the ring.

Introduction

Interest in substituted fluorobenzenes dates back to 1952 when Gutowsky, *et al.*,³ reported that the influence of substituents on the electron distribution in benzene produces changes in the nuclear magnetic shielding of fluorine atoms in the molecules. Since this initial work, many substituted fluorobenzenes have been studied and their H-H, H-F, and F-F coupling constants have been reported.⁴⁻¹² In most cases, these compounds have been polyfluorobenzenes and the data obtained have served to define approximate ranges for the H-F couplings.

In a recent communication, Abraham, *et al.*,¹³ noted that proton couplings in substituted benzenes are relatively invariant to the nature of the ring substituents, and from the limited fluorobenzene data available, the H-F couplings appear to behave similarly. However, small systematic variations of the H-H couplings in benzene derivatives have been reported.^{11,14} As a result of a precise analysis of the benzene ¹³C-H satellites¹⁵ and analyses of a number of monosubstituted benzenes,^{16,17} it has been possible to study these substituent coupling effects in some detail. Because of the observed short-range character of the substituent effects, it appears that changes in the H-H couplings probably arise from inductive influences and are transmitted primarily through the σ electrons. Moreover, it has been found that substituent effects on the H-H coupling parameters are approximately additive.¹⁸

In view of the results cited for H-H couplings in the substituted benzenes, it appeared worthwhile also to examine the effects of substituents on H-F couplings in a series of substituted fluorobenzenes in order to determine whether similar trends exist. The H-F couplings are particularly interesting because the available data indicate that the variability of H-F couplings is considerably greater than is the case for H-H couplings. In addition, it appears that H-F couplings, quite unlike H-H couplings, are considerably influenced by long-range effects. This is particu-

larly evident in the *para* H-F couplings which have been observed to have either sign relative to the *ortho* and *meta* couplings. The latter couplings have been shown to be of the same sign.¹⁹⁻²³

At the present time, there have appeared very few complete analyses of the nmr spectra of monosubstituted fluorobenzenes. These have been limited to the *para* compounds,^{4,6-12} and, even so, there are discrepancies in the parameters reported by various workers. In this article, we describe the results of a

- (1) NASA Predoctoral Trainee, 1966-1969.
- (2) Eastman Kodak Fellow, 1966-1967.
- (3) H. S. Gutowsky, D. W. McCall, B. R. McGarvey, and L. H. Meyer, *J. Amer. Chem. Soc.*, **74**, 4809 (1952).
- (4) R. E. Richards and T. Schaefer, *Proc. Roy. Soc. (London)*, **A246**, 429 (1958).
- (5) S. S. Dharmatti, M. M. Dhungra, G. Govil, and C. L. Khetrapal, *Current Sci. (India)*, **31**, 414 (1962).
- (6) I. G. Aruldas and P. Venkateswarlu, *Mol. Phys.*, **7**, 65 (1963).
- (7) B. Gestblom and S. Rodmar, *Acta Chem. Scand.*, **18**, 1767 (1964).
- (8) G. W. Smith, *J. Mol. Spectrosc.*, **12**, 146 (1964).
- (9) W. G. Patterson and E. J. Wells, *ibid.*, **14**, 101 (1964).
- (10) G. Aruldas, *Proc. Indian Acad. Sci., Sect. A*, **63**, 349 (1966).
- (11) B. Dischler, *Z. Naturforsch.*, **20a**, 888 (1965).
- (12) M. Kimura, S. Matsuoka, S. Hattori, and K. Senda, *J. Phys. Soc. Jap.*, **14**, 684 (1959).
- (13) R. J. Abraham, D. B. Macdonald and E. S. Pepper, *Chem. Commun.*, 542 (1966).
- (14) P. F. Cox, *J. Amer. Chem. Soc.*, **85**, 380 (1963).
- (15) J. M. Read, Jr., R. E. Mayo, and J. H. Goldstein, *J. Mol. Spectrosc.*, **22**, 419 (1967).
- (16) S. Castellano and C. Sun, *J. Amer. Chem. Soc.*, **88**, 4741 (1966).
- (17) J. M. Read, Jr., and J. H. Goldstein, *J. Mol. Spectrosc.*, **23**, 179 (1967).
- (18) J. M. Read, Jr., R. W. Creceley, R. S. Butler, J. E. Loemker, and J. H. Goldstein, *Tetrahedron Letters*, in press.
- (19) H. S. Gutowsky, C. H. Holm, A. Saika, and G. A. Williams, *J. Amer. Chem. Soc.*, **79**, 4596 (1957).
- (20) W. G. Patterson and H. Spedding, *Can. J. Chem.*, **41**, 2706 (1963).
- (21) D. F. Evans, *Mol. Phys.*, **6**, 179 (1963).
- (22) E. Lustig and P. Diehl, *J. Chem. Phys.*, **44**, 2974 (1966).
- (23) C. Barbier, H. Faucher, D. Gagnaire, and A. Rousseau, *J. Chim. Phys.*, **63**, 283 (1966).

systematic investigation of H-F coupling constants which were obtained by detailed computer analyses of the proton (and, in two cases, ^{19}F) spectra of a series of *o*-, *m*-, and *p*- halo-substituted fluorobenzenes. A total of ten halogen-substituted fluorobenzenes have been analyzed in this investigation, and the effects of the substituents on the nmr parameters at each position have been determined by comparison with the corresponding values in fluorobenzene.²⁴ Although the number of substituents employed is somewhat restricted, the results appear to determine adequately at least the effects produced by halogen substituents. In addition, the new parameters serve to supplement values previously reported for other dihalobenzenes.²⁵

Experimental Section

The ten monosubstituted fluorobenzenes were the commercially available materials, their purity being indicated by their respective nmr spectra. Most of the proton spectra were obtained at 60 MHz, using a Varian Model A60-A spectrometer at a probe temperature of 38°. All samples were examined as solutions in tetramethylsilane (TMS) at a concentration of 10 mol % and were degassed before examination. Calibrations were performed by the usual side-band technique and the measured frequencies are the averages of three forward and three reverse sweeps. All of the spectral parameters reported here are based on these calibrated spectra.

Two additional spectra were obtained as verification for the *ortho*-substituted fluorobenzenes: the fluorine spectrum of *o*-chlorofluorobenzene obtained on a Varian Model HA 100 operating at 94.1 MHz and the proton spectrum of *o*-fluoroiodobenzene at 100 MHz obtained on a Jeolco 4H-100 nmr spectrometer.

Results and Calculations

The compounds studied here are five-spin systems of the type ABCDX for the *ortho*- and *meta*-substituted compounds and AA'BB'X for the *para*-substituted compounds.

The *m*-difluorobenzene is an ABB'CXX' six-spin system. The spectra were analyzed with the aid of Prospect-1, a least-squares computer program modified for an IBM 1620 computer after LAOCOON II.²⁶ The initial analyses were simplified somewhat by the availability of chemical shift and proton-proton coupling data for benzene¹⁵ and by the use of additivity relationships found for the disubstituted benzenes.

Substituent effects are calculated from the benzene¹⁵ and monohalobenzene¹⁷ parameters. The substituent effects on the chemical shifts were calculated in the manner previously described.²⁷⁻³⁰ The H-H coupling in a disubstituted benzene is calculated as the sum of the substituent effects from the two pertinent monosubstituted benzenes and the corresponding coupling in benzene.¹⁸ The initial estimates of the H-F coupling

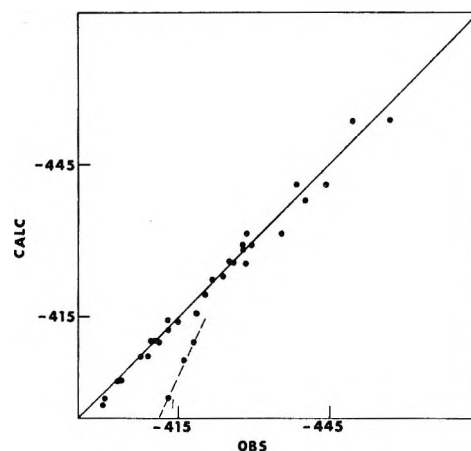


Figure 1. Additivity-calculated chemical shifts vs. observed chemical shifts in the monosubstituted fluorobenzenes.

constants were obtained from reported values in similar molecules and were refined through trial and error calculations.

Table I contains the observed chemical shifts along with the chemical shifts calculated from the additive substituent effects. These calculated shifts are plotted against the observed shifts in Figure 1, the solid line at a 45° angle to the axes corresponding to exact agreement of the two sets of values. As can be seen from this figure, with the exception of the proton *ortho* to the halogens in the 1,2-disubstituted benzenes, these calculated shifts are a good first approximation to the final values. The deviations found in the *ortho* proton shifts are comparable to those reported by Martin and Dailey³⁰ for other disubstituted benzenes.

Table II contains the observed H-H and H-F couplings along with the corresponding H-H couplings calculated from the additive substituent effects. These calculated and observed substituent effects on the H-H couplings are plotted in Figure 2, and again the correspondence is good enough to allow a close first approximation to the coupling parameters.

In the case of *o*-chlorofluorobenzene, the parameters which reproduced the proton spectrum at 60 MHz were also adequate to predict the fluorine spectrum at 94.1 MHz, with the proton shifts at 60 MHz being converted to proton shifts at 100 MHz. The same type of correspondence also held for the proton spectrum of *o*-

(24) J. E. Loemker, J. M. Read, Jr., and J. H. Goldstein, *Mol. Phys.*, **13**, 433 (1967).

(25) J. M. Read, Jr., R. W. Creceley, R. S. Butler, and J. H. Goldstein, *Spectrochim. Acta*, in press.

(26) S. Castellano and A. A. Bothner-by, *J. Chem. Phys.*, **41**, 3863 (1964).

(27) J. B. Leane and R. E. Richards, *Trans. Faraday Soc.*, **55**, 707 (1959).

(28) I. Yamaguchi and N. Hayakawa, *Bull. Chem. Soc. Jap.*, **33**, 1128 (1960).

(29) P. Diehl, *Helv. Chim. Acta*, **44**, 829 (1961).

(30) J. S. Martin and B. P. Dailey, *J. Chem. Phys.*, **39**, 1722 (1963).

Table I: Observed and Calculated Proton Chemical Shifts in the Monosubstituted Fluorobenzenes^a

Compound	2	3	4	5	6
Fluorobenzene ^b	-415.27	-430.96	-418.99	-430.96	-415.27
1,2-Bromofluorobenzene		-416.23 (-406.54)	-426.00 (-425.66)	-410.61 (-410.26)	-444.23 (-441.14)
1,2-Chlorofluorobenzene		-418.27 (-410.17)	-423.97 (-422.82)	-415.00 (-413.89)	-435.51 (-431.54)
1,2-Fluoriodobenzene		-413.03 (-398.85)	-428.01 (-428.23)	-403.16 (-402.57)	-457.11 (-453.74)
1,3-Difluorobenzene	-400.49 (-397.75)		-403.64 (-401.47)	-428.03 (-429.13)	-403.64 (-401.47)
1,3-Bromofluorobenzene	-428.46 (-425.45)		-411.33 (-409.97)	-421.90 (-422.23)	-429.76 (-429.17)
1,3-Chlorofluorobenzene	-418.78 (-415.85)		-408.85 (-407.13)	-425.61 (-425.86)	-420.52 (-419.57)
1,3-Fluoriodobenzene	-440.23 (-438.05)		-413.01 (-412.54)	-412.87 (-414.54)	-441.72 (-441.77)
1,4-Bromofluorobenzene	-438.67 (-441.14)	-407.62 (-406.54)		-407.62 (-406.54)	-438.67 (-441.14)
1,4-Chlorofluorobenzene	-428.84 (-431.54)	-409.92 (-410.17)		-409.92 (-410.17)	-428.84 (-431.54)
1,4-Fluoriodobenzene	-449.49 (-453.74)	-400.24 (-398.85)		-400.24 (-398.85)	-449.49 (-453.74)

^a The nonfluorine substituent is assigned the number 1, and succeeding positions are numbered consecutively around the ring in the direction which gives the fluorine the lower position number, in Hz, at 60 MHz, relative to TMS. Numbers in parentheses are the calculated values. ^b From ref 22, numbering begins with fluorine.

Table II: Observed and Calculated H-H and H-F Coupling Constants in the Monosubstituted Fluorobenzenes^a

	J_{23}	J_{24}	J_{25}	J_{26}	J_{34}	J_{35}	J_{36}	J_{45}	J_{46}	J_{56}
Fluorobenzene ^b	8.35	1.03	0.40	2.58	7.50	1.76	0.40	7.50	1.03	8.35
1,2-Bromofluorobenzene	8.58	4.82	-0.63	6.82	8.25 (8.31)	1.48 (1.42)	0.29 (0.26)	7.50 (7.38)	1.61 (1.54)	8.02 (7.96)
1,2-Chlorofluorobenzene	9.06	4.72	-0.85	7.29	8.26 (8.33)	1.46 (1.40)	0.32 (0.27)	7.54 (7.46)	1.64 (1.58)	8.01 (8.04)
1,2-Fluoriodobenzene	7.97	4.99	-0.24	6.29	8.24 (8.32)	1.42 (1.43)	0.26 (0.24)	7.41 (7.39)	1.64 (1.56)	7.89 (7.82)
1,3-Difluorobenzene	9.14	2.45 (2.34)	0.33 (0.20)	2.45 (2.34)	8.22	6.45	-0.93	8.39 (8.25)	0.79 (0.75)	8.39 (8.25)
1,3-Bromofluorobenzene	8.38	2.51 (2.38)	0.24 (0.26)	1.76 (1.77)	8.31	5.99	-0.46	8.28 (8.31)	0.90 (0.79)	8.06 (7.96)
1,3-Chlorofluorobenzene	8.66	2.45 (2.42)	0.39 (0.27)	2.01 (1.93)	8.23	6.08	-0.59	8.42 (8.39)	0.89 (0.83)	8.02 (8.04)
1,3-Fluoriodobenzene	8.14	2.50 (2.40)	0.30 (0.24)	1.57 (1.57)	8.42	5.85	-0.27	8.38 (8.32)	0.95 (0.81)	7.88 (7.82)
1,4-Bromofluorobenzene	8.79 (8.89)	4.83	0.26 (0.26)	2.55 (2.52)	8.18	3.16 (3.01)	0.26 (0.26)	8.18	4.83	8.79 (8.89)
1,4-Chlorofluorobenzene	8.81 (8.97)	4.66	0.32 (0.27)	2.70 (2.68)	8.08	3.11 (2.99)	0.32 (0.27)	8.08	4.66	8.81 (8.97)
1,4-Fluoriodobenzene	8.69 (8.75)	5.10	0.29 (0.24)	2.31 (2.32)	8.39	3.10 (3.02)	0.29 (0.24)	8.39	5.10	8.69 (8.75)

^a The nonfluorine substituent is assigned the number 1, and succeeding positions are numbered consecutively around the ring in the direction which gives fluorine the lower position number, in Hz. Numbers in parentheses are the calculated values. ^b From ref 22, numbering begins with fluorine.

fluoriodobenzene at 60 MHz and that at 100 MHz. Such correspondence indicates that these parameter sets very probably constitute a unique solution.

It should be noted that, in these calculations, all of the H-H couplings were assumed to be of the same sign, taken to be positive, as is usually the practice in the

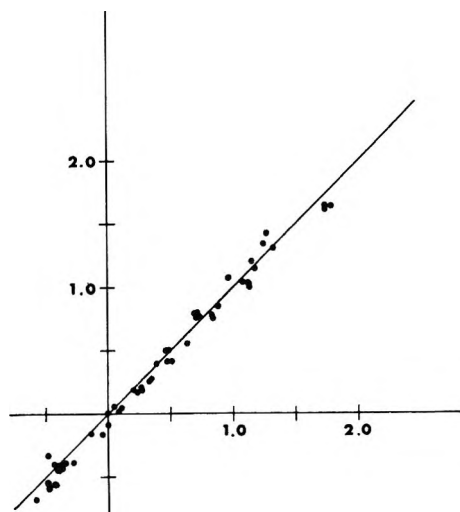


Figure 2. Additivity-calculated coupling substituent effects vs. observed coupling substituent effects in the monosubstituted fluorobenzenes.

case of benzene derivatives.^{31,32} Bak, *et al.*,³³ showed that in fluorobenzene the H-F and H-H couplings are of the same relative sign and hence the H-F couplings in fluorobenzene are taken to be positive. In our recent analysis of fluorobenzene, we confirmed these relative signs, and, in addition, found that the *para* H-F coupling had a small (0.20 Hz) positive value.²⁴ In the present set of monosubstituted fluorobenzenes, we have found it necessary, for successful fitting of the spectra, to assume that the *para* H-F couplings in the *ortho*- and *meta*-disubstituted compounds are of opposite sign to that of the *ortho* and *meta* H-F couplings in the same molecules. This point is covered in some detail in the Discussion.

In general, the errors associated with the analyses are quite small. In no case was the root-mean-square error deviation between the experimental and calculated frequencies greater than 0.06 Hz, and individual deviations greater than 0.10 Hz occurred only in situations where there were unresolved lines. The probable errors in the parameter sets are conservatively estimated to be no greater than 0.04 Hz.

Several examples of the observed and corresponding calculated spectra of the compounds analyzed are shown in Figures 3 and 4.

Discussion

Although considerable work has been done on the disubstituted benzenes, and, in particular, on the dihalosubstituted benzenes, relatively little attention has been directed to compounds containing one or two fluorine atoms. The symmetrical *para*-substituted fluorobenzenes have been rather extensively studied^{7,8,10-12} and, in the case of *p*-bromo- and *p*-chloro-fluorobenzene, complete analyses have been reported by Gestblom and Rodmar.⁷ In the case of the *ortho*-

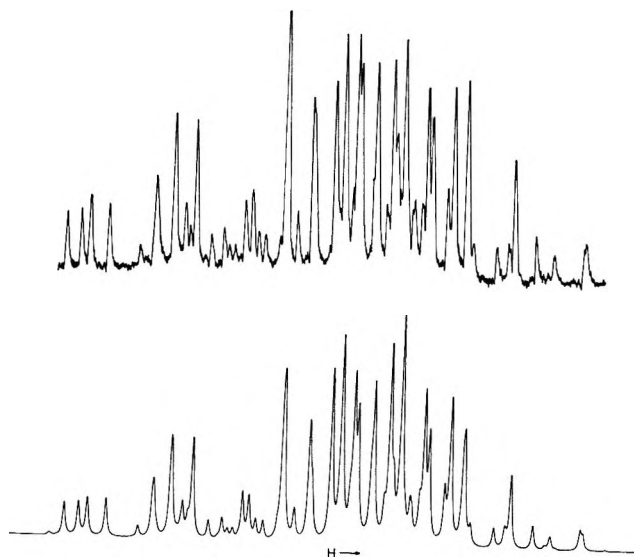


Figure 3. Experimental (top) and theoretical (bottom) proton spectra of *o*-chlorofluorobenzene at 60 MHz.

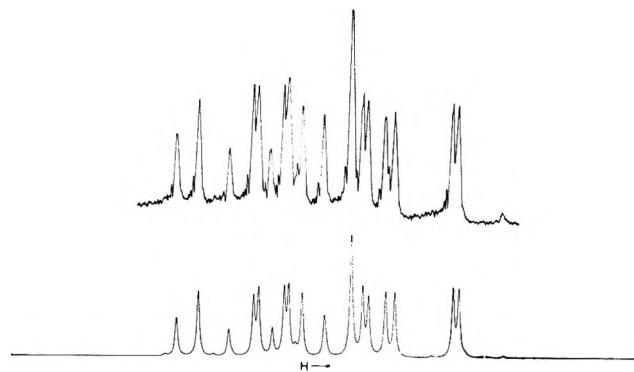


Figure 4. Experimental (top) and theoretical (bottom) fluorine spectra of *o*-chlorofluorobenzene at 94.1 MHz.

and *meta*-substituted fluorobenzenes, very little work has been done. Dharmatti, *et al.*,⁵ studied *ortho*- and *meta*-substituted fluorobenzenes and attempted to correlate the *para* H-F couplings with the σ - and π -electron densities in the ring. They concluded that the fluorine interaction with the *para* proton decreases steadily with an increase of the electronegativity of the substituent and that the effect is greater in the *meta*-substituted compounds with the substituent *ortho* to the *para* proton. However, their *para* H-F couplings for *o*-bromofluorobenzene (0.9 Hz), *o*-chlorofluorobenzene (1.0 Hz), *m*-bromofluorobenzene (1.9 Hz), and *m*-chlorofluorobenzene (1.8 Hz) are significantly different from those which are reported here. It should be noted that these previously reported *para* H-F couplings⁵ were obtained from a first-order analysis of the fluorine spectra.

(31) R. W. Fessenden and J. S. Waugh, *J. Chem. Phys.*, **31**, 966 (1959).

(32) C. N. Banwell, *Mol. Phys.*, **4**, 265 (1961).

(33) B. Bak, J. N. Schoolery, and G. A. Williams, *J. Mol. Spectrosc.*, **2**, 525 (1958).

While this paper was being written, an analysis of the 100-MHz spectrum of *m*-difluorobenzene appeared in the literature.³⁴ The H-H and H-F couplings reported in Macdonald's paper agree quite well with those in Table II, and, in addition, he reports an F-F coupling of 6.57 Hz compared to our value of 6.50 Hz. Although Patterson and Wells⁹ have reported H-H, H-F, and F-F couplings for the deceptively simple proton and fluorine spectra of *p*-difluorobenzene, complete analyses of the *o*- and *p*-difluorobenzenes have not been carried out.

Many empirical correlations have been attempted in an effort to find some regularities governing the H-H couplings in substituted benzenes. We have carried out an analogous examination of the effect of substituents on the H-F couplings in this series of substituted fluorobenzenes. From the available data for H-H and H-F couplings in substituted benzenes, the ranges for the H-F couplings appear to be considerably greater than those for the H-H couplings. Also, unlike the H-H couplings, these H-F couplings are influenced to a great extent by long-range effects.

Substituent effects on the H-F couplings may be readily found by comparing the values listed in Table II with the corresponding fluorobenzene data.²⁴ (The nomenclature used is explained in footnote *a* of Table II.) For example, the *ortho* H-F couplings in the *ortho*-substituted compounds have a range of 7.97–9.06 Hz, compared to a fluorobenzene value of +8.90 Hz. The *ortho* H-F coupling, J_{23} , in the *meta*-substituted compounds has a similar range, 8.14–9.14 Hz. It is worth noting that, in each of these two couplings, the substituent is *ortho* to either the fluorine or the proton in question and that the coupling increases with increasing substituent electronegativity. The *ortho* H-F coupling, J_{34} , in the *meta*-substituted and *para*-substituted compounds decreases slightly with increasing substituent electronegativity. In these two cases, neither of the nuclei in question is *ortho* to the substituent, and the couplings are all smaller than the corresponding fluorobenzene coupling. The ranges of these two *ortho* couplings are 8.23–8.42 Hz and 8.08–8.39 Hz for the *meta*- and *para*-substituted compounds, respectively.

Hence one correlation which appears to be significant is shown in Figure 5, which is a plot of these *ortho* H-F couplings vs. the Pauling electronegativity of the second substituent. Unlike the *ortho* H-H couplings, which show a definite increase with increasing electronegativity, these *ortho* H-F couplings show either an increase or a decrease depending on the position of the second substituent.

Two of the *meta* H-F couplings exhibit consistent increases over the fluorobenzene value of +5.57 Hz, and two of the couplings exhibit decreases. These *meta* H-F couplings are plotted against the substituent electronegativity in Figure 6. The range of the values

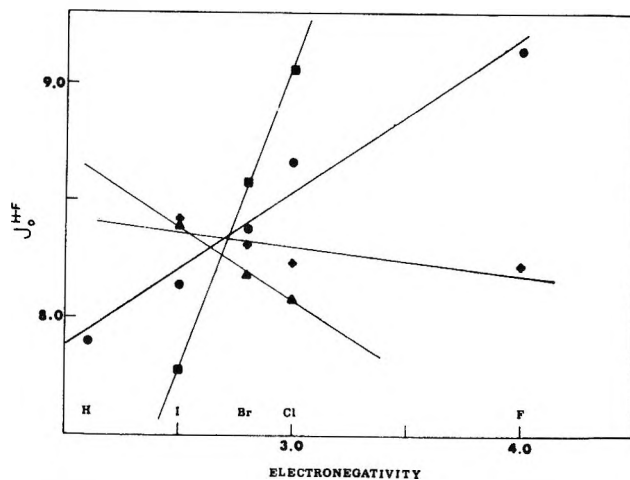


Figure 5. Plot of J_o^{HF} vs. the Pauling electronegativity of the second substituent: ■, $-J_{23}$ in the *ortho*-substituted compounds; ●, $-J_{23}$ in the *meta*-substituted compounds; +, $-J_{34}$ in the *meta*-substituted compounds; ▲, $-J_{34}$ in the *para*-substituted compounds.

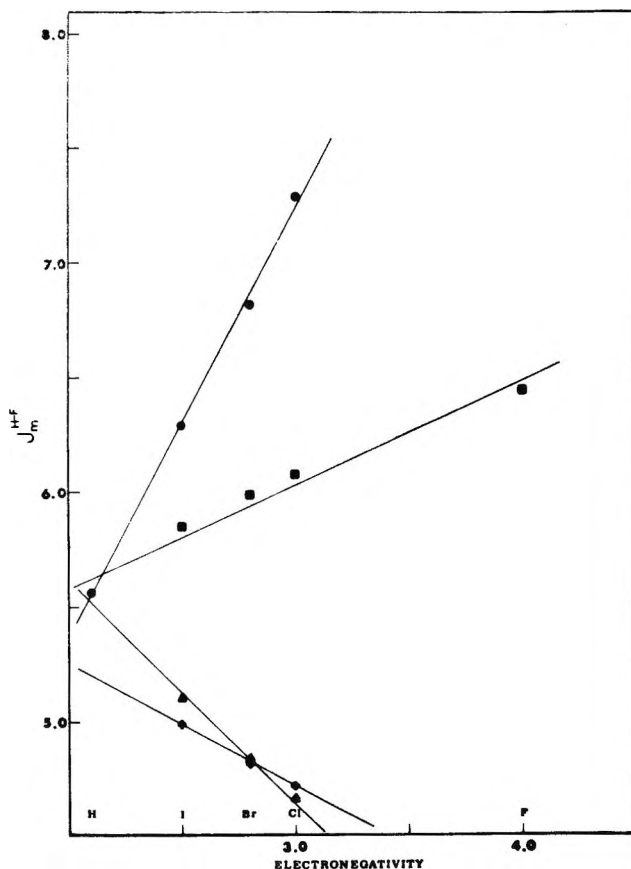


Figure 6. Plot of J_m^{HF} vs. the Pauling electronegativity of the second substituent: ●, $-J_{26}$ in the *ortho*-substituted compounds; ■, $-J_{35}$ in the *meta*-substituted compounds; ▲, $-J_{24}$ in the *ortho*-substituted compounds; +, $-J_{24}$ in the *para*-substituted compounds.

for J_{26} in the *ortho*-substituted compounds is 6.29–7.29 Hz, while J_{35} in the *meta*-substituted compounds

(34) D. B. Macdonald, *Chem. Commun.*, 686 (1967).

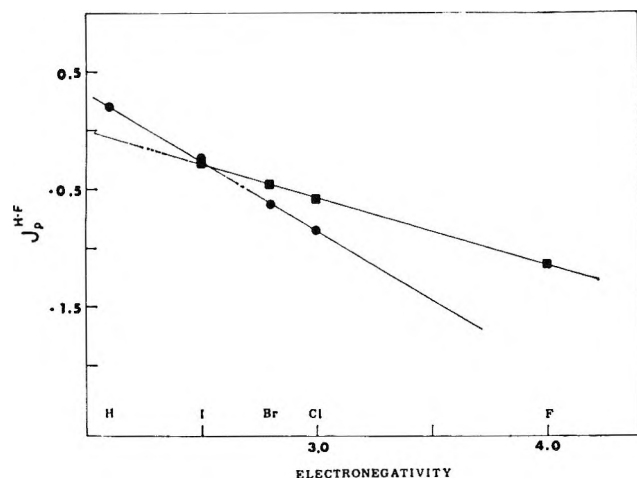


Figure 7. Plot of J_p^{HF} vs. the Pauling electronegativity of the second substituent: ●, $-J_{25}$ in the *ortho*-substituted compounds; ■, $-J_{36}$ in the *meta*-substituted compounds.

assumes values in the range 5.85–6.45 Hz. The other two *meta* H–F couplings, J_{24} in the *ortho*-substituted compounds and J_{24} in the *para*-substituted compounds, have ranges of 4.72–4.99 Hz and 4.66–5.10 Hz, respectively. In these cases, it is difficult to perceive any well-defined relation between the substituent position and the corresponding increase or decrease in the parameter. However, it will be noted that in the two cases where the coupling increases, both nuclei are either *ortho* to the substituent or *meta* to the substituent.

The *para* H–F couplings in both the *ortho*- and *meta*-substituted compounds decrease from the fluorobenzene value of +0.20 Hz. These *para* H–F couplings are plotted against the substituent electronegativity in Figure 7. In the *ortho*-substituted compounds, J_{25} has a range from -0.63 to -0.24 Hz, and in the *meta*-substituted compounds, J_{36} has a range from -0.93 to -0.27 Hz. As mentioned previously, Dharmatti, *et al.*,⁵ discussed the effect of the substituent position on the magnitude of the *para* H–F couplings. Our data are essentially in agreement with their conclusion that the relatively larger effect is caused by the substituent *ortho* to the proton.

While this manuscript was in preparation, there appeared a publication by Hutton, Richardson, and Schaefer³⁵ in which these authors demonstrated an empirical relationship between the sum $J_o^{\text{HF}} + J_m^{\text{HF}}$ and the electronegativity of substituents *ortho*, *meta*, and *para* to fluorine in the substituted fluorobenzenes. We have prepared similar plots (not shown here) using the data in Table II and the fluorobenzene data. In the case of the *para*-substituted compounds, the result is a smooth curve, which supports a previous conclusion that an increase in substituent electronegativity corresponds to a reduction in $J_o^{\text{HF}} + J_m^{\text{HF}}$.³⁵ For the *ortho*- and *meta*-substituted fluorobenzenes, the corresponding sums cannot be obtained, since there are two

meta H–F couplings in the *ortho* compounds and two *ortho* H–F couplings in the *meta* compounds. However, if in these two types of systems the sums are formed with either combination of *ortho* and *meta* couplings, or with the one coupling and an average of the two *ortho* or two *meta* couplings, the results partially agree with those of Hutton, *et al.*³⁵ Although it is true that, in general, increasing substituent electronegativity corresponds to increasing values of $J_o^{\text{HF}} + J_m^{\text{HF}}$, the sum for the substituent, hydrogen, deviates considerably to the positive side of any of the possible curves. The reason for this deviation can be seen in Figure 5. For the *ortho* and *meta* compounds, each of the plots of the *ortho* H–F couplings vs. electronegativity also lies considerably below the point for hydrogen.

In the *ortho*- and *meta*-substituted fluorobenzenes studied here, the *para* H–F couplings, although relatively small in magnitude, were found to have a sign opposite to that of the *ortho* and *meta* H–F couplings. In order to verify this result, several additional calculations were carried out for the fluorine spectrum of *o*-chlorofluorobenzene. These calculated spectra are shown in Figure 8. The observed spectrum and the calculated spectrum with $J_p^{\text{HF}} = -0.85$ are shown in Figure 8A and B. Figure 8C is the calculated spectrum in which all of the H–F couplings are of the same sign, here taken to be positive. As can be readily seen from the figure, the latter calculated spectrum does not correspond to the observed spectrum. The final

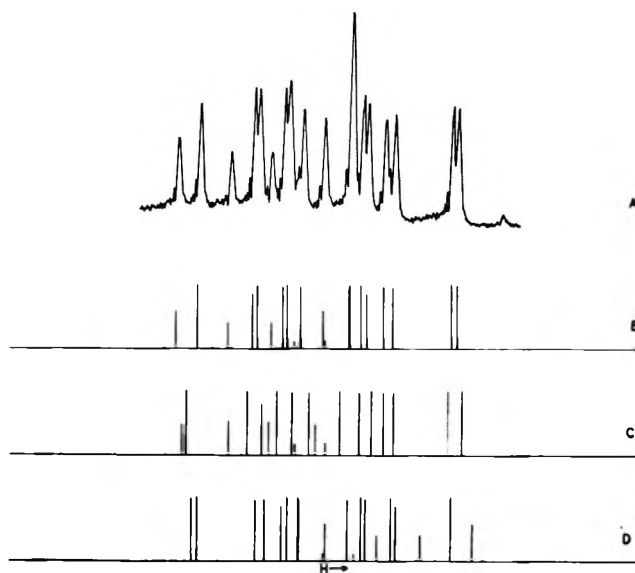


Figure 8. A. Observed fluorine spectrum of *o*-chlorofluorobenzene at 94.1 MHz. B. Corresponding calculated spectrum with $J_p^{\text{HF}} = -0.85$ Hz. C. Calculated spectrum with all J_p^{HF} 's taken as positive. D. Calculated spectrum with the relative signs of the J^{HF} 's the same as in spectrum B, but with $J_p^{\text{HF}} = +0.85$ Hz.

(35) H. M. Hutton, B. Richardson, and T. Schaefer, *Can. J. Chem.*, **45**, 1795 (1965).

calculated spectrum in this Figure (8D) is one in which the relative signs were taken to be the same for the H-F couplings, as in Figure 8B, but with $J_p^{\text{HF}} = +0.85$ Hz. The effect of this choice was merely to invert the entire spectrum. Hence, it seems reasonable to conclude that the *para* H-F couplings are of opposite sign from that of the other H-F couplings and that the *ortho* and *meta* H-F couplings have the same sign relative to the H-H couplings.

In summary, the H-F coupling constants reported here exhibit rather wide ranges of values which are consistent with the ranges previously reported for other derivatives. Unlike the corresponding H-H couplings in the monosubstituted benzenes, all of the H-F couplings in the fluorobenzenes are significantly affected by the substituent. The correlations found between the H-F couplings and substituent electronegativity are interesting, but not readily explicable. It is possible that these couplings may be influenced not only by inductive factors, which seem largely responsible for variations in aromatic H-H couplings, but also

by some combination of mesomeric and geometric variations. Previous theoretical studies have indicated that the interpretation of H-F couplings presents, in general, a more difficult task than is the case for H-H couplings,^{36,37} and there are further complications in aromatic systems. The present status of this problem indicates a need for additional investigations, both theoretical and experimental.

Acknowledgments. This research was supported in part by a grant from the National Institutes of Health. The authors also wish to express their appreciation to Mr. Bill Jankowski, Analytical Instruments Application Laboratory, Varian Associates, Pittsburgh, Pa., for the fluorine spectra of *o*-chlorofluorobenzene and *m*-difluorobenzene at 94.1 MHz. The proton spectrum of *o*-fluoriodobenzene at 100 MHz was provided by Jeolco, Medford, Mass.

(36) J. A. Pople, *Mol. Phys.*, **1**, 216 (1958).

(37) G. A. Williams and H. S. Gutowsky, *J. Chem. Phys.*, **30**, 717 (1959).

Photochromism: Spectroscopy and Photochemistry of

Pyran and Thiopyran Derivatives

by Ralph S. Becker and Jaroslav Kolc

Department of Chemistry, University of Houston, Houston, Texas 77004 (Received September 1, 1967)

Several pyran and thiopyran derivatives, including an indolinospirobenzothiopyran, exhibit photochromic behavior. It is possible to sensitize coloration of the latter compound in a rigid matrix. The substitution of sulfur for oxygen causes dramatic red shifts in the absorption bands of the colored but not of the colorless compound. Structures for the colored products have been assigned. The photochemical process appears to be highly efficient.

Introduction

As part of our continuing investigation to evaluate the various spectroscopic parameters of molecules, energy transfer, and the importance of these in photochemistry, we have investigated several new molecular systems. One particular aspect worthy of clarification is the site of photochemical activity in the chromenes and indolinospirobenzopyrans. Another important area is the evaluation of the effects of substitution of sulfur for oxygen. Of particular concern are the spectroscopic properties of both the uncolored and colored forms, as well as the photochemical behavior of the uncolored form.

We wish to report reversible photochemical behavior for four new molecular ring systems: 2H-pyran, 2H-thiopyran, 2H-thiochromene, and indolinospirobenzothiopyran.

Experimental Section

All experiments were carried out in 3-methylpentane at 77°K, unless otherwise noted. The absorption spectra were determined by means of a Cary Model 15 recording spectrophotometer with quartz cells 2 mm and 10 mm in path length. Concentrations were approximately 10^{-3} M. For production of the photo-colored forms, a 1-kW Hg-Xe lamp with a Corning

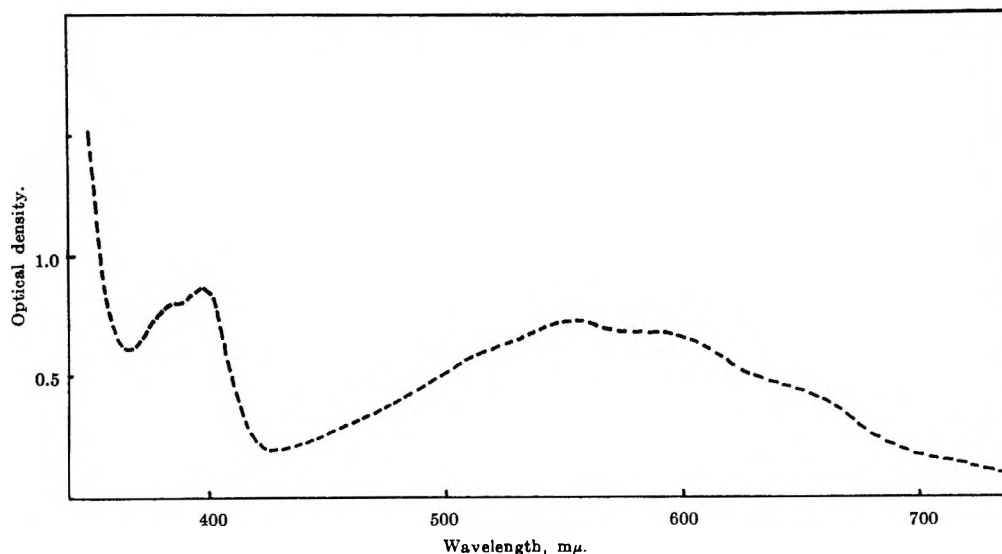


Figure 1. Absorption spectrum of the colored form of 2H-thiochromene in 3-methylpentane at 77°K.

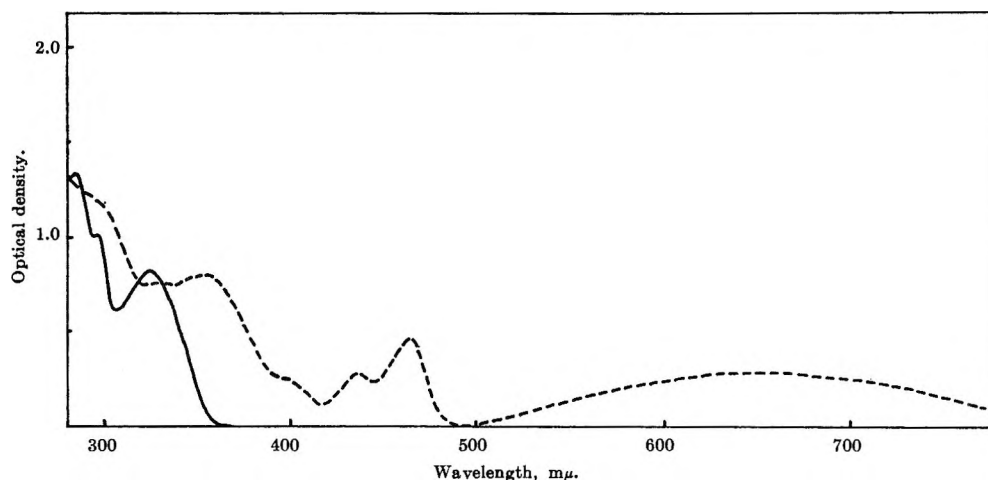


Figure 2. Absorption spectra of 2,2-diphenyl-2H-thiochromene in 3-methylpentane at 77°K: —, colorless form; ---, colored form.

no. 9863 glass filter was used. Conversion from the colored back to the colorless forms was achieved by warming the sample to room temperature.

The 2,4,6-triphenyl-2-benzyl-2H-pyran and 2,4-dimethyl-2,6-diphenyl-2H-pyran were gifts from Prof. J. Dreux of Ecole Supérieure de Chimie Industrielle, Lyon, France. The 2,4,6-triphenyl-2-benzyl-2H-thio-pyran was given to us by Prof. K. Dimroth, Chemisches Institut der Universität Marburg, Marburg, Germany. The 6,11-dihydro[1]benzothiopyrano[4,3-*b*]indole, its 2-methyl and 2-chloro derivatives, and 5,11-dihydro[2]-benzothiopyrano[4,3-*b*]indole were received from Prof. N. P. Buu-Hoi, Institut de Chimie des Substances Naturelles du C.N.R.S., Gif-sur-Yvette, France. All compounds were checked for purity on thin-layer chromatography. Where purification was necessary, liquid-column chromatography was used.

The 2H-thiochromene was prepared,¹ but the principal product was not thiochromene but thiochromane.

This was confirmed by high-resolution nmr (100 Mc) and mass spectral analysis. Nonetheless, the mixture showed reversible photocoloration with the production of a blue-red compound. Thiochromane has no visible absorption nor does it exhibit photochemistry. The absorption spectrum of the colored form of 2H-thiochromene is shown in Figure 1. The 2,2-diphenyl-2H-thiochromene was prepared from 1,1-diphenylethylene and *o*-mercaptobenzaldehyde following a parallel preparation of the analogous oxygen compound.² Purification was accomplished using solid-liquid chromatography. High-resolution nmr (100 Mc) spectral analysis showed absorption corresponding to 14 aromatic, 2 olefinic, and no other protons. This conforms to that expected for the desired compound.

The 1',3',3'-trimethylspiro[2H-1-benzothiopyran-

(1) E. Luttringhaus and N. Engelhard, *Ber.*, **93**, 1525 (1960).

(2) R. Wizinger and H. Wenning, *Helv. Chim. Acta*, **23**, 247 (1940).

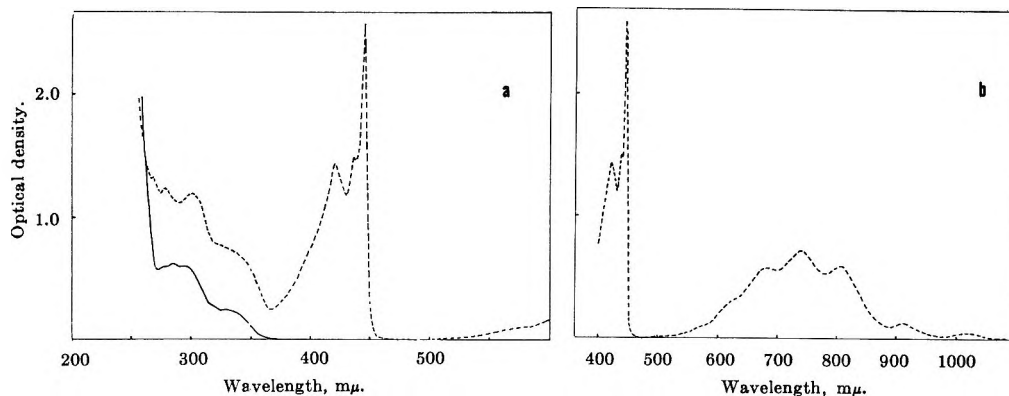


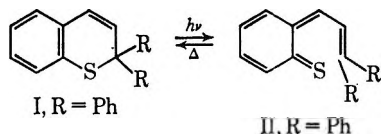
Figure 3. Absorption spectra of 1',3',5'-trimethylspiro[2H-1-benzothiopyran-2,2'-indoline] in 3-methylpentane at 77°K: —, colorless form; - - -, colored form.

2,2'-indoline] was prepared by adding 2.1 g (15 mmol) of *o*-mercaptobenzaldehyde³ in 5 ml of ether to 1.7 g (10 mmol) of 2-methylene-1,3,3-trimethylindoline in 30 ml of absolute methanol and refluxing. The mixture was then evaporated to dryness and chromatographed on a silica-gel column with ligroin as a solvent. The desired product was recrystallized from absolute ethyl alcohol and, after drying, had a melting point of 91–92°. *Anal.* Calcd for C₁₉H₁₉NS (293.2): C, 77.76; H, 6.53; N, 4.78; S, 10.9%. Found: C, 77.51; H, 6.46; N, 4.72; S, 11.23. High-resolution nmr (100 Mc) analysis gave singlets of C-methyls (τ 8.88, 3H; and τ 8.62, 3H), singlet of N-methyl (τ 7.42, 3H), olefinic proton doublets (τ 4.34, 1H; and τ 3.73, 1H), and aromatic proton multiplet (τ 2.9–3.5, 8H). These data confirm the structure of the compound.

Results and Discussion

Irradiation of a substituted 2H-pyran and a 2H-thiopyran resulted in the formation of yellow photo-products. More will be said concerning these shortly.

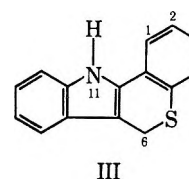
These results prompted us to investigate the sulfur analogs of the chromenes and indolinobenzospiropyranes. The 2,2-diphenyl-2H-thiochromene (I) gave a green product which is assigned as the *o*-thioquinoneallide (II). This is based on two principal facts. The ab-



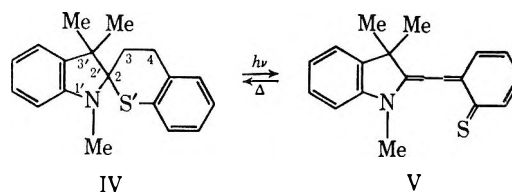
sorption spectrum of the photoproduct, Figure 2, is parallel to that product from the oxygen analog. Further, the photocolored products from the oxygen analogs, the 2H chromenes, have been shown to be *o*-quinoneallides by subsequent reactions.⁴

In the contrast to these results, some more complicated thiochromenes as 6,11-dihydro[1]benzothiopyrano[4,3-*b*]indole (III), its 2-methyl and 2-chloro derivatives, and 5,11-dihydro[2]benzothiopyrano[4,3-

b]indole do not exhibit photochromic behavior under the same conditions. Thus, it appears that the additional pyrrole ring imposes restrictions on the rearrangement of double bonds which is necessary for creation of the colored form.



In addition, we synthesized the previously unknown 1',3',3'-trimethylspiro[2H-1-benzothiopyran-2,2'-indole] (IV) and found it to be photochromic. The



green form, assigned as structure V, can be produced by irradiation and can be eradicated by warming. The assignment of structure V as the photocolored form is based on the identification of the colored products from the chromenes⁴ and indolinobenzospiropyranes^{4,5} and the parallel spectral characteristics compared with the colored forms of the chromenes, thiochromenes, and indolinobenzospiropyranes.^{5,6} The absorption spectrum of the colored form, Figure 3a and b, is quite unique regarding the fact that the longest wavelength band extends into the near infrared to approximately 10,500 Å. In addition, the shorter wavelength absorption band (maximum ~4420Å) is unusually intense compared with the other compounds

(3) P. Friedlander and E. Lenk, *Ber.*, **45**, 2083 (1912).

(4) J. Kolc and R. Becker, *J. Phys. Chem.*, **71**, 4045 (1967).

(5) R. Heiligman-Rim, Y. Hirschberg, and E. Fischer, *J. Chem. Soc.*, 156 (1961); *J. Phys. Chem.*, **66**, 2465 (1962).

(6) N. Tyer and R. Becker, unpublished data.

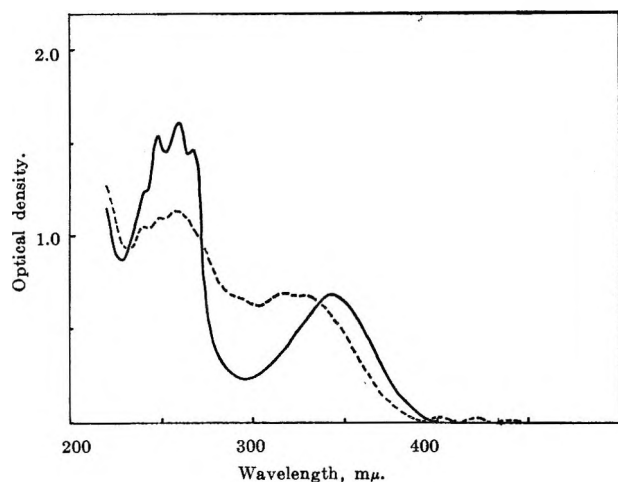


Figure 4. Absorption spectra of 2-benzyl-2,4,6-triphenyl-2H-pyran in 3-methylpentane at 77°K: —, colorless form; ---, colored form.

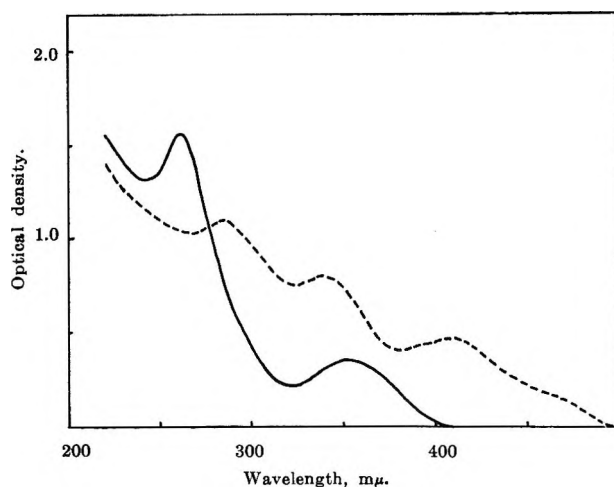


Figure 5. Absorption spectra of 2-benzyl-2,4,6-triphenyl-2H-thiopyran in 3-methylpentane at 77°K: —, colorless form; ---, colored form.

that have been studied; for example see Figures 1 and 2 and indolinobenzospiryan.^{5,6}

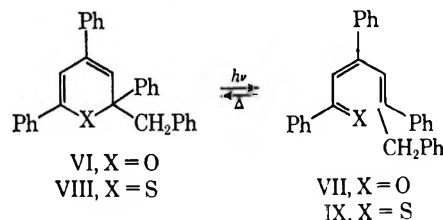
The substitution of sulfur for oxygen causes only minor red shifts in the spectrum of the uncolored molecule but dramatic red shifts for the colored compound. The same is true for the thiochromene system. Although it is known that the $\pi^* \leftarrow n$ transition in thiobenzophenone is at considerably longer wavelength than in benzophenone, the longest wavelength band referred to in our case does not correspond to a $\pi^* \leftarrow n$ but a $\pi^* \leftarrow \pi$ transition. This is primarily based on the vibrational spacings within the transition. There appears to be little or no spectral considerations of aromatic thio ketone systems, probably because of their general rarity.

Attempts were made to observe emission from all of the compounds discussed. However, no emission characteristic of the compounds was detected. Although this does not imply that there is no emission, it is at least extremely weak. Therefore, photochemistry (and any concomitant internal conversion) must be highly efficient.

A 10^{-2} M solution of this compound in rigid EPA at 77°K showed no coloration after irradiation for 20 min at 3900 Å. However, a solution of 10^{-2} M thio-spiran plus 2×10^{-3} M thioxanthone irradiated at 3900 Å showed coloration in 2 min. Thus triplet \rightarrow triplet energy transfer occurred.

Although earlier results⁷ indicated that the pyran ring itself exhibited reversible photochemistry, the compound was a rather complex natural product, flindersine. Irradiation of a simply substituted pyran, 2-benzyl-2,4,6-triphenyl-2H-pyran (VI) produces a light yellow product. The structure of the colored product is assigned as VII, primarily based upon analogy with the *o*-quinoneallide produced from the chromenes.⁴ Furthermore, the absorption spectrum, Figure 4, is consistent with what would be expected for

such a structure. The absorption spectra of both the pyran and the photoproducted ketone are shown in Figure 4. The reaction can be reversed by warming.



However, some irreversible reaction(s) occurs as well, since the band maximum at approximately 350 mμ does not return to its original intensity. The 2,4-dimethyl-2,6-diphenyl-2H-pyran shows still less reversibility, indicating that aromatic substituents apparently play an important role in the degree of reversibility for pyran \rightleftharpoons dienone transformation. The nature of the irreversible product(s) is not known.

Irradiation of 2-benzyl-2,4,6-triphenyl-2H-thiopyran (VIII) produces a strongly yellow form assigned as thioketone (IX). The bases for the assignment are parallel to those given above for the pyran. The absorption spectra of VIII and IX are shown in Figure 5. Reversibility is accomplished as for the pyran. It is worthwhile noting that cycling experiments show that the amount of irreversible character in this case is considerably less than for the pyran. Photocoloration is best accomplished by irradiation of a low-temperature viscous solution rather than a rigid matrix at 77°K. Considerably more colored product is produced at a faster rate under the former environmental condition. This obviously indicates a viscosity barrier is present and thus that a notable geometrical rearrangement occurs in the formation of the colored product.

(7) R. Becker and J. Michl, *J. Am. Chem. Soc.*, **88**, 5931 (1966).

In conclusion, photochromic behavior has been established for some new compounds. Some of these compounds show unique spectral properties when in the colored forms. Furthermore, these results establish the fact that for all complex molecules studied that

contain a pyran or thiopyran ring system, the photochemical change originates in such a ring and results from C-O or C-S bond breakage. This would imply similar behavior for other molecules with parallel structural features.

Nuclear Magnetic Resonance Studies of Proton-Exchange Kinetics of N-Methylacetamide and N-Acetylglycine N-Methylamide¹

by James E. Bundschuh and Norman C. Li

Department of Chemistry, Duquesne University, Pittsburgh, Pennsylvania 15219 (Received September 1, 1967)

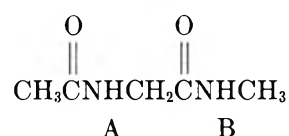
Proton-exchange kinetics of compounds with peptide-like bonds, N-methylacetamide (NMA) and N-acetylglycine N-methylamide (AGMA), have been studied by the nmr method. NMA has one proton capable of exchanging, while AGMA has two. For AGMA, $\text{CH}_3\text{CONHCH}_2\text{CONHCH}_3$, the amino proton adjacent to the methylene group is labeled site A, while the amino proton adjacent to the N-methyl group is labeled site B. The specific rate of protolysis of NMA is proportional to hydrogen ion concentration, while there is a 1.3-1.4 power dependence of the specific rate on hydrogen ion concentration for both sites A and B of AGMA. The activation energies of protolysis for NMA and AGMA sites A and B were found to be 16.4, 16.2, and 17.7 kcal/mol, respectively.

Introduction

Nmr provides an effective method of elucidating the kinetics of rapidly exchanging protons. Grunwald, *et al.*,² studied the collapse of the methyl spin-spin quartet of the methylammonium ion in aqueous solution in determining the rate of NH exchange as a function of pH. This technique was soon applied to di- and trimethylammonium ions³ by observing the collapse of the methyl spin-spin triplet and the collapse of the methyl spin-spin doublet, respectively. Protolysis kinetics of amino acids have been studied extensively.⁴⁻⁷ Methylamides have also been studied because of their peptide-like bonds.⁸⁻¹⁰

This is a report of our work evaluating the proton-exchange kinetics of the amino protons of N-methylacetamide (NMA) and N-acetylglycine N-methylamide (AGMA). The rates of exchange have been found to be accelerated by the addition of HCl to the aqueous solutions. The rates are reported as a function of hydrogen ion concentration and temperature; rate constants are calculated and the activation parameters are reported. Although the exchange rates for NMA have been reported by previous workers,⁸⁻¹⁰ it is felt that further studies were warranted for the comparison of the results and to fill a gap left by their investigations. Our investigation of NMA as a proton-exchanging

molecule has at least one common axis with each of the previous works and provides some interesting comparisons. AGMA has two amino protons in separate environments labeled in the manner



The mean lifetime, τ , of a proton on a particular site can be determined by observing how much it disturbs the nmr signal of an adjacent site. Considering NMA,

- (1) This investigation was supported by PHS Research Grant No. GM-10539-05 from the National Institute of General Medical Sciences, Public Health Service. Abstracted in part from the Ph.D. Thesis of J. E. Bundschuh, Duquesne University, Pittsburgh, Pa., 1967.
- (2) E. Grunwald, A. Loewenstein, and S. Meiboom, *J. Chem. Phys.*, **27**, 630 (1957).
- (3) A. Loewenstein and S. Meiboom, *ibid.*, **27**, 1067 (1957).
- (4) M. Scheinblatt and H. S. Gutowsky, *J. Am. Chem. Soc.*, **86**, 4814 (1964).
- (5) M. Scheinblatt, *J. Chem. Phys.*, **39**, 2005 (1963).
- (6) M. Scheinblatt, *J. Am. Chem. Soc.*, **88**, 2123 (1966).
- (7) M. Scheinblatt, *ibid.*, **87**, 572 (1965).
- (8) A. Berger, A. Loewenstein, and S. Meiboom, *ibid.*, **81**, 62 (1959).
- (9) M. Takeda and E. O. Stejskal, *ibid.*, **82**, 25 (1960).
- (10) A. Saika, *ibid.*, **82**, 3540 (1960).

one would expect to observe a doublet corresponding to the N-methyl, in the absence of exchange. At fast exchange, the N-methyl signal would appear as a singlet. At intermediate exchange rates, a signal corresponding to the N-methyl would appear somewhere between a doublet and a singlet. The mean lifetime of the proton on the nitrogen can be evaluated by matching the signal observed for the N-methyl with a signal calculated for the N-methyl corresponding to a particular mean lifetime. The signal shapes can be calculated by appropriate modifications of the Bloch equations.¹¹ The procedure followed in calculating line shapes is reported by Grunwald, *et al.*,² and modified by Loewenstein and Meiboom³ for the collapse of the spin-spin doublet.

For AGMA, the collapse of the doublet of the methylene protons adjacent to site A and the collapse of the doublet of the methyl adjacent to site B were taken as measures of the mean lifetimes for the corresponding NH. For both NMA and AGMA, the measured quantities were the peak width at half-height, $\delta\omega_{1/2}$, for a singlet and the peak separation of a doublet, $2\delta\omega$.

Experimental Section

Materials. NMA was distilled and used immediately. AGMA was prepared using a method analogous to that developed by Vaughn and Osato¹² for the synthesis of amides. N-Acetylglycine was treated with isovaleryl bromide to give the mixed anhydride. The mixed anhydride was treated with methylamine gas to give the desired product, which was recrystallized from ethyl acetate several times: mp 158°; lit. 158°.¹³ The solutions were prepared in water and aqueous HCl was added. pH measurements were made with a Beckman Model G pH meter equipped with micro glass and calomel electrodes. The values of $-\log(\text{HCl})$ were interpolated from plots of $-\log(\text{HCl})$ vs. pH, which had been determined independently for solutions of the same amide concentrations.

Instruments. All nmr spectra were obtained with a Varian Associates A-60 nmr spectrometer. During the recording of spectra, the temperature remained constant to within $\pm 1^\circ$, as indicated by the separation in cycles per second between two peaks in ethylene glycol. The radiofrequency field (H_1) chosen was sufficiently small so that decreasing H_1 further caused no apparent change in the width at half-height of the acetyl methyl resonance. The instrumental resolution is 0.3 cps.

The line-shape equation was programmed and a CDC G-20 computer used for computation. The least-squares equation was also programmed and computed.

Results and Discussion

In order to evaluate successfully the mean lifetimes, it is necessary to know two experimentally determinable parameters: (1) the transverse relaxation time, T_2 , in the absence of exchange and (2) the peak separation of

the doublet in the absence of exchange, $2\delta\omega_0$. Using the method employed by Saika,¹⁰ T_2 was evaluated from the peak width at half-height of each of the components of the spin-spin doublet in the absence of exchange, $2\delta\omega_0$ being the peak separation. The situation where no exchange exists was recorded for solutions with no added acid and at temperatures for which a further decrease in temperature caused no change in the experimentally determined parameters. T_2 is related to the peak width at half-height in the absence of exchange, $\delta\omega_{1/2}^0$, by the equation

$$T_2 = 2/\delta\omega_{1/2}^0 \quad (1)$$

The remaining parameters needed to calculate a set of theoretical spectra can be evaluated in terms of $\delta\omega_{1/2}^0$ and $2\delta\omega_0$. These experimentally determined parameters are shown in Table I.¹⁴

Table I: Experimentally Determined Exchange Parameters for NMA and AGMA¹⁴

	$\delta\omega_{1/2}^0$, radians sec ⁻¹	$2\delta\omega_0$, radians sec ⁻¹
NMA	9.36	29.7
AGMA, site A	11.7	37.7
AGMA, site B	8.79	30.1

The theoretical spectra were calculated from eq 2¹⁵

$$M = R \frac{r(2 + rt - irs)}{(1 + rt - i(rs + r))(1 + rt - i(rs - r)) - 1} \quad (2)$$

where M is a relative value for the peak amplitude, R indicates the real part, $i = (-1)^{1/2}$, $r = 2\tau\delta\omega_0$, $t = \delta\omega_{1/2}^0/2\delta\omega_0$, and $s = \Delta\omega/\delta\omega_0$ ($\Delta\omega$ is the frequency relative to the center of the multiplet). The values of τ were evaluated by interpolating from graphs of either $\delta\omega_{1/2}$ or $2\delta\omega$ plotted vs. r .^{16,17} Plots of $\delta\omega_{1/2}$ and $2\delta\omega$ vs. τ are shown in Figures 1 and 2, for AGMA site A. Corresponding plots for AGMA, site B, and NMA are similar.

(11) H. M. McConnell, *J. Chem. Phys.*, **28**, 430 (1958).

(12) J. Vaughn and R. Osato, *J. Am. Chem. Soc.*, **73**, 5553 (1951).

(13) S. Mizushima, T. Shimonouchi, M. Tsuboi, T. Sugita, N. Mataga, and R. Sonda, *ibid.*, **74**, 4639 (1952).

(14) In NMA, each of the components of the N-methyl doublet actually consists of a closely spaced quadruplet, as has been pointed out by Berger, *et al.*⁸ A spin-spin interaction of about 0.45 cps exists between the C-methyl and the N-methyl hydrogens. Nevertheless, equations for the exchange broadening of a doublet was used, and the quadruplet splitting was taken into account by the introduction of an effective natural line width of the magnitude of the width of the multiplet. In AGMA, each of the components of the N-methyl doublet actually consists of a closely spaced triplet with spin-spin interaction of 0.45 cps between the methylene and N-methyl hydrogens, and the same procedure as for NMA was adopted. Fine splitting was not observed for the N-CH₂ doublet, possibly because of coupling from two directions, *i.e.*, N-CH₃ and C-CH₃.

(15) Weizmann Institute of Science, Technical Note No. 2, Rehovoth, Israel, 1958.

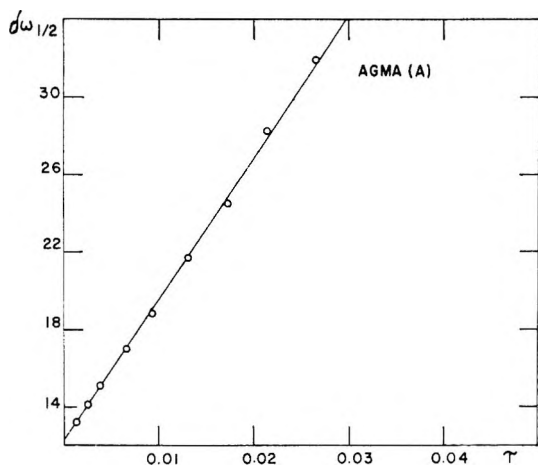


Figure 1. Widths of half-height vs. τ for N-acetylglycine N-methylamide site A.

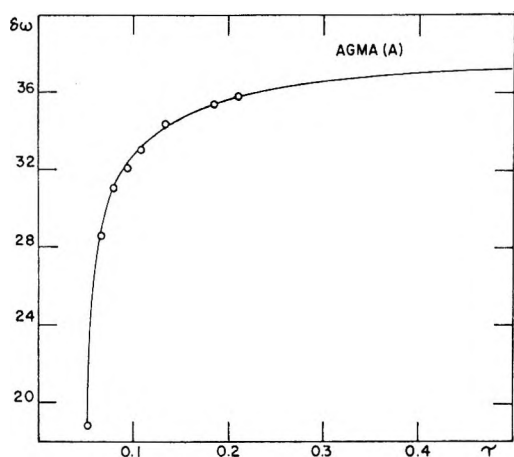


Figure 2. Splitting of the doublets vs. τ for N-acetylglycine N-methylamide site A.

Equation 2 gives the line shape for two-site exchange with equal concentrations. It is identical with the equation of Gutowsky, *et al.*,¹⁸ when one remembers that in this paper as in ref 15, $\delta\omega_0$ is half the frequency spacing between adjacent lines, whereas in ref 18, it is the total spacing.

Tables II and III show that the reciprocal of the mean lifetime for NMA and AGMA, sites A and B, is approximately independent of the amide concentration. For NMA, the specific rate is proportional to hydrogen ion concentration and, therefore, can be written $R = k(\text{HCl})$. This is consistent with the expression arrived at by previous workers^{8,9} and the intercept obtained from a least-square plot of $\log(1/\tau)$ vs. $-\log(\text{HCl})$ is then $\log k$, where k has the units liters per mole per second. The values of k are listed in Table IV, together with literature values.

Our value of k at 25° is in excellent agreement with ref 8, where the temperature is $23 \pm 2^\circ$. It must be mentioned that in ref 9, the value of k is obtained from plot of $\log(1/\tau)$ vs. pH, whereas in ref 8 and the present

Table II: Specific Rates of Exchange for NMA as a Function of $-\log(\text{HCl})$ and Temperature

$-\log(\text{HCl})$	$\delta\omega_{1/2}$, radians sec ⁻¹	$\delta\omega_0$, radians sec ⁻¹	$\log(1/\tau)$
1.29 M NMA, 25°			
0.13	11.3		2.40
0.31	11.3		2.40
0.46	12.6		2.16
0.63	13.8		2.00
0.90	18.8		1.68
1.29 M NMA, 18°			
0.13	12.6		2.16
0.46	14.7		1.93
0.63	18.4		1.72
0.90	33.2		1.22
2.00		28.6	0.48
1.29 M NMA, 10°			
0.13	15.3		1.88
0.31	17.3		1.76
0.46	23.4		1.51
0.63	29.3		1.36
0.90		22.0	1.08
1.29 M NMA, 4°			
0.13	22.4		1.54
0.31	33.0		1.25
0.63		20.5	1.12
0.90		27.0	0.75
2.78 M NMA, 18°			
0.01	13.4		2.05
0.31	14.0		1.98
0.48	15.7		1.86
0.61	18.8		1.69
0.92	30.8		1.30
2.78 M NMA, 10°			
0.01	15.9		1.83
0.31	21.0		1.59
0.48	23.4		1.51
0.89		21.7	1.09
2.78 M NMA, 4°			
0.01	20.1		1.67
0.31	27.6		1.40
0.61		20.6	1.11
0.92		27.7	0.64

work, $-\log(\text{HCl})$ is used instead of pH. The activation energy, E_a , for NMA is calculated from a $\log k$ vs. $1/T$ plot to be 16.4 kcal/mol. It is interesting to compare this value with the value of 14 ± 2 kcal/mol obtained in neat NMA.¹⁰

(16) Although Allerhand, *et al.*,¹⁷ have urged that the spin-density matrix treatment be used as reference for all systems, we have found that the correction of τ , as employed by Scheinblatt,⁵ is actually negligible for NMA and AGMA.

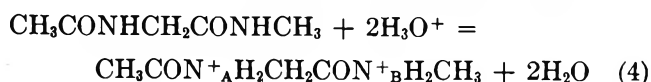
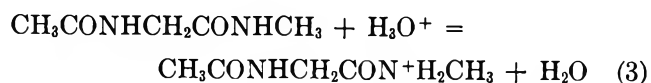
(17) A. Allerhand, H. S. Gutowsky, J. Jonas, and R. A. Meinzer, *J. Am. Chem. Soc.*, **88**, 3185 (1966).

(18) H. S. Gutowsky, D. W. McCall, and C. P. Slichter, *J. Chem. Phys.*, **21**, 279 (1953).

Table III: Specific Rates of Exchange for AGMA

Site A			Site B				
$-\log$ (HCl)	$\delta\omega_{1/2}$, radians sec ⁻¹	$2\delta\omega$, radians sec ⁻¹	\log (1/ τ)	$-\log$ (HCl)	$\delta\omega_{1/2}$, radians sec ⁻¹	$2\delta\omega$, radians sec ⁻¹	\log (1/ τ)
0.293 M AGMA, 35°							
-0.13	16.3		2.22	0.10	12.3		2.26
0.67		28.9	1.16	0.34	15.7		1.90
0.92		34.8	0.88	0.67	23.9		1.52
				0.92		20.0	1.10
				1.20		28.2	0.65
0.293 M AGMA, 20°							
				-0.13	13.4		2.10
0.34		30.3	1.12	0.10	17.0		1.81
0.69		35.9	0.72	0.34	25.2		1.48
				0.67		21.5	1.11
				0.97		28.0	0.68
0.293 M AGMA, 10°							
-0.13		26.1	1.11	-0.13	22.9		1.55
0.34		36.7	0.48	0.34		27.3	0.78
				0.67		29.1	0.44
0.389 M AGMA, 35°							
-0.13	16.3		2.22	0.10	11.9		2.30
0.10	21.4		1.90	0.32	13.8		2.05
0.69		30.2	1.12	0.69	25.1		1.48
0.87		33.7	0.92	0.94		18.8	1.15
0.94		35.5	0.70				
0.389 M AGMA, 20°							
0.10		28.4	1.17	-0.13	13.4		2.10
				0.10	22.6		1.56
				0.69		26.5	0.88
				0.87		27.9	0.70
0.389 M AGMA, 10°							
-0.13		29.9	1.13	-0.13	22.7		1.55
0.10		34.4	0.85	0.10		16.8	1.17
0.32		36.4	0.54	0.32		26.1	0.90
0.579 M AGMA, 49°							
0.13	17.0		2.15	0.30	11.0		2.52
0.30	18.7		2.05	0.65	13.8		2.05
0.65	33.9		1.52	0.93	19.5		1.68
				1.23	31.4		1.33
				1.52		23.2	1.06
0.579 M AGMA, 41°							
0.13	17.9		2.10	0.30	11.8		2.40
0.30	22.0		1.87	0.65	15.6		1.90
0.65	41.4		1.39	0.93	31.4		1.33
0.84		30.5	1.11	1.23		13.2	1.08
				1.52		28.8	0.54
0.579 M AGMA, 35°							
-0.13	17.2		2.16	0.30	15.7		1.89
0.30	29.9		1.61	0.65	26.0		1.46
0.93		34.9	0.80	0.93		22.0	1.10
1.23		36.4	0.54	1.23		28.2	0.65

Plots of $\log(1/\tau)$ vs. $-\log(\text{HCl})$, using the data of Table III, show that there is a 1.3–1.4 power dependence of the specific rate on hydrogen ion concentration for both sites A and B of AGMA. The exchange reactions for AGMA may be written



that dipole moments of unsaturated systems be accurately known, particularly in heteroatomic aromatic systems where the σ moment is likely to be large. Accordingly, the investigation reported here was concerned with the dipole moments of 1-alkylpyrazoles as solutes in nine solvents in order (1) to gauge the solvent effects⁶ upon the moments of these heterocycles, and thence to estimate their gas-phase moments, and (2) to determine the changes in the dipole moment attending N-substitution by methyl, ethyl, and isopropyl groups on the pyrazole nucleus.

Experimental Section

Materials. 1-Methylpyrazole (1-MePy), 1-ethylpyrazole (1-EtPy), and 1-isopropylpyrazole (1-*i*PrPy) were prepared and purified as described elsewhere.⁷ Benzene and toluene were refluxed over P_4O_{10} for 8 hr and fractionally distilled from sodium; dioxane, cyclohexane, and ether were refluxed over sodium for 8 hr and fractionally distilled from sodium; carbon tetrachloride and chlorobenzene were washed with H_2SO_4 , then H_2O , 2.0 N NaOH, and finally H_2O , dried over K_2CO_3 , and fractionally distilled from K_2CO_3 ; chloroform was refluxed over P_4O_{10} for 8 hr and fractionally distilled from P_4O_{10} ; trichloroethylene was triply distilled from K_2CO_3 . The constant-boiling evolute of each solvent was redistilled fractionally and stored in glass bottles under nitrogen in polyethylene bags for no longer than 2 days.

Dipole Moment Measurements. Dielectric constants were measured in solution at 25.0° with a heterodyne-beat apparatus which consisted of a General Radio Model 1304B beat frequency generator and a General Radio Model 1422D variable precision capacitor. The dielectric cell consisted of a glass-enclosed variable capacitor⁸ with a maximum air capacitance of 75 $\mu\mu F$, fitted with fixed stops corresponding to positions of minimum and maximum capacitance. The dielectric constant was calculated by

$$\epsilon = \Delta C_{\text{solution}} / \Delta C_{\text{air}}$$

where ΔC is the difference in the capacitance at the two fixed settings. ΔC_{air} was determined anew prior to each solution determination and was reproducible to less than 1 part in 7000; $\Delta C_{\text{solution}}$ was reproducible to about 1 part in 3000.

Dipole moments were calculated by the method of Halverstadt and Kumler,⁹ programmed for the CDC-6400 and IBM-1620 computers. Molar refractivities were calculated from measured refractive indices (Na D line). No correction was made for atomic polarization. All measurements were made at 25.0°.

Results

The dipole moments obtained for 1-methylpyrazole, 1-ethylpyrazole, and 1-isopropylpyrazole in each of nine solvents are listed in Table I, together with pertinent

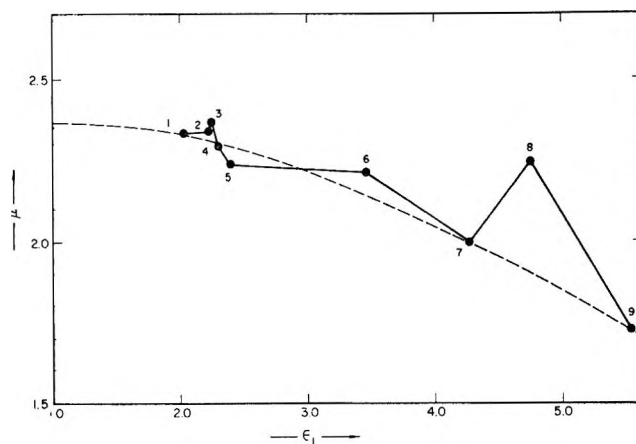


Figure 1. Dipole moments of 1-methylpyrazole in various solvents.

dielectric data. Weight fractions ranged from ~ 0.002 to ~ 0.05 in these measurements.

A plot of the dipole moment of 1-methylpyrazole as a function of the dielectric constant of the solvent is shown in Figure 1; the general shape of this curve is typical for 1-ethylpyrazole and 1-isopropylpyrazole as well. This shape indicates that the "classical" solvent effect⁶ is negative, that is, that $\mu_{\text{gas}} > \mu_{\text{solution}}$, but that the dependence of the dipole moment of the solute is not a smooth function of the extrapolated dielectric constant of the medium. In particular, the dipole moments of 1-alkylpyrazoles measured in carbon tetrachloride, trichloroethylene, and chloroform have high values relative to hydrocarbon solvents. Anomalous results for solutes that contain a nitrogen lone pair are attributable to donor-acceptor interactions.¹⁰ If a donor-acceptor interaction is unlikely, $\Delta\mu = \mu_{\text{CCl}_4} - \mu_{\text{benzene}} < 0.05$ D.¹⁰ For the 1-alkylpyrazoles, $\Delta\mu = 0.074$ for 1-MePy, 0.082 for 1-EtPy, and 0.069 for 1-*i*PrPy, giving evidence of a weak donor-acceptor interaction. This weak interaction is compatible with the weak basicity of 1-alkylpyrazoles; thus, $\Delta\mu = 0.12$ for pyridine¹⁰ ($pK_a = 5.23$) compared with $\Delta\mu = 0.07$ for 1-methylpyrazole ($pK_a = 2.04$). According to Figure 1, the "classical" value of $\Delta\mu$ for 1-MePy should be about 0.02–0.03 D. The quite large value of the dipole moments of 1-alkylpyrazoles measured in chloroform may be attributed to a combination of donor-acceptor interactions and intermolecular hydrogen-bond interactions,¹¹ both involving the nitrogen lone pair of the pyrazole nucleus. Ring chlorine,

(6) A. D. Buckingham and R. J. W. LeFevre, *J. Chem. Soc.*, 1932 (1952).

(7) J. D. Vaughan, G. L. Jewett, and V. L. Vaughan, *J. Am. Chem. Soc.*, 89, 6218 (1967).

(8) E. C. Johnson and Co., No. 167-4.

(9) I. F. Halverstadt and W. D. Kumler, *J. Am. Chem. Soc.*, 64, 2988 (1942).

(10) A. N. Sharpe and S. Walker, *J. Chem. Soc.*, 157 (1962).

(11) D. P. Earp and S. Glasstone, *ibid.*, 2781 (1935).

Table I: Dielectric Properties and Dipole Moments (D.) of 1-Alkylpyrazoles at 25.0°

Solute	ϵ_1^a	V_1^a	α^a	β^a	$P_{2\infty}^a$	R_M^a	μ^b
Cyclohexane							
1-MePy	2.0186	0.3016	5.5980	-0.1815	134.45	23.574	2.330
1-EtPy	2.0131	1.3027	5.1152	-0.1970	146.16	28.110	2.404
1- <i>i</i> PrPy	2.0161	1.3022	4.6839	-0.1517	157.04	32.528	2.469
Dioxane							
1-MePy	2.2208	0.9748	8.2822	0.9748	135.19	23.574	2.337
1-EtPy	2.2156	0.9736	7.4152	0.07807	146.31	28.110	2.405
1- <i>i</i> PrPy	2.2139	0.9738	6.9288	0.1947	162.66	32.528	2.528
Carbon Tetrachloride							
1-MePy	2.2388	0.6327	12.9786	0.4192	137.81	23.492	2.365
1-EtPy	2.2375	0.6319	11.9467	0.4439	151.44	28.110	2.457
1- <i>i</i> PrPy	2.2362	0.6332	11.0806	0.4215	163.12	32.468	2.529
Benzene							
1-MePy	2.2836	1.1469	6.8449	-0.1137	130.81	23.565	2.291 ^c
1-EtPy	2.2803	1.1461	6.2021	-0.05316	143.33	28.110	2.375
1- <i>i</i> PrPy	2.2793	1.1471	5.7499	-0.02145	156.10	32.468	2.460
Toluene							
1-MePy	2.3793	1.1633	6.5888	-0.1109	125.66	23.570	2.235
1-EtPy	2.3778	1.1615	6.0957	-0.08767	139.03	28.110	2.330
1- <i>i</i> PrPy	2.3783	1.1608	5.6152	0.009795	152.96	32.528	2.428
Trichloroethylene							
1-MePy	3.4563	0.6910	1.4761	0.3605	123.26	23.565	2.209
1-EtPy
1- <i>i</i> PrPy	3.4315	0.6915	1.2739	0.3355	149.33	32.546	2.391
Ether							
1-MePy	4.2676	1.4182	7.1816	-0.4569	105.01	23.561	1.997
1-EtPy	4.2603	1.4197	6.6025	-0.5137	114.34	28.105	2.054
1- <i>i</i> PrPy
Chloroform							
1-MePy	4.7519	0.6777	21.9573	0.3287	126.31	23.574	2.242
1-EtPy	4.7563	0.6773	19.2463	0.3623	137.92	28.094	2.318
1- <i>i</i> PrPy	4.7470	0.6779	19.1686	0.3866	159.45	32.468	2.493
Chlorobenzene							
1-MePy	5.6263	0.9092	8.1822	0.1546	84.497	23.574	1.727
1-EtPy	5.7241	0.9100	6.3400	0.1694	91.346	28.156	1.759
1- <i>i</i> PrPy	5.6262	0.9099	4.9616	0.1586	97.057	32.468	1.778

^a ϵ_1 , dielectric constant; V_1 , specific volume; α , slope of dielectric constant, weight fraction plot; β , slope of specific volume, weight fraction plot; $P_{2\infty}$, molar polarization at infinite dilution; R_M , molar refractivity at infinite dilution. ^b Estimated error $\pm 0.2\%$ (0.005 D.). ^c Literature value is 2.30 D.: K. A. Jensen and A. Friediger, *Kgl. Danske Videnskab. Selskab, Mat. Fys. Medd.*, **20**, No. 20, 1 (1943).

as in chlorobenzene, has been shown to be a poor acceptor in donor-acceptor interactions.¹⁰

Two procedures are open for estimating the gas-phase dipole moment from solution values. First, one may calculate μ_{gas} from semiempirical equations that relate the dipole moment in solution to the dielectric constant of the medium. The results of such calculations have doubtful value for nitrogen heterocycles at this time. For example, the equations of Ross and Sack⁶ and Buckingham and LeFèvre⁸ predict a relatively large negative solvent effect for pyridine, whereas a relatively large positive solvent effect is observed.^{5,12}

Second, one can extrapolate $\mu-\epsilon_1$ curves to ϵ_1 1.0. This procedure leads to large uncertainties for the alkylpyrazoles because the dependence of μ upon ϵ_1 is not smooth. If we neglect dipole moment values measured in carbon tetrachloride, trichloroethylene, and chloroform, it is possible to make reasonable rough graphical extrapolations. The gas-phase dipole moments obtained in this way are 2.36 ± 0.04 D. for 1-MePy, 2.44 ± 0.04 D. for 1-EtPy, and 2.50 ± 0.04 D. for 1-*i*PrPy.

(12) B. B. DeMore, W. S. Wilcox, and J. H. Goldstein, *J. Chem. Phys.*, **22**, 876 (1954).

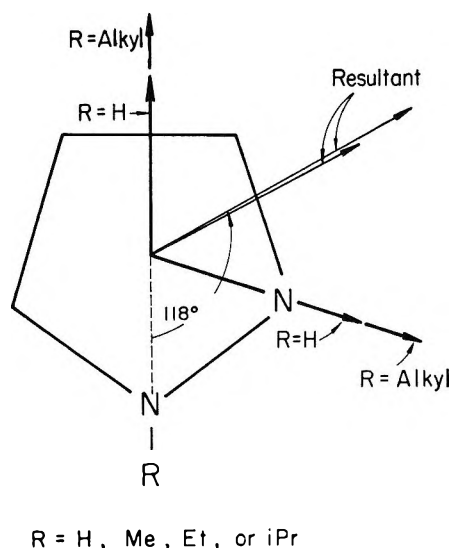


Figure 2. Vector model of pyrazole and N-alkylpyrazoles.

The gas-phase dipole moment of pyrazole has recently been determined to be 2.214 D.¹³ Comparison of this value and the extrapolated gas-phase moments of the alkylpyrazoles indicates that N-substitution leads to an increase in the moment in the order $H < Me < Et < i\text{-Pr}$. This increase is readily interpreted in terms of a vector model of pyrazole originally proposed by Grandberg, *et al.*,¹⁴ in which the contributions of the pyrrole-type nitrogen and the pyridine-type nitrogen atoms are taken to be proportional to the experimental moments of pyrrole and pyridine, respectively. The model takes no account of the perturbing effects of the two adjacent nitrogen atoms upon one another and therefore can provide only a qualitative indication of the magnitude and direction of the moment in pyrazole. The experimental gas-phase moments of pyrrole and pyridine are 1.84 D.¹⁵ and 2.25 D.,¹⁶ respectively. If pyrazole is considered to be a perfect pentagon in this approximation, the moments of pyrrole and pyridine add vectorially to yield a resultant of 2.41 D. directed

118° relative to the N-H bond of pyrazole (Figure 2). This resultant is 0.20 D. larger than the experimental gas-phase moment of pyrazole,¹³ but if the contributions of the pyrrole-type and pyridine-type nitrogen atoms are proportional to the corresponding moments in pyrrole and pyridine to a similar extent, the direction of the resultant is probably within a few degrees of that predicted. If we assume that alkyl groups exhibit σ - and π -inductive effects relative to hydrogen,¹⁷ the N-R (R = alkyl) contribution to the total moment would be greater than that of N-H. In addition, we would expect an added contribution from the N lone pair resulting from the inductive effect of the alkyl group. The resultant moment would be increased by both these contributions and shifted slightly in direction according to their relative magnitudes (Figure 2). The observed order of total moment increase ($H < Me < Et < i\text{Pr}$) is consistent with the inductive model of electron release.

The vector model also accounts for the observed increased polarization of pyrazoles in chlorinated or hydrogen-bonding solvents. Here, interaction of solvent molecules with the nitrogen lone pair of the solute would lead to an enhanced contribution of the lone pair to the resultant moment.

Acknowledgment. We wish to thank Mr. Robert M. Rodgers for assistance in preliminary experiments. This research was supported in part by a Colorado State University Faculty Grant.

(13) W. Kirchoff, *J. Am. Chem. Soc.*, **89**, 1312 (1967).

(14) S. Hiller, I. Mazeika, and I. Grandberg, Institute of Organic Synthesis, Academy of Sciences, Latvian SSR, Riga, II and III, 1964.

(15) A. D. Buckingham, B. Harris, and R. J. W. LeFèvre, *J. Chem. Soc.*, 1626 (1953).

(16) A. D. Buckingham, J. Y. H. Chau, H. C. Freeman, R. J. W. LeFèvre, D. A. A. S. Narayana Rao, and J. Tardif, *ibid.*, 1405 (1956).

(17) M. J. S. Dewar, "Hyperconjugation," The Ronald Press Co., New York, N. Y., 1962.

Critical Bond Length in Radical Combination and Unimolecular

Dissociation Reactions

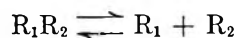
by E. Tschuikow-Roux

Department of Chemistry, The University of Calgary, Calgary, Alberta, Canada (Received September 5, 1967)

An expression for the most probable internuclear distance for loose activated complexes is derived in terms of the inverse R^6 attractive potential constant a . Of three contributing terms considered, the principal contribution is due to dispersion forces; however, for polar species the electrostatic contribution may be significant. The $\langle R \rangle_{av}$ values, which depend on temperature as $\sim T^{-1/6}$, have been evaluated for 14 reactions and found to be several times greater than the usual "fractional bond" estimates.

Introduction

In discussions of gas-phase bimolecular reactions in terms of activated complex theory or unimolecular reactions in terms of the quantum statistical (RRKM) theory, a model for the transition state must be assumed. In particular, the length of the bond to be formed or broken must be estimated. It is customary to assign a "fractional" bond value, for example, using Pauling's empirical rule relating bond length to bond order.¹ However, this arbitrary method is not suitable for reactions involving a very loose transition state, such as in unimolecular dissociations or their reverse, radical combinations. Here we note that the principle of microscopic reversibility requires that the transition



state be the same for reaction in either direction. Therefore, it appears to be desirable to obtain an expression for the most probable value of the internuclear distance for such processes based on the transition-state model applicable to such reactions.

Theoretical Considerations

The absolute rate theory treatment of reactions with no or essentially zero activation energy,² such as radical combination and atom addition to olefins,³ assumes that the radicals (reactants) are attracted by a force, F_a , due to the intermolecular attractive potential, $V_a = -a/R^6$, and that this force is opposed by a centrifugal force arising from the rotation of the two radicals about a common center of mass. The centrifugal force, F_c , is given by

$$F_c = M^2/\mu R^3$$

where μ is the reduced mass, M is the total angular momentum of the complex equal to $[J(J+1)]^{1/2}\hbar$, and J is the angular momentum quantum number. The multiplicity of J is $(2J+1)$. The activated complex is

defined to exist at a critical separation, R_c , at which the centrifugal force is equal and opposite to the attractive force: $F_a = -6a/R^7$. Hence R_c is given by

$$R_c = [6a\mu/J(J+1)\hbar^2]^{1/4} \quad (1)$$

It is a basic assumption in the Gorin theory^{2,4} that the distance R_c is sufficiently large so that the radicals in the activated complex may be regarded to have the same vibrational and rotational degrees of freedom as the free radicals.^{2,4}

The total energy of the system is equal to the sum of the attraction V_a and the kinetic energy of rotation, $E_c = M^2/2\mu R^2$. Making use of eq 1

$$E(R_c) = 2\hbar^3[J(J+1)]^{3/2}/(6\mu)^{3/2}a^{1/2} \quad (2)$$

For a Boltzmann distribution of energies, the fraction of activated complexes in the J th quantum level is

$$N_J/N = (2J+1) \exp\{-\alpha[J(J+1)]^{3/2}\}/Q \quad (3)$$

where

$$\alpha = 2\hbar^3/(6\mu)^{3/2}a^{1/2}kT \quad (4)$$

and Q is the partition function obtained by integrating the numerator of eq 3 over all J 's

$$Q = 4\Gamma(2/3)\mu a^{1/3}(kT/2)^{2/3}\hbar^{-2} \quad (5)$$

The total population of systems with quantum numbers between J and $J+dJ$ is $(N_J/N)dJ$. Associated with each element dJ is an element dR corresponding to the range of R . Upon substitution of eq 1, 4, and 5

(1) H. S. Johnston, *Advan. Chem. Phys.*, **3**, 131 (1960).

(2) E. Gorin, *Acta Physicochim. URSS*, **6**, 691 (1938).

(3) H. S. Johnston and P. Goldfinger, *J. Chem. Phys.*, **37**, 700 (1962).

(4) S. Glasstone, K. J. Laidler, and H. Eyring, "The Theory of Rate Processes," McGraw-Hill Book Co., Inc., New York, N. Y., 1941, p 131.

Table I: Input Parameters and Internuclear Distance in Activated Complexes at 400°K

R ₁	R ₂	$\bar{\mu}_1$, D ^a	$\bar{\mu}_2$, D ^a	10 ²⁴ α ₁ , cm ³ b	10 ²⁴ α ₂ , cm ³ b	N ₁	N ₂	10 ²⁸ a _{es} , ergs cm ⁶	10 ²⁸ a _{ind} , ergs cm ⁶	10 ²⁸ a _{dis} , ergs cm ⁶	10 ²⁸ a _a , ergs cm ⁶	10 ⁸ (R) _v , cm	
CH ₃	CH ₃	2.2	...	7	...	~0	...	1.09	~1.09	5.20	(5.20) ^e
CH ₂ Cl	CH ₂ Cl	1.7	...	4.0	...	13	...	1.01	0.23	3.63	4.87	6.68	
CHCl ₂	CHCl ₂	1.4	...	5.9	...	19	...	0.46	0.23	7.86	8.55	7.34	
CCl ₃	CCl ₃	0.90	...	7.8	...	25	...	0.08	0.13	13.71	13.92	7.96	(7.94) ^e
CF ₃	CF ₃	1.5	...	2.65 ^c	...	25	...	0.61	0.12	2.72	3.45	6.31	(6.06) ^e
C ₂ H ₅	C ₂ H ₅	4.0	...	13	...	~0	...	3.63	~3.63	6.36	
C ₂ H ₄ Cl	C ₂ H ₄ Cl	1.85	...	5.8	...	19	...	1.41	0.40	7.66	9.47	7.46	
C ₂ Cl ₅	C ₂ Cl ₅	0.85	...	13.3	...	43	...	0.06	0.19	40.03	40.28	9.50	
CH ₃	H	...	0	2.2	0.667 ^d	7	1	0	...	0.27	~0.27	4.12	
C ₂ H ₅	H	...	0	4.0	0.667 ^d	13	1	0	...	0.49	~0.49	4.56	
CH ₃	C ₂ H ₅	2.2	4.0	7	13	~0	...	1.97	~1.97	5.75	
CH ₃	NO	...	0.16	2.2	1.68 ^c	7	11	~0	...	0.98	~0.98	5.11	
C ₂ H ₄	H	0	0	4.1	0.667 ^d	12	1	0	0	0.49	0.49	4.56	
C ₂ H ₄	Cl	0	0	4.1	2.3	12	7	0	0	2.05	2.05	5.78	

^a Values of corresponding RH molecules less 10% ^b Values taken from ref 3, except as indicated. ^c T. S. Ree, T. Ree, H. Eyring, and T. Fueno, *J. Chem. Phys.*, **36**, 281 (1962). ^d Reference 7. ^e Radical assumed to be planar ($\bar{\mu} = 0$).

in eq 3, we obtain the distribution function in terms of R

$$f(R) dR = \frac{6}{\Gamma(2/3)} \left(\frac{2a}{kT} \right)^{2/3} \frac{\exp[-2a/kTR^6]}{R^5} dR \quad (6)$$

where $f(R)$ is normalized. The average, or most probable value R is then found from

$$\langle R \rangle_{av} = \int_{R_m}^{\infty} R f(R) dR \quad (7)$$

The lower limit, R_m , is dictated by the physical model, namely, that the radicals in the activated complex be so far apart that there is no electronic overlap and only the long-range attractive potential need be considered. For the present we shall not further specify the magnitude of R_m , except for stating the condition $R_m > R_E$, where R_E is the equilibrium internuclear distance in the stable molecule.

Introducing $R' = R - R_m$ in eq 7

$$\begin{aligned} \langle R \rangle_{av} &= \int_0^{\infty} (R' + R_m) f(R' + R_m) dR' \\ &= C \int_0^{\infty} (R' + R_m)^{-4} \exp[-\theta/(R' + R_m)^6] dR' \end{aligned} \quad (8)$$

where $C = 6\theta^{2/3}/\Gamma(2/3)$ and $\theta = 2a/kT$. The change of variable $y = \theta^{1/2}/(R' + R_m)^3$ leads to the probability integral

$$\begin{aligned} \langle R \rangle_{av} &= (1/3)C\theta^{-1/2} \int_0^{\theta^{1/2}/R_m^3} e^{-y^2} dy \\ &= \frac{\pi^{1/2}}{\Gamma(2/3)} \left(\frac{2a}{kT} \right)^{1/6} \operatorname{erf} \left[\left(\frac{2a}{kT} \right)^{1/2} / R_m^3 \right] \end{aligned} \quad (9)$$

As will be shown below, for practical cases $(2a/kT)^{1/2}/$

$R_m^3 > 2$, so that, to a very good approximation, the error function is equal to unity, and hence

$$\langle R \rangle_{av} = 1.3092(2a/kT)^{1/6} \quad (10)$$

Thus the problem in evaluating $\langle R \rangle_{av}$ is one of calculation of the attractive constant, a . For reactants which have permanent dipole $\bar{\mu}$ and polarizability α and which are in thermal equilibrium, the attractive potential, averaged over all orientations, is given by⁵

$$\begin{aligned} V_a &= -a/R^6 \\ &= -(a_{es} + a_{ind} + a_{dis})/R^6 \end{aligned} \quad (11)$$

where $a_{es} = 2\bar{\mu}_1^2\bar{\mu}_2^2/3kT$ is the electrostatic contribution due to dipole-dipole interaction, $a_{ind} = \alpha_1\bar{\mu}_2^2 + \alpha_2\bar{\mu}_1^2$ is the inductive contribution due to dipole-induced dipole interaction, and a_{dis} is the dispersion contribution due to instantaneous induced dipole moments interaction between R_1 and R_2 . A simple expression for the estimation of a_{dis} has been given by Slater and Kirkwood^{6,7} for atom-atom and molecules with axial-symmetry interactions

$$a_{dis} = (3/2)(e\hbar/m_e)^{1/2} \alpha_1 \alpha_2 / [(\alpha_1/N_1)^{1/2} + (\alpha_2/N_2)^{1/2}] \quad (12)$$

where e and m_e are the charge and mass of an electron and N is the number of outer-shell electrons. More recently, N has been reinterpreted as the total number of electrons in the case of two-atom interactions.⁸ Johnston and Goldfinger³ have used eq 12 with N as the

(5) J. O. Hirschfelder, C. F. Curtiss, and R. B. Bird, "Molecular Theory of Gases and Liquids," John Wiley and Sons, Inc., New York, N. Y., 1954, p 986.

(6) J. C. Slater and J. G. Kirkwood, *Phys. Rev.*, **37**, 682 (1931).

(7) L. Salem, *Mol. Phys.*, **3**, 441 (1960).

(8) C. Mavroyanis and M. J. Stephen, *ibid.*, **5**, 629 (1962).

"effective" number of electrons to calculate the rates of radical recombinations. Fortunately, $\langle R \rangle_{av}$ depends on N as $N^{1/2}$ and hence is not very sensitive to its precise definition. We shall, therefore, use N as the sum of the outer-shell electrons of all the atoms in the reactant.

Results

The calculated values of $\langle R \rangle_{av}$ for twelve radical combinations, as well as hydrogen and chlorine atom addition to ethylene, are listed in Table I. The assigned dipole moments for the halohydrocarbon radicals were taken as 90% of the values for the corresponding halohydrocarbon molecules.⁹

Polarizabilities were taken from ref 3 and are based on known atom polarizabilities.^{7,10} In all cases, the principal contribution to the long-range attractive potential and hence to $\langle R \rangle_{av}$ is due to dispersion forces. The induction contribution is small, less than 5% for CH_2Cl and $\text{C}_2\text{H}_4\text{Cl}$ and negligible in all other cases. The electrostatic contribution, while also small in most cases, may be quite significant (21% for CH_2Cl , 15% for $\text{C}_2\text{H}_4\text{Cl}$)

and should not be dismissed lightly without investigating the magnitude of the dipole moments. The relatively large values of $\langle R \rangle_{av}$ are noteworthy; thus an assumption of a "half bond" in these cases would lead to a severe underestimate.

A justification for setting the error function in eq 10 equal to unity may be sought as follows. For $(2a/kT)^{1/2}/R_m^3 = 2$, an error of less than 1/2% would be introduced by setting $\text{erf}(2) = 1$. Now for the most unfavorable case, $(\text{CH}_3 + \text{H})$ in Table I, $(2a/kT)^{1/2} = 31.2 \times 10^{-24} \text{ cm}^3$. Using this value and solving for R_m , we find $R_m = 2.5 \times 10^{-8} \text{ cm}$, which is 2.3 times R_E in methane. The assumption of the validity of the Gorin model for such separations then justifies the approximation in eq 10.

(9) "Handbook of Chemistry and Physics," 46th ed, The Chemical Rubber Publishing Co., Cleveland, Ohio, p E57.

(10) J. A. A. Katelaar, "Chemical Contribution," Elsevier Publishing Co., Amsterdam, The Netherlands, 1958, p 91.

Radical Yield in γ -Irradiated Aqueous Alkaline Solutions of Fremy's Salt

by N. Th. Rakintzis

Nuclear Research Center "Democritos," Radiation Chemistry Laboratory, Aghia Paraskevi Attikis, Athens, Greece

and Gabriel Stein

Department of Physical Chemistry, Hebrew University, Jerusalem, Israel (Received September 7, 1967)

Using deaerated aqueous solutions of $\text{ON}(\text{SO}_3)_2^{2-}$ at pH 10–11, the total radical yield was determined in γ -irradiated solutions, $G_{(\text{H} + \cdot + \text{OH})} = 6.1$.

Introduction

The dependence of the radical yield in irradiated aqueous solutions on the pH is being very actively investigated.^{1–3} In alkaline solutions there is a dearth of simple systems suitable for the determination of exact values of the radical yield.²

In a previous publication,⁴ the behavior of the inorganic free radical, Fremy's salt (hereafter denoted by F), nitrosodisulfonate, $\text{ON}(\text{SO}_3)_2^{2-}$, irradiated with γ rays in aerated solution at pH 10–11 was investigated and the correlation of the $G(-F)$ with $G_{(\text{H} + \cdot + \text{OH})}$ was discussed. In the present paper, results in deaerated solutions are reported and discussed in relation to the problem of radical yields in irradiated aqueous solutions.

Experimental Section

Irradiations were carried out by means of a 3150-curie ^{60}Co γ -ray source (Gamma-cell 200, Atomic Energy of Canada Limited). The dose rate was about 5000 rads min^{-1} throughout the experiments, determined by the Fricke dosimeter. The cylindrical irradiation cell was made of Pyrex glass with an absorption cell of silica (10-mm light path) sealed on. The cleaning technique used, the dosimetry, and the prep-

(1) M. Haissinsky, *J. Chim. Phys.*, **62**, 224 (1965).

(2) A. O. Allen, *Radiation Res. Suppl.*, **4**, 54 (1964).

(3) D. G. Marketos, N. Th. Rakintzis, and G. Stein, "On a pH Dependent Increase in the Yield of Available Radicals in the Radiation Chemistry of Aqueous Solutions," to be published.

(4) N. Th. Rakintzis and G. Stein, *J. Phys. Chem.*, **70**, 727 (1966).

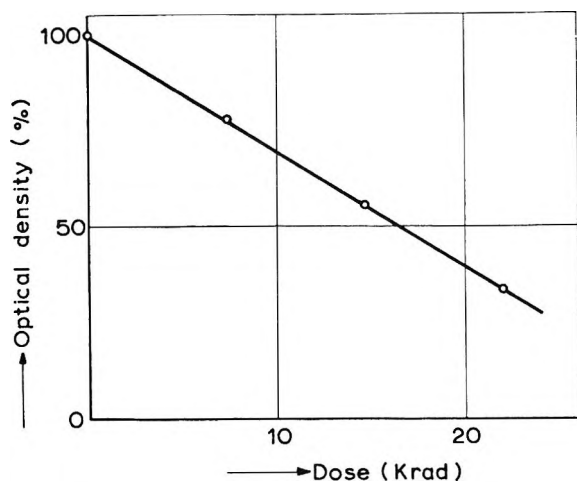


Figure 1. Variation of decomposition with radiation dose. $[F] = 2.09 \times 10^{-4} M$; pH 10.5; dose rate, 4540 rads min^{-1} .

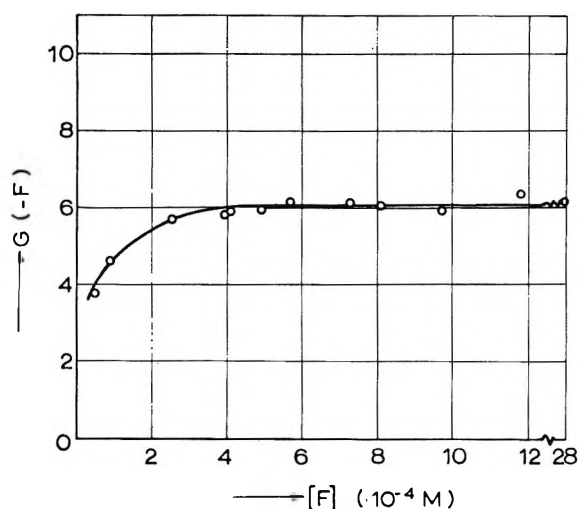


Figure 2. Variation of the decomposition yield of Fremy's salt in aqueous deaerated solutions with its initial concentration.

aration of the triply distilled water are described in a previous paper.⁵ Optical densities of the solutions were measured with a Hilger Uvispek spectrophotometer, Model H 700.308. The pH's of the solutions were adjusted by adding KOH and measured with a Photovolt Model 110 pH meter.

Fremy's salt was prepared according to the procedure of Luz, Silver, and Eden,⁶ but using more NH_4OH , to keep the solution alkaline. Better yields were thus obtained. The solutions were deaerated by alternate freezing with liquid nitrogen and melting on a vacuum line.

Results

Kinetics of the Radiation Reaction. The radiolysis was followed by measuring the decrease in OD at 242 μ . As in the case of the aerated solutions, strictly zero-order kinetics were obtained when the experiments

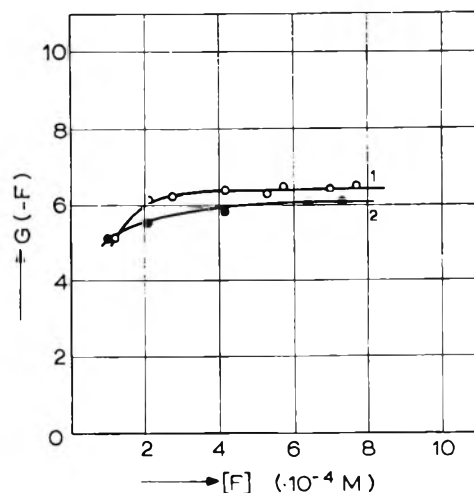


Figure 3. Decomposition yield of Fremy's salt in aqueous deaerated solutions in the presence of 2-propanol vs. its initial concentration: curve 1, $2 \times 10^{-1} M$ 2-propanol; curve 2, $1 \times 10^{-1} M$ 2-propanol.

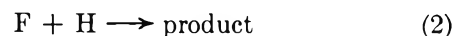
were carried out at pH 10–11. One experimental curve is shown in Figure 1.

Dependence of $G(-F)$ on Concentration. The effect of F concentration on the G of the decomposition up to $\sim 3 \times 10^{-3} M$ is shown in Figure 2. From about $5 \times 10^{-3} M$ upward, reproducible results became difficult to obtain owing to concentration-dependent side reactions.⁴

The Influence of Added 2-Propanol. The results shown in Figure 3 are obtained at a constant concentration of 10^{-1} and $2 \times 10^{-1} M$ of 2-propanol with varying F concentrations.

Discussion

Comparison of the results shown in Figure 2 with the results in ref 4, obtained in the presence of air and at a different dose rate (650 rads min^{-1}), shows excellent agreement with the limiting yield of $G(-F) = 6.1$. This limiting yield is attained in the present case at $[F] \approx 5 \times 10^{-4} M$ and then remains constant. In the presence of air, as Figure 3 of ref 4 shows, the limiting value is only slowly approached with increasing $[F]$. We propose that in the absence of air complications due to the possible formation⁴ of O_3^- are excluded and the one-electron equivalent oxidation and reduction reactions of the inorganic free radical F



all proceed efficiently. As mentioned previously,⁴

(5) N. Th. Rakintzis, D. G. Marketos, and A. P. Konstas, *Z. Physik. Chem. (Frankfurt)*, **35**, 234 (1962).

(6) Z. Luz, B. Silver, and C. Eden, *J. Chem. Phys.*, **44**, 4421 (1966).

H₂O₂ at the concentrations produced by the radiation does not react with F in the course of the experiments. $G(-F) = 6.1$ corresponds therefore at pH 10.5 to $G_{(H^+ + e + OH)}$.

In the presence of $2 \times 10^{-1} M$ 2-propanol (Figure 3, curve 1), the limiting yield rises to $G = 6.3$. This is exactly the value obtained by Asmus and Henglein,⁷ using tetranitromethane in the presence of $2 \times 10^{-1} M$ 2-propanol. At such relatively high concentrations of a good OH scavenger, the radical yield, higher than the limit reached by $[F] \approx 5 \times 10^{-4} M$ alone, may be due to the interception of additional radicals. Note, however, that even in the presence of $10^{-1} M$ 2-propanol the limiting value is still 6.1 (Figure 3, curve 2). The error in this value should be insignificant, since in all experiments strictly zero-order kinetics were obtained, showing on one hand that the products do not interfere in the reaction and on the other hand that their contribution to absorption at 242 m μ is negligible.

The present experiments confirm the usefulness of

solutions of Fremy's salt at its relatively stable alkaline pH as a radical scavenger. Available as a crystalline material and reacting by irreversible one-electron reactions with both reducing and oxidizing radicals, it has some advantages over other agents used for similar purposes, e.g., N₂O and C(NO₂)₄.

The total radical yield $G = 6.1$ now obtained in alkaline solution is similar to that obtained previously⁸ at neutral pH, using a system in which all the available radicals were scavenged. The results thus support the view that at least over this pH range the radical yield appears to remain constant, when suitable scavengers are used.

Acknowledgments. We wish to thank Mr. D. Arapoglou for his assistance in carrying out the experiments.

(7) K. D. Asmus and A. Henglein, *Ber. Bunsenges. Physik. Chem.*, **68**, 348 (1964).

(8) M. J. Day and G. Stein, *Radiation Res.*, **6**, 666 (1957).

Study of Dielectric Relaxation in Benzene Solutions of Some Hydroxy- and Methoxybenzaldehydes

by J. P. Shukla, S. I. Ahmad, D. D. Shukla, and M. C. Saxena

Physics Department, Lucknow University, Lucknow, India (Received September 7, 1967)

The dielectric constants (ϵ'), and the loss factors (ϵ'') of dilute benzene solutions of *o*-hydroxy-, *o*-methoxy-, *p*-methoxy-, 2,4-dimethoxy-, and 3,5-dimethoxybenzaldehydes have been measured at a number of temperatures in the 3-cm microwave region by the concentration-variation method. The data obtained have been utilized for determining the relaxation times. The values of relaxation times at different temperatures have been used to determine the free energy, heat, and entropy of activation for dielectric relaxation. For comparison, the free energy, heat, and entropy of activation have been determined for the process viscous flow of the solvent from the viscosity data also. The relaxation times have been discussed in terms of molecular and intramolecular rotation.

Introduction

The authors have carried out the measurements of the relaxation time of five substituted benzaldehydes, *vis.*, *o*-hydroxybenzaldehyde, *o*-methoxybenzaldehyde, *p*-methoxybenzaldehyde, 3,5-dimethoxybenzaldehyde, and 2,4-dimethoxybenzaldehyde in solutions of benzene, at varying temperatures and at a fixed frequency in the 3-cm microwave region. These relaxation-time values have been utilized for determining the molar free energies of activation for dipole relaxation (ΔF_e) using Eyring's theory of rate process,¹ according to which

$$\tau = \frac{A}{T} e^{\Delta F_e/RT} \quad (1)$$

where A is known as the frequency factor and is given by h/k , h and k are Planck's constant and Boltzmann's constant, respectively, and R is the gas constant.

The heats of activation (ΔH_e) and entropies of acti-

(1) S. Glasstone, K. J. Laidler, and H. Eyring, "The Theory of Rate Process," McGraw-Hill Book Co., Inc., New York, N. Y., 1941, p 548.

vation (S_e) for dipole relaxation have also been determined by putting

$$\Delta F_e = \Delta H_e - T\Delta S_e$$

in eq 1, which reduces it to

$$\tau = \frac{A}{T} e^{-\Delta S_e/R} e^{\Delta H_e/RT} \quad (2)$$

The molar free energies of activation (ΔF_η), the heats (ΔH_η), and the entropies (ΔS_η) of activation for the viscous flow of the solvent have also been determined for the purpose of comparison using the relations¹

$$\eta = B e^{\Delta F_\eta/RT} \quad (3)$$

and

$$\eta = B e^{-\Delta S_\eta/R} e^{\Delta H_\eta/RT} \quad (4)$$

Where B is known as the frequency factor and has been shown by Eyring¹ to have values given by hN/V where N and V are Avagadro's number and the molar volume, respectively.

Whiffen and Thompson,² Gopala Krishna,³ and Sobhanadri⁴ have found the energy of activation, ΔF_η for viscous flow of the solvent to be always greater than ΔF_e . Saxton⁵ and Van Eick and Poley⁶ have observed that ΔF_e and ΔF_η are nearly equal in the case of some pure liquids. Saxton has also observed that they are independent of temperature. The factor A was found to vary with temperature and to be always greater than Eyring's estimated value of h/k ($\approx 4.8 \times 10^{-11}$). Recent observations of Bhanumati⁷ have indicated that ΔF_e and ΔF_η are nearly equal only in the case of low-viscosity solvents. A was found to depend upon the nature of the solute. Smyth and collaborators⁸⁻¹⁰ have found ΔF_e to increase with the size of the molecule.

A study of the above results indicate that no definite conclusions can be drawn regarding the energies of activation and the factors A and B . The present investigation, therefore, was undertaken to study the dielectric relaxation in relation to molecular structure and to further our knowledge about the energies of activation for dielectric relaxation and viscous flow and the factors A and B .

Theory

The relaxation times have been determined using the fixed-frequency method of Gopala Krishna¹¹ for dilute solutions using the relations

$$\tau = \frac{\lambda}{2\pi c} \frac{dy}{dx} \quad (5)$$

$$x = \frac{\epsilon'^2 + \epsilon''^2 + \epsilon' - 2}{(\epsilon' + 2)^2 + \epsilon''^2} \quad (6)$$

$$y = \frac{3\epsilon''}{(\epsilon' + 2)^2 + \epsilon''^2} \quad (7)$$

where λ is the free-space wavelength, ϵ' is the dielectric constant, and ϵ'' is the loss factor.

Because dielectric relaxation is a rate process, the Eyring¹ equations have been used for determining the molar free energies and factors A and B . The values of ΔH_e have been evaluated using eq 2, plotting log

Table I: Experimental Data for the Determination of Relaxation Times (τ)

o-Hydroxybenzaldehyde							
25°		35°		40°			
ϵ'	ϵ''	ϵ'	ϵ''	ϵ'	ϵ''		
2.3122	0.0477	2.3201	0.0307	2.3446	0.0310		
2.3225	0.0562	2.3724	0.0653	2.3454	0.0356		
2.3446	0.0785	2.3836	0.0746	2.3618	0.0616		
2.3836	0.0994	2.4158	0.0887	2.3900	0.0651		
				2.4214	0.0869		
o-Methoxybenzaldehyde							
25°		30°		35°		40°	
ϵ'	ϵ''	ϵ'	ϵ''	ϵ'	ϵ''	ϵ'	ϵ''
2.2389	0.0251	2.2434	0.0266	2.2646	0.0251	2.2659	0.0225
2.2454	0.0336	2.2486	0.0339	2.2710	0.0297	2.2684	0.0282
2.2734	0.0556	2.2678	0.0540	2.2897	0.0533	2.2985	0.0521
2.2771	0.0728	2.2741	0.0705	2.3104	0.0707	2.3114	0.0773
2.2884	0.0885	2.3141	0.0865	2.3298	0.0742	2.3273	0.1371
p-Methoxybenzaldehyde							
25°		30°		40°			
ϵ'	ϵ''	ϵ'	ϵ''	ϵ'	ϵ''		
2.2258	0.0254	2.2304	0.0246	2.2428	0.0279		
2.2337	0.0334	2.2454	0.0288	2.2576	0.0352		
2.2684	0.0482	2.2499	0.0457	2.2595	0.0448		
2.2779	0.0728	2.2966	0.0768	2.3022	0.0762		
2.3151	0.1069	2.3298	0.1657	2.3255	0.1286		
3,5-Dimethoxybenzaldehyde							
25°		30°		35°			
ϵ'	ϵ''	ϵ'	ϵ''	ϵ'	ϵ''		
2.2284	0.0254	2.2368	0.0369	2.2530	0.0396		
2.2445	0.0488	2.2499	0.0518	2.2685	0.0513		
2.2499	0.0618	2.2631	0.0713	2.2841	0.0707		
2.2600	0.0707	2.2639	0.0825	2.2934	0.0880		
2.2981	0.1108	2.3091	0.1176	2.3138	0.1198		
2,4-Dimethoxybenzaldehyde							
25°		30°		35°			
ϵ'	ϵ''	ϵ'	ϵ''	ϵ'	ϵ''		
2.2184	0.0356	2.2384	0.0361	2.2353	0.0371		
2.2314	0.0368	2.2484	0.0377	2.2522	0.0372		
2.2600	0.0687	2.2592	0.0729	2.2553	0.0776		
2.2669	0.1116	2.2732	0.1157	2.2809	0.1200		

- (2) D. H. Whiffen and H. W. Thompson, *Trans. Faraday Soc.*, **42A**, 114 (1946).
- (3) K. V. Gopala Krishna, *Indian J. Phys.*, **32**, 387 (1958).
- (4) J. Sobhanadri, *Trans. Faraday Soc.*, **56**, 569 (1960).
- (5) J. A. Saxton, *Proc. Roy. Soc. (London)*, **213**, 473 (1952).
- (6) A. J. Van Eick and J. P. H. Poley, *Appl. Sci. Res.*, **6B**, 359, (1957).
- (7) A. Bhanumati, *Indian J. Pure Appl. Phys.*, **1**, 148 (1963).
- (8) E. L. Grub and C. P. Smyth, *J. Am. Chem. Soc.*, **83**, 4122 (1961).
- (9) O. F. Kalmann and C. P. Smyth, *ibid.*, **82**, 783 (1960).
- (10) E. J. Heston, W. M. Heston, Jr., and C. P. Smyth, *ibid.*, **70**, 4102 (1948).
- (11) K. V. Gopala Krishna, *Trans. Faraday Soc.*, **53**, 767 (1957).

Table II: Relaxation Times and Molar Activation Energy Parameters

Substance	Temp, °K	$\tau \times 10^{12}$, sec	ΔF_e , kcal/mol	ΔF_η , kcal/mol	ΔS_e , cal/mol	ΔS_η , cal/mol	ΔH_e , kcal/mol	ΔH_η , kcal/mol
<i>o</i> -Hydroxy-benzaldehyde	298	11.62	2.55	2.91	-2.67	-1.30	1.74	2.52
	308	10.79	2.58	2.93	-2.78	-1.33	1.74	2.52
	313	9.96	2.59	2.94	-2.74	-1.34	1.74	2.52
<i>o</i> -Methoxy-benzaldehyde	298	19.92	2.83	2.91	-1.90	-1.30	2.29	2.52
	303	17.43	2.84	2.92	-1.79	-1.32	2.29	2.52
	308	16.18	2.85	2.93	-1.80	-1.33	2.29	2.52
	313	14.94	2.86	2.94	-1.79	-1.34	2.29	2.52
<i>p</i> -Methoxy-benzaldehyde	298	14.94	2.67	2.91	-1.69	-1.30	2.18	2.52
	303	13.28	2.68	2.92	-1.62	-1.32	2.18	2.52
	313	11.62	2.70	2.94	-1.64	-1.34	2.18	2.52
3,5-Dimethoxy-benzaldehyde	298	24.90	2.98	2.91	-3.11	-1.30	2.06	2.52
	303	22.41	3.00	2.92	-3.05	-1.32	2.06	2.52
	308	21.58	3.01	2.93	-3.12	-1.33	2.06	2.52
2,4-Dimethoxy-benzaldehyde	298	22.26	2.92	2.91	-3.96	-1.30	1.74	2.52
	303	21.58	2.94	2.92	-4.03	-1.32	1.74	2.52
	308	19.09	2.96	2.93	-3.91	-1.33	1.74	2.52

Table III: Relaxation Times and Factors A' and B'

Substance	Temp, °K	$\tau \times 10^{12}$, sec	$10^{11}A'$ ($= Ae^{-\Delta S_e/R}$)	$10^8B'$ ($= Be^{-\Delta S_e/R}$)	$\frac{hN}{V} \times 10^6$
<i>o</i> -Hydroxy-benzaldehyde	298	11.62	18.40	8.58	4.47
	308	10.79	19.41	8.59	4.41
	313	9.96	19.05	8.60	4.38
			18.85 ^a	8.60 ^a	
<i>o</i> -Methoxy-benzaldehyde	298	19.92	12.47	8.58	4.47
	303	17.43	11.81	8.58	4.44
	308	16.18	11.86	8.59	4.41
	313	14.94	11.81	8.60	4.38
			11.95 ^a	8.60 ^a	
<i>p</i> -Methoxy-benzaldehyde	298	14.94	11.12	8.58	4.47
	303	13.28	10.81	8.58	4.44
	313	11.62	10.96	8.60	4.38
				11.04 ^a	8.60 ^a
3,5-Dimethoxy-benzaldehyde	298	24.90	22.92	8.58	4.47
	303	22.41	22.23	8.58	4.44
	308	21.58	22.99	8.59	4.41
				22.71 ^a	8.60 ^a
2,4-Dimethoxy-benzaldehyde	298	22.26	35.19	8.58	4.47
	303	21.58	36.43	8.58	4.44
	308	19.09	34.32	8.59	4.41
				35.02 ^a	8.60 ^a

^a Denotes the average values of the factors concerned.

τT vs. $1/T$, and the intercept of the curve, namely, A' , has been used to determine the entropy, ΔS_e , using

$$A' = \frac{h}{k} e^{-\Delta S_e/R} \quad (8)$$

The values of ΔH_e and ΔS_e so obtained give ΔF_e according to

$$\Delta F_e = \Delta H_e - T\Delta S_e \quad (9)$$

Similarly, in the case of the process of viscous flow of the solvent, the straight line drawn between $\log \eta$ and $1/T$, using eq 4, gives the values of ΔH_η and the intercept B' . The values of ΔS_η can be determined using the relation

$$B' = \frac{hN}{V} e^{-\Delta S_{\eta}/R} \quad (10)$$

An equation similar to eq 9 gives the values of ΔF_{η} , also.

Experimental Section

A microwave bench of a 3-cm wavelength region was used for measuring the dielectric constant, ϵ' , and the loss factors, ϵ'' , of the dilute solutions of the compounds in benzene. The standing-wave technique of Roberts and Von Hippel,¹² described earlier,¹³ was used. The simplified method of Dakin and Works¹⁴ was used for calculating the values of the dielectric constant and loss factors.

Chemicals. The chemicals used were of the purest quality and were obtained from standard firms. *o*-Hydroxybenzaldehyde was obtained from British Drug House Ltd., England. *o*-Methoxybenzaldehyde, *p*-methoxybenzaldehyde, 3,5-dimethoxybenzaldehyde, and 2,4-dimethoxybenzaldehyde of Fluka AG and SG were obtained from Switzerland. Analar benzene, purest quality, was obtained from British Drug House Ltd., England, and was distilled before use.

Results

The dielectric constant (ϵ') and the loss factors (ϵ'') at different temperatures are given in Table I. In Table II, the values of relaxation times and the thermodynamic parameters have been reported. The values of the factors A' and B' along with Eyring's estimated values for the frequency factors are given in Table III.

Discussion

As observed from Table II, the results show that the relaxation time of all the substituted benzaldehydes decreases with increasing temperature. This is due to the decreasing viscosity of the solvent with increase in temperature and indicates that the distribution of relaxation times around the most probable value decreases with increase in temperature. The relaxation time of methoxybenzaldehydes is found to decrease as the two substituted groups go farther apart from each other. This may be explained to be due to the decreasing interaction between the two rotating groups in the same order. Further, the relaxation time of both *o*- and *p*-methoxybenzaldehydes is greater than that of *o*-hydroxybenzaldehyde at the same temperature, as expected in view of the greater size of the former molecules.

As all of the investigated compounds contain substituted groups having freedom of rotation around their bonds with the ring, the dielectric relaxation should take place by both molecular as well as intramolecular rotations. The two dimethoxybenzaldehydes are found to have greater relaxation time than *o*- or *p*-methoxybenzaldehyde at the same temperature, because of their greater molecular size. The possession of one more ro-

tating group, namely, the methoxy group by the methoxybenzaldehyde molecule, may increase the contribution of intramolecular rotation, but the increase in size appears to have greater effect on relaxation time than the capability of a group to rotate round its bond with the ring.

The relaxation time of unsubstituted benzaldehyde in benzene has been reported earlier by one of the authors¹⁵ to be 10.6×10^{-12} sec at 27°. Neglecting the small differences in temperatures, the results show that the relaxation, at 25°, of the substituted benzaldehydes considered in the present investigation is always greater than that of the unsubstituted one. This is in conformity with the greater size of the hydroxy- or methoxybenzaldehyde. The addition of a hydroxy or methoxy group, besides increasing the size of the molecule, may also increase the contribution of intramolecular rotation tending to decrease the observed relaxation time. The higher values of relaxation times of hydroxy- or methoxybenzaldehyde than that of the unsubstituted benzaldehyde indicate that the effect of increase in size is greater than that of the capability of a group to rotate, as concluded above, or that the intramolecular rotation does not contribute much to the observed microwave absorption in the present case of dilute solutions.

The free energies of activation for dielectric relaxation and viscous flow of the solvent are found to increase with temperature. Further, the free energy of activation for viscous flow of the solvent is slightly greater than that for dielectric relaxation in the case of *o*-hydroxy- and *o*- and *p*-methoxybenzaldehydes. They are nearly equal in the case of 2,4-dimethoxybenzaldehyde. In the case of 3,5-dimethoxybenzaldehyde, the free energy of activation for dielectric relaxation (ΔF_{ϵ}) is observed to be slightly greater than that for viscous flow, ΔF_{η} , which appears to be anomalous. However, in view of the possible experimental error involved in such measurements, this small discrepancy is unavoidable and can be safely ignored. Similar anomalies have been observed earlier by Smyth and coworkers,^{9,16} in certain cases. The higher values of ΔF_{η} than ΔF_{ϵ} indicate that, in viscous flow, there is greater hindrance from the neighbors than in dielectric relaxation, because while the former involves both translation and rotation, the latter takes place by the rotation of the dipole with little or no translation.

The values of A' ($= Ae^{-\Delta S_{\epsilon}/R}$) given in Table III are found to vary little with temperature for one solution but are different for solutions having different polar molecules varying from 10.81 to 36.43×10^{-11} .

(12) S. Roberts and A. Von Hippel, *J. Appl. Phys.*, **17**, 610 (1946).

(13) N. K. Mehrotra, J. P. Shukla, and M. C. Saxena, *Indian J. Pure Appl. Phys.*, **5**, 61 (1967).

(14) T. W. Dakin and C. N. Works, *J. Appl. Phys.*, **18**, 610 (1947).

(15) S. I. Ahmad, *Indian J. Pure Appl. Phys.*, **1**, 434 (1963).

(16) A. J. Petro and C. P. Smyth, *J. Am. Chem. Soc.*, **79**, 6142 (1957).

This indicates that the observed values of this factor differ widely from the theoretical value $(h/k)e^{-\Delta S_e/R} = 4.8 \times 10^{-11}$, where A is equal to h/k , as shown by Eyring, and the exponential factor has been taken to be nearly equal to 1 as ΔS_e is a very small quantity.

As given in Table III, factor B' ($=Be^{-\Delta S_e/R}$), which is very nearly equal to B , varies little within the observed range of temperature and is nearly twice Eyring's estimated values of hN/V for the frequency factor B .

The heats of activation for viscous flow of the solvent, ΔH_η , are found to be greater than that for dielectric relaxation, ΔH_e , in all of the molecules as expected. The entropies of activation for both of the processes are observed to be always negative, indicating that the activated state is more ordered than the normal state.

Acknowledgments. We are deeply indebted to Dr. B. G. Gokhale, Professor Head of the Physics Department, for his continued interest and encouragement throughout the work.

The Activity of Lithium in Lithium Amalgams

by David R. Cogley and James N. Butler

Tyco Laboratories, Inc., Waltham, Massachusetts 02154 (Received September 8, 1967)

Activity coefficients of lithium in its amalgams have been measured using the cell $\text{Li(s)}|\text{Li}^+, \text{X}^-\text{Li(Hg)}$, where X^- is Cl^- or ClO_4^- , with anhydrous dimethyl sulfoxide as solvent. The activity coefficient (mole fraction scale, reference state infinite dilution) is given by the relation, $\log \gamma_{\text{Li}} = (14.6 \pm 0.4)X_{\text{Li}}$, for $X_{\text{Li}} < 0.013$ (saturation), and the solutions appear to be regular within experimental error. The standard potential difference between the solid lithium and lithium amalgam electrodes is 0.8438 ± 0.0002 V. A saturated amalgam at 25° contains 1.33 mole % lithium.

Introduction

In the course of our studies on the kinetics of the lithium amalgam–lithium ion electrode in nonaqueous solvents,¹ we have measured the activity coefficient of lithium in its amalgams at room temperature, as well as the potential difference between the amalgams and solid lithium.

The potential difference between a lithium amalgam (1.00 mole %) and solid lithium electrode in a propylamine–lithium iodide electrolyte was measured by Lewis and Keyes² as part of their determination of the standard potential of the lithium electrode in aqueous solutions. Since they used the same amalgam composition for the aqueous cell, it was unnecessary for their purpose to determine the activity coefficient of lithium in the amalgam, and they made measurements with only one amalgam composition. Spiegel and Ulich³ measured the potential difference between various lithium amalgams ranging in composition from 0.03 to 2.3 mole %, using electrolytes consisting of LiCl dissolved in acetone, methanol, or acetonitrile, but the potential with respect to solid lithium was not measured. Although the activity coefficients obtained in the different electrolytes were consistent within experimental error, the dependence of activity coeffi-

cient on amalgam concentration showed strong deviations from regular solution behavior. Both sodium and potassium amalgams appear to be regular in this concentration range.⁴ In view of these discrepancies, we decided to redetermine the potential between lithium and its amalgams and the activity coefficients of the amalgams, using dimethyl sulfoxide (DMSO) as a solvent. A high degree of reversibility and stability of the lithium amalgam¹ and lithium electrodes⁵ has been demonstrated in LiCl–DMSO solutions.

Experimental Section

Lithium amalgams were prepared from triple-distilled mercury (Doe and Ingalls), which had been freed of oxygen by passing it through a porous frit in an argon atmosphere, and lithium ribbon (Foote Mineral Co.,

(1) D. R. Cogley and J. N. Butler, *J. Electrochem. Soc.*, **113**, 1074 (1966).

(2) G. N. Lewis and F. G. Keyes, *J. Am. Chem. Soc.*, **35**, 340 (1913).

(3) G. Spiegel and H. Ulich, *Z. Physik. Chem.*, **A178**, 187 (1937).

(4) M. O. Davies, *et al.*, "The Physical and Chemical Properties of Dilute Alkali Metal Amalgams," Technical Reports No. 7 (June 1957) and 20 (July 1963), Contract Nonr 581(00). Part I: AD 138 849; part II: AD 609 294.

(5) W. H. Smyrl and C. W. Tobias, *J. Electrochem. Soc.*, **115**, 33 (1968).

99.97%) by combining weighed quantities of the two materials or by dilution of a more concentrated amalgam with mercury. The amalgams were analyzed by decomposition with aqueous acid and analysis of the resulting solution for Li^+ by flame photometry. The flame photometer (Instrumentation Laboratories Model 143-A) was calibrated with solutions of approximately the same composition in Li^+ and exactly the same internal standard concentration (1 mM K^+) as the samples to be analyzed. The difference between duplicate analyses was always less than 1%, and often as small as 0.1%. The analysis agreed with the composition as prepared within experimental error.

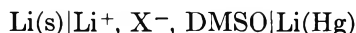
Electrolytes were prepared from anhydrous LiCl or LiClO_4 (Anderson Physics Laboratories, ultrapure grade) and anhydrous dimethyl sulfoxide (Matheson Coleman and Bell, Chromatographic grade). The solvent was treated for 1 week with Linde 5A Molecular Sieve (which had been dried for 16 hr at 500° in argon) to remove the last traces of water. To avoid contamination by any solid particles from the molecular sieve, the treated solvent was filtered through a 10–20- μ glass frit. The water content of the solutions was less than 0.001%, as determined by gas chromatography⁶ on a column of Porapak Q (Waters Associates). No organic impurities could be detected, and it is estimated that their concentration was less than 0.005%.

Potentials were measured with a high-impedance differential voltmeter (John Fluke), which was calibrated against a Weston standard cell (Eppley Laboratories) and found to be accurate to ± 0.05 mV. Potentials were normally read to the nearest 0.1 mV.

All manipulations were carried out in an argon atmosphere containing less than 1 ppm of water, oxygen, or nitrogen (Vacuum Atmospheres Corp. drybox) and at ambient temperature. The temperature was measured to within 0.03° and was $25 \pm 1^\circ$ for all experiments.

Results

We measured the potential of 39 cells of the type



(where X^- is either Cl^- or ClO_4^-) as a function of amalgam concentration from 0.002 to 1.33 mole % Li . The concentrations and potentials are summarized in Table I. The potential of the cell is given by the expression

$$E = E^\circ_{\text{Li(Hg)}} - E^\circ_{\text{Li}} - \frac{RT}{F} \ln (X_{\text{Li}} \gamma_{\text{Li}}) \quad (1)$$

where $E^\circ_{\text{Li(Hg)}}$ is the standard potential of the lithium amalgam (reference state: infinite dilution, mole fraction scale), E°_{Li} is the standard potential of solid lithium, R is the gas constant, T is the absolute tem-

perature, F is the Faraday constant, X_{Li} is the mole fraction of lithium in the amalgam, and γ_{Li} is the activity coefficient of lithium in the amalgam. If the electrode

Table I: Experimental Results

$X_{\text{Li}} \times 10^4$	$T, ^\circ\text{C}$	E, V	γ^a	$\text{Log } \gamma_{\text{Li}}^b$
Series 1A: 1 M LiClO_4 in DMSO				
127.6	24.65	0.9454	14.091	0.178
70.43	24.68	0.9655	14.172	0.097
28.90	24.68	0.9912	14.221	0.048
11.33	24.70	1.0170	14.250	0.019
5.538	24.71	1.0358	14.258	0.011
1.996	24.72	1.0625	14.266	0.003
0.720	24.72	1.0888	14.268	0.001
0.025	24.73	1.1229	14.300	...
Series 1B: 1 M LiClO_4 in DMSO				
127.6	24.55	0.9450	14.084	0.190
70.43	24.57	0.9657	14.176	0.098
28.90	24.58	0.9914	14.226	0.048
11.33	24.60	1.0172	14.255	0.019
5.538	24.61	1.0360	14.262	0.012
1.996	24.63	1.0627	14.271	0.003
0.720	24.64	1.0891	14.274	0.000
0.205	24.65	1.1237	14.315	...
Series 1C: 0.1 M LiClO_4 in DMSO				
127.6	24.50	0.9451	14.086	0.183
70.43	24.51	0.9653	14.170	0.099
28.90	24.52	0.9910	14.219	0.050
11.33	24.52	1.0168	14.248	0.021
5.538	24.53	1.0357	14.258	0.011
1.996	24.53	1.0623	14.265	0.004
0.720	24.54	1.0887	14.269	0.000
0.205	24.55	1.1228	14.301	...
Series 2A: 1 M LiCl in DMSO				
133.2 ^c	26.1	0.9430	14.061	0.208
133.2 ^c	26.2	0.9431	14.062	0.207
118.8	26.2	0.9478	14.092	0.177
52.25	26.2	0.9743	14.182	0.087
0.66	26.2	1.0908	14.245	0.024?
Series 2B: 0.2 M LiCl in DMSO				
86.57	26.0	0.9588	14.141	0.128
52.25	26.0	0.9745	14.187	0.082
29.31	25.9	0.9912	14.218	0.051
0.66	26.0	1.0908	14.248	0.021?
Series 2C: 0.2 M LiCl in DMSO				
133.2 ^c	25.3	0.9434	14.072	0.197
118.8	25.5	0.9478	14.096	0.173
86.57	25.7	0.9587	14.141	0.128
52.25	25.2	0.9743	14.188	0.081
29.31	25.8	0.9912	14.218	0.051
0.66	25.6	1.0912	14.260	0.009?

^a Corrected to 25° using $\Delta H^\circ = -19.8$ kcal. ^b Corrected to 25° . Calculated using $\Delta E^\circ = 0.8440$ V except for series 1B, where $\Delta E^\circ = 0.8443$ V. ^c Saturated amalgam, over-all composition $X_{\text{Li}} = 0.01394$.

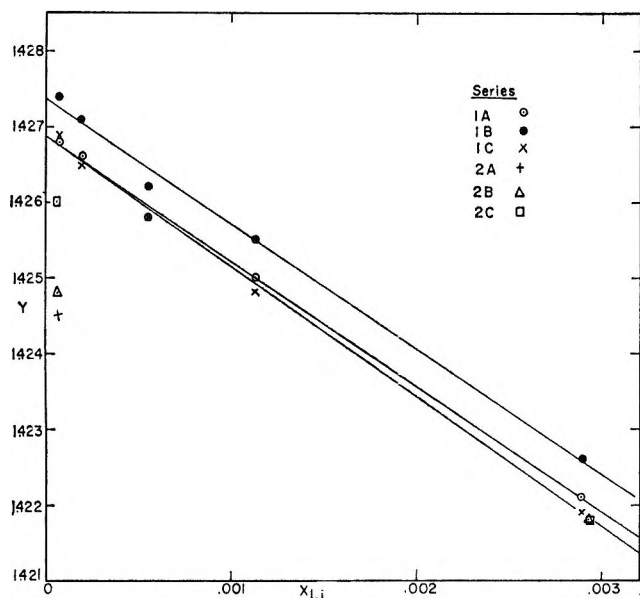


Figure 1.

reactions are ideally reversible and no side reactions take place, the potential of the cell is independent of electrolyte composition.

All of the measurable parameters were combined into the function

$$Y = \frac{F}{2.303RT}E + \log X_{Li} + \frac{\Delta H^\circ}{2.303R} \left(\frac{1}{T} - \frac{1}{298} \right) \quad (2)$$

which is listed in Table I. The last term is a small correction for the temperature variations, and for this we used the standard enthalpy of the reaction^{4,7} $\text{Li(s)} + \text{Hg} = \text{Li(Hg)}$ ($\Delta H^\circ = -19.8$ kcal/mole). Extrapolation of the function Y to $X_{Li} = 0$ gives the standard potential difference $\Delta E^\circ = E^\circ_{\text{Li(Hg)}} - E^\circ_{\text{Li}}$; and eq 1 can then be used to calculate an activity coefficient value from each experimental measurement.

Figure 1 shows the extrapolation to zero concentration. If the solutions are regular, a linear extrapolation function is appropriate, and the three sets of measurements in series 1 do give a linear extrapolation. Series 2 did not contain enough low-concentration points for a separate extrapolation but appears to be consistent with series 1. The extrapolated value of Y was 14.269 ($\Delta E^\circ = 0.8440$ V) for series 1A and 1C, and 14.274 ($\Delta E^\circ = 0.8443$ V) for series 1B. For series 2, ΔE° was assumed to be 0.8440 V. Activity coefficients calculated using eq 1 are listed in Table I and plotted in Figure 2.

We have also determined the concentration of lithium in a saturated amalgam at $26.0 \pm 0.2^\circ$ by interpolating the potential-concentration curve at high concentrations. The circles in Figure 3 are experimental data from series 2A and 2B. The curve is the shape predicted by eq 1 using the activity coefficients as shown in Figure 2. The intersecting horizontal line

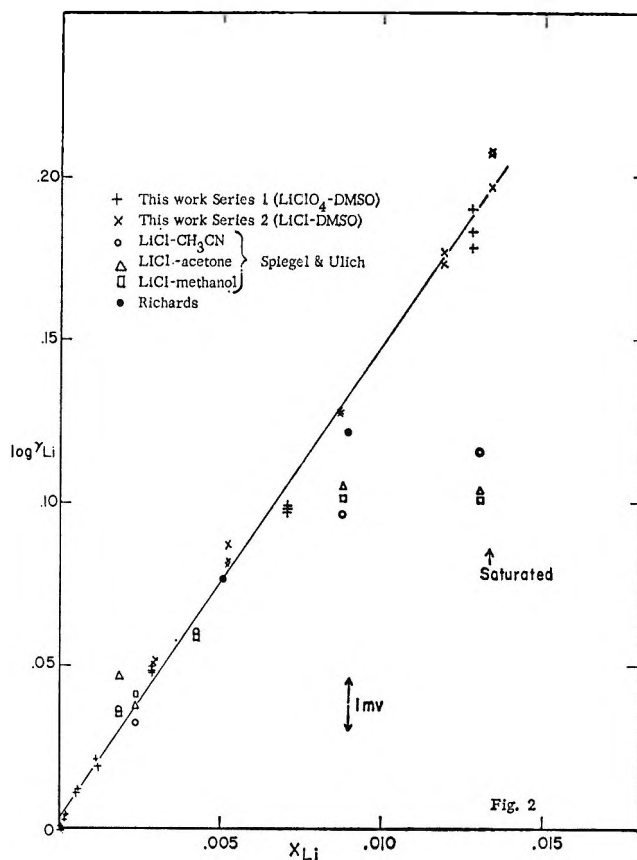


Figure 2.

represents the constant potential of a saturated amalgam. The point of intersection is the concentration of lithium in the saturated liquid phase: $X_{Li} = 0.0133$.

Discussion

The results of our measurements are compared with those of previous workers in Figure 2. Although the data of Spiegel and Ulich³ agree with our results at $X_{Li} < 0.005$, their results are substantially lower than ours at higher concentrations. We have also included two points based on a measurement by Richards and Garrod-Thomas⁸ of the potential difference between two lithium amalgams in lithium chloride-pyridine solutions. The lower point ($X_{Li} = 0.005$) was fixed to be consistent with our data, and the upper point ($X_{Li} = 0.009$) was calculated from their observed potential difference. The agreement with our data is good.

From Figure 2, it is clear that the data are adequately represented by a straight line through the origin. However, since there is a firmer theoretical basis for treating

(7) F. D. Rossini, *et al.*, "Selected Values of Chemical Thermodynamic Properties," National Bureau of Standards Circular 500, U. S. Government Printing Office, Washington, D. C., 1952.

(8) T. W. Richards, J. H. Wilson, and R. N. Garrod-Thomas, "Electrochemical Investigation of Liquid Amalgams," Carnegie Institute of Washington, Publication No. 118, 1909, pp 55-57; T. W. Richards and R. N. Garrod-Thomas, *Z. Physik. Chem.*, **72**, 182 (1910).

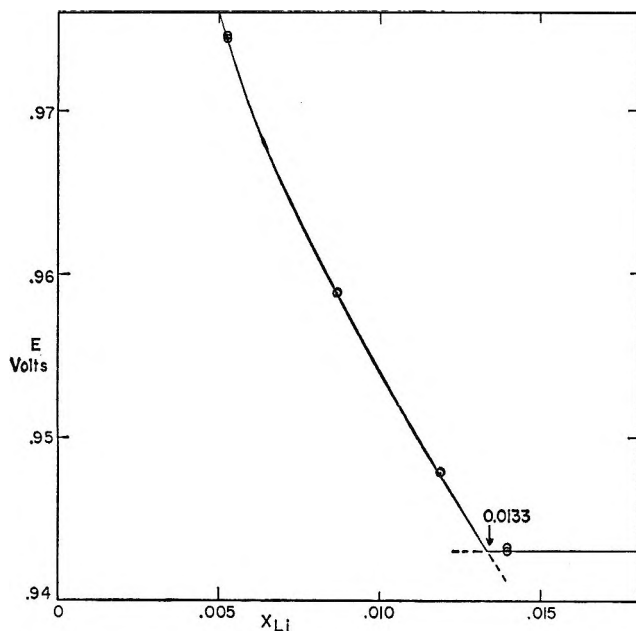


Figure 3.

the results in terms of the theory of regular solutions,⁹ we have made our statistical analysis of the data in terms of the equation

$$\log \gamma_{\text{Li}} = B(1 - X_{\text{Hg}}^2) \quad (3)$$

This is the simplest power-series function which satisfies the Gibbs–Duhem relation. In the concentration range covered by Figure 2, this function deviates by less than 1% from a straight line through the origin.

The 30 points with $X_{\text{Li}} > 0.001$ were fitted to eq 3 by the method of least squares, allowing both the slope and the intercept of the straight line to vary. The intercept obtained at $X_{\text{Li}} = 0$ was $\log \gamma_{\text{Li}} = 0.0033 \pm 0.0030$ (errors are 95% confidence limits), and the slope was $B = 7.3 \pm 0.2$. This is the line drawn in Figure 2. The nonzero intercept implies that our extrapolation was not quite correct and that the values of $\log \gamma_{\text{Li}}$ in Table I should be diminished by approximately 0.003.

An alternative method was also used. We calculated values of B from eq 3 for each of the 30 points and obtained the mean of these values, $B = 8.1 \pm 0.4$. This is significantly larger than the value obtained when the intercept was allowed to vary. A better agreement is obtained if the values of $\log \gamma_{\text{Li}}$ are diminished by 0.0033 and the three points at $X_{\text{Li}} = 0.00001996$ are discarded. These 27 points give $B = 7.4 \pm 0.2$, in good agreement with the results of the first method. Our value of B may be compared with $B = 8.3$ for Na amalgam and $B = 15.4$ for K amalgam.⁴

Since X_{Li} is small, we may summarize our results with no loss in accuracy by an equation of the form

$$\log \gamma_{\text{Li}} = 2BX_{\text{Li}} = (14.6 \pm 0.4)X_{\text{Li}} \quad (4)$$

By the Gibbs–Duhem relation,⁹ we can obtain the

activity coefficient of mercury in the amalgams (reference state, pure Hg)

$$\log \gamma_{\text{Hg}} = (-7.3 \pm 0.2)X_{\text{Li}}^2 \quad (5)$$

The difference in standard potentials between solid lithium and lithium amalgam may be compared with the measurements of Lewis and Keyes.² Their initial value corresponds to $\Delta E^\circ = 0.8412$ V, and they noted that over a period of 4 days the potential decreased by 5 mV. Since this may have been due to transport of lithium through the propylamine solution to the amalgam, their initial value is most probably best, and the true value may be even larger.

Our least-squares analysis indicated that we may have overestimated the extrapolated zero-concentration value of Y , and thus the standard potential difference we obtained ($\Delta E^\circ = 0.8440$) may actually be as low as 0.8438. Since the 95% confidence limits on the intercept of the $\log \gamma_{\text{Li}}$ curve correspond to an error of 0.19 mV in ΔE° , our best estimate of the standard potential difference between solid lithium and lithium amalgam is $\Delta E^\circ = 0.8438 \pm 0.0002$. This corresponds to a standard free energy of the reaction



$\Delta G^\circ = -19.459 \pm 0.005$ kcal/mole (standard state of the amalgam: hypothetical ideal solution at unit mole fraction).

The standard entropy and enthalpy of this reaction can be calculated from the temperature coefficient of the cell used by Lewis and Keyes.² At $X_{\text{Li}} = 0.0100$, their data give $dE/dT = 0.317 \pm 0.005$ mV/deg. Using eq 1 and our activity coefficient values, this gives $\Delta S^\circ = 1.18 \pm 0.12$ eu. Combining this with the standard free energy given above, we obtain $\Delta H^\circ = -19.81 \pm 0.04$ kcal/mole, which is in agreement with published values.^{4,7,10}

Our measurement of the solubility of lithium in mercury at 26° (1.33 mole %) is in agreement with the value (1.34 mole %) determined by Smith and Bennett,¹¹ but higher than other values obtained by chemical analysis of saturated amalgams and lower than values obtained by thermal analysis.¹²

Acknowledgment. This research was supported by the U. S. Air Force Cambridge Research Laboratories, Office of Aerospace Research, under Contract AF 19-(628)-5525, but does not necessarily reflect endorsement by the sponsor.

(9) J. H. Hildebrand and R. L. Scott, "The Solubility of Nonelectrolytes," 3rd ed, Reinhold Publishing Corp., New York, N. Y., 1950.

(10) H. L. Freidman and K. Schug, *J. Am. Chem. Soc.*, **78**, 3881 (1956).

(11) G. M. Smith and H. C. Bennett, *ibid.*, **31**, 804 (1909); **32**, 622 (1910); *Z. Anorg. Allgem. Chem.*, **74**, 172 (1912).

(12) M. Hansen and K. Anderko, "Constitution of Binary Alloys," McGraw-Hill Book Co., Inc., New York, N. Y., 1958.

Dissociation of Lithium and Sodium Salts in Ethereal Solvents

by D. Nicholls, C. Sutphen, and M. Szwarc

Department of Chemistry, State University College of Forestry, Syracuse University, Syracuse, New York 13210
(Received September 8, 1967)

The density, viscosity, and dielectric constant of 2-methyltetrahydrofuran (MeTHF) and tetrahydropyran (THP) were determined over a wide temperature range. The significance of the data is discussed. The conductance of the lithium salts of biphenyl, naphthalene, anthracene, and perylene in THF and the conductance of sodium and lithium tetraphenyl borides in THF and MeTHF have also been investigated over a wide temperature range. The conductance data indicate that in each solvent the Stokes radii of solvent-coordinated free Li^+ and Na^+ ions are nearly the same; however, both are larger in MeTHF than in THF. The dissociation constants of the lithium salts of the aromatic radical anions were found to be essentially independent of the nature of Ar^- and their heats of dissociation were low (-3 to 0 kcal/mol). These observations indicate that the salts form solvent-separated pairs in THF over the whole temperature range. The lithium and sodium tetraphenyl borides were also found to exist as solvent-separated pairs in THF, while in MeTHF it was shown that the proportion of contact ion pairs is significant, particularly in the case of the sodium salt. A comparison of the solvent-separated sodium salts of aromatic radical ions with those of the corresponding lithium salts shows that the latter are 3-4 times less dissociated than the former. This might indicate a higher degree of compressibility of the solvated lithium ion when compared with the sodium ion.

The conductance of various sodium salts has been investigated previously in tetrahydrofuran (THF) and in dimethoxyethane (DME).¹ The present study was initiated with the following aims: (1) to determine the mobilities of alkali cations in THF, 2-methyltetrahydrofuran (MeTHF), and tetrahydropyran (THP), and (2) to determine the heat and entropy of dissociation of sodium and lithium salts in the above solvents, thus gaining insight into the structure of the respective ion pairs in these media. We investigated, therefore, the conductance of the lithium salts of perylene, anthracene, biphenyl, and naphthalene in THF, and lithium and sodium tetraphenyl boride in THF and MeTHF. The attempt to measure conductance in THP was unsuccessful in that the data were irreproducible and could not be used to determine the relevant dissociation constants which seem to be of the order of 10^{-8} to 10^{-9} M. The present data for Na^+ , BPh_4^- in THF agree well with those previously reported.^{1b}

Extensive knowledge of solvent properties is needed for such investigations. The data characterizing THF and DME have been reported elsewhere^{1b} and the respective values for MeTHF and THP are reported here.

Experimental Section

The purification of the solvents² and the techniques used in studying their properties have been fully described.^{1b} The lithium salts of perylene, anthracene, biphenyl, and naphthalene were prepared from the recrystallized hydrocarbons which, with the exception of perylene, were sublimed *in vacuo* before use. Small pieces of lithium were introduced into the reaction vessel under argon and the system was evacuated and sealed off. The surface of the metal was

scaled by treating it with a THF solution of the appropriate hydrocarbon. The reacted solution was decanted from the shiny metal into a side ampoule and the pieces washed by condensing on them the solvent distilled from this ampoule. Thereafter, a fresh THF solution of the same hydrocarbon was contacted with the clean metal surface for 10-15 min. Only a fraction of hydrocarbon reacted and, therefore, the decanted solution contained the radical anions together with an excess of hydrocarbon, but free of dianions.

The conductance was measured using the technique described in ref 1. The measurements were performed in the temperature range -75 to 25° . All these operations, as well as the previously described preparations, were performed under high vacuum in all-glass equipment with break-seals instead of stopcocks.

The concentrations of the lithium salts of the aromatic hydrocarbons were determined spectrophotometrically.^{1c} The respective extinction coefficients were assumed to be the same for the lithium and sodium salts, and the pertinent data justifying this assumption are listed in Table I where similar data of Hoijtink³ are also included. Consideration of these data suggests that the extinction coefficients of the lithium salts do not differ by more than 5-6% from those of the respec-

(1) (a) D. N. Bhattacharyya, C. L. Lee, J. Smid, and M. Szwarc, *J. Phys. Chem.*, **69**, 608 (1965); (b) C. Carvajal, K. J. Tolle, J. Smid, and M. Szwarc, *J. Amer. Chem. Soc.*, **87**, 5548 (1965); (c) P. Chang, R. V. Slaters, and M. Szwarc, *J. Phys. Chem.*, **70**, 3180 (1966).

(2) C. Geacintov, J. Smid, and M. Szwarc, *J. Amer. Chem. Soc.*, **84**, 2508 (1962).

(3) (a) P. Balk, G. J. Hoijtink, and J. W. H. Schreurs, *Rec. Trav. Chim.*, **76**, 813 (1957); (b) G. J. Hoijtink and P. J. Zandstra, *Mol. Phys.*, **3**, 376 (1960); (c) K. H. J. Buschow, J. Dieleman, and G. J. Hoijtink, *ibid.*, **7**, 1 (1963).

Table I

Radical anion in THF (25°)	λ_{\max} , m μ		Our data ^a ϵ (decimal) for the sodium salt	Hojtink's data		Ref
	Na ⁺	Li ⁺		λ_{\max}	ϵ (decimal)	
Anthracene ^{·-}	658	657	7,000	662(Na ⁺ , 25°)	7,250	3a
				667 ^b (Na ⁺ , -180°)	6,870	3b
Perylene ^{·-}	577	580	59,500	581(Na ⁺ , 25°)	43,000 (?)	3a
				590 ^b (Na ⁺ , -180°)	57,500	3b
Biphenyl ^{·-}	400	407	38,000	400 ^b (Li ⁺ , 25°)	36,500	3c
Naphthalene ^{·-}	323	325	16,000	324(Na ⁺ , 25°)	15,500	3a
				329 ^b (Na ⁺ , -180°)	15,800	3b

^a The extinction coefficients of sodium and lithium perylene^{·-} were redetermined by introducing a known amount of stearic acid to their solutions and measuring the decrease in the respective optical densities. The results show that within 6% the extinction coefficients were the same. At $\lambda_{\max} = 577$ m μ , $\epsilon = 60,000$ for perylene^{·-}, Na⁺ and at $\lambda_{\max} = 580$ m μ , $\epsilon = 63,000$ for perylene^{·-}, Li⁺.

^b In 2-methyltetrahydrofuran solution.

tive sodium salts. If this difference is real the corresponding values of Λ_0 would be higher by 5-6%.

Solutions of lithium and sodium tetraphenyl borides were prepared by the gravimetric rather than the volumetric dilution technique. Some experimental difficulties were encountered in determining the conductance of these salts in the lowest concentration range (10^{-6} to 10^{-5} M). Apparently adsorption of the salts on glass, particularly that of lithium, led to some errors. Consequently, all the conductance measurements were repeated several times, rinsing the glassware with the appropriate dilute solutions to ascertain the reliability of the calculated salt concentrations in the prepared samples. It was also essential to exclude oxygen from solutions of Li⁺, BPh₄⁻, since this compound seemed to oxidize readily. Purified helium, therefore, was bubbled through the solvent prior to preparing the solution.

The method used in determining conductance is given in ref 1. Fuoss plots (*viz.*, F/Λ vs. $c\Delta f^2/F$) involving the values of Λ_0 determined from Ostwald plots were used to find initial values of Λ_0 . The values of Λ_0 thus obtained were plotted in the form of $\eta\Lambda_0$ vs. $1/T$ and the "smoothed" values, derived from such plots, were used in the calculations of the corrected Fuoss plot and of K_{diss} .

Characterization of the Solvents

Properties of MeTHF and THP are given in Tables II and III. The latter solvent freezes at about -45° and, therefore, the respective data could not be extended to lower temperatures. The lower density of MeTHF as compared with THF indicates a poorer packing of MeTHF molecules, probably because of their lower symmetry. Nevertheless, the thermal expansion coefficients of both liquids are remarkably similar. As expected, the dielectric constant and its temperature coefficient ($\partial \ln \epsilon / \partial \ln T$) are lower for MeTHF than for THF.

Table II: Physical Properties of 2-Methyltetrahydrofuran (MeTHF)^a

T, °C	d, g/cm ³	10 ³ η , P	ϵ
25.0	0.848	4.57	6.24
10.0	0.862	5.36	6.63
0.0	0.871	6.01	6.92
-10.0	0.880	6.80	7.22
-20.0	0.889	7.77	7.55
-30.0	0.898	8.98	7.91
-40.0	0.908	10.51	8.30
-50.0	0.917	12.47	8.72
-60.0	0.926	15.04	9.19
-70.0	0.935	18.47	9.70
-75.0	0.940	20.63	9.97

^a $d \ln \epsilon / d \ln T = -1.125$; $\epsilon = -1.14 + (2200/T)$; $d \ln v / dT = \alpha = 0.00109 \text{ deg}^{-1}$; $\log \eta = -3.635 + (386/T)$.

Table III: Physical Properties of Tetrahydropyran (THP)^a

T, °C	d, g/cm ³	10 ³ η , P	ϵ
25	0.878	7.64	5.61
20	0.883	8.26	5.71
10	0.892	9.73	5.90
0	0.901	11.61	6.12
-10	0.910	14.03	6.35
-20	0.919	17.21	6.59
-30	0.928	21.48	6.86
-40	0.938	27.31	7.15
-45	0.942	31.05	7.30

^a $d \ln \epsilon / d \ln T = -0.97$; $\epsilon = 0.11 + (1640/T)$; $d \ln v / dT = \alpha = 0.00104 \text{ deg}^{-1}$; $\log \eta = -4.10 + (591/T)$.

The density of THP is higher than that of the isomeric MeTHF; in fact, the former is comparable to that of THF. In its flow properties, THP resembles dioxane, both liquids being much more viscous than THF, MeTHF, or DME. The nonplanar chair con-

formation of THP molecules probably leads to substantial stacking in the liquid which accounts for the observed high viscosity and its high activation energy (2.7 kcal/mol for THP, as compared with 1.8 kcal/mol for THF and MeTHF). In spite of their isomerism, $\epsilon_{25} = 5.61$ for THP, whereas its value is 6.24 for MeTHF. Even more significant is the low temperature coefficient of the dielectric constant, *viz.*, $-\partial \ln \epsilon / \partial \ln T = 0.97$. The relevant coefficients for MeTHF and THF have higher values, *viz.*, 1.125 and 1.16, respectively. The relevant data for THF are given in ref 1b.

Conductance of the Lithium Salts of Radical Ions Derived from Perylene, Anthracene, Naphthalene, and Biphenyl in THF

The plots of $\eta\Lambda_0$ vs. $1/T$ are given in Figure 1 for Li^+ , naphthalene \cdot^- , Li^+ , anthracene \cdot^- , and Li^+ , perylene \cdot^- . The maximum experimental scatter of the initial values of Λ_0 is within 10% and it seems likely, therefore, that the smoothed values of Λ_0 are reliable within 5% in all cases.

The lithium salts decompose slowly in tetrahydrofuran, but it seems that the products of decomposition did not affect our results. To ascertain this point, we determined the conductance of lithium anthracene twice, using independently prepared solutions, and the agreement between these two sets of data was most satisfactory (within 5%). The same conclusion was drawn from the studies of the conductance of lithium perylene. The conductance of a series of solutions was measured consecutively as the concentration was decreased. In the course of these determinations, the lithium salt was partially destroyed by spontaneous reaction with the solvent. Thereafter, the solution was concentrated and the conductance redetermined. The results agreed with the previous set of data within 2%, indicating no discernible effect of the products of decomposition on the conductance.

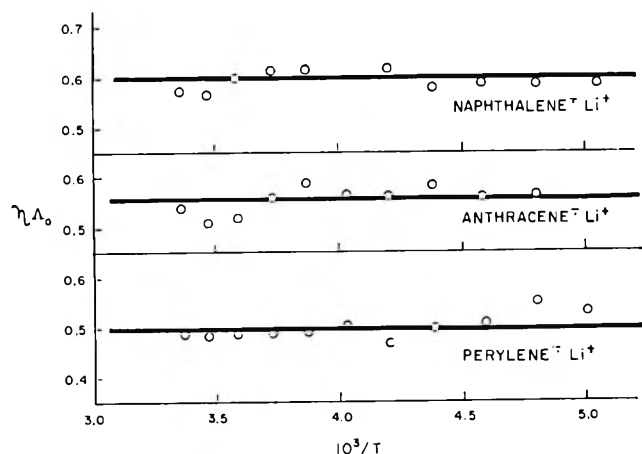


Figure 1. Plots of the Walden product of lithium salts of radical ions in THF vs. $1/T$.

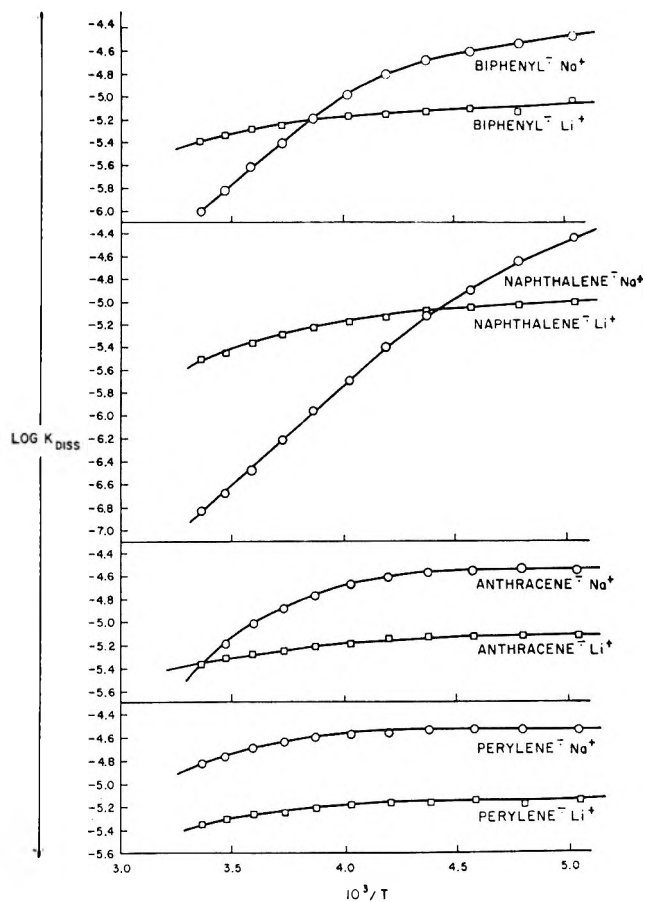


Figure 2. Plots of $\log K_{\text{diss}}$ vs. $1/T$ for salts of radical ions in THF.

Comparison of the smoothed Λ_0 's obtained for the lithium and sodium salts of perylene \cdot^- , anthracene \cdot^- , and naphthalene \cdot^- show that they are virtually identical (see Table IV), indicating that in THF $\lambda_0^+(\text{Na}^+) = \lambda_0^+(\text{Li}^+)$, contrary to the earlier findings from this laboratory.^{1a} This identity was shown to be valid in the temperature range -60 to 25° .

Table IV: Comparison of Λ_0 (cm^2/ohm) for Sodium and Lithium Salts in THF at 25°

Radical ion	$\Lambda_0(\text{Na}^+ \text{ Ar}\cdot^-)^a$	$\Lambda_0(\text{Li}^+ \text{ Ar}\cdot^-)$
Perylene \cdot^-	106	107 ± 5
Anthracene \cdot^-	120	121 ± 6
Naphthalene \cdot^-	128	129 ± 6

^a Obtained from ref 1c.

The large degree of destruction of lithium biphenyl in solutions more dilute than $5 \times 10^{-5} M$ made it impossible to obtain points at lower concentrations. Consequently, the lack of data prevented an accurate determination of the relevant Λ_0 's. In the computation of Fuoss plots, it was assumed, therefore, that $\Lambda_0(\text{B}\cdot^-)$,

Table V: Dissociation Constants of Lithium Salts of Radical Ions in THF^{a,b}

T, °C	Biphenyl ^{•-} , Li ⁺		Naphthalene ^{•-} , Li ⁺		Anthracene ^{•-} , Li ⁺		Perylene ^{•-} , Li ⁺	
	Slope of Fuoss line	10 ⁶ K _{diss} , M	Slope of Fuoss line	10 ⁶ K _{diss} , M	Slope of Fuoss line	10 ⁶ K _{diss} , M	Slope of Fuoss line	10 ⁶ K _{diss} , M
25	13.5	4.2	19.1	3.1	15.7	4.4	19.3	4.5
15	14.8	4.7	19.7	3.8	17.0	4.95	21.3	5.0
5	16.8	5.3	21.3	4.3	19.8	5.3	24.9	5.4
-5	19.8	5.6	23.2	5.2	23.7	5.6	29.9	5.7
-15	22.4	6.5	25.5	6.0	27.5	6.3	36.4	6.1
-25	28.4	6.8	30.6	6.7	37.3	6.2	46.3	6.4
-35	37.0	7.0	37.3	7.4	43.7	7.2	57.8	7.0
-45	48.5	7.6	40.7	8.2	61.0	7.2	82.0	6.8
-55	66.2	8.0	62.1	9.0	115	7.0
-65	103	7.6 (?)	87.7	9.4	133	7.1	189	6.4 (?)
-75	135	9.0	127	10.3	263	7.1

^a The supporting data necessary in calculation of Fuoss plots are given in ref 4. ^b The calculated dissociation constants are reliable within 10–15%.

Table VI: Heats (kcal/mole) and Entropies (cal/deg) of Dissociation of Lithium and Sodium Salts of Radical Ions in THF^a

	Biphenyl ^{•-}		Naphthalene ^{•-}		Anthracene ^{•-}		Perylene ^{•-}	
	Li ⁺	Na ⁺	Li ⁺	Na ⁺	Li ⁺	Na ⁺	Li ⁺	Na ⁺
ΔH(15°)	-2.5	-7.3	-2.8	-8.2	-1.9	-6.1	-1.4	-2.2
ΔS(15°)	-33	-52	-35	-58	-31	-45	-29	-29
ΔH(-65°)	-0.4	-1.6	-0.5	-1.8	0.0	0.0	0.0	0.0
ΔS(-65°)	-26	-28	-26	-30	-24	-21	-24	-21

^a ΔH values are reliable within 0.3–0.5 kcal/mol, the corresponding ΔS values within 1–2 eu.

Li⁺) = Λ₀(B^{•-}, Na⁺). The final calculations led us to the values of the respective dissociation constants given in Table V and presented graphically in Figure 2. The calculated heats and entropies of dissociation are given in Table VI, together with the corresponding data for the sodium salts.

The striking equality of the Λ₀'s derived for the respective lithium and sodium salts is most significant. It proves that the mobilities of the Li⁺ and Na⁺ ions in tetrahydrofuran are almost identical, *i.e.*, the solvated ions have almost the same Stokes radii. Experimental determination of Λ₀ in ethereal solvents is difficult and an error of 5% is not uncommon. Hence the errors in λ₀⁻ and λ₀⁺ may be of the order of 10–20%. However, our present work permits us to claim that λ₀⁺(Li⁺) = λ₀⁺(Na⁺) within 5%, since we compare a series of lithium and sodium salts with common anions.

The lithium salts in solvents of low dielectric constant might be agglomerated. This appears not to be the case for the salts of the investigated aromatic radical ions in tetrahydrofuran. A typical Fuoss plot shown in Figure 3 demonstrates that the linear relation between F/Λ and cΔF²/F is well obeyed in the concentration range 10⁻³ to 7 × 10⁻⁶ M. This should not be the case if the dissociation is represented by the equation

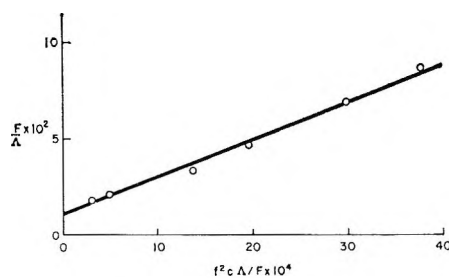
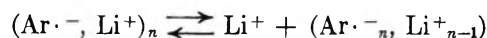


Figure 3. A typical Fuoss plot; Li⁺, anthracene^{•-} in THF at +5°.

Alternatively, one could argue that the dissociation of agglomerates follows the equation



but then the value of Λ₀ for A^{•-}, Li⁺ should be substantially smaller than the respective Λ₀ of A^{•-}, Na⁺, contrary to our observation. There is no evidence whatsoever for any aggregation of sodium salts, and the remarkable agreement between the Λ₀ values of the lithium and the corresponding sodium salts shown in Table IV implies that the transport in both systems is due to single ions.

The dissociation constants of the sodium salts of radical anions were shown to be virtually independent

of the nature of the anion if the pair is of the solvent-separated type.^{1c} This is illustrated by the data obtained in dimethoxyethane and by those in tetrahydrofuran at low temperatures. The heat of dissociation of such pairs is low, *viz.*, between 0 and -2 kcal/mol. Our present results show the same behavior for the lithium salts in tetrahydrofuran. As may be seen from the data given in Tables V and VI, the dissociation constants of all the lithium salts are virtually identical and their heats of dissociation are all low. We conclude, therefore, that the lithium salts in tetrahydrofuran are virtually solvent separated, at least at temperatures below 25° .

Our present data rationalize the observations of Hoijtink, *et al.*,⁴ who found the conductance of a 10^{-4} M solution of lithium anthracene to decrease monotonically with decreasing temperature. The temperature coefficient of conductance is given by $E_\eta + \frac{1}{2}\Delta H_{\text{diss}}$, and for anthracene \cdot^- , Li $^+$ in THF, its value increases from 0.9 kcal/mol at 15° to about 1.8 kcal/mol at -65° .

The relation between the dissociation constants of the sodium and lithium salts in tetrahydrofuran may be seen from inspection of Figure 2. The sodium salts of naphthalene \cdot^- and biphenyl \cdot^- form contact pairs at higher temperatures ($-\Delta H$ is high) and, consequently, the respective dissociation constants are lower than those of the corresponding lithium salts. A smaller fraction of contact pairs present at temperatures above 25° may account for the behavior of anthracene \cdot^- , Na $^+$. Under conditions when the solvent-separated pairs dominate, the lithium salts are less dissociated than the sodium salts. Since the solvated free Na $^+$ and Li $^+$ ions are approximately of the same size, our observation tentatively indicates that the solvation shell of the lithium ion is more compressible than that of the sodium ion. It is also possible that the solvated lithium ion is slightly smaller than the sodium cation, since a difference of, say, 0.2 Å in the Stokes radii might not be detectable in values of Λ_0 which are uncertain within 5%. This is plausible, since the unsolvated Li $^+$ cation is smaller than the Na $^+$ cation. It is obvious, however, from the dissociation constants and the respective ΔS values that the solvated lithium ion cannot be larger than the sodium cation.

The conductance data for Ar \cdot^- , Li $^+$ are in good agreement with those reported for lithium fluorenyl in tetrahydrofuran.⁵ This may be seen from Table VII. The slightly higher $-\Delta H_{\text{diss}}$ found for the fluorenyl salt could be expected; the more localized negative charge in fluorenyl carbanion when compared with anthracene \cdot^- should lead to a higher proportion of the contact pairs in the former case. Hence, the dissociation constant at 25° of fluorenyl lithium should be lower than that of lithium anthracene, in agreement with the observations. These results suggest, therefore, that fluorenyl lithium is not agglomerated in tetrahydrofuran, contrary to recent claims.⁶

Table VII: $10^6 K_{\text{diss}} (M)$

$T, ^\circ\text{C}$	Li $^+$, fluorenyl $^-$		Li $^+$, anthracene \cdot^-
25	3.9 ^a	1.7 ^b	4.5
0	6.6 ^a	2.9 ^b	5.5
-30	12 ^a	5.2 ^b	6.7
-60	19 ^a	8.6 ^b	7.2

^a The original results, calculated on the basis of the assumed $\Lambda_0 = 88.4$ at 25° . ^b The recalculated values, based on the $\Lambda_0 = \Lambda_0(\text{anthracene}\cdot^-, \text{Li}^+) = 121$ at 25° . In view of similar sizes of A \cdot^- and fluorenyl, this identity is plausible.

Conductance of Li $^+$, BPh $_4^-$, and of Na $^+$, BPh $_4^-$ in THF and MeTHF

The values of Λ_0 and K_{diss} of Li $^+$, BPh $_4^-$ in THF and MeTHF are given in Table VIII, and the corresponding data for Na $^+$, BPh $_4^-$ are given in Table IX.

In view of the difficulties discussed previously, some of the quoted Λ_0 's may be uncertain within 15%. It is desirable, therefore, to look for some regularities which could indicate the reliability of these data. Indeed, one notes a monotonic change with temperature of the ratios $(\Lambda_{07})_{\text{THF}} : (\Lambda_{07})_{\text{MeTHF}}$ both for the lithium and sodium salts (see the last columns of Tables X and XI). Stokes radii of the solvent-coordinated free Na $^+$ and Li $^+$ ions appear to be similar, confirming our previous observations. In THF, the Na $^+$ cation seems to be slightly larger (6–7%) than the Li $^+$ ion, whereas the relation appears to be reversed (–5%) in MeTHF. These deviations may reflect the experimental uncertainty. Both ions appear to be larger in MeTHF than in THF. This is plausible; the coordination shell is expected to be larger when MeTHF replaces THF.

Most interesting are the data dealing with the heats of dissociation of the respective ion pairs. The dissociation constants, determined at various temperatures,

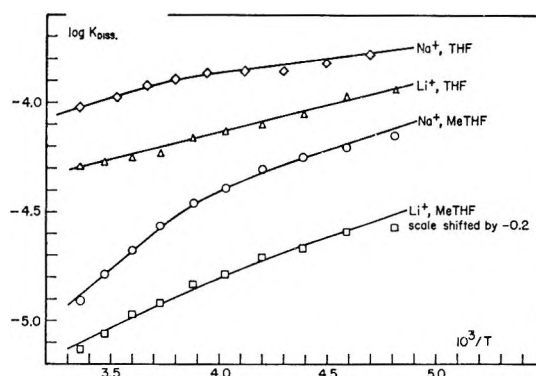


Figure 4. Dissociation of tetraphenyl borides.

(4) K. H. J. Buschow, J. Dieleman, and G. J. Hoijtink, *J. Chem. Phys.*, **42**, 1993 (1965).

(5) T. E. Hogen-Esch and J. Smid, *J. Amer. Chem. Soc.*, **88**, 318 (1966).

(6) T. E. Hogen-Esch and J. Smid, *ibid.*, **89**, 2764 (1967).

Table VIII: Dissociation Constant of Li^+ , BPh_4^- ^a

$T, ^\circ\text{C}$	THF			MeTHF			$K_{\text{diss}}(\text{THF}) : K_{\text{diss}}(\text{MeTHF})$
	Λ_0 , cm^2/ohm equiv	Slope	$10^6 K_{\text{diss}}$, M	Λ_0 , cm^2/ohm equiv	Slope	$10^6 K_{\text{diss}}$, M	
25.0	90	2.39	5.1	77	14.6	1.2	4.4
15.0	82	2.86	5.3	68	15.1	1.4	3.7
5.0	73	3.34	5.8	60	16.5	1.7	3.3
-5.0	64	4.14	6.0	52	19.0	1.9	3.0
-15.0	56	4.64	6.9	45	21.2	2.3	3.0
-25.0	48	5.80	7.5	38	25.8	2.6	2.8
-35.0	41	7.55	8.0	32	31.4	3.1	2.6
-45.0	34	10.05	8.8	26	41.2	3.5	2.5
-55.0	28	12.0	10.8	21	52.8	4.1	2.6
-65.0	22	17.5	11.5	17	80.2	4.3	2.7

^a Λ_0 values reliable within 15%; K_{diss} values within 30%. The variations in K_{diss} are more reliable than its absolute value.

Table IX: Dissociation Constant of Na^+ , BPh_4^- ^a

$T, ^\circ\text{C}$	THF			MeTHF			$K_{\text{diss}}(\text{THF}) : K_{\text{diss}}(\text{MeTHF})$
	Λ_0 , cm^2/ohm equiv	Slope	$10^6 K_{\text{diss}}$, M	Λ_0 , cm^2/ohm equiv	Slope	$10^6 K_{\text{diss}}$, M	
25	86	1.52	8.8	80	12.5	1.2	7.1
15	76	1.73	10.0	71	12.0	1.6	6.1
5	67	2.00	11.0	63	12.0	2.1	5.2
-5	59	2.38	12.0	55	12.2	2.7	4.4
-15	52	2.85	13.2	47	12.8	3.5	3.8
-25	44	3.56	14.4	40	15.2	4.0	3.5
-35	38	4.47	15.5	34	17.4	5.0	3.1
-45	32	5.88	16.6	28	22.6	5.6	2.9
-55	26	11.5	17.0	23	31.0	6.3	2.7
-65	20	15.4	16.2	18	43.5	7.0	2.3

^a Λ_0 values reliable within 15%; K_{diss} within 30%. The variations in K_{diss} are more reliable than its absolute value.

Table X: Walden Products, Λ_{07} , of Li^+ , BPh_4^- ^a

$T, ^\circ\text{C}$	THF	MeTHF	Ratio
25	0.417	0.350	1.19
15	0.418	0.345	1.21
5	0.417	0.339	1.23
-5	0.415	0.332	1.25
-15	0.412	0.326	1.27
-25	0.408	0.319	1.28
-35	0.403	0.311	1.29
-45	0.396	0.302	1.31
-55	0.390	0.294	1.33
-65	0.382	0.284	1.35

^a Ratio (25°/-65°): THF, 1.09; MeTHF, 1.23.

Table XI: Walden Products, Λ_{07} , of Na^+ , BPh_4^- ^a

$T, ^\circ\text{C}$	THF	MeTHF	Ratio
25	0.397	0.367	1.08
15	0.389	0.362	1.08
5	0.387	0.356	1.09
-5	0.383	0.350	1.10
-15	0.381	0.343	1.11
-25	0.376	0.336	1.12
-35	0.377	0.328	1.15
-45	0.375	0.320	1.17
-55	0.365	0.310	1.18
-65	0.343(?)	0.300	1.14(?)

^a Ratio (25°/-65°): THF, 1.16; MeTHF, 1.23.

are listed in Tables VIII and IX, and the plots of $\log K_{\text{diss}}$ vs. $1/T$ are shown in Figure 4. The heats of dissociation in THF are -1.2 ± 0.9 kcal/mol for Li^+ , BPh_4^- and -1.3 ± 0.9 kcal/mol (decreasing, however, at lower temperatures) for Na^+ , BPh_4^- . This implies that both ion pairs are solvent separated, being coordinated with THF, and dissociate into THF

coordinated alkali ions. Hence, the entropies of dissociation should be relatively small; in fact, they are -24 and -23 eu, respectively. In MeTHF the heat of dissociation of the lithium salt is also relatively low, *viz.*, -2.2 ± 0.9 kcal/mol, the exothermicity being higher than in THF only by 0.9 kcal/mol. However, a substantial increase of exothermicity is

observed for the sodium salt, *viz.*, $\Delta H = -3.8 \pm 0.9$ kcal/mol, decreasing to somewhat lower values at -70° . Apparently, the degrees of solvent coordination of the Li^+ , BPh_4^- pair and Li^+ free ions are still comparable in MeTHF. The larger Na^+ ion, which also appears to be coordinated by MeTHF when free, associates into a noncoordinated, contact Na^+ , BPh_4^- ion pair. The latter becomes gradually more solvated as temperature decreases, this being reflected in the

respective value of ΔH (see Figure 4). The decrease of the value of $-\Delta H$ at lower temperatures is a general phenomenon observed in many other systems.¹

Acknowledgment. We wish to acknowledge financial support of this investigation to the National Science Foundation, to the United States Air Force (Contract AF 33(615)-3788), and to the Petroleum Research Fund (Grant 2475-C) administered by the American Chemical Society.

Gas-Phase Radiolysis of Benzene

by Robert R. Hentz and Stefan J. Rzad

Department of Chemistry and the Radiation Laboratory,¹ University of Notre Dame, Notre Dame, Indiana 46556 (Received September 11, 1967)

The γ radiolysis of benzene vapor was studied at room temperature as a function of pressure (5–80 torr), dose, dose rate, and added NO and N_2O . $G(-\text{C}_6\text{H}_6)$ and the yields and variety of ring-fragmentation products are considerably greater than in radiolysis of the liquid. At pressures greater than ~ 60 torr, product yields are independent of pressure. At 66 torr, values of $G(\text{H}_2) = 0.11$ and $G(\text{C}_2\text{H}_2) = 0.63$ are obtained which are independent of dose, dose rate, and the presence of NO or N_2O . It is concluded that, at >60 torr, H_2 and C_2H_2 are not formed *via* free-radical or ion-neutralization reactions, but are formed by molecular elimination from either superexcited states or ion-molecule reactions of C_6H_6^+ with C_6H_6 or both. G values of the following products also were studied: CH_4 , C_2H_4 , propadiene, butadiyne, cyclohexene, cyclohexadienes, biphenyl, and dihydrobiphenyls. The yields of all such products show, in addition to a pressure dependence below ~ 60 torr, a dependence on certain of the other radiolysis variables; free radicals or secondary ions or both are involved at some stage in their formation. At the lowest dose studied, except for $G(\text{biphenyl}) = 0.17$, all such products are formed with $G < 0.1$. At a total pressure of 66 torr, radiolysis of benzene in the presence of N_2O yields N_2 and phenol in a 2:1 ratio; $G(\text{N}_2) = 13.3$ at 10 mol % N_2O appears to require some kind of short-chain mechanism.

Introduction

Considerable attention has been devoted to study of the radiation chemistry of benzene in the liquid phase.² However, no detailed study of the gas-phase radiolysis has been published, although several authors have reported G values for a few products under a specific set of conditions.^{3–6} Indeed, isopropylbenzene appears to be the only aromatic hydrocarbon whose gas-phase radiolysis has been studied in any detail.⁷ The present study of benzene radiolysis in the gas phase was undertaken for comparison with a recently completed study of the gas-phase photolysis of benzene with the Xe and Kr resonance lamps.⁸ Such a comparison is of interest because negligible ionization of benzene occurs with the Xe lamp, while the Kr lamp produces ionization in benzene with a quantum efficiency of $\sim 60\%$.⁹

Experimental Section

Materials. The benzene used was Fisher Certified Reagent; it was purified with an Aerograph Autoprep

Model A 700 using a $3/8$ -in. \times 12-ft column which was packed with 20 wt % β, β' -oxydipropionitrile on 60–80 mesh Chromosorb W and operated at 70° . Benzene of purity better than 99.99 mol % was obtained. Nitrous oxide and nitric oxide, obtained from Matheson, were purified by low-temperature distillation.

(1) The Radiation Laboratory of the University of Notre Dame is operated under contract with the U. S. Atomic Energy Commission. This is AEC Document No. COO-38-542.

(2) For a summary of the results of such studies, see E. A. Cherniak, E. Collinson, and F. S. Dainton, *Trans. Faraday Soc.*, **60**, 1408 (1964).

(3) J. P. Manion and M. Burton, *J. Phys. Chem.*, **56**, 560 (1952).

(4) V. P. Henri, C. R. Maxwell, W. C. White, and D. C. Peterson, *ibid.*, **56**, 153 (1952).

(5) P. Huyskens, P. Claes, and F. Cracco, *Bull. Soc. Chim. Belges*, **68**, 89 (1959).

(6) L. M. Theard, *J. Phys. Chem.*, **69**, 3292 (1965).

(7) R. R. Hentz, *ibid.*, **66**, 1622 (1962).

(8) R. R. Hentz and S. J. Rzad, *ibid.*, **71**, 4096 (1967).

(9) J. C. Person, *J. Chem. Phys.*, **43**, 2553 (1965).

Procedures. Spherical flasks of 220 ml volume were used as irradiation cells; each flask was fitted with a tube for sample introduction, a break-seal, and a small-bore Pyrex tube for liquid-product condensation. Prior to sample introduction, the cells were evacuated to 10^{-6} torr on a mercury-free vacuum line for ~ 16 hr, with periodic heating by means of a hand torch; evacuation was continued until no increase in pressure was indicated by the vacuum gauge after a long heating period.

A storage bulb containing 20 ml of the pure benzene was joined to the vacuum line *via* a Hoke bellows valve; the benzene was degassed by the microstill-reflux method.¹⁰ The gases were admitted to the desired pressure into a calibrated volume and then condensed into the cold finger of the cell at 77°K or, at the higher pressures, were admitted to the desired pressure directly into the cell. Pressures were measured at room temperature ($\sim 23^\circ$) with a Bourdon tube gauge obtained from Wallace and Tiernan, Inc.

Samples were irradiated at room temperature in the Notre Dame 10-kc ^{60}Co facility. Dose rates to benzene were determined by use of the ethylene dosimeter, $G(\text{H}_2) = 1.28$ for the radiolysis of ethylene at 1 atm,¹¹ and application of a correction for the electron density of benzene relative to ethylene. Baily and Brown¹² have obtained the following empirical equation for the stopping power per electron of an element of atomic number Z relative to that of air for the electronic-equilibrium spectrum of ^{32}P : $S = 1.296 - 0.1372 \ln Z$. Use of this equation gives $S(\text{C}_6\text{H}_6)/S(\text{C}_2\text{H}_4) = 0.977$. On this basis, neglect of the stopping-power ratio, as in this work and that of Theard,⁶ gives dose rates to benzene that are 2.3% high and, correspondingly, G values that are 2.3% low. Unless otherwise specified, samples were irradiated at a dose rate of 1.42×10^{11} eV ml⁻¹ sec⁻¹ torr⁻¹.

After irradiation, the cell was sealed to the vacuum line and, after rupture of the break-seal, gases volatile at 77°K were removed and measured with a standard Toepler pump and gas buret arrangement. These gases then were transferred into a sample bulb for analysis. The radiolysis cell was warmed to room temperature and then was immersed in Dry Ice-acetone for removal of gases volatile at -78° . Measurement of this fraction was made in a calibrated volume on the mass spectrometer with a Consolidated membrane micromanometer. The two volatile fractions were analyzed on a Consolidated 21-103 A mass spectrometer. Identifications and determinations were made by comparison with fragmentation patterns of known amounts of the pure substances.

After removal of the two volatile fractions, the small-bore cold finger of the radiolysis cell was immersed in liquid nitrogen for collection of the condensable fraction while the cell was warmed to $\sim 90^\circ$; after about 1 hr, the cold finger was sealed off. The liquid was analyzed

for cyclohexene and cyclohexadienes with an F & M Model 609 gas chromatograph and for biphenyl, dihydrobiphenyls and phenol (formed in the presence of N_2O) with an F & M Model 810 gas chromatograph; flame-ionization detection was used with both instruments. Cyclohexadienes were analyzed with a 0.25-in. \times 10-ft column packed with 20 wt % of succinate polyester of diethylene glycol on 60-80 mesh Chromosorb P and operated at 60° . Cyclohexene was separated with a 0.25-in. \times 20-ft column packed with 17 wt % β, β' -oxydipropionitrile on 60-80 mesh Chromosorb P and operated at room temperature. Biphenyl, phenol, and dihydrobiphenyls were determined with a 0.25-in. \times 4-ft column which was packed with 9 wt % silicone grease on 60-80 mesh Chromosorb P and operated at 165° .

Results

The effect of dose was studied in radiolysis of benzene vapor at 66 torr from 1.2×10^{19} eV to 1.2×10^{20} eV; for $G(-\text{C}_6\text{H}_6) \approx 5$, 10^{19} eV corresponds to $\sim 0.1\%$ conversion. Results at the two extremes of dose are presented in Table I. The dose-dependent G values are averages of five measurements; the dose-independent values represent averages of about 25 measurements. In all irradiations a pale yellow fine powder (polymer) was deposited on the bottom of the cell.

The effect of dose rate was studied over the range 4.8×10^9 to 1.42×10^{11} eV sec⁻¹ ml⁻¹ torr⁻¹ at 66 torr and a total dose of 4.5×10^{19} eV. Those product yields

Table I: Yields in the Radiolysis of Benzene Vapor at 66 Torr^a

Products	Dose, 10^{19} eV	
	1.2	12
H_2	0.11 ^c	0.11 ^c
CH_4	0.012 ^c	0.012 ^c
C_2H_2	0.63 ^c	0.63 ^c
C_2H_4	0.046 ^c	0.046 ^c
Propadiene	0.041	0.025
Butadiyne	0.093	0.006
Cyclohexene	0.013	0.003
Cyclohexadienes	0.03	0.004
Biphenyl	0.17	0.07
Dihydrobiphenyls	0.006	0.003

^a Dose rate of 1.42×10^{11} eV sec⁻¹ ml⁻¹ torr⁻¹ in 220 ml at 23° . ^b Maximum deviation is ± 0.01 - 0.02 for values given to the second decimal place (± 0.005 for H_2) and ± 0.001 - 0.005 for values given to the third decimal place. ^c The dose-independent G values given are averages of the values obtained at all doses.

(10) W. Van Dusen, Jr., and W. H. Hamill, *J. Am. Chem. Soc.*, **84**, 3648 (1962).

(11) R. A. Back, T. W. Woodward, and K. A. McLaughlan, *Can. J. Chem.*, **40**, 1380 (1962).

(12) N. A. Baily and G. C. Brown, *Radiation Res.*, **11**, 745 (1959).

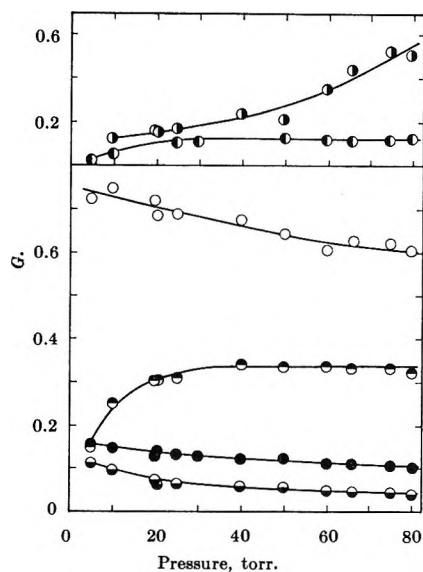


Figure 1. The pressure dependence of yields in the radiolysis of benzene vapor: \circ , $G(\text{C}_2\text{H}_2)$; \bullet , $G(\text{H}_2)$; \ominus , $G(\text{C}_2\text{H}_4)$; \oplus , $G(\text{C}_3\text{H}_4) \times 10$; \otimes , $G(\text{C}_4\text{H}_2) \times 10$; and \odot , $G(\text{biphenyl})$.

found to be dose independent are also independent of dose rate, and those product yields that are dose dependent are also dependent on dose rate. For example, a change in dose rate from the maximum to minimum value of the range, under the specified conditions, produces a decrease in $G(\text{propadiene})$ from 0.033 to 0.023 and in $G(\text{butadiene})$ from 0.044 to 0.010; $G(\text{dihydrobiphenyls})$ increases from 0.004 to 0.010, while the yields of cyclohexene and the cyclohexadienes become too small for measurement at the lowest dose rate.

All product yields are affected as pressure is varied from 5 to 80 torr. Results for gas products and biphenyl are shown in Figure 1 for a dose rate of $1.42 \times 10^{11} \text{ eV sec}^{-1} \text{ ml}^{-1} \text{ torr}^{-1}$ and a constant dose of $4.5 \times 10^{19} \text{ eV}$; for $G(-\text{C}_6\text{H}_6) \approx 5$, conversions correspond to ~ 0.4 and $\sim 6\%$ at 80 and 5 torr, respectively. Yields of the other liquid products behave very similarly to that of biphenyl.

The effect of 7 mol % NO on product yields was determined at a dose of $4.5 \times 10^{19} \text{ eV}$ and a total pressure of 66 torr. G values of H_2 and C_2H_2 are essentially unaffected; $G(\text{C}_3\text{H}_4)$ decreases to 0.021 while the yield of biphenyl is reduced by $\sim 70\%$, and CH_4 , cyclohexene, cyclohexadienes, and dihydrobiphenyls become undetectable. However, $G(\text{C}_2\text{H}_4)$ and $G(\text{butadiene})$ increase to values of 0.27 and 0.18, respectively, and vinylacetylene appears with $G = 0.10$. As in the case of NO addition, at a total pressure of 66 torr and a dose of $4.5 \times 10^{19} \text{ eV}$, the presence of up to 10 mol % N_2O has no effect on the yields of H_2 and C_2H_2 . With the exception of the dihydrobiphenyl yield, which disappears, and the propadiene yield, which remains constant, all other product yields increase with increase in N_2O concentration; the individual yields remain small at 10 mol % N_2O ($G \leq 0.3$) and do not warrant detailed discussion.

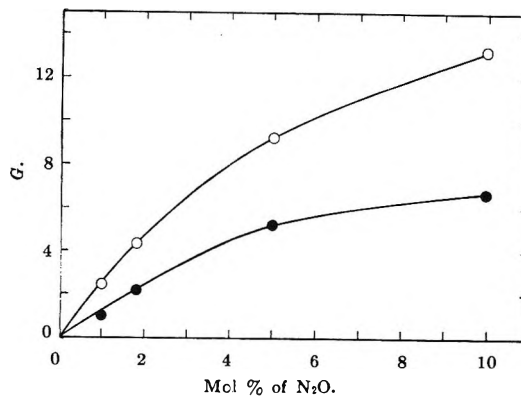


Figure 2. Yields in radiolysis of $\text{C}_6\text{H}_6\text{-N}_2\text{O}$ mixtures at 66 torr: \circ , $G(\text{N}_2)$; and \bullet , $G(\text{C}_6\text{H}_5\text{OH})$.

Of particular interest, however, is the dependence of nitrogen and phenol yields on N_2O concentration, which is shown in Figure 2.

Discussion

Comparison of Vapor and Liquid Radiolyses. The radiation chemistry of benzene vapor is obviously complex, more so than that of the liquid. Because of such complexity and the absence of adequate background information on the various possible elementary processes, a detailed interpretation of the results obtained in radiolysis of benzene vapor is not possible; however certain general conclusions can be drawn from such a study.

In Table II a comparison is presented between yields obtained in previous studies of benzene radiolysis, both in the gas and liquid phase, and the corresponding yields obtained in this work. Examination of Table II reveals that $G(-\text{C}_6\text{H}_6)$ is considerably greater in the gas

Table II: Comparison with Reported Yields in the Radiolysis of Benzene

Product	P, torr			
	66 ^a	1000 ^b	~80 ^c	Liq ^d
	Temp, °C			
	23	100	~25	~25
	G			
H_2	0.11	0.084	0.30	0.039
CH_4	0.012	...	0.01	...
C_2H_2	0.63	0.61	0.42	0.020
C_2H_4	0.046	0.02	0.02	...
$-\text{C}_6\text{H}_6$	(>0.7) ^e	...	4.9	0.8

^a γ Rays (this work). ^b γ Rays (ref 6). ^c α Rays (ref 4).

^d γ Rays and $\sim 1\text{-MeV}$ electrons (ref 2). ^e Calculated from C and H in the measured products of Table I at the lower dose.

than in the liquid phase. $G(-\text{C}_6\text{H}_6) = 4.9$ of Henri, *et al.*,⁴ given in Table II, compares favorably with $G(-\text{C}_6\text{H}_6) = 4.23$ obtained by Huyskens and coworkers⁵ in α radiolysis of benzene vapor at 100° and 400 torr. Our value of $G(-\text{C}_6\text{H}_6) > 0.7$, based only on C and H in

the measured products of Table I, is about equal to the liquid-phase value based on conversion to polymer. Evidently, conversion to polymer of more than two monomer units¹³ represents the predominant mode of benzene disappearance in the vapor as well as in the liquid, but with an approximately sevenfold greater yield in the vapor (assuming approximate equality of γ - and α -radiolysis conversions in the gas phase). Thus, as suggested earlier in study of the gas-phase γ radiolysis of isopropylbenzene,⁷ marked radiation resistance of aromatics relative to aliphatics appears to be characteristic only of the condensed state. For example, compare gas-phase values of $G(-C_6H_6) = 4.9^4$ and $G(-c-C_6H_{12}) = 9^4$ with the liquid-phase values of $G(-C_6H_6) = 0.8^2$ and $G(-c-C_6H_{12}) \approx 8.1^4$. In addition, the comparison of gas and liquid radiolysis in Table II and the results of Table I show that the yields and variety of ring-fragmentation products are considerably greater in the vapor phase; *e.g.*, $G(C_2H_2)$ is enhanced by ~ 30 -fold. A similar effect has been observed in *c*- C_6H_{12} radiolysis.^{6,14,15}

The H_2 and C_2H_2 Yields. The yields of H_2 and C_2H_2 at 66 torr are independent of dose, dose rate, and the presence of NO and N_2O . An estimation using reasonable specific rates indicates that 7% NO, under the conditions employed, should have scavenged all free radicals in competition with addition to benzene or combination. For N_2O as an electron scavenger, Johnson and Warman¹⁶ give $\sqrt{k_c/k_s} = 3 \times 10^{10}$ molecule⁻¹ ml sec⁻¹, in which k_s and k_c are specific rates of the scavenging and ion-electron combination reactions, respectively. Use of such a value indicates that 92% of all electrons should have been scavenged in the experiments with 10% N_2O , which would be expected to affect the yields of products formed in neutralization reactions.¹⁶ Thus, on the basis of the observed insensitivity of H_2 and C_2H_2 yields to the four variables studied at 66 torr (dose, dose rate, and presence of NO or N_2O), it appears that these products are not formed *via* free-radical or ion-neutralization reactions.

With the exception of butadiyne,¹⁷ all product yields seem to approach a plateau with increase in pressure (*cf.* Figure 1), becoming essentially independent of pressure above ~ 60 torr. It is interesting to note that $G(C_2H_2) = 0.60$ and $G(H_2) = 0.10$ at 80 torr, as compared to $G(C_2H_2) = 0.61$ and $G(H_2) = 0.084$ at 1000 torr in the work of Theard⁶ (*cf.* Table II). The decrease in H_2 and C_2H_2 yields to the pressure-independent plateaus attained near 60 torr may be related to suppression of two kinds of primary decomposition processes. One such process involves excited states of benzene that lie below the ionization potential; photolyses of benzene vapor with the Xe resonance lamp⁸ and at 1849 Å¹⁸ indicate that decomposition of such excited states is inhibited by increase in pressure and is considerably suppressed at 66 torr. On the other hand, quantum yields in Kr-lamp photolyses of benzene vapor are in-

dependent of pressure from 1 to 66 torr;⁸ *i.e.*, pressure variation from 1 to 66 torr has no effect on decomposition, with $\phi \approx 0.40$,⁸ of the superexcited states (lying above the ionization potential) produced in Kr-lamp photolysis or on the reactions of $C_6H_6^+$ produced with $\phi_i \approx 0.60$ ⁹ (fragmentation being negligible with the Kr resonance lines). A second process suppressed at higher pressures is parent-ion fragmentation. Acetylene is formed in $\sim 50\%$ of all such fragmentation processes¹⁹ with either 70-eV²⁰ or 1-keV²¹ electrons. By use of the equations of Stevenson,²² derived from the quasi-equilibrium theory of mass spectra, values of 15 and 0% fragmentation of $C_6H_6^+$ are calculated for the time available between collisions at 70 and 760 torr, respectively. The results in Figure 1 suggest that fragmentation may be negligible at 66 torr.

It is possible, then, to draw the following conclusions from all the results for $G(H_2)$ and $G(C_2H_2)$. In gas-phase radiolysis at pressures in excess of ~ 60 torr (as in Kr-lamp photolysis from 1 to 66 torr⁸), the number of possible processes whereby excitation or ionization of a benzene molecule may lead to its chemical conversion is reduced to essentially three: (1) decomposition of superexcited states in competition with ionization, (2) reaction of $C_6H_6^+$ with C_6H_6 ,²³ and (3) decomposition of $C_6H_6^+$ on neutralization.²⁴ The reaction modes and relative yields of processes 1–3 are essentially independent of pressure from 1000 torr (*cf.* results of Theard⁶ in Table II) down to at least 1 torr (as shown in Kr-lamp photolysis⁸). At pressures greater than ~ 60 torr, the products H_2 and C_2H_2 are formed only by molecular elimination in one or both of the processes 1 and 2.

(13) Note that the value of $G(-C_6H_6) = 0.8$ given in ref 2 for radiolysis of the liquid includes a contribution of $G(C_6H_6 \rightarrow \text{dimers}) \approx 0.2$.

(14) Calculated from the results of S. K. Ho and G. R. Freeman, *J. Phys. Chem.*, **68**, 2189 (1964).

(15) J. M. Ramaradhy and G. R. Freeman, *J. Chem. Phys.*, **34**, 1726 (1961).

(16) G. R. A. Johnson and J. M. Warman, *Trans. Faraday Soc.*, **61**, 1709 (1966).

(17) The exceptional behavior of this compound is probably attributable to its lability; *cf.* J. W. Copenhaver and M. H. Bigelow, "Acetylene and Carbon Monoxide Chemistry," Reinhold Publishing Corp., New York, N. Y., 1949, p 303.

(18) K. Shindo and S. Lipsky, *J. Chem. Phys.*, **45**, 2292 (1966); J. K. Foote, M. H. Mallon, and J. N. Pitts, Jr., *J. Am. Chem. Soc.*, **88**, 3698 (1966).

(19) F. H. Field and J. L. Franklin, "Electron Impact Phenomena," Academic Press, Inc., New York, N. Y., 1957.

(20) Based on an average of six patterns reported in "Catalog of Mass Spectral Data," American Petroleum Institute Research Project 44, Thermodynamics Research Center, Texas A & M University, College Station, Texas, 1962.

(21) R. H. Schuler, *Trans. Faraday Soc.*, **61**, 100 (1965).

(22) D. P. Stevenson, *Radiation Res.*, **10**, 610 (1959).

(23) The little information available on ion-molecule reactions in benzene indicates considerable complexity; *cf.* R. Barker, *Chem. Ind. (London)*, 233 (1960), and A. Henglein, *Z. Naturforsch.*, **17a**, 44 (1962).

(24) Because ion-electron combination lifetimes under our conditions are of the order of 10^{-3} sec, neutralization of $C_6H_6^+$ may be precluded by its ion-molecule reactions.

On passage to the liquid state (*cf.* Table II), the reductions in $G(\text{H}_2)$, $G(\text{C}_2\text{H}_2)$, and $G(-\text{C}_6\text{H}_6)$ are attributable to characteristics of the liquid structure which may alter both the nature of the energy deposition process²⁵ (giving rise, *e.g.*, to nonlocalized energy deposition or collective excitations²⁶) and the nature and extent of the decomposition processes.

Other Product Yields. In addition to a pressure dependence below ~ 60 torr, all measured product yields other than those of H_2 and C_2H_2 show a dependence on certain of the other radiolysis variables. Free radicals or secondary ions (formed only in process 2 at higher pressures with an increasing contribution of C_6H_6^+ fragmentation as pressure is lowered) or both are clearly implicated at some stage in the formation of such products. The variety of possible transient species and of their possible competitive reactions precludes a detailed interpretation of the observed effects; however, certain aspects of the results merit discussion.

Because dose (eV ml^{-1}) was kept constant in study of the pressure effect, a decrease in pressure at fixed dose rate ($\text{eV sec}^{-1} \text{ml}^{-1} \text{torr}^{-1}$) is equivalent to a decrease in dose rate at fixed pressure with respect to a competition between combination-disproportionation reactions of free radicals and their scavenging by a reactive product of the radiolysis;²⁷ the rate of energy absorption per unit volume is simply the product of pressure and dose rate as defined here.

The effect of dose, dose rate, pressure, and NO on liquid-product yields is indeed such as to indicate their formation in reactions between free radicals (of the type proposed for their formation in radiolysis of the liquid^{2,28}) in competition with scavenging of the free-radical precursors by reactive products of the radiolysis or by NO. The behavior of propadiene yields is similar in all respects to that of the liquid products and may be similarly interpreted. The behavior of butadiyne yields differs in the enhancement produced by NO, which may implicate butadiyne as one of the reactive scavengers. Ethylene behaves like C_2H_2 with regard to the effect of dose, dose rate, and pressure; however, the yield enhancement with added NO or N_2O suggests the participation in C_2H_4 formation of secondary-ion precursors.²⁹

Phenol and N_2 Yields. In the radiolysis of $\text{C}_6\text{H}_6\text{-N}_2\text{O}$ mixtures at 66 torr, surprisingly large yields of phenol

and N_2 are produced, as shown in Figure 2. The average value of $G(\text{N}_2)/G(\text{C}_6\text{H}_5\text{OH})$ is 2.0 with an average deviation of $\pm 8.5\%$. Such a result suggests the involvement of a single reaction sequence in formation of both products over the concentration range studied (1–10 mol % of N_2O). The value of $G(\text{N}_2)$ at 10 mol % N_2O is 3.3-fold greater than a value of $G(\text{e}^-) \approx 4$. A plot of $1/G(\text{N}_2)$ vs. $1/[\text{N}_2\text{O}]$ gives a good straight line. Such a plot can be interpreted in terms of a competition between ion-electron combination and scavenging of electrons by N_2O ;¹⁶ with such an interpretation, the values of slope and intercept give the maximum N_2 yield as $G_m(\text{N}_2) = 29$, which is $\sim 7G(\text{e}^-)$, and a value of $\sqrt{k_c/k_s} = 3.6 \times 10^{11} \text{ molecule}^{-1} \text{ ml sec}^{-1}$.

Johnson and Warman¹⁶ have obtained values of $G_m(\text{N}_2) = 2G(\text{e}^-)$ and $\sqrt{k_c/k_s} = 3 \times 10^{10} \text{ molecule}^{-1} \text{ ml sec}^{-1}$ in the radiolysis of $\text{C}_3\text{H}_8\text{-N}_2\text{O}$ mixtures, and Warman³⁰ reports $G_m(\text{N}_2) = 1.55 G(\text{e}^-)$ in radiolysis of the C_2 , C_3 , and C_4 alkanes with added N_2O . On the other hand, Meaburn and Mellows³¹ find that radiolysis of methanol vapor containing 6.5 mol % N_2O gives $G(\text{N}_2) = 48.3$; these authors argue that N_2O has a very low cross section for electron capture and invoke a free-radical chain reaction to explain their large N_2 yields.

It is evident that the role of added N_2O in gas-phase radiolysis is not always simple. The interesting results shown in Figure 2 seem to require some kind of short-chain mechanism that produces N_2 and phenol in a 2:1 ratio. Specification of the nature of the chain must await further work directed specifically to this problem.

(25) K. H. Jones, *J. Phys. Chem.*, **71**, 709 (1967), *e.g.*, reports a phase-dependent protection effect in cyclohexane-benzene mixtures at the critical temperature.

(26) M. Burton, *Discussions Faraday Soc.*, **36**, 7 (1963).

(27) Though product yields may be affected by a transition from gas-phase to wall neutralization with changes in pressure and dose rate, the situation is somewhat confused with regard to the conditions under which such a transition occurs; see, *e.g.*, C. E. Klots and V. E. Anderson, *J. Phys. Chem.*, **71**, 265 (1967).

(28) T. Gäumann, *Helv. Chim. Acta*, **44**, 1337 (1961); M. K. Eberhardt, *J. Phys. Chem.*, **67**, 2856 (1963).

(29) The participation of NO in various ionic reactions has been demonstrated by P. Ausloos, S. G. Lias, and R. Gorden, Jr., *J. Chem. Phys.*, **39**, 3341 (1963), and by G. G. Meisels, *ibid.*, **42**, 3237 (1965). In general, the effect of N_2O on product yields may be related to a change in the neutralization reactions (*cf.* ref 16).

(30) J. M. Warman, *Nature*, **213**, 381 (1967).

(31) M. Meaburn and F. W. Mellows, *Trans. Faraday Soc.*, **61**, 1701 (1965).

Tellurium Vapor Pressure and Optical Density at 370–615°

by R. F. Brebrick

Lincoln Laboratory,¹ Massachusetts Institute of Technology, Lexington, Massachusetts 02173 (Received September 13, 1967)

The optical density of the vapor at 755° originating from a Te reservoir between 370 and 615° has been measured between 2100 and 1990 Å and near 4357 Å. The results strongly indicate that Beer's law is satisfied so that vapor pressures can be obtained. It is found that $\log P$ varies linearly with $1/T$ down to the triple point of 450°. This is in disagreement with the apparently most precise measurements on liquid tellurium. Between 450 and 370° $\log P(\text{atm}) = -8.001 \times 10^3/T + 7.540$.

Introduction

In general, the vapor pressure of tellurium is probably known with good accuracy between 200 and 890°.² However, there are few measurements between 400 and 512° and none between 427 and 484°. In the former temperature interval, the vapor pressure lies between 4×10^{-5} and 10^{-3} atm and for liquid tellurium shows a marked deviation from the nearly linear dependence of $\log P$ upon $1/T$ observed at higher temperatures according to one study.³ Our determinations of the partial pressures of $\text{Te}_2(\text{g})$ over a number of crystalline tellurides⁴–⁷ from the optical density of the coexisting vapor have depended upon the published vapor pressure of liquid tellurium. Here we report the results of optical density measurements between 2100 and 1990 Å and at 4357 Å of the vapor over pure tellurium. The optical density near 2000 Å is about ten times larger than that at 4357 Å, where our previous measurements were made, and accurate measurements are easily made at Te_2 pressures as low as 10^{-4} atm. This covers the range where $\log P$ vs. $1/T$ is claimed to be nonlinear for liquid tellurium. Moreover, if the absorption can be shown to follow Beer's law, the usual procedure can be reversed; *i.e.*, the optical density measurements can be used to determine the relative vapor pressure of tellurium. Although we cannot prove absolutely the validity of Beer's law for our optical density measurements, we conclude it is probably valid with a high degree of certainty. Accepting this conclusion, we then find that the reported low temperature curvature³ of $\log P$ vs. $1/T$ for liquid tellurium is not real. Using the published vapor pressure at the one temperature of 508°, our results yield the vapor pressure between 370 and 615°.

Experimental Section

In essence, the method was to measure the optical density ($D \equiv \log I_0/I$) of the vapor contained in a cylindrical silica optical cell at a fixed temperature of 755° using a double-beam spectrophotometer. The vapor originated from pure Te contained in a side arm whose temperature was independently controlled and

measured at temperatures from room temperature to about 615°.

Chunk tellurium, from American Smelting and Refining Co., N. J., and 99.99 at. % pure by their emission spectrographic analysis, was kept molten under vacuum for 15 min in a previously outgassed silica tube and then cooled. The surface layers were discarded and about 1 g was put into a silica optical cell previously outgassed at 1040° and 3×10^{-7} torr for 16 hr. The cell and tellurium were then outgassed at 220° for 3 hr and the cell was sealed off below 10^{-6} torr.

The cylindrical, fused-silica optical cells were 22 mm o.d. with flat parallel windows and a 21.6 cm long side arm at right angles to the cylindrical axis. One optical cell had an inside optical path length of 22.1 mm; the other had a length of 98.3 mm. The end of the side arm away from the cell was the seal-off point and during measurements contained the condensed tellurium phase. A schematic of the furnaces used to keep the optical cell proper at 755° during the measurements, while the temperature of the tellurium reservoir was held at room temperature or above, has been published.⁴ᵃ The temperature of the optical cell proper was constant to within $\pm 2^\circ$ during the measurement. The gradient across the optical cell was 20° . A close-fitting cylindrical silver liner, 10 cm long, with walls 6.4 mm thick, was put around the end of the side arm or tellurium reservoir to minimize the temperature gradient. Along the 2.5-cm length containing the tellurium the temperature gradient was 0.5° or less during the measurements. At the middle position of the tellurium reservoir the temperature was measured

(1) Operated with support from the U. S. Air Force.

(2) An. N. Nesmeyanov, "Vapour Pressures of the Elements," translated by J. I. Carasso, Academic Press, New York, N. Y., 1963.

(3) R. E. Machol and E. F. Westrum, Jr., *J. Am. Chem. Soc.*, **80**, 2950 (1958).

(4) (a) R. F. Brebrick and A. J. Strauss, *J. Chem. Phys.*, **40**, 3230 (1964); (b) *ibid.*, **41**, 197 (1964).

(5) R. F. Brebrick, *ibid.*, **41**, 1140 (1964).

(6) R. F. Brebrick and A. J. Strauss, *J. Phys. Chem. Solids*, **25**, 1441 (1964).

(7) R. F. Brebrick and A. J. Strauss, *ibid.*, **26**, 989 (1965).

to a precision of $\pm 0.1^\circ$ using a calibrated Pt—Pt-13% Rh thermocouple with an ice junction and a Leeds and Northrup K-3 potentiometer. The emf from this thermocouple was recorded and generally varied by less than $\pm 0.2^\circ$ during the 4 min needed to measure the optical density between 2100 and 1990 Å.

The optical cell proper with surrounding furnace was placed in the sample beam of a Cary Model 14H double-beam spectrophotometer with the side arm tilting downward about 15° from the horizontal. With the center of the optical cell proper at 755° and the reservoir at room temperature, the zero of optical density between 2100 and 1990 Å was recorded. The zero run was repeated with a reservoir temperature of about 300° . The temperature was then raised and the optical densities measured after the reservoir temperature and optical density at 2007 Å had reached a steady value. This generally took 20 to 40 min. The reservoir temperature was then raised about 5° and the whole procedure was repeated. Optical densities in the visible part of the spectrum were measured at 6000, 5500, and 5000 Å and between 4400 and 4300 Å in a similar fashion but in separate runs.

The ultraviolet spectra were obtained using the hydrogen light source of the Cary 14H, a scanning speed of 0.5 Å/sec, a 12.7-cm/min chart speed giving 2.36 Å/cm, and a 1-sec period for the recorder pen. The spectral band pass at 2100 and 2000 Å was 1.28 and 1.68 Å, respectively. The visible spectra were obtained using a tungsten light source, a scanning speed of 0.63 Å/sec, a 12.7-cm/min chart speed, and a 1-sec pen period. At 4357 Å the spectral band pass was 1.7 Å.

The spectra were generally obtained with increasing reservoir temperatures. On several occasions the furnaces sat at temperature overnight and runs were continued the next day.

Results

Seventeen absorption maxima were observed between 1990 and 2100 Å. For optical densities between a few hundredths and 2, no shifts in the positions of these maxima were observed. A shift of 0.5 Å could easily be detected. The positions of each of these maxima with one exception agree to within 1.5 Å or better with one of the 36 band heads measured photographically and with higher resolution by Migeotte.⁸ The exception is a maximum we observe at 1995.5 Å which was not reported by Migeotte. The envelope of the absorption band maxima decreases with increasing wavelength between 1990 and 2100 Å. The optical densities were analyzed for three maxima at 1995.5, 2025, and 2056 Å. The structure of the corresponding bands as well as that at 4357 Å is shown in Figure 1. As indicated in Table I, characteristic features of the band shapes are preserved as the optical density increases. The 1995.5-Å band is significantly

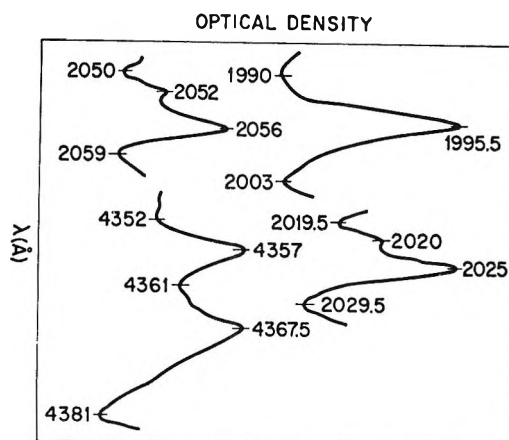


Figure 1. Structure of $\text{Te}_2(\text{g})$ absorption bands used. Optical density is plotted vs. wavelength for each band.

different in structure from the bands at 2025 and 2056 Å whose maxima are close to just resolved secondary maxima. On the other hand, the ultraviolet bands differ significantly from that at 4357 Å in that they are better resolved, the optical densities at the adjacent minima being 25–35% of the optical density at the maximum for the ultraviolet bands and 78% for the 4357-Å band.

Table I: Characteristics of the 1995.5-, 2025-, 2056-, and 4357-Å Bands. The Significance of the Various Wavelengths Is Shown in Figure 1

$D_{2003}/D_{1995.5} = 0.25$
Half-width of 1995.5-Å peak is $6 \pm 0.5 \text{ Å}$
for $0.03 \leq D_{1995.5} \leq 1.5$
$D_{2020}/D_{2025} = 0.62 \pm 0.02$
$D_{2029.5}/D_{2025} = 0.35 \pm 0.02$
$D_{2052}/D_{2056} = 0.62 \pm 0.02$
$D_{2059}/D_{2056} = 0.32 \pm 0.02$
$D_{4352}/D_{4357} = 0.91 \pm 0.03$
$D_{4381}/D_{4357} = 0.78 \pm 0.03$

It was found that the optical density at 1995.5 Å increased as the spectral band pass was decreased below the value of 1.68 Å used. On the other hand, that at 4357 Å was unchanged as the spectral band pass varied from $1/2$ to 2 times the value of 1.7 Å used. The effect of tracking errors in the recording system was shown to be negligible by the fact that decreasing the scanning speed to 0.13 Å/sec gave no significant increase in the optical densities at the band maxima. On the other hand, optical density values above unity for both cells are increasingly low, the error being the same for the four wavelengths above (as well as at 5000 Å where the absorption shows no structure) and being of the form of a stray light error. For this

(8) R. Migeotte, *Mem. Soc. Roy. Sci. Liege*, 5, 547 (1942).

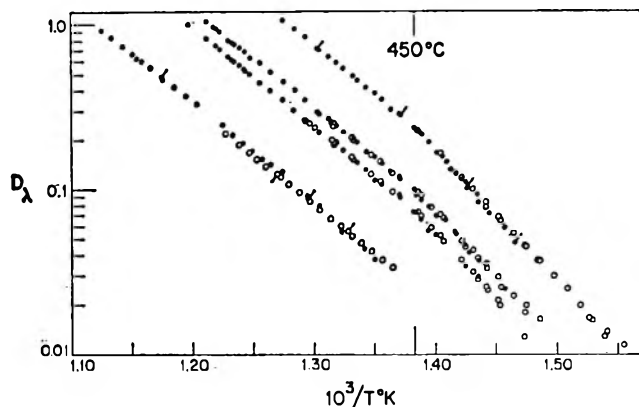


Figure 2. Optical density of $\text{Te}_2(\text{g})$ absorption band maxima, D_λ , plotted on a log scale against $10^3/T$, where T is the absolute temperature of the $\text{Te}(\text{c}, \text{l})$ reservoir. Solid circles are from the 22.1-mm path length cell, and other points from the 98.3-mm cell. In order of decreasing D , λ is 1995.5, 2025, 2056, and 4357 Å.

reason only optical densities below unity are presented in what follows.

Figure 2 shows the optical density plotted logarithmically for the four band maxima against the reciprocal absolute temperature (of the Te reservoir). Optical densities for the 98.3-mm cell were multiplied by the factor 22.1/98.3 and plotted with those for the 22.1-mm cell. Slanting lines attached to the 1995.5-Å points indicate the furnaces were at temperature overnight before the ultraviolet measurements were taken. Slanting lines attached to the 4357-Å points have a similar meaning for the measurements in the visible. These points agree well with those taken 20–40 min after the reservoir temperature was changed. The results for the two cells agree with two exceptions. Below 450° the optical densities are larger for the 98.3-mm cell. However, the discrepancy is comparable to the expected experimental error of ± 0.005 . At 4357 Å, the values are smaller for the 98.3-mm cell. The data for the 22.1-mm cell show a downward curvature at low values and are in agreement with the 98.3-mm cell data. At higher optical densities the two sets of data give parallel lines differing by 5%. The cause of this latter discrepancy is not understood. In general, the data for the various wavelengths are well represented by two sets of parallel straight lines that connect at the triple point of tellurium at 450° ($10^3/T = 1.3828$). Above 450° the data for each wavelength were fit by a straight line of slope -5.9602 , the slope found for the vapor pressure of liquid tellurium by Brooks⁹ and Ustygov.¹⁰ For 4357 Å, the optical densities for the two cells were fit separately. For a 22.1-mm path length the equations of these lines are given by

$$\log D_{1995.5} = -5.9602 \times 10^3/T + 7.6337 \quad (1)$$

$$D_{2025} = 0.4098D_{1995.5} \quad (2)$$

$$D_{2056} = 0.3174D_{1995.5} \quad (3)$$

$$D_{4357} \text{ (from 22.1-mm cell)} = 0.1108D_{1995.5} \quad (4)$$

$$D_{4357} \text{ (from 22.1-mm cell)}/$$

$$D_{4357} \text{ (from 98.3-mm cell)} = 1.049 \quad (5)$$

The adequacy with which eq 1–5 fit the experimental data is indicated in Table II. For each experimental value of optical density a value was calculated from eq 1–5. The difference between experimental and calculated values was then expressed as a percentage of the former, Δ . It is seen that the data are fit very well. In general, the largest discrepancies are associated with the smallest optical densities as one would expect.

Table II: Percentage Difference between Experimental and Calculated (Eq 1–5) Optical Densities, Δ , for $T \geq 450^\circ$

λ , Å	No. of exptl points	No., $\Delta \leq$ 2.2%	No., $\Delta \leq$ 3.5%	No., $\Delta \leq$ 5%	Largest Δ
1995.5	17	16	17
2025	30	26	30
2056	31	20	...	28	6.1%
4357 (22.1 mm)	21	17	19	...	9%
4357 (98.3 mm)	19	17	19

Below 450° the 1995.5-Å data were fit by a straight line using a least-squares analysis and relative weights of 20 and 1 for the 98.3- and 22.1-mm cell data, respectively. The result is

$$\log D_{1995.5} = -8.001 \times 10^3/T + 10.455 \quad (T \leq 450^\circ) \quad (6)$$

which fits the 98.3-mm cell data very well. Only 5 of 29 measurements differ by more than 5% from the value of D given by eq 6. As is seen in Figure 2, the 22.1-mm cell data are low at the lowest temperatures. Using eq 2, 3, and 6, the 2025 and 2056 optical densities below 450° can be calculated and are in good agreement with those observed.

Vapor Pressure of Tellurium. Using the free energy of dissociation¹¹ of $\text{Te}_2(\text{g})$, one can show that the vapor in a 755° optical cell is essentially all $\text{Te}_2(\text{g})$, even for the lowest tellurium reservoir temperature used here. The partial pressure of $\text{Te}_2(\text{g})$ is then equal to the vapor pressure of tellurium. If Beer's law is valid, our data give the relative vapor pressure of tellurium, and one calibration point suffices to obtain the absolute vapor pressure. In principle, one expects intermolecu-

(9) L. S. Brooks, *J. Amer. Chem. Soc.*, **74**, 227 (1952).

(10) A. A. Kudryavtsev and G. P. Ustygov, *Russ. J. Inorg. Chem.*, **6**, 1227 (1961).

(11) D. R. Stull and G. C. Sinke, "Thermodynamic Properties of the Elements," American Chemical Society, Washington, D. C., 1956.

lar forces will change the optical density in a given wavelength interval from the value expected from the behavior of isolated molecules so that Beer's law may not hold. The effect can be very large at relatively low concentrations for monoatomic gaseous species with sharp absorption lines and has been the subject of much theoretical and experimental attention.^{12,13} The theoretical situation is more complicated for the relatively broad and overlapping lines encountered in the electronic spectra of molecules. Yet from a practical point of view, Beer's law holds in many cases. In particular, optical density measurements of the same nature as described here have been made on a number of systems. Comparison with other determinations have shown Beer's law to hold at certain wavelengths for Se₂,¹⁴ PbTe,³ SnTe,⁴ and GeTe.⁵ The likelihood of its validity for the measurements described here is strong in view of the following considerations.

(1) Log D vs. $1/T$ has the same slope for all four band maxima even though these have different structures and would be expected to behave differently if intermolecular forces were contributing significantly to the optical density.

(2) The bands themselves do not appear to change shape with increasing optical density. This is verified quantitatively for a few features in Table I. Again it would appear that shifts in optical density due to intermolecular forces and leading to deviations from Beer's law are negligible.

(3) The slope of log D_{4357} vs. $1/T$ is constant up to 615°. Near this temperature the most accurate vapor pressure data^{3,9,10} essentially agree and have the same slope as log D_{4357} . It would be expected that D_{4357} , satisfying Beer's law for Te reservoir temperatures near 615°, would also satisfy Beer's law at lower reservoir temperatures. The Te₂ partial pressure is then lower and intermolecular forces are less important.

On the basis of the above considerations, we shall assume Beer's law is valid for our data, *i.e.*

$$P_{\text{Te}_2}(\text{atm}) = r_\lambda D_\lambda$$

where D_λ is the optical density at wavelength λ for a 22.1-mm optical path length at 755° and r_λ is the Beer's law constant. From eq 1, $D_{1995.5} = 1$ at $10^3/T = 1.2808$. The constant $r_{1995.5}$ is then numerically equal to the vapor pressure of tellurium at this temperature, which is 1.216×10^{-3} atm according to Brooks.⁹ The Beer's law constants for the other wavelengths can then be calculated using eq 2-5. (At 4357 Å, the Beer's law constant obtained with the 98.3-mm cell is in excellent agreement with that used previously⁷ in a study of the Hg-Te system while that obtained from the 22.1-mm cell is 6.6% lower.) As a result, we find the vapor pressure equation of Brooks⁹

$$\log P(\text{atm}) = -5.9602 \times 10^3/T + 4.7192 \quad (T \geq 450^\circ) \quad (7)$$

is valid to within better than $\pm 2\%$ in P between 450 and 615°. (Brooks' experimental study using silica gauges covered the range 512-832°.) The vapor pressure at the triple point of 450° is 2.99×10^{-4} atm. Between 370 and 450° the vapor pressure of Te(c) is obtained from eq 6 as

$$\log P(\text{atm}) = -8.001 \times 10^3/T + 7.540 \quad (370^\circ \leq T \leq 450^\circ) \quad (8)$$

Table III: Measured Vapor Pressure of Tellurium^a

$T, ^\circ\text{C}$	$p(\text{atm}) \times 10^4$	$T, ^\circ\text{C}$	$p(\text{atm}) \times 10^4$	$T, ^\circ\text{C}$	$p(\text{atm}) \times 10^4$
22.1-mm Cell ^b					
Run 1					
434.3	1.63	460.5	3.76	489.0	7.82
440.5	2.05	464.4	4.27	493.5	8.60
444.0	2.37	467.7	4.72	494.2	8.74
447.0	2.64	471.5	5.12	500.5	10.3
449.2	2.80	475.6	5.60	505.7	11.6
450.1	2.93	477.7	5.97	511.6	13.1
456.8	3.50	482.0	6.70		
456.5	3.48	485.3	7.26		
Run 2					
413.6	0.717	428.2	1.25	438.4	2.03
419.3	0.875	432.5	1.56		
423.6	1.02	436.8	1.80		
98.3-mm Cell ^c					
Run 1					
365.1	0.087	400.7	0.454	428.6	1.37
376.6	0.158	405.8	0.552	437.8	1.95
382.1	0.205	414.8	0.790	442.9	2.35
391.2	0.298	423.8	1.14	447.2	2.70
Run 2					
363.7	0.115	394.6	0.366	420.6	1.02
370.0	0.139	400.0	0.448	425.7	1.23
375.8	0.167	405.2	0.549	429.8	1.42
380.8	0.197	409.9	0.662	439.1	2.05
385.3	0.246	415.4	0.836	448.5	2.80
390.0	0.303	419.8	0.962		

^a The accuracy of the values listed depends upon the assumption that the vapor pressure at 507.8° is 1.216×10^{-3} atm. If subsequently it is found that a more accurate value is p , the values listed above could be adjusted accordingly by multiplication by the ratio, $p/1.216 \times 10^{-3}$. ^b An error of $\pm 6.7 \times 10^{-6}$ atm is expected from the error of ± 0.005 in optical density. ^c An error of $\pm 1.5 \times 10^{-6}$ atm is expected from the error of ± 0.005 in optical density.

(12) A. G. Kuhn, "Atomic Spectra," Academic Press, Inc., New York, N. Y., 1962.

(13) A. C. S. Mitchell and M. W. Zemansky, "Resonance Radiation and Excited Atoms," Cambridge University Press, Cambridge, England, 1961.

(14) R. F. Brebrick, *J. Chem. Phys.*, **43**, 3031 (1965).

The vapor pressures calculated from the measured value of $D_{1995.5}$ are given in Table III. Between 450 and 511.6° only one value out of 17 deviates by more than 2.2% from the vapor pressure given by eq 7. This one value at 460.5° is 3.5% low. Between 363.7 and 450°, only 5 of the 29 values obtained with the 98.3-mm cell deviate by more than 5% from the vapor pressure given by eq 8.

Discussion

An evaluation of tellurium vapor pressure measurements has been given.¹ We shall discuss only those that seem most accurate. Brooks'⁹ vapor pressure measurements summarized in eq 7 have been confirmed to within a few per cent between 646 and 890° by Kudryavtsev and Ustygov,¹⁰ who used a boiling point method. The vapor pressure of solid tellurium has been determined by Niwa and Sibata¹⁵ between 320 and 410° by measuring the weight loss and angular displacement of a torsion effusion cell. The vapor was found to be $\text{Te}_2(\text{g})$. It has also been determined by Korneeva, *et al.*,¹⁶ between 298 and 427°, who measured the weight loss in "free evaporation." Both sets of measurements are in fair agreement although they contain a total of only four experimental points above 400° and the scatter is about 22% near 400°. Using these authors' equations the extrapolated vapor pressure at 450° is 2.4×10^{-4} and 2.5×10^{-4} atm. This is significantly below the value of 2.99×10^{-4} atm obtained here or by extrapolation of Brooks' equation.

Our value for the vapor pressure of solid tellurium given by eq 8 lies above those of Niwa and Sibata and Korneeva, *et al.*, in the overlapping temperature range, being 17–20% high near 426° and about 13% high at 372° ($10^3/T = 1.550$). Near 330° eq 8 gives vapor pressures in agreement with the above authors.

The most precise measurements of the vapor pressure of liquid tellurium would seem to be those of Machol and Westrum,³ who used a silica Bourdon gauge between 484 and 855°. Above 650° their results agree with those of Brooks to better than 2% but are increasingly lower at lower temperatures (2.5% at 617° and 27% at 450°). The only explanation for this curvature would be an unusually large second virial coefficient for $\text{Te}_2(\text{g})$. As noted by Machol and Westrum themselves, their data only include nine points below 600° and the estimated error is $\pm 1.3 \times 10^{-4}$ atm. This error is about equal to the discrepancy between their value of the vapor pressure at 450°, 2.24×10^{-4} atm, and ours. Because of the precision of our data, it is obvious that they (coupled with the assumed validity of Beer's law) are inconsistent with the results of Machol and Westrum.

Acknowledgment. The author wishes to express his gratitude to Mr. R. Capes for his competent assistance in performing the experiments.

(15) K. Niwa and Z. Sibata, *J. Chem. Soc. Japan*, **61**, 667 (1940).

(16) I. V. Korneeva, A. S. Pashinkin, A. V. Novoselova, and Yu. A. Priselkov, *Zh. Neorg. Khim.*, **2**, 1720 (1957).

The Conductance of the Trialkylsulfonium Iodides in Water, Methanol, and Acetonitrile at 10 and 25°

by D. Fennell Evans and T. L. Broadwater

Department of Chemistry, Case Western Reserve University, Cleveland, Ohio 44106 (Received September 26, 1967)

Precise conductance measurements were carried out on Me_3SI , Et_3SI , and Pr_3SI in water, methanol, and acetonitrile at 10 and 25° and on Bu_3SI in water and methanol at 25°. In the nonaqueous solvents, the trialkylsulfonium iodides are found to be considerably more associated than the corresponding tetraalkylammonium iodides, a result consistent with the shorter cation-anion contact distance of the sulfonium iodides. In aqueous solution, there is no evidence for any greater ionic association of the sulfonium over the ammonium salts, indicating that the large deviations from ideality that have been observed for the R_4N halides are not the result of coulombic stabilized ion pairs. The change in the limiting conductance viscosity product in water with temperature is interpreted in terms of water structural effects.

Introduction

Aqueous solutions of the tetraalkylammonium salts have been carefully investigated by a number of physical methods.¹⁻¹³ These measurements have, in general, been interpreted in terms of the enforcement of water structure around the hydrocarbon side chains of these ions. This type of interaction has readily been detected in those measurements which have limiting ionic properties such as conductance⁵ and viscosity.⁹ However, there is considerable disagreement concerning the interpretation of the concentration dependence of aqueous solutions of these electrolytes. The large deviations from limiting-law behavior have been discussed in terms of cation-anion pairing,¹⁴ cation-cation pairing,³ micelle formation,² and salting-in effects.¹⁵ In order to investigate to what extent coulombic forces are responsible for these large departures from ideality, we have carried out measurements on the trialkylsulfonium iodides (R_3SI) in water and in nonaqueous solvents. The trialkylsulfonium salts are pyramidal in configuration¹⁶ with the sulfur atom located at one of the apices. Consequently, the positively charged atom resides at the surface of the molecule rather than being buried in the center of a tetrahedron as in the case of the tetraalkylammonium compounds. Therefore, if coulombic stabilized cation-anion pairing is an important factor in these aqueous solutions, it should be accentuated in the trialkylsulfonium series.

Experimental Section

All of the trialkylsulfonium iodides were prepared by treating the alkyl iodide with the corresponding dialkyl sulfide in methanol. The reaction of the trimethyl compound was carried out at room temperature and

was complete within 3 hr. The triethylsulfonium iodide was formed by refluxing the methanol solution overnight. Both salts were recrystallized three times from methanol by the addition of ether, dried for 12 hr in a vacuum oven at room temperature, and stored in a darkened desiccator.

The tripropyl and tributyl salts were prepared by heating the reactants in sealed flasks for 1 month at 50°. The unreacted starting materials were removed by extraction with ether, and the desired salts were obtained from the resulting residues by recrystallizing six times from acetone-ether mixtures. The salts were dried in a vacuum oven overnight at room temperature and stored in the dark.

Upon standing, all of the salts showed some sign of

- (1) H. S. Frank and W. Y. Wen, *Discussions Faraday Soc.*, **24**, 133 (1957).
- (2) S. Lindenbaum and G. E. Boyd, *J. Phys. Chem.*, **68**, 911 (1964).
- (3) W. Y. Wen and S. Saito, *ibid.*, **68**, 2639 (1964).
- (4) H. G. Hertz and M. D. Zeidler, *Ber. Bunsenges. Physik. Chem.*, **68**, 821 (1964).
- (5) R. L. Kay and D. F. Evans, *J. Phys. Chem.*, **69**, 4216 (1965); **70**, 2325 (1966).
- (6) D. F. Evans and R. L. Kay, *ibid.*, **70**, 366 (1966).
- (7) S. Lindenbaum, *ibid.*, **70**, 814 (1966).
- (8) W. Y. Wen, S. Saito, and C. Lee, *ibid.*, **70**, 1244 (1966).
- (9) R. L. Kay, T. Vituccio, C. Zawoyski, and D. F. Evans, *ibid.*, **70**, 2336 (1966).
- (10) B. E. Conway and R. E. Verrall, *ibid.*, **70**, 3952, 3961 (1966).
- (11) G. E. Boyd, J. W. Chase, and F. Vaslow, *ibid.*, **71**, 573 (1967).
- (12) R. H. Wood, H. L. Anderson, J. D. Beck, J. R. France, W. E. de Vry, and L. J. Soltzberg, *ibid.*, **71**, 2149 (1967).
- (13) R. Zana and E. Yeager, *ibid.*, **71**, 4241 (1967).
- (14) R. M. Diamond, *ibid.*, **67**, 2513 (1963).
- (15) J. E. Desnoyers and M. Arel, *Can. J. Chem.*, **45**, 359 (1967).
- (16) S. Lindenbaum, *J. Phys. Chem.*, **72**, 212 (1968).

Table I: Equivalent Conductances

10°C	A	10°C	A	10°C	A	10°C	A	10°C	A	10°C	A
Me ₃ SI		Et ₃ SI		Pr ₃ SI		Me ₃ SI		Et ₃ SI		Pr ₃ SI	
		CH ₃ CN						H ₂ O			
		10°						10°			
2.877	164.65	2.302	158.03	7.795	142.96	5.076	87.31	4.289	77.72	4.520	71.64
9.882	157.14	7.931	152.51	14.787	138.73	11.227	86.52	15.802	76.37	11.139	70.82
19.951	150.06	15.432	147.73	22.920	134.93	17.411	85.97	20.322	75.98	18.440	70.14
30.581	144.45	23.450	143.82	32.622	131.28	24.640	85.42	25.782	75.58	26.884	69.49
42.342	139.42	31.605	140.56	43.336	127.93	31.997	84.94	32.888	75.11	37.028	68.84
56.526	134.51	40.515	137.53	55.997	124.60	40.302	84.46	41.092	74.63	49.288	68.12
70.752	130.37	51.282	134.38	70.204	121.41	49.675	83.96	50.250	74.14	61.523	67.50
85.174	126.74	64.027	131.17								
		25°				A = 0.088		A = 0.086		A = 0.082	
A = 0.067		A = 0.079		A = 0.076		9.806	121.59	13.725	108.14	6.884	100.65
2.418	191.67	2.068	184.09	1.972	172.82	20.490	120.27	22.493	107.12	14.770	99.49
6.201	186.08	5.865	179.11	6.723	167.17	31.082	119.26	33.373	106.11	23.191	98.54
10.160	181.73	11.990	173.82	13.902	161.65	45.578	118.12	44.952	105.17	32.112	97.68
15.718	176.82	18.279	169.65	21.439	157.32	53.022	117.59	55.094	104.44	39.666	97.04
21.453	172.61	25.731	165.64	29.263	153.64	66.643	116.74	63.984	103.87	49.030	96.31
27.474	168.80	33.218	162.23	37.261	150.45	78.464	116.08	71.944	103.40	59.072	95.60
34.646	164.88	41.420	159.01	46.325	147.33	89.946	115.48	82.818	102.77		
		51.833	155.45	56.457	144.25						
		62.297	152.31								
		MeOH				H ₂ O, 25°		Bu ₃ SI		MeOH, 25°	
		10°				A = 0.074				A = 0.15	
5.180	100.31	3.419	96.69	3.593	87.46	6.486	97.23			4.933	99.91
11.388	97.01	10.731	92.55	11.376	83.38	13.549	96.07			10.271	96.52
18.782	94.15	19.475	89.21	20.825	80.09	21.803	95.04			15.849	93.92
26.780	91.72	29.122	86.45	30.701	77.48	29.724	94.20			20.987	91.94
35.489	89.53	38.773	84.21	40.689	75.34	36.318	93.57			26.625	90.07
48.644	86.80	48.993	82.20	50.754	73.51	45.402	92.78			33.764	88.03
63.162	84.31	61.116	80.17	60.938	71.90	52.312	92.23				
		73.916	78.30	76.798	69.76	57.344	91.85				
		25°									
A = 0.102		A = 0.104		A = 0.105							
5.739	122.32	6.032	116.57	4.821	106.32						
11.624	118.49	12.065	112.80	9.598	103.22						
18.563	115.12	18.734	109.68	16.177	100.02						
26.697	112.01	27.249	106.53	23.909	97.05						
33.106	109.94	33.953	104.44	33.353	94.18						
40.434	107.89	42.937	102.05	40.681	92.30						
48.899	105.80	48.912	100.66	49.585	90.30						
57.312	103.97	60.808	98.18	56.196	88.97						

decomposition as evidenced by the disulfide odor that could be detected upon opening the salt container. The rate of decomposition appeared to increase with increasing cation size and caused such difficulty in the case of the tributyl compound that we obtained only enough material for two conductance runs. The salts were always recrystallized before use, and the actual conductance runs were completed within 3 hr. Conductivity water was prepared by passing distilled water through a 1.2-m column of analytical grade ion-exchange resin, Amberlite MB1. The preparation of conductance grade methanol¹⁷ and acetonitrile¹⁸ was the same as previously described.

The electrical equipment, conductance cells, and

general techniques were similar to those reported elsewhere^{17,19} except for the conductance bridge, which consisted of a Leeds and Northrup ratio box, Catalog No. 1553, and a General Radio decade resistance box, Catalog No. 1432. Briefly, the conductance runs were carried out in Kraus type conductance cells²⁰

(17) R. L. Kay, C. Zawoyski, and D. F. Evans, *J. Phys. Chem.*, **69**, 4208 (1965).

(18) J. F. Coetzee, G. P. Cunningham, D. K. McGuire, and G. R. Padmanabhan, *Anal. Chem.*, **34**, 1139 (1962).

(19) C. G. Swain and D. F. Evans, *J. Am. Chem. Soc.*, **88**, 383 (1966).

(20) H. M. Daggett, Jr., E. Bair, and C. A. Kraus, *ibid.*, **73**, 799 (1951).

which were stirred constantly with a Teflon-covered magnetic stirring bar. The cells, which had cell constants of 1.3, were calibrated²¹ with reagent grade potassium chloride.²⁰ The usual small frequency correction was applied to all resistance measurements. The salts were added to the cell in small Pyrex cups with the aid of a Hawes-Kay cup dropping device.²²

The temperature of the baths was set with a calibrated platinum resistance thermometer and controlled to $\pm 0.005^\circ$.

Results

The density increments used to calculate the volume concentration at 25° are given in Table I. They were obtained by density measurements on the most concentrated solution used in the conductance measurement and were assumed to follow the relationship $d = d_0 + A\bar{m}$, where d_0 is the density of the pure solvent and \bar{m} is the concentration in moles per kilogram of solution. The value of A for the trialkylsulfonium iodides was assumed to be independent of temperature, an assumption that has been verified⁶ in the case of the tetraalkylammonium salts.

The measured equivalent conductances and corresponding concentrations in moles per liter are also given in Table I. The data were analyzed by the Fuoss-Onsager equation²³ in the form

$$\Lambda = \Lambda_0 - S(C\gamma)^{1/2} + EC\gamma \log C\gamma - (J - B\Lambda_0)C\gamma - K_A C\gamma \Delta f^2 \quad (1)$$

where ionic association was detected, and with $\gamma = 1$ and $K_A = 0$ otherwise. Since the viscosity of these solutions has not been determined, the value of B , which corrects for the effect of the electrolyte on the viscosity of the solution, was set equal to zero. This correction does not alter the value of Λ_0 nor the association constant and only changes the value of J and consequently of d , the ion size parameter. The solvent properties of dielectric constant, viscosity, and density required in the computation have been given in convenient tabular form already.²⁴

The conductance parameters Λ_0 , d , and K_A were obtained by a least-squares fit using a computer program²⁵ and are shown in Table II. Also given are σ , the standard deviation of the individual points, and λ_0^+ , the limiting conductance of the cation. The following $\lambda_0(I^-)$ values were used in this calculation: water, 25° , 76.98; water, 10° , 55.39; methanol, 25° , 62.78; methanol, 10° , 50.9; and acetonitrile, 25° , 102.7.^{5,23} The agreement between the least-squares fit of the Fuoss-Onsager equation and the data in water at 25° can be seen by inspection of the Λ' plot, Figure 1, where Λ' is

$$\Lambda' \equiv \Lambda - \Lambda_0 + S\sqrt{C} - Ec \log c = Jc \quad (2)$$

The solid line drawn through the experimental points is the least-squares best value of J .

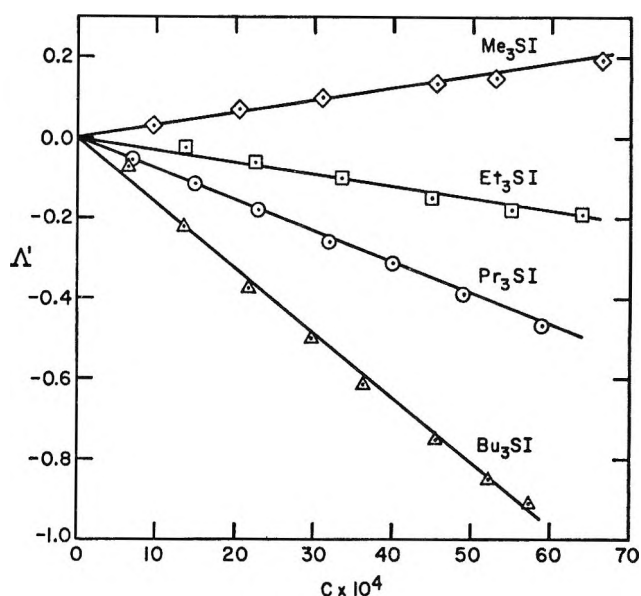


Figure 1. A plot of eq 2 for trialkylsulfonium iodides in water at 25° .

Discussion

Limiting Ion Conductances. Although enforcement of water structure about the hydrocarbon chains of the tetraalkylammonium salts is perhaps the most cited feature of their behavior in aqueous solution, this type of interaction is not observed with all of the members of the series.⁵ In fact, there appears to be a critical size of hydrocarbon chain below which enforcement of water structure is not observed for these cations.²⁶ This effect is most readily detected by studying aqueous solutions of these salts as a function of temperature since water structural effects decrease as the temperature increases. From a number of such studies the following picture has emerged. The smallest member of this series, Me_4N^+ ion, disorganizes water structure in its immediate vicinity in a manner similar to the larger alkali metal ions. This results, for example, in a negative temperature coefficient for the limiting ionic conductance-viscosity product, $\lambda_0\eta$,⁵ a positive viscosity B temperature coefficient,⁹ and a negative $d\Delta t/dt$,²⁷ where Δt is a structural temperature difference between water and Me_4N^+ solutions for the 0.97 near-infrared band. The tetrapropylammonium ion and

(21) J. E. Lind, Jr., J. J. Zwolenik, and R. M. Fuoss, *J. Am. Chem. Soc.*, **81**, 1557 (1959).

(22) J. L. Hawes and R. L. Kay, *J. Phys. Chem.*, **69**, 2420 (1965); G. P. Cunningham, B. J. Hales, and R. L. Kay, *ibid.*, **71**, 3925 (1967).

(23) R. M. Fuoss and F. Accascina, "Electrolytic Conductance," Interscience Publishers, Inc., New York, N. Y., 1959.

(24) G. P. Cunningham, D. F. Evans, and R. L. Kay, *J. Phys. Chem.*, **70**, 3998 (1966).

(25) R. L. Kay, *J. Am. Chem. Soc.*, **82**, 2099 (1960).

(26) D. F. Evans, G. P. Cunningham, and R. L. Kay, *J. Phys. Chem.*, **70**, 2974 (1966).

(27) K. W. Bunzl, *ibid.*, **71**, 1358 (1967).

Table II: Conductance Parameters at 25 and 10° for Water, Methanol, and Acetonitrile

Salt	Temp, °C	Δ°	d	K_A	σ	λ_0^+
CH ₃ CN						
Me ₃ SI	25	199.23 ± 0.02	3.6 ± 0.1	35.7 ± 0.6	0.02	96.53
	10	171.67 ± 0.04	3.0 ± 0.1	31.7 ± 0.6	0.04	
Et ₃ SI	25	190.25 ± 0.05	3.5 ± 0.2	19.8 ± 0.8	0.05	87.55
	10	163.57 ± 0.04	3.3 ± 0.1	17.9 ± 0.7	0.03	
Pr ₃ SI	25	178.64 ± 0.03	3.4 ± 0.1	18.7 ± 0.6	0.03	75.94
	10	153.27 ± 0.01	2.76 ± 0.02	13.5 ± 0.1	0.01	
MeOH						
Me ₃ SI	25	130.32 ± 0.03	3.69 ± 0.09	23.4 ± 0.6	0.02	67.54
	10	106.23 ± 0.04	3.6 ± 0.2	23 ± 1	0.03	55.33
Et ₃ SI	25	124.62 ± 0.03	3.6 ± 0.1	23.9 ± 0.7	0.02	61.84
	10	101.28 ± 0.04	3.5 ± 0.1	24 ± 1	0.03	50.38
Pr ₃ SI	25	113.09 ± 0.02	3.52 ± 0.08	24.2 ± 0.6	0.01	50.31
	10	91.97 ± 0.03	3.35 ± 0.08	24.2 ± 0.7	0.02	41.07
Bu ₂ SI	25	106.67 ± 0.05	4.3 ± 0.4	31 ± 2	0.02	43.89
H ₂ O						
Me ₃ SI	25	124.49 ± 0.01	0.88 ± 0.02		0.01	47.51
	10	88.71 ± 0.02	0.30 ± 0.05		0.02	33.32
Et ₃ SI	25	111.51 ± 0.01	0.27 ± 0.02		0.02	34.53
	10	78.95 ± 0.03	0.03 ± 0.01		0.03	23.56
Pr ₃ SI	25	102.99 ± 0.003	0.054 ± 0.001		0.002	26.01
	10	72.92 ± 0.01	0.005 ± 0.001		0.02	17.53
Bu ₃ SI	25	99.57 ± 0.01	2.0 ± 0.4	3.6 ± 0.2	0.002	22.59

higher homologs behave in just the opposite manner, promoting water structure and producing a $\lambda_0\eta$ product which has a positive temperature coefficient, a negative viscosity B temperature coefficient, and a positive $d\Delta t/dt$. Tetraethylammonium ion shows no temperature dependence, indicating that structure breaking and promoting effects apparently cancel each other.

A comparison of the behavior of the symmetrical R_4N^+ ions to the asymmetrical Me_3RN^+ ions (where $R = C_2H_5$ to $C_{14}H_{29}$) has shown that the geometry of the molecule is also an important factor.²⁵ For example, the limiting ionic mobility of the trimethyltetradecylammonium ion (17 carbon atoms) is 9% larger than that of the Bu_4N^+ (16 carbon atoms). The promotion of water structure around all portions of the Bu_4N^+ ion results in its moving slower than it would in the absence of structural effects, a conclusion that can be verified by comparing the $\lambda_0\eta$ value for non-aqueous solvents with that for water. For methanol, ethanol, acetonitrile, and nitromethane, $\lambda_0\eta$ for Bu_4N^+ ion is 0.2120, which is 23% larger than the corresponding value for water at 25°.⁵ The asymmetrical trimethyltetradecylammonium ion appears to exhibit more complex behavior in that the three methyl groups attached to the charged nitrogen atom disorganize water structure while the fourth larger alkyl group promotes water structure.²⁴ The polar end of

the asymmetrical series behaves like a Me_4N^+ ion, moving more rapidly than it would in the absence of structural effects. Thus the effect of an R_4N^+ ion on water structure depends upon both the size and shape of the ionic species.

A comparison of the behavior of the pyramidal trialkylsulfonium ions with the tetrahedral tetraalkylammonium ions allows these generalizations to be extended. Shown in Figure 2 is a plot of $\lambda_0\eta$ vs. temperature for both series of compounds. The quantity R_{25}^{10} given by

$$R_{25}^{10} = (\lambda_0\eta)_{10}/(\lambda_0\eta)_{25}$$

should be greater than 1 for structure-breaking ions and less than 1 for structure-making ions. R_{25}^{10} is 1.02 for Me_4N^+ and 1.03 for Me_3S^+ . This result is consistent with the Me_3S^+ ion being a smaller species with greater surface charge density than Me_4N^+ ion, and hence somewhat more like a large alkali metal ion in its behavior in aqueous solution. R_{25}^{10} for cesium ion is 1.07. Like the Et_4N^+ , the Et_3S^+ ion shows no temperature dependence, a result in accord with the idea that the structure-promoting and destroying properties of an ethyl group cancel each other. R_{25}^{10} is 0.968 for Pr_4N^+ and 0.988 for Pr_3S^+ , indicating that the hydrocarbon-water interaction dominates in aqueous

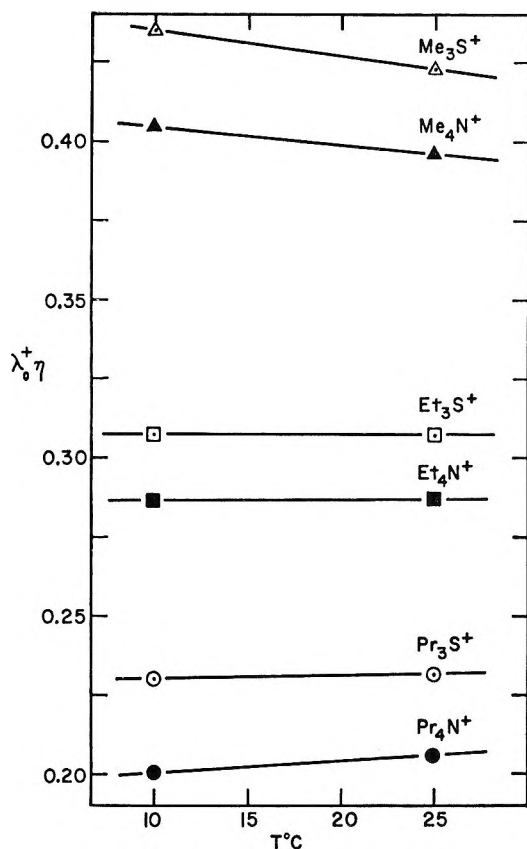


Figure 2. Change of the limiting Walden product for the trialkylsulfonium and tetraalkylammonium ions with temperature.

solution although to a lesser extent in the case of the pyramidal ion.

That water structure effects are responsible for the variation in R_{25}^{10} can be verified by considering this same ratio in nonaqueous solvents. The average R_{25}^{10} in methanol for all the R_3S^+ ions is almost constant, 1.01 ± 0.003 , in contrast to the 4% variation observed in aqueous solution. The same type of analysis for acetonitrile solutions is not possible because of the lack of transference data for this solvent at 10°. Thus the conclusions drawn concerning the behavior of the R_4N^+ ions in aqueous solution are confirmed by the R_3S^+ ions.

Concentration Dependence. Since the stabilization of ion pairs is mainly coulombic in origin, it is anticipated that a trialkylsulfonium iodide should be more associated than the corresponding tetraalkylammonium iodide. The pyramidal shape of the R_3S^+ , with the charged sulfur atom at one of the apices, should allow the cation-anion centers to approach one another more closely than in the case of R_4N^+ , where the charged nitrogen is shielded by hydrocarbon on all sides.

Such behavior has been verified in nonaqueous solvents.⁵ In methanol all of the ammonium iodides, methyl through amyl, gave $K_A = 17 \pm 1$.¹⁷ Similarly, as can be seen in Table II, a constant value of K_A is also obtained for the trialkylsulfonium iodides,²⁸ but they are about 35% more associated than the corresponding ammonium salts. In acetonitrile, K_A decreases with increasing cation size, as was the case with the ammonium salts,²⁹ but the R_3SI salts are 50 to 100% more associated than the corresponding R_4NI salts. Thus the association behavior of the sulfonium salts is the same as that of the ammonium salts, but the degree of association is greater for the sulfonium iodides as expected, due to the shorter contact distance. In both methanol and acetonitrile the slight change in the association constants with temperature is not considered significant. It is interesting to note that the \bar{d} for all the sulfonium salts is 3.5 ± 0.3 in exact agreement with the value 3.5 ± 0.2 found for all the tetraalkylammonium halides in nonaqueous solvents.³⁰

In aqueous solution, in contrast to the results in nonaqueous solvents, there is no evidence for any greater association of the sulfonium over the ammonium salts. Only one of the salts, Bu_3SI , analyzed for any association in water, giving $K_A = 3.6 \pm 0.2$. A K_A of the same magnitude was found for Bu_4NI in water.⁶ As can be seen in Table II, the values of \bar{d} for the other sulfonium salts are all unrealistically small. Equally small values of \bar{d} were obtained for the R_4N^+ iodides in water, Pr_4NI $\bar{d} = 0.03$, Et_4NI $\bar{d} = 0.5$, and Me_4NI $\bar{d} = 1.32$; B set equal to zero. Comparison of the two cation series shows that they have the same concentration dependence to within 0.1%. This latter fact shows that the peculiar concentration dependence of salts of these large cation series is not the result of coulombic interaction. A similar argument excludes ion-pair stabilization by dispersion forces depending on polarizability.

Acknowledgment. We wish to acknowledge the technical assistance of Mr. John Nadas under the sponsorship of the Undergraduate Research Participation Program of the National Science Foundation. This work was supported in part by Contract No. 14-01-0001-1281 with the Office of Saline Water, U. S. Department of the Interior.

(28) The somewhat larger value of K_A obtained for Bu_3SI reflects a bad split in the least-squares estimation of the best values of \bar{d} and K_A .

(29) D. F. Evans, C. Zawoycki, and R. L. Kay, *J. Phys. Chem.*, **69**, 3878 (1965).

(30) The published value for the R_4N^+ halides is 3.5 plus 0.2 for the viscosity correction.

High-Temperature Infrared Spectroscopy of Pyridine Adsorbed on Faujasites

by P. E. Eberly, Jr.

*Esso Research Laboratories, Humble Oil & Refining Company, Baton Rouge Refinery, Baton Rouge, Louisiana
(Received April 4, 1967)*

Results are presented on the infrared spectral studies of pyridine adsorbed on various ion-exchanged faujasites at 100–260°. Pyridinium ions reflecting Brønsted acidity are detected by an infrared band near 1540 cm^{-1} . Coordinately bound pyridine has a band near 1450 cm^{-1} which can be used as a measure of Lewis acidity. With hydrogen-faujasite, the adsorbed species consist predominantly of pyridinium ions formed by reaction with the structural OH groups having an infrared absorption frequency of 3635 cm^{-1} . Little reaction is observed with the groups at 3540 cm^{-1} . With the alkali metal exchanged faujasites, no pyridinium ions are observed, indicating the surface acidity to be predominantly Lewis in nature. The K form appears to be the least reactive toward pyridine. The Ca, Mg, and Cd forms after evacuation at elevated temperatures exhibit both Brønsted and Lewis acidity. With Ca and Mg faujasites, the ability to form pyridinium ions is greatly enhanced by the addition of small amounts of water. These cations are believed to perturb neighboring hydroxyl groups enabling the hydrogen atoms to protonate adsorbed pyridine. The marked similarity between the spectrum of pyridine on the water-treated Ca form and that on hydrogen-faujasite suggests that the materials may have some of the same structural features. The formation of $-\text{Ca}-\text{OH}$ and $-\text{OH}$ groups upon exposure to water at 260° is indicated.

I. Introduction

The relationship between catalyst acidity and activity in carbonium ion type reactions such as cracking and isomerization has been the subject of a number of investigations.¹ Although a wide variety of techniques to measure acidity have been reported, the recent method involving infrared studies of adsorbed pyridine has several advantages. In view of the distinct difference between the spectrum of the protonated form of pyridine and that of coordinately bound pyridine, one can readily distinguish between the Brønsted and Lewis types of acidity. Parry² and, more recently, Basila, Kantner, and Rhee³ have employed this technique for characterizing the surfaces of silica, alumina, and amorphous silica-alumina cracking catalysts. The interaction between pyridine and silica is very weak, mainly involving the formation of hydrogen bonds. Alumina, on the other hand, possesses strong Lewis acidity. Silica-alumina catalysts exhibit both Brønsted and Lewis acidity, and small amounts of water can transform the Lewis into Brønsted sites. Liengme and Hall⁴ and, more recently, Hughes and White⁵ demonstrated that pyridine reacts with hydroxyl groups on hydrogen-faujasite to form pyridinium ions. The extent of this reaction is reported to decrease as the hydroxyl groups are removed by more severe calcination.

The present investigation deals with infrared studies of the interaction of pyridine at temperatures up to 260° with various ion-exchanged faujasites. The effect of small amounts of water on the distribution of Brønsted and Lewis type sites is explored. The experimental techniques and equipment used for high-temperature infrared studies have been previously described.⁶

II. Experimental Section

Materials. Two different samples of Na-faujasite (NaY) were investigated and their compositions are given in Table I. Although the composition of NaY-(II) was nearly the same as NaY(I), its infrared transmission properties were inferior. Possibly, it had a greater concentration of larger particles causing more scattering of the incident radiation. HY(I) was prepared by first exchanging the sodium with ammonium ions. Upon calcination, the NH_4Y liberates NH_3 forming HY. For this purpose, 180 g of NaY(I) was treated with a solution of 333 g of NH_4NO_3 dissolved in 3 l. of water. The exchange was conducted for 2 hr at 70°. After allowing it to settle and decanting the supernatant liquid, a fresh solution of NH_4NO_3 was added and the treatment was repeated. After a total of five such treatments, the solid was filtered, thoroughly washed, and oven-dried at 150° overnight. Analysis of this sample is given in Table I.

For our earlier studies on other ion-exchanged faujasites, NaY(II) was used as the starting material. The various forms were prepared by ion exchanging with the chloride salts of the desired ion. In general, a threefold excess of the ion was employed and the treatment was repeated three times. The degree of exchange accomplished is included in Table II.

(1) L. B. Ryland, M. W. Tamele, and J. N. Wilson, "Catalysis," Vol. 7, Reinhold Publishing Corp., New York, N. Y., 1960.

(2) E. P. Parry, *J. Catalysis*, **2**, 371 (1963).

(3) M. R. Basila, T. R. Kantner, and K. H. Rhee, *J. Phys. Chem.*, **68**, 3197 (1964).

(4) B. V. Liengme and W. K. Hall, *Trans. Faraday Soc.*, **62**, 3229 (1966).

(5) T. R. Hughes and H. M. White, *J. Phys. Chem.*, **71**, 2192 (1967).

(6) P. E. Eberly, Jr., *ibid.*, **71**, 1717 (1967).

Table I: Composition of Na and NH₄ Faujasites

	Compn as expressed by empirical formula, moles		
	NaY(I)	NaY(II)	NH ₄ Y(I)
Na ₂ O	1.13	1.07	0.08
(NH ₄) ₂ O	0	0	0.87
Al ₂ O ₃	1.00	1.00	1.00
SiO ₂	4.72	4.88	4.67

Table II: Absorbance of Pyridine Bands at 150°^a

Ion-exchanged form	% exchange	ε/r, Å ⁻¹	Absorbance/g of solid		
			1545 cm ⁻¹	1490 cm ⁻¹	1450 cm ⁻¹
HY(I)	92	...	7.0	∞	0.8
CdY(II)	73	2.1	0.57	1.8	6.8
MgY(II)	67	3.1	0.41	1.3	3.0
CaY(II)	75	2.0	0.33	1.0	4.1
Li(II)	64	1.7	0	0.29	2.1
Na(II)	100	1.1	0	0.27	1.2
K(II)	95	0.75	0	0	0

^a Exposed to 0.1 mm of pyridine and then evacuated for 30 min.

Experimental Procedure. For infrared examination, the solids were ground with a mortar and pestle. Then they were compressed under 30,000 psi pressure into 1.25 in. diameter disks. These disks were about 8–16 mils thick and contained 13–19 mg of solid/cm². These were placed in a sample holder and inserted into the high-temperature infrared cell. Details of the cell and associated equipment have been previously described.⁶ The samples were initially degassed for several hours at 427°. The temperatures were then lowered to the desired value and spectra were recorded with a Cary-White Model 90 infrared spectrophotometer. Generally, spectra were obtained in the region of 4000–1200 cm⁻¹ at a spectral slit width of 4 cm⁻¹ and a scan speed of 3 cm⁻¹ sec⁻¹. Spectra were measured both before and after exposure to 0.1 mm of pyridine vapor. In certain cases, the samples were pretreated with small amounts of water to determine its effect on the distribution of Brønsted and Lewis sites. To cancel out the absorption of infrared radiation by the gas phase, a dummy cell was placed in the reference beam and connected to the same vacuum and gas dosing system.

III. Results

Pyridine Adsorption on NaY(I) and HY(I). From previous studies on the spectra of pyridine complexes and pyridine adsorbed on various solids, it has been possible to distinguish between various types of adsorbed species.^{2–4} The protonated form of pyridine is best characterized by a band near 1540 cm⁻¹. Coordinately bound pyridine formed by interaction with Lewis type sites has a band near 1450 cm⁻¹.

Infrared spectra of pyridine adsorbed on HY(I) at 260° are given in Figure 1. HY(I) was prepared from the ammonium form by evacuation at 427° and has three characteristic OH bands at 3740, 3635, and 3540 cm⁻¹. Because of the nature of these bands, the uncertainty in frequency assignment is estimated to be ±5 cm⁻¹. Other investigators^{4–9} have reported their occurrence at 3750–3744, 3677–3640, and 3570–3540 cm⁻¹, respectively. Upon exposure to 0.1 mm of pyridine at 260°, large changes in the spectrum can be observed. Pyridine reacts quite selectively with the OH groups responsible for the 3635-cm⁻¹ band. Very little change occurs in the intensity of the two remaining OH bands. This interaction results in the formation of pyridinium ions almost exclusively as evidenced by a strong band at 1540 cm⁻¹ (not shown) and the near absence of a band at 1450 cm⁻¹. This is consistent with previous spectral studies at lower temperature.^{4,5} In contrast to the broad ill-defined bands generally seen on amorphous silica-alumina catalysts,^{2,3} three distinct NH stretch vibrations are observed at 3230, 3160, and 3130 cm⁻¹. These probably result from varying degrees of hydrogen bonding and indicate some degree of order in the interaction of the adsorbed species with oxygen ions in the lattice. These are nearly 30 cm⁻¹ lower than those previously listed for the N–H stretch for chemisorbed protonated pyridine.^{2–4} In addition, a new band is observed near 2160 cm⁻¹ (not shown) which is in the region characteristic of amine salts.^{10,11} Pyridine hydrochloride, for example, has a pronounced band at 2100 cm⁻¹.

In the CH stretch region, the band at 3080 cm⁻¹ is characteristic of such vibrations in the pyridine molecule. It is surprising, however, to observe bands at 2970 and 2880 cm⁻¹ showing the formation of saturated CH linkages. In fact, the positions of the bands appear to be more nearly characteristic of CH₃ rather than CH₂ groupings. This indicates that HY(I) at 260° possesses some hydrogenation-dehydrogenation activity.

The adsorbed material is rather tenaciously held on the surface and is not extensively removed even after a 16-hr evacuation at 260°. Some desorption occurs, however, as indicated by a general lowering in intensity of the infrared bands and also by the partial reappearance of the OH band at 3635 cm⁻¹.

A similar set of experiments was performed with

- (7) C. L. Angell and P. C. Schaffer, *J. Phys. Chem.*, **69**, 3463 (1965).
- (8) J. B. Uytterhoeven, L. G. Christner, and W. K. Hall, *ibid.*, **69**, 2117 (1965).
- (9) J. L. White, A. N. Jelli, J. M. André, and J. J. Fripiat, *Trans. Faraday Soc.*, **63**, 461 (1967).
- (10) R. N. Jones and C. Sandorfy, "Chemical Applications of Spectroscopy," W. R. West, Ed., Interscience Publishers Inc., New York, N. Y., 1956, Chapter V.
- (11) C. N. R. Rao, "Chemical Applications of Infrared Spectroscopy," Academic Press, Inc., New York, N. Y., 1963, Chapter IV.

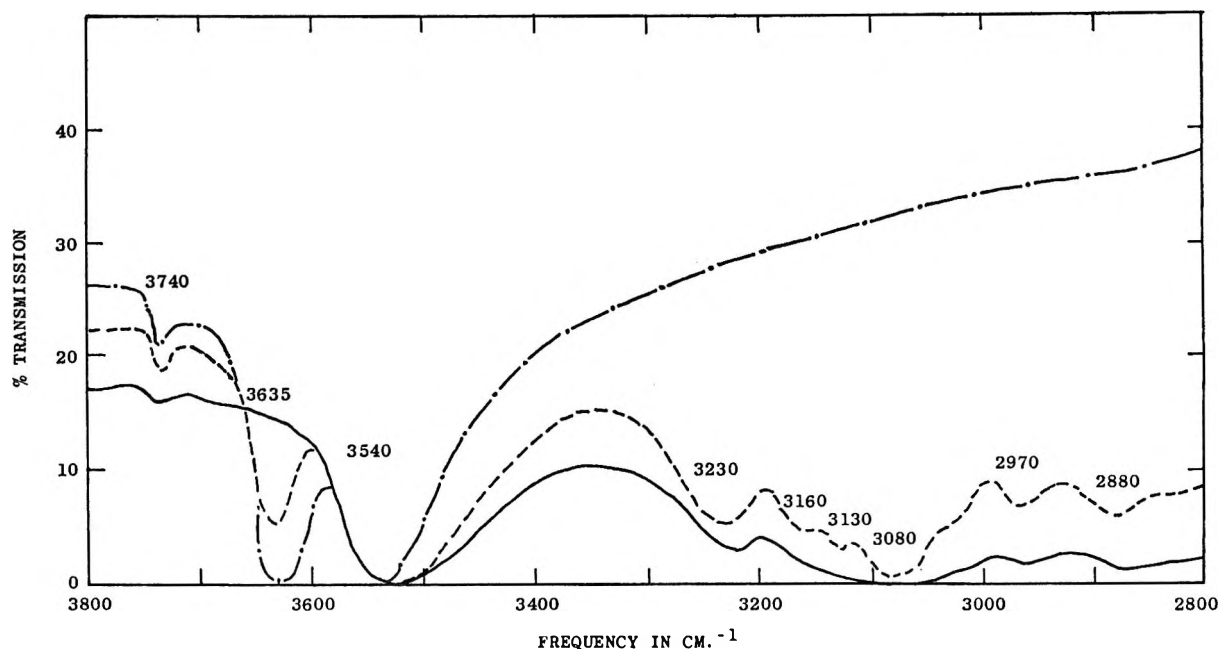


Figure 1. Infrared spectra of pyridine adsorbed on HY(I). Spectra were recorded at 260° with a disk originally containing 19 mg/cm^2 . The lines have the following significance: - - - -, original spectrum under vacuum; —, spectrum under 0.1 mm of pyridine; - · - ·, spectrum after overnight evacuation.

NaY(I). No structural hydroxyl groups, however, could be observed by infrared techniques. The interaction of pyridine at 260° was considerably weaker. Much less material was adsorbed and nearly all of this existed in the form of Lewis-bonded rather than protonated species. The adsorbed material could be completely removed by only a 15-min evacuation at 260° .

Pyridine Adsorption on Other Ion-Exchanged Faujasites. Changing the nature of the cation in the faujasite cages is known to affect markedly the material's catalytic properties.^{12,13} Consequently, it becomes of interest to investigate the effect of ion exchange on the surface acidity as determined by pyridine adsorption. A summary of intensities of key infrared bands recorded at 150° is given in Table II for a series of ion-exchanged faujasites.

The 1540-cm^{-1} band reflecting the amount of Brønsted acidity is most pronounced on HY(I). With the divalent faujasites, its intensity is reduced almost 10–20-fold. The existence of this small amount of Brønsted acidity indicated that some hydroxyl groups still exist on the surface and are capable of protonating the adsorbed pyridine. Several investigations have demonstrated the great difficulty in completely removing the hydroxyl groups by extensive evacuation at elevated temperatures.^{8,14} The most pronounced band on the divalent faujasites is that at 1450 cm^{-1} characteristic of coordinately bound pyridine. Its intensity is much larger than that on HY(I).

With the monovalent faujasites, no Brønsted acidity is observed even though trace amounts of hydroxyl

groups would still be expected to be present.⁸ Lewis acidity, however, is still present in LiY(II) and NaY(II). The potassium form is the least acidic and exhibits no pyridine absorption bands at these conditions.

Effects of H_2O on Pyridine Adsorption. With amorphous silica-alumina catalysts, it has been shown that Lewis sites can be partially transformed to Brønsted sites by exposure to small amounts of water.³ This effect is not observed with NaY. However, with CaY and MgY, trace amounts of water have a very pronounced effect on the relative distribution of the two types of acidity. Spectra illustrating this for CaY(II) at 260° are shown in Figure 2 for the $3800\text{--}2800\text{-cm}^{-1}$ region and in Figure 3 for the $1800\text{--}1200\text{-cm}^{-1}$ region.

From the initial spectrum (A) under vacuum, little evidence is seen for hydroxyl groups in the OH stretch region of $3800\text{--}3500 \text{ cm}^{-1}$. Upon exposure to 0.1 mm of pyridine (spectrum B), the adsorbed species consist primarily of coordinately bound pyridine as evidenced by a strong band near 1440 cm^{-1} . Some pyridinium ions, however, are present having the characteristic 1540-cm^{-1} absorption band. The concentration is not sufficient to produce observable vibrations in the NH stretch region. Spectrum C was

(12) V. J. Frilette, P. B. Weisz, and R. L. Golden, *J. Catalysis*, **1**, 301 (1962).

(13) P. E. Pickert, J. A. Rabo, E. Dempsey, and V. Schomaker, *Proc. Third Intern. Congr. Catalysis*, 714 (1964).

(14) J. L. Carter, P. J. Lucchesi, and D. J. C. Yates, *J. Phys. Chem.*, **68**, 1385 (1964).

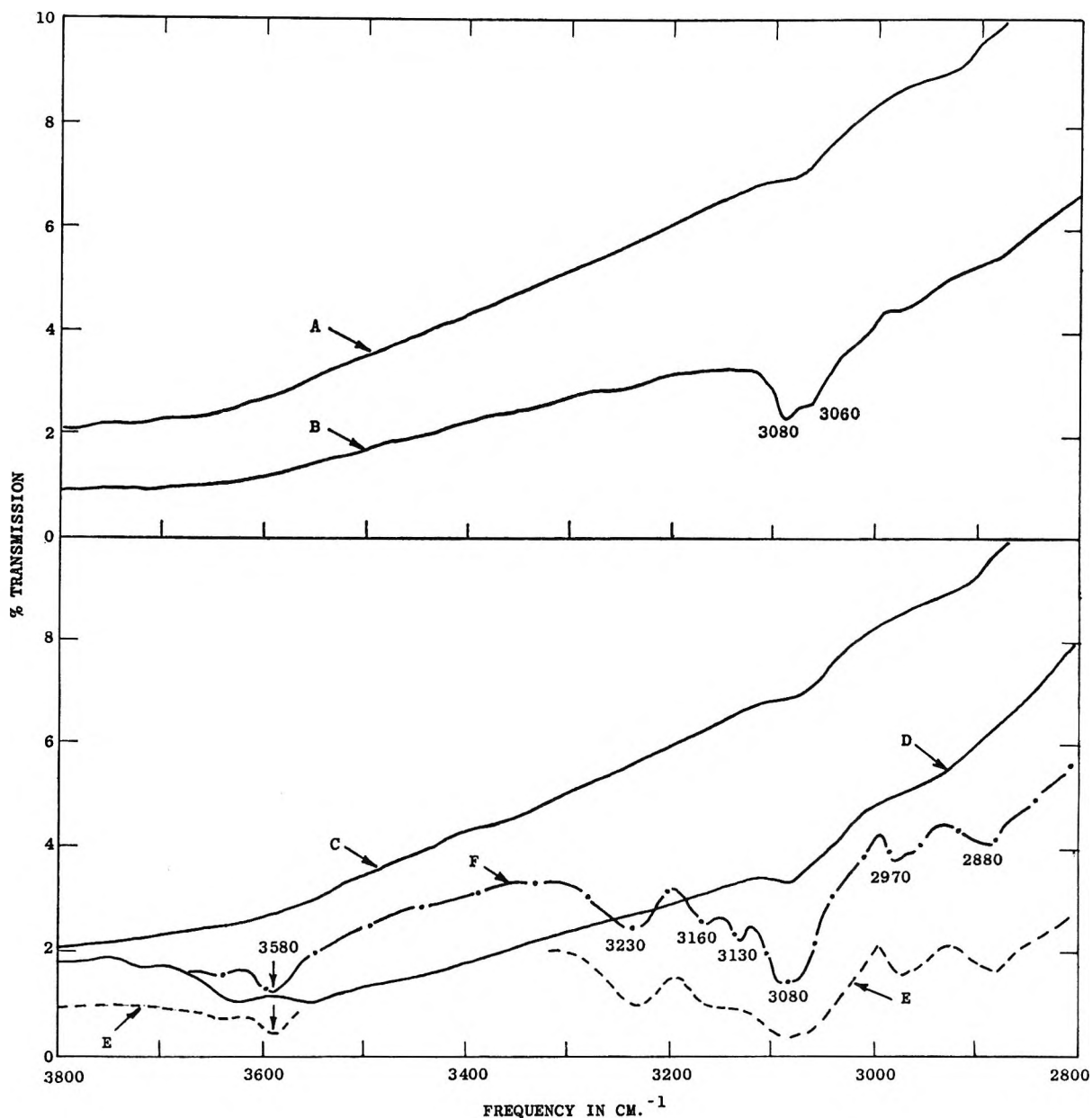


Figure 2. Effect of H_2O on pyridine adsorption on CaY(II) at 260° . Spectra were recorded on a disk containing 15 mg/cm^2 . The various spectra were obtained in series at the following conditions: A, initially under vacuum; B, exposed to 0.1 mm of pyridine; C, reevacuated for 16 hr; D, exposed to 1.5 mm of H_2O ; E, reevacuated briefly and exposed to 0.1 mm of pyridine; F, evacuated 1 hr.

obtained after evacuation for 16 hr and is nearly identical with the original spectrum (A). When the solid is exposed to a pressure of 1.5 mm of water, OH groups are formed and also some bulk water is adsorbed. The spectrum taken under these conditions (D) shows OH groups near 3550 and 3650 cm^{-1} and also a water bend vibration near 1630 cm^{-1} . The faujasite was then briefly evacuated (10 min) at 260° and the material was reexposed to 0.1 mm of pyridine. The resulting spectrum (E) is totally different from that originally observed before water addition. The final spectrum (F) was taken after an evacuation of 1 hr.

The creation of Brønsted acidity by water addition is clearly seen by the pronounced increase in intensity

of the 1540-cm^{-1} band. Additional evidence is provided by the appearance of three NH stretch vibrations at 3230 , 3160 , and 3130 cm^{-1} . This type of acidity apparently results from water reacting with the sites formerly responsible for Lewis acidity since the 1440-cm^{-1} band is much less pronounced after the water addition.

Similar phenomena are also observed with the magnesium form of faujasite. Initially, the material reacts with pyridine to produce largely coordinately bound species. However, water transforms the Lewis to Brønsted sites resulting in a much increased intensity of the 1540-cm^{-1} band.

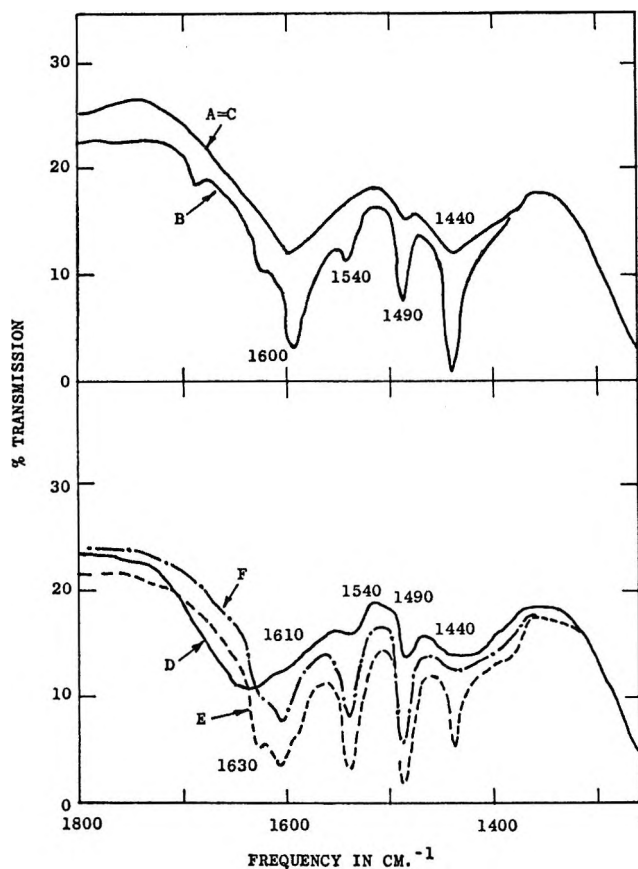


Figure 3. Effect of H_2O on pyridine adsorption on CaY(II) . Spectra were recorded under the same conditions as listed in Figure 2.

IV. Discussion

The hydroxyl group structure of HY has been the subject of a number of investigations.^{5-9,14} The low-intensity band near 3740 cm^{-1} is almost universally observed on silica-containing materials and hence it is not necessarily characteristic of HY. Since zeolites are rarely completely free of amorphous material, it could easily result from an OH group on the impurity. Different interpretations have been applied to the remaining two intense OH frequencies near 3635 and 3540 cm^{-1} . Angell and Schaffer⁷ have attributed the lower frequency band to interaction between two adjacent hydroxyl groups. Liengme and Hall,⁴ however, suggested that the two bands may result from OH groups in different crystallographic positions. Our present results on the preferential interaction of pyridine with the OH groups at 3635 cm^{-1} are similar to those of the latter authors. Consequently, the data favor the explanation that the OH groups at 3635 cm^{-1} are inside the adsorption cavities in a position capable of direct interaction with pyridine. Similar groups at 3540 cm^{-1} could be in inaccessible bridge positions located between sodalite units. However, in a recent investigation by Hughes,⁵ the lower frequency groups were found to interact with piperidine and, conse-

quently, must be close to the large adsorption chambers.

The variation in the type and amount of acidity with the nature of the cation is particularly interesting. The Brønsted acidity, for example, appears to increase with the polarizing power of the cation as defined by the ratio of ionic charge to radius (e/r). This latter quantity can only be considered as an estimate since the ionic radius has been shown to depend on the nature of the crystal.¹⁵ Since no information is currently available on the size of these ions in zeolites, Pauling's crystal radii were used.¹⁶ These results suggest that cations of high polarizing power are able to perturb nearby hydroxyl groups causing the hydrogens to become acidic enough to protonate pyridine. Richardson¹⁷ has suggested this type of reaction and his esr results on the effect of polarizing power of the cation on the ionization of aromatics are in line with our acidity measurements. With the monovalent ions, no Brønsted acidity is observed. Basila and Kantner¹⁸ reported on the acidity of amorphous silica-alumina materials and for a K-poisoned sample containing only Lewis acidity, the absorption coefficient for the 1490-cm^{-1} band was only one-fourth of that for the 1450-cm^{-1} band. This is the same ratio that we observed on sodium faujasite. However, with LiY(II) which also shows only Lewis acidity, the intensity of the 1490-cm^{-1} band is only about one-eighth of the 1450-cm^{-1} band. Apparently, the ratio of these bands cannot be considered to be independent of the nature of the cation and complicates the estimation of the relative amounts of Lewis and Brønsted acidity.

The effect of trace amounts of water on the distribution of the two types of acidity for the Ca and Mg faujasites is especially significant. Since these ions are thought to perturb OH groups resulting in their protonation of adsorbed pyridine, the amount of Brønsted acidity is limited by the number of OH groups. When these are increased by addition of water, the pyridine bound to Lewis sites becomes protonated and the intensity of the infrared band at 1540 cm^{-1} increases. The striking similarity between the spectrum of pyridine on water-treated CaY (spectrum F, Figure 2) and pyridine on HY (dashed line, Figure 1) suggests that the materials may have some of the same structural features. For example, water could be reacting with the calcium ions to form $-\text{Ca}-\text{OH}$ and $-\text{OH}$

(15) K. B. Harvey and G. Porter, "Introduction to Physical Inorganic Chemistry," Addison & Wesley, Reading, Mass., 1965, Chapter II, p 24.

(16) L. Pauling, "The Nature of the Chemical Bond," 3rd ed, Cornell University Press, Ithaca, N. Y., 1960, p 514.

(17) J. T. Richardson, paper presented at Symposium on Mechanisms of Heterogeneous Catalysis, 153rd National Meeting of the American Chemical Society, New York, N. Y., Sept 1966, Preprint Vol. 11, No. 4, A-123 (1966).

(18) M. R. Basila and T. R. Kantner, *J. Phys. Chem.*, **70**, 1681 (1966).

groups on the surface. The latter would be similar to those on HY and if in cage positions could react with pyridine to form pyridinium ions. Indications of the formation of these OH groups are given in spectra D, E, and F of Figure 2. Analogous effects occur on MgY. With the Na form and presumably the Li and K forms as well, the polarizing power of the ions is not sufficient to dissociate significant amounts of water to

form structural OH groups. However, Basila, Kantner, and Rhee³ do report that water on a K-poisoned amorphous silica-alumina catalyst transforms a small portion of the Lewis into Brønsted sites. Their studies were done at 150° rather than the 260° used in the present study. This low temperature could have caused the concentration of adsorbed species to be sufficiently high to detect their existence.

Measurement of Activities in Gallium-Indium Liquid Alloys¹

by G. J. Macur, R. K. Edwards, and P. G. Wahlbeck

Department of Chemistry, Illinois Institute of Technology, Chicago, Illinois 60616 (Received September 25, 1967)

Activities for both components have been determined for the Ga-In system. Activities were derived from effusion measurements utilizing the multiple Knudsen-cell effusion technique. Positive deviations from ideality occur for the activities of both components. Entropies of mixing were derived from the free-energy data of this study and calorimetric data recently reported in the literature. Integral entropies of mixing were found to be less than values for ideal solutions.

Introduction

Thermodynamic information for binary liquid metal alloys is important to the advancement of theories of metals. In the work being reported, thermodynamic activities in the Ga-In system have been determined experimentally. No direct experimental measurements have been reported in the literature.

Activities were obtained from Knudsen effusion measurements leading to evaluations of partial pressures of the alloy components. The effusion measurements were performed by means of a "multiple Knudsen-cell" technique.² Essentially, the technique consists of performing simultaneous measurements for a large number (up to 14) of alloy compositions, each of which is contained within its own effusion cell, and all cells are contained within the same isothermal zone (large molybdenum block). This technique was developed specifically to achieve for each selected temperature a high relative precision in that set of data. Thus, improved consistency should be achieved in evaluations making use of the Gibbs-Duhem integration method, since the integration appropriately is being performed for a set of data which are truly isothermal. This improvement is desirable, particularly if no direct measurement is made of the composition of the effusing vapor, but instead, compositions are obtained by the "calculation method."³ Since both components are volatile in the Ga-In system, compo-

sitions of the gas phase must necessarily be evaluated. The calculation method was chosen because it greatly simplifies the experimentation, although it does demand data of high relative precision.

Previous information bearing on the thermodynamic activities of the gallium-indium system is of an indirect nature. Svirbely and Read,⁴ utilizing information on the ternary Zn-In-Ga system, calculated activities for this binary system. Bros^{5a} and Bros, Castanet, and Laffitte^{5b} have recently reported calorimetric measurements of enthalpies of mixing for the Ga-In system.

Experimental Section

Apparatus and Procedure. The total rates of effusion of gallium and indium from 14 alumina Knudsen cells under isothermal conditions were measured with an ap-

(1) Based on a thesis by G. J. Macur submitted to the Illinois Institute of Technology, Chicago, Ill., in partial fulfillment of the requirements for the Ph.D. degree, 1955. Presented before the Physical Chemistry Division at the 150th National Meeting of the American Chemical Society, Atlantic City, N. J., Sept 1965.

(2) G. J. Macur, R. K. Edwards, and P. G. Wahlbeck, *J. Phys. Chem.*, **70**, 2956 (1966).

(3) R. K. Edwards and M. B. Brodsky, *J. Am. Chem. Soc.*, **78**, 2983 (1956).

(4) W. J. Svirbely and S. M. Read, *J. Phys. Chem.*, **66**, 658 (1962).

(5) (a) J. P. Bros, *Compt. Rend.*, **263**, 977 (1966); (b) J. P. Bros, R. Castanet, and M. Laffitte, *ibid.*, **264**, 1804 (1967).

paratus which has been previously described;² all procedures used in obtaining the data were also described.²

Effective orifice areas were determined by allowing mercury to effuse through the orifice; the vapor pressure of mercury was calculated from an equation evaluated by Carlson, *et al.*,⁶ based on the data of Busey and Giaque.⁷ The orifice areas were corrected for thermal expansion appropriate for the temperature of the run by using the linear coefficient of thermal expansion of $7.8 \times 10^{-6} \text{ deg}^{-1}$.⁸

Materials. Indium wire and gallium metal with stated purities of 99.999% were purchased from A. D. MacKay, Inc. Indium wire was washed with pure benzene prior to insertion into the Knudsen cells. Since gallium metal reacts slowly with moist air, the amount of exposure to the laboratory atmosphere of the gallium was minimized.

Alloy Compositions. Alloy solutions of desired compositions were prepared initially by adding appropriate masses of indium and gallium to the Knudsen cells. Each Knudsen cell contained at least 6 g of alloy. The composition of a given alloy was assumed to remain constant during an effusion run.

In the worst case, the mole fraction of indium, X_{In} , changed by less than 2 ppt during the course of a run at a particular temperature. For $1.0 > X_{\text{In}} > 0.4$, indium in the amount corresponding to the observed mass loss was added to the Knudsen cell at the end of each run. The addition of indium was an attempt to restore the composition of the alloy to its original value in preparation for a subsequent run at a new temperature and was based on the assumption that gallium volatilization was negligible. The validity of the latter assumption became obvious during the course of the final evaluations of activities.

Results

The experimental data are presented in Table I. Activities of In in the Ga–In liquid solutions were calculated using the definition for activity: $a_{\text{In}} = p_{\text{In}}/p_{\text{In}}^0$, where p_{In} is the partial pressure of In in equilibrium with the alloy and p_{In}^0 is the vapor pressure of pure In. The p_{In}^0 values were obtained from earlier experiments² in which the same apparatus was used. The activity coefficient, γ_{In} , was computed by setting $\gamma_{\text{In}} = a_{\text{In}}/X_{\text{In}}$, where X_{In} is the atom fraction of In in the liquid metallic solution. For computation purposes the α function of Darken and Gurry⁹ was used: $\alpha_i = \log \gamma_i/(1 - X_i)^2$.

For solutions containing less than 5% indium, the partial pressure of gallium must be less than that of pure Ga, and it was assumed initially to be greater than the partial pressure given by Raoult's law. (Later the assumption was validated completely by the activity data.) Because of the very low concentrations of In, α_{In} varies only slightly between these two indium

pressure limits. For example, with cell I at 1269°K, $X_{\text{In}} = 0.0399$, α_{In} was 0.36 and 0.34, respectively, and the average value was taken.

For solutions containing more than 5% indium, the calculation method of Edwards and Brodsky³ was used. The calculation method uses a successive approximation to obtain the true activities. A first-calculated α , $\alpha_{\text{In}}(1)$, was determined from the Knudsen-cell data by assuming that the vapor in equilibrium with the Ga–In alloys was pure indium; this assumption is a good one since the vapor pressure of pure indium is *ca.* 11 times that of pure gallium.² The values of $\alpha_{\text{In}}(1)$, after smoothing the data to a curve, were used to calculate a first curve for $a_{\text{Ga}}(1)$ ¹⁰ and $a_{\text{In}}(1)$. For a second approximation in the calculations for α_{In} , the values of $a_{\text{Ga}}(1)$ and $a_{\text{In}}(1)$ were used to determine the vapor composition. Values of $\alpha_{\text{In}}(2)$ were used to calculate $a_{\text{Ga}}(2)$ and $a_{\text{In}}(2)$. Any further successive treatments produced changes in activities which were much smaller than the experimental uncertainties in the data, and hence values of α and a used in later calculations for solutions containing more than 5% indium are from the second approximation.

A difficulty arose in run 3. It was found that the measuring thermocouple did not reach the same position in the molybdenum block as in the two previous runs. For this reason, the measured temperature was suspected to be incorrect, and this inference is supported by the observation of inconsistent α values for indium when the measured value for the temperature is used. The mass-loss rates calculable from the data in Table I indicate that the temperature of run 3 is between that of runs 1 and 2. In order to obtain a corrected value of the temperature for run 3, an interpolative procedure was devised. A "calculated" temperature for each cell, B through G, for run 3 was evaluated by interpolating from a linear $\log \gamma_{\text{In}}$ vs. $1/T$ plot between sets 1 and 2 for the given cell. Actually, since γ_{In} is a function of temperature, the procedure involved the appropriate successive interpolations. The average of these calculated temperatures, 1247°K, was selected as the temperature of run 3 and was only 4° higher than the measured temperature. The data from run 3 are, in comparison with those from the other

(6) K. D. Carlson, P. W. Gilles, and R. J. Thorn, *J. Chem. Phys.*, **38**, 2725 (1963).

(7) R. H. Busey and W. F. Giaque, *J. Am. Chem. Soc.*, **75**, 806 (1953).

(8) "Physical Properties," Bulletin No. D 763, McDanel Refractory Porcelain Co., Beaver Falls, Pa., 1963.

(9) L. S. Darken and R. W. Gurry, "Physical Chemistry of Metals," McGraw-Hill Book Co., Inc., New York, N. Y., 1953.

(10) Values for $\log \gamma_{\text{Ga}}$ were calculated by

$$\log \gamma_{\text{Ga}} = -\alpha_{\text{In}}X_{\text{In}}X_{\text{Ga}} - \int_{X_{\text{Ga}}=1}^{X_{\text{Ga}}=X_{\text{Ga}}} \alpha_{\text{In}}dX_{\text{Ga}}$$

from data for α_{In} .

Table I: Experimental Effusion Data for Ga-In Alloys and Derived Values of the α Functions of Indium

Effusion cell	Orifice area at 50°, cm ² × 100	Atom % indium	Total mass effused, g × 10 ⁶			$\alpha_{In} = \frac{\log \gamma_{In}}{(1 - X_{In})^2}$		
			Run no. 1 ^b	Run no. 2 ^c	Run no. 3 ^d	Run no. 1 ^{b,h}	Run no. 2 ^{c,h}	Run no. 3 ^{d,h}
B	0.09568	98.0	1350	1087	1256	15	21	51
B*	0.1051	94.7	1101	927	1075	6.48	6.85	9.94
C	0.1458	92.0	1811	1469	1702	4.37	3.40	4.12
D	0.1947	90.0	2320	1924	2218	2.55	3.46	2.50
E	0.2000	88.0	2962	2533	2962	0.75	1.82	1.96
F	0.3950	88.0	3695	3116	3588	2.12	2.93	2.51
G	0.4962	50.0	4359	3492	4024	0.47	0.415	0.47
H	0.4955	49.9	3918 ^f	3455	4007	0.31 ^f	0.42	0.47
I	0.5750	3.99	1116	988	1106	0.35	0.44	0.43
J**	0.7436	4.01	1389	1081	1233	0.46	0.46	0.40
K**	0.9583	1.97	1203	1502 ^g	1128	0.35	0.76 ^g	0.34
L	1.0310	2.00	1456	1216	1375	0.37	0.44	0.35
M***	1.1729	0.98	1431	1126	1269	0.48	0.51	0.36
N	1.4022	1.00	1692	1318	1485	0.47	0.49	0.34

^a Expansion-of-orifice corrections were made using the coefficient of thermal expansion of $7.8 \times 10^{-6} \text{ deg}^{-1}$. ^b At 1269°K for 225.29 min. ^c At 1223°K for 434.76 min. ^d At 1247°K for 330.15 min. ^e Cells J*, K*, and M*** were calibrated with pure Ga by comparison with cells I, L, and N which were calibrated with Hg. ^f This value is too low, because it should agree with cell G. The values of G and F are nearly identical in runs 2 and 3. ^g This value is too high, because it is out of sequence both horizontally and vertically. ^h The α values are the final results of the iterative procedure discussed in the text.

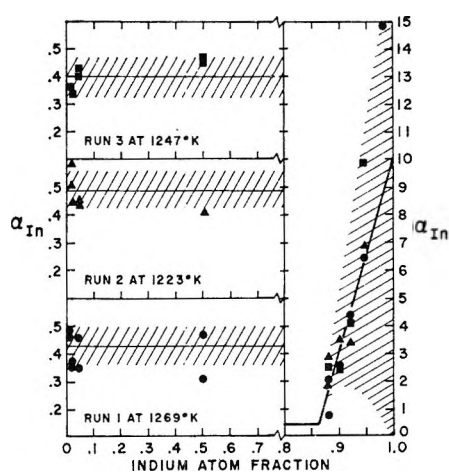


Figure 1. α -function values for indium. The solid line represents the average α_{In} value for each run for $0 < X_{In} < 0.86$. The solid line $0.86 < X_{In} < 1$ is from a least-squares fit of data from all three runs to a linear equation. The shaded regions represent the uncertainty in α_{In} based on a 3% uncertainty in vapor-pressure measurements.

two runs, of restricted value, and they are given a lower weight in the evaluation of the enthalpy data.

In Table I are indicated the values of α_{In} which were calculated for each of the experimental determinations. In Figure 1 are plotted α_{In} vs. X_{In} for the three runs. The derived activity curves are shown in Figure 2.

Discussion

In the Introduction, the particular advantages of the multiple Knudsen-cell technique for activity measurements in a binary system were pointed out. In a previous paper,² it was demonstrated that with

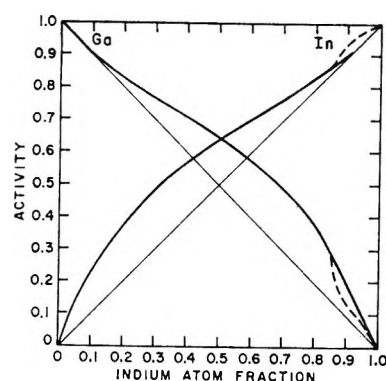


Figure 2. Activities in liquid Ga-In solutions at 1269°K were calculated using α_{In} data of Figure 1. The solid line represents the calculated activities based on $\alpha_{In} = 0.42$ at all compositions. The dashed curve, $0.86 < X_{In} < 1$, represents the calculated activities based on the given straight line through the α_{In} data of Figure 1.

sets of vapor-pressure measurements precisions as good as 1.0 and no worse than 8.9%, averaging to ca. 3%, were obtained under the isothermal conditions achievable in this technique. It would follow that, in a single experiment, activities may be determined at several compositions with this same level of precision since, of course, they are all relative to the same reference state.

The consistent behavior of the α -function data seen in Figure 1 indicates that the expected precision was achieved. The α function is extremely sensitive to experimental error.

The activity curves in Figure 2 show positive deviations from Raoult's law at all compositions for both

components. These curves were calculated in two ways for the composition region $0.86 < X_{\text{In}} < 1$: (1) activities calculated from the α_{In} data represented by the given least-squares line of Figure 1 (dashed line) and (2) activities calculated by assuming that $\alpha_{\text{In}} = 0.42$ (solid line). An error analysis of the α_{In} data shows that the latter method is nearly permitted (see error bands on Figure 1). There is no basis for a choice between the two curves. Svrbely and Read⁴ have derived activity curves for the Ga-In system from their data for the Ga-In-Zn, In-Zn, and Ga-Zn systems, which they obtained from emf measurements. Their calculated data show strong positive deviations from Raoult's law behavior for Ga over the entire composition range. For indium, a strong positive deviation was derived for $0 < X_{\text{In}} < 0.5$, and for $0.5 < X_{\text{In}} < 1$ the activities approximated Raoult's law behavior. Svrbely and Read make only a "semiquantitative claim" for their derived activity values of Ga and In.

Some excellent data for the enthalpy of mixing in this binary system recently have been determined by Bros, *et al.*,^{5a,b} by microcalorimetric measurements. They obtained an integral enthalpy curve which is symmetrical with respect to the mole fraction with a maximum of 265 cal. These data indicate that ΔH is independent of temperature from 150° to 469° within experimental error. From the integral enthalpy curve, they derived partial molar enthalpies which were also positive. The only purpose in deriving enthalpy data from the activity data is to check for inconsistencies. The enthalpy data derived¹¹ from the activity results were found to be in satisfactory accord with Bros' results; for example, the maximum in the integral enthalpy was at *ca.* 2.2 kcal, but the uncertainty is probably *ca.* 2 kcal.

From the enthalpy data of Bros^{5a} and Bros, *et al.*,^{5b} and the free-energy data from this study, one may cal-

culate entropy data; these data are given in Table II. The entropies of mixing are less than ideal solution values and give an indication of ordering effects in the solutions.

Table II: Integral Quantities for Ga-In Alloys at 1269°K

X_{In}	ΔG , ^a cal	ΔH , ^b cal	ΔS , cal deg ⁻¹
1.00	0	0	0
0.90	-567	84	0.51
0.80	-862	168	0.81
0.70	-1016	220	0.97
0.60	-1098	248	1.06
0.50	-1124	265	1.09
0.40	-1098	248	1.06
0.30	-1016	220	0.97
0.20	-862	168	0.81
0.10	-595	96	0.54
0	0	0	0

^a Calculated by means of $\Delta G = RT\{X_{\text{In}} \ln a_{\text{In}} + X_{\text{Ga}} \ln a_{\text{Ga}}\}$. Values of a_{In} and a_{Ga} were obtained from Figure 2. ^b Based on calorimetric data of Bros, *et al.*^{5a,b}

Acknowledgments. The authors gratefully acknowledge the support of this research by the Air Force Office of Scientific Research through Contract No. AF 49(638)-346 and the Atomic Energy Commission through Contract No. AT(11-1)-1029. G. J. M. wishes to thank the Illinois Institute of Technology for a fellowship for the 1958-1959 academic year. G. J. M. and R. K. E. acknowledge the support of the Chemical Engineering Division of Argonne National Laboratory during the preparation of the manuscript.

$$(11) \Delta H = -R \frac{\partial}{\partial(1/T)} \{X_{\text{In}} \ln a_{\text{In}} + X_{\text{Ga}} \ln a_{\text{Ga}}\}.$$

Isotopic Exchange of Oxygen on Platinum Powder¹

by Y. L. Sandler and D. D. Durigon

Westinghouse Research Laboratories, Pittsburgh, Pennsylvania 15235 (Received September 26, 1967)

A kinetic study of the isotopic oxygen exchange on platinum powders between -195 and $+300^\circ$ is presented. Three different weak modes of chemisorption were found which change with time and temperature. Adsorption and isotopic dilution experiments showed that no oxygen beyond the equivalent of one monolayer was in or on the powders which were well annealed and freed of carbon and hydrogen. The uptake of several monolayers of oxygen described in the literature appears to be caused by the presence of impurities or a high concentration of defects. Nitrogen does not exchange on platinum or interfere with the oxygen exchange up to 600° .

Introduction

In a recent study of the oxygen chemisorption on silver,^{2,3} different modes of chemisorption were found and studied on silver above 160° . At this temperature the adsorption becomes, in part, reversible, and the isotopic oxygen-exchange reactions thus can be measured. Reactions of this type are particularly suited for studying different modes of chemisorption and their mutual interaction. The present study deals with a similar investigation on platinum. The investigation of the modes of adsorption on platinum was motivated by the finding that the cathodic behavior of the platinum-oxygen electrode is very sensitive to its thermal and electrochemical prehistory.⁴ A preliminary pressure-temperature scan⁵ taken with a platinum powder indicated that the onset of reversibility lies at about 250° . The temperature range investigated was up to 300° , where the exchange became too fast to be measured in our system. The methods in this work are similar to those used in the previous investigation on silver. The behavior of platinum, however, turned out to be rather different from silver, as will be discussed in the present paper. The possibility of "surface solution" of oxygen on platinum was also investigated.

A slow uptake of oxygen by platinum at elevated temperatures was reported in the literature on foils,⁶ evaporated films,^{7,8} and powders^{9,10} amounting to several monolayers or more. The phenomenon (if not simply due to the oxidation of impurities) could be an excess uptake beyond one monolayer in the first outer layers of the metal, where it may affect the properties of the outer surface, or an excess uptake could be due to occlusion in structural defects, such as crevices, grain boundaries, or dislocations. The appearance of new phases on prolonged contact of platinum with oxygen was observed;¹⁰ these were claimed to be due to certain platinum oxides. Surface solution of oxygen was also reported to exist on platinum electrodes in aqueous electrolytes.^{11,12}

For the present work, special care was taken to

remove carbon and hydrogen from the system. In the case of silver, residual hydrogen was found³ to have a considerable influence on the adsorption of oxygen. A study of the isotopic exchange of nitrogen on platinum is also briefly discussed.

Experimental Section

The platinum powder was supplied by Engelhard Industries. It was produced from 99.999% ammonium chloroplatinate and was subjected to prolonged heating in air at 800° . Only the particles passing 350 mesh were used. The measurements were made in a static system, in a quartz vessel of 30–40-cm³ volume which could be isolated by a Hoke metal valve from a gas-handling system, mercury diffusion pump, and liquid nitrogen traps. BET surface areas were determined by krypton adsorption by means of thermistor gauges. A mass spectrometer was coupled to the system for analyzing the isotopic oxygen mixtures and monitoring the impurities desorbing during evacuation of the powder. The experiments with one sample (Pt(III))

(1) Work in part supported by the Advanced Research Projects Agency and sponsored by the Office of Naval Research.

(2) Y. L. Sandler and D. D. Durigon, *J. Phys. Chem.*, **69**, 4201 (1965).

(3) Y. L. Sandler, S. Z. Beer, and D. D. Durigon, *ibid.*, **70**, 3881 (1966).

(4) Y. L. Sandler and E. A. Pantier, *J. Electrochem. Soc.*, **112**, 928 (1965).

(5) In this method, a fixed amount of gas is admitted to the reaction vessel and the pressure is recorded while the temperature is driven up. At the onset of reversibility, the pressure goes through a minimum and begins to increase with temperature as required in a reversible system. Cf. ref 2.

(6) A. Berliner, *Wied. Ann.*, **35**, 807 (1888).

(7) T. V. Kalish and R. K. Burstein, *Dokl. Akad. Nauk SSSR*, **81**, 1093 (1951).

(8) A. V. Khasin and G. K. Borekov, *ibid.*, **152**, 1387 (1963).

(9) H. Reischauer, *Z. Physik. Chem. (Leipzig)*, **B26**, 399 (1934).

(10) Cf. S. Z. Roginsky, *Proc. Intern. Congr. Catalysis, 3rd, Amsterdam, 1964*, **2**, 939 (1965).

(11) W. Böld and M. Breiter, *Electrochim. Acta*, **5**, 145 (1961).

(12) S. Schuldiner and T. B. Warner, *J. Electrochem. Soc.*, **112**, 212 (1965).

were carried out on a mass spectrometer of higher accuracy after transfer from the vacuum system.

O^{18} (94%) was procured from the Weizmann Institute, Israel, in the form of HgO . In most adsorption and exchange experiments, a small amount of argon, which is not adsorbed, was added to the oxygen mixtures as a reference gas. The amounts of the different isotopes in the gas phase and in the adsorbed phase present at any time can then be determined by measuring the ratio of the gas concentrations, the amounts withdrawn for sampling, and the amount of gas left in the system at the end of a run. These amounts, given in cubic centimeter atmospheres, were measured by expanding the gas into a standard volume and reading the pressure on a capacitance manometer.

Four samples of platinum powder were tested and gave essentially the same results. The powders were subjected to degassing for about 1 week, at temperatures up to 630° , with frequent contact with low-pressure oxygen to remove carbon, which often is the main impurity¹³ in high-purity metals.

Contrary to usual practice, no hydrogen was at first used for cleaning the surface. The effect of hydrogen pretreatment on the activity of the surface was later checked.

Results

The Exchange Reaction $O^{16}_2 + O^{18}_2 \rightarrow 2O^{16}O^{18}$. To measure this reaction (homomolecular exchange), an approximately equimolar mixture of O^{16}_2 and O^{18}_2 was admitted to a quartz vessel of 135-cm^3 volume containing 20 g of platinum powder (Pt(III)). After degassing and low-pressure oxygen pretreatment, it had a BET surface area of $1100\text{ cm}^2/\text{g}$.

The rate of approach to isotopic equilibrium often was not an exponential function of time, as would be expected when the adsorption equilibrium is established. (At equilibrium, $K = [O^{16}O^{18}]^2/[O^{16}_2][O^{18}_2] = 4$, which gives $[O^{16}O^{18}] = 50\%$ for equimolar mixtures.) The apparent rate constant, k , was evaluated from successive measurements, under the assumption that between these an exponential decay law is obeyed.

In Figure 1, the rate at which isotopically equilibrated molecules appear in the gas phase, *i.e.*, k times the number of oxygen molecules in the gas phase, is plotted logarithmically *vs.* the inverse absolute temperature for an oxygen mixture at 9 torr. After pumping the sample at 600° , an appreciable activity is found at relatively low temperatures. On increasing the temperature, at about 250° , a higher slope is reached. On decreasing the temperature the low-temperature activity is depressed. The high-temperature oxygen strongly reduces the low-temperature activity. The cycle can be repeated after pumping the surface at 600° .

A rapid change of activity with time was observed throughout the entire temperature range down to

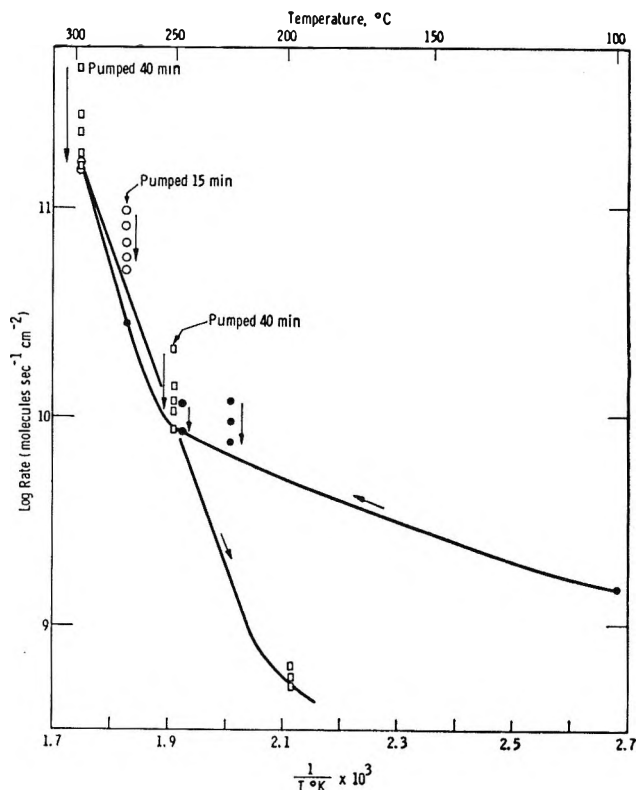


Figure 1. Isotopic exchange rate *vs.* inverse absolute temperature (sample, Pt(III)).

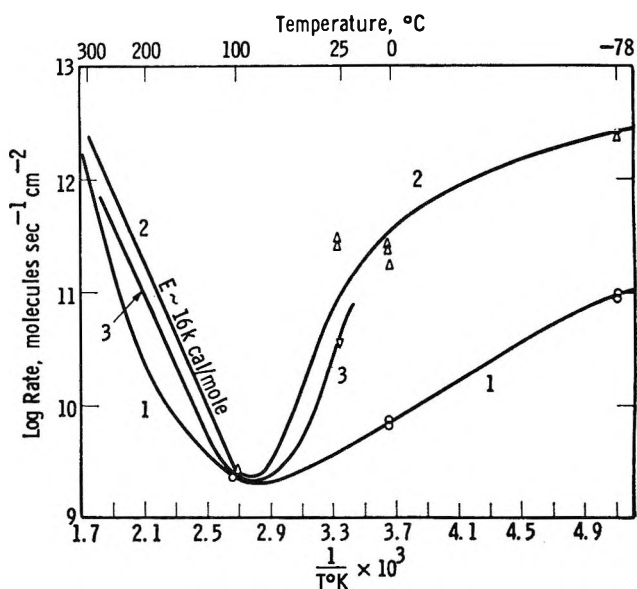


Figure 2. Isotopic exchange rate *vs.* inverse absolute temperature (on Pt(IV)) after different pretreatments: (1) after oxygen treatment and pumping; (2) after hydrogen cleaning and pumping for 2 days at 600° ; (3) after repeated oxygen contact and pumping at 620° for 16 days.

-78° (cf. Figure 2). The points in Figure 1 taken with the same dose of gas are marked in the same manner. At 275° , for example, the point marked by the

(13) Y. L. Sandler and D. D. Durigon, *Trans. Faraday Soc.*, **62**, 215 (1966).

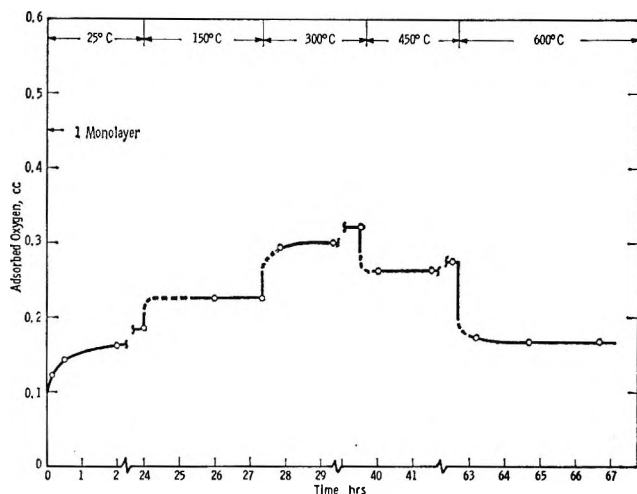


Figure 3. Oxygen adsorption vs. time and temperature.

black circle was taken with the charge of oxygen previously used at lower temperatures. The system was then pumped for 15 min. The activity obtained with a new dose of gas characteristically was considerably higher in the beginning and decreased with time. The change in the amount of oxygen adsorbed from point to point was quite small. The decrease in activity is due to a change in the mode of adsorption with time. The chemisorbed oxygen assumes a more stable form and the reversibility of the adsorption is therefore reduced.

Oxygen Adsorption. Figure 3 shows the amounts of oxygen adsorbed on the same platinum sample at different temperatures. Such curves are the by-product of exchange measurements. (See Experimental Section.) From the curve shown and similar ones taken in other experiments, it is seen that the adsorbed amount increases up to 250°, where it reaches a maximum of about 70% of a monolayer and then decreases. (Monolayer coverage will be defined by 1.3×10^{15} oxygen atoms/cm².) To the measured value a certain amount has to be added, which cannot be desorbed by pumping at 600° before the start of a run. At low temperatures most of the gas is irreversibly adsorbed. For a reversible adsorption, for thermodynamic reasons, we would expect a decrease in coverage with temperature. The reversible adsorption below 250° represents only a very small fraction of the chemisorbed gas. Adsorption of about one monolayer of water vapor was found to suppress the catalytic activity completely below 100°. The decrease in activity with time was not confined to the low-temperature region and was also observed at higher temperatures, where other modes of adsorption of different strength become reversible.

Effect of Hydrogen Pretreatment on the Exchange. In Figure 2, three curves are shown representing the logarithm of the oxygen-exchange rate vs. the inverse absolute temperature for three cases (on Pt(IV)), all at

ascending temperatures. The lines drawn through measured points are arbitrary to a certain degree because of the change of activity with time. Curve 1 was taken after prolonged oxygen pretreatment and pumping at 600°; it is similar to the corresponding curve in Figure 1. Curve 2 was taken after hydrogen treatment at 400° for 3 days and pumping for 2 days at 550°. The activity above 100° may be seen to be increased by the treatment.

Curve 3 was subsequently obtained after treating the sample again with oxygen and degassing at 620° for 16 days. No significant change in the shape of the curve was observed as compared to curve 2, except for a decrease in activity by a factor of 2. The activation energy for the temperature region shown is roughly 16 kcal/mol. The cause of the change in shape between curve 1 and the others is believed to be the removal of an impurity, presumably chlorine, by the hydrogen pretreatment. The treatment did not remove the time dependence of the adsorption modes.

The different changing modes of adsorption can be separated, to a certain extent, by determining the pressure dependence of the reactions after different pretreatment of the powders.

Pressure Dependence of the Exchange Reaction at 250°. Individual rate constants on samples which were evacuated at a high temperature initially declined rapidly, as indicated in Figures 1 and 2 and previously discussed. For evaluating reaction orders in this state, average values of several rate constants were determined between 30 and 240 min after admitting the isotopic mixture, *i.e.*, where the rate of decline of the constants was already relatively slow.

In Table I a few of many rate measurements at 250° are summarized, taken on sample Pt(IV). The pretreatment immediately preceding the measurement (column 2) is of decisive importance. Samples degassed at 600° gave zero-order kinetics, *i.e.*, exchange rates independent of pressure, as may be seen from examples I and II. When the platinum was pretreated with 10 torr or more of oxygen (O¹⁶) at 600° and very slowly cooled in oxygen to 250°, the reaction order was about 0.6 (examples III-1, -2). The most weakly bound component (zero-order component) giving rise to the highest activity was no longer present. It is interesting that in spite of this the adsorbed phase still contained another relatively weakly chemisorbed component which caused the measured reaction. From example III-2 it may be seen that reduction of the pressure from 30 to 10 torr, after pumping for only 40 sec, gave approximately the same reaction order as obtained for an increased pressure (example III-1). The desorption experiments described below confirm that the active oxygen is so weakly bound that most of it is removed by the short pumping of 40–70 sec at 250° preceding each desorption experiment.

In none of the experiments did a measurable ex-

Table I: Oxygen Pressure Dependence at 250°

	Sample	Pretreatment before run	Pressure, torr	Exchange rate, cm ⁻² sec ⁻¹	Reaction order
I	Pt(IV) O ₂ pretreated to 600°	Pumped 17 hr at 600°; cooled to 250° in helium	4.2	2.77 × 10 ¹²	0.0
		Pumped 17 hr at 600°; cooled to 250°	14.4	2.72 × 10 ¹²	
II	Pt(IV) H ₂ pretreated to 500°; pumped 2 days at 550°; in O ₂ up to 300°	Pumped 17 hr at 611°; cooled to 250°	10.3	1.90 × 10 ¹²	0.0
		Pumped 60 sec	25.5	1.92 × 10 ¹²	
III	Pt(IV) O ₂ pretreated 20 days at 600° following treatment II	Pumped 17 hr at 600°; 10 torr of O ₂ for 19 hr at 400°; 3 days at 250°			
		(1) Pumped 40 sec	9.6	1.13 × 10 ¹¹	0.64
		Pumped 40 sec	17.1	1.70 × 10 ¹¹	
		(2) Pumped 17 hr at 17 torr of O ₂ at 250°			
		Pumped 40 sec	30.9	1.60 × 10 ¹¹	0.51
Pumped 40 sec	10.3	8.25 × 10 ¹¹			

change take place, in the course of the homomolecular exchange, between the preadsorbed O¹⁶ and the admitted isotopic mixture. If the more strongly bound preadsorbed oxygen is involved in the homomolecular exchange (*cf.* Discussion), it must be less than 15% of one monolayer.

Desorption Rate of Oxygen. In a previous study of the oxygen exchange on silver,² it was shown that the rate of the homomolecular exchange $O^{16}_2 + O^{18}_2 \rightarrow 2O^{16}O^{18}$ is exactly equal to the rate of desorption of oxygen at the same surface coverage, down to the lowest temperature (150°) at which the desorption was measurable. The rate was measured by first pumping the system for at least 40 sec, the time required for practically complete removal of the oxygen from the gas phase; the pressure increase in the vessel was then measured by means of a thermistor gauge after closing the valve on the vessel. With silver, the pressure increase was linear with time up to several per cent loss in coverage. The behavior of platinum is quite different.

Table II gives the results of a typical desorption experiment with platinum at 250°. The given rates were evaluated from the tangent to the recorded pressure-time curve. It may be seen that the rate is rapidly decreasing with time as the coverage decreases. A comparison of the measured initial desorption rates with the exchange rate is given in Table III. The rates were measured on samples which were well saturated with oxygen and gave approximately 0.6-order kinetics. The desorption rate was determined immediately after the exchange, after pumping the iso-

topic oxygen mixture for 40–70 sec. The ratio of the two rates is given in the last column. The first example shown (Pt(II)) refers to the desorption experiment just discussed. The desorption rate after 70 sec of pumping was 17 times lower than the rate of exchange. Since the measured exchange cannot possibly be faster than the true initial desorption rate, the result means that most of the gas responsible for the desorption step in the exchange reaction is very weakly bound and is immediately removed on pumping.

Table II: Desorption of Oxygen from Pt(II) after Cooling in 15 Torr of O₂ from 650° and Pumping for 70 Sec at 250°

	Time, min					
	0.5	1.5	3	6	11	21
Rate × 10 ⁻⁹ , molecules/ sec cm ²	12	11	8.7	7.6	6.0	3.9
Decrease in coverage × 10 ³ , monolayers	1.1	3.0	5.7	9.8	18	24

Exchange of Nitrogen. Nitrogen interacts strongly with some d metals, but only weakly with platinum.¹⁴ It is, therefore, of interest to see whether or not an isotopic exchange analogous to the molecular oxygen exchange at low temperature takes place.

(14) B. M. W. Trapnell, "Chemisorption," Butterworth and Co. Ltd., London, 1955, p 183.

Table III: Comparison of Isotopic Exchange Rate with Initial Desorption Rate of Oxygen on Platinum at 250°

Sample	Pretreatment	Pressure, torr	r (isotopic exchange rate), molecules $\text{cm}^{-2} \text{sec}^{-1}$	r' ^a (initial desorption rate), molecules $\text{cm}^{-2} \text{sec}^{-1}$	r/r'
Pt(II)	Added 15 torr of O ₂ at 650°; cooled to 250°	15	2.0×10^{11}	1.2×10^{10}	17
Pt(IV)	(1) Added 10 torr of O ₂ at 400°; 19 hr at 400°; 3 days at 250°	10	8.2×10^{10}	6.9×10^9	12
	(2) Added 3.5 torr of O ₂ at 400°; 1 hr at 400°; 17 hr at 250°	20	3.6×10^{11}	1.5×10^{10}	23
	(3) Added 26.5 torr of O ₂ at 400°; 1 hr at 400°; 17 hr at 250°	35	3.1×10^{11}	7.8×10^9	40

^a Measured after 40–70 sec of pumping.

No measurable reaction $\text{N}^{14}_2 + \text{N}^{15}_2 \rightarrow 2\text{N}^{14}\text{N}^{15}$ occurred between -78 and 600° within 90 min. Nitrogen, therefore, does not dissociate on platinum up to 600° .

The effect of nitrogen on the oxygen exchange at 250° was also determined in two runs. No significant effect on the oxygen reaction was found.

Long-Term Oxygen Uptake at Higher Pressures. No oxygen uptake beyond a monolayer was found in the course of 1 day in any of the exchange experiments so far described, at temperatures up to 600° (cf. Figure 3). The pressure in these experiments was of the order of a few torr.

Two runs were made at higher pressures and for longer periods. The first of these was carried out before hydrogen treatment of sample Pt(IV). (A 4-g sample was used in a 34-cm³ vessel. The surface area was measured to be 890 cm²/g after hydrogen pretreatment.) After pumping at 600° overnight, a mixture of 30 torr of oxygen and some argon was admitted at room temperature. The system was cycled several times between the extremes of 23 and 600° . The data in Table IV show that no change in the oxygen:argon ratio occurred within the limit of accuracy. The latter was 5%, which is equivalent to about one monolayer of oxygen under our conditions.

A similar experiment was also performed after the same sample was pretreated with hydrogen and again with oxygen (as described before). In an experiment lasting 14 days, 40 torr of O₂ was used. Again the oxygen:argon ratio fluctuated within the limits of accuracy of 5%. No uptake beyond one monolayer therefore took place.

No residual hydrogen was left in the sample from the preceding hydrogen pretreatment. To test this, deuterium at 10 torr was left in contact with the sample, for 64 hr at room temperature and for 16 hr at 600° . The total amount of hydrogen appearing in the gas phase only amounted to the equivalent of less than 10^{-3} monolayer.

Table IV: Long-Term Oxygen Uptake by Pt(IV) at 30 Torr (Expt No. 1)

Time	Temp, °C	Mole %		
		O ₂	Ar	O ₂ :Ar
0	...	90.2	9.8	9.2
4 days	Cycling between 23 and 400	89.8	10.2	8.8
		89.5	10.5	8.5
1 day	260	89.9	10.1	8.9
1 day	21	89.6	10.4	8.6
2 hr	247	89.8	10.2	8.8
2 hr	457	89.7	10.3	8.7
1 day	595	89.9	10.1	8.9
		89.9	10.1	8.9
1 day	253	89.5	10.5	8.5

Isotopic Dilution of Residual Oxygen. So far all platinum samples were pumped at 600° overnight before measurement of the oxygen uptake or of the exchange. In order to test the possibility that at 600° a major amount of oxygen might remain occluded or chemisorbed, a final isotopic dilution experiment was carried out with the same sample (Pt(IV)), at even higher temperatures.

After pumping at 600° overnight, O¹⁸, containing about 10% O¹⁶O¹⁸, was admitted to the system at 600° to give a pressure of 12 torr. Samples of the gas phase were taken after different contact times at temperatures between 610 and 860° . A few of the analyses are shown in Table V. Above 610° , increasing amounts of trapped nitrogen were released by the sample. Failure of the nitrogen to be released below 600° appears to be connected with the inability to dissociate below this temperature, as seen in the isotopic nitrogen-exchange experiments. The source of the trapped nitrogen presumably was ammonia used in the preparation of the sample. Presence of the nitrogen had no apparent effect on the behavior of the surface below 600° .

The oxygen analyses in the table are given in mole per cent, excluding the nitrogen. Owing to the exchange

of the added O^{18} with O^{16} in or on the platinum, the $O^{16}O^{18}$ concentration may be seen to increase up to 800° (to 26.2% after 1280 min). The small further increase at higher temperatures is due to exchange with the quartz vessel, which was also determined.

Table V: Exchange of 12 Torr of O^{18} on Pt(IV) after Pumping for 16 Hr at 600°

Time, min	Temp, $^\circ\text{C}$	Mole % without N_2			$\text{N}_2:\text{O}_2$
		O^{16}_2	$O^{16}O^{18}$	O^{18}_2	
0	...	0.2	10.2	89.6	...
194	6.0	0.3	12.2	87.5	0.03
208	703	0.6	15.8	83.6	0.07
245	798	1.7	22.9	75.4	0.87
1280	798	2.4	26.2	71.4	0.22
270	857	2.7	27.3	70.0	0.28
1505	858	3.1	29.2	67.7	0.38

Assuming complete isotopic equilibrium at 800° between gas and solid phases, an amount of 0.026 cm^3 atm of O^{16}_2 is calculated which must have been on or in the solid after pumping at 600° . On a surface of 3200-cm^2 area of the platinum sample, the residual O^{16} amounts to 0.3 monolayer.

The largest adsorption previously measured after pumping at 600° was 0.7 monolayer (at 250° ; cf. section Oxygen Adsorption). The maximum total amount of sorbed oxygen therefore was one monolayer. We conclude that there was little or no oxygen occluded or in surface solution, contrary to what is generally found in literature.

Discussion

The experiments show the existence of a large number of adsorption modes on the surface. When platinum is pumped at high temperatures, the activity is higher at -78° than at liquid nitrogen temperature, but it drops with increasing temperature to about 0° , owing to conversion of the adsorbed oxygen to a second mode. The two very weak modes give rise to zero-order kinetics. Weak adsorption modes have been observed on many defect oxides.^{15,16} They are observed wherever isolated metal sites exist in the surface lattice of an oxide and the same appears to hold for noble metals covered by chemisorbed oxygen. In some cases the lifetime of the weak modes may be very short, as indicated by preliminary experiments¹⁷ with silver.

A large number of different ordered modes of oxygen adsorption on platinum and the ease of their rearrangement was found by Tucker,¹⁸ by means of low-energy electron diffraction. These experiments were performed on atomically clean surfaces and at a much lower pressure than used in the present experiments. The stronger modes of chemisorption are not in direct evidence in the present exchange experiments, except

for their effect of eliminating the activity which is due to the weaker chemisorptions. Most of the strongly chemisorbed oxygen does not participate in the homomolecular oxygen exchange. In this respect, platinum behaves differently from silver,² where one whole monolayer is involved in the exchange above 160° . The reason for the difference in behavior presumably is the higher mobility of the silver surface and the lower strength of the silver-oxygen bond for the major portion of the chemisorbed phase.

The weak chemisorption giving 0.6-order kinetics after saturating the platinum with oxygen at a high temperature was also easily removed by pumping. This must again be a different mode; otherwise it would be difficult to understand why, after removal of the sites responsible for the weak zero-order component, the reaction order would be higher. The zero-order mode appears to be destroyed by surface rearrangements that accompany the incorporation of more strongly bound oxygen.

The fact that no exchange with preadsorbed oxygen was detected in the present work is due to the small number of sites participating in the reaction and the relative insensitivity of the experimental setup. A small exchange of this type was found by Khasin and Boreskov³ with oxygen-saturated platinum films. The initial rate was equal to the rate of the homomolecular exchange. Equality of the two rates usually means that desorption is the rate-determining step in the two reactions. Failure of our attempt to measure the correct desorption rate proves that desorption proceeds from few sites at a very high rate, as previously discussed (cf. Desorption Rate of Oxygen section).

The apparent activation energy of about 16 kcal/mol of the homomolecular oxygen exchange is the same as found by Khasin and Boreskov.⁸ The rate constants and reaction orders are also similar. The agreement is noteworthy in view of the different systems used (powders and films, respectively), the usual lack of reproducibility of the results of various authors, particularly with platinum, and the small number of sites which appear to be responsible for the exchange in the investigated temperature region. The authors did not investigate the behavior of pumped films, presumably because of their instability.

No uptake beyond one monolayer was found in the present experiments, while Khasin and Boreskov did find a strong additional uptake, in agreement with many previous authors.⁶⁻¹⁰ The additional oxygen uptake caused no change in the surface properties.

Absence of occlusion of oxygen in the present experi-

(15) Cf. G. K. Boreskov, *Advan. Catalysis*, **15**, 319 (1964).

(16) Y. L. Sandler and D. D. Durigon, submitted for publication.

(17) Y. L. Sandler and D. D. Durigon, unpublished results.

(18) C. W. Tucker, *J. Appl. Phys.*, **35**, 1897 (1964).

ments is believed to be a consequence of the careful annealing treatment of the sample, the relatively high purity of the material, and the precautions taken to remove carbon and hydrogen. The uptake of oxygen found by other investigators, if not due to oxidation of impurities in the metal, is to be connected with the presence of structural defects. In the absence of these "internal surfaces" no occlusion occurs.

The uptake of several monolayers of oxygen was also found in electrochemical studies with platinum electrodes in aqueous electrolytes. Observed changes in catalytic activity were correlated by some authors^{11,19} with the surface solution of oxygen. The present

results, as well as the results with silver,² indicate that these changes should be correlated with variations in the mode of chemisorption and not with the concomitant excess uptake. With a well-annealed pure platinum surface it remains to be seen whether and to what extent an uptake of excess oxygen would actually occur at a given potential.

Acknowledgement. The authors are indebted to W. M. Hickam and his group for carrying out the exchange experiments on one of the samples.

(19) T. B. Warner and S. Schuldiner, *J. Phys. Chem.*, **69**, 4048 (1965).

Pressure Dependence of Dielectric Constant and Density of Liquids¹

by James F. Skinner,² E. L. Cussler, and Raymond M. Fuoss

Sterling Chemistry Laboratory, Yale University, New Haven, Connecticut 06520 (Received September 27, 1967)

Densities and dielectric constants at 30° and at pressures up to 5000 kg/cm² have been measured for toluene, *o*-xylene, *p*-xylene, cumene, diethyl ether, di-*n*-propyl ether, anisole, *n*-butyl chloride, chlorobenzene, 1,1-dichloroethane, 1,2-dichloroethane, and 1,2-dibromoethane. Two new high-pressure piezometers are described; one measures density through change in electrical capacity, the other through change in resistance between a constantan wire and a mercury piston. Densities are reproduced by the Tait equation within about 0.2%. An equation with the same pressure-dependent term for the electrical susceptibility ($\epsilon - 1$) represents the dielectric data to about the same precision. The coefficient multiplying the Tait function for dielectric dependence on pressure is greater than for the density dependence because, in addition to the density effect, it also includes the effects of increased short-range interaction between dipoles.

A number of investigations of the pressure dependence of the dielectric constants ϵ of liquids have appeared.³⁻⁸ For nonpolar liquids,^{4,5} the Clausius-Mosotti polarization $(\epsilon - 1)M/(\epsilon + 2)\rho$ is nearly independent of pressure, showing that the density ρ is the controlling variable; as the liquid is compressed, more molecules are compacted into a given volume, and the electronic polarization is correspondingly increased. For polar liquids, for which the Clausius-Mosotti function does not provide an adequate description, density still appears to be one of the fundamental parameters. Owen and Brinkley⁹ showed that the dielectric constant follows an equation of the same logarithmic form as the Tait equation, which gives density as a function of pressure. The parameter B , which measures the pressure sensitivity, is the same for both dielectric constant and density. The purpose of this paper is to present data on the pressure dependence of dielectric constant and density of a variety of liquids and to consider the effects of structure on the pressure coefficients.

For polar liquids, we find that the increased short-range interaction between neighboring molecules leads to an increase in dielectric constant which is added to the increase produced by increased density.

Experimental Section

The pressure-generating system, the temperature

(1) This work was supported by Grant No. AF-AFOSR-244-63.65 from the Directorate of Chemical Sciences, Air Force Office of Scientific Research.

(2) Part of the material presented here is from a thesis submitted by J. F. Skinner to the Graduate School of Yale University in June 1964, in partial fulfillment of the requirements for the degree of Doctor of Philosophy in Chemistry.

(3) S. Kyropoulos, *Z. Physik*, **40**, 507 (1926).

(4) W. E. Danforth, Jr., *Phys. Rev.*, **38**, 1224 (1931).

(5) Z. T. Chang, *Chinese J. Phys.*, **1**, 1 (1933).

(6) B. K. P. Scaife, *Proc. Phys. Soc.*, **B68**, 790 (1955).

(7) H. Hartmann, A. Neumann, and G. Rinck, *Z. Physik. Chem. (Frankfurt)*, **44**, 204, 218 (1965).

(8) B. B. Owen, R. C. Miller, C. E. Milner, and H. L. Cogan, *J. Phys. Chem.*, **65**, 2065 (1961).

(9) B. B. Owen and S. R. Brinkley, Jr., *Phys. Rev.*, **64**, 32 (1943).

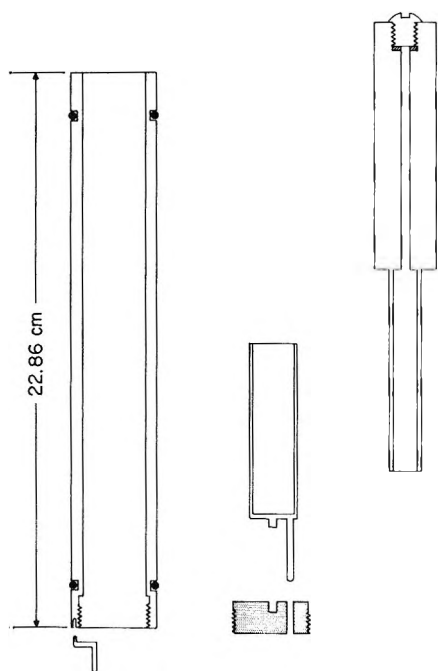


Figure 1. Capacitance piezometer.

control, and the design and calibration of the high-pressure cell for dielectric measurements have been described.¹⁰ Capacitance measurements were made on the Schering bridge¹¹ at 500 Hz and 400 V. Resistance measurements for the resistance piezometer were made on a Kelvin bridge (Leeds and Northrup No. 4287). Temperature control for the density measurements by means of the resistance piezometer was considerably improved over that by the earlier design¹⁰ by using water as the heat-transfer liquid and by replacing the 0.635-cm copper tubing by larger tubing, 1.27 cm in diameter.

For the determining densities by change of capacitance, the cell shown in Figure 1 was used. Pressure drives a piston carrying a cylindrical electrode into a cell containing the test liquid and a fixed cylindrical electrode. Capacitance increases with increasing pressure (a) because the dielectric constant of the liquid increases and (b) because the overlap area of the electrodes increases. The first effect is known from measurements in a cell with fixed electrodes,¹⁰ and the second effect, which obviously measures the volume change of the test liquid, can be calculated. The outer casing is stainless steel, 23 cm high and of 2.54-cm i.d. It is insulated from the walls of the high-pressure bomb by two neoprene O rings. A threaded Supramica plug screws into the bottom and seats against an O ring, which forms the bottom seal between the test liquid and the pressurizing fluid (Hercoflex 600). The plug carries a stainless steel electrode which is brazed to a rod which passes through the plug and dips into a mercury cup on the low-potential lead through the bottom closure of the bomb. The rod is sealed into the plug with epoxide cement. The movable high-

potential electrode is carried on a bronze piston. The distance between the outer surface of the movable electrode and the inner surface of the fixed electrode is 1.6 mm. The clearance between the piston and casing is 0.05 mm (2 mils). On assembly, the piston is coated with grease (18:15:5 smoked sheet rubber–vaseline–paraffin) to seal the test liquid from the pressurizing fluid. In order to make the series impedance of the capacity between piston and casing negligibly small compared to that between the test electrodes, the distance from piston to casing must be very small; at such small clearances, O rings jammed. The heavy grease makes an excellent seal and does not appreciably contaminate the cell contents, as shown by agreement between measurements made at decreasing pressure after the run at increasing pressure. The cell is filled through the central 3-mm hole, and the assembly is closed by a threaded plug at the top which seats on a Teflon disk. The casing is connected to a rod which dips into a second mercury cup, connected to the high-potential side of the Schering bridge. For safety, the bomb is grounded. The capacity from the casing to bomb is merely a shunt across the input transformer and is not "seen" by the bridge.¹¹ The guard line is connected to the shield around the test line; the latter is unshielded for the short distance (*ca.* 12 cm) it traverses the bottom closure of the bomb through ceramic insulation; the corresponding capacity is a high-impedance shunt around the R3 arm of the bridge, but the error is negligible because R3 is of the order of only several thousand ohms.

The cell capacitance consists of (1) lead capacitance which is fixed, (2) capacitance between the stationary electrode and the casing, which depends on pressure through the dielectric constant of the liquid between it and the casing, and (3) capacitance between the moving and the fixed electrodes, which depends on pressure through the dielectric constant and through the position of the piston. After a small overlap has been established, bench tests at constant pressure showed that (3) was *linear* in the height of the piston; with the geometry shown in Figure 1, the capacity from the lower face of the piston to the fixed electrode is negligible as long as the piston is at least 2.0 cm above the top of the fixed electrode. Capacitances (1) and (2) were determined by measurements with the cell in the thermostated bomb, using a piston without attached inner electrode, and with air (ϵ 1.000), toluene (ϵ 2.373), di-*n*-propyl ether (ϵ 3.255), and diethyl ether (ϵ 4.152) as dielectrics. The result is

$$C_{1,2} = 5.76 + 10.72\epsilon \quad (1)$$

where 5.76 pF is the lead capacity, 10.72 ϵ is the capacity

(10) J. F. Skinner and R. M. Fuoss, *J. Phys. Chem.*, **69**, 1437 (1965).

(11) D. Edelson, W. N. Maclay, and R. M. Fuoss, *J. Chem. Educ.*, **27**, 644 (1950).

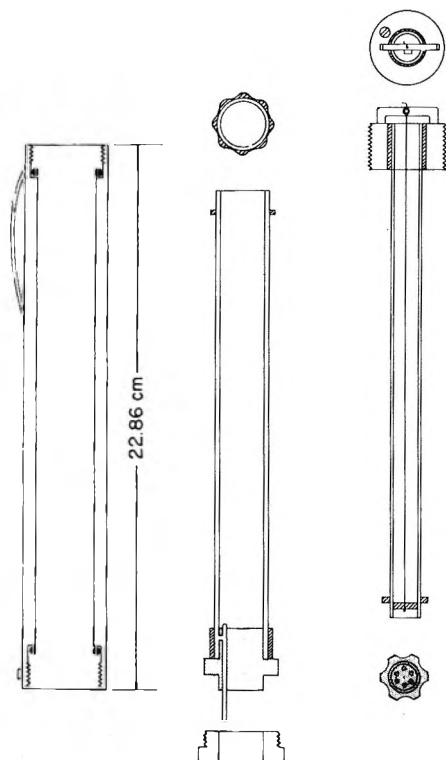


Figure 2. Resistance piezometer.

between the casing and the fixed electrode, and ϵ is the dielectric constant of the test liquid. Then the inner electrode was attached to the piston, and a series of measurements was made using the same four dielectrics, with the piston at different heights, the latter determined to 0.05 mm by means of a height gauge. The final calibration equation is

$$C = C_{1,2} + \epsilon(10.57 - 6.254h) \quad (2)$$

where h is the distance (in inches) from the top of the casing to the top of the piston. If h is the distance for the cell filled at 30° and 1 atm and h' is the distance when the cell is under pressure P , then (2) gives

$$\Delta h = h - h' = h - [6.254\epsilon(1)h + 21.29\Delta\epsilon - \Delta C]/6.254\epsilon(P) \quad (3)$$

where $\epsilon(1)$ is the dielectric constant of the test liquid at 1 atm, $\epsilon(P)$ that at pressure P , $\Delta\epsilon$ the difference $[\epsilon(P) - \epsilon(1)]$, and ΔC is the increase in capacity at pressure P . Using the cell with fixed electrodes,¹⁰ $\Delta\epsilon$ is known as a function of pressure. Therefore, measurement of ΔC determines Δh , and then from this and the known diameter of the cell, the volume change ΔV is known. The volume of the cell (about 50 cc) was determined as a function of h by weighing the cell plus various amounts of liquids of known density for different piston heights. The average precision in $V(P)/V(1)$ by this method is 0.5%.

For determining densities by resistance measurements, the cell shown in Figure 2 was used. The test

liquid is compressed by a mercury piston, and the motion of the latter is measured by the change in resistance of a wire passing through the surface between the mercury and the pressurizing liquid. The middle tube, which is the mercury well, is carried on a Supramica bushing, which is sealed into the outer casing by an O ring and the bottom closure nut. Electrical contact to the mercury is made by a pin through the bushing; when the piezometer is positioned in the high-pressure bomb, this pin fits into a jack carried on an insulated lead through the bottom closure of the bomb.¹⁰ Electrical contact between the pin and the middle tube was made by drilling a hole through the tube, ceramic, and pin, and filling the hole with lead; contact resistance between the top of the pin and the mercury was erratic, but by using the inner surface of the middle tube as the contact to mercury and connecting the tube to the pin with lead, resistances reproducible to 0.002 ohm, independent of pressure, were obtained. The resistance wire is carried by the inner tube; it is spanned between a yoke at the top, where it is fastened by a set screw, and a perforated Teflon disk at the bottom. The inner tube is insulated from the top closure to which the yoke is screwed by a Teflon tube. This nut makes good electrical contact with the casing, which in turn makes contact with the inner surface of the autoclave by means of a stiff leaf spring; the contact surface of the spring is coated with lead. The resistance wire is constantan (General Electric Copnic thermocouple wire), 0.13 mm in diameter (36 gauge, Brown and Sharp). It should be mentioned that a variety of wires were tried: nichrome, platinum, stainless steel, tungsten, and iron; all gave erratic contact resistances. Constantan gives reproducible results, independent of pressure and time; evidently mercury does not attack the alloy. As will be described below, it is essential, however, that the constantan-mercury interface be completely clean and oil free.

To measure volume changes, the middle tube and casing are locked together, and the inner tube assembly is screwed in a few turns. Then the piezometer is weighed. The inner tube assembly is next removed, and mercury is filled into the well formed by the middle tube and the Supramica bushing. The filling is done under vacuum to avoid trapping air under the mercury. The inner assembly is then locked into place and the piezometer is reweighed in order to determine the amount of mercury in it. Finally, the test liquid is added, also under vacuum. A metal filling cylinder screws into a hole through the top closure; the whole assembly is placed in a vacuum chamber; after evacuating, the test liquid is admitted and completely fills the space between the casing and the middle cylinder, above the mercury. The hole in the top closure nut is sealed by a screw, and the pycnometer is again weighed in order to determine the weight of test liquid. The filled pycnometer is then placed in the bomb and

allowed to come to temperature. Our working temperature, 30°, is above room temperature; expansion of the test liquid will therefore cause the mercury to rise in the inner tube. It is essential for reproducible resistance readings that the mercury-constantan surface be dry during this expansion; only after temperature equilibrium is pressurizing fluid added to the autoclave and the latter closed. Otherwise, a film of the pressurizing fluid would be trapped between the wire and the mercury during expansion and erratic resistances would be found when the mercury surface was forced down by subsequent increases in pressure. A similar precaution must be taken on pressurizing; this operation of course causes adiabatic heating. If the pressure is run up too rapidly, the liquid will be compressed, lowering the mercury level, and then it will expand thermally, thereby raising the mercury again, with the result that fluid is trapped between the wire and the mercury. In order to avoid this source of error, pressure is increased in a sequence of small steps (for example, by increments of 7000, 2000, and 1000 psi for a total increment of 10,000 psi). When the resistance changes as a consequence of the mercury level *falling* around a wire which has been initially immersed in mercury under vacuum, readings are reproducible to 0.01 ohm; if however, the interface is ever wet with any liquid, the results become erratic. The total resistance change for 5000 kg/cm² pressure increment is 2–4 ohms, depending on the liquid.

The wire is calibrated by measuring the resistance for different heights of mercury in the cell. The mercury heights were determined by a precision height gauge carrying a pointed probe, which was connected to one side of a resistance meter; the other side was connected to the contact pin at the bottom of the cell. Blank runs, made in the autoclave, with the filling screw in the top of the pycnometer left out (so that the mercury level would only change due to its own compression, by a calculable amount) showed that the change of resistance of the constantan due to pressure was negligible.

Relative densities are calculated from the observed differences ΔR between the cell resistance at 1 atm and that at pressure P by the equation

$$1 - [\rho(1)/\rho(P)] = [\pi D^2 K \Delta R / 4 V_1] - \Delta \quad (4)$$

where D is the diameter of the inner tube (1.100 cm), K is the calibration constant of the wire (1.412 cm/ohm), V_1 is the volume of test liquid in the cell at 1 atm and 30° (determined from its weight and density), and Δ is a correction for the change in volume due to compression of the mercury. It is given by the equation

$$\Delta = [V(\text{Hg})/V_1][1 - (\rho_{\text{Hg}}(1)/\rho_{\text{Hg}}(P))] \quad (5)$$

where $V(\text{Hg})$ is the volume at 1 atm and 30° of the mercury in the cell and $\rho_{\text{Hg}}(1)$ and $\rho_{\text{Hg}}(P)$ are, respec-

tively, the densities¹² of mercury at 1 atm and at pressure P .

Materials. Toluene (Fisher) was refluxed over sodium-lead alloy for 12 hr and fractionated through an 80-cm column; bp 110.2–110.4°; density at 25°, 0.8623 g/ml. The two xylenes (Matheson) were used as received. Cumene (Matheson) was rolled for 12 hr over four 200-ml portions of concentrated sulfuric acid, washed with water, rolled with sodium bicarbonate, and again washed with water. After drying with calcium chloride, it was distilled; the fraction boiling at 151–152° was used. Diethyl ether (Mallinckrodt) and di-*n*-propyl ether (Matheson) were used as received and immediately after opening a container, to minimize peroxidation. Anisole (Matheson) was dried over calcium chloride, distilled, and rolled with sodium hydroxide overnight. After two washes with water, it was refluxed over sodium-lead alloy for 24 hr and then fractionated, bp 153.5–154.0°. Butyl chloride (Matheson) was rolled with successive portions of concentrated sulfuric acid until no color developed. It was washed with water and dried over calcium chloride, followed by activated alumina and then barium oxide. After distillation (bp 78.0–79.0°), the solvent was stored over alumina and Analabs 4A Molecular Sieve; after discarding a forerun, the material with specific conductance of 2×10^{-9} mho was used for measurements. Chlorobenzene (Matheson) was fractionated (bp 131.0–131.5°) and run through a 60-cm column of activated alumina before use; specific conductance, 1.0×10^{-10} mho. Ethylidene chloride (Matheson) was treated with calcium carbonate, potassium bicarbonate, and barium oxide and then fractionated; bp 57.0–57.5°. After storing for 48 hr over a mixture of alumina and 4A Sieve, it was run through a column of 4A Sieve; specific conductance, 2.0×10^{-9} mho. Ethylene chloride (Matheson) was treated the same way as 1,1-dichloroethane; bp 83.2–83.5°, specific conductance, 4.7×10^{-10} mho. Ethylene dibromide (Matheson) was treated with concentrated sulfuric acid, washed with water, dilute sodium hydroxide, and water again, dried over calcium chloride, distilled (bp 129–130°), recrystallized, and finally stored over alumina; specific conductance, 3.5×10^{-10} mho.

The experimental results are summarized in Tables I and II which give dielectric constants and densities at 30.0° as a function of pressure (kg/cm²) for the 12 liquids studied. Most of the data go up to about 5000 atm (our blow-out patch is rated at 70,000 psi); the range was limited by freezing for *p*-xylene (*ca.* 700 atm), *o*-xylene (*ca.* 2500 atm), and ethylene dibromide (*ca.* 900 atm). For ethylidene and ethylene dichlorides, we report only the ratio $\epsilon(P)/\epsilon(1)$. The initial 1-atm values were too high (10.8 and 11.4, respectively, *vs.* 10.2 expected); both solvents attacked all the O rings we tried, and contamination of solvent by material

(12) L. A. Davis and R. B. Gordon, *J. Chem. Phys.*, **46**, 2650 (1967).

Table I: Dielectric Constants at 30°

P	ϵ	P	ϵ	P	ϵ
Toluene					
1	2.379	1	4.17	1	7.06
1040	2.509	950	4.84	1040	7.79
2070	2.597	2880	5.59	4780	8.94
3190	2.671	4090	5.94	3090	8.54
4150	2.726	2285	5.39	1620	8.05
1030	2.515	1	4.18	1	7.09
2080	2.600	3375	5.79	1990	8.19
3160	2.672	4780	6.14	3180	8.56
4080	2.721	3790	5.88	4210	8.81
4920	2.758	1690	5.19	4640	8.90
o-Xylene					
1	2.514	1	3.255	1690	8.09
478	2.578	1060	3.670	Chlorobenzene	
940	2.628	2040	3.913	1	5.65
1490	2.675	3140	4.144	1040	6.02
1990	2.712	4120	4.315	3150	6.45
2040	2.713	4850	4.427	4230	6.60
2310	2.733	1780	3.863	4850	6.68
Cumene					
1	2.322	1	3.255	1640	6.16
980	2.442	970	3.641	1	5.65
1360	2.468	1970	3.898	1,1-Dichloroethane	
2040	2.525	3330	4.178	1	1.000 ^a
2770	2.563	4240	4.335	650	1.091
3100	2.589	4780	4.418	1390	1.166
4130	2.638	2530	4.025	1890	1.205
4840	2.664	Anisole		2360	1.234
3800	2.622	1	4.28	2960	1.267
3310	2.588	1480	4.59	3520	1.286
2990	2.581	2710	4.78	3940	1.304
1970	2.514	4750	4.98	1,2-Dichloroethane	
1590	2.495	3780	4.89	1	1.000 ^a
1	2.328	2240	4.71	600	1.058
p-Xylene					
1	2.213	1000	4.52	1140	1.101
315	2.255	2010	4.68	1800	1.141
655	2.289	3140	4.83	3330	1.186
315	2.250	4090	4.93	4220	1.206
680	2.287	2270	4.73	4790	1.221
1,2-Dibromoethane					
		1	4.93	1	4.93
		345	5.11	345	5.11
		600	5.23	600	5.23
		840	5.33	840	5.33

^a $\epsilon(P)/\epsilon(1)$.

leached from the O rings and leakage of pressurizing fluid are suspected. While the absolute values of ϵ are therefore incorrect, we believe that the ratios $\epsilon(P)/\epsilon(1)$ are probably reliable to 1-2% and show the correct trend of the ratio with pressure for these two liquids.

Discussion

Relative volumes for anisole, toluene, n-butyl chloride, di-n-propyl ether, and diethyl ether are shown in

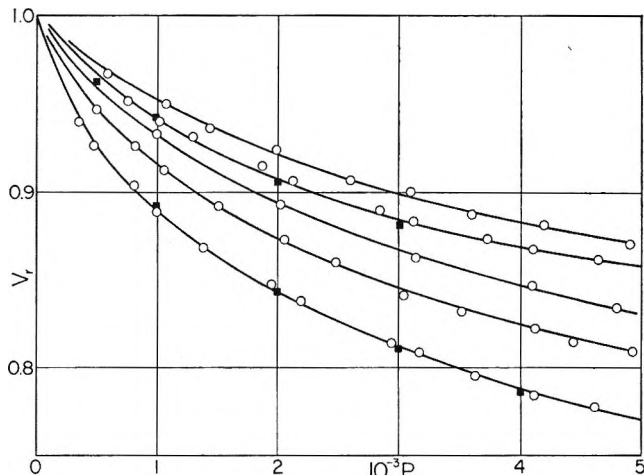


Figure 3. Relative volumes, dependence on pressure. Top to bottom: anisole, toluene (squares, Chang⁵), n-butyl chloride, di-n-propyl ether, diethyl ether (squares, Bridgman¹³).

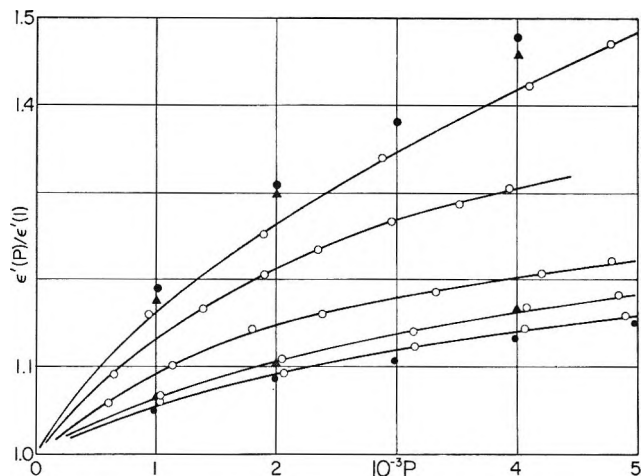


Figure 4. Dielectric constants, dependence on pressure. Top to bottom: diethyl ether (solid circles, Chang⁵; triangles, Danforth⁴), 1,2-dichloroethane, 1,1-dichloroethane, chlorobenzene (triangles, Danforth⁴), toluene (solid circles, Chang⁵).

Figure 3. Excellent agreement with literature values for toluene (Chang⁵) and diethyl ether (Bridgman¹³) is observed. Figure 4 shows the change of relative dielectric constant with pressure for diethyl ether, 1,2-dichloroethane, 1,1-dichloroethane, chlorobenzene, and toluene. Agreement with earlier values is good for chlorobenzene and toluene, but we find a somewhat smaller increase for diethyl ether. The general pattern of the change in dielectric constant and density is the same for all the liquids investigated: both increase with increasing pressure, as expected. As shown in Figure 5, where dielectric constant is plotted against density at the same pressure, the dependence is very nearly linear.

(13) P. W. Bridgman, *Proc. Am. Acad. Arts Sci.*, **49**, 62 (1913).

Table II: Densities at 30°

<i>P</i>	ρ	<i>P</i>	ρ	<i>P</i>	ρ
Toluene		<i>p</i> -Xylene		Anisole	
1	0.858	1	0.852	1	0.985
750	0.900	352	0.870	585	1.018
1290	0.921	527	0.878	1440	1.052
1860	0.939	703	0.884	2590	1.087
2830	0.965	Diethyl Ether		3590	1.110
3730	0.982	1	0.702	4480	1.126
4640	0.996	810	0.777	1070	1.036
1020	0.912	1390	0.808	1990	1.066
2120	0.947	1950	0.830	3090	1.094
3120	0.972	2940	0.862	4200	1.118
4100	0.989	3620	0.882	4910	1.132
4780	1.000	4610	0.903	<i>n</i> -Butyl Chloride	
<i>o</i> -Xylene		1000	0.790	1	0.876
1	0.872	2190	0.838	1000	0.939
352	0.895	3160	0.868	2020	0.981
703	0.908	4110	0.895	3130	1.016
1055	0.924	4940	0.908	4100	1.034
1406	0.937	Di- <i>n</i> -propyl Ether		4800	1.049
2108	0.959	1	0.737	Chlorobenzene	
Cumene		490	0.779	1	1.096
1	0.853	1060	0.809	352	1.118
352	0.871	2050	0.845	703	1.140
703	0.887	3140	0.876	1055	1.158
1055	0.902	4220	0.896	1406	1.175
1406	0.917	4930	0.912	1758	1.190
1758	0.928	810	0.797	2108	1.203
2108	0.942	1510	0.827	2812	1.235
2812	0.960	2480	0.858	3515	1.256
3515	0.977	3520	0.885	4218	1.271
4218	0.992	4430	0.903	4920	1.283
4920	1.007	1,2-Dibromoethane		1	2.160
				527	2.206
				703	2.221

From the observed linear dependence on pressure of the reciprocal of the compressibility, the equation¹⁴

$$y = 1 - (\rho(1)/\rho(P)) = C \ln [(B + P)/(B + 1)] \quad (6)$$

can easily be derived, where $\rho(1)$ is density at 1 atm, $\rho(P)$ is density at pressure P , and B and C are empirical constants. Owen and Brinkley⁹ suggested that the dielectric constant ϵ is given by an equation of similar form. Their equation is based on the integral of a differential equation for $v = 1/\rho$

$$(\partial^2 v / \partial P^2) / (\partial v / \partial P)_T = \frac{\partial^2(1/\epsilon) / \partial P^2}{[\partial(1/\epsilon) / \partial P]} \quad (7)$$

which was derived by considering the electrostatic term in the partial molal volume. Integration gives

$$1 - (\epsilon(1)/\epsilon(P)) = A'y/C \quad (8)$$

and combining with (6), there results

$$1 - (\epsilon(1)/\epsilon(P)) = A' \ln [(B + P)/(B + 1)] \quad (9)$$

Consideration of dielectric polarization, in which density and dielectric constant appear explicitly, leads to an equation of similar form and suggests the physical basis for the observation that the coefficient of the logarithmic function is greater for dielectric behavior than for density. Kirkwood's¹⁵ equation is

$$\epsilon - 1 = 9pM\rho/(2 + (1/\epsilon)) \quad (10a)$$

where M is molecular weight and

$$p = (4\pi N/3)(\alpha + (g\mu^2/3kT)) \quad (10b)$$

Here N is Avogadro's number, α is electronic polarizability per molecule, μ is dipole moment, k is Boltzmann's constant, T is absolute temperature, and g is a measure of the interaction between a given dipole and its nearest neighbors. If (6) is substituted in (10a), using $F(P)$ to represent the Tait function, we find the ratio

$$(\epsilon_1 - 1)/(\epsilon_P - 1) = \frac{[p_1(1 + (1/2\epsilon_P))/p_P(1 + (1/2\epsilon_1))](1 - CF)}{(1 - CF)} \quad (11)$$

The ratio $(2 + (1/\epsilon_P))/(2 + (1/\epsilon_1))$ is less than unity and is of the form

$$1 - [AF(\epsilon_1 - 1)/\epsilon_1(2\epsilon_1 + 1)] + O(F^2) \quad (12)$$

The ratio p_1/p_P is also less than unity, because intermolecular interaction presumably increases with increasing pressure. If we assume that the increase in g is also logarithmic, corresponding to the decrease in average intermolecular distances with compression, (11) can be written in the form

$$(\epsilon_1 - 1)/(\epsilon_P - 1) = (1 - DF)(1 - CF) \quad (13)$$

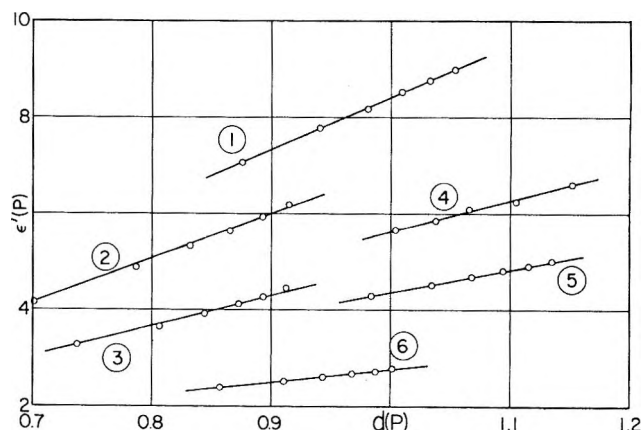


Figure 5. Dielectric constant, dependence on density at same pressure: 1, *n*-butyl chloride; 2, diethyl ether; 3, di-*n*-propyl ether; 4, chlorobenzene; 5, anisole; 6, toluene.

(14) P. G. Tait, "Reports on Some of the Physical Properties of Fresh Water and Sea Water," "Physics and Chemistry of the Voyage of H.M.S. Challenger," Vol. II, Part IV, S.P., LXI, 1888.

(15) J. G. Kirkwood, *J. Chem. Phys.*, **7**, 911 (1939).

Table III: Constants of Interpolation Equation

Compound	<i>C</i>	<i>A</i>	<i>A/C</i>	<i>B</i>	% σ (ρ)	% σ (ϵ)
Toluene	0.0779	0.1167	1.50	913	0.10	0.08
<i>o</i> -Xylene	0.0860	0.1127	1.31	1115	0.15	0.05
<i>p</i> -Xylene	0.0628	0.1039	1.65	888	0.05	0.09
Cumene	0.0906	0.1267	1.40	1166	0.26	0.19
Diethyl ether	0.0923	0.1555	1.68	449	0.18	0.27
Di- <i>n</i> -propyl ether	0.0879	0.1578	1.80	625	0.15	0.11
Anisole	0.0814	0.1127	1.38	1234	0.15	0.11
<i>n</i> -Butyl chloride	0.0750	0.1081	1.44	602	0.17	0.06
Chlorobenzene	0.0934	0.1181	1.26	1276	0.23	0.20
1,1-Dichloroethane ^a	0.0485	0.0833	1.72	493	0.17	0.38
1,2-Dichloroethane ^a	0.0678	0.1184	1.74	526	0.15	0.31
1,2-Dibromoethane	0.0482	0.1441	2.99	936	0.06	0.03

^a D. M. Newitt and K. E. Weale, *J. Chem. Soc.*, 3092 (1951).

and since *F* is small compared to unity

$$(\epsilon_1 - 1)/(\epsilon_P - 1) \approx 1 - AF \quad (14)$$

where

$$A = C + D \quad (15)$$

This shows that the coefficient for the dielectric constant function is greater than *C*, that for density, by an amount *D* which depends on the effect of pressure on the Kirkwood correlation factor (plus some contribution from the $1/2\epsilon$ terms). Equation 14 can be rearranged to

$$z = 1 - [\epsilon(1) - 1]/[\epsilon(P) - 1] = A \ln [(B + P)/(B + 1)] \quad (16)$$

which makes dielectric susceptibility, rather than dielectric constant, proportional to the Tait function.

The data of Tables I and II were analyzed to find the constants *A*, *B*, and *C* of eq 6 and 16 by the method of least squares.¹⁶ The quantity Σ is defined by

$$2\Sigma = \Sigma_j [(Y_j - y_j)^2 + (Z_j - z_j)^2]$$

where Y_j and Z_j are calculated and y_j and z_j are observed values of the variables of (6) and (16). Minimizing Σ with respect to *A*, *B*, and *C* gives three equations which determine these parameters; since (6) and (16) are nonlinear in *B*, an iterative method is used. The calculations were programmed for an electronic computer. The results are summarized in Table III. As shown by the standard deviations for density and dielectric constant in the last two columns, the equations may be used to reproduce values for the physical properties within a few tenths of 1% up to 5000 kg/cm².

Some correlations between the constants and the structure of the compounds can be found. The *B* parameter of the Tait function, which measures the effect of pressure, is largest for the aromatic compounds. This might be expected from their compact structure as compared to that of the aliphatic compounds. A large value of *B* means, of course, that a correspondingly

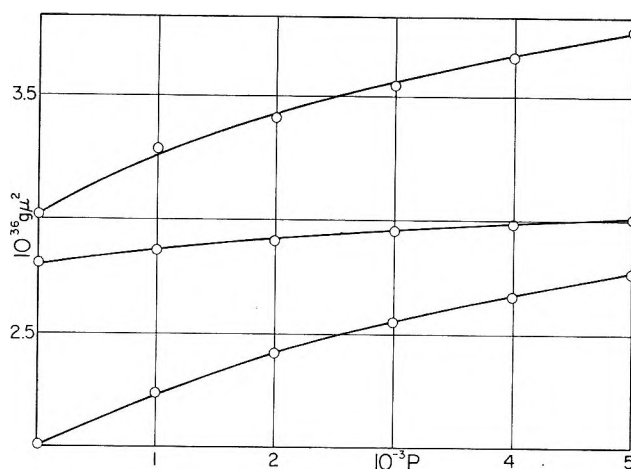


Figure 6. Dependence of Kirkwood function $g\mu^2$ on pressure. Top to bottom: diethyl ether, anisole, di-*n*-propyl ether.

large value of *P* is required for a given change in the Tait function. The ratio *A/C* is uniformly greater than unity, in agreement with eq 15. Figure 6 shows several examples of the dependence of the *g* factors on pressure; they were calculated from our values of dielectric constant and density by eq 10a and b, using literature values for indices of refraction to calculate α . We note again that the aromatic ether is less sensitive to pressure than the aliphatics.

The first four compounds in Table III are all hydrocarbons and are relatively nonpolar. For them, the Clausius-Mosotti polarization $(\epsilon - 1)M/(\epsilon + 2)\rho$ is nearly independent of pressure, but this quantity masks the effect of the small dipole moments of the methyl groups. The ratio *A/C* is greater than unity for these compounds, which shows the presence of the $g\mu^2/3kT$ term in the Kirkwood polarization. The fact that *A/C* for *p*-xylene is not equal to unity, despite the net moment of zero for this molecule, shows that the *g* factor is indeed a measure of short-range interactions. Fur-

(16) J. B. Scarborough, "Numerical Mathematical Analysis," 5th ed, Johns Hopkins Press, Baltimore, Md., 1962, p 539.

thermore, the result suggests that the Kirkwood $g\mu^2$ factor should not be calculated using the net moment of the molecule, but rather as an average sum over interactions of the individual moments on the neighboring molecules. A similar effect was observed in the viscosities of a number of polar molecules; the increment in the viscosity due to short-range interactions depends on the sum of the scalar moments rather than on the vector sum.¹⁷

The two dichloroethanes provide an interesting correlation with structure. Using the dielectric constants at 30° from Table I and literature values of relative volumes¹⁸ at 25°, the *A* and *C* coefficients of Table III were computed. The *C* coefficient for 1,2-dichloroethane is considerably larger than for its isomer; that is, it compresses at a higher intrinsic rate. It exists in two conformations, *cis* with a large net moment and *trans* with opposing C-Cl dipoles. The relative values of the coefficients suggest that pressure favors the *cis*

form. This parallels the observation¹⁹ that the *cis-trans* equilibrium in 1,2-dichloroethene is shifted toward *cis* with increasing pressure.

The two xylenes froze under pressure. The change in dielectric constant correlates with their structures. We recall that *p*-xylene has zero net dipole moment, while *o*-xylene has a moment of about 0.5 D. At 680 kg/cm², *p*-xylene is a liquid with dielectric constant 2.287; at 795, it is a solid with ϵ 2.587. The increase corresponds, of course, to the increase in polarization due to the increase in density on solidification, but *o*-xylene at 2310 kg/cm² has a dielectric constant of 2.733 which drops to 2.674 at 2600 kg/cm². The increased electronic polarization on freezing is more than compensated by the loss of dipole polarization.

(17) J. F. Skinner and R. M. Fuoss, *J. Phys. Chem.*, **68**, 2998 (1964).

(18) D. M. Newitt and K. E. Weale, *J. Chem. Soc.*, 3092 (1951).

(19) A. G. Ewald, S. D. Hamann, and J. E. Stutchbury, *Trans. Faraday Soc.*, **53**, 991 (1957).

Thermodynamics of Aqueous Mixtures of Electrolytes and Nonelectrolytes.

IV. Transfer of Hydrochloric Acid from Water to

Aqueous Acetic Acid at 25°

by J. H. Stern and J. Nobileone

Department of Chemistry, California State College, Long Beach, California 90801 (Received September 29, 1967)

Partial molal enthalpies of transfer of hydrochloric acid from water to aqueous acetic acid were determined calorimetrically at 25°. The enthalpies were combined with partial molal free energies of transfer to yield entropies over the mixed-solvent range from water to nearly pure acetic acid. The free energy is a linear function of the mole fraction of acetic acid, X_3 , and does not reflect the complexity of the transfer. Both the enthalpies and entropies indicate the two processes likely to occur over the range of mixed solvent. The left-hand side of the enthalpy and entropy curves (X_3 , from 0 to ca. 0.8) corresponds to transfer from water to mixed solvent in which hydrochloric acid is predominantly ionized. The enthalpy is thus interpreted as a measure of nonelectrolyte-electrolyte and ion-ion interaction. Primary and secondary medium effects are briefly discussed. The decreasing entropy is in qualitative agreement with that predicted from the Born solvation entropies. Beyond $X_3 = 0.8$, hydrochloric acid becomes predominantly ion associated, and both enthalpies and entropies rise sharply with the latter increasing by ca. 28 cal/deg mol between $X_3 = 0.8$ and 1.0. This value is in the range of ion association of 1-1 weak acids in water, indicating similarities between the behavior of hydrochloric acid in pure acetic acid and 1-1 weak acids in water.

Introduction

Previous papers in this series have dealt with the thermodynamics of transfer of nonelectrolytes from water to a variety of electrolytes.¹ The transfer of electrolytes from water to aqueous mixed solvents is a related process,² and this contribution describes the

thermodynamic changes at 25° when HCl is transferred at constant low molality, m_2 , from pure water to aqueous acetic acid.

(1) Previous papers in this series: J. H. Stern and A. Hermann *J. Phys. Chem.*, **71**, 306, 309, 3623 (1967).

There have been numerous investigations of the physicochemical properties of electrolytes in water-nonaqueous solvent mixtures. These were mainly concerned with conductance, transport numbers, and activity coefficients.³

Limited miscibility of low-dielectric-constant nonelectrolytes with water and the low solubility of electrolytes in such mixtures has precluded many studies over wide dielectric constant ranges. This study appears to be the first to report the free energy, calorimetric enthalpy, and entropy of transfer, $\overline{\Delta F}_2$, $\overline{\Delta H}_2$, and $\overline{\Delta S}_2$, over a range of mixed solvents from $X_3 = 0.0902$ to 0.997 , where X_3 is the mole fraction of acetic acid. This assures a wide range of conditions, since the dielectric constant changes from *ca.* 80 to 6 between pure water and glacial acetic acid, respectively. Thus the coulombic energy of two ions becomes approximately 13 times greater in the latter solvent than in water, and effects due to ionic interaction as X_3 increases eventually lead to the formation of ion pairs. In pure acetic acid, HCl becomes very weak, with a dissociation constant of 2.8×10^{-9} .⁴ Higher order association products may also be formed; however their concentrations are likely to be very small.

For a given HCl concentration, m_2 , the logarithm of the mean ionic activity coefficient, γ_{m_2, X_3} , in any given solvent mixture relative to pure water may be expressed as⁵

$$\log \gamma_{m_2, X_3} = \log \gamma_{0, X_3} + \log \frac{\gamma_{m_2, X_3}}{\gamma_{0, X_3}} \quad (1)$$

where the subscripts m_2 and X_3 refer to the molality of the electrolyte and the mole fraction of the nonelectrolyte, respectively. The term $\log \gamma_{0, X_3}$ is the primary medium effect, which characterizes the nonelectrolyte-electrolyte interaction at very low values of m_2 . No general theory has yet been developed which predicts the magnitude of the primary medium effect.⁶ The term $\log (\gamma_{m_2, X_3}/\gamma_{0, X_3})$ is the secondary medium effect which represents the activity coefficient of the electrolyte at concentration m_2 in a mixed solvent of composition X_3 , referred to unity at infinite dilution in that solvent. This term appears to converge to the limiting Debye-Hückel slopes for HCl in dioxane-water.⁷

The total medium effect is represented by the left-hand term, $\log \gamma_{m_2, X_3}$, and gives an indication of both ion-ion and ion-solvent interactions. Both primary and secondary medium effects for HCl in the HOAc-H₂O systems are discussed by Pitzer and Brewer.⁵ The primary medium effect is shown by a linear plot of $\log \gamma_{0, X_3}$ vs. X_3 over the range from pure water to pure HOAc, based on emf and vapor pressure data.⁵ Over this range, $\log \gamma_{0, X_3}$ increases from 0 to nearly 3. At concentrations less than $0.005 m$, the secondary medium effect is negligible when compared to the very large primary effect. Thus at low m_2

$$\log \gamma_{m_2, X_3} = KX_3 \quad (2)$$

where K is a constant independent of m_2 . This equation is similar to that describing the limiting behavior of the activity coefficient of a nonelectrolyte in the presence of an aqueous electrolyte.²

The nonideal free energy of transfer of HCl at low m_2 from pure water to the mixed solvent may be obtained from

$$\overline{\Delta F}_2 = 2 \times 2.303RT \log \gamma_{m_2, X_3} = 2 \times 2.303RTKX_3 \quad (3)$$

This, combined with the calorimetric enthalpies of transfer, yields the entropies of transfer

$$\overline{\Delta S}_2 = \frac{\overline{\Delta H}_2 - \overline{\Delta F}_2}{T} \quad (4)$$

Experimental Section

Materials. Concentrated HCl and pure HOAc were both AR grade. All mixtures were prepared with distilled CO₂-free water.

Calorimetric Procedure. The calorimeter has been described elsewhere.⁸ Weighed quantities of concentrated HCl ($16.18 \pm 0.02 m$) were sealed into glass ampoules and crushed against the bottom of a dewar containing 450 g of mixed solvent. The final concentration of HCl in the majority of runs was *ca.* $0.003 m$. The HCl concentration in the ampoules was periodically checked by titration with standard NaOH and the composition of the mixed solvent was determined similarly. All runs were made at $25 \pm 0.1^\circ$, and each one was corrected by subtracting the enthalpy of mixing of the small quantities of water initially contained in the ampoule, with the mixed solvent in the dewar. These corrections were obtained *via* an IBM 1620 computer from the analytical least-squares equation calculated by Campbell and Gieskes to represent their calorimetric HOAc-H₂O enthalpies of mixing at 25° ⁹

$$\Delta H_m \text{ (cal/mol)} = X_3X_1[296 + 166(X_3 - X_1) + 19(X_3 - X_1)^2 + 321(X_3 - X_1)^3] \quad (5)$$

(2) G. N. Lewis and M. Randall, "Thermodynamics," revised by K. S. Pitzer and L. Brewer, 2nd ed, McGraw-Hill Book Co., Inc., New York, N. Y., 1961, p 586.

(3) H. S. Harned and B. B. Owen, "The Physical Chemistry of Electrolytic Solutions," 3rd ed, Reinhold Publishing Corp., New York, N. Y., 1958.

(4) S. Bruckenstein and I. M. Kolthoff, *J. Am. Chem. Soc.*, **78**, 10 (1956).

(5) See ref 2, p 591.

(6) F. A. Long and W. F. McDevitt, *Chem. Rev.*, **51**, 119 (1952).

(7) See ref 3, p 471.

(8) J. H. Stern and C. W. Anderson, *J. Phys. Chem.*, **68**, 2528 (1964).

(9) A. N. Campbell and J. M. T. M. Gieskes, *Can. J. Chem.*, **43**, 1004 (1965).

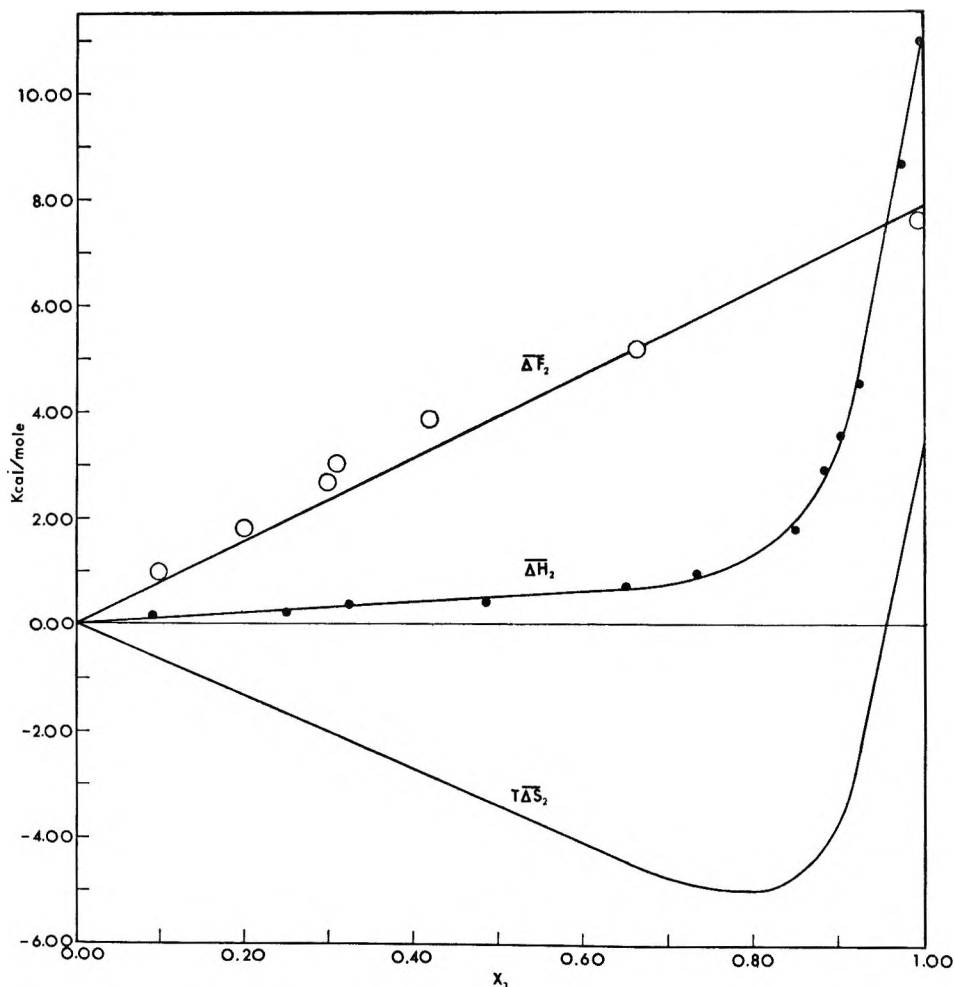
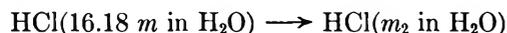


Figure 1. Variation of $\overline{\Delta F}_2$, $\overline{\Delta H}_2$, and $T\overline{\Delta S}_2$ with X_3 .

where X_1 is the mole fraction of H_2O . Enthalpies of transfer were obtained from

$$\overline{\Delta H}_2 = \Delta H_2 - \Delta H_2^0 \quad (6)$$

where ΔH_2 is the corrected enthalpy of dilution in the mixed solvent, $HCl(16.18 m \text{ in } H_2O) \rightarrow HCl(m_2, X_3)$, and ΔH_2^0 is the corresponding enthalpy of dilution in pure water



Results and Discussion

The enthalpies of dilution in pure water and in the mixed solvent are shown in Table I. The experimental ΔH_2^0 is within 0.5% of the value based on tables in Circular NSRDS-NBS2.¹⁰ Uncertainties associated with all averages consist of the standard deviation of the enthalpies together with the estimated error in ΔH_m corrections.

In Figure 1 $\overline{\Delta F}_2$, $\overline{\Delta H}_2$, and $T\overline{\Delta S}_2$ are plotted vs. X_3 . The open circles and straight line represent free energies based directly on the points and corresponding straight line from Figure 34-13 by Pitzer and Brewer,⁵ while the full circles for $\overline{\Delta H}_2$ are at experimental compositions,

Table I: Enthalpies of Dilution of Aqueous HCl with Aqueous Acetic Acid

No. of runs	$m_2 \times 10^4$	X_3	ΔH_2 , kcal/mol
8	3-4	0.000 (ΔH_2^0)	-3.950 ± 0.020
5	3-5	0.0902	-3.760 ± 0.025
11	3-4	0.250	-3.720 ± 0.025
10	3-5	0.323	-3.565 ± 0.025
6	3-5	0.485	-3.530 ± 0.035
6	3	0.651	-3.230 ± 0.035
6	2-3	0.733	-2.980 ± 0.030
5	2-4	0.848	-2.145 ± 0.090
6	3-12	0.882	-1.035 ± 0.060
5	2-4	0.902	-0.395 ± 0.050
5	2-3	0.925	0.585 ± 0.080
2	2-3	0.974	4.665 ± 0.130
4	2-3	0.997	6.995 ± 0.120

shown in Table I. Table II shows values of $\overline{\Delta F}_2$, $\overline{\Delta H}_2$, and $\overline{\Delta S}_2$ taken from the curves in Figure 1, at regular mole fraction intervals of 0.1 mol fraction.

(10) V. B. Parker, "Thermal Properties of Aqueous Uni-Univalent Electrolytes," NSRDS-NBS2, National Bureau of Standards, U. S. Government Printing Office, Washington, D. C., 1965.

Figure 1 shows several notable features. The $\overline{\Delta F}_2$ curve, in contrast to those for $\overline{\Delta H}_2$ and $T\overline{\Delta S}_2$, does not reflect the complicated nature of the transfer process. Apparently competing equilibria among the different species tend to offset nonlinear changes in the free energy. All values of $\overline{\Delta H}_2$ are positive and fall on a curve which consists of two linear portions joined by a smooth arc. The nature of the $\overline{\Delta H}_2$ curve reflects the two processes most likely to occur over the entire span of mixed solvents. The left-hand side corresponds to transfer from water to a mixed solvent where HCl is predominantly ionized. Thus $\overline{\Delta H}_2$ is a measure of nonelectrolyte-electrolyte and ion-ion interactions.

Table II

X_3	$\overline{\Delta F}_2$, kcal/mol	$\overline{\Delta H}_2$, kcal/mol	$\overline{\Delta S}_2$, cal/mol deg
0.1	0.8	0.118	-2.3
0.2	1.6	0.218	-4.6
0.3	2.4	0.321	-7.0
0.4	3.2	0.416	-9.3
0.5	3.9	0.511	-11
0.6	4.7	0.618	-14
0.7	5.5	0.744	-16
0.8	6.3	1.31	-17
0.9	7.1	3.37	-12
1.0	7.9	11.14	+11

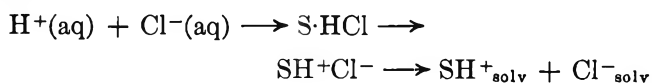
It would be of interest to divide $\overline{\Delta H}_2$ into contributions due to these two effects, where a measure of the latter is the relative partial molal enthalpy difference, $\overline{\Delta L}_2$. Comparisons with two HCl-mixed aqueous solvent systems for which $\gamma_{m_2, X_3}/\gamma_{0, X_3}$ and \overline{L}_2 data are available from emf studies does not lead to any meaningful estimates of $\overline{\Delta L}_2$ for this system.¹¹ The entropy of the left-hand side is negative and decreases from zero to a minimum at *ca.* $X_3 = 0.8$. The sign and decrease of $\overline{\Delta S}_2$ may be compared with that predicted by the Born treatment of the entropy of solvation¹²

$$\overline{\Delta S}_2 = A \left[\frac{1}{D_{X_3}^2} \left(\frac{\partial D_{X_3}}{\partial T} \right)_{X_3} - \frac{1}{D_0^2} \left(\frac{\partial D_0}{\partial T} \right) \right] \quad (7)$$

where A is a constant characteristic of the electrolyte, D_{X_3} and $(\partial D_{X_3}/\partial T)_{X_3}$ are the dielectric constant and its temperature derivative for the mixed solvent, and D_0 and $(\partial D_0/\partial T)_{X_3}$ are analogous quantities for pure water. The dielectric constant of the mixed solvent decreases with increasing X_3 and is less than D_0 . The temperature derivative of D is negative¹² and it is reasonable to assume that $(\partial D_{X_3}/\partial T)_{X_3}$ is also negative,¹³ since this quantity for other water-nonelectrolyte mixtures usually is also negative.¹⁴ Based on this assumption, eq 7 predicts values of $\overline{\Delta S}_2$ in qualitative agreement with this study. The emf data on HCl in dioxane-water also yield negative values of $\overline{\Delta S}_2$.¹⁵ The negative values of $\overline{\Delta S}_2$ indicate that the HCl in aqueous acetic

acid may find itself in a more "structured" environment than in pure water.¹⁶

Past *ca.* $X_3 = 0.8$, the solute rapidly becomes predominantly ion associated as HCl becomes a weaker acid than HOAc. At very high X_3 , the transfer from pure water may be represented by the following sequence¹⁷



where S can be either H_2O or HOAc. The final dissociation to solvated ions is very small owing to the low dissociation constant of HCl in pure HOAc. The entropy of transfer on the right-hand side supports the association reaction. Beyond $X_3 = 0.8$, $\overline{\Delta S}_2$ rises sharply and for the transfer from the minimum of the curve at *ca.* $X_3 = 0.8-1.0$, $\overline{\Delta S}_2$ is approximately 28 cal/deg mol. Examination of ion-association entropies for 1-1 weak acids in water shows that they range from *ca.* 20 to 30 cal/deg mol.¹⁸ Thus, both in sign and in magnitude, $\overline{\Delta S}_2$ corresponds to that of ion-association reactions for aqueous weak acids. Consequently the $\overline{\Delta C}_{p,2}$ of transfer may have the same order of magnitude as that of ion-association reactions in water, *ca.* 30-50 cal/deg mol, and similarly the temperature variation of the dissociation constant of HCl in HOAc may follow the trend observed for weak acids in water.

Similar studies on electrolytes in various mixed-solvent media (*e.g.*, HCl-ethylene glycol-water) are in progress.

Acknowledgment. The authors wish to express their deep appreciation to Professor Leo Brewer for helpful discussions and encouragement of this work. We also wish to thank A. Hermann for his participation in the preparation of this paper. The financial assistance of the National Science Foundation is gratefully acknowledged.

(11) The HCl-MeOH-H₂O system (R. G. Bates and R. A. Robinson in "Chemical Physics of Ionic Solutions," B. E. Conway and R. G. Barradas, Ed., John Wiley and Sons, Inc., New York, N. Y., 1966, p 211) has both small $\gamma_{m_2, X_3}/\gamma_{0, X_3}$ and \overline{L}_2 values, while HCl in dioxane-water (see ref 3, p 717) has values of $\gamma_{m_2, X_3}/\gamma_{0, X_3}$ which appear to be about 10 times larger than in the present study and large \overline{L}_2 values which change rapidly with mixed solvent composition and m_2 .

(12) See ref 2, p 523.

(13) Dipole moment measurements at $X_3 < 0.98$ were not possible because the resistances of solutions fell below the specified limit of the instrument (Dipolmeter, Type DM 01, Wissenschaftlich-Technische Werkstätten, Berlin). At very high X_3 , qualitative measurements showed that $(\partial D_{X_3}/\partial T)$ is negative.

(14) Landolt-Börnstein, "Zahlenwerte und Funktionen," Vol. II, part 6, Elektrische Eigenschaften, Springer-Verlag, Berlin, 1959, p 750.

(15) See ref 3, p 715.

(16) For a recent discussion of structural effects in mixed-solvent systems see, for example: E. M. Arnett, W. G. Bentrude, J. J. Burke, and P. McDuggleby, *J. Am. Chem. Soc.*, **87**, 1541 (1965).

(17) G. J. Janz and S. S. Danyluk in "Electrolytes," B. Pesce, Ed., Pergamon Press Inc., New York, N. Y., 1962, p 255.

(18) See ref 3, p 667.

Physicochemical Properties of Sulfolane

by Mario Della Monica, Liliana Jannelli, and Ugo Lamanna

Institute of Physical Chemistry, University of Bari, Bari, Italy

Accepted and Transmitted by The Faraday Society (June 26, 1967)

Cryoscopic behavior of solutions of *n*-heptane, carbon tetrachloride, naphthalene, diphenylmethane, benzene, pyridine, and cyclohexane in sulfolane was investigated in the molality range 0–1. Data supply evidence that sulfolane solidifies at 28.45° in plastic crystals, which undergo a transition in a new solid phase at 15.45°, owing to the "globular" structure of the molecule. Negative conclusions are drawn concerning the use of sulfolane as a reliable solvent in cryoscopy, in the domain of mesomorphic phase, because molar depressions are indicative of a partition of solute between solid and liquid phases. Below the transition temperature, dissolved substances lose their individuality, in the limits of their different activity coefficients.

Introduction

During the past 15 years, a considerable number of papers have been written on the subject of molecular crystals.¹ These crystals resemble a liquid in some aspects and they may be regarded as a mesomorphic-state intermediate between typical solids and liquids.²

The mesomorphic phase is characterized by a high dielectric constant value. This implies that the molecules which have quasi-spherical (globular) repulsion envelopes when close-packed in the crystals possess sufficient energy to rotate frequently over the restricting potential energy barriers. Therefore, the entropy of fusion does not exceed 3–5 eu,³ because changes of vibrational entropy are negligible and only positional disordering in melting is important. Some degrees below the melting point, the mesomorphic phase undergoes a transition in a nonrotational crystalline phase; enthalpy change on the transition considerably exceeds the enthalpy of fusion.

As globular substances are very often polymorphic, more than one transition point may be encountered with decreasing temperature. Therefore, in the proximity of a transition point, nucleation of two forms may occur within the crystal matrix, and hybrid single crystals may be formed. In this case, the transition is called continuous, in the sense of Ubbelohde.^{2,4}

Evidence of globular properties of sulfolane and of some molecular rotational freedom between the freezing point (28.45°) and a transition point (15.43°) is given by our previous studies on this substance.⁵

In the present paper, thermal behavior of a highly purified sample of sulfolane in the temperature range 10–30° is reported. Also, cryoscopic data are collected on several binary mixtures in which the solvent is the sulfolane and the other component may be: *n*-heptane, cyclohexane, carbon tetrachloride, benzene, benzoic acid, pyridine, diphenylmethane, or naphthalene.

Experimental Section

Materials. Sulfolane (tetramethylene sulfone), fur-

nished by Shell Industrial Chemical Division, was carefully purified and dehydrated on P₂O₅ by repeated distillation *in vacuo* (10⁻⁴ torr) through a 1.5-m Podbielniack column packed with glass helices. Benzene, *n*-heptane, and cyclohexane were boiled under reflux over phosphorous pentoxide and finally distilled in a stream of dry air. The purified material was stored under dry air. Carbon tetrachloride, free of carbon disulfide, was dried over fused calcium chloride and distilled. Benzoic acid was twice recrystallized from hot water and dried in a vacuum desiccator. Naphthalene was kept overnight at 140° under a stream of nitrogen, in order to remove water. The product was twice recrystallized from anhydrous methanol and distilled. Diphenylmethane, obtained from the Eastman Kodak Co., was subjected to three fractional crystallizations. The resulting product melted at 25.1°. Reagent grade pyridine was purified by repeated fractional freezing, refluxing over freshly heated barium oxide, and distilling through a column, 1 m in length, packed with glass helices.

Cryoscopic Apparatus and Procedure. The measuring cell (300 cm³) was constructed in order to prevent errors due to intrusion of water vapor and, generally, to secure a satisfactory standard of accuracy. It was cleaned with chromic acid and carefully washed with distilled water. It was then evacuated with a mercury diffusion pump and subsequently heated to 150° for a period of 24 hr.

(1) A. R. Ubbelohde, *Quart. Rev. (London)*, **11**, 246 (1957); *Angew. Chem.*, **4**, 587 (1965); G. B. Guthrie and J. P. McCullough, *J. Phys. Chem. Solids*, **18**, 53 (1961); L. A. K. Staveley, *Ann. Rev. Phys. Chem.*, **13**, 351 (1962).

(2) A. R. Ubbelohde, *Quart. Rev. (London)*, **11**, 246 (1957).

(3) B. Timmermans, *J. Phys. Chem. Solids*, **18**, 1 (1961).

(4) G. B. Guthrie and J. P. McCullough, *ibid.*, **18**, 53 (1961).

(5) J. Jannelli, M. Della Monica, and A. Della Monica, *Gazz. Chim. Ital.*, **94**, 552 (1964); U. Lamanna, O. Sciacovelli, and L. Jannelli, *ibid.*, **96**, 114 (1966).

An opening in the cell head provided a way to introduce the solvent and solutes with a suitable delivery apparatus. In order to prevent intrusion of water vapor during measurements, it was essential to grease all ground joints with Apiezon M grease. The stirrer consisted of a glass spiral.

Temperatures were measured by a platinum resistance thermometer calibrated by NBS. The resistance was measured by a Mueller G2 bridge (Leeds & Northrup Co.).

Heating curves were preferred to cooling curves, in the case of solutions, in order to avoid undercooling and related errors.⁶ Before starting the measurement of a heating curve, the solid-liquid mixture was kept at a temperature slightly below the initial melting point for at least 1 hr.

The molality of the solutions investigated ranged between 0 and 1.

Results and Discussion

Data on Pure Substance. The mesomorphic-phase domain may be detected by the cooling curve in Figure 1. It reveals a transition at 15.43° whose latent heat considerably exceeds that of fusion at 28.45°. This melting point was first determined by us on a highly purified sample of the material; it is in good agreement with the value (28.85°) predicted by Birch and Mac Allen⁷ using Rossini's extrapolation method. We report here, for the first time, the value of the transition temperature, directly determined on the pure substance. It checks well with the cryoscopic preliminary data of Burwell and Langford,⁸ which are consistent with the existence of a new solid phase below 15°.

Dielectric behavior indeed⁹ evidences that sulfolane molecules still possess rotational freedom below the melting point, until the transition temperature is reached, at which point a nonrotational crystalline phase is formed.

Data on Solutions. Several binary systems were studied by thermal analysis, as previously described, up to $m = 1$. In the case of the *n*-heptane and cyclohexane solutions, measurements are restricted to dilute solutions, on account of their low solubility.

Initial freezing points (liquid-solid equilibrium temperatures) of these solutions are plotted *vs.* molality in Figure 2. The values lie on straight lines, but the slope of the lines appears to depend upon the solute in the first composition range (0–0.2 m). The steeper the slopes are, the more the dissolved substance is different, in size and shape, from the solvent. Afterward, the plots exhibit a sharp break, which, in most cases, checks well with the transition temperature (15.43°) of sulfolane itself.

The initial freezing points of the solutions, having a composition higher than the molality at the transition point, lie on a straight line, which is practically common

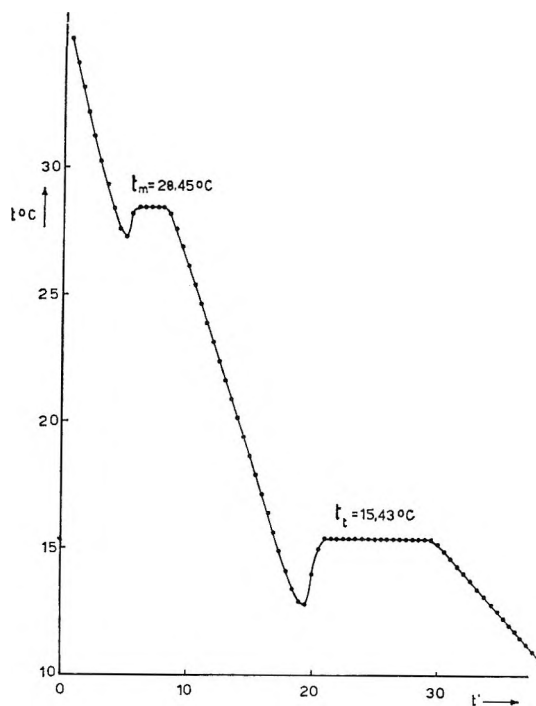


Figure 1. Cooling curve of pure substance.

to all dissolved substance, up to $m = 1$. Because of their low solubility, solutions of *n*-heptane and cyclohexane may not gain transition points.

Discussion

Cryoscopic behavior may be better described by Figure 3, where molal depressions, ϑ/m , calculated from the fusion point, 28.45°, of the pure substance, are plotted *vs.* molality. In the composition range 0–0.2 m , these values lie on straight lines and they appear to be influenced slightly by temperature. The straight lines, for several solutes—naphthalene, diphenylmethane, *n*-heptane, and benzoic acid—extrapolate to a value of 65, which may be indicated, reasonably, as the cryoscopic constant of sulfolane in the stability region of the plastic phase. Practically all acids are not dissociated in sulfolane.¹⁰

The values of ϑ/m for carbon tetrachloride, pyridine, and cyclohexane solutions lie on straight lines, but these do not extrapolate to normal values of ϑ/m when $m \rightarrow 0$. Therefore, they are suspected of forming plastic mixed crystals with the solvent. From the limiting values of ϑ/m , distribution coefficients of

(6) W. M. Smit, "Purity Control by Thermal Analysis," Vol. 7, Elsevier Publishing Co., Amsterdam, The Netherlands, 1957, pp 23–35.

(7) A. R. Birch and J. Mac Allen, *J. Chem. Soc.*, 2556 (1951).

(8) R. L. Burwell and C. Langford, *J. Amer. Chem. Soc.*, **81**, 3799 (1959).

(9) U. Lamanna, O. Sciacovelli, and L. Jannelli, *Gazz. Chem. Ital.*, **94**, 552 (1964).

(10) E. M. Arnett and C. F. Douty, *J. Amer. Chem. Soc.*, **86**, 409 (1964).

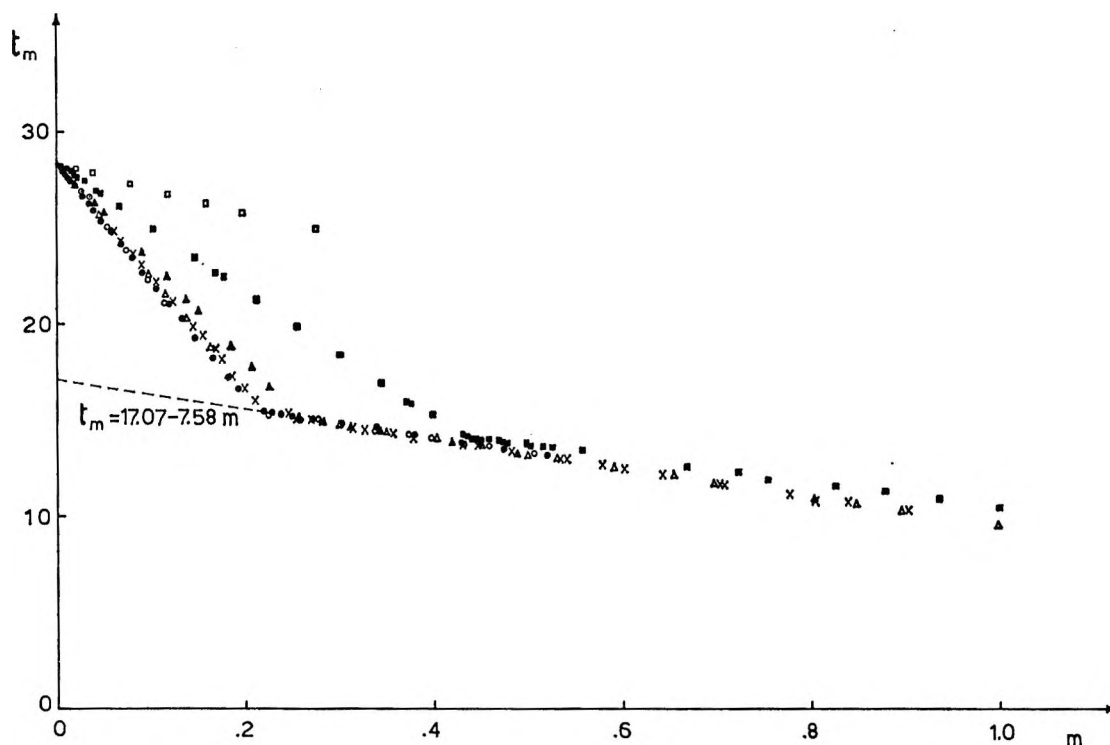


Figure 2. Initial freezing points vs. molality: \circ , diphenylmethane; \bullet , naphthalene; Δ , benzoic acid; \odot , *n*-heptane; \times , benzene; \blacktriangle , pyridine; \blacksquare , carbon tetrachloride; \square , cyclohexane.

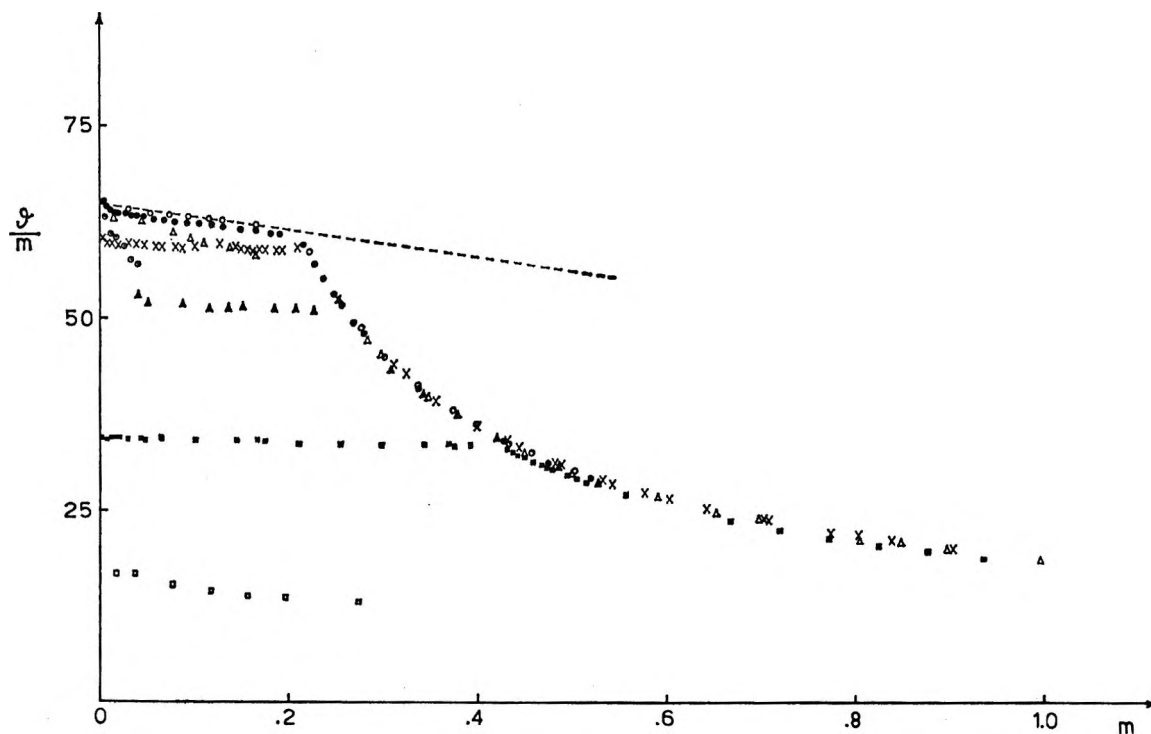


Figure 3. Molal depression vs. molality. (Symbols have the same meanings as they have in Figure 2.)

solutes between solid and liquid sulfolane could be calculated, which are consistent with the hypothesis that the greater the disturbing effect of a solute on the mesomorphic phase, the more the second component departs from criteria of mesomorphism.

In the phase-II domain, experimental points lie practically on one curve which crosses the straight lines, previously described, corresponding to the transition temperature. This value, in the case of carbon tetrachloride, pyridine, and cyclohexane solutions,

varies from substance to substance, still affording support to hypothesis that plastic sulfolane can dissolve solutes.

Since an ideal solution is defined as one in which the activities of the components are equal to their mole fractions, their freezing points can be calculated by replacing the activity of the solvent by its mole fraction in Lewis and Randall's equation.¹¹

In the case of solutions in sulfolane, thermal data on molal heat of solidification and on heat capacities of the solid and liquid phases are lacking. An equation $\vartheta = 65m - 17.9m^2$, valid in the range 0–0.2 m , can be obtained if we put $(\vartheta/m)_{m=0} = 65$ and we disregard the small difference between the heat capacities of liquid and plastic sulfolane. As can be seen from Figure 3, the experimental points, in the case of solutions of diphenylmethane and naphthalene in sulfolane, lie close to the dotted line calculated by this equation; *n*-heptane and benzoic acid are indeed some examples of nonideal solutes, as might be expected.

The initial freezing points of solutions, having

molality higher than the transition value, may be represented well by the expression $17.07 - 7.57m$ (dotted line in Figure 2), where 17.07 is the virtual fusion temperature of the crystalline nonrotational phase II and 7.57 may be reasonably indicated as the cryoscopic constant of sulfolane in equilibrium with the phase II.

Starting from these values, an entropy change associated with the transition phase II \rightarrow liquid can be calculated as 9.1 eu, whereas the corresponding value for the fusion of phase I does not exceed 1.1 eu. Therefore, the entropy that characterizes the transition II \rightarrow I amounts to 8 eu. Both transition and fusion entropies are in good agreement with the figures referred to by Staveley¹² and Guthrie and McCullough⁴ for some substances forming plastic crystals.

(11) S. N. Lewis and M. Randall, "Thermodynamics and Free Energy of Chemical Substances," McGraw-Hill Book Co., Inc., New York, N. Y., 1923, p 283, eq 17.

(12) L. A. K. Staveley, *Ann. Rev. Phys. Chem.*, **13**, 351 (1962).

NOTES

On the Reaction of D_2^+ with Cyclohexane

by Jean H. Futrell,^{1a} Fred P. Abramson,^{1b}
and Thomas O. Tiernan

*Aerospace Research Laboratories, Wright-Patterson Air Force Base,
Ohio 45433 (Received September 22, 1967)*

In a recent communication, Wolfgang and Menzinger² presented a preliminary account of an ion-impact experiment in which cyclohexane deposited on a surface was bombarded with T_2^+ and T^+ ions as a function of ion kinetic energy in order to evaluate the threshold energy and energy dependence of a typical hot-atom reaction. The initial stage of the reaction could involve charge exchange and/or various ion-atom interchange processes— T^+ transfer, H atom abstraction, and T stripping. To aid in the interpretation of this initial stage of the reaction, we have performed the related gas-phase experiment of impacting D_2^+ on cyclohexane at various ion energies and examining the ionic products of this reaction.

The experiments which we report here were carried out using the ARL tandem mass spectrometer described in detail elsewhere.³ In the present experiments, D_2^+

ions were formed by electron impact on D_2 in the ion source of the first-stage mass spectrometer, accelerated, both energy and mass selected, decelerated to terminal energy, and impacted on cyclohexane vapor in a differentially pumped collision chamber. The energy spread in the ion beam, determined by the defining slit of the electrostatic analyzer, was 0.5 eV in these experiments. The lowest energy investigated approached thermal velocities (ion energy 0–0.5 eV) and is reported in Table I. Ions monochromatic in energy to this degree were then impacted on cyclohexane at various energies up to 20-eV nominal ion kinetic energy. Cyclohexane pressure in the collision chamber was maintained at 0.005 torr, and the chamber temperature was ca. 230°; under these conditions secondary reactions of the ions initially produced are negligible.

The distribution of cyclohexane ions from the reaction of 0–0.5-eV D_2^+ ions is reported in Table I. At this energy no signal was detected at m/e 2 (D^+) or at

(1) (a) Department of Chemistry, University of Utah, Salt Lake City, Utah 84112. (b) Consolidated Electrodynamics Corp., Monrovia, Calif. 91017.

(2) R. Wolfgang and M. Menzinger, *J. Am. Chem. Soc.*, **89**, 5992 (1967).

(3) J. H. Futrell and C. D. Miller, *Rev. Sci. Instr.*, **37**, 1521 (1966).

Table I: Products from the Reaction of Low-Energy D_2^+ Ions with Cyclohexane

m/e	Ion	Relative intensity, %
27	$C_2H_3^+$	0.4
28	$C_2H_4^+$	0.8
41	$C_3H_5^+$	12.5
42	$C_3H_6^+$	8.1
43	$C_3H_7^+$	4.4
54	$C_4H_8^+$	0.9
55	$C_4H_7^+$	19.4
56	$C_4H_6^+$	30.8
57	$C_4H_9^+$	1.6
69	$C_5H_9^+$	3.5
83	$C_6H_{11}^+$	4.5
84	$C_6H_{12}^+$	13.1

m/e 5 (D_2H^+). At 2 eV, a D^+ signal is barely discernible above the noise level and appears to increase slightly with increasing energy. This collision-induced dissociation (stripping) reaction is $\leq 10^{-3}$ of the integrated intensity of products reported in Table I at low velocity and $\leq 10^{-2}$ of the intensity at 5-eV ion kinetic energy. Within experimental error the spectrum of hydrocarbon product ions at 5 eV is the same as that reported for low-energy ions; hence we conclude that translational energy of the ions is not effectively converted into internal energy of the reacting system.

In other experiments, we have shown that stable protonated cyclohexane can be formed using several proton donors and that with increasing exothermicity (*i.e.*, reagents of lower proton affinity) the dissociative proton-transfer reaction forms mainly $C_3H_7^+$ and $C_6H_{11}^+$ ions. Both of these ions are quite small in the present experiment. Bombarding cyclohexane with low-velocity H_2^+ also gave the same spectrum of ions as D_2^+ , from which we conclude that no deuterium is incorporated in the ions reported in Table I. We therefore conclude that the principal reaction of molecular hydrogen ions with cyclohexane is dissociative charge transfer, and ion-atom interchange processes are relatively unimportant for this system.

Intensity limitations prevented our carrying out comparable experiments with D^+ and H^+ . However, related experiments by Chupka and Lindholm⁴ with *n*-butane neutrals have shown that charge transfer is the dominant reaction for both H^+ and H_2^+ . We therefore suggest that the initial stage of the tritium ion beam experiments² is best interpreted as charge transfer to the target molecule. In solid cyclohexane it is quite possible, of course, that energy transfer could stabilize the excited cyclohexane molecule ion prior to

dissociation and reduce the reaction to simple charge exchange. Evidence for stabilization in the gas phase of excited cyclohexane ions produced by electron impact has been presented elsewhere.⁵

An Infrared Study of Hydroxyl Groups on Sepiolite

by F. R. Cannings

The British Petroleum Company Limited, BP Research Centre, Sunbury-on-Thames, Middlesex, England

Accepted and Transmitted by The Faraday Society (August 8, 1967)

The idealized crystal structure of sepiolite was determined by Nagy and Bradley¹ and their deductions were substantially confirmed by the work of Brauner and Preisinger.² Other details are given in a review by Robertson,³ including information on industrial applications as a selective adsorbent, filler, and catalyst support. The dimensions of the channels in sepiolite (cross-sectional area, 5.6×11.0 Å; repeat unit-cell distance, 5.3 Å) confer importance on molecular sieving and selective adsorption processes. The general formula $H_4Mg_9Si_{12}O_{30}(OH)_{10} \cdot 6H_2O$ represents sepiolite in its ideal form, but variations in magnesium and hydrogen contents occur, depending on the source of the mineral.

To date, very little information has been published on the infrared spectra of sepiolite,⁴ and a brief examination of this property in these laboratories showed that certain features, particularly the form and location of chemisorbed molecular water, were worthy of further investigation. This note describes this work.

Experimental Section

Disks (11 mg/cm²) were formed from an acid-washed Vallecas sepiolite at a pressure of 10 tons/cm². A Grubb-Parsons GS2 double-beam infrared spectrometer was used in the investigation. All spectra were run at room temperature. Evacuation to better than 5×10^{-6} torr and gaseous dosing of the sample were done with conventional equipment. The disk was transported, horizontally, between a cell with sodium chloride windows and a furnace-enclosed quartz side arm, by a magnetic device. The cell was machined from a $9 \times 5 \times 5$ cm stainless steel bar. The windows were held in place by metal flanges tightened

(4) W. A. Chupka and E. Lindholm, *Arkiv Fysik*, **25**, 349 (1963).

(5) F. P. Abramson and J. H. Futrell, *J. Phys. Chem.*, **71**, 3791 (1967).

(1) B. Nagy and W. F. Bradley, *Amer. Mineral.*, **40**, 885 (1955).

(2) K. Brauner and A. Preisinger, *ibid.*, **44**, 752 (1959).

(3) R. H. S. Robertson, *Chem. Ind.* (London), 1492 (1957).

(4) M. Koltermann and K.-P. Müller, *Tonind. Zt. Keram. Rundschau*, **89**, 406 (1965).

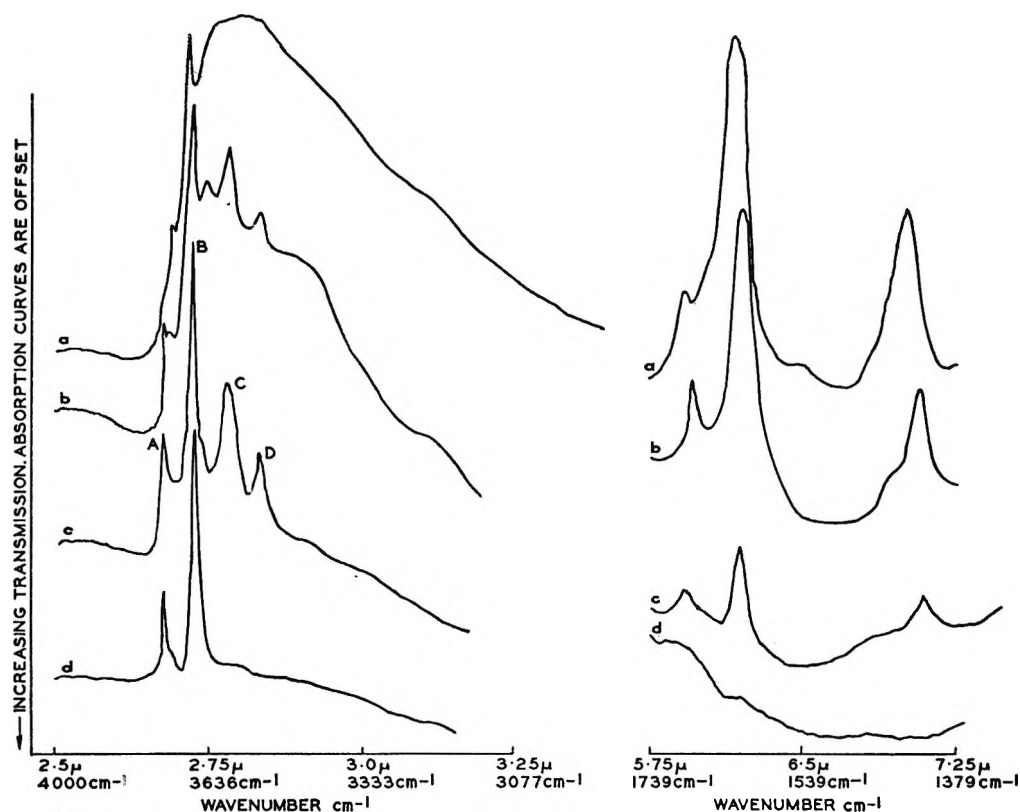


Figure 1. Spectra of sepiolite after (a) evacuation at 25°, (b) evacuation at 200°, (c) evacuation at 400°, (d) evacuation at 600°.

against rubber O rings located in grooves cut in the body of the cell. The disk could be heated, evacuated, and dosed under controlled conditions with subsequent reproducible positioning in the analytical beam.

Results and Discussion

Spectra obtained after the sepiolite was calcined and evacuated for 1 hr at the temperatures indicated are shown in Figure 1. Evacuation at 25° revealed a sharp absorption band arising from hydroxyl stretching. Pumping at higher temperatures further resolved the fundamental OH stretching region; after treatment at 400° four distinct bands at 3740, 3674, 3599, and 3532 cm^{-1} were observed (A–D in the Figure). The intensity of the peak at 1616 cm^{-1} , assignable to molecular water deformation, decreased with the rise in temperature of calcination.

Under vacuum at 600°, the lower frequency hydroxyls disappeared, together with hydroxyl bending at 1616 cm^{-1} . If the disk was subsequently exposed to a low pressure of pyridine vapor, the 3740- cm^{-1} band was immediately removed. The remaining band at 3674 cm^{-1} was unaffected, even after 30-min exposure.

In experiments carried out after evacuation at 400°, adsorbed pyridine did not alter the intensities of the 3599- and 3532- cm^{-1} bands, and in a separate test, attenuation of only the 3740- cm^{-1} band occurred, when ethylene at 760 torr was admitted to the cell.

To provide additional information, we studied the exchange of the disked sepiolite with D_2O vapor. A

fresh sepiolite disk was heated to 350° and successively dosed with heavy water and then evacuated at this temperature. Spectra of the initial and exchanged samples are given in Figure 2, together with procedural details. During this experiment the ratio of the absorbancies of the bands at 3599 (C) and 3532 (D) cm^{-1} effectively remains constant, but the intensity of band C does not decrease linearly with the loss of molecular water, as indicated by the 1616- cm^{-1} band. After evacuation at 350°, some H-bonded water is still retained by the sepiolite and this is exchanged first. Band A is also rapidly converted to its deuterioxyl equivalent. Band B is not so readily replaced.

One puzzling feature is that the intensities and the wavelengths of the exchanged lower frequency hydroxyl stretch bands (C' and D') are so low and are somewhat displaced from the anticipated positions. The frequencies of the OD bands are 2756, 2707, 2671, and 2585 cm^{-1} (A'–D' of Figure 2). The ratio of the wave numbers of the OH bands and their deuterioxyl equivalents are 1.357, 1.357, 1.347, and 1.366, respectively.

Nevertheless, the bands at 3599 and 3532 cm^{-1} are tentatively assigned to molecular water antisymmetric and symmetric stretching frequencies. Their disappearance coincides with the loss of all molecular water (1616 cm^{-1}) and it is probable that they arise from the same source. (Toropov⁵ noted the same

(5) Ya. I. Ryskin, G. P. Stautskaya, and N. A. Toropov, *Zh. Neorg. Khim.*, 5, 2727 (1960).

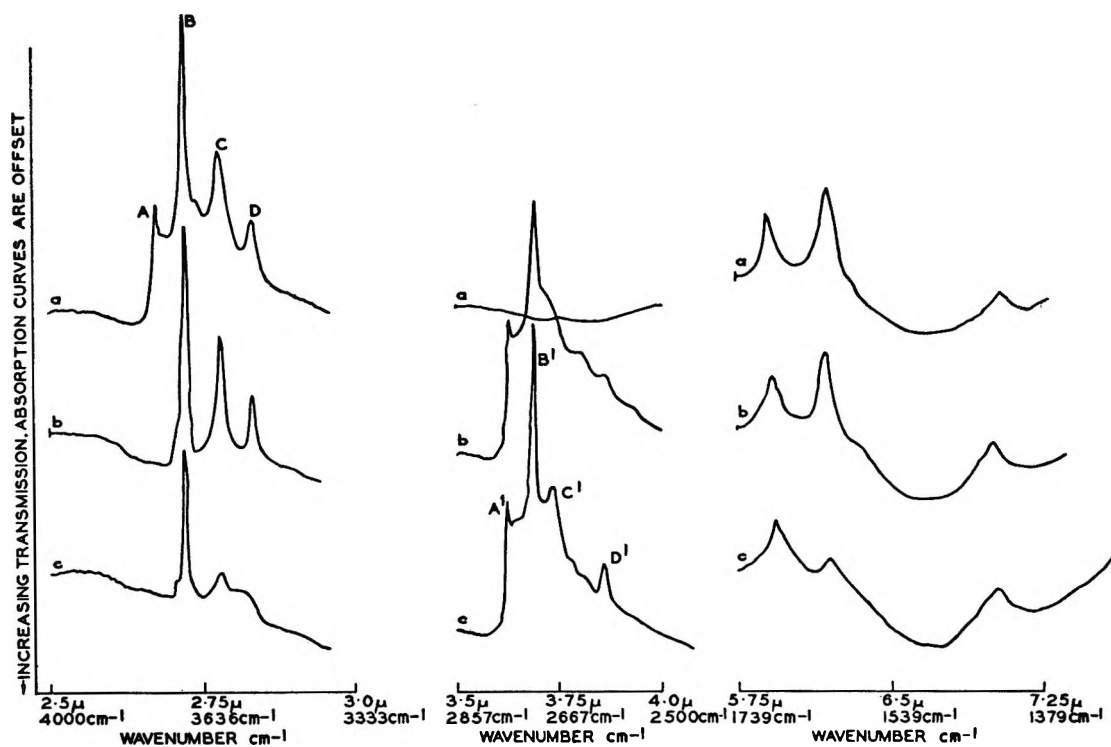


Figure 2. Spectral changes resulting from the exchange of sepiolite with D_2O : (a) sepiolite after 30-min evacuation at 350° ; (b) after 30-min exchange with D_2O and 30-min evacuation, both at 350° ; (c) after 24-hr exchange with D_2O and 30-min evacuation, both at 350° .

phenomenon for diopase.) If this is correct, it would indicate that the adsorbed molecule of water is linked through its oxygen atom to the surface. The most likely site is an electrophilic species, probably a magnesium ion. This spatial arrangement allows the hydrogens freedom to produce two sharp bands in the normal hydroxyl stretch region, similar to the spectrum observed from a dilute solution of H_2O in carbon tetrachloride.

Dehydration above 400° is predominantly irreversible and the regeneration of bands C and D lost in this treatment does not occur on the addition of water vapor at 25° to the calcined specimen.

The hydroxyl stretch bands A and B, one of which, A, rapidly exchanges with D_2O and interacts with adsorbed ethylene and pyridine, must originate from hydroxyl groups located in different environments. Angell and Schaffer⁶ observed hydroxyl bands at 3745, 3688, 3643, and 3540 cm^{-1} for a magnesium-exchanged Y-type zeolite and assigned them, respectively, to SiOH groups, possibly AlOH, a proton which has combined with surface oxygen to give SiOH adjacent to 3-coordinated aluminium, and H-bonded OH. It seems likely that the band detected at 3740 cm^{-1} (A) in this investigation arises from free hydroxyls located on silicon atoms, since all forms of dehydrated silica display absorption in the range $3740\text{--}3750\text{ cm}^{-1}$. The sharp band at 3674 cm^{-1} is assigned either to a hydroxyl on a magnesium ion, corresponding to the 3688-cm^{-1} band of Angell, or to hydroxyl produced by the reaction of

dehydrated protons with the neighboring oxygen lattice. As the band is observed after room-temperature evacuation, the latter explanation is less plausible. Adsorbed pyridine did not exhibit spectra typical of a pyridinium species,^{7,8} but, as adsorption affected only one of the four bands, this does not constitute a very comprehensive test.

Bands at 1695 and 1425 cm^{-1} have not been identified.

(6) C. L. Angell and P. C. Schaffer, *J. Phys. Chem.*, **69**, 3463 (1965).

(7) E. P. Parry, *J. Catal.*, **2**, 371 (1963).

(8) M. R. Basila, T. R. Kantner, and K. H. Rhee, *J. Phys. Chem.*, **68**, 3197 (1964).

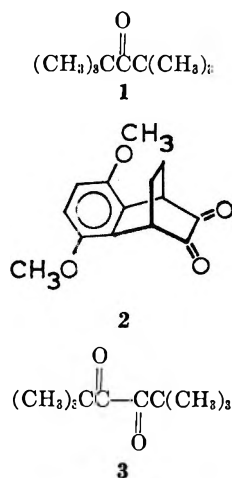
Aliphatic Semidiones. VIII. Hyperfine Splitting by Oxygen and Carbon Atoms in Semidiones¹

by Glen A. Russell and Graham R. Underwood

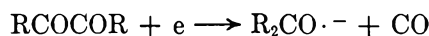
Department of Chemistry, Iowa State University,
Ames, Iowa 50010 (Received September 5, 1967)

Hyperfine splitting by ^{17}O has been observed in the esr spectra of nitroxides,² *p*-benzosemiquinone,³ nitrobenzene radical anions,⁴ and substituted phenoxy radicals.⁵

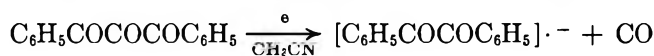
We have measured a^O for the radical anions produced by reduction of structures 1-3. It is recognized that structure 3 yields a *trans*-semidione ($RC(O\cdot)=C(O^-)-R$).⁶



In other cases, the reduction of the α -diketone could conceivably occur with decarbonylation to yield the ketyl



Processes of this type occur readily for triketones: for example, in the electrolytic reduction of 1,3-diphenyl-1,2,3-propanetrione.⁷ The investigation of a^O in structures 1-3 was undertaken to establish if this splitting



constant might serve as a definitive test for the ketyl (1) or semidione (3) structure.

The introduction of ^{17}O into structures 2 and 3 occurred readily by treatment of the diketone with ^{17}O -enriched ($\sim 10\%$) water (YEDA Research and Development Co., Ltd., Rehovoth, Israel) in dimethoxyethane solution. For structure 1, the ketone and water in the presence of 1.5 M hydrogen chloride in dimethoxyethane solution were heated at 200° (sealed tube) for 3 days. Upon cooling, structures 1 and 3 separated from an aqueous layer. For structure 2, the solvent was removed under reduced pressure. The substrates were reduced in dimethoxyethane at 25° by sodium-potassium alloy. Typical spectra are given in Figures 1 and 2 and the coupling constants are listed in Table I.

On the basis of the general theory of Karplus and Fraenkel,⁸ the value of a^O is expected to be given by eq 1 for the radical anions derived from structures 1-3.⁹ Values of $Q_{O^O} = -40$ and $Q_{CO^O} = -17$ G have been

$$a^O = Q_{O^O}\rho_O + Q_{CO^O}\rho_C \quad (1)$$

suggested.³ These values lead to a predicted value of -9.95 G for structure 2 and -12.9 G for structure 3 (estimating $\rho_O = 0.11$ and $\rho_C = 0.35$ for the *cis*-semi-

Table I: Hyperfine Splitting Constants (G) in Dimethoxyethane Solution at 25°

Substrate	$ a^H $	$ a^C $	a^{Oa}
1 ^b	0.12 (18)	52.7 (1), 7.7 (6)	-11.1
2	2.82 (2), 0.29 (2) ^c	6.15 (2) ^d	-9.95
3	0.34 ^e	3.8 (2), ^d 2.4 (6)	-10.5

^a All a^O values assumed to be negative. Line widths increased with increasing magnetic field: E. de Boer and E. L. Mackor, *J. Chem. Phys.*, **38**, 1450 (1963). ^b Previously reported (N. Hirota and S. I. Weissman, *J. Amer. Chem. Soc.*, **82**, 4424 (1960)) $a^H = 0.12$ and $a^C = 7.6$ (6) and 49.6 G in tetrahydrofuran solution. ^c Previously reported: G. A. Russell, G. W. Holland, and K.-Y. Chang, *ibid.*, **89**, 6629 (1967). ^d Total intensity was approximately 2% of spectral intensity. ^e Reference 6. Also reported as 0.31 G (G. A. Russell and E. T. Strom, *ibid.*, **86**, 744 (1964)) in dimethyl sulfoxide (80%)-*t*-butyl alcohol (20%).

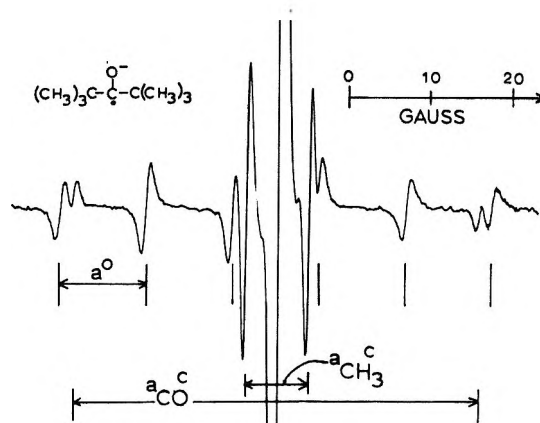


Figure 1. First-derivative esr spectrum of ^{17}O -enriched potassium ketyl in dimethoxyethane solution at 25°. Two ^{13}C splittings (natural abundance) are also seen. The ^{17}O hyperfine splittings show line width broadening as the magnetic field increases. At the concentration of ketyl employed, $a^H = 0.12$ G (18 hydrogens) is not seen.

dione (2), and $\rho_O = 0.20$ and $\rho_C = 0.29$ for the *trans*-semidione (3).⁹

(1) This work was supported by grants from the National Institutes of Health (GM 13,000-02) and the National Science Foundation (GP 6402X).

(2) J. C. Baird, *J. Chem. Phys.*, **37**, 1879 (1962).

(3) W. M. Gulick, Jr., and D. H. Geske, *J. Amer. Chem. Soc.*, **88**, 4119 (1966).

(4) W. M. Gulick, Jr., and D. H. Geske, *ibid.*, **87**, 4049 (1965).

(5) (a) K. Dimroth, F. Bär, and A. Berndt, *Angew. Chem.*, **77**, 217 (1965); (b) K. Dimroth, A. Berndt, F. Bär, R. Volland, and A. Schweig, *ibid.*, **79**, 69 (1967).

(6) G. R. Luckhurst and L. E. Orgel, *Mol. Phys.*, **7**, 297 (1963).

(7) G. A. Russell and S. A. Weiner, *J. Amer. Chem. Soc.*, **89**, 6623 (1967).

(8) M. Karplus and G. K. Fraenkel, *J. Chem. Phys.*, **35**, 1312 (1961).

(9) G. A. Russell, E. T. Strom, E. R. Talaty, and S. A. Weiner, *J. Amer. Chem. Soc.*, **88**, 1998 (1966); G. A. Russell and R. S. Stephens, *J. Phys. Chem.*, **70**, 1320 (1966).

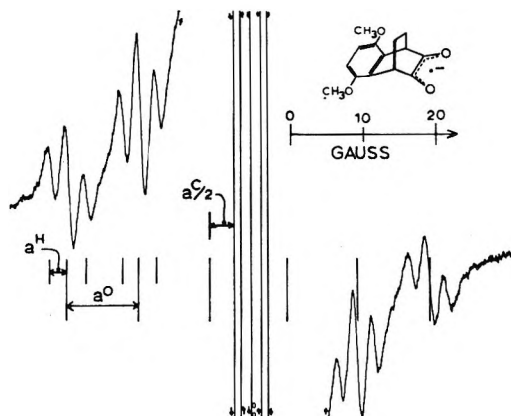


Figure 2. First-derivative esr spectrum of potassium salt of ^{17}O -enriched semidione in dimethoxyethane solution at 25° . The central three lines of the spectrum due to $a^{\text{H}} = 2.82$ G (2 hydrogens) are off scale, as are a pair of ^{13}C satellites that coincide with two of the ^{17}O splittings. The ^{13}C satellites ($a^{\text{C}} = 6.15$ G) are easily seen in the absence of ^{17}O splittings. At lower concentrations (better resolution), a second triplet, $a^{\text{H}} = 0.29$ G, is seen.

McLachlan spin densities,¹⁰ calculated to give the best fit with the available data,^{2,4} yielded values of $Q_{\text{CO}}^{\text{O}} = -20$ and $Q_{\text{O}}^{\text{O}} = -32$ G. Applying these constants yielded predicted values of a^{O} of -10.5 (*cis*) and -12.2 (*trans*) G.

However, it is obvious from the magnitude of Q_{CO}^{O} and Q_{O}^{O} preferred by others³ that no reasonable spin distributions in the di-*t*-butyl ketyl could possibly account for an oxygen hfsc of -11.1 G. It does appear that using $Q_{\text{CO}}^{\text{O}} = 0$ and $Q_{\text{O}}^{\text{O}} = -40 \pm 4$ ^{5b} G actually provides a reasonable fit with all data if ρ_{O} is assumed to be about 0.25 for the radical anions derived from structures 1–3.

The values of $a_{\text{CH}_3}^{\text{H}}$ and $a_{\text{CH}_3}^{\text{C}}$ for the radical anions derived from structures 1 and 3 are surprising. The ketyl with the highest carbonyl carbon spin density gives the smallest hydrogen coupling and the largest $^{13}\text{CH}_3$ coupling. Perhaps there is a sign reversal in the hydrogen coupling. In any event, the mechanism of this coupling is not clear.¹¹

The ^{13}C hyperfine splittings assigned to two identical carbon atoms in the semidiones derived from structures 2 and 3 could be due to the carbonyl carbon atoms¹² or the α -carbon atoms. In view of the assignment of $a_{\text{CH}_3}^{\text{C}}$ in ethyl radical as 13.57 G,¹³ the splitting by the α -carbon atoms would be expected to be $\rho_{\text{C}}(Q_{\text{C}^{\text{C}}})$. From Fessenden's data, we estimate $Q_{\text{C}^{\text{C}}} = 13.57 / [1 - (3(26.9)/508)] = 16$ G, and using $\rho_{\text{C}} \sim 0.25$, a value of $a_{\alpha}^{\text{C}} \sim 4$ G is predicted. The values found are 6.15 G for structure 2 and 3.8 G for structure 3. The difference in values of a^{C} found for structures 2 and 3 is in accord with the conclusions that the *cis*-semidiones possess a higher spin density on the carbonyl carbon atom than the *trans* isomer.⁹ This is reflected in the values of $a_{\text{CH}_3}^{\text{H}}$ in the *cis*-biacetyl (7.0 G) and

trans-biacetyl (5.6 G) radical anions in dimethyl sulfoxide solution. The absence of a third a^{C} for structure 1 is surprising. Perhaps the 7.7-G a^{C} is due to eight magnetically equivalent carbon atoms (the six methyl carbons and the two quaternary carbon atoms). The absence of detectable splitting due to a_{CO}^{C} in structures 2 and 3 is a puzzling feature. For the *trans*-biacetyl radical anion very sharp lines have been reported, but only a single a^{C} is seen (4.5 G). Here, any other value of a^{C} would have to be less than 2 G and probably less than 1 G.¹⁴

(10) A. D. McLachlan, *Mol. Phys.*, **3**, 233 (1960).

(11) K. H. Hausser, H. Brunner, and J. C. Jochims, *ibid.*, **10**, 253 (1966).

(12) E. T. Strom and G. A. Russell, *J. Chem. Phys.*, **41**, 1514 (1964).

(13) R. W. Fessenden, *J. Phys. Chem.*, **71**, 74 (1967).

(14) Diisopropylsemidione ($(\text{CH}_3)_2\text{CHC}(\text{O}^-)=\text{C}(\text{O}^-)\text{CC}(\text{CH}_3)_2\text{H}$) has been prepared by Mr. H. Malkus with ^{13}C at the carbonyl and methine positions. The observed values of a^{C} are 0.8 and 4.0 G, respectively. Biacetyl radical anion ($\text{CH}_3\text{C}(\text{O}^-)\text{CH}_3$) has been labeled with ^{13}C at the methyl position by Mr. D. Lawson. The values of a^{C} observed are 5.2 ± 0.1 and 4.5 G for the *cis* and *trans* structures, respectively. The carbonyl carbon atoms in biacetyl radical anion have also been labeled, $a^{\text{C}} = 0.50$ (*trans*) and ~ 1.2 (*cis*) G.

The Argon-Sensitized Radiolysis of Methane and Ethane in the Liquid Phase¹

by Norman V. Klassen²

Radiation Research Laboratories, Mellon Institute, Pittsburgh, Pennsylvania (Received September 22, 1967)

A study of the argon-sensitized radiolysis of liquid ethylene was reported previously.³ Energy transfer from argon to ethylene in the liquid phase was found to be very efficient. The *G* values (based on the total energy absorbed by the solutions) of acetylene, ethane, and *n*-butane were similar for the radiolysis of an argon solution containing only 0.05 mol % ethylene and for the radiolysis of pure ethylene. It seemed significant that the *G* values of all measured products were constant when the ethylene concentration of the irradiated solutions was varied between 1 and 0.05%. The present report of the radiolysis of argon–methane and argon–ethane solutions in the liquid phase shows a similar pattern of product formation with change in hydrocarbon concentration.

Experimental Section

The methane and ethane were purified by gas chromatography to reduce hydrocarbon impurities to levels

(1) Supported in part by the U. S. Atomic Energy Commission.

(2) Division of Applied Physics, National Research Council of Canada, Ottawa, Ontario.

(3) N. V. Klassen, *J. Phys. Chem.*, **71**, 2409 (1967).

Table I: Radiolysis of Liquid Methane-Argon at -182°

Concentrations, electron %			CH ₄ converted, ^a %	<i>G</i> values ^b				
CH ₄	Argon	Solute		C ₂ H ₆	C ₂ H ₄	C ₃ H ₈	<i>i</i> -C ₄ H ₁₀	<i>n</i> -C ₄ H ₁₀
100	0	...	0.1	2.24	0.00	0.21	0.010	0.012
35.7	64.3	...	0.06	1.86	0.00	0.20	0.004 ^c	0.010 ^c
35.7	64.2	0.1 NO	0.03	0.69	0.24	0.034	0.036	0.028
35.2	63.8	1.0 NO	0.03	0.47	0.21	0.022	0.018	0.018
30.5	59.1	10.4 NO	0.03	0.24	0.12	0.013	0.011	0.020
10.5	89.5	...	1.3	1.60	0.005	0.19	0.0015	0.0090
0.51	99.49	...	0.3	1.05	0.003	0.053	0.0017	0.0044
0.50	99.49	0.01 C ₂ H ₄ ^d	7.1	1.62	...	0.82	0.0066	0.27
0.22	99.78	...	10	1.0	0.00	0.04
0.055	99.945	...	0.8	1.03	0.00	0.065

^a These values are merely estimates made in order to indicate the approximate conversions of methane. For this purpose a value of 10 was chosen for $G(-\text{CH}_4)$. ^b *G* values are based on the total energy absorbed by the solutions. ^c This value was determined by graphical interpolation and not by experiment. ^d Cyclopropane was carefully looked for in this experiment but was not found.

at which impurities were undetected by the analytical procedures used to measure radiolysis products. The argon was Matheson Prepurified grade. It was passed through a bed of glass beads at -183° . The argon and methane were further purified by exposure to freshly deposited films of misch metal in order to remove oxygen.⁴

The irradiations and analyses were performed in the same manner as described previously.³ Irradiations were carried out in a uniform field of Co⁶⁰ γ rays at a dose rate in liquid argon of 6×10^{17} eV/g min (10^4 rads/min). The homogeneous liquid solutions of argon-methane and argon-ethane were irradiated in Pyrex ampoules at -182° , using a constant temperature bath of liquid oxygen held slightly above atmospheric pressure. After an irradiation, the liquid oxygen was discarded because of the ozone which accumulated in it.

All *G* values reported here are based on the total energy absorbed by the solutions.

Results and Discussion

Argon-Methane Radiolysis. Argon-sensitized radiolysis has already been observed for gaseous⁵⁻⁸ and solid⁹ methane. The present results, given in Table I, show that considerable sensitization occurs in the liquid phase also. It is seen that $G(\text{C}_2\text{H}_6)$ and $G(\text{C}_3\text{H}_8)$ are constant at low methane concentrations. The product yields determined here for pure methane at -182° are in agreement with the radiolytic yields found by Gillis⁴ for liquid methane at -161° . Also included in Table I are several experiments in which nitric oxide or ethylene were present in the solutions.

Ethylene was found as a product in the presence of NO, while, at the same time, the ethane and propane yields were depressed. The effect of NO may be complicated since it probably reacts with free radicals and

ions. Radical scavenging by NO would prevent the formation of ethane by methyl radical dimerization. It is probable that the presence of NO actually led to ethylene formation, rather than merely protected ethylene from further reaction. If ethylene were produced in the absence of NO, it would react with hydrogen atoms to form ethyl radicals. Under the present conditions, ethyl radicals would disproportionate to ethane and dimerize to *n*-butane with approximately equal probability.³ However, in the absence of NO only minor amounts of *n*-butane were found. The formation of *n*-butane in the presence of added ethylene indicates a substantial yield of hydrogen atoms which react with ethylene to form ethyl radicals.

Argon-Ethane Radiolysis. Efficient energy transfer has been observed in the radiolysis of gaseous argon containing 4% ethane.¹⁰ The present results, given in Table II, show that efficient energy transfer occurs in the liquid phase also. The *G* values of hydrocarbon products are essentially constant at low ethane concentrations. It is suspected that the small decrease in $G(\text{C}_4\text{H}_{10})$, as the ethane concentration was reduced below 1%, was due to traces of oxygen in the ethane. This suspicion is held because some of the *n*-butane is likely to have free-radical precursors which would be susceptible to scavenging by oxygen and because the ethane was not subjected to oxygen removal by misch

(4) H. A. Gillis, *J. Phys. Chem.*, **71**, 1089 (1967).

(5) J. Maurin, *J. Chim. Phys.*, **59**, 15 (1962).

(6) V. Aquilanti, *J. Phys. Chem.*, **69**, 3434 (1965).

(7) R. W. Hummel, *Trans. Faraday Soc.*, **62**, 59 (1966).

(8) G. G. Meisels, W. H. Hamill, and R. R. Williams, *J. Phys. Chem.*, **61**, 1456 (1957).

(9) P. Ausloos, R. E. Rebbert, and S. G. Lias, *J. Chem. Phys.*, **42**, 540 (1965).

(10) G. von Bunau, *Ber. Bunsenges. Physik. Chem.*, **69**, 16 (1965).

metal treatment as were the methane and argon. The product yields given in Table II for 100% liquid ethane are in qualitative agreement with the results of Gillis¹¹ for the radiolysis of liquid ethane at higher temperatures.

Table II: Radiolysis of Liquid Ethane-Argon at -182°

C ₂ H ₆ , electron %	C ₂ H ₆ con- verted, ^a %	G values ^{b,c}			
		CH ₄	C ₂ H ₄	C ₂ H ₂	n-C ₄ H ₁₀
100	0.1	0.33	0.89	0.24	1.81
55.8 ^d	0.2	0.49	1.03	0.30	1.57
10.0	0.03	...	0.15	0.29	1.00
10.0	0.06	...	0.12	0.29	0.99
10.0	0.12	...	0.09	0.28	0.86
10.0	0.18	...	0.10	0.34	1.10
0.89	1.4	...	0.00	0.14	0.59
0.10	5.6 ^e	0.046	0.00	0.12	0.40
0.048	1.4	...	0.00	0.12	0.39

^a These values are merely estimates made in order to indicate the approximate amount of ethane decomposed in each experiment. They are based on a hypothetical value of 10 for $G(-C_2H_6)$ (see footnote e). ^b G values are based on the total energy absorbed by the solutions. ^c Acetylene was detected in several experiments. In all cases $G(C_2H_2)$ was less than 0.1. ^d A product, probably butenes, was produced with a G value of 0.08. ^e This conversion was experimentally determined. It corresponds to a value of 3.3 for $G(-C_2H_6)$. This suggests that some high molecular weight products may have been formed.

The radiolyses of argon solutions containing less than 1% of methane, ethane, or ethylene provide interesting data. The initial absorption of energy in these solutions is almost entirely by argon. Yet it is obvious that, in each case, a large fraction of the absorbed energy is ultimately utilized to destroy the hydrocarbon solute. For all solutes, the G value of each product was constant over the range 1–0.05% solute. Thus, it has been shown that the constancy of G values at low solute concentrations is not peculiar to the ethylene solutions studied previously.³ It seems that, at low hydrocarbon concentrations, energy transfer occurs through one or more long-lived species which can react completely even with 0.05% hydrocarbon. The constant G values seem to preclude argon ions as the energy-transfer species, since geminate recombination of argon ions and electrons should compete with charge transfer to hydrocarbon solute in the low-concentration range. For this reason, it was stated previously³ that electronically excited argon is the most likely energy-transfer species at low solute concentrations.

(11) H. A. Gillis, *J. Phys. Chem.*, **67**, 1399 (1963).

The Action of Lead Monoxide as an Inorganic Photosensitizer

by W. C. Tennant

Chemistry Division, Department of Scientific and Industrial Research, Wellington, New Zealand (Received October 12, 1967)

In a recent paper,¹ a mechanism was proposed for the zinc oxide photosensitized photolysis of PbCl₂ and certain other inorganic salts in aqueous mixtures. Photolysis was shown to result from electron transfer from ZnO to the decomposing molecule following the absorption of radiation by the sensitizer. Aqueous interaction of the two components is a necessary prerequisite to the electron transfer.

Lead monoxide also undergoes aqueous interaction with many heavy-metal salts,² it has a favorable absorption spectrum³ and possesses n-type photoconducting properties.⁴ Hence it might be expected that PbO could parallel ZnO in its action as an inorganic photosensitizer, although no instances have apparently been reported in the literature.

This note discusses the action of lead monoxide in photosensitizing the photolyses of PbCl₂, PbBr₂, and HgCl₂ in aqueous mixtures. The photosensitizing action is shown to be a function of the yellow form of lead monoxide only, and possible reasons for this are discussed.

Experimental Section

A Norelco X-ray diffractometer was used to study the products of aqueous interaction of PbO with PbCl₂, PbBr₂, and HgCl₂.

The energy dependences of the photolyses studied were determined with a Philips 120-W medium-pressure quartz mercury lamp in conjunction with the appropriate color filters.

Absorption spectra of the red and yellow forms of PbO and of the three salts studied were measured with a Beckmann DU spectrophotometer, using the standard reflectance attachment and using magnesium oxide as the reference. The spectra are shown in Figure 1. The extent of decomposition of irradiated mixtures was taken as proportional to the blackening produced and was measured as the percentage decrease in reflected light at 7000 Å, where the salts and both forms of PbO are completely reflecting.

(1) W. C. Tennant, *J. Phys. Chem.*, **70**, 3523 (1966).

(2) H. R. Oswald and W. Feitknecht, *Helv. Chim. Acta*, **44**, 847 (1961).

(3) C. F. Goodeve, *Trans. Faraday Soc.*, **33**, 340 (1937).

(4) L. Heijne, *Philips Res. Rept. Suppl.*, No. 4 (1961).

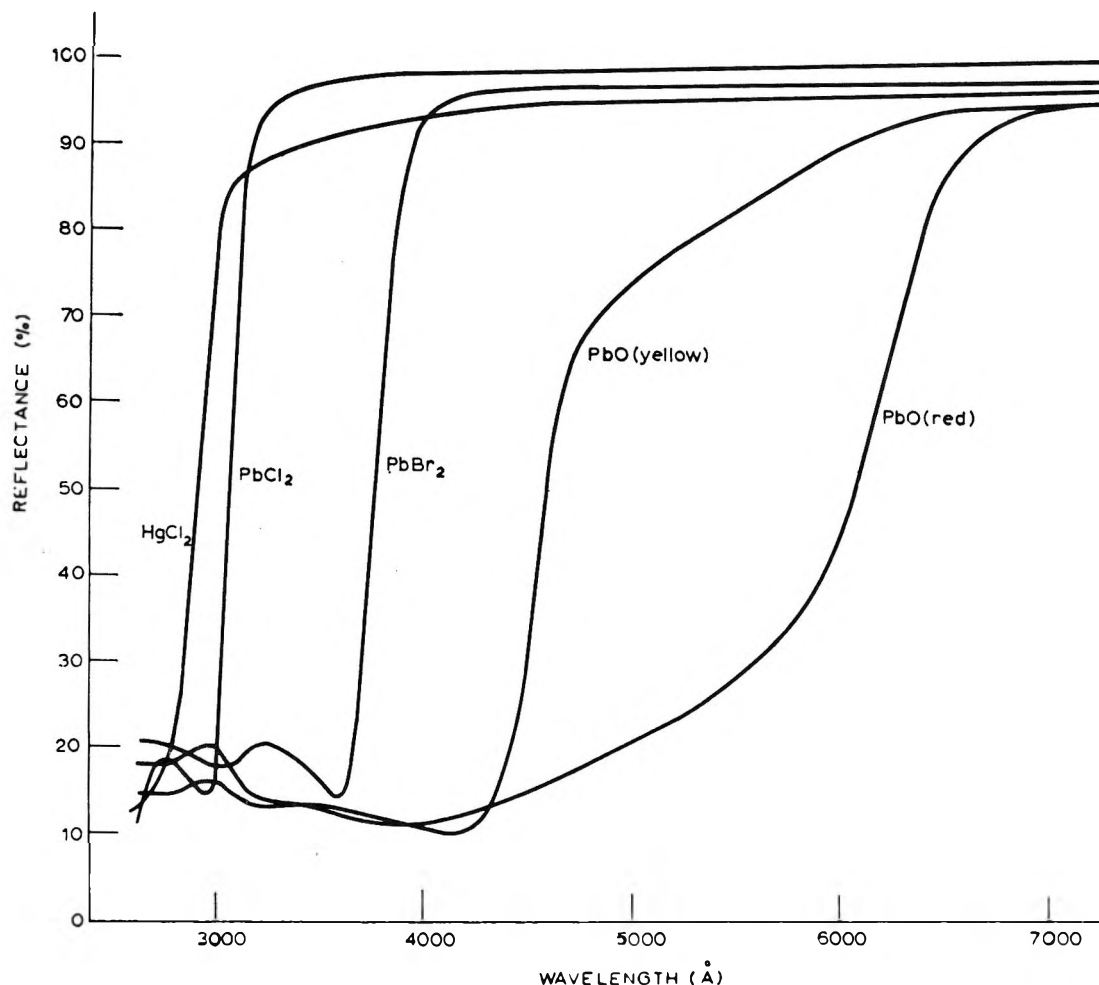


Figure 1. Absorption spectra of solid powders.

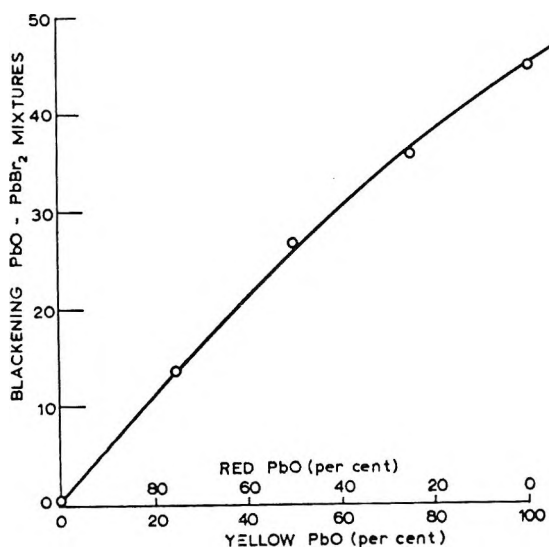
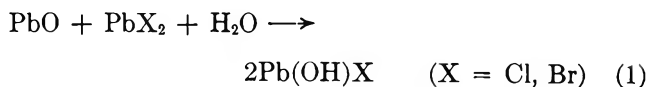


Figure 2. Relation between PbO-PbBr₂ blackening and the crystal form of PbO.

Results and Discussion

X-Ray examination of wetted powder mixtures showed that the yellow orthorhombic form of PbO

reacts with PbCl₂ and PbBr₂ to form Pb(OH)Cl and Pb(OH)Br, respectively. A stoichiometric equation of the form



can be proposed, although the reactions are never complete. X-Ray powder patterns of wetted yellow PbO-HgCl₂ mixtures showed almost complete disappearance of PbO and HgCl₂ and the formation of a new compound (or compounds) which, however, could not be identified from the ASTM powder file. However, a reaction similar to eq 1, with the formation of a basic chloride of mercury, appears almost certain to occur. The red tetragonal form of PbO also reacts with the three salts in aqueous mixtures, but the reaction products were in each case amorphous and could not be identified by X-rays.

Wetted mixtures of yellow PbO with PbCl₂, PbBr₂, or HgCl₂ blackened markedly within 10 min when exposed to light of wavelength shorter than about 4300 Å. Each of the three salts alone is decomposed by radiations on the short-wavelength side of its absorption edge

(see Figure 1). The photosensitized reactions only took place in mixtures which had been wetted, and only the yellow form of PbO was effective as the photosensitizer. This is shown clearly in Figure 2, where the photosensitized decomposition (blackening) of PbBr₂ in admixture with various proportions of red and yellow PbO is shown to be nearly proportional to the amount of yellow oxide present.

From the description of the photochemical reactions given above, it is clear that the photosensitizing action of the yellow form of PbO closely parallels that of ZnO.¹ In the case of ZnO photosensitization, the decomposition of lead chloride arises from electron transfer from the ZnO to PbCl₂ and this only takes place following aqueous interaction of the two. It was proposed¹ that this aqueous interaction was necessary to lock the two components rigidly together in a solid mass of basic chlorides, thus providing an efficient contact for electron transfer to occur. An entirely similar interpretation is obviously applicable

to the PbO-photosensitized photolyses of PbCl₂, PbBr₂, and HgCl₂.

The ineffectiveness of the red form of PbO as a photosensitizer is, at first sight, somewhat surprising, since both forms of PbO are strongly absorbing in the photoactive region (see Figure 1) and both are known to exhibit n-type photoconductivity, at least to some extent.^{4,5} However, in the case of the tetragonal PbO, the photoconductivity has its maximum value at about 6000 Å,⁵ which is outside the photosensitizing range, and hole conduction is predominant.⁶ A further possibility, as suggested by the X-ray evidence, is that aqueous interaction of the red form with the salts studied does not result in efficient contact between the sensitizer and decomposing crystal, so that electron transfer does not readily occur.

(5) V. A. Izvozhikov and G. A. Bordovskii, *Dokl. Akad. Nauk SSSR*, **145**, 1253 (1962).

(6) O. I. Kolesova, *Chem. Abstr.*, **58**, 6302e (1963).

COMMUNICATIONS TO THE EDITOR

The Reaction of Nitrogen Atoms with N₂O₅¹

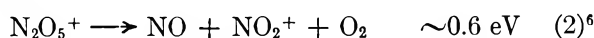
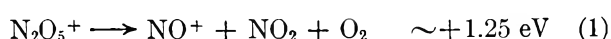
Sir: In the radiolysis of nitrogen-oxygen mixtures using polonium-210 α particles and examination of the absorption spectra in the infrared, N₂O₅ was observed along with O₃.² As the radiolysis proceeded, the O₃ disappeared and the N₂O₅ was found to decay giving rise to NO₂. In addition, the radiolysis of ¹⁴N₂-¹⁵N₂ and mixtures of ¹⁴N₂-¹⁵NO indicated the presence of nitrogen atoms with a *G* value of approximately 2.³ The question then arose whether the reaction of N atoms with N₂O₅ contributes to the disappearance of N₂O₅ in the radiolysis experiments.

The apparatus used in this experiment has been previously described.⁴ Nitrogen atoms were prepared by the use of a condensed discharge in a Woods-Bonhoeffer tube. The concentration of the nitrogen atoms was determined by titration with NO⁵ and checked with a time-of-flight mass spectrometer. The partial pressure of the nitrogen atoms was 0.025 torr. The N₂O₅ was prepared by the interaction of O₃ and NO₂. The N₂O₅ was trapped in a Dry Ice bath and fractionally distilled. Only the middle fraction was used in these experiments. The N₂O₅ was added directly to the flowing system which was kept at 0.2 torr. The partial pressure of N₂O₅ was between 0.005 and 0.010 torr. The linear velocity of the flowing gases was 40 m/sec.

To observe the mass spectrum at low ionizing electron energies, a digital voltmeter was added to the Bendix time-of-flight mass spectrometer since the potentiometer built into the instrument was not exactly linear in its lower values. In this way the average energy of the ionizing electrons could be directly measured.

In examining the mass spectrum of N₂O₅, no parent ion N₂O₅⁺ was observed. The fragment ions NO⁺ and NO₂⁺ were formed at a nominal ionizing electron energy of 11.5 V. The relative intensities of these ions at the electron energy used in our experiments, 11.5 eV, was *m/e* 30, 83.3%, and *m/e* 46, 16.7%.

The processes which can give rise to the observed fragmentation pattern are



Reaction 4



did not occur since no signal at *m/e* 32 was observed. This is consistent with the higher value for the ionization potential of O₂ of 12.2 eV.⁷

In examining the reaction of nitrogen atoms with N₂O₅, we observed no change in the signal from *m/e* 30 (NO⁺) or 46 (NO₂⁺). We used the *m/e* 30 signal to measure the concentration of N₂O₅ in the gas phase. Under our experimental conditions of an excess of nitrogen atoms, any nitric oxide formed from the reaction of N + N₂O₅, would be consumed at once by the reaction N + NO → N₂ + O. If N₂O₅ were attacked by nitrogen atoms, the NO⁺ signal would be reduced. The N₂O₅ as measured by the signal at *m/e* 30 showed only a very minor change when mixed with an excess of nitrogen atoms. An examination of *m/e* 14 (N atoms) showed only a minute change, less than 1%, when N₂O₅ was added to the system. In addition, no chemiluminescence was observed at the point of the addition of N₂O₅. Also, there was no change in the intensity of the nitrogen afterglow. These observations indicate that either there is no reaction or the reaction is very slow.

Since our instrumentation can determine reaction rate constants between 10⁻¹¹ and 10⁻¹⁵ cc/particle sec, we would estimate that the rate constant for the reaction of N atoms with N₂O₅ is smaller than 10⁻¹⁵ cc/particle sec.

Thus the reaction of N atoms with N₂O₅ plays no important role in the radiation chemistry of N₂-O₂ mixtures since any N atoms present will react faster with O₂ and even with O₃. The disappearance of N₂O₅ in the radiolysis experiments must be by a mechanism other than a reaction with N atoms. In general, the mechanism previously indicated by Harteck and Dondes⁸ still is pertinent although charge transfer from

(1) This research was supported by the U. S. Atomic Energy Commission under Contract AT(30-3)-321.

(2) P. Harteck, S. Dondes, and B. Thompson, *Science*, **147**, 393 (1965).

(3) P. Harteck and S. Dondes, *ibid.*, **146**, 30 (1964); R. D. Brown, S. Dondes, and P. Harteck, USAEC Document RPI-321-9 (Oct 1966); M. Anbar and P. Perlstein, *J. Phys. Chem.*, **68**, 1234 (1964); D. H. Dawes and R. A. Back, *ibid.*, **69**, 2385 (1965).

(4) G. Liuti, S. Dondes, and P. Harteck, *J. Am. Chem. Soc.*, **88**, 3212 (1966).

(5) P. Harteck, R. R. Reeves, and G. Mannella, *J. Chem. Phys.*, **29**, 608 (1958).

(6) The ionization potential for NO₂⁺ used here is 9.78 eV, from the work of T. Nakayama, M. Y. Kitamura, and K. Watanabe, *ibid.*, **30**, 1180 (1959).

(7) V. I. Vedenev, L. V. Gurvich, V. N. Kondrat'yev, V. A. Medvedev, and Ye. L. Frankevich, "Bond Energies, Ionization Potentials and Electron Affinities," St. Martin's Press, New York, N. Y., 1966.

(8) P. Harteck and S. Dondes, *ibid.*, **28**, 975 (1958).

N_2^+ and O_2^+ ions to N_2O_5 , followed by the fragmentation of the N_2O_5 molecule adds to the complexity of the system.

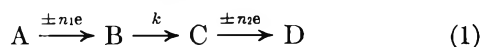
RENSSELAER POLYTECHNIC INSTITUTE
TROY, NEW YORK 12181

G. LIUTI
S. DONDES
P. HARTECK

RECEIVED DECEMBER 4, 1967

Homogeneous Chemical Kinetics with the Rotating Disk Electrode. The ECE Mechanism

Sir: The application of the rotating disk electrode to the study of the ECE electrolysis mechanism



has recently been discussed by Malacheský, Marcoux, and Adams.¹ They presented this approximation for the limiting current

$$i_e = 0.62nFAC_A^b D^{2/3} \gamma^{-1/6} \omega^{1/2} [2 - \exp(-0.834 \times \gamma^{1/3} k / D^{1/3} \omega)] \quad (2)$$

where C_A^b is the bulk concentration of A, D is the diffusion coefficient, γ is the kinematic viscosity, ω is the angular velocity, and k is the first- or pseudo-first-order rate constant. Equation 2 was obtained by combining results from hydrodynamic studies² with an equation arising in the chronoamperometric treatment of the ECE mechanism for a stationary electrode of constant area.³ The latter describes the instantaneous situation at an electrode with constantly changing concentration profiles. When a limiting current is measured with a rotating disk electrode, however, the concentration profiles are at a steady state and the use of chronoamperometric results can provide only an approximation to the truth.

An expression, for the ECE mechanism, describing the variation of current with time in a controlled-potential electrolysis using a macroelectrode has been presented.^{4,5} It may be used to describe the steady-state current at a rotating disk electrode if one sets $t = 0$ and substitutes the appropriate expression for the diffusion layer thickness δ . Considering, as did Malacheský, Marcoux, and Adams, that²

$$\delta = 1.62D^{1/3} \gamma^{1/6} \omega^{-1/2} \quad (3)$$

the result is

$$i_e = 0.62nFAC_A^b D^{2/3} \gamma^{-1/6} \omega^{-1/2} \times \left[2 - \frac{\tanh(1.62D^{-1/6} \gamma^{1/6} \omega^{-1/2} k^{1/2})}{1.62D^{-1/6} \gamma^{1/6} \omega^{-1/2} k^{1/2}} \right] \quad (4)$$

As in eq 2, it is assumed that $n_1 = n_2 = n$ and that the diffusion coefficients of all species are identical. Equation 4 does not involve an approximation comparable to the one inherent in eq 2.

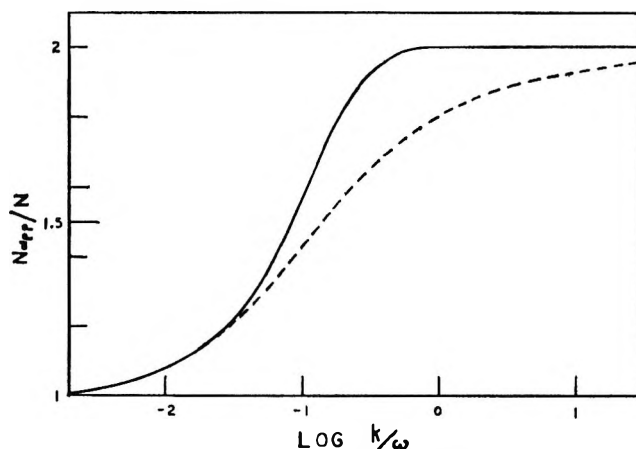


Figure 1. Plot of n_{app}/n vs. $\log(k/\omega)$. Solid line shows curve calculated from eq 5; dashed line shows curve calculated from eq 6. It is assumed that $D = 10^{-5}$ cm²/sec and that $\gamma = 10^{-2}$ cm²/sec.

Malacheský, Marcoux, and Adams used the apparent n value, n_{app} , to correlate their experimental results. From eq 2, they obtain

$$\frac{n_{app}}{n} = 2 - \exp(-0.834 \gamma^{1/3} k / D^{1/3} \omega) \quad (5)$$

Similarly, from eq 4

$$\frac{n_{app}}{n} = 2 - \frac{\tanh(1.62D^{-1/6} \gamma^{1/6} \omega^{-1/2} k^{1/2})}{1.62D^{-1/6} \gamma^{1/6} \omega^{-1/2} k^{1/2}} \quad (6)$$

Values of n_{app}/n for various values of k/ω were calculated from eq 5 and 6 with typical values for the constants γ and D and are plotted in Figure 1. Although both approaches give qualitatively similar results, they exhibit significant quantitative differences. However, as is apparent from their Figure 1, Malacheský, Marcoux, and Adams varied k/ω over only a rather narrow range (approximately 0.02–0.04) in which their equation yields values indistinguishable from those obtained by the present treatment.

In brief, this note presents a treatment of the ECE mechanism for the rotating disk electrode similar in some respects to that previously presented,¹ but not involving a major approximation made there.

Acknowledgment. It is a pleasure to acknowledge the interest and numerous suggestions of Professor Louis Meites.

(1) P. A. Malacheský, L. S. Marcoux, and R. N. Adams, *J. Phys. Chem.*, **70**, 4068 (1966).

(2) V. G. Levich, "Physicochemical Hydrodynamics," Prentice-Hall, Inc., Englewood Cliffs, N. J., 1962.

(3) G. S. Alberts and I. Shain, *Anal. Chem.*, **35**, 1859 (1963).

(4) S. Karp and L. Meites, *J. Electroanal. Chem.*, in press.

(5) S. Karp, Ph.D. Thesis, Polytechnic Institute of Brooklyn, 1967.

DEPARTMENT OF CHEMISTRY
LONG ISLAND UNIVERSITY
BROOKLYN, NEW YORK 11201

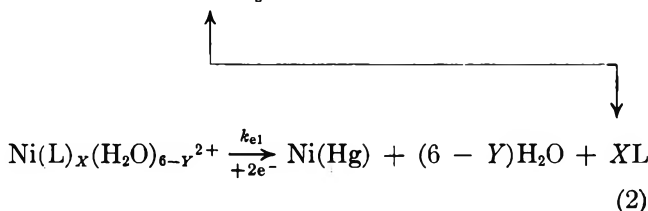
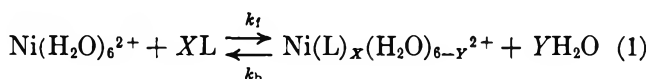
STEWART KARP

RECEIVED DECEMBER 18, 1967

Evidence for the Formation of a Surface Complex as the Rate-Determining Step in the Polarographic Reduction of Certain Nickel(II)-Organic Amine Complexes.

Effect of the Structure of the Electrical Double Layer¹

Sir: Several groups of investigators have reported prewaves which arise at potentials positive to the usual $\text{Ni}(\text{H}_2\text{O})_6^{2+}$ reduction when a variety of complexing agents, such as pyridine, *o*-phenylenediamine, ethylenediamine, triethylenetetramine, chloride ion, etc., are present.²⁻⁶ When the $\text{Ni}(\text{H}_2\text{O})_6^{2+}$ ion concentration is in large excess with respect to the complexing agent, L, the limiting current of the prewave is much larger than would be expected for the diffusion-controlled reduction of a nickel(II)-ligand complex of some form.^{2,3,5} Thus, the prewave mechanism is thought to involve the cyclic regeneration of the ligand according to the reaction sequence²⁻⁴



While there is agreement among the different groups that the above mechanism is correct and the formation of the complex (eq 1) is the rate-determining step, one group contends that the formation of this more easily reduced complex occurs only at the surface (the excess $\text{Ni}(\text{H}_2\text{O})_6^{2+}$ diffusing to the electrode reacts with adsorbed ligand).^{2,3,6,7} The other group argues that the ligand, on release from the complex on reduction (eq 2), diffuses away from the electrode and reacts with the excess $\text{Ni}(\text{H}_2\text{O})_6^{2+}$ in the "bulk" of the solution.^{8,9} Both groups employed indirect plausibility arguments to support their proposed mechanisms.^{3,8} However, no direct or unique experimental evidence has been reported. Tur'yan and Malyavinskaya actually state that their calculated reaction layer thickness^{8,9} "lies in acceptable ranges . . . of the elimination of the influence of the electrical double layer on the kinetics of the chemical reaction . . ." but they did not carry out double-layer-effect studies. Thus, a study of the properties of the electrical double layer was undertaken in an effort to resolve this point. The structure of the double layer can be varied significantly by varying both the nature and the concentration of the supporting electrolyte in these experiments.¹⁰

Experimental Section

All experimental techniques and procedures employed here are identical with those previously described,^{2,3,7} except that the drop time of the dme was controlled mechanically at 4.0 sec,⁷ and no Ca^{2+} salts were added.¹¹ Also all chemicals (supporting electrolytes, solvent, and ligand) were carefully purified⁷ according to standard practices.

Results and Discussions

As mentioned above, a variety of ligands have been studied, but each gave similar results. It was decided to employ *o*-phenylenediamine for the study of the double-layer effect on the prewave as this species gives a well-defined prewave.^{3,7} Gierst¹⁰ has shown that for a surface rate-determining reaction preceding the electron-transfer reaction (where L is an uncharged species specifically adsorbed on the electrode), the velocity, V^* , of this reaction will be a function of the potential of the reaction plane, Ψ° [Ψ° is actually the potential of the outer Helmholtz plane^{7,10} but is considered to be also the plane of closest approach for most electrochemical reactive species^{7,10}], as given by

$$V^* = V_0 \exp\left(-\frac{ZF}{RT}\Psi^\circ\right) \quad (3)$$

(1) This research was supported in part by the National Science Foundation, Grants No. GP-4620 and GP-6425, and the U. S. Army Office of Research (Durham), Contract No. DA-31-124-ARO-D-284.

(2) H. B. Mark, Jr., and C. N. Reilley, *J. Electroanal. Chem.*, **4**, 189 (1962); *Anal. Chem.*, **35**, 195 (1963).

(3) H. B. Mark, Jr., *Anal. Chem.*, **36**, 940 (1964); *J. Electroanal. Chem.*, **7**, 276 (1964); **8**, 253 (1964).

(4) Ya. J. Tur'yan and G. G. Serova, *Fiz. Khim.*, **31**, 1976 (1957); Ya. I. Tur'yan, *Dokl. Akad. Nauk SSSR*, **148**, 848 (1962); *Zh. Fiz. Khim.*, **39**, 257 (1965).

(5) J. V. Nelson and R. T. Iwamoto, *J. Electroanal. Chem.*, **6**, 234 (1963).

(6) D. C. Olson, *Anal. Chem.*, **39**, 1785 (1967).

(7) L. R. McCoy, Ph.D. Thesis, University of Michigan, 1967; L. R. McCoy, H. B. Mark, Jr., and L. Gierst, unpublished results, 1967.

(8) Ya. I. Tur'yan and O. N. Malyavinskaya, *Elektrokhimiya*, **2**, 1185 (1966); *Sov. Electrochem.*, **2**, 1082 (1966).

(9) Reaction in the "bulk" of the solution is defined here and in ref 8 as any reaction plane or thickness that is at a distance beyond the influence of the electrical double layer, *i.e.*, greater than a minimum of 100 Å. Tur'yan and Malyavinskaya calculate a reaction layer thickness of 2.8×10^{-4} cm based on their model and their estimate the equilibrium constant of formation of the nickel(II)-ligand complex (eq 1).

(10) L. Gierst "Transactions of the Symposium on Electrode Processes," John Wiley and Sons, Inc., New York, N. Y., 1959, Chapter 5; J. Dandoy and L. Gierst, *J. Electroanal. Chem.*, **2**, 116 (1961); according to these authors, if an electrochemical reaction such as eq 1 involves an adsorbed ligand or occurs only at the surface, the rate of this reaction k_f will be dependent on the potential gradient and, hence, the structure of the electrical double layer. If the reaction is a "bulk" reaction, no effect of double-layer structure on the rate will be observed (note that Tur'yan and Malyavinskaya agree on this point; see ref 8).

(11) The Ca^{2+} acts as a maximum suppressor for the $\text{Ni}(\text{H}_2\text{O})_6^{2+}$ wave to increase the definition of the prewave (see ref 2, 3, and 7) but would be an added confusion in double-layer studies.

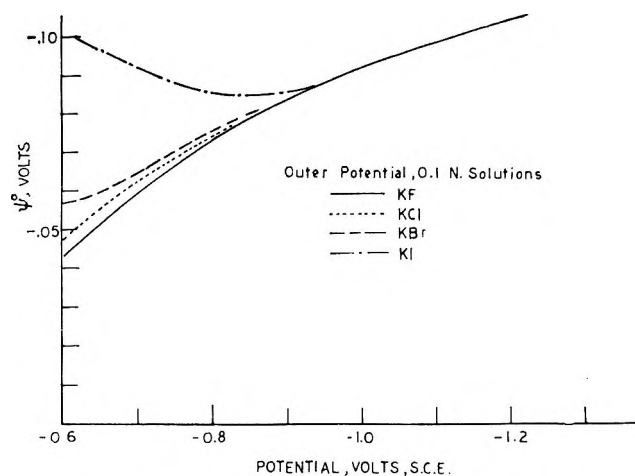


Figure 1. Variation of the outer Helmholtz potential, Ψ° , with electrode potential for 0.1 *N* solutions of potassium halides.

where $V_0 = \sqrt{DKk_t}$, Z is the charge of the reaction species, F , R , and T have their usual electrochemical meaning,¹¹ and D and K are the diffusion coefficient of the $\text{Ni}(\text{H}_2\text{O})_6^{2+}$ and the equilibrium constant of eq 1, respectively. Thus, the limiting current of a catalytic prewave will vary, according to eq 3, with the nature (with both the cation and anion) of the supporting electrolyte and with its concentration,^{7,10} if the rate-determining reaction takes place at the electrode surface.

Figure 1 shows the effect of variation of the nature of the anion of the supporting electrolyte on the potential of the outer Helmholtz plane Ψ° , as determined by differential capacitance measurements.^{7,12} These data show that the order of strength of specific adsorption of the anions is $\text{I}^- > \text{Br}^- > \text{Cl}^- > \text{F}^-$. Thus, Ψ° is considerably more negative at a given applied potential between -0.6 and -0.9 V *vs.* sce for iodide than bromide, than chloride, than fluoride. Thus, if the rate-determining step takes place within the electrical double layer, the limiting current should vary according to eq 3. Figure 2 shows the polarographic behavior of the nickel(II)-*o*-phenylenediamine system as a function of the variation of the anion of the supporting electrolyte (constant concentration of supporting electrolyte). The observed increase of the limiting current as well as

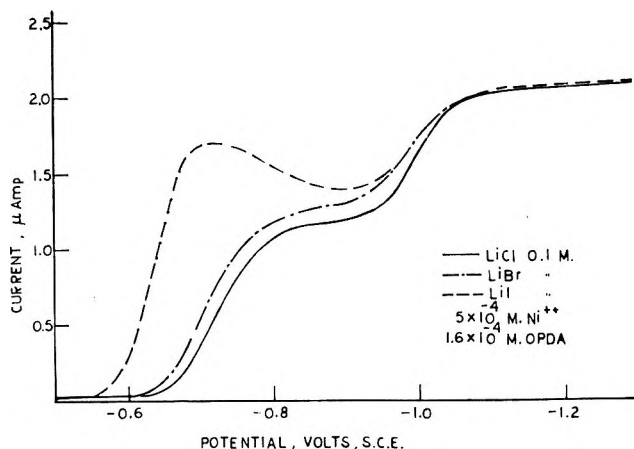


Figure 2. Effect of anion adsorption on the shape and amplitude of the prewave (0.1 *N* solutions of the halide salts).

the shape of the prewave as a function of the anion of the supporting electrolyte is exactly that predicted by eq 3. Also, variations of the prewave limiting current and wave shape with the cation and concentration of the supporting electrolyte were found to agree with those predicted by eq 3.^{7,13} Thus, there can be no doubt that the rate-determining reaction (eq 1) takes place at the surface of the electrode.

Further studies on the exact digital computer solution for each kinetic model of the over-all, both heterogeneous and homogeneous, electrode mechanism (both surface and bulk control), the adsorption properties of ligands that show a catalytic prewave, and the study of effect of the structure of various ligands on both the heterogeneous and homogeneous kinetic properties of the prewave are now in progress and will be reported in the near future.

(12) P. Delahay "New Instrumental Methods in Electrochemistry," Interscience Publishers, Inc., New York, N. Y., 1954.

(13) L. R. McCoy, H. C. MacDonald, Jr., E. Kirowa-Eisner, and H. B. Mark, Jr., unpublished results, 1967.

DEPARTMENT OF CHEMISTRY
UNIVERSITY OF MICHIGAN
ANN ARBOR, MICHIGAN 48104

HARRY B. MARK, JR.
LOWELL R. MCCOY
EMILIA KIROWA-EISNER
HUBERT C. MACDONALD, JR.

RECEIVED DECEMBER 18, 1967